5-2015

Application of Nonlinear Site Response Analysis in Coastal Plain South Carolina

Md. Ariful Haque Bhuiyan
Clemson University

APPLICATION OF NONLINEAR SITE RESPONSE ANALYSIS IN COASTAL PLAIN SOUTH CAROLINA

A Dissertation
Presented to
the Graduate School of
Clemson University

In Partial Fulfillment
of the Requirements for the Degree
Doctor of Philosophy
Civil Engineering

---

by
Md. Ariful Haque Bhuiyan
May 2015

Accepted by:
Dr. Nadarajah Ravichandran, Committee Chair
Dr. Ronald D. Andrus
Dr. C. Hsein Juang
Dr. Weichiang Pang

This research was supported by the South Carolina Department of Transportation (SCDOT) and the Federal Highway Administration (FHWA) under SCDOT project No. 686. The views and conclusions contained in this dissertation are those of the author and should not be interpreted as necessarily representing the official policies, either expressed or implied, of SCDOT or FHWA.

ABSTRACT

The 1933 Long Beach, 1957 San Francisco, 1967 Caracas, 1985 Mexico City, 1989 Loma Prieta, and 1994 Northridge earthquake events left evidences of how the local site condition can affect the characteristics of propagating earthquake wave from the bedrock through the top soil. The ground motion amplitude, frequency content or the duration can be affected by the local site condition and thus can cause significant amplification or de-amplification to the original bedrock motion which can seriously affect the structures. Quantification of such site effect on ground motions is a challenging task. This dissertation is dedicated to improve the existing ground response quantification techniques and the related knowledge base.

The first major attempt towards ground response quantification was the development of the 1994 NEHRP (BSSC, 1995) seismic site factor provision. Since the development of the NEHRP provisions, several studies have found these factors to produce inadequate predictions for the state of South Carolina. In an attempt to generate seismic site factors based on conditions specific to South Carolina Coastal Plain (SCCP), a series of nonlinear one-dimensional ground response analyses are performed by this author as part of a research team considering appropriate soil profiles and location specific ground excitations. After the generation of this new site factor model, a systematic repercussions study is performed by applying earthquake loads, considering both NEHRP and the new site factors, on typical highway bridge structures.

Being exposed to the realm of nonlinear site response studies, the author feels that this sector lacks sufficient benchmarking studies over the code usage protocols and

therefore its use in the practitioners' community has been limited to date (Stewart et al., 2008; Matasovic and Hashash, 2012). This author performs a benchmarking study over several widely used nonlinear one-dimensional site response analysis tools considering the ground motions and soil profiles specific to the Charleston, SC region. A few key issues are addressed: (i) the modeling techniques of several NL site response programs are reviewed for the site; (ii) comparative study over the site factors computed based on several nonlinear and equivalent linear analysis programs produce important insights; and (iii) a guideline stating the conditions required for selecting a nonlinear analysis over an equivalent linear analysis program.

One dimensional site response analysis is limited to horizontally layered ground conditions. Earlier studies showed that topographic variations such as ground slopes can significantly affect the computed surface response. Considering the conditions specific to the Charleston, South Carolina area, two-dimensional finite element models of a range of sloping (mild and infinite) ground cases are analyzed. Based on the outcomes, a slope adjustment factor is proposed which modifies the existing one-dimensional site factors to account for the ground inclination in the design.

Shear wave velocity (V_S) is an important input for any seismic site response study. The author observed significant shear strain accumulation at V_S contrast locations at the layer interfaces in previous studies. A numerical investigation dedicated to the effect of such stiffness contrast on the seismic surface response is performed. Smoothening these contrast locations reduced the imposed shear strain, thus lesser damping and higher surface spectral accelerations are obtained.

DEDICATION

This dissertation is dedicated to my mother, my elder brother, my wife and my siblings in recognition of their love, care and inspiration.

ACKNOWLEDGMENTS

During the four and half year-long graduate study I was surrounded by numerous professors, colleagues and friends who served as an inspirational source of support in all levels; academic, moral or personal. Nonetheless, if I have to personify my life in Clemson University, my advisor Dr. Nadarajah Ravichandran stands out. With his professionalism, energetic involvement and immense patience, he generously guided me to my academic adulthood. He is 'the one' who planted a researcher in me and has trained me well how to nurture it. It was a great privilege for me working with him. No word in the dictionary is suitable enough to express my gratitude to him. I honestly pray to God for his and his family's wellbeing.

I would also like to express my sincere gratitude to Dr. Ronald Andrus for his valuable guidance, technical insights and constant support throughout this study. I also would like to thank my committee members Dr. C. Hsein Juang and Dr. WeiChiang Pang for their great support and valuable comments. I send my honest gratitude to Dr. Youssef Hashash for making the program DEEPSOIL available to the research community.

I want to thank my friend Dr. Akhter Hossain for his constant helps and supports since the day one of my stay in Clemson. I would also like to mention Dr. Shimelies Aboye for his un-parallel helps in my research. I am grateful to Michael Esposito for reviewing my dissertation.

I acknowledge the support, love and care I received from my family members. Finally, I remember the Bangladesh Association of Clemson (BAC) members, especially Mr.'s Mizan, Sunny, Sajib and Asif, for their constant support, care and friendship.

TABLE OF CONTENTS

Table of Contents (Continued) Page

Table of Contents (Continued) Page

Table of Contents (Continued) Page

Table of Contents (Continued) Page

Table of Contents (Continued) Page

Table of Contents (Continued) Page

LIST OF TABLES

Table Page

List of Tables (Continued) Page

LIST OF FIGURES

Figure Page

List of Figures (Continued) Page

List of Figures (Continued) Page

CHAPTER 1

INTRODUCTION

1.1 Overview

The earthquake events like 1933 Long Beach, 1957 San Francisco,1967 Caracas, 1985 Mexico City, 1989 Loma Prieta, and 1994 Northridge are important examples of how local site conditions affect the characteristics of wave propagation through the top soil. The ground motion parameters such as amplitude, frequency content or the duration can be affected by the local site condition and may result in amplification or de-amplification to the original bedrock motion. Therefore the structures on the ground surface (or even the buried structures i.e. tunnels) can be seriously affected by such phenomena and need to be accounted for during the design phase. Quantification of site effects on ground motions is a challenging task. This dissertation is dedicated to improve the existing ground response quantification techniques and the related knowledge base.

1.2 Motivation

1.2.1 Necessity of a new seismic site factor model for SCCP

The concept of seismic site factor, ratio of the spectral acceleration at the ground surface to that of the rock outcrop at a specific spectral period, is used in the design of geotechnical and structural systems to consider the effect of geologic and seismic conditions. The first major step towards ground response quantification was the development of the NEHRP (BSSC, 1995) provision. This provision proposed site factors

at 0.2 s (F_a) and 1.0 s (F_v) periods and since then this provision was adopted by several other specifications including SCDOT (2008a).

Since the development of the NEHRP site factors in 1994, a number of studies (Borcherdt, 2002; Stewart et al., 2003; Park and Hashash, 2004) found that the recommended site factors under-predict in certain soil and loading conditions and over-predict in some other cases. In South Carolina, several studies (Hwang et al., 1997; Power et al., 1998; Lester and Chapman, 2005; Chapman et al., 2006) showed that the NEHRP site factors are un-conservative. A possible reason is NEHRP assumes a single value (i.e. site factor) for an entire site class which covers a wide range of soil conditions (stiffness). Engineers at the South Carolina Department of Transportation (SCODT) also found un-conservativeness in the NEHRP code provisions during several of their projects. Therefore, a new set of site factors needs to be developed for the State of South Carolina considering the local geologic and seismic conditions.

1.2.2 Benchmarking of nonlinear site response analysis for Charleston, SC area

Although both equivalent linear and nonlinear one-dimensional site response analyses are used for conducting seismic site response analysis, the nonlinear codes better predict the seismic response when the system behaves in the highly nonlinear zone. For decades, practitioners debated the conditions for which nonlinear analysis is required. Recently, a few guidelines have been developed (Kramer and Paulsen, 2004; Matasovic and Hashash, 2012; Kaklamanos et al., 2013 and 2015; Kim et al., 2013) for choosing the appropriate analysis procedure. These guidelines have several limitations and therefore

more work is needed to develop comprehensive criteria for choosing appropriate procedure with standard inputs.

Moreover, the use of nonlinear site response analysis by practicing engineers has been limited due to lack of clear guidance on the code usage protocols and parameter selections (Stewart et al., 2008). Engineers at the SCDOT have been looking for a benchmarking study over a nonlinear site response analysis tool for the state of South Carolina. Another issue is that the computed surface response and the resulting site factors vary significantly with the type and the computer program used for the analysis (Kottke, 2010; Zalachoris, 2014). Therefore, a comprehensive study to compare and quantify the difference in computed site factors from industry standard site response analysis tools is needed for better practice.

1.2.3 Effect of mild infinite ground slope on site response analysis

One dimensional site response analysis is limited to horizontally layered ground conditions where the earthquake wave energy is assumed to propagate only in the vertically upward (1-D) direction which may not always be an appropriate assumption. Numerous earthquake events like: 1971 San Fernando earthquake, 1987 Whittier Narrows earthquake and 1999 Athens earthquake etc. showed abundant effects on the earthquake wave propagation characteristics due to topographic variations. One of the commonly seen topographic features is mild infinitely sloping ground conditions where economic importance exists. These sloping ground conditions are often approximated to horizontal ground conditions so that the seismic site response analysis can be conducted

using one-dimensional codes. A two-dimensional plain strain approximation is necessary to effectively handle such a sloping (mild and infinite) ground condition.

1.2.4 Effect of V_S contrast in ground response analysis

Shear wave velocity (V_S) is an important parameter of seismic site response analysis. Commonly, shear wave velocity measurements (from field tests such as: seismic cone, crosshole seismic, multichannel analysis of surface waves, refraction microtremor etc. or resonant column test in laboratory) for a site are simplified by discretizing the entire soil profile to a number of homogeneous layers with a constant V_S value for each layer. Therefore, to represent an increased or decreased shear wave velocity in the immediate layers a sudden rise and drop of V_S values at the layer interfaces i.e. the V_S contrasts are inevitable. In this manner the geotechnical engineer compiles the 'working' V_S profile. This has been a wide spread practice in the community for decades as this simplification is advantageous to the day-to-day geotechnical engineering related computations (both analytical and numerical). However, this assumption of sudden contrast of V_S in the layer interfaces is often unnatural; as opposed to a gradual increase or drop in V_S. During site response analysis such sudden changes in V_S incur unrealistically high shear strain at those interface locations, especially on the softer side of the interface (Stewart et al., 2008; Kottke, 2010; Matasovic and Hashash, 2012; Bozzano et al., 2012; Gouveia et al., 2012; Brandenberg et al., 2013), a major issue of such assumption. The excessive shear strain can cause significant amount of energy loss (damping) during the seismic wave propagation through that interface which may

eventually reduce the amplitude of the surface response from ground response analysis (Gouveia et al., 2012).

1.2.5 Repercussions of new seismic site factor model on highway structures

The development of new seismic site factors for the SC locations may greatly affect the design of highway structures (i.e. bridges) in this area. The new site factors may produce significant variation in the structural design demand as compared to the NEHRP site factors and thus a major impact from the economic stand-point is expected. Analysis of typical bridge structures with earthquake loads considering both the NEHRP and the new site factors to perform a systematic comparison of the computed seismic demands from both sides can deliver the best opportunity to visualize the repercussions of the new site factors in actual application.

1.3 Objectives

The objectives of this dissertation are as follows:

1. Perform nonlinear time domain one dimensional site response analysis for four locations selected from the coastal plain South Carolina: Charleston, Myrtle Beach, Columbia and Aiken. These nonlinear one dimensional simulation outcomes are combined with the equivalent linear simulations (performed by Dr. Shimelies Aboye as part of the research group) to develop a new seismic site factor model for the coastal plain of South Carolina (Aboye et al., 2011, 2013a, 2013b and 2014; Andrus et al., 2014).

2. Perform a benchmarking study over nonlinear one-dimensional site response analysis code usage protocols. This involves:
    a. The Rayleigh damping parameters calibration based on comparison with the computed responses from equivalent linear code while the system behaves linearly (i.e. within linear elastic strain range).
    b. Comparison of the outcomes from nonlinear and equivalent linear site response analysis programs over a range of earthquake loadings and site conditions typical of subsurface conditions in Charleston.
    c. Generation of several seismic site factor models each of which are based on a separate site response program and then are compared. Several nonlinear and equivalent linear site response analysis tools are employed to obtain important insights from such relative comparison.
    d. Propose a set of criteria to determine for which conditions a nonlinear site response analysis is warranted over equivalent linear analysis.
3. Perform ground response analysis for sloping (mild and infinite) ground condition using two dimensional finite element simulations with OpenSees. A range of 'infinite' ground slopes, seismic loadings and site conditions specific to Charleston area are considered. Based on the outcomes, the new site factor model for horizontal ground conditions is updated to account for the infinitely sloping ground conditions in structural design.

4. To observe the effect of soil layer interface V_S contrast on the computed surface response by comparing the ground responses computed using V_S profiles with interface contrasts and the corresponding 'smoothed' interfaces.
5. Finally, to study the repercussions of the newly generated site factor model for the South Carolina Coastal Plain (SCCP) by applying earthquake loadings, generated based on both the new and the current (NEHRP) site factors, on typical bridge structures to compare the computed structural responses from Multi-Modal Response Spectrum analysis.

1.4 Contributions

This dissertation will over-all contribute to the existing knowledge base of seismic ground response studies. The specific anticipated contributions are:

1. This author contributed to the generation of the new seismic site factor model (Aboye et al., 2011, 2013a, 2013b and 2014; Andrus et al., 2014) for the SCCP which will replace the existing NEHRP site factor provisions for this region.
2. The benchmarking study over the one dimensional nonlinear site response analysis will provide a comprehensive guideline for the engineers of the Charleston, SC area which is currently unavailable for the region.
3. Proposed a unique guideline under which conditions a nonlinear site response analysis is warranted over an equivalent linear analysis.
4. An update to the new seismic site factor model to extend its applicability to the sloping ground (mild and infinite) conditions specific to Charleston area.

5. The observed effect of sudden stiffness contrast in soil layer interfaces on computed seismic responses is a brand new addition to the site response knowledge base and a potential source of error in site response estimation.

1.5 Dissertation Organization

This dissertation report is organized into nine chapters. Chapter 2 provides a background overview of the existing knowledge base of the seismic ground response study.

Chapter 3 presents the thousands of nonlinear time domain one dimensional site response analysis outcomes performed for the selected SCCP locations: Charleston, Myrtle Beach, Columbia and Aiken. These simulation outcomes are used to develop new seismic site factor provisions for the SCCP.

Chapter 4 presents the comparison of the outcomes of thousands of nonlinear and equivalent linear one-dimensional site response analyses for Charleston, SC. This chapter covers: the Rayleigh damping parameters calibration; comparison of the outcomes from nonlinear and equivalent linear programs over a range of earthquake loadings and soil profile variations; development of several site factor models each based on separate nonlinear and equivalent linear site response programs and then to compare; and finally, development of a set of criteria for under which conditions a nonlinear site response program is warranted over an equivalent linear type program.

Chapter 5 presents site response analysis for sloping (mild and infinite) ground conditions for Charleston, SC region. Based on the outcomes, an update to the new site factor provision is proposed to extend its applicability for the sloping ground conditions.

Chapter 6 presents the evaluation of the effect of sudden shear wave velocity contrast on seismic site responses.

The repercussions of the newly proposed site factor model for the South Carolina Coastal Plain (SCCP) are discussed in Chapter 7. The earthquake loadings, generated based on both the new and the current (NEHRP) site factors, are applied on two highway bridge structures to compare the structural responses using the Multi-Modal Response Spectrum analysis.

Chapter 8 presents a few studies in which the author was responsible to perform nonlinear ground response analyses with one dimensional approximation.

Finally, the major outcomes of the dissertation and recommendations for future research are summarized in Chapter 9.

CHAPTER 2

BACKGROUND REVIEW

2.1 Introduction

Local site condition can significantly affect the seismic wave while it is propagating from bedrock to the ground surface (Kramer, 1996). Depending on the type and sequence of soil layers at a site, ground motions can be amplified or de-amplified as was illustrated in the 1933 Long Beach, 1957 San Francisco,1967 Caracas, 1985 Mexico City, 1989 Loma Prieta, and 1994 Northridge earthquakes. Therefore, ground response evaluation is one of the most important geotechnical earthquake engineering problems for the both the professional and research communities. The goal is to develop the design response spectra at the ground surface which is a quantification of the induced forces on the structure. Then the seismic analysis of the structure is performed to establish the respective design demand.

In this chapter, at first a few terminologies common in ground response study are discussed; the current code provisions are reviewed; and a generalized overview of the current seismic site response analysis methodologies, advancements and validation efforts are presented.

2.2 Common Terminologies of Ground Response Analysis

Ground response analysis techniques are mostly problem oriented and often are grouped on the basis of dimensionality of the specific problem type: one, two or three-dimensional analysis techniques. Within each technique, further variation exists with

respect to the soil material modeling approximations i.e. linear, equivalent-linear or nonlinear stress-strain relationships (Kramer, 1996). In this study the primary focus is on nonlinear one- and two-dimensional ground response analysis techniques and their applications. Before going in-to further details some important terminologies and analysis techniques are reviewed:

Response spectra: A response spectrum represents for a particular input motion the maximum response of a SDOF (single-degree-of-freedom) system which is dependent on the natural frequency (or period) and damping ratio of the system. Maximum responses are calculated on different SDOF systems with different natural periods and a response spectra versus period plot is generated (Kramer, 1996). Although the acceleration response spectra are widely used in earthquake engineering practice (and also in this study) velocity and displacement response spectra can also be generated.

Average shear wave velocity at top 30 m (V_{S30}): The average shear wave velocity in the top 30 m (V_{S30}) of soil profile is defined as (Borcherdt, 1994):

$$V_{S30} = \frac{30}{\sum_{i=1}^{n} \frac{H_i}{V_{Si}}} \tag{2.1}$$

where H_i is the thickness of soil layer 'i' in meter; V_{Si} is the shear wave velocity of layer 'i' in m/s; and n is the number of soil layers in the top 30 m from the ground surface.

Seismic site factor: The site factor for a specific period is defined by the following equation (SCDOT, 2008a):

$$F=\frac{S_{Site}}{S_{Outcrop}} \quad (2.2)$$

where S_{Site} is the spectral acceleration computed at the ground surface and $S_{Outcrop}$ is the B-C soft-rock outcrop spectral acceleration. Both the parameters correspond to the same period as the site factor to be calculated.

Acceleration Design Response Spectra (ADRS) curves: The acceleration design response spectra (ADRS) are generated based on seismic site factors of different periods. ADRS curves are used to perform seismic analysis of structures to determine the required design demand. South Carolina Department of Transportation (SCDOT) is currently using site factors which are originally adopted from the NEHRP provisions (BSSC, 1995 and 2010). The historical development of the NEHRP provisions is discussed in a later section. Figure 2.1 describes the procedure of generating three point ADRS curves using three factors F_{PGA}, F_a and F_v at 0.0 sec, 0.2 sec and 1.0 sec periods (T), respectively (SCDOT, 2008a).

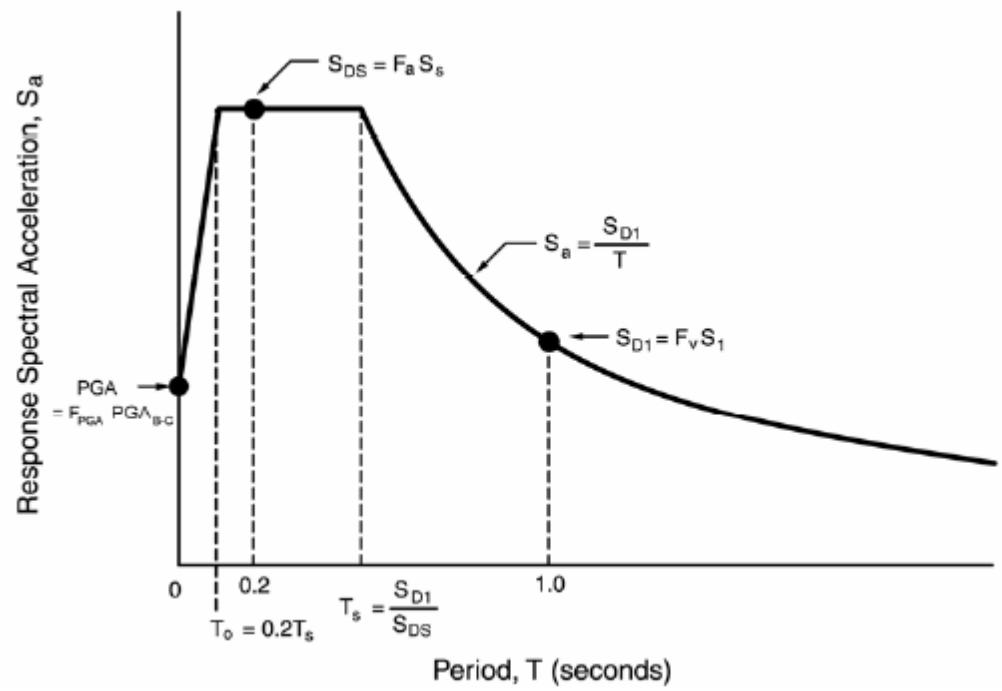

Figure 2.1: Three-point ADRS curve development methodology (SCDOT, 2008a).

Site-response analysis: After a fault rupture takes place (i.e. initiation of an earthquake event), body waves spread in every directions and propagate through different layers of geologic materials while reflections and refractions at the layer interfaces define their travel path to the ground surface. Generally speaking, waves propagate with decreasing velocity as they approach to the ground surface, causing the waves to refract at the horizontal layer interfaces until the wave path becomes near vertical (Figure 2.2). This is the basis for the approximation of one-dimensional site response analysis in the case of horizontally layered soil deposit where vertical shear-wave propagation from the underlying bedrock to the ground surface is assumed (Kramer, 1996).

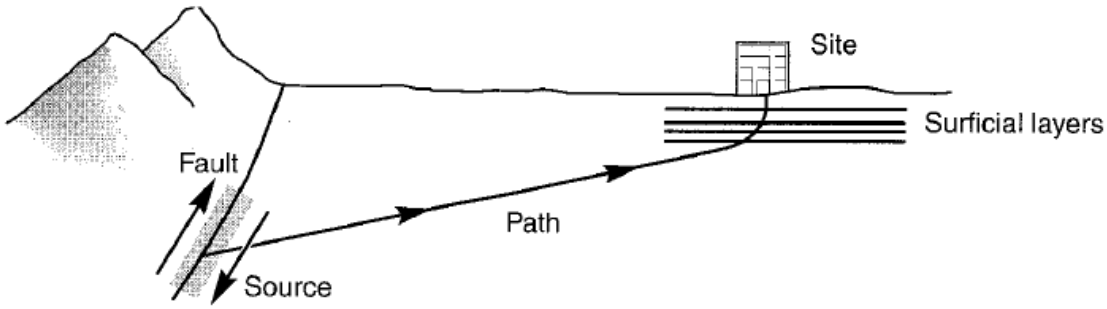

Figure 2.2: Wave propagation towards ground surface through parallel soil layers and intermediate boundaries (Kramer, 1996).

2.3 Development of NEHRP provisions

The first major attempt to quantify the effect of soil response on earthquake motion was the development of the NEHRP provision. The site factors for short-period or 0.2 sec (F_a) and long-period or 1.0 sec (F_v) first appeared in the 1994 NEHRP seismic provisions (BSSC, 1995 and 2010). SCDOT (2008a) adopted the NEHRP F_a values for peak horizontal ground acceleration site factor (F_{PGA}), which corresponds to the 0.0 sec spectral period or free-field condition. Values of F_a and F_v were set based on two different approaches:

(i) At small levels of shaking (peak ground accelerations ≈ 0.1 g) F_a and F_v were derived from empirical investigations using strong motion data recorded in San Francisco during the 1989 Loma Prieta earthquake (Borcherdt, 1994; Borcherdt and Glassmoyer, 1992; Joyner et al., 1994).

(ii) At stronger levels of shaking, due to lack of strong motion data on soft soil sites, F_a and F_v were derived from the results of one-dimensional equivalent linear and nonlinear site response analyses (Dobry et al., 1994; Seed et al., 1994).

In both these approaches, empirical regression curves were fitted to the amplification data as a function of mean shear wave velocity in top 30 m (V_{S30}) of the site. Using these regression lines the amplification factors (or site factors) were calculated at the middle value of the V_{S30} range corresponding to each site class and adopted in the NEHRP provisions as site factors. For example, in Borcherdt (1994) for site class III, which has a V_{S30} range of 200-375 m/s, the middle point selected was 290 m/s and the corresponding amplification factor was taken as the site factor for that entire site class. Finally a consensus process was held among the experts where the NEHRP factors were finalized and adopted in several other specifications (ASCE, 2010; AASHTO, 2011; ICC, 2012; BSSC, 2010; SCDOT, 2008a).

2.4 Equivalent Linear (EL) Site Response Analysis

Frequency domain equivalent linear (EL) analysis can better approximate soil nonlinearity than a linear system (Kramer, 1996). SHAKE (Schnabel et al., 1972) is a widely used program of this kind. In this method an equivalent linear shear modulus, G and an equivalent linear damping ratio, ζ representing energy loss of a single cycle (i.e. hysteresis loop) are required. Calculating G and ζ is a five step procedure (according to Kramer, 1996):

i. At first initial estimates of G and ζ are made correspond to the small strain values.

ii. These G and ζ are then used to perform ground response which computes the shear strain time history for each layer.

iii. The maximum shear strain is measured from the shear strain time history for each layer. This maximum strain is then multiplied by a ratio, R to compute an effective shear strain for that layer. R is a function of the earthquake magnitude, M_w (Idriss and Sun, 1992):

$$R = \frac{M_w - 1}{10} \tag{2.3}$$

iv. Using this effective strain, the corresponding G and ζ are read from the user specified G-γ and ζ-γ curves for the next iteration.

v. Now steps (ii) through (iv) are repeated until the computed G and ζ from two successive iterations become very close. Thus generated equivalent linear G and ζ values are then used for the final run of this ground response analysis. These properties are kept constant during the entire earthquake excitation (i.e. final run) and thus this method cannot account for soil stiffness changes during an event.

EL analysis is widely used because of simplicity, low computational requirement and also availability of good documentation on the code usage protocol. Limitations are: high amplification of responses when frequency matching occurs from both the loading and soil profile sides; filtering of high frequency motion; and over and under damping of the system due to erroneous selection of effective shear strain.

2.5 Nonlinear (NL) Site Response Analysis

Nonlinear (NL) site response analysis can provide improved predictions compared to the corresponding equivalent linear or linear analyses counterparts when the system behaves nonlinearly due to either larger loading and/or softer materials, given that the nonlinear model parameters are obtained/ modeled accurately. However, due to the lack of knowledge in determining the necessary model parameters and the limitations of the stress-strain models, the nonlinear analysis has always been the least used or preferred by the practitioners (Stewart et al., 2008; Matasovic and Hashash, 2012). This section briefly discusses the methodologies and current advancements related to total stress type nonlinear site response analysis.

2.5.1 Methodologies

The following dynamic equation of motion is solved in nonlinear time domain site response analysis:

$$\mathbf{M}u'' + \mathbf{C_R}u' + \mathbf{K}u = \mathrm{f} \qquad (2.4)$$

where **M** is the mass matrix, $\mathbf{C_R}$ is the viscous damping matrix, **K** is the nonlinear stiffness matrix, **f** is the excitation at the base of the layer and u, u' and u'' are the relative displacement, velocity and acceleration vectors, respectively. This dynamic equation of motion is solved at each time step using a time-integration scheme (e.g. Newmark's Beta method).

Soil layers are discretized into multi-degree of freedom lumped masses or using finite elements (Kramer, 1996). Figure 2.3 (adopted from Stewart et al., 2008) presents a schematic representation of a lumped mass and a distributed mass system (i.e. using finite

elements) system in the case of one-dimensional earthquake wave propagation through a multi-layered stratum. Here lumped masses are assumed at each layer interface with mass contributions (half of the mass) from each of the adjacent layers and thus mass matrix, **M** is developed for the problem. These masses are then connected to each other through a set-up with a nonlinear spring and a viscous damping dashpot. Soil behavior is accounted for using a constitutive model that can simulate cyclic behavior of soil. The stiffness matrix, **K** is updated at each time step (i.e. dynamically) and thus incorporates the system nonlinearity. DMOD2000 (Matasović and Ordóñez, 2011) and DEEPSOIL (Hashash, 2011) implement lumped-mass concept while OpenSees (McKenna and Fenves, 2001) uses finite elements to represent the soil continua and will be described in a later chapter.

Over the years a broad range of soil constitutive models have been employed into the study of nonlinear site effects over ground motion propagation. There have been some advanced plasticity based models which can capture important soil features such as pore water pressure, anisotropy or dilation (e.g. DYNA1D, Prevost, 1989; SUMDES, Li et al., 1997; and OpenSees, McKenna and Fenves, 2001). But use of such advanced soil constitutive models is not always required and simplified 'Hyperbolic' model based codes (e.g. DESRA-2, Lee and Finn, 1978; DMOD, Matasovic, 1993; and DEEPSOIL, Hashash, 2011) are sufficiently accurate and understandably more popular.

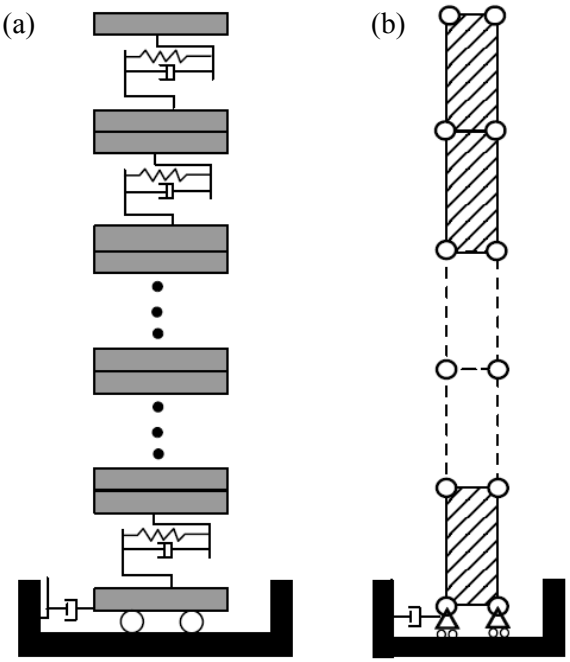

Figure 2.3: Schematic representation of (a) multi-degree of freedom lumped parameter mass system and (b) distributed mass system, which numerically represents the vertical wave propagation through a horizontally layered soil deposit (adopted from Stewart et al., 2008).

2.5.2 Damping estimation

2.5.2.1 *Viscous damping*

Full Rayleigh damping (Hudson et al., 1994) is widely accepted for small strain damping (i.e. viscous damping, $\mathbf{C_R}$) estimation in different nonlinear time domain site response analysis packages. $\mathbf{C_R}$ is expressed as a function of mass and stiffness as follows:

$$\mathbf{C_R} = \alpha_R \mathbf{M} + \beta_R \mathbf{K} \tag{2.5}$$

where α_R and β_R are calculated using Equations 4.6 and 4.7, respectively (Matasović and Ordóñez, 2011).

$$\alpha_R = \xi_{tar}\left(\frac{4\pi}{T}\right)\left(\frac{n}{(n+1)}\right) \tag{2.6}$$

$$\beta_R = \left(\xi_{tar}T\right)\left(\frac{1}{\pi(n+1)}\right) \tag{2.7}$$

where ξ_{tar} is the target damping ratio obtained through calibration and ranging from 0.1 to 5%, T is the fundamental period of the soil profile given by $T = 4H / V_{S,avg}$, H is the total depth of the soil profile considered, $V_{S,avg}$ is the weighted average of the shear wave velocity of the profile-layers and n is an odd integer (1, 3, 5, 7 etc.) related to mode number.

The natural frequency of the soil profile (first mode) corresponds to n = 1 and the higher numbers are related to higher mode. DMOD2000 requires n value correspond to the higher mode in addition to the first mode (n = 1) for full Rayleigh damping calibration. The parameter ξ_{tar} is the small (insignificant) strain damping of each of the soil layers. DMOD2000 uses a single ξ_{tar} value as an input for the entire profile for the simulation (rather than setting ξ_{tar} for each of the layers). Calibration is required to obtain a suitable pair of n and ξ_{tar}. This calibration is done by running DMOD2000 at a low $PGA_{Outcrop}$ and simultaneously adjusting n and ξ_{tar} until the response spectrum matches well with the corresponding SHAKE2000 response. It is assumed that the NL and EL responses should be comparable due to linear elastic behavior of soil at this small loading.

The calibration of full Rayleigh damping parameters has been a challenge for the practitioners. Both Phillips and Hashash (2009) and Hashash et al. (2010) reported that

Rayleigh damping (small-strain damping) has the tendency to over-dampen the system in the case of deep profiles and thus computed responses may be under-predicted.

Phillips and Hashash (2009) addressed the issue of full Rayleigh damping by proposing a new frequency independent small-strain damping estimation scheme which does not require calibration; consequently the issues/challenges oriented to the Rayleigh damping parameter calibration are eliminated.

In order to formulate the new frequency independent viscous damping, Phillips and Hashash (2009) started from the damping matrix expression by Clough and Penzien (1993):

$$\mathbf{C_R} = \mathbf{M}\sum_{b=0}^{N-1} a_b \left(\mathbf{M}^{-1}\mathbf{K}\right)^b \tag{2.8}$$

where N is the number of modes/frequencies and a_b is a scalar value as defined by a constant damping ratio, ζ_n throughout the soil profile such as:

$$\xi_n = \frac{1}{4\pi f_n}\sum_{b=0}^{N-1} a_b \left(2\pi f_n\right)^{2b} \tag{2.9}$$

For the scalar index $b = ½$, the ζ_n in Equation 2.9 reduces to $\zeta_n = a_b/2$ which is frequency independent and thus frequency independent damping matrix is obtained (Phillips and Hashash, 2009).

2.5.2.2 *Hysteretic damping*

Traditional nonlinear site response analysis tools are observed to have issues regarding estimation of the high strain damping as well. The hysteretic damping estimated through conventional nonlinear approaches overestimates laboratory measurements and thus over-dampens the system responses at high strains. A recent scheme developed by Phillips and Hashash (2009) has overcome this issue which enables

the nonlinear programs to better estimate both the hysteretic damping and the modulus variation as well. Details of these damping estimation improvements in nonlinear programs are discussed in Chapter 4.

2.5.3 Benchmarking studies

Park and Hashash (2004) compared EL and NL responses for deep soil sites from the Mississippi embayment. They found EL responses to be on the lower side at higher frequencies than NL analysis in the cases of large loading intensities while both the NL and EL produced similar responses at smaller loading levels.

Stewart et al. (2008) made an excellent effort on a benchmarking study over some widely used NL packages which was partly a compilation of some earlier but similar works (Kwok et al. 2007, Stewart et al. 2006 and Stewart and Kwok 2008). Most NL packages had limited documentation and practitioners were not able to work within a defined framework. Stewart et al. (2008) primarily worked on the parameter selection protocols to develop a state-of-the-art framework for using the popular one-dimensional NL site response packages. The key suggestions were:

- Outcropping motion should be used as input with an assumption of elastic base
- Full Rayleigh damping should be used if available in the program and
- For MKZ model parameters calibration, the modulus-reduction curve matching techniqueshould be followed and if available, to match both the modulus-reduction and damping curves simultaneously.

They also compared responses generated from several NL and EL packages. They found EL responses are deviating from the NL responses at around $PGA_{Outcrop}$ (peak

ground acceleration) of 0.1g to 0.2g. However, the responses from several NL programs agreed well with each other, in general.

Kottke (2010) compared the EL analysis outcomes with NL analysis and found difference in the responses at frequencies less than 5 Hz for small intensity motions (i.e. $PGA_{Outcrop} < 0.1g$). For higher intensities, NL produced lower spectral amplification than EL for cases greater than 25 Hz due to phase incoherence in the NL and EL stress strain response. Due to the varying stiffness in NL method and also for damping mismatch, NL produced higher and lower amplification than EL in the 5 to 25 Hz range and at site frequency, respectively.

Recently, Matasovic and Hashash (2012) made a comprehensive survey to identify and describe the current practice and also the methods available for evaluating the influence of local ground conditions on the site response. Based on the collected information it has been identified that practitioners still prefer using EL codes over NL counterparts due to: (i) familiarity with the EL method, (ii) uncertainty of the input parameters for the NL analysis, and (iii) lack of comprehensive validation study of NL techniques. Based on the survey responses, they made a series of recommendations for future research:

- A need for further benchmarking study in the field of total stress nonlinear site response analysis and improved code usage documentation.
- A rigorous benchmarking study for the effective stress nonlinear site response analysis mostly emphasizing the site class E (soft soil) and F (very soft clay and liquefiable soils).

- The implied shear strength of the widely used modulus reduction curves has been observed to be unreasonable by many researchers. Improvement of modulus reduction curves especially at higher strains is needed.
- Guidelines are necessary to use site response tools for liquefaction evaluation.
- Benchmarking of vertical site response study is necessary as the current resources are insufficient.
- Extensive validation study of the current site response tools using the recently available ground motion array recordings from all over the world is necessary.

2.5.4 Validation studies

Borja et al. (1999), Lee et al. (2006) and Stewart et al. (2008) compared EL and NL outcomes with recorded responses from various vertical arrays. All these studies found differences in the predicted and observed responses (mostly predicted responses on the un-conservative side) at higher frequencies. Generally, the NL analyses produced the lowest of all at the higher frequencies. Kottke (2010) evaluated EL and NL responses based on Lotung, La Cienega and Kik-Net array recordings. He found overall competency in each of the EL and NL tools although their performance greatly varies with site characteristics.

Recently, Kaklamanos et al. (2013 and 2015) attempted to develop a set of thresholds to define the applicability of linear, EL and NL codes by comparing the simulated responses with KiK-net down-hole array data in Japan. They developed a set of threshold beyond which they claimed equivalent linear analysis is unable to produce

adequate prediction and nonlinear analysis should be performed instead. The details of the findings are discussed in the next section.

Kim and Hashash (2013) considered Kik-net downhole array data during 11 March 2011 M_w 9.0 and some other smaller earthquake events to evaluate the performance of both EL and NL analyses. It was observed that both EL and NL produced good agreement with recorded spectral acceleration for soft rock/ stiff soil sites. However, for soft soil sites both EL and NL were on the unconservative side, especially for the lower periods. The authors pointed out that improper characterization of soil dynamic properties may have been the reason, especially for such long duration earthquakes which imposed large strain accumulation.

Zalachoris (2014) compiled borehole array recordings from various locations and moderate to high intensity motions were considered. Both the EL and NL analysis tools were compared and validated with these recorded data. For shear strain less than 0.1% cases, predicted and recorded lines matched considerably well in general at high frequencies. For shear strain more than 0.1% cases, predicted lines from both EL and NL analyses under-predicted the observed ground response. Interestingly, for higher strain (more than 0.4%) and lower period (less than 0.5 sec) cases where EL starts to deviate from the observed responses, NL lines also failed to predict those cases adequately. The author pointed out to the fact that this might be related to inappropriateness of the one dimensional approximation.

Brandenberg et al. (2013) developed centrifuge models for soft-clay deposits to study seismic site response over a wide strain range. They made an effort to evaluate the

performance of several EL and NL site response packages with respect to the physical model generated data. Both the EL and NL predictions matched well with the measured data for low intensity loading cases while in the case of higher loading NL produced more accurate predictions than the EL responses, as expected.

2.5.5 When NL analysis is required over EL analysis

Site factors computed from the EL and NL analyses can vary significantly, especially when the system behavior becomes more and more nonlinear. Thus conditions for which a NL analysis should be performed rather than an EL analysis has been a matter of great controversy. Kramer and Paulsen (2004) based on a survey done among the practitioners claimed that equivalent linear codes can be used up-to 1-2% strain level and a peak ground acceleration ($PGA_{Outcrop}$) of 0.3-0.4g. However, some other studies observed nonlinearity in soil at a much lower strain and/or loading levels. A study by Tokimatsu and Sugimoto (2008) found strong nonlinearity of a Holocene sand dune (with shear wave velocity, V_S of 310-350 m/s) at a depth of about 70 m which experienced a shear strain of about 0.3% based on down-hole array data recorded during the 2007 Niigata-ken Cheutsu-oki earthquake. The surface responses computed using nonlinear and equivalent linear approaches were found to diverge at strong ground motions (higher amplitude shaking) and/or at soft soil sites (lower V_S). Stewart et al. (2008) observed the responses computed using equivalent linear code deviate from that of nonlinear code at a Peak Ground Acceleration ($PGA_{Outcrop}$) of 0.1g to 0.2g. Hashash et al. (2010), Hartzell et al. (2004) and Ardoino et al. (2008) recommended nonlinear approaches for soft soil sites which experiences nonlinear behavior even at low $PGA_{Outcrop}$ ranges. Moreover, Hartzell

et al. (2004) found nonlinear approaches to be the best predictor in the cases of site classes D and E (site class definition can be found in BSSC, 2010). More recently, Matasovic and Hashash (2012) made a comprehensive survey to collect information on the current practice and also the methods available for evaluating the influence of local ground conditions on the site specific earthquake design ground motions. They found the need for a well-defined guideline to effectively select the appropriate type of site response program: an equivalent linear or a nonlinear analysis, as this survey revealed that there is a large controversy on this matter in the community. Matasovic and Hashash (2012) suggested nonlinear and equivalent linear approaches starts to diverge at 0.1-0.2% strains and after 0.5%, responses calculated by equivalent linear approach are no more reliable. Their survey revealed a trend in the practitioners for using nonlinear site response tools in the cases of site classes E and F while some use equivalent linear codes up to 1% strains. Professors Matasovic and Hashash strongly differed from that opinion by claiming that with a strain of 1%, soils would be too close to the failure and a high level of nonlinearity is expected.

Kaklamanos et al. (2013), based on Kik-Net array recordings, observed equivalent linear code to produce acceptable estimates up to 0.1% to 0.4% shear strain levels and/or around 0.1g $PGA_{Outcrop}$ level. More recently, Kaklamanos et al. (2015) found slight deviation of NL responses from EL responses even at 0.05% strain. Limitation involved in their approach are: (1) to obtain shear strain a pre-run of a site response analysis tool is necessary which the user may not be able to perform in many cases; and (2) shear strains computed based on EL and NL programs may differ significantly. Assimaki and Li

(2012) identified some key parameters of nonlinearity susceptibility of site response analysis tools such as: V_{S30}, the site amplification at the fundamental period, $PGA_{Outcrop}$, and an index related to the wavelength compatibility between soil layer thickness and incident wave. In a subsequent study, Kim et al. (2013) identified an estimated strain, γ_{est}, a ratio of peak ground velocity of incident motion and V_{S30}, a good predictor of soil nonlinearity. They developed a predictive model of relative variation of surface spectral accelerations computed from EL and NL tools as a function of γ_{est} and spectral period, T.

2.6 Multidimensional Site Response Analysis

Surface topography can significantly affect earthquake ground motion propagating from the bedrock to the ground surface. Evidences of such effects were observed during some past earthquake events such as: 1971 San Fernando earthquake (Boore, 1972), 1987 Whittier Narrows earthquake and 1999 Athens earthquake etc. (Assimaki, 2004). Structural damage concentrations were more abundant in areas with uneven topography (hills, slopes, canyons etc.). One of the commonly seen topographic features is mild infinitely sloping ground conditions where economic importance exists. These sloping ground conditions are often approximated to horizontal ground conditions so that the seismic site response analysis can be conducted using one-dimensional codes. The seismic site factors recommended by NEHRP (BSSC, 1995) were also developed based on one-dimensional analyses ignoring the two-dimensional effect due to sloping ground surface.

For the cases with ground inclination, a static shear stress is always active towards the downslope direction. This additional stress causes the horizontal ground deformation

to accumulate in the downslope direction although a temporary deformation may be observed in the opposite direction during an earthquake event (Biscontin and Pestana, 2006; Kramer et al., 2011) and thus can significantly alter the propagating ground motion characteristics.

Numerous studies (Boore, 1972; Geli et al., 1988; Bard, 1999; Assimaki, 2004, Bouckovalas and Papadimitriou, 2005) have been done in the past for addressing the effect of steep slopes (hills, ridges, dams etc.) on ground motion characteristics. A general outcome/observation from all of these studies is that the earthquake motion amplifies at the crest of a steep slope. A more recent study by Assimaki and Jeong (2013) reveals that to effectively evaluate the effect of steep slope on earthquake ground motion acceleration, both of the soil stratigraphy and topography effects should be accounted for in a coupled manner. However, there has been scarcely any study that has solely focused on the effect of mild infinite slopes on earthquake motion characteristics. So far, mild infinite slopes under seismic events have been studied mostly to address the stability related problems (Hadj-Hamou and Kavazanjian, 1985; Taboada and Dobry, 1998; Mutsuo et al., 2002; Ko, 2001). To the author's knowledge, only a very few (Taboada and Dobry, 1998; Ko, 2001) have looked into, at least to some extent, the effect of mild infinite slopes on ground motion acceleration amplitudes. Taboada and Dobry (1998) summarized eleven centrifuge model tests performed at Rensselaer Polytechnic Institute (RPI) to investigate liquefaction and earthquake-induced lateral spreading in sand using a laminar box. Ko (2001) performed parametric study by varying ground inclination with a one dimensional ground response analysis program that has been modified to account for

slope inclination. Both of these studies reveal an increase in computed surface acceleration with the increase of the slope angle until the onset of liquefaction.

2.7 Summary

Some common terminologies related to seismic site response study were introduced in this chapter. Also the existing practice for seismic design demand estimation i.e. NEHRP site factors are briefly discussed. The two most widely used one-dimensional site response analysis techniques: equivalent linear and nonlinear analyses were elaborated. Additionally, available nonlinear site response analysis methodologies, recent benchmarking and validation studies were reviewed. For low intensity motions both equivalent linear and nonlinear analyses should produce acceptable prediction while for higher intensity cases only nonlinear analysis is observed to produce an acceptable match with the recorded scenario. However, some studies revealed even with nonlinear analysis adequate predictions may not be achieved, especially for the softer sites and when adequate/quality site dynamic characterization is available. A list of studies and their findings were compiled on the development of a threshold for the use of nonlinear analysis instead of equivalent linear analysis. Finally, a literature survey over the site response analysis of a sloping ground condition following the multi-dimensional site response approach is presented.

CHAPTER 3

SEISMIC SITE FACTOR MODEL FOR SCCP BASED ON NONLINEAR SITE RESPONSE ANALYSIS RESULTS

3.1 Introduction

South Carolina Department of Transportation (SCDOT) is currently using seismic site factors which are originally adopted from the NEHRP provisions (BSSC, 1995 and 2010). During some projects SCDOT have found significant deviations in the site factors computed from site-specific studies with the recommended NEHRP provisions (Aboye et al., 2011).

After being assigned by the SCDOT, a new generalized model of seismic site factors for the Coastal Plain of South Carolina has been developed which is going to be implemented in the next version of the Geotechnical Design Manual of SCDOT. The research group developed this site factor model based on thousands of one-dimensional total stress equivalent linear (with SHAKE2000) and nonlinear (with DMOD2000) site response simulations. SHAKE2000 was used for input peak ground accelerations ($PGA_{Outcrop}$): 0.05g, 0.1g, 0.2g and 0.3g whereas DMOD2000 was used for simulating the $PGA_{Outcrop}$'s: 0.4g and 0.5g cases. This author was responsible for the 17000 DMOD2000 simulations for the four selected sites of the SCCP: Charleston, Columbia, Aiken and Myrtle Beach area. Only the part that this author was responsible for, i.e. the DMOD2000 simulations, is the focus of this Chapter; the generated site factor model based on the

combined team effort is presented in Aboye et al. (2011, 2013a, 2013b and 2014) and Andrus et al. (2014).

3.2 Geology and Seismology

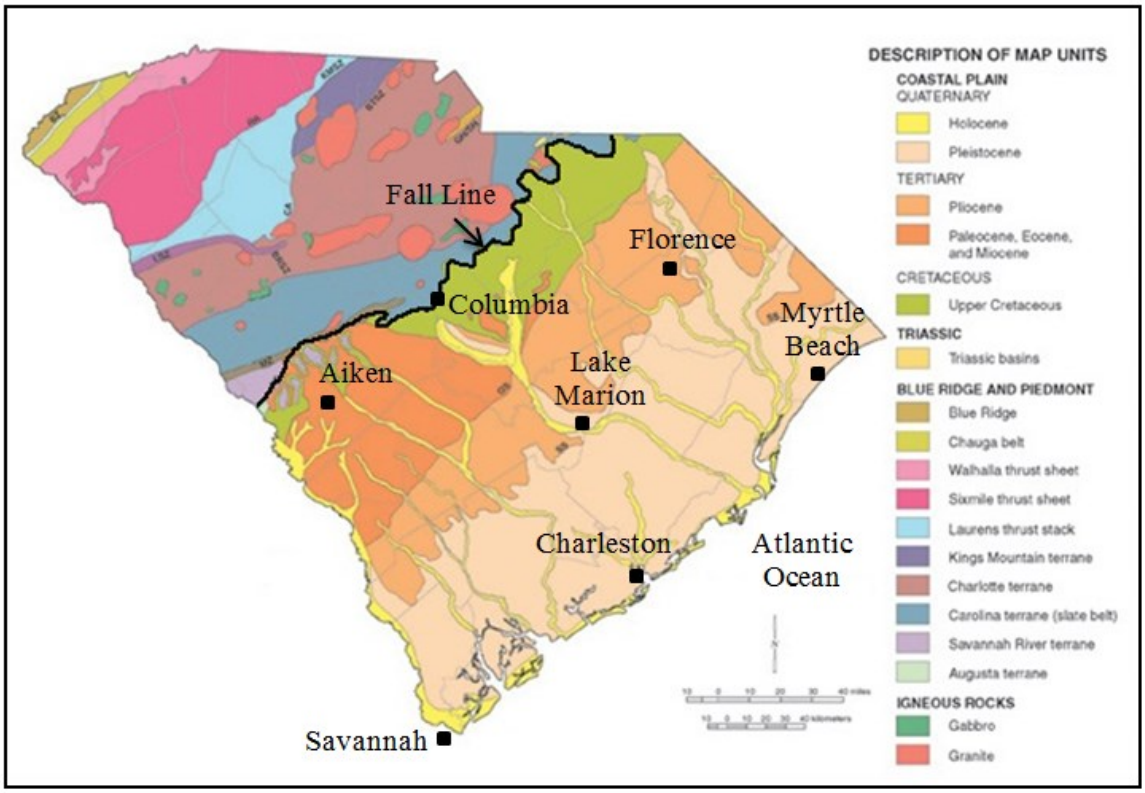

Figure 3.1: South Carolina Geologic map (SCDNR, 2005) with areas considered for ground response analysis (Adopted from Aboye et al., 2014).

The geologic map of South Carolina is presented in Figure 3.1 which was published by the South Carolina Department of Natural Resources (SCDNR, 2005). The Fall Line divides the Coastal Plain and the Piedmont physiographic provinces. The solid squares represent the locations selected for ground response analysis. In the Coastal Plain, sediments of Quaternary, Tertiary and Cretaceous ages lie on top of Mesozoic/Paleozoic

basement rocks (Wheeler and Cramer, 2000; Odum et al., 2003). The SCCP was divided into the four general areas: 1) Charleston-Savannah, 2) Myrtle Beach, 3) Columbia-Florence-Lake Marion, and 4) Aiken. The Charleston-Savannah area, which lies in the lower part of the SCCP, mainly consists of beach/barrier, fluvial and back-barrier deposits. The marine deposits of marl, cemented sand and limestone form the underlying Cretaceous and Tertiary sediments. This area has a sediment thickness of 600-1200 m.

The Myrtle Beach area has near-surface sediments older and stiffer than the sediments of Charleston-Savannah at the same depths. Myrtle Beach area has a sediment thickness of 300-600 m. In the Columbia-Florence-Lake Marion area, near-surface weathered crystalline rock gently dips towards the south-east direction with a thickening overlying 0-700 m deep deposits of Pleistocene, Pliocene and upper Cretaceous sediments. A 0-700 m thick deposit of Paleocene, Eocene and Miocene sediments form the majority of surface exposures in Aiken area.

Mostly the Charleston Seismic Zone located about 30 km northwest of downtown Charleston (Woodstock fault on Figure 3.1) dominates the seismicity of the SCCP. As mentioned earlier, on 31 August 1886, Charleston experienced an earthquake with moment magnitude of 7.3 ± 0.3 (Johnston, 1996) which is the largest in the eastern United States (Bollinger, 1977).

3.3 Soil Profiles and Material Properties

Figures 3.2(a), 3.2(b), 3.2(c) and 3.2(d) present the V_S profiles of Charleston-Savannah, Myrtle Beach, Columbia-Florence-Lake Marion and Aiken areas, respectively. The profiles for Charleston area were generated based on the data collected and compiled

from Andrus et al. (2006) and also from suspension logger tests done by South Carolina Department of Transportation (SCDOT) in 2006. 137 m deep profiles were selected laying over the soft-rock half space with assumed V_S of 700 m/s for the area. The 'dark' line in Figure 3.2(a) presents the 'reference' V_S profile while all other V_S profile variations are by considering ±1, -2 and -3 standard deviations of ln(V_S) and also by assuming a 0m, 10m, 20m and 30m Quaternary soil layer variations. The other geometric and geotechnical parameters of the 'reference' soil profile are presented in Section 4.3.

Similar to Charleston-Savannah, V_S profiles for all other location were also generated. The reference V_S profile for Myrtle Beach was developed based on averages of profiles presented in Silva et al. (2003) and Odum et al. (2003). Columbia-Florence-Lake Marion reference profile was developed using information presented in Silva et al. (2003), Odum et al. (2003), Lester and Chapman (2005) and Andrus et al. (2006). The source of the development of the Aiken reference profile was the work of Silva et al. (2003). All other variations to the 'reference' profiles were generated similar to the methodology followed in Charleston-Savannah region. The Zhang et al. (2005 and 2008) relationships were used for the shear modulus with shear strain (G/G_{max}-γ) and damping with shear strain (D-γ) curves generation for each site of the SCCP. Readers are suggested to visit Aboye et al. (2013a and 2014) and Andrus et al. (2014) for further information.

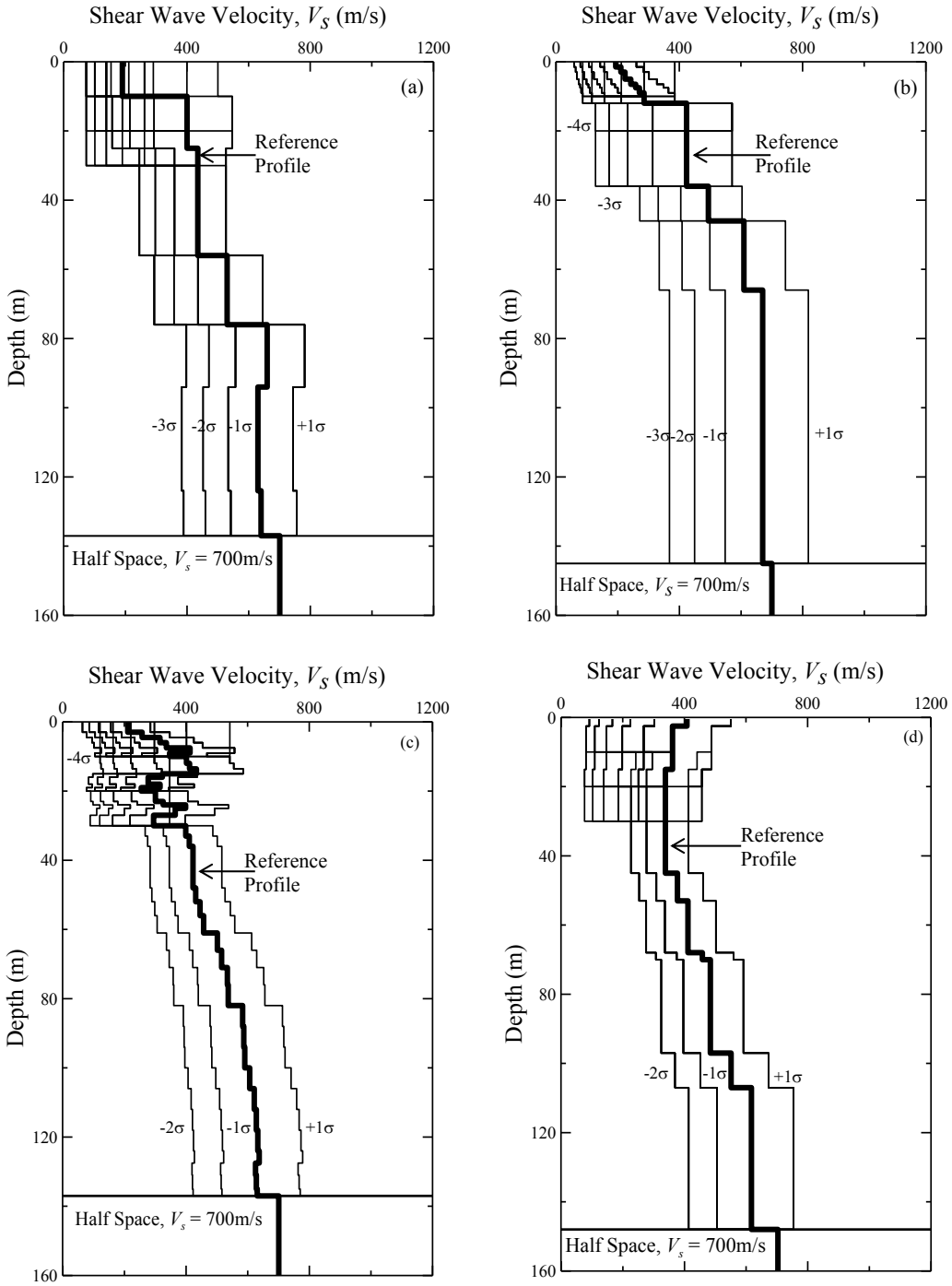

Figure 3.2: Shear wave velocity profiles considered for (a) Charleston-Savannah, (b) Myrtle Beach, (c) Columbia-Florence-Lake Marion, and (d) Aiken (adopted from Aboye et al., 2014)

3.4 Ground Motion

A computer program called Scenario_PC (Chapman, 2006) was employed to generate outcroppping motions for all four regions of SCCP as there is no actual strong motion record available. Scenario_PC was developed for South Carolina Department of Transportation (SCDOT) to perform seismic hazard analysis in the area. Scenario_PC was employed in 16, 4, 5 and 15 quadrangles of Charleston, Myrtle Beach, Columbia and Aiken areas, respectively. A return period of 2% and 10% probability of exceedance in 50 years and a modal moment magnitude of 7.3 were used as inputs for Scenerio_PC. The generated motions were then scaled to the peak ground acceleration ($PGA_{Outcrop}$) levels of 0.05g, 0.1g, 0.2g, 0.3g, 0.4g and 0.5g to be used for site factor model generation. A sample synthetic acceleration time history and corresponding acceleration response spectra from the Charleston quadrangle are showed in the Figure 3.3.

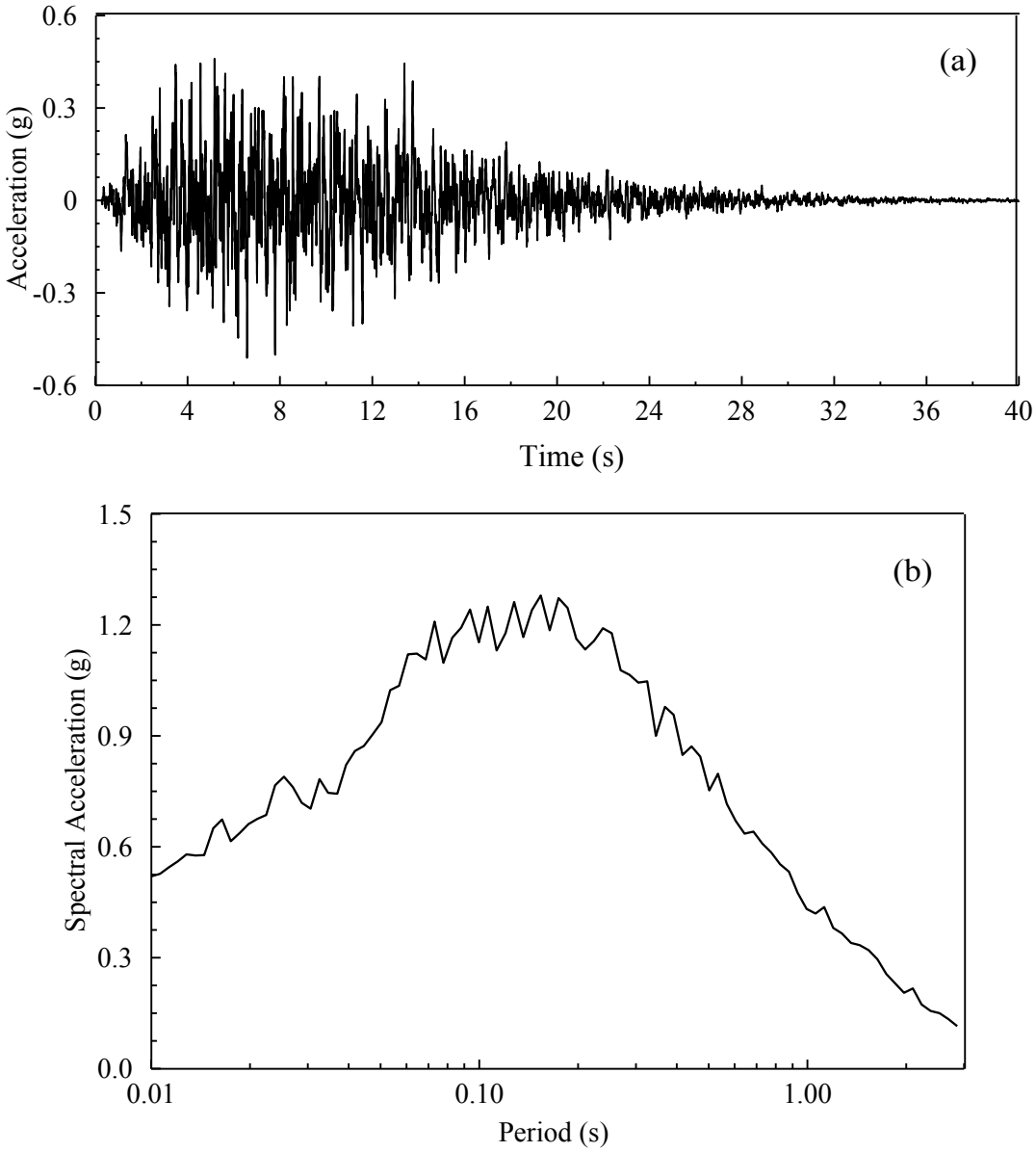

Figure 3.3: The ground motion generated for Charleston quadrangle: (a) acceleration time history and (b) acceleration response spectra.

3.5 Ground Response Analysis with DMOD2000 on SC Locations

The equivalent linear site response analysis program SHAKE2000 (Ordóñez, 2011) has been originally developed based on the SHAKE (Schnabel et al., 1972). This total stress site response analysis tool was used for simulating ground motions with

$PGA_{Outcrop}$ of 0.05, 0.1, 0.2 and 0.3g cases for all four regions (Charleston-Savannah, Myrtle Beach, Columbia-Florence-Lake Marion, and Aiken) of SCCP. With higher loading (i.e. $PGA_{Outcrop}$) the system is expected to start experiencing nonlinearity to the amount that the equivalent linear program can no longer produce responses with acceptable accuracy. Thus to deal with higher loading cases of $PGA_{Outcrop}$ scaled to 0.4 and 0.5g, the nonlinear site response analysis program DMOD2000 (Matasović and Ordóñez, 2011) was implemented. DMOD2000 simulations are computation intensive with no scheme available for 'batch mode' simulation as compared to its equivalent linear counterpart SHAKE2000 which has extensive 'batch mode' capabilities. Thus due to time and resource constraints DMOD2000 simulations were only employed when there is an absolute necessity. Overall 17000 DMOD2000 simulations were performed through-out this study by manually performing each simulation one by one over a time span of nearly 2.5 years.

3.6 Results

Immediately after completion of the SHAKE2000 and DMOD2000 simulations for a location, necessary calculations for seismic site factor, F were performed. The site factor, F is calculated for six spectral period ranges: $\leq$ 0.01 s as for F_{PGA}, 0.01-0.4 s for $F_{0.2}$ (or F_a), 0.41-0.8 s for $F_{0.6}$, 0.81-1.2 s for F_1 (or F_v), 1.21-2.0 s for $F_{1.6}$ and 2.01-4.0 s for $F_{3.0}$. These factors are the averaged values over the corresponding period ranges and then further averaged over all motions used in that region. These site factors are then plotted against corresponding V_{S30} and grouped for six different $S_{Outcrop}$ ranges for the corresponding spectral periods.

Figures 3.4-3.7 present the F-V_{S30} plots based on DMOD2000 simulations corresponding to 0, 0.2 and 1.0 s periods for all four locations. The NEHRP provisions are also plotted with the simulated data for comparison purposes. These F-V_{S30} scatters based on both SHAKE2000 and DMOD2000 simulations for all $PGA_{Outcrop}$ levels and periods were fitted with regression analysis and thus the proposed site factor model for the SCCP was developed (Aboye et al., 2014).

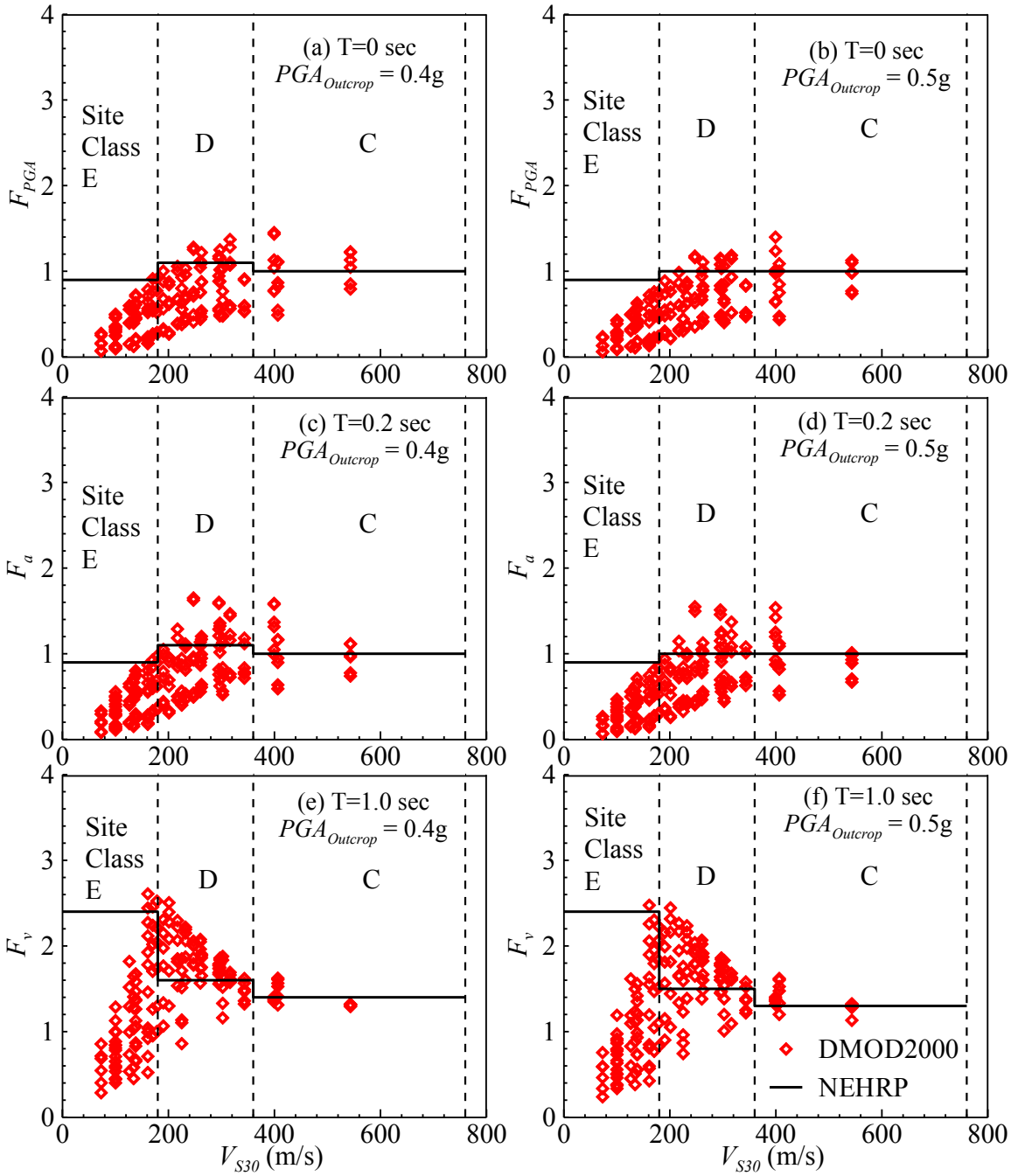

Figure 3.4: Site factors calculated from DMOD2000 plotted with NEHRP provisions for Charleston area: (a) T= 0 sec and $PGA_{Outcrop}$ = 0.4g; (b) T= 0 sec and $PGA_{Outcrop}$ = 0.5g; (c) T= 0.2 sec and $PGA_{Outcrop}$ = 0.4g; (d) T= 0.2 sec and $PGA_{Outcrop}$ = 0.5g; (e) T= 1.0 sec and $PGA_{Outcrop}$ = 0.4g; (f) T= 1.0 sec and $PGA_{Outcrop}$ = 0.5g.

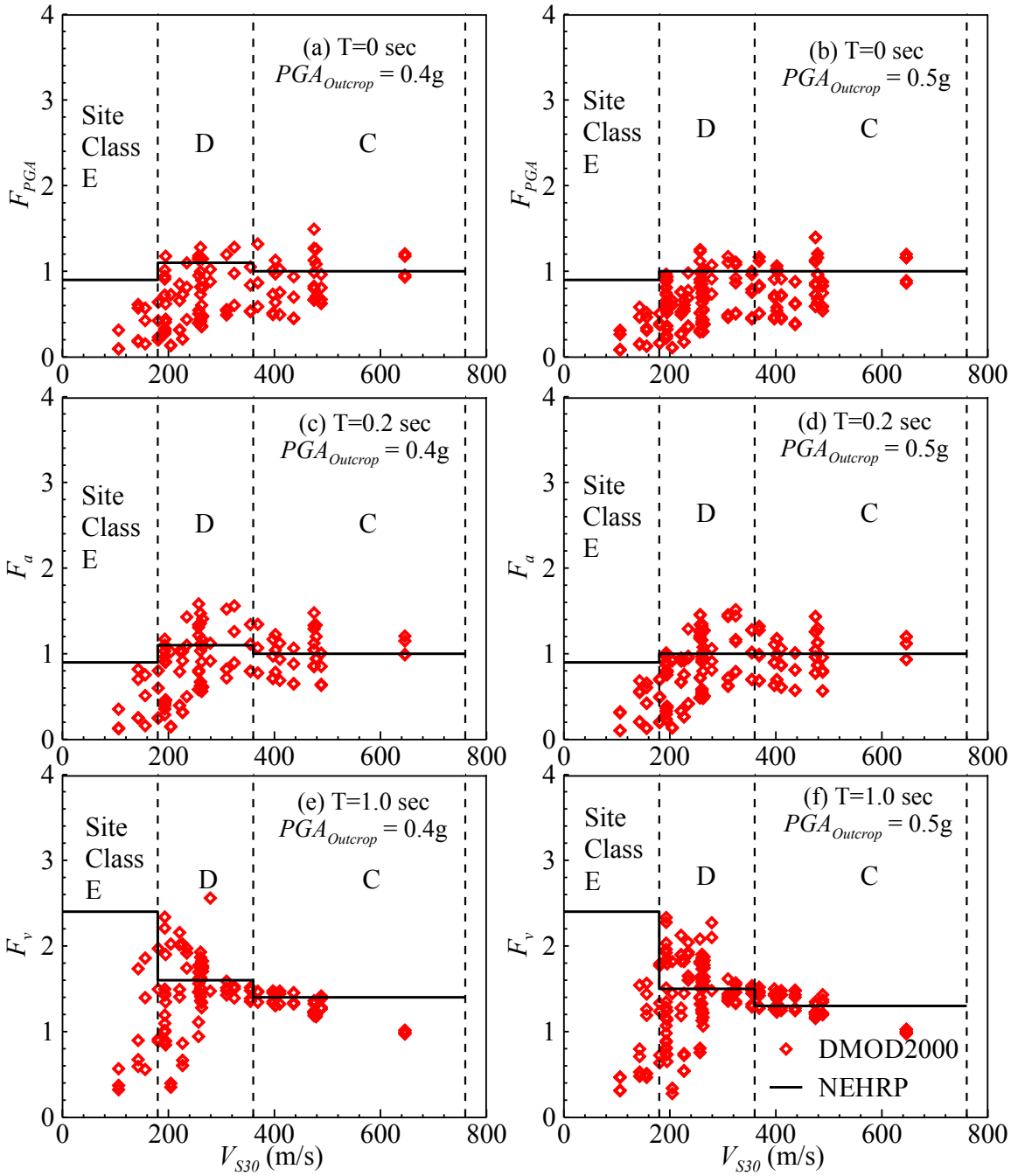

Figure 3.5: Site factors calculated from DMOD2000 plotted with NEHRP provisions for Myrtle Beach area: (a) T= 0 sec and $PGA_{Outcrop}$ = 0.4g; (b) T= 0 sec and $PGA_{Outcrop}$ = 0.5g; (c) T= 0.2 sec and $PGA_{Outcrop}$ = 0.4g; (d) T= 0.2 sec and $PGA_{Outcrop}$ = 0.5g; (e) T= 1.0 sec and $PGA_{Outcrop}$ = 0.4g; (f) T= 1.0 sec and $PGA_{Outcrop}$ = 0.5g.

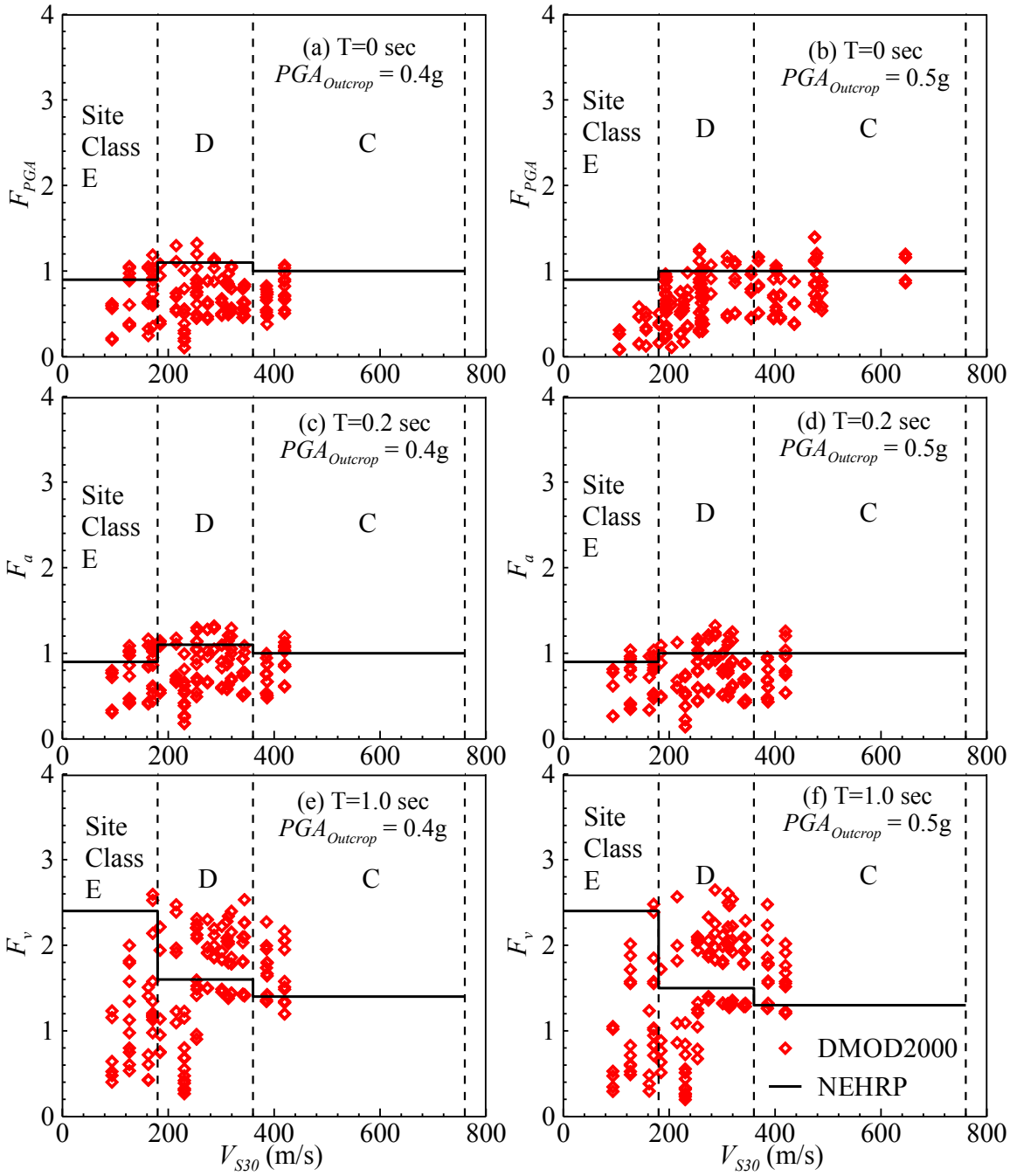

Figure 3.6: Site factors calculated from DMOD2000 plotted with NEHRP provisions for Columbia area: (a) T= 0 sec and $PGA_{Outcrop}$ = 0.4g; (b) T= 0 sec and $PGA_{Outcrop}$ = 0.5g; (c) T= 0.2 sec and $PGA_{Outcrop}$ = 0.4g; (d) T= 0.2 sec and $PGA_{Outcrop}$ = 0.5g; (e) T= 1.0 sec and $PGA_{Outcrop}$ = 0.4g; (f) T= 1.0 sec and $PGA_{Outcrop}$ = 0.5g.

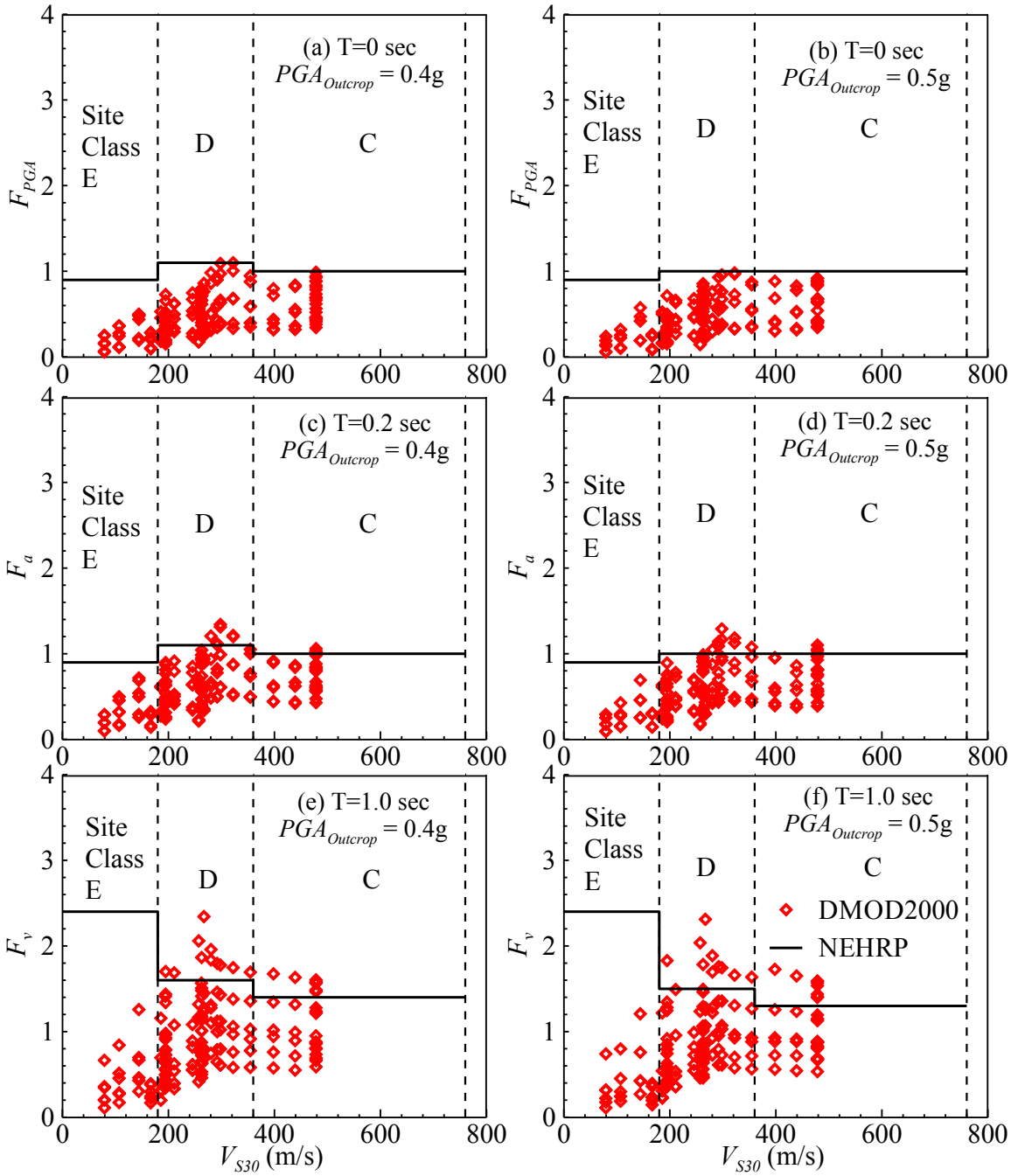

Figure 3.7: Site factors calculated from DMOD2000 plotted with NEHRP provisions for Aiken area: (a) T= 0 sec and $PGA_{Outcrop}$ = 0.4g; (b) T= 0 sec and $PGA_{Outcrop}$ = 0.5g; (c) T= 0.2 sec and $PGA_{Outcrop}$ = 0.4g; (d) T= 0.2 sec and $PGA_{Outcrop}$ = 0.5g; (e) T= 1.0 sec and $PGA_{Outcrop}$ = 0.4g; (f) T= 1.0 sec and $PGA_{Outcrop}$ = 0.5g.

3.7 Discussions

The F-V_{S30} scatter plots form Figures 3.4-3.7 show some common features in general: the scatter has a trend to start from a very low site factor in low V_{S30} range, and then it increases with V_{S30} until it reaches the peak and then again decreases with the V_{S30}. This general trend was observed for all periods and at all four locations simulated. Moreover, the peak is shifting towards left on the V_{S30} axis with the change of period, T from smaller (0 sec) to higher (3.0 sec) cases. Additionally, with higher $S_{Outcrop}$ the peak shifts towards the right on the V_{S30} axis in general. The observations with respect to the NEHRP provisions are:

- In the case of C site class (V_{S30} within 360 m/s and 700 m/s) the scatters fall above the NEHRP F_{PGA}, and F_a values while the NEHRP F_v values give conservative estimates in general.
- In case of D site class (V_{S30} within 180 m/s and 360 m/s) the scatters fall much above the NEHRP F_{PGA}, F_a and F_v values and sometimes the differences are more than 50%.
- In case of E site class (V_{S30} within 180 m/s and 360 m/s) the scatters fall much lower than the NEHRP F_{PGA}, F_a and F_v values and the differences increase with the profile V_{S30} decrease.

Using all these insights from these figures and in combination with the cases handled with SHAKE2000 the research group has developed the site factor model for the SCCP and has been published in Aboye et al. (2011, 2013a, 2013b and 2014) and Andrus et al. (2014).

3.8 Conclusions

The seismic site factor model for the Coastal Plain South Carolina has been developed by the research group in which performing thousands of nonlinear site response analyses with DMOD2000 was the responsibility of the author. This chapter presents the data generated by DMOD2000 simulations and the insights taken.

CHAPTER 4

COMPARISON OF SEISMIC SITE FACTORS BASED ON NONLINEAR AND EQUIVALENT LINEAR SITE RESPONSE ANALYSIS IN CHARLESTON, SOUTH CAROLINA

4.1 Introduction

Typically, site response analysis is conducted to predict the local site effect on the earthquake motion propagating from the hypocenter to the ground surface where most of the civil infrastructure is built. The equivalent linear (EL) site response analysis, typically using SHAKE2000, is a widely used method among practitioners. The EL method requires only a few well-defined input parameters and predicts the surface response reasonably well when the soil profile behaves with a linear or near linear range. On the other hand, a nonlinear (NL) site response analysis can better predict the surface response compared to the equivalent linear or linear analysis when the soil profile behaves well beyond the linear range for the given ground motion characteristics, given that the input parameters for the nonlinear analysis are obtained accurately. Although the nonlinear analysis procedure can better predict the response, because of the lack of knowledge in determining the necessary input parameters and the limitations of the stress-strain model for accurately representing the cyclic behavior of the soil, the nonlinear analysis method has always been the least used or preferred by the practitioners (Stewart et al., 2008; Matasovic and Hashash, 2012).

The purpose of the site response analysis is to predict the acceleration response spectra at the ground surface level for the given soil and earthquake conditions. The acceleration response spectra is a plot of the maximum acceleration response of a set of single-degree-of-freedom (SDOF) systems with a specified (5% typically) damping and are plotted against the corresponding fundamental period, for a particular input ground motion (Kramer, 1996). The seismic site factor at a specific period (F_T) is a ratio of the computed surface spectral acceleration (S_{Site}) and the bedrock spectral acceleration ($S_{Outcrop}$) at the same period. The $S_{Outcrop}$ and the site factors are then used to develop an Acceleration Design Response Spectrum (ADRS curves; details of ADRS curve generation process can be found in SCDOT, 2008a) which is an input for performing seismic analyses (e.g. multi-modal response spectrum analysis) of structures. The seismic site factors computed from the results of EL and NL analyses can vary significantly, especially when the soil profile behaves well beyond the linear range for the given conditions. Thus it has been a matter of great controversy for years that under which condition a NL analysis should be performed rather than an EL analysis. Kramer and Paulsen (2004), based on a survey conducted among the practitioners, claimed that equivalent linear analysis can be used up-to 1-2% strain and a peak ground acceleration ($PGA_{Outcrop}$) of 0.3-0.4g. Following their suggestion, seismic site factor models specific to the Charleston, South Carolina area were developed by the author and his research team based upon thousands of one-dimensional equivalent linear (SHAKE2000 for $PGA_{Outcrop} \leq 0.3$g cases) and nonlinear (DMOD2000 for $PGA_{Outcrop} > 0.3$g cases) site response analysis results (Aboye et al., 2011 and 2013). The developed site factor model is a

function of the average shear wave velocity in the top 30 m (V_{S30}) which is defined as (Borcherdt, 1994):

$$V_{S30} = \frac{30}{\sum_{i=1}^{n} \frac{H_i}{V_{Si}}} \tag{4.1}$$

where H_i is the thickness of soil layer 'i' in meter; V_{Si} is the shear wave velocity of layer 'i' in m/s; and n is the number of soil layers in top 30 m from the ground surface. However, some other studies observed difference in the computed response from the EL and NL methods at experienced shear strain much lower than 1-2% and also shaking lower than 0.3 g $PGA_{Outcrop}$. A study by Tokimatsu and Sugimoto (2008) found strong nonlinearity of a Holocene sand dune (the shear wave velocity, V_S of 310-350 m/s) at a depth of about 70 m experiencing a shear strain of about 0.3% from a down-hole array data during the 2007 Niigata-ken Cheutsu-oki earthquake. The surface responses computed using nonlinear and equivalent linear approaches were found to diverge at strong ground motions (higher amplitude shaking) and/or at soft soil sites (lower V_S). Stewart et al. (2008) observed the responses computed using equivalent linear code deviate from that of nonlinear code at around a Peak Ground Acceleration ($PGA_{Outcrop}$) of 0.1g to 0.2g. Hashash et al. (2010), Hartzell et al. (2004) and Ardoino et al. (2008) recommended nonlinear approaches for soft soil sites which experiences nonlinear behavior even at low $PGA_{Outcrop}$ ranges. Moreover, Hartzell et al. (2004) found nonlinear approaches to be the best predictor in the cases of site classes D and E (site class definition can be found in BSSC, 1995). More recently, Matasovic and Hashash (2012) made a comprehensive survey to collect information on the current practice and also the

methods available for evaluating the influence of local ground conditions on the site specific earthquake design ground motions. They found the need for a well-defined guideline to effectively select the appropriate type of site response program: an equivalent linear or a nonlinear analysis, as this survey revealed that there is a large controversy on this matter in the community. Matasovic and Hashash (2012) suggested nonlinear and equivalent linear approaches starts to diverge at 0.1-0.2% strains and after 0.5%, responses calculated by equivalent linear approach are no more reliable. Their survey revealed a trend in the practitioners for using nonlinear site response tools in the cases of site classes E and F while some use equivalent linear codes up to 1% strains. Professors Matasovic and Hashash strongly differed from that opinion by claiming that with a strain of 1%, soils would be too close to the failure and a high level of nonlinearity is expected.

Recently, Kaklamanos et al. (2013 and 2015) attempted to develop a set of thresholds to define the applicability of linear, EL and NL codes by comparing the simulated responses with KiK-net down-hole array data in Japan. In Kaklamanos et al. (2013), they observed equivalent linear code to produce acceptable estimates up to 0.1% to 0.4% shear strain levels and/or around 0.1g $PGA_{Outcrop}$ level while in Kaklamanos et al. (2015), they found slight deviation of NL responses from EL responses even at 0.05% strain. Limitations involved in their approach are: (1) to obtain shear strain a pre-run of a site response analysis tool is necessary which the user may not be able to perform in many cases; and (2) shear strains computed based on EL and NL programs may differ significantly. Assimaki and Li (2012) identified some key parameters of nonlinearity

susceptibility of site response analysis tools such as: V_{S30}, the site amplification at the fundamental period, $PGA_{Outcrop}$, and an index related to the wavelength compatibility between soil layer thickness and incident wave. A following work, Kim et al. (2013), identified an estimated strain, γ_{est}, a ratio of peak ground velocity of incident motion and V_{S30}, which was found to be a good predictor of soil nonlinearity. They developed a predictive model of relative variation of surface spectral accelerations computed from EL and NL tools as a function of γ_{est} and spectral period, T.

This Chapter is dedicated to address the differences that may occur in the computed site factors from EL and NL programs for the deep soil profiles of Charleston, SC area. Therefore, similar to the Aboye et al. (2014) site factor model, three separate seismic site factor models: 'SF-SK', 'SF-DM' and 'SF-DS' are generated and are then compared. SF-SK is a product of purely EL analyses with SHAKE2000 whereas SF-D and SF-DS are generated based on purely NL site response programs DMOD2000 and DEEPSOIL, respectively. Important insights are taken from the comparison of these site factor models generated with the same set of profiles and ground motions from the problem area. Finally, based on the data sets generated from SHAKE2000, DMOD2000 and DEEPSOIL simulations, a set of criteria or in other words a threshold chart is developed for the engineers which distinguishes the conditions that warrant the use of a NL analysis program over its EL counterpart for the most accurate prediction. The uniqueness of this chart is its simplistic nature in the sense of input requirements: V_{S30} (site parameter) and $PGA_{Outcrop}$ (motion parameter), which are usually commonly available engineering parameters.

4.2 Geology and Seismology of Charleston Area

Charleston, South Carolina is located in the Atlantic coastal plain physiographic province. Figure 4.1 presents the geology of the area of interest with 7.5-minute quadrangle boundaries. The Ashley, the Cooper, the Stono and the Wando are the major rivers. This location of interest has a 700-1000m deep ocean-ward thickening subsurface geology with Cretaceous and younger sediments (Chapman and Talwani, 2002). The near-surface Quaternary sediments are typically unconsolidated in nature which range from beach/barrier island sand to estuarine sand and clay to fluvial sand and silt (McCartan et al., 1984). Right beneath the Quaternary layer are the compacted and weakly lithified Tertiary and Cretaceous layers over a hard Mesozoic/Paleozoic basement rock.

The historic Charleston earthquake on 31st August, 1886 with a moment magnitude of about 7.0 is the largest in the south-eastern United States (Bollinger, 1977). Figure 4.1 shows the Woodstock fault zone which is the likely source of this catastrophic event. Moreover, in the past 6000 years, this area experienced several liquefaction-inducing earthquakes and the recurrence rate of an 1886-like earthquake is about 500 years for this area (Talwani and Schaeffer, 2001).

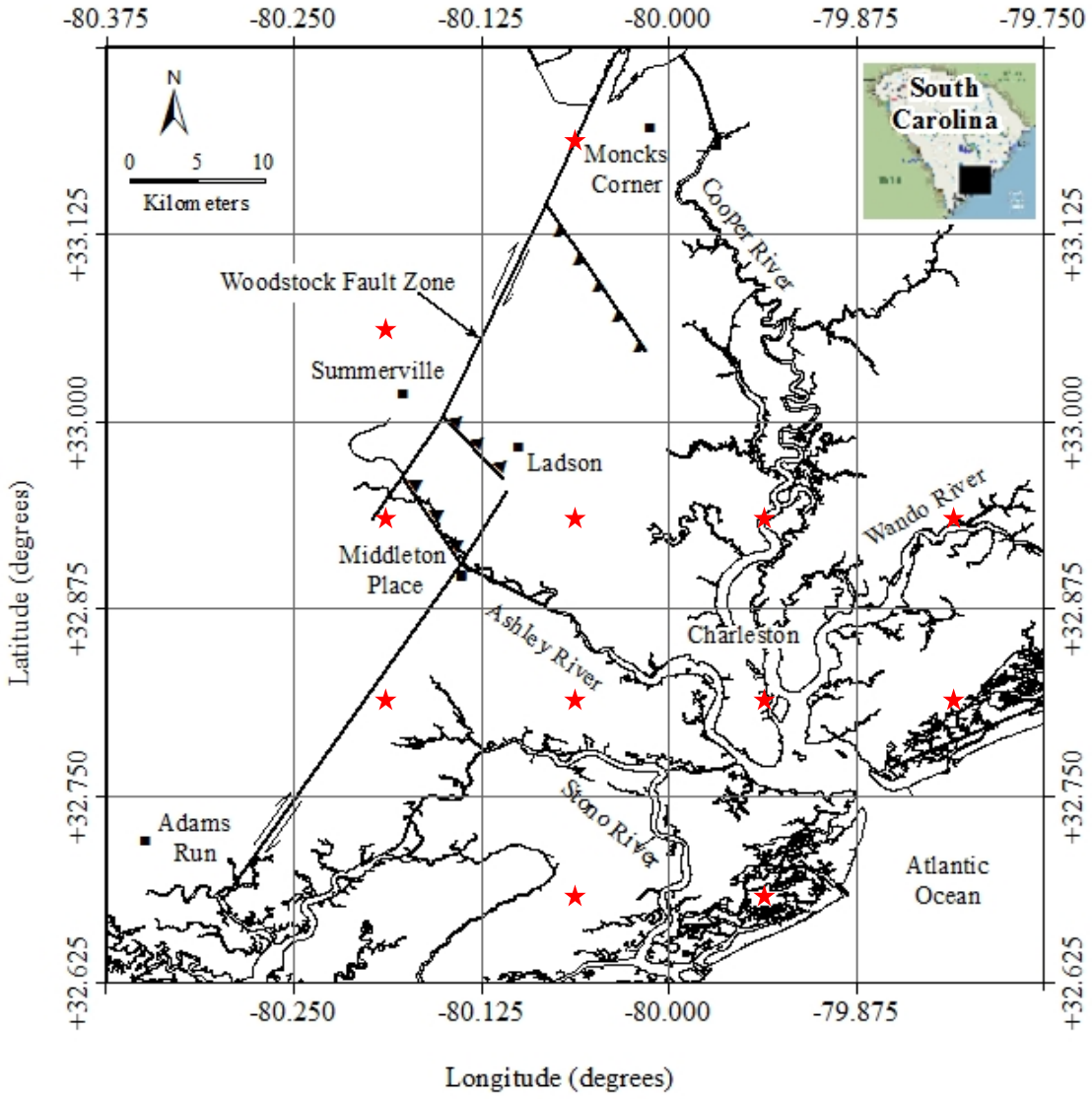

Figure 4.1: The Woodstock fault zone of Charleston, SC area as delineated in Durá-Gómez and Talwani (2009) (adopted from Aboye et al., 2013a). The red stars show the locations of synthetic ground motions generated with Scenario_PC.

4.3 Soil Profile and Material Properties

Figure 4.2 presents the twenty eight shear wave velocity, V_S profiles for the Charleston area. Based on the data collected and compiled from Andrus et al. (2006) and also from suspension logger tests done by South Carolina Department of Transportation (SCDOT) in 2006, a 137m deep profile is selected laying over the soft-rock half space

with an assumed Vs of 700 m/s. The 'dark' line in Figure 4.2 presents the 'reference' V_S profile while all other V_S profile variations are by considering ±1, -2 and -3 standard deviations (σ) of the natural logarithm of V_S and also by assuming 0m, 10m, 20m and 30m Quaternary soil layer depth variations. The geometric and geotechnical parameters of the 'reference' soil profile are presented in Table 4.1. These parameters include number of soil layers and layer thickness, total unit weight (γ_t), and plasticity index (PI). Also, Table 4.2 presents all the variations applied to the 'reference' V_S profile to generate a total of twenty-eight V_S profiles for this study.

Figure 4.3(a) and 4.3(b) present the mean variations of the normalized shear modulus (G/G_{max}) and damping (D) variation with shear strain amplitude (γ) based on the Zhang et al. (2005) relationships, respectively, for each of all nine layers of the soil profile. Additionally, the mean±1σ (σ = standard deviation) variations of the G/G_{max}-γ and D-γ curves (Zhang et al., 2008) are also considered. The Zhang et al. (2005 and 2008) relationships are the function of soil plasticity index, mean effective confining pressure and geologic age. For the half space (V_{S30} = 700 m/s), purely linear relationships for G/G_{max}-γ (G/G_{max} = 1.0) and D-γ (D = 0.5%) – pairs are assumed (SCDOT, 2008a).

Table 4.1: Reference soil/soft rock profile (From Aboye et al., 2011 based on Andrus et al., 2006).

Layer #	Layer thickness	Total unit weight	Shear wave velocity, V_s	Standard deviation (σ) of ln(V_s)	Plasticity index, *PI*	Mean effective stress, σ_m'	Geologic age
	(m)	(kN/m³)	(m/s)	(m/s)	(%)	(kPa)	
1	3	18.2	190	0.32	15	15	Quaternary (Wando Formation)
2	7	18.2	190	0.32	15	50	
3	15	18.5	400	0.312	50	220	Tertiary
4	11	18.5	435	0.191			
5	20	18.5	435	0.191	15	600	
6	20	18.9	530	0.197			
7	18	18.9	660	0.169			
8	6	18.9	680	0.262			
9	37	19.6	680	0.262	15	1400	
10	Half space	22.5	700	-	-	-	Tertiary and older

Table 4.2: V_s profile variations considered.

Depth of Quaternary layers (m)	V_s profile variation: Mean+kσ		Total Number of Profiles
	Variation limited to only Quaternary layers	Variation extends to all layers	
0	k = 0	k = -2,-1 and +1	4
10	k = -3,-2,-1,0 and +1	k = -2,-1 and +1	8
20	k = -3,-2,-1,0 and +1	k = -2,-1 and +1	8
30	k = -3,-2,-1,0 and +1	k = -2,-1 and +1	8
			Total = 28

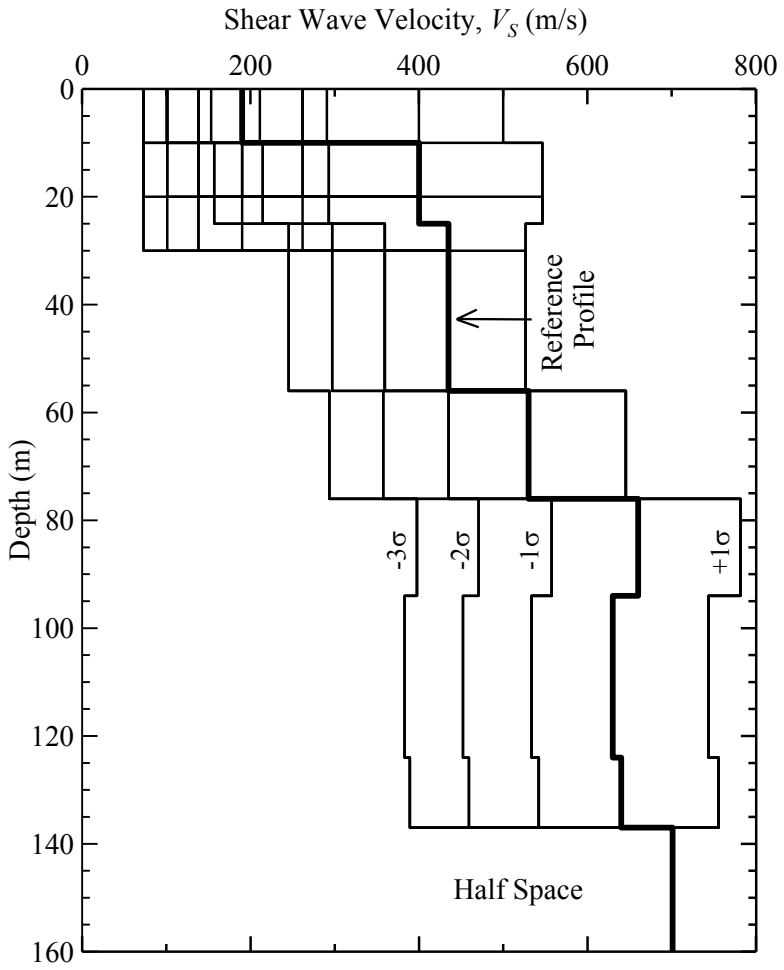

Figure 4.2: Shear wave velocity profiles considered for Charleston, SC. (Aboye et al., 2013a).

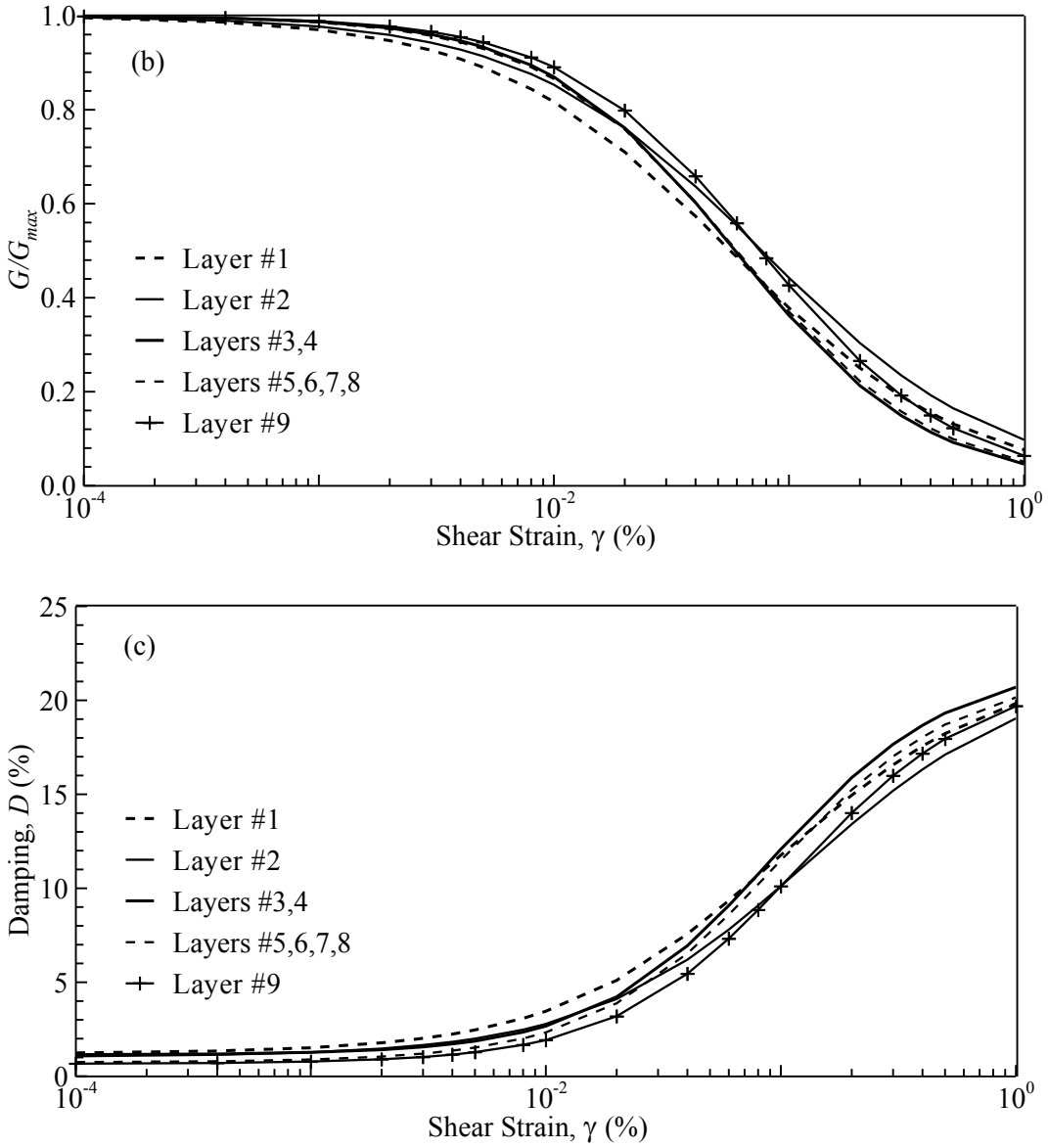

Figure 4.3: Soil dynamic properties: (a) the *G/Gmax-γ*; and (b) *D-γ* curves, based on Zhang et al. (2005) relationships.

4.4 Ground Motion

A computer program called Scenario_PC (Chapman, 2006) is employed to generate outcroppping motions for Charleston as strong ground motion records are not available currently for the area. Scenario_PC was developed for South Carolina Department of Transportation (SCDOT) to perform seismic hazard analysis in this area.

Required inputs for Scenario_PC are: (1) the rock model, (2) earthquake moment magnitude, (3) site-to-source distance and (4) return period. The Geologic realistic condition (Chapman and Talwani, 2002), a very thick outcropping layer of soft rock (V_s = 700 m/s) at a depth of 137 m from ground surface, is selected as the rock model for Scenario_PC. Twelve quadrangles are selected for this study and thus the site to source distance is determined within 6 to 36 km for the center of each quadrangle (locations marked in Figure 4.1 with red stars). Considering a return period of 2% probability of exceedance in 50 years (known as the Safety Evaluation Earthquake or SEE according to SCDOT, 2008a), the site to source distance based on quadrangles (Charleston) and a modal moment magnitude of 7.3 are used as inputs to this Scenario_PC. A sample synthetic acceleration time history and corresponding acceleration response spectra from the Charleston quadrangle are showed in the Figure 4.4. All these motions are scaled to the $PGA_{Outcrop}$ levels of 0.05g, 0.1g, 0.2g, 0.3g, 0.4g and 0.5g in order to keep consistency with the existing NEHRP recommended site factor tables.

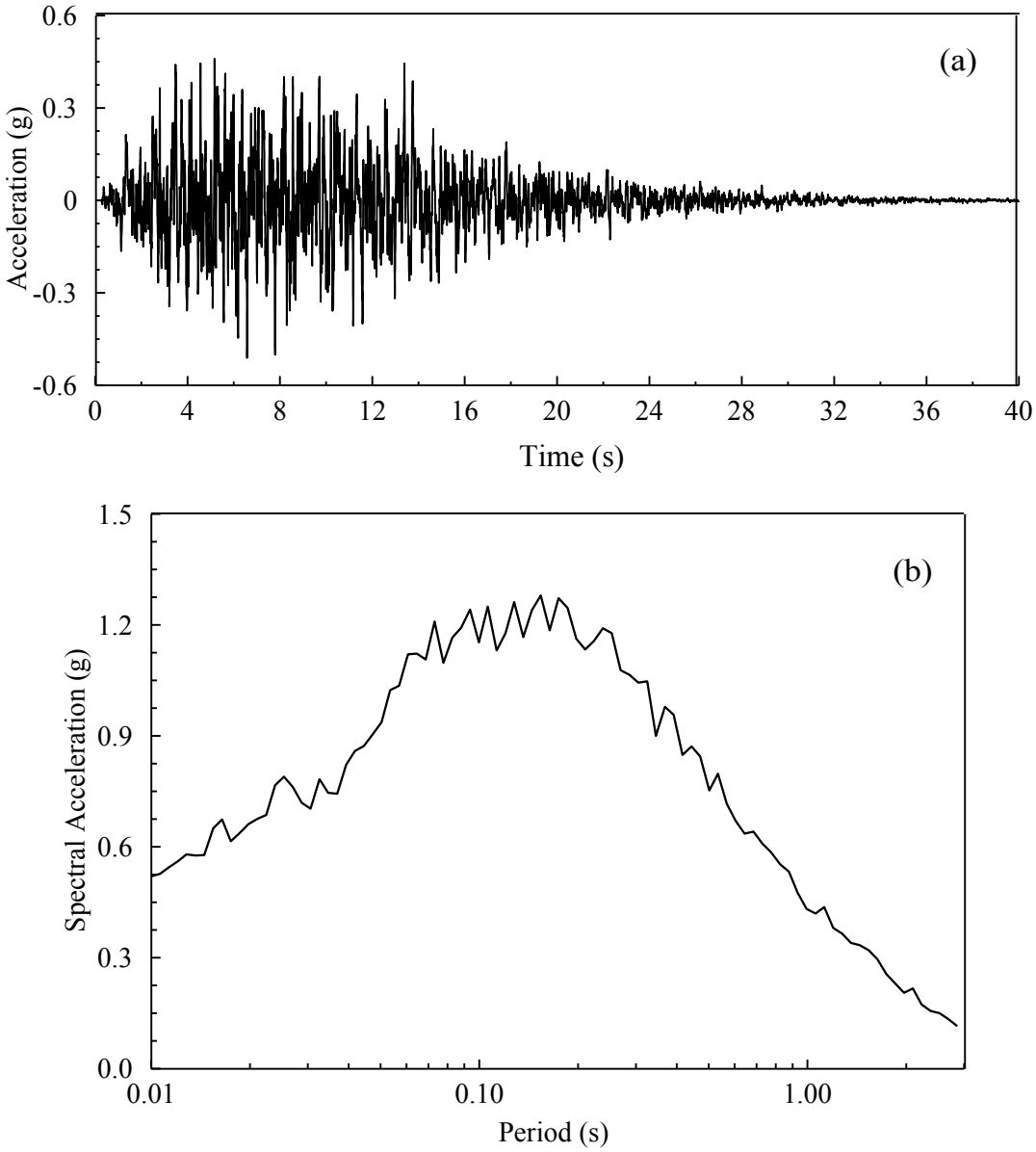

Figure 4.4: The ground motion generated for Charleston quadrangle: (a) acceleration time history and (b) acceleration response spectra.

4.5 Site Response Analysis Tools and Model Parameter Calibration

The one-dimensional equivalent linear analyses were conducted using popular computer program SHAKE2000 and the one-dimensional nonlinear analyses were conducted using DMOD2000 and DEEPSOIL. Although DMOD2000 and DEEPSOIL

are based on similar theories, differences exist in the way the shear modulus and damping curves are matched with input curves and also in the computation of the small stain damping. Summary of the similarities, differences and modeling technique of these computer programs are described in subsequent sections.

4.5.1 Equivalent linear site response analysis tool: SHAKE2000

SHAKE2000 (Ordóñez, 2011), the latest version of SHAKE (Schnabel et al., 1972), is developed and commercialized by GeoMotions, LLC in the USA and around the world. An equivalent linear analysis can better approximate soil nonlinearity than its linear analysis counterparts (Kramer, 1996). EL method is widely used because of its simplicity, low computational requirement and also availability of good documentation on usage protocol.

In SHAKE2000, a symmetric hysteretic stress-strain cycle is approximated by an equivalent linear shear modulus, G and an equivalent linear damping ratio, ξ. G is determined as the secant modulus whereas ξ is the energy lost i.e. proportional to the area of the hysteretic loop. The single pair of G and ξ values allows the equivalent linear analysis to actually run in the realm of linear dynamic analysis platform. G and ξ are primarily determined using iterative procedure by performing trial runs in the program. At first based on some initial estimates of G and ξ the first trial run of the linear analysis produce shear strain time history for each layer. Then the effective shear strains are obtained based on a fraction of the maximum observed strain in each layer. Based on the input G/G_{max}-γ and D-γ curves (Section 4.3) the estimates of G and ξ corresponding to the effective strain values are used for the next trial run and such iterations are continued

until a convergence is obtained. The final G and ξ values are then kept constant for the final run of the entire earthquake excitation. Therefore this method neither can account for soil stiffness changes during an event nor can predict the responses at failure due to that originally linear material model. Therefore, an equivalent linear analysis is merely an approximation to the actual nonlinear behavior.

4.5.2 Nonlinear site response analysis tools: DMOD2000 and DEEPSOIL

GeoMotions, LLC developed DMOD2000 (Matasović and Ordóñez, 2011), a Windows^{TM}-based platform around DMOD_2 which is an enhanced form of DMOD (Matasovic and Vucetic, 1993a). DMOD2000 is a nonlinear one dimensional site response analysis tool which models the vertical propagation of horizontal shear wave through deep soil deposits. DEEPSOIL v5.0 (Hashash et al., 2011) is another widely accepted one-dimensional site response analysis program. Although it is capable of performing both nonlinear and equivalent linear analyses, and both total stress and effective stress analyses, only nonlinear total stress capabilities are applied. DEEPSOIL has an intuitive graphical user interface.

Both DMOD2000 and DEEPSOIL implement the same soil constitutive model to represent the soil stress-strain behavior. In both cases, the deep soil deposit is represented by a multi-degree of freedom lumped-mass system. The dynamic equation of motion is solved by the Newmark's β method. However, DEEPSOIL implements advanced techniques to estimate both the small strain (viscous) and the hysteretic damping which gives theoretical advantage to DEEPSOIL over DMOD2000 in producing quality predictions.

4.5.2.1 *Constitutive models*

Both DMOD2000 and DEEPSOIL incorporate Modified KZ (i.e. MKZ) model (Matasovic and Vucetic, 1993a) to define the initial stress-strain backbone curve (Figure 4.5) in the simulation. The normalized MKZ model is given by:

$$\tau^* = \frac{G^*_{max}\gamma}{1+\alpha\left(\frac{\gamma}{\gamma_r}\right)^s} \tag{4.2}$$

where α and s are two curve fitting constants added to the Kondner and Zelasko (1963) or KZ model, τ is the shear stress, γ is the shear strain, $\tau^* = \tau/\sigma'_{vc}$, $G^*_{max}=G_{max}/\sigma'_{vc,}$ $\gamma_r= \tau_{max}/G_{max}$, σ'_{vc} is the initial vertical effective stress and G_{max} is the initial (maximum) shear modulus of the soil. The α and s parameters are obtained by a calibration process which is described in section 4.5.2.3. The material degradation with repeated cycle is incorporated into this model by using degradation index functions (Matasovic and Vucetic, 1993b) as shown in Figure 4.5.

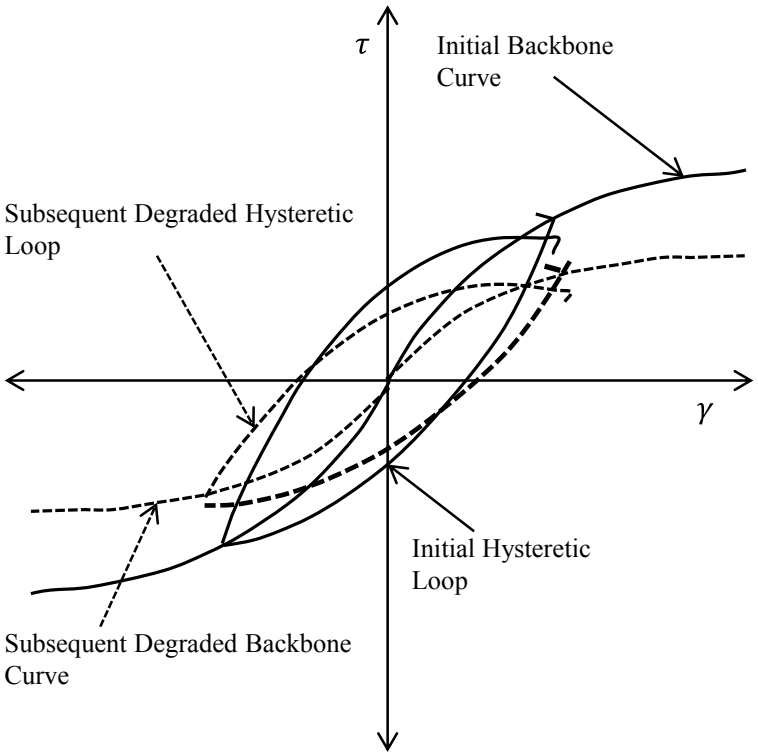

Figure 4.5: Shear stress-strain behavior during first cycle and a subsequent cycle (after Stewart et al., 2008).

However, in DEEPSOIL a modified reference shear strain definition (Hashash and Park, 2001) has been incorporated:

$$\gamma_r = a\left(\frac{\sigma'_{vc}}{\sigma_{ref}}\right)^b \tag{4.3}$$

where σ'_{vc} = effective vertical stress, σ_{ref} = reference confining pressure and a and b are the curve fitting parameters.

4.5.2.2 *Small strain damping estimation*

Presented in Equation 4.4 is the equation of motion in terms of matrix notations which is solved by Newmark's β method in both DMOD2000 and DEEPSOIL.

$$\mathbf{M}u'' + \mathbf{C_R}u' + \mathbf{K}u = \mathrm{f} \tag{4.4}$$

where **M** is the mass matrix, $\mathbf{C_R}$ is the viscous damping matrix, **K** is the nonlinear stiffness matrix, **f** is the excitation at the base of the layer and u, u' and u'' are the relative displacement, velocity and acceleration vectors, respectively. Since the hyperbolic constitutive model employed in both DMOD2000 and DEEPSOIL is very simplified in nature, the inherent hysteretic damping becomes insignificant and under-predict the system damping at small strain ranges. Therefore, the concept of small strain or viscous damping, $\mathbf{C_R}$ is introduced and is externally incorporated into the dynamic equation of motion (i.e. equation 4.4). In DMOD2000, $\mathbf{C_R}$ is expressed as a function of the frequency of the input motion although $\mathbf{C_R}$ is frequency independent in reality. A frequency independent type expression for $\mathbf{C_R}$ is implemented in DEEPSOIL.

In DMOD2000, $\mathbf{C_R}$ is calculated by following the full Rayleigh damping formulation (Hudson et al., 1994) and is expressed as a function of mass and stiffness as follows:

$$\mathbf{C}_\mathrm{R} = \alpha_R \mathbf{M} + \beta_R \mathbf{K} \tag{4.5}$$

where α_R and β_R are calculated using Equations 4.6 and 4.7, respectively (Hudson et al., 1994; Park and Hashash, 2004).

$$\alpha_R = \xi_{tar}\left(\frac{4\pi}{T}\right)\left(\frac{n}{(n+1)}\right) \tag{4.6}$$

$$\beta_R = \left(\xi_{tar}T\right)\left(\frac{1}{\pi(n+1)}\right) \tag{4.7}$$

where ξ_{tar} is the target damping ratio obtained through calibration and the range is 0.1 to 5%, T is the fundamental period of the soil profile given by $T = 4H / V_{S,avg}$, H is the total depth of the soil profile considered, $V_{S,avg}$ is the weighted average of the shear wave velocity of the profile-layers and n is an odd integer (1, 3, 5, 7 etc.) related to mode number.

The natural frequency of the soil profile (first mode) corresponds to n = 1 and the higher numbers are related to higher mode. DMOD2000 requires n value correspond to the higher mode in addition to the first mode (n = 1) for full Rayleigh damping calibration. On the other hand, ξ_{tar} is the small (insignificant) strain damping of each of the soil layers. DMOD2000 requires a single ξ_{tar} value as an input (rather than setting ξ_{tar} for each of the layers) for the entire profile for the simulation. Therefore, calibration is required to obtain a suitable pair of n and ξ_{tar}. This calibration is done by running DMOD2000 at a low $PGA_{Outcrop}$ and simultaneously adjusting n and ξ_{tar} until the response spectrum matches well with the corresponding SHAKE2000 response; assumption is the NL and EL responses should be comparable due to linear elastic behavior of soil at this small loading. Presented in Figures 4.6(a), (b) and 4.7 are such comparison of spectral accelerations computed using the equivalent linear code SHAKE2000 and the nonlinear code DMOD2000 at low $PGA_{Outcrop}$s for three profiles (i.e. different V_{S30} values).

At first, a $PGA_{Outcrop}$ of 0.1g is selected for calibration of n and ξ_{tar} for the reference profile (V_{S30} = 295 m/s) assuming the loading to be small enough to create linear elastic soil behavior and is presented in Figure 4.6(a). It is observed that any of the

n and ξ_{tar} combinations: (5, 0.5), (7, 0.5) and (7, 0.75) have produced acceptable amount of matching with the SHAKE2000 response.

However, differences in responses from SHAKE2000 and DMOD2000 are observed in the cases of lower velocity (softer) profiles even for motions with $PGA_{Outcrop}$ of 0.05g and 0.1g. This suggests that for softer profiles nonlinearity can occur at a $PGA_{Outcrop}$ much lower than even 0.05g. Therefore, two profiles with lower V_{S30} (100 and 201 m/s) are selected along with a very small $PGA_{Outcrop}$ of 0.001g. Figure 4.6(b) and 4.7 present these two cases for calibration at 0.001g level and interestingly the same sets of n and ξ_{tar} combinations: (5, 0.5), (7, 0.5) and (7, 0.75) are still found to produce acceptable matching in responses between SHAKE2000 and DMOD2000.

Point to be noted here that, in some cases especially for higher $PGA_{Outcrop}$ values and/or softer profiles, DMOD2000 experiences convergence issues. Altering the n and ξ_{tar} values seemed to improve the scenario. This is the justification of considering multiple sets of calibrated n and ξ_{tar} combinations during the DMOD2000 simulations in this study.

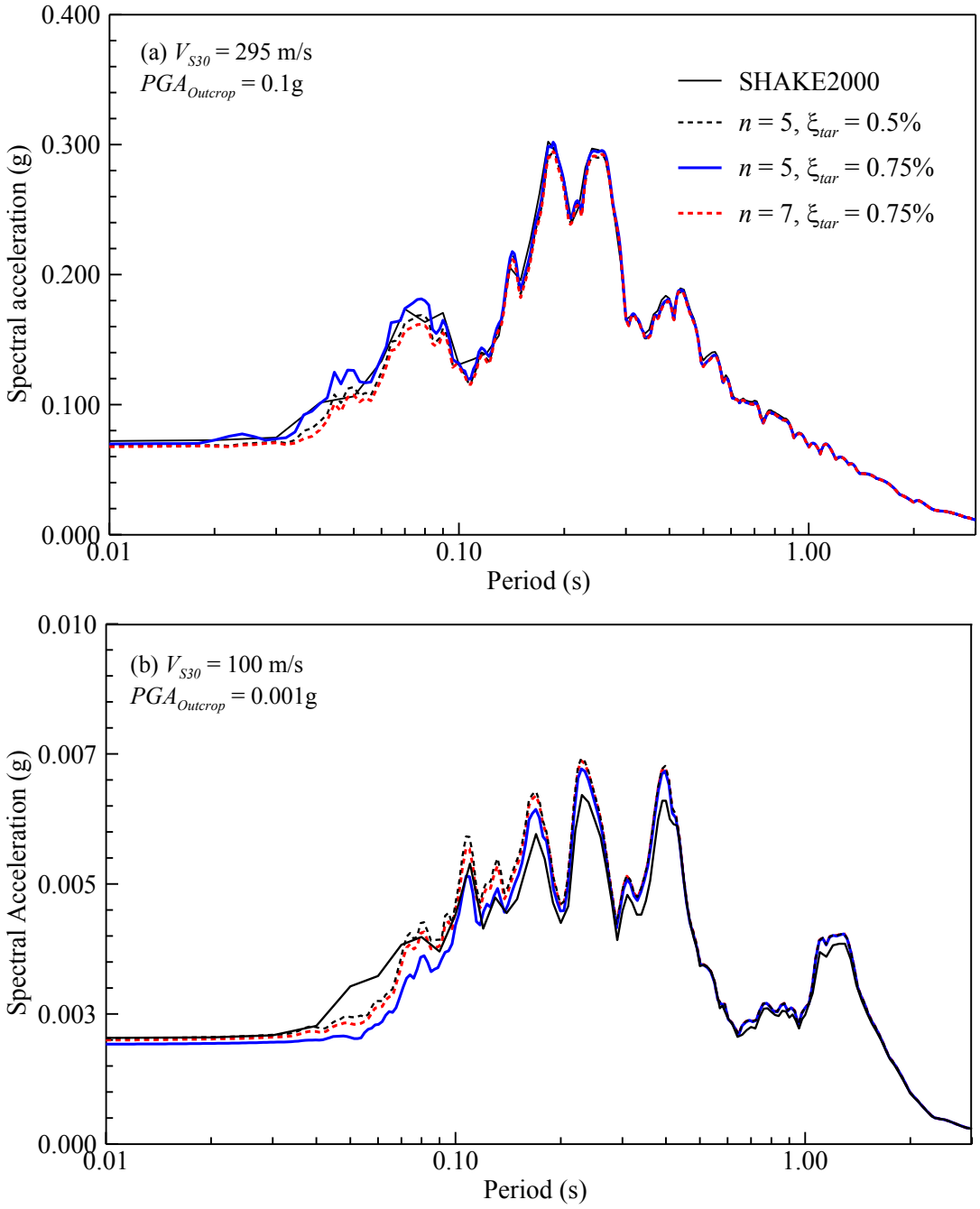

Figure 4.6: Rayleigh damping parameters n and ξ_{tar} calibration procedure: (a) V_{S30} = 295 m/s at $PGA_{Outcrop}$ = 0.1g; and (b) V_{S30} = 100 m/s at $PGA_{Outcrop}$ = 0.001g.

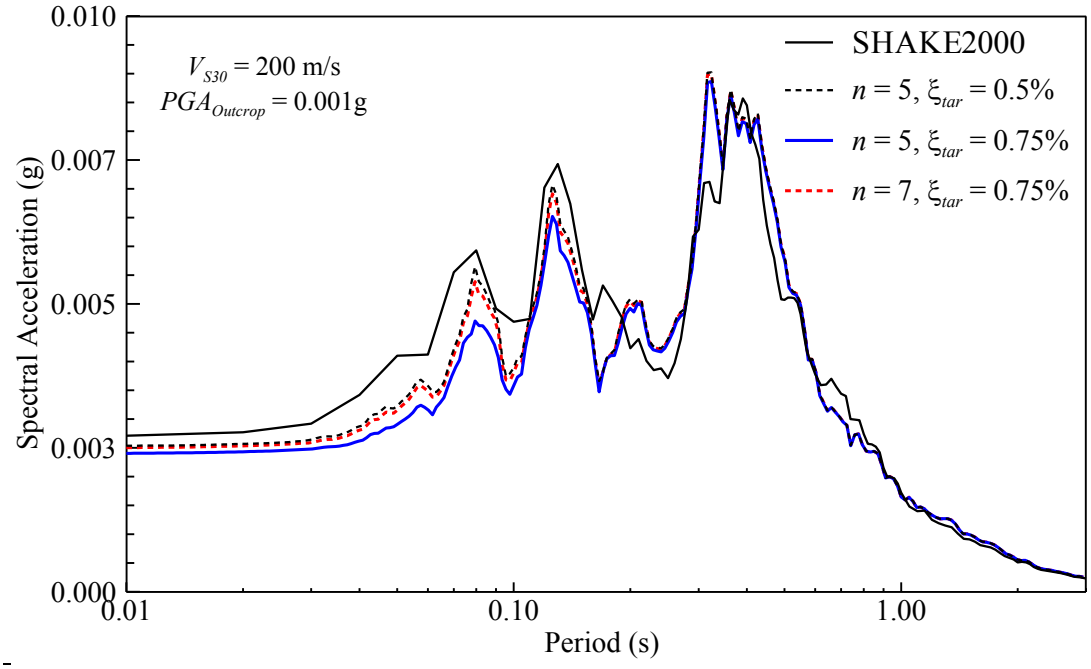

Figure 4.7: Rayleigh damping parameters n and ξ_{tar} calibration procedure for V_{S30} = 201 m/s at $PGA_{Outcrop}$ = 0.001g.

Both Phillips and Hashash (2009) and Hashash et al. (2010) reported that Rayleigh damping (small-strain damping) has the tendency to over-dampen the system in the case of deep profiles and thus computed responses may be under-predicted. DEEPSOIL has a frequency independent small-strain damping estimation scheme implemented based on Phillips and Hashash (2009) which addresses this issue. Consequently the issues/challenges oriented to the Rayleigh damping parameter calibration are eliminated.

In order to formulate the new frequency independent viscous damping, Phillips and Hashash (2009) started from the damping matrix expression provided by Clough and Penzien (1993):

$$\mathbf{C_R} = \mathbf{M}\sum_{b=0}^{N-1} a_b \left(\mathbf{M}^{-1}\mathbf{K}\right)^b \tag{4.8}$$

where N is the number of modes/frequencies and a_b is a scalar value as defined by a constant damping ratio, ζ_n throughout the soil profile such as:

$$\xi_n = \frac{1}{4\pi f_n}\sum_{b=0}^{N-1} a_b \left(2\pi f_n\right)^{2b} \tag{4.9}$$

For the scalar index b = ½, the ζ_n in Equation 4.9 reduces to $\zeta_n = a_b/2$ which is frequency independent and thus frequency independent damping matrix is obtained (Phillips and Hashash, 2009).

4.5.2.3 *Hysteretic damping estimation*

In DEEPSOIL, a special 'modulus reduction and damping curve fitting' or MRDF fitting is selected for the MKZ model parameters (α and s) calibration which employs a reduction factor, R_F (Phillips and Hashash, 2009) to modify the extended Masing (1926) loading/unloading stress-strain relationship.

$$R_F = b_1\left(\frac{G_{secant}}{G_{max}}\right)^{0.1} \tag{4.10}$$

where G_{secant} is the secant shear modulus corresponding to the maximum shear strain level and b_1 is a variable related to soil and input motion properties. R_F is multiplied with the damping computed using the Masing's criteria to obtain the modified ξ_{Masing} value in the case of MRDF option in DEEPSOIL. This increases the flexibility of the model to match both the modulus reduction and damping curves simultaneously with better accuracy as compared to the MR or MRD matching options available in DMOD2000.

Figure 4.8 presents a comparison of different MKZ model parameters calibration techniques used for this study: the MR and MRD lines from DMOD2000 and MRDF

from DEEPSOIL along with the Zhang et al. (2005) lines, for a soil layer at 4-10m depth of the reference profile (V_{S30} = 295 m/s). Figures 4.8(a) and 4.8(b) present the G/G_{max}-γ and D-γ plots, respectively. As is seen, the 'MR' line matched with the 'Zhang et al. (2005)' line in the case of G/G_{max}-γ (Figure 4.8a) curve while in the case of D-γ (Figure 4.8b) curve, it shows significantly higher damping than the 'Zhang et al. (2005)' line especially at higher strains. The MRD line was unable to fit the 'Zhang et al. (2005)' line on both occasions as expected. On the other hand, the 'MRDF' from DEEPSOIL fits the 'Zhang et al. (2005)' line almost perfectly in both figures. This confirms DEEPSOIL's capability of better estimation of high strain damping than it's nonlinear counterpart DMOD2000.

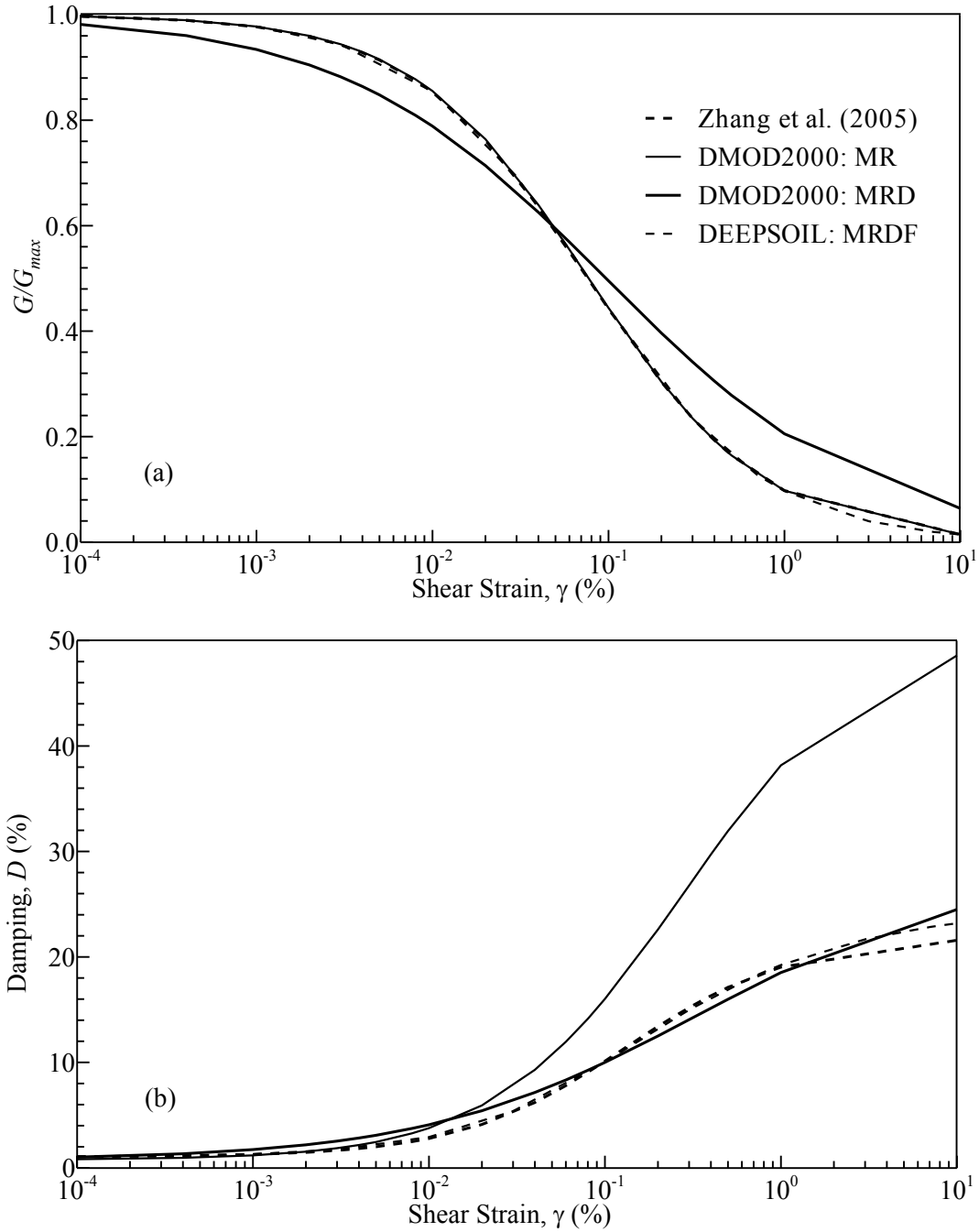

Figure 4.8: MKZ model parameter calibration techniques for: (a) G/G_{max}-γ and (b) D-γ curves.

4.6 Results and Discussions

A total of 18000 site response simulations with SHAKE2000, DMOD2000 and DEEPSOIL are considered among which the SHAKE2000 simulations for $PGA_{Outcrop} \leq$ 0.3g cases and the DMOD2000 simulations for $PGA_{Outcrop}$ of 0.4g and 0.5g cases were also utilized during the site factor model generation as discussed in Chapter 3.

4.6.1 Comparison of responses computed using SHAKE2000, DMOD2000 and DEEPSOIL

From the site response analyses performed, at first, the ground surface acceleration response spectra are computed. In this section, the computed responses using SHAKE2000, DMOD2000 and DEEPSOIL for three sample cases from site class C, D and E (site class definition can be found in BSSC, 1995) with V_{S30} = 134, 295 and 406 m/s, respectively are selected for comparison. Comparison is performed for only two levels of shaking i.e. $PGA_{Outcrop}$ of 0.05g and 0.5g with the Charleston SEE motion (the ground motion in Figure 4.4) and only the mean variation of the G/G_{max}-γ and D-γ curves (Zhang et al., 2005) are considered. Such comparison of the surface acceleration response spectra for the $PGA_{Outcrop}$ of 0.05g case are presented in Figure 4.9(a)-4.9(c) for V_{S30} of 134, 295 and 406 m/s cases, respectively while the similar plots for the $PGA_{Outcrop}$ of 0.5g case are presented in 4.10(a)-4.10(c). Couple of observations can be made from these comparisons: (1) the divergence of the EL and NL lines occur mostly for higher loading ($PGA_{Outcrop}$ of 0.5g) cases although for softer profiles such deviations occur even for $PGA_{Outcrop}$ of 0.05g case (Figure 4.9a) which is the evidence of nonlinearity even at this small loading level; (2) the divergence of the EL and NL lines become lesser with profile

stiffness (V_{S30}) increase; (3) EL lines mostly produced higher amplitude although they fall below the NL lines at the smaller periods (see the response spectra plots); and (4) the divergence between the two NL lines: DMOD2000 and DEEPSOIL, occur mostly for higher loading ($PGA_{Outcrop}$ of 0.5g) cases at lower periods.

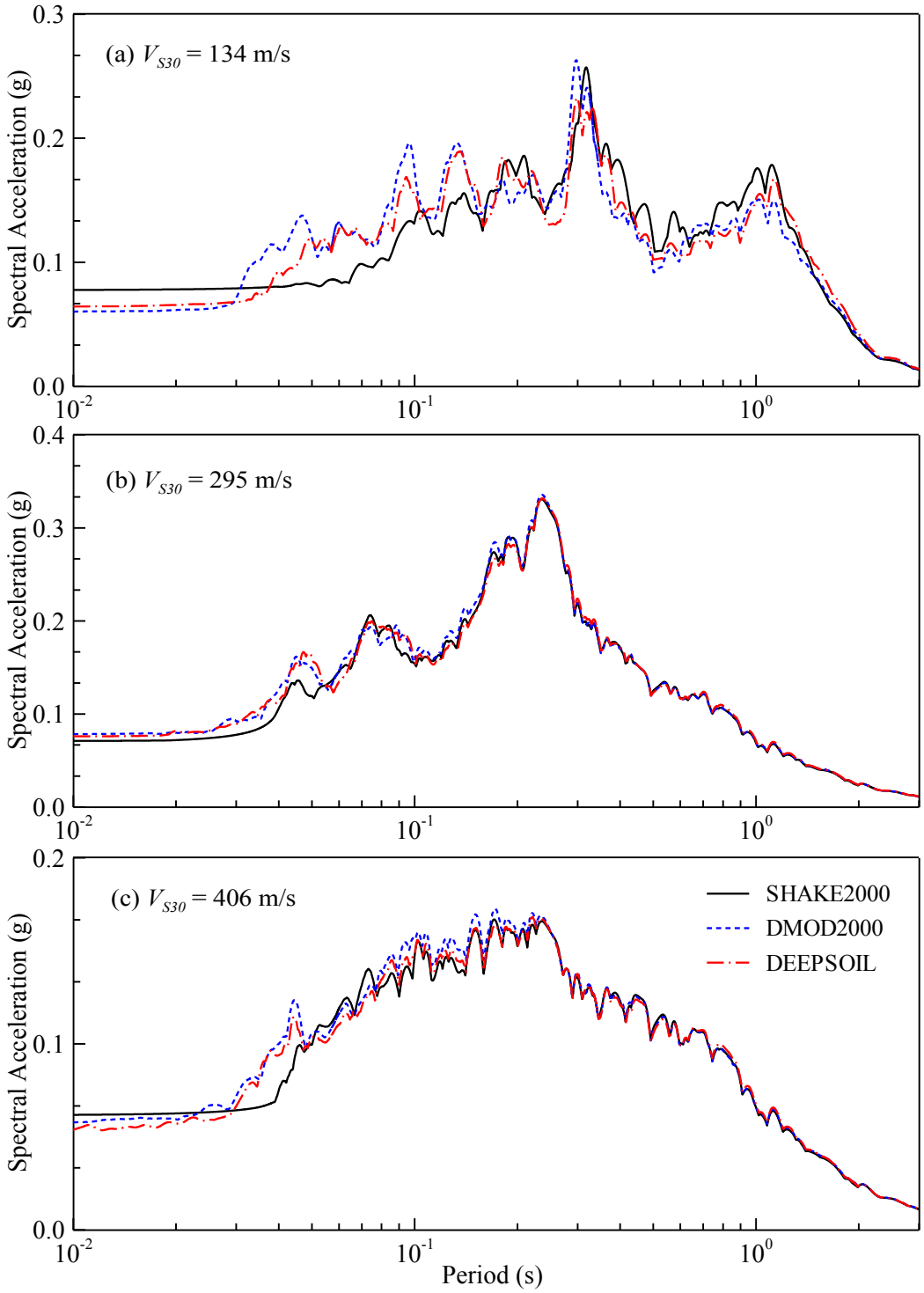

Figure 4.9: Comparison of the computed acceleration response spectra in sub-plots (a), (b) and (c) for V_{S30} of 134, 295 and 406 m/s, respectively; the Charleston ground motion scaled to $PGA_{Outcrop}$ of 0.05g is used.

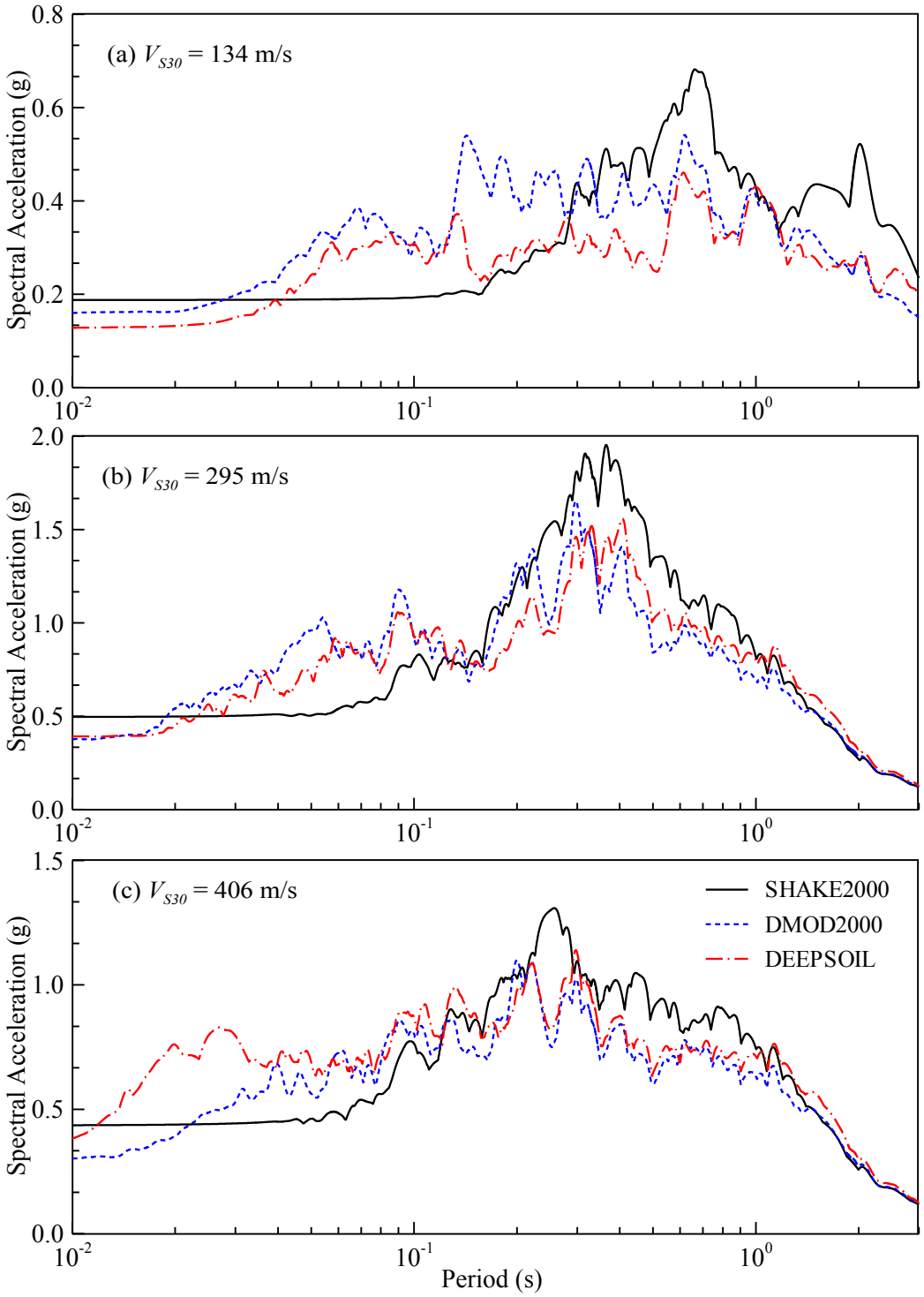

Figure 4.10: Comparison of the computed acceleration response spectra in sub-plots (a), (b) and (c) for V_{S30} of 134, 295 and 406 m/s, respectively; the Charleston ground motion scaled to $PGA_{Outcrop}$ of 0.5g is used.

4.6.2 Generation of site factor models

Based on the simulations with the site response tools: SHAKE2000, DMOD2000 and DEEPSOIL, three separate brand new site factor models: 'SF-SK', 'SF-DM' and 'SF-DS', respectively, are developed following the procedure of Aboye et al. (2013a) and are presented in this section. Point to be noted here that, proposing a new site factor model for the location is not the intention of this study. The intention is: comparing the Aboye et al. (2013a) –type site factor models that are generated purely based on EL and NL analyses in order to evaluate the potential deviation of the predicted site factors.

At first based on the generated data points from each of the SHAKE2000, DMOD2000 and DEEPSOIL, the site factor, F for six spectral period ranges: ≤ 0.01 s as for F_{PGA}, 0.01-0.4 s for $F_{0.2}$ (or F_a), 0.41-0.8 s for $F_{0.6}$, 0.81-1.2 s for F_1 (or F_v), 1.21-2.0 s for $F_{1.6}$ and 2.01-4.0 s for $F_{3.0}$, are generated which are the averaged (arithmetic) values of the corresponding ranges. These factors are then averaged (arithmetic) over all twelve motions considered and plotted against the corresponding V_{S30} and also grouped into six different $S_{Outcrop}$ ranges for the corresponding spectral periods. Figures 4.11-4.13 present sample cases of these F-V_{S30} scatterplots based on the SHAKE2000 simulation results for F_{PGA}, $F_{0.2}$, *and* $F_{1.0}$ cases, respectively while Figures A.1-A.3 from Appendix A present the cases from $F_{0.6}$, $F_{1.6}$, *and* $F_{3.0}$. Similar F-V_{S30} plots from the DMOD2000 and DEEPSOIL simulations are also presented in Figures A.4-A.9 and A.10-A.15, respectively. Similar to the F-V_{S30} plots in Aboye et al. (2013a), the data points obtained from each of SHAKE2000, DMOD2000 and DEEPSOIL show the same three distinct features. Those are: (a) an increasing trend of F *with* V_{S30} for low V_{S30} values, (b) a zone

of peak F, and (c) a decreasing trend of F *with* V_{S30} beyond the peak. Thus, the same set of equations and procedure described in Aboye et al. (2013a) are used to fit these F-V_{S30} scatter (i.e. for each of the SF-Sk, SF-D and SF-DS cases) in this study. For the sake of completeness, the equations are presented below (Aboye et al., 2013a):

$$F = \left(\frac{F_p}{V_{S30P}}\right) V_{S30} \qquad \text{for all values of } T \text{ when } V_{S30} < V_{S30P} \qquad (4.11a)$$

$$F = \frac{\left(F_p - 1\right)\left(760 - V_{S30}\right)}{760 - V_{S30P}} + 1 \quad \text{when } T \leq 0.2\ s \text{ and } V_{S30} \geq V_{S30P} \qquad (4.11b)$$

$$F = a + b(\exp^{cV_{S30}}) \qquad \text{when } T > 0.2\ s \text{ and } V_{S30} \geq V_{S30P} \qquad (4.11c)$$

where F is the median site factor value, F_p is the peak F value, T stands for the spectral period and V_{S30P} is the V_{S30} corresponding to F_p; a, b and c are the regression coefficients. F_p, V_{S30P}, b and c are obtained using following expressions (Aboye et al., 2013a):

$$F_p = x_1 S_{Outcrop} + x_2 \qquad (4.12a)$$

$$V_{S30P} = x_3 S_{Outcrop} + x_4 \qquad (4.12b)$$

$$b = \frac{1 - a}{\exp^{760c}} \qquad (4.12c)$$

$$c = \frac{\ln\left(\frac{1 - a}{F_p - a}\right)}{760 - V_{S30P}} \qquad (4.12d)$$

where x_1, x_2, x_3 *and* x_4 are the regression coefficients.

To fit the above equations, a two-stepped procedure is followed: first, a residual analysis to fit the median curves for the individual sub-set of data from each of the F-V_{S30} plots; secondly, linear regression analysis is performed to fit F_p versus $S_{Outcrop}$ and V_{S30P} versus $S_{Outcrop}$ data to obtain x_1, x_2, x_3 *and* x_4 coefficients. As for the residual analysis, the computed medians of the residuals are very close to 1.0 proving the central tendencies of the corresponding median relationships. The coefficients of the above equations for these fittings of SHAKE2000, DMOD2000 and DEEPSOIL data points are tabulated in Table 4.3. For further details of the model fitting procedure, the reader is suggested to review the Aboye et al. (2013a).

Table 4.3: Regression coefficients of the site factor models based on SHAKE2000, DMOD2000 and DEEPSOIL simulations.

		Regression coefficients (comma separated values are for the models based on: SHAKE2000, DMOD2000 and DEEPSOIL, respectively)				
Spectral period, T (s)	$S_{Outcrop}$	x_1 (g^{-1})	x_2	x_3 (g^{-1}.m/s)	x_4 (m/s)	a
0.0	*PGA*	-1.91, -1.39, -1.40	1.95, 1.62, 1.27	200, 270, 270	170, 174, 174	-
0.2	S_s	-0.79, -0.76, -0.61	2.00, 1.97, 1.48	129, 84, 84	195, 207, 207	0.65
0.6	$S_{0.6}$	-2.26, -2.52, -2.92	2.86, 2.68, 2.71	207, 139, 156	156, 183, 182	0.85
1.0	S_1	-2.39, -2.50, -3.40	3.43, 2.89, 3.41	129, 124, 97	153, 147, 156	0.90
1.6	$S_{1.6}$	-4.46, -4.92, -4.92	3.49, 3.22, 3.21	198, 323, 324	121, 113, 133	0.97
3.0	$S_{3.0}$	-8.2, -4.389, -0.97	2.80, 2.10, 2.21	394, 346, 482	80, 85, 131	0.99

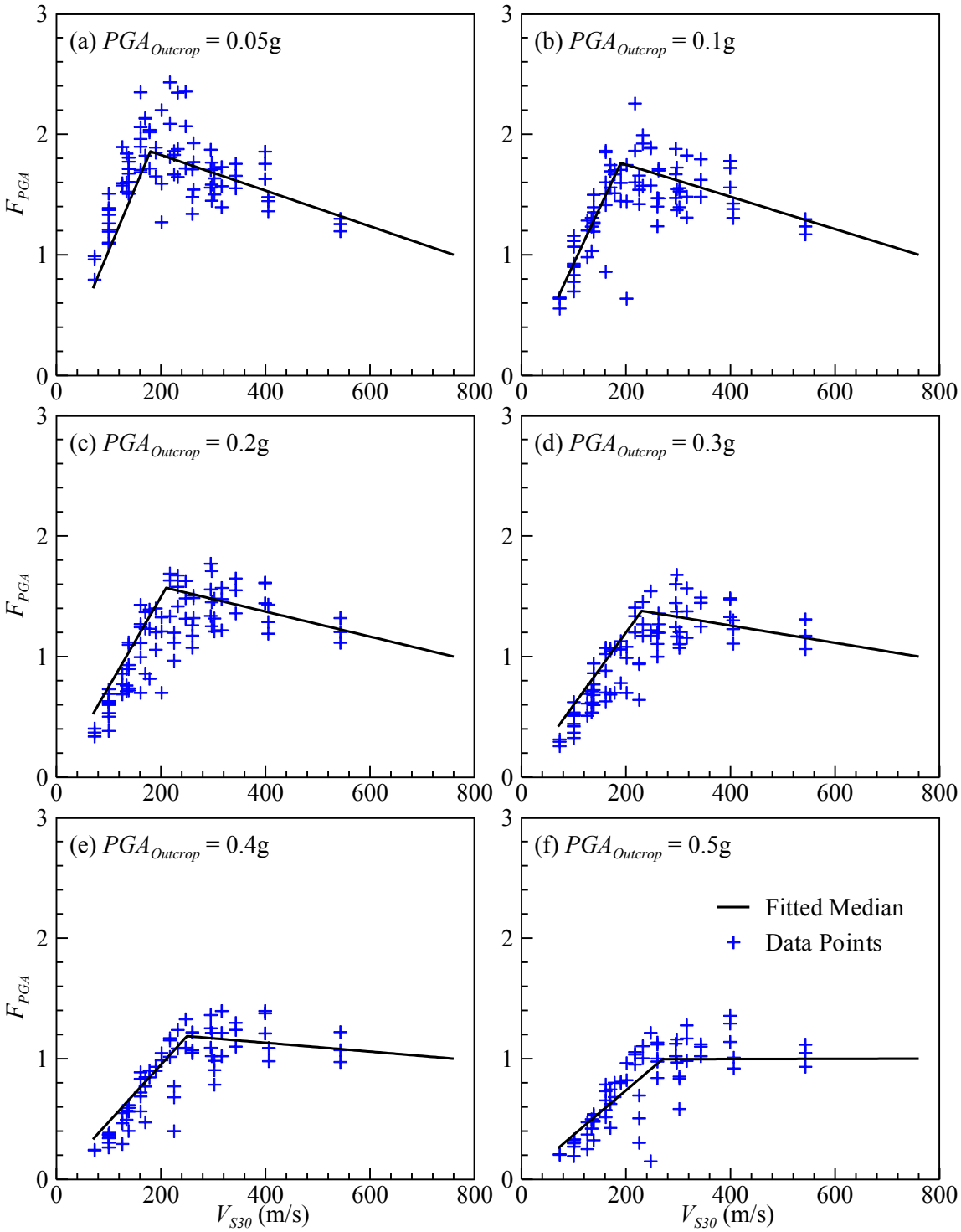

Figure 4.11: Site Factor model based on SHAKE2000 data points for F_{PGA}: (a) $PGA_{Outcrop}$ = 0.05g, (b) $PGA_{Outcrop}$ = 0.1g, (c) $PGA_{Outcrop}$ = 0.2g, (d) $PGA_{Outcrop}$ = 0.3g, (e) $PGA_{Outcrop}$ = 0.4g, and (f) $PGA_{Outcrop}$ = 0.5g.

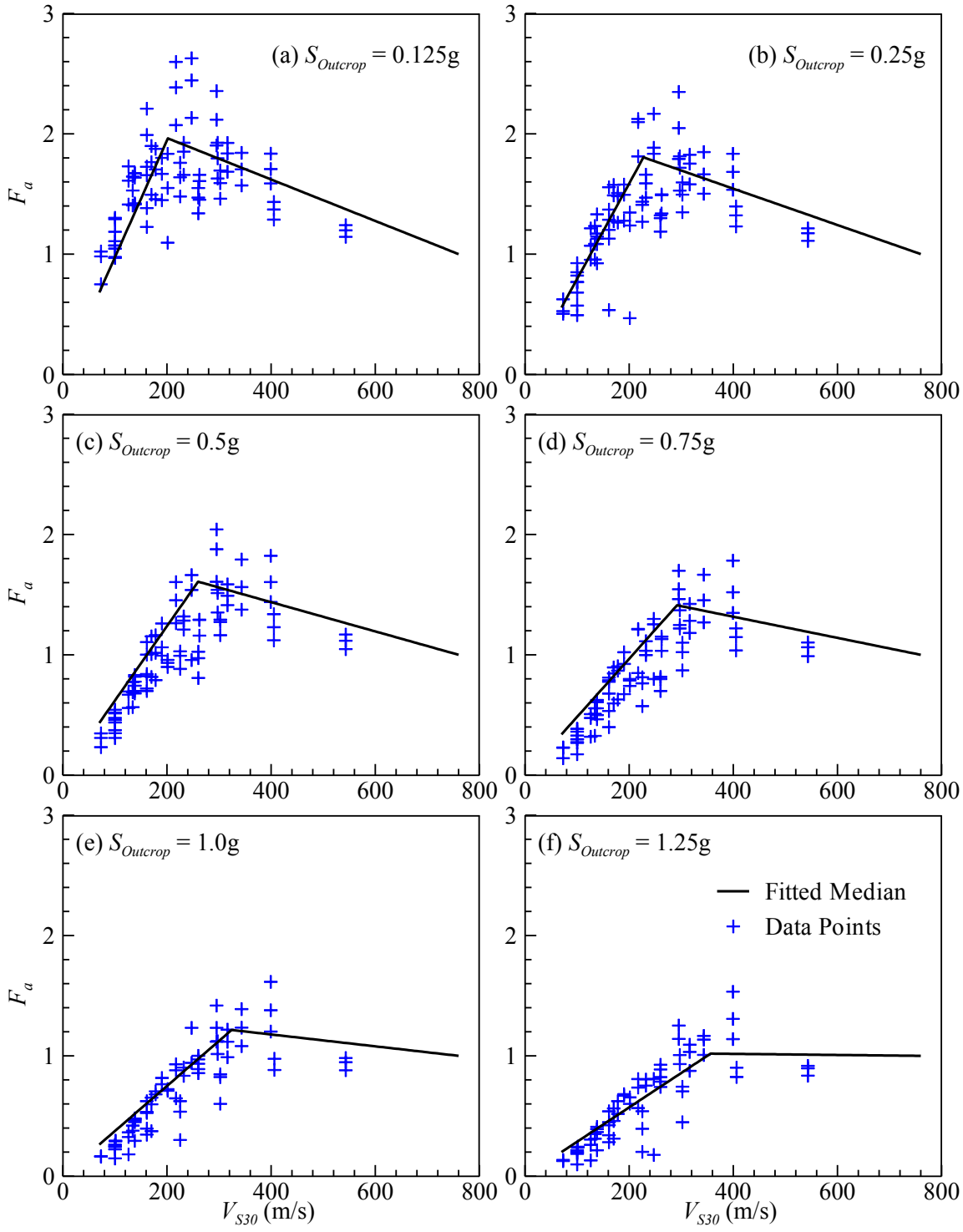

Figure 4.12: Site Factor model based on SHAKE2000 data points for F_a or $F_{0.2}$: (a) $S_{Outcrop}$ = 0.125g, (b) $S_{Outcrop}$ = 0.25g, (c) $S_{Outcrop}$ = 0.5g, (d) $S_{Outcrop}$ = 0.75g, (e) $S_{Outcrop}$ = 1.0g, and (f) $S_{Outcrop}$ = 1.25g.

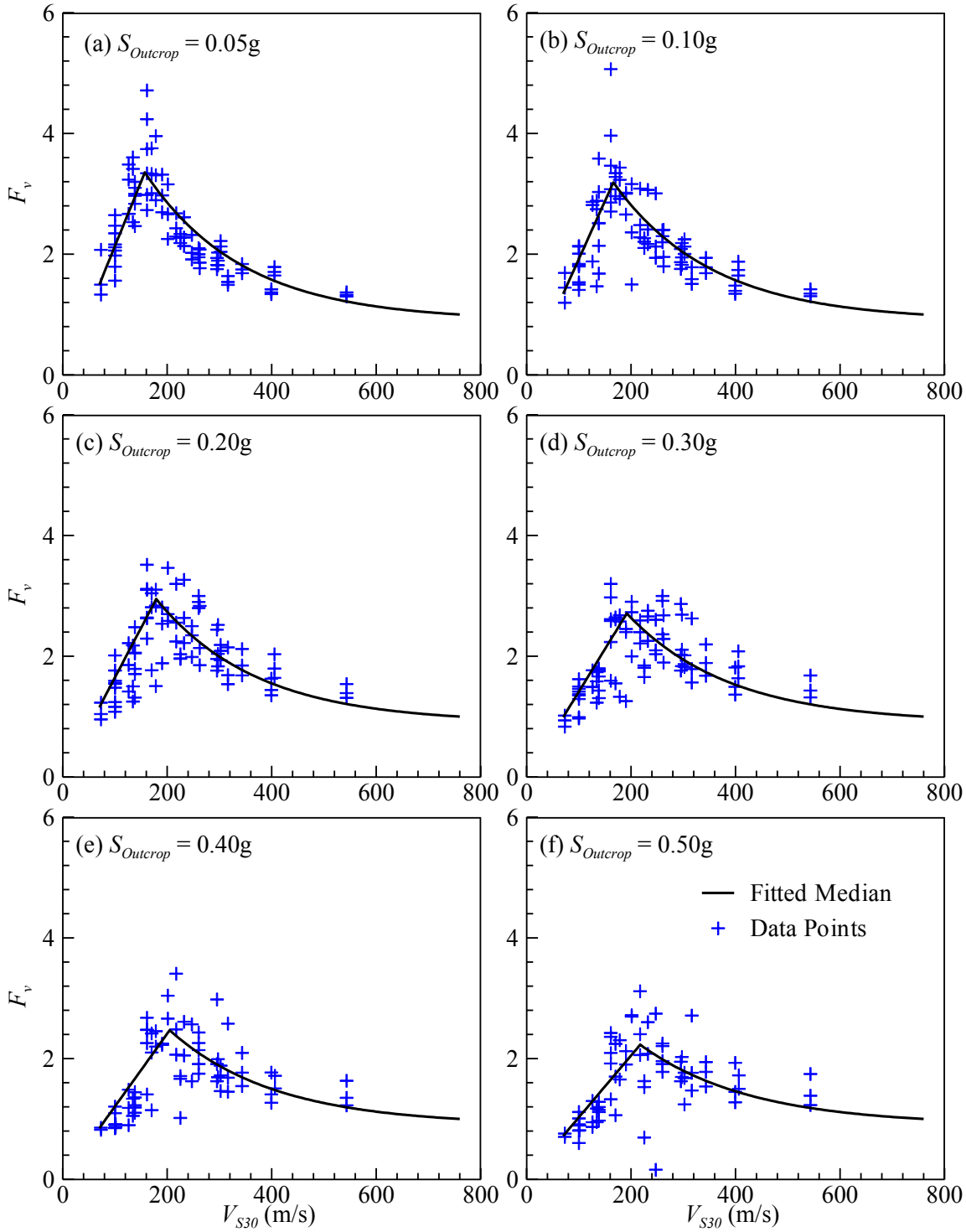

Figure 4.13: Site Factor model based on SHAKE2000 data points for F_v or $F_{1.0}$: (a) $S_{Outcrop}$ = 0.05g, (b) $S_{Outcrop}$ = 0.1g, (c) $S_{Outcrop}$ = 0.2g, (d) $S_{Outcrop}$ = 0.3g, (e) $S_{Outcrop}$ = 0.4g, and (f) $S_{Outcrop}$ = 0.5g.

4.6.3 Comparison of the seismic site factor models

Figures 4.14-4.16 present the comparison of the fitted median lines of each of the SF-SK, SF-DM and SF-DS site factor models for F_{PGA}, $F_{0.2}$ and $F_{1.0}$ cases, respectively while the similar plots for the $F_{0.6}$, $F_{1.6}$, *and* $F_{3.0}$ cases are presented in Figures A.16-A.18 in the Appendix A. Each figure contains six sub-plots corresponding to six $S_{Outcrop}$ (or $PGA_{Outcrop}$ in the case of Figure 4.14) ranges.

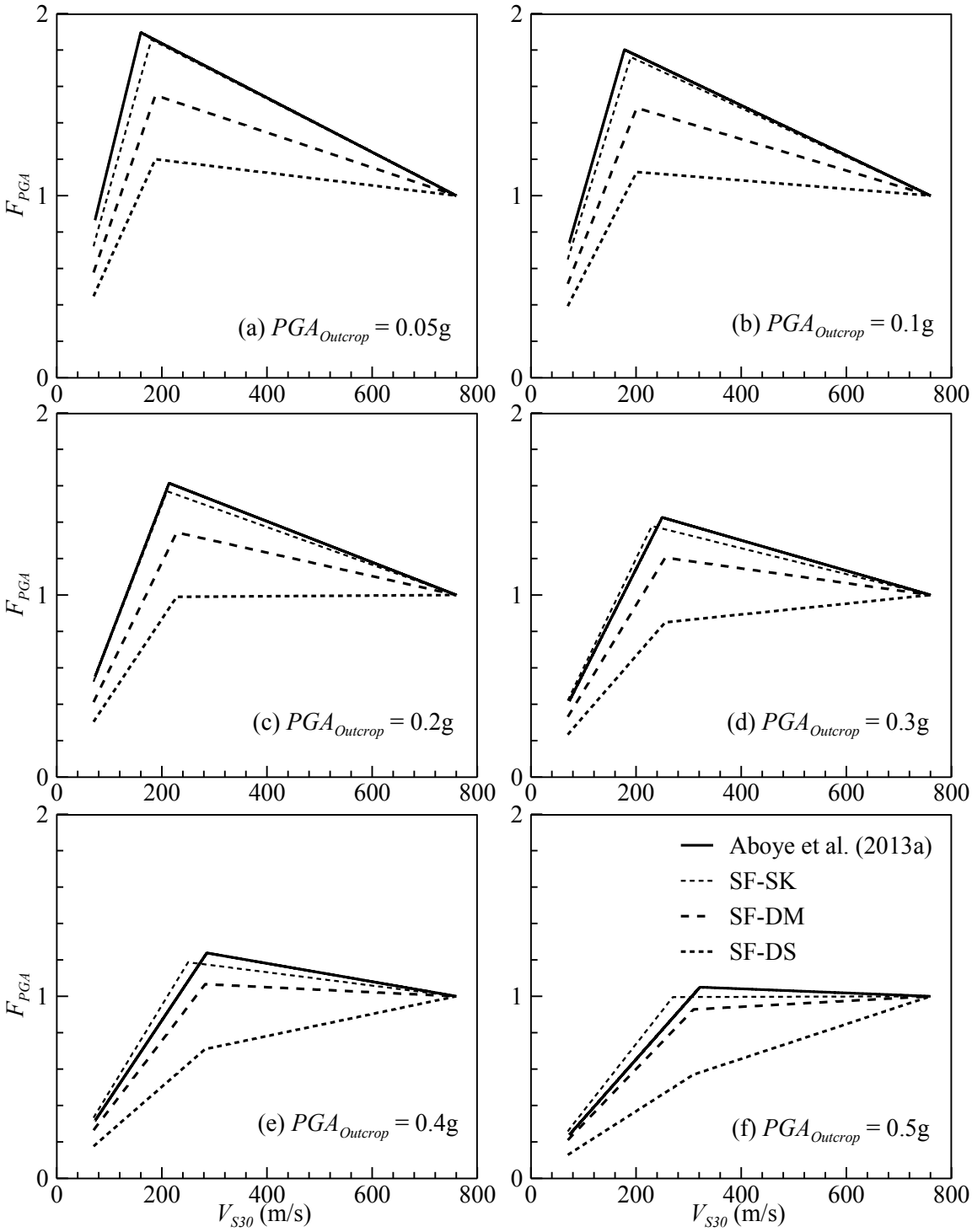

Figure 4.14: Comparison of the site factor models based on Aboye et al. (2013a), SF-SK, SF-DM and SF-DS in the case of F_{PGA} for $PGA_{Outcrop}$ of (a) 0.05g, (b) 0.1g, (c) 0.2g, (d) 0.3g, (e) 0.4g and (f) 0.5g.

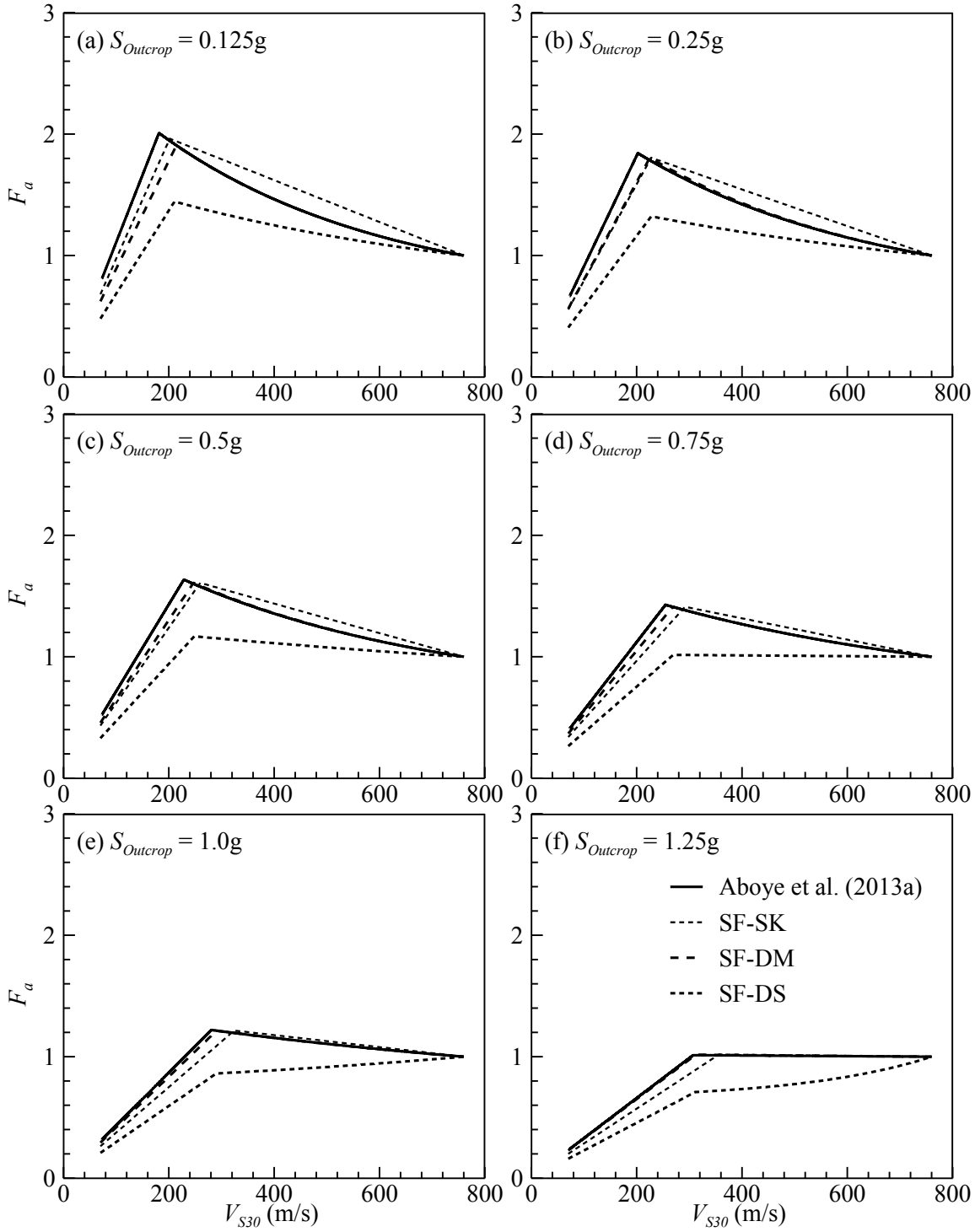

Figure 4.15: Comparison of the site factor models based on Aboye et al. (2013a), SF-SK, SF-DM and SF-DS in the case of F_a or $F_{0.2}$ for $S_{Outcrop}$ of (a) 0.125g, (b) 0.25g, (c) 0.5g, (d) 0.75g, (e) 1.0g, and (f) 1.25g.

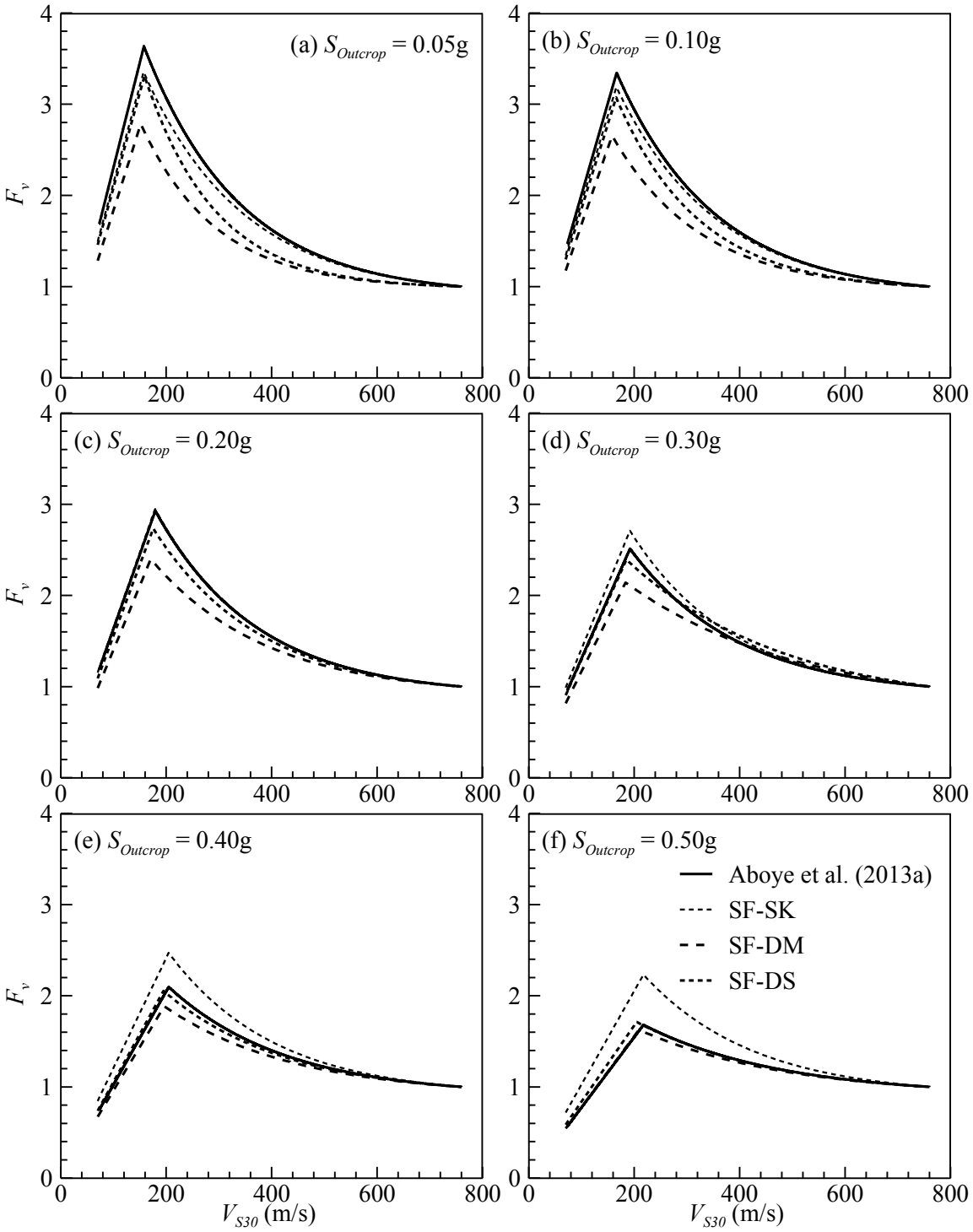

Figure 4.16: Comparison of the site factor models based on Aboye et al. (2013a), SF-SK, SF-DM and SF-DS in the case of F_v or $F_{1.0}$ for $S_{Outcrop}$ of (a) 0.05g, (b) 0.1g, (c) 0.2g, (d) 0.3g, (e) 0.4g, and (f) 0.5g.

Based on the Figures 4.14-4.16 and Figures A.16-A.18 in Appendix A, a few observations can be made. Firstly, SF-SK generally produces conservative estimates than the NL counterparts SF-DM and SF-DS models, even at the lowest loading intensities except for the $F_{0.2}$ (Figure 4.15) and softer profiles cases where SF-DM line predicts higher numbers than the SF-SK. This observation is consistent with the observations seen in the surface spectral acceleration comparison in Figures 4.9 and 4.10 where SHAKE2000 predictions are higher than the corresponding DMOD2000 or DEEPSOIL predictions except for the cases with higher loadings and lower periods. Secondly, significant differences in the computed responses from the NL models i.e. SF-DM and SF-DS, also exist. The SF-DS shows lower values than the SF-DM for low periods such as T = 0.0 and 0.2 s. This difference may be attributed to the difference in the Rayleigh damping formulation (Kwok et al., 2008) in DMOD2000 and DEEPSOIL. On the other hand, the SF-DS shows higher values than the SF-DM for T ≥ 1.0 s cases. This may be attributed to better fitting of input hysteretic damping by DEEPSOIL as discussed in the Section 4.5.3. Finally, the difference among the site factor models decreases as the profiles behave within the linear range where the responses computed from the EL and NL programs are expected to converge. All of these observations in the site factor model are consistent with that observed in the computed surface responses shown in the Figures 4.9 and 4.10.

The Aboye et al. (2013a) site factor models are also plotted in each of the Figures 4.14-4.16 and Figures A.16-A.18 for the comparison purpose. It should be noted that the Aboye et al. (2013a) site factor models are based on the combined EL and NL analysis

results and they are expected to be in the next version of the Geotechnical Design Manual of the SCDOT. Comparison of the Aboye et al. (2013a) site factor models with the models proposed in this study shows that both the NL models (SF-DM and SF-DS) fall, in general, below the Aboye et al. (2013a) models. This indicates that the Aboye et al. (2013a) site factor models predicts conservative estimate.

The implication of the models based on EL analysis results generally producing higher estimates than the NL based models is that the site factors computed entirely based on EL analysis results may overestimate the actual responses, Conversely, existence of significant differences in the site factor models computed from the two NL analysis programs indicates that the selection of computer program is also important and the users must be aware of such differences. This observation demands that the widely used computer programs for conducting site response analysis must be validated against experimental results and/or actual measurements for various soil and loading conditions. The recent efforts to validate the widely used computer programs (Stewart et al., 2008; Kottke, 2010; Kaklamanos et al., 2013 and 2015; Zalachoris, 2014 etc.) must be continued by various research teams. Even the EL responses have been observed (e.g. Zalachoris, 2014) to produce better predictions of the true scenario than an NL analysis especially when the system behavior is nonlinear. Therefore, in the case of site specific analysis, an efficient approach would be to compute site factors based on both EL and NL analyses and make engineering judgments to decide the final site factors for the subsequent seismic analysis of the structure (Matasovic and Hashash, 2012).

4.6.4 Factors contributing to the site factor model variations

In order to explain the behavior observed from the comparison of the models based on EL and NL analyses (Figures 4.14-4.16 and Figures A.16-A.18), at first, the profile maximum shear strains ($\gamma_{Max\_Profile}$) for all six $PGA_{Outcrop}$ levels (i.e. 0.05, 0.1, 0.2, 0.3, 0.4 and 0.5g in six sub-plots) from the SHAKE2000, DMOD2000 and DEEPSOIL simulations are plotted against the respective V_{S30} in Figure 4.17. $\gamma_{Max\_Profile}$ is the maximum shear strain observed in the soil profile during the entire excitation period and are then arithmetically averaged for all 12 motions considered.

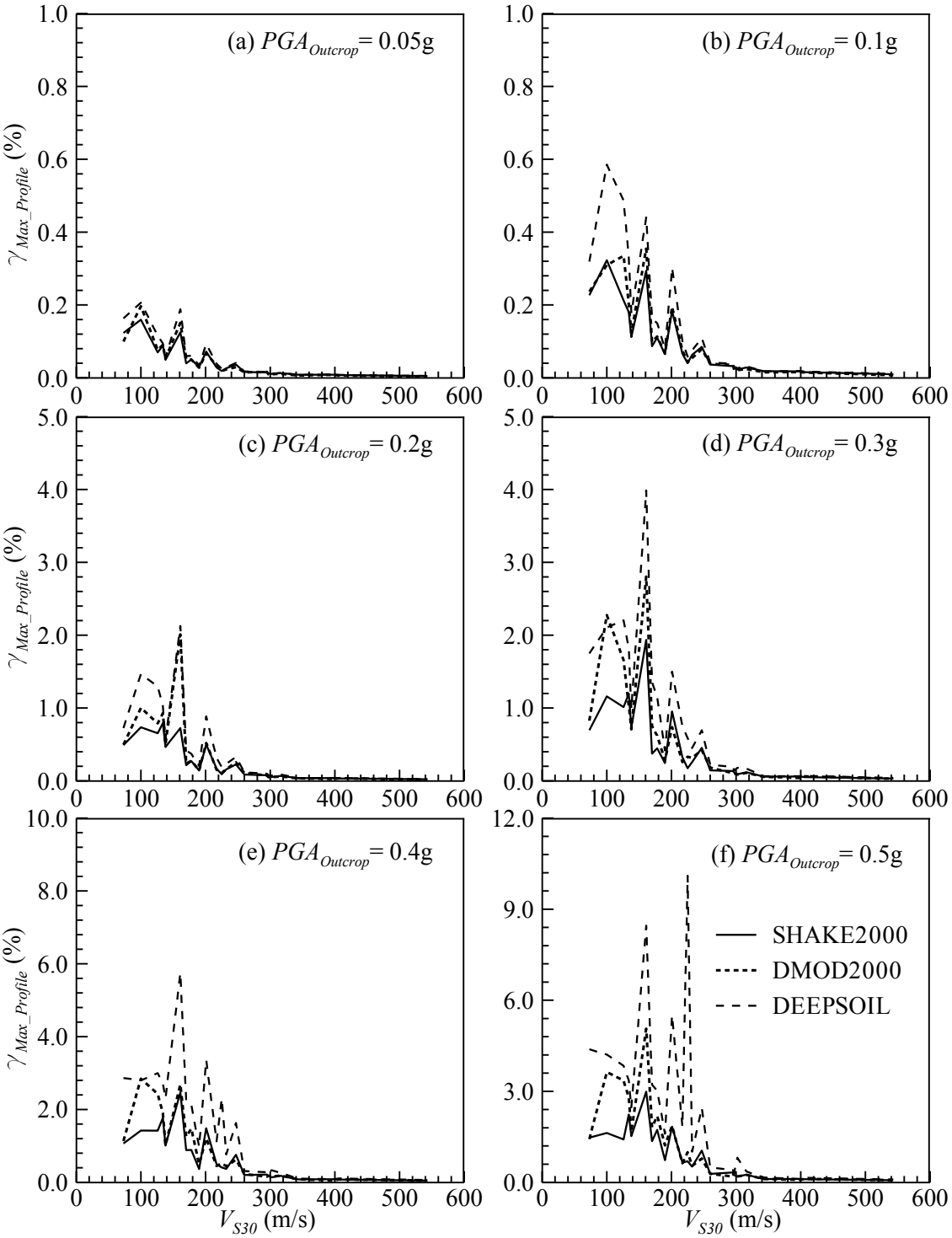

Figure 4.17: Profile maximum shear strain vs. V_{S30} plot for $PGA_{Outcrop}$ levels of: (a) 0.05g, (b) 0.1g, (c) 0.2g, (d) 0.3g, (e) 0.4g and (f) 0.5g, from each of SHAKE2000, DMOD2000 and DEEPSOIL.

As is seen in Figure 4.17, higher values of $\gamma_{Max\_Profile}$ are observed in the softer profiles especially for $V_{S30} \leq 200$ m/s profiles for all three cases (i.e. SHAKE2000, DMOD2000 and DEEPSOIL) while strains are insignificant for the stiffer profiles. In the $V_{S30} \leq 200$ m/s profile cases, the observed $\gamma_{Max\_Profile} \geq 0.1\%$ even for $PGA_{Outcrop}$ of 0.05g; this is the suggested threshold after which the EL and NL responses are expected to diverge (Matasovic and Hashash, 2012; Kaklamanos et al., 2013). Thus, the site factor models (Figures 4.14-4.16 and Figures A.16-A.18) based on EL (i.e. SF-SK) and NL (i.e. SF-DM and SF-DS) analyses started to diverge even at such small intensity loading levels for the softer profile cases. Shear strain estimates from SHAKE2000 is lower than both the NL programs which indicates that SHAKE2000 is using a 'higher equivalent linear modulus and/or lower damping' and explains the higher site factors observed in the previous section (Section 4.6.3). However, the smaller loading cases involve smaller spectral accelerations and thus site factors are typically higher in these cases than the larger loading scenarios; this has potentially contributed to the contrasts observed in Figures 4.14-4.16 and Figures A.16-A.18 between different site factor models at the smaller loading cases. Nonetheless, for the higher intensity loading levels such as 0.3, 0.4 and 0.5g, $\gamma_{Max\_Profile}$ becomes much higher than 0.5% strain; this is a point where EL methods are unable to model the soil responses successfully as suggested by Matasovic and Hashash (2012). High amplitude strains involve higher hysteretic damping in the NL analysis thus a lesser amplification of the ground motion to the surface level was observed than the EL analysis for the softer profiles. Point to be noted here that, a slight deviation among the EL and NL models are observed (Figures 4.14-4.16 and Figures

A.16-A.18) even for the stiffer profiles. This is mostly due to the deviation of the data sets at the softer profiles which imposes a propagation of deviation of the fitted models even in the stiffer profile cases.

Another factor may have an implication on the NL (i.e. SF-DM and SF-DS) lines falling below the EL lines (i.e. SF-SK) and/or even the deviations observed among the NL lines. The standard protocol of a site response analysis require the implied shear strength, computed by the program based on the input G/G_{max}-γ curve, should reasonably match the actual shear strength for each soil layer of the profile. Implied shear strength is computed from the last pair of data of the G/G_{max}-γ curves which corresponds to the highest shear strain considered i.e. failure. Due to the unavailability of shear strength parameters from the study location, the author was unable to verify the program generated implied shear strength values which were computed based on the Zhang et al. (2005 and 2008) G/G_{max}-γ curves for shear strength estimation at large strains. This possibly has induced unrealistic 'softness' in the profile behavior and an unreasonably damped response may have occurred, especially in the cases of NL analyses where the whole G/G_{max}-γ curve is being considered rather than a single value (e.g. equivalent linear shear modulus in SHAKE2000). For detailed discussions over adjusting the input G/G_{max}-γ curves for matching the implied shear strength can be found in Hashash et al. (2010) and Zalachoris (2014).

4.6.5 Factors contributing to the differences observed in responses from DMOD2000 and DEEPSOIL

An attempt has been made to investigate the differences in the surface responses observed from the DMOD2000 and DEEPSOIL programs. Although the framework is the same in both the computer programs, differences exists in the way the input modulus reduction (MR) and Damping are matched by the analytical model used in the computer programs. The small strain damping formulations implemented in these programs are also different. To investigate the effect of these differences, a number of analysis were conducted on the reference profile (V_{S30} = 295 m/s) with the Charleston ground motion (Figure 4.4) scaled to $PGA_{Outcrop}$ of 0.5g by varying the procedure.

First, two cases were considered for DEEPSOIL analyses: (i) Case-I which applies the MRDF matching (refer to Section 4.5.2 for detail) for MKZ model calibration and the frequency independent technique for incorporating small strain damping; and (ii) Case-II which applies the MR matching with the full Rayleigh damping. Thus the damping estimation technique followed in the Case-II of DEEPSOIL is the closest to the technique followed in DMOD2000. Figure 4.18(a) presents the comparison of the surface spectral accelerations computed for each of the three cases. Clearly, the Case-II from DEEPSOIL and DMOD2000 responses are very close to each other while the Case-I from DEEPSOIL shows deviation in both lower and higher periods. Figure 4.18(b) presents the comparison of the computed shear strains for a layer at 10 m depth (where the largest shear strain concentration is observed for each of the cases) from the ground surface. Once again the Case-II from DEEPSOIL and DMOD2000 responses are very

close to each other while the Case-I from DEEPSOIL shows deviation as expected. These observations reveal: (i) both the DMOD2000 and DEEPSOIL produce very similar responses when the damping estimation techniques are identical; and (ii) the incorporation of advanced damping estimation techniques (both for small and large strain ranges) are the sources of the deviations observed in the DEEPSOIL responses from its NL counterpart DMOD2000. The above observation supports the fact that both DMOD2000 and DEEPSOIL frameworks are capable of producing almost identical predictions given that the estimated damping are close to each other.

However, DEEPSOIL predicting higher shear strain values than DMOD2000 has an implication over the relative difference observed in their surface responses. Once again the layer at 10 m depth for the reference profile (V_{S30} = 295 m/s) is selected for comparison of DMOD2000 and DEEPSOIL (here the MRDF matching and frequency independent techniques are followed in DEEPSOIL) responses. Figure 4.19(a) presents the shear strain-time history comparison where DEEPSOIL produces higher strain than DMOD2000, in general. The corresponding damping versus strain curves from both the DMOD2000 (MR fitted) and DEEPSOIL (MRDF fitted) are plotted in Figure 4.19(b). One of the implications of DEEPSOIL predicting higher strain values than DMOD2000 is, although the damping versus shear strain curves from both these programs have major differences, higher shear strain from DEEPSOIL minimizes the actual damping differences computed from both the programs or can even impose a greater damping than DMOD2000 in some cases. For example, after 7.7 s of excitation, the shear strain computed by DEEPSOIL is 0.37% (as seen in Figure 4.18a). The corresponding damping

values according to Figure 4.18(b) for 0.37% strain from 'DEEPSOIL' line is 15.5% while from 'DMOD2000' line it is 28.8%, which means 13.3% difference in damping. On the other hand, the shear strain computed by DMOD2000 is 0.27% at 7.7 s, and the corresponding damping is 25.5%, instead. Thus DEEPSOIL and DMOD2000 have estimated damping difference of 10% while it could be higher (~13.5%) if both the codes would produce closer shear strain estimates.

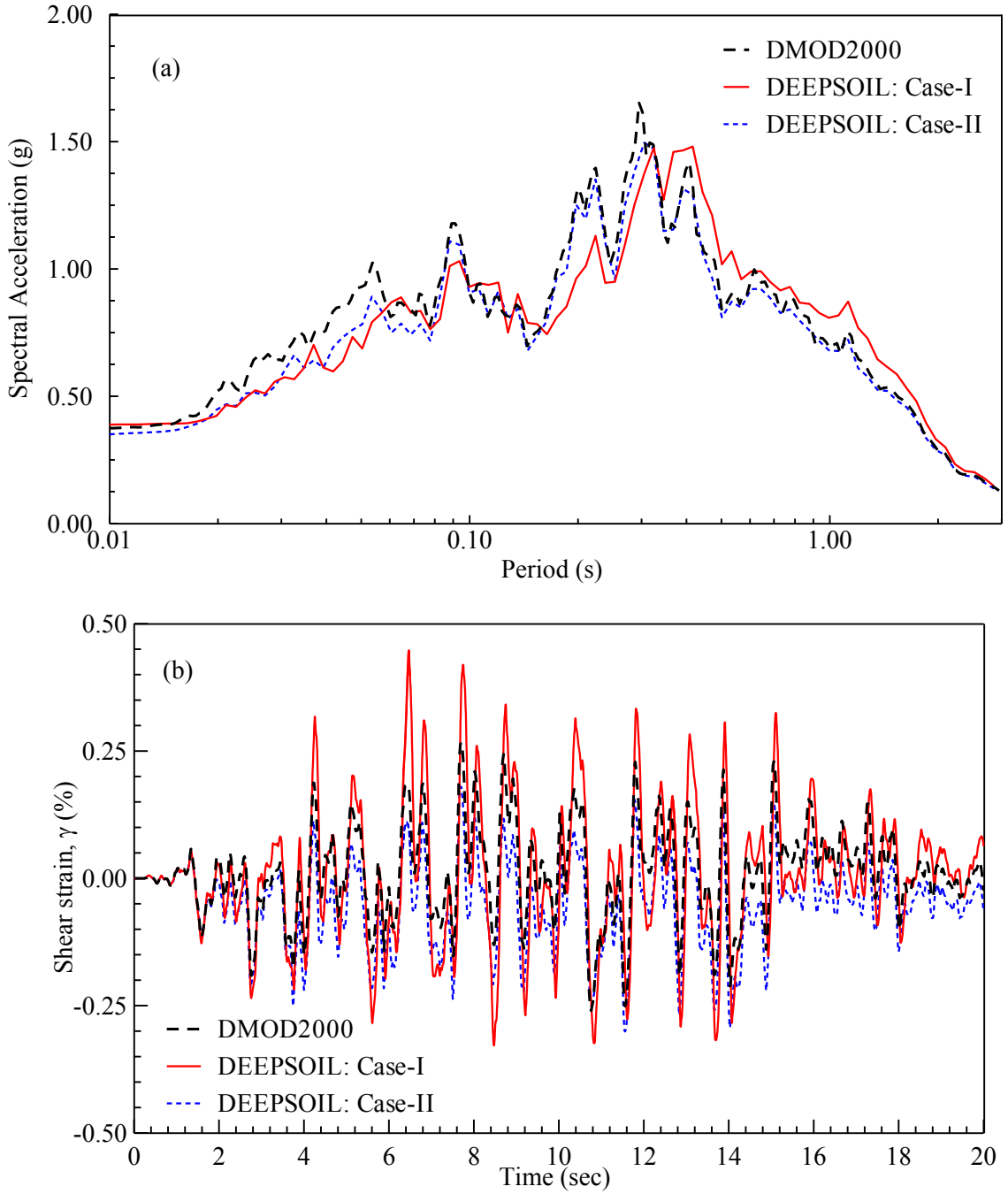

Figure 4.18: Differences in the computed surface responses observed from the DMOD2000 and DEEPSOIL programs: (a) surface spectral accelration and (b) shear strain time history (upto 20 sec) for a layer at 10 m depth from ground surface.

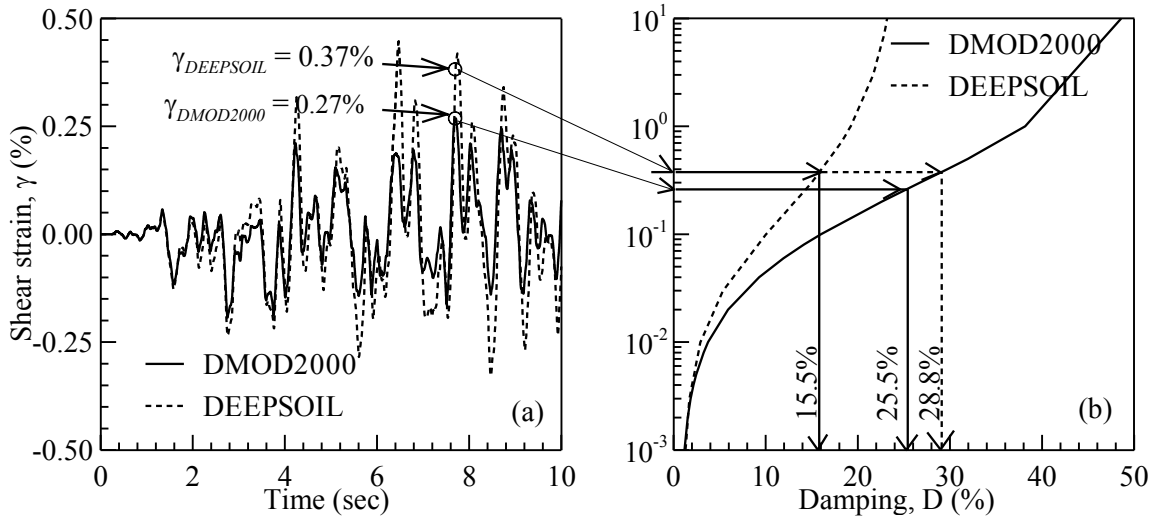

Figure 4.19: Implication of shear strain differences between DEEPSOIL and DMOD2000 on computed responses: (a) shear strain time history (partial) comparison, and (b) damping versus strain curves from both programs for the reference profile at 10 m depth from ground surface.

4.7 Criteria for Selection of an EL or NL Analysis: A Simple Threshold Chart

Based on the literature survey performed, the need for a comprehensive guideline to select an appropriate site response analysis tool: EL or NL, is enormous. Although a few guidelines have emerged from some of the most recent studies (Matasovic and Hashash, 2012; kaklamanos et al., 2013 and 2015; Kim et al., 2013), more work is necessary to build a comprehensive guideline for the practitioners to be able to apply in different sets of conditions all over the world. In this goal, an effort is made in this section to develop a guideline using the comparison of simulations from the EL (SHAKE2000) and NL (DMOD2000, DEEPSOIL) tools. The guideline is formed as a threshold chart which is a function of two commonly available parameters: V_{S30} and $PGA_{Outcrop}$.

4.7.1 Development steps

Following is a step-by-step procedure of threshold chart generation for the cases with mean G/G_{max}-γ and D-γ curves:

(i) First of all, the area enclosed within the band of 0 s and 10 s period of the surface response spectral acceleration plots, i.e. the shaded region of the response spectral acceleration curve in Figure 4.20, is calculated for each of the simulations with SHAKE2000, DMOD2000 and DEEPSOIL.

(ii) Then for each of the V_{S30} cases, the arithmetic means of the area from all 12 motions are calculated from SHAKE2000, DMOD2000 and DEEPSOIL simulations, for all six $PGA_{Outcrop}$ levels.

(iii) Then for each V_{S30}, the corresponding averaged area ratios of the pairs SHAKE2000 to DMOD2000 and also SHAKE2000 to DEEPSOIL are computed, again for all six $PGA_{Outcrop}$ levels.

(iv) Finally the threshold chart (Figure 4.21) is generated by setting V_{S30} and $PGA_{Outcrop}$ as the x- and y-axes, respectively; then the area ratios from: SHAKE2000 to DMOD2000 and also SHAKE2000 to DEEPSOIL, are combined and plotted using separate markers for three distinct ranges of ratios: less than 1.1, within 1.1 to 1.2, and greater than 1.2. Based on these area ratios, regions of deviations of the EL responses from the responses of NL programs being 'less than 10%' (i.e., area ratio of 1.1), 'within 10 to 20%' (i.e., area ratio within 1.1 to 1.2), and 'above 20%' (i.e., area ratio above 1.2), can be easily distinguished. Higher V_{S30} cases fall 'less than 10%' range for up to a $PGA_{Outcrop}$ of 0.5g whereas

low velocity profiles fall 'within 10 to 20%' or even 'above 20%' range even at a low $PGA_{Outcrop}$ such as 0.1g. $PGA_{Outcrop} \geq$ 0.4g cases show more than 20% variation for the profiles with $V_{S30} \leq$ 300 m/s and thus labeled under 'above 20%'. For cases with $V_{S30} <$ 200 m/s and $PGA_{Outcrop} \geq$ 0.1g, at least a 10% variation between the EL and NL programs is expected and for above 0.3g it's above 20%. An attempt is made to differentiate these ≤10%, >10% and <20%, ≥20% zones with three significant color patches. These regions should help distinguish whether to switch for a nonlinear code such as DEEPSOIL or DMOD2000, or to stick with an equivalent linear code such as SHAKE2000, for a given set of V_{S30} and $PGA_{Outcrop}$ values from the project location to perform a site specific ground response analysis.

Similarly, two other threshold charts are generated for the mean+1σ and mean-1σ G/G_{max}-γ and D-γ cases based on the same SHAKE2000, DMOD2000 and DEEPSOIL simulations and are presented in Figures A.19(a) and A.19(b) in Appendix A.

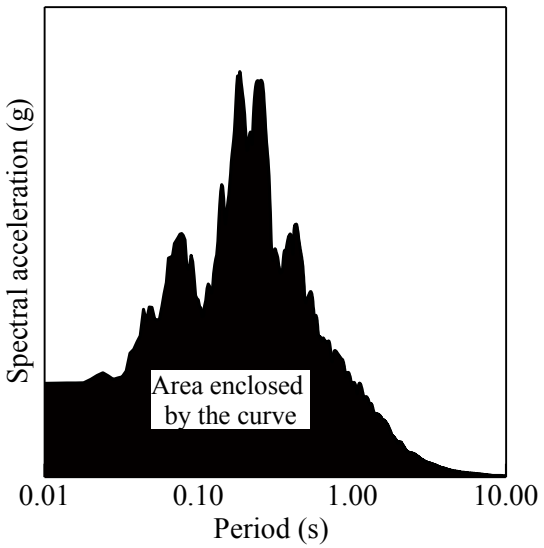

Figure 4.20: Area enclosed by a typical spectral acceleration curve.

Point to be noted here that, the developed threshold chart accounts for the spectral acceleration difference over the entire range of 0.01-10 sec period rather than specifying period dependent distinctions as the ones suggested in Kaklamanos et al. (2013) and Kim et al. (2013). Therefore, unlike to Kim et al. (2013) who proposed a 30% deviation (i.e. deviation of computed responses) is required to trigger the use of NL tools, the here proposed threshold is kept to 10% (or greater) as a greater deviation at a specific period may be concealed under this full-range (i.e. 0.01-10 sec) deviation. As is seen from Figures 4.21 and Figures A.19, the cases with the mean and mean±1σ of G/G_{max}-γ and D-γ can produce significantly different set of outcomes. The mean+1σ case in Figure A.19(a) states that the nonlinear and equivalent linear codes are expected to produce very close estimates practically for most of the soil profiles and loading conditions that are covered in this study. On the other hand, for the mean-1σ cases in Figure A.19(b) it's the opposite. These mean±1σ cases represent two extremes of soil dynamic properties

(G/G_{max}-γ and D-γ) and are less likely to be found in reality. These two figures (Figures A.19a and A.19b) are included here in the intention that the user should be aware of the potential variation of the mean case (Figure 4.21) that might occur due to such dynamic properties variation. However, the threshold chart for the mean case (Figure 4.21) is the recommended one for general engineering application, especially when a very limited knowledge is available over the variation of G/G_{max}-γ and D-γ curves in the project site. All the above charts are generated considering the spectral period band of 0 to 10 sec (Figure 4.20). An attempt was made to reduce it to 0-4 sec band and no practical deviation was observed in the threshold charts from the 0-10 sec cases. A sample case with mean G/G_{max}-γ and D-γ case based on 0-4 sec period band is presented in the Appendix A Figure A.20. This proves the fact that after 4 sec period no practical deviation in spectral acceleration exists between the EL and NL cases.

Moreover, an attempt is made to generate a regression equation for the recommended threshold chart (Figure 4.21) to be able to quickly estimate the approximate differences involved in these two types (equivalent linear and nonlinear) of programs. At first, the area ratios of SHAKE2000 to DMOD2000 and also SHAKE2000 to DEEPSOIL are combined, grouped into six $PGA_{Outcrop}$ levels and then plotted against the corresponding V_{S30} values. Figure 4.22 presents the area ratio versus V_{S30} plot for all $PGA_{Outcrop}$ levels. It is observed that the ratios show a clear deviation from '1.0' at around 200 m/s or below, especially in the $PGA_{Outcrop}$ levels of 0.05, 0.1, 0.2 and 0.3g. For $PGA_{Outcrop}$ levels of 0.4 and 0.5g, such deviation starts at even higher velocity. This supports the earlier observations in this study that the low velocity profiles start to

experience nonlinearity at a very small loading while the stiffer profiles (i.e. with higher velocity) stay close to linear zone even at a significant loading. The following equation has been developed based on a regression analysis:

$$\text{Area ratio, Equivalent Linear/Nonlinear} = a\left(V_{S30}\right)^{(-0.8)} + b \tag{4.13a}$$

$$\text{where, } a = (28.2)PGA_{Outcrop} + 3.744 \tag{4.13b}$$

$$b = \begin{cases} 0.948, \textit{ when } PGA_{Outcrop} \leq 0.2g \\ 0.913, \textit{ when } PGA_{Outcrop} > 0.2g \end{cases} \tag{4.13c}$$

The coefficient of determination, R^2 values that stated on each sub-plot of Figure 4.22 supports the quality of these fits. The residual (difference between data and the fit) plots are also seemed random in general (not presented here).

The Equation 4.13 can be used to obtain an exact estimation of the difference between the SHAKE2000 and the corresponding DMOD2000 responses or SHAKE2000 and DEEPSOIL responses. Therefore, together the fitted equation (Equation 4.13) and the threshold chart (Figure 4.21) provides the complete guideline on selecting the most appropriate site specific response spectrum analysis tool for the project in hand. The tool requires the $PGA_{Outcrop}$ and the profile V_{S30} which are more likely to be available to the user prior to performing a site specific response spectrum analysis. This is an advantage over the previous protocols (Kramer and Paulsen, 2004; Matasovic and Hashash, 2012; kaklamanos et al., 2013 and 2015) which state shear strain as a parameter in the selection of an appropriate site response tool.

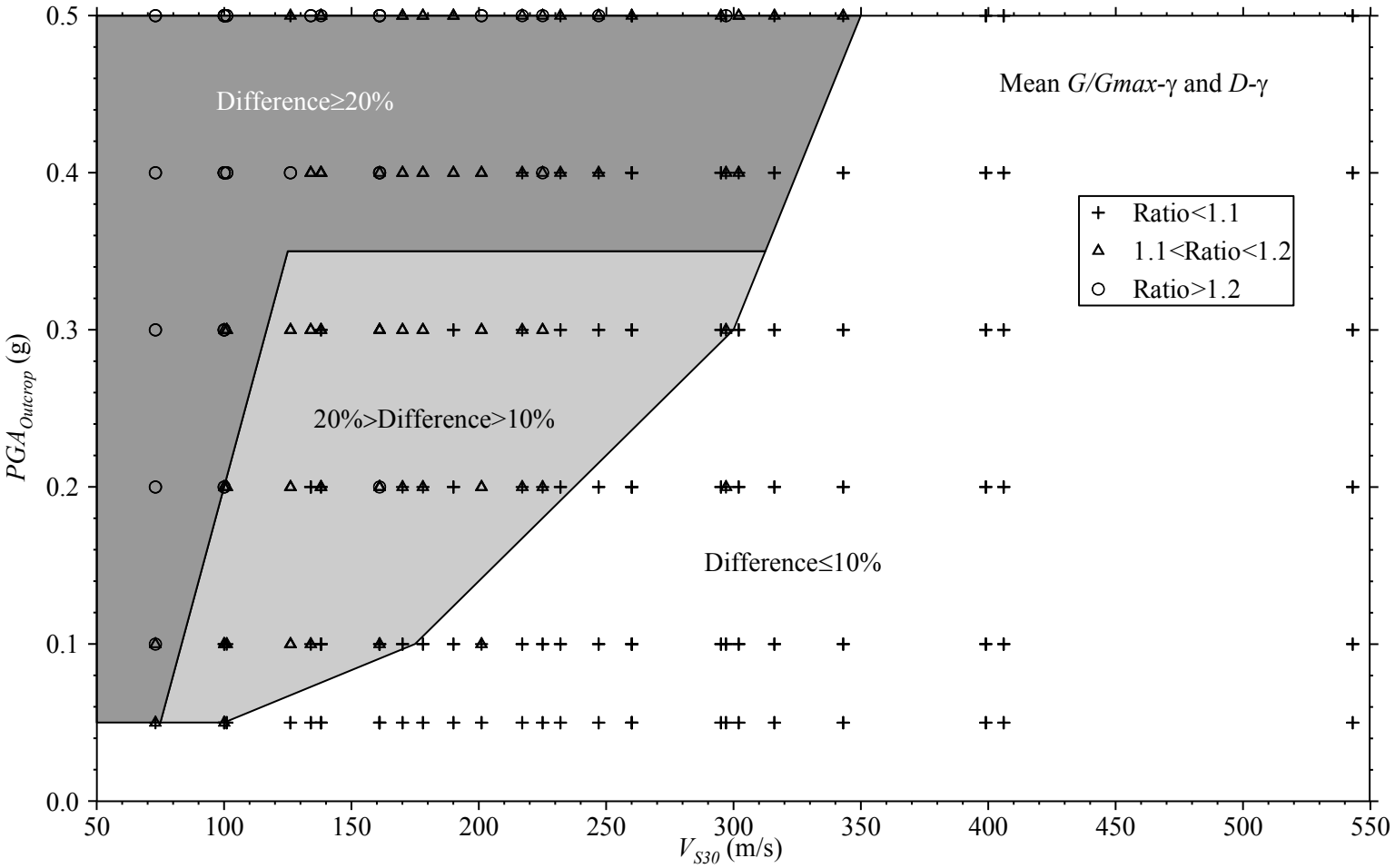

Figure 4.21: Threshold chart developed with regions showing variation of the area ratios between the EL (SHAKE2000) and NL codes (DMOD2000 and DEEPSOIL) for a range of V_{S30} and $PGA_{Outcrop}$ considered for the mean G/G_{max}-γ and D-γ.

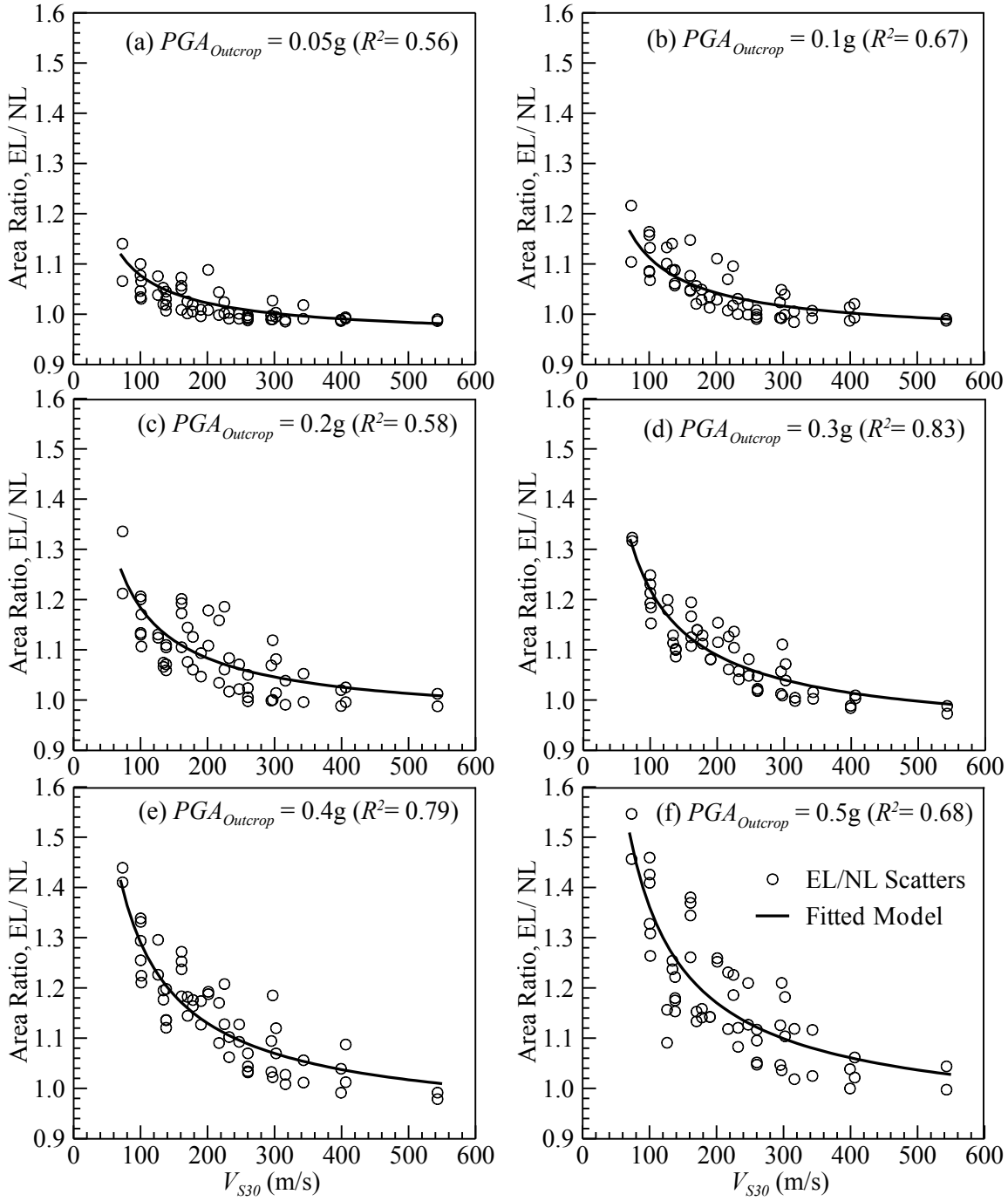

Figure 4.22: Plots showing variation of the area ratios between the equivalent linear (EL) code: SHAKE2000 and the nonlinear (NL) codes: DMOD2000 and DEEPSOIL for the mean G/G_{max}-γ and D-γ case and for a range of V_{S30} and $PGA_{Outcrop}$ as: (a) 0.05, (b) 0.1, (c) 0.2, (d) 0.3, (e) 0.4 and (f) 0.5g.

4.7.2 Validations and limitations

This study generally agrees with the observation of Kaklamanos et al. (2013 and 2015) although the site conditions are different. From Figure 4.17, the strain levels are observed to be ≥ 0.4% for the cases with $V_{S30} \leq 200$ m/s and $PGA_{Outcrop}$ level ≥ 0.1g; after Kaklamanos et al. (2013 and 2015), responses from NL codes considerably deviates from the corresponding EL codes at this level. Interestingly, these cases (i.e. $V_{S30} \leq 200$ m/s and $PGA_{Outcrop} \geq 0.1$g) fall within the '>10% and <20%' or even '≥20%' zones in the developed threshold chart (Figure 4.21) which suggests the application of nonlinear programs for such conditions.

Another research group (Afacan et al., 2013 and Brandenberg et al., 2013) developed centrifuge models for soft clay deposits to study seismic site response over a wide strain range. They made an effort to evaluate the performance of several equivalent linear and nonlinear site response analysis packages. Figures 4.23(a) and 4.23(b) present two of the cases (Brandenberg et al., 2013) where both the EL and the NL responses computed using DEEPSOIL were compared with the measured surface response from the centrifuge model for two $PGA_{Outcrop}$ levels: 0.28g and 0.55g, respectively. In the case of $PGA_{Outcrop}$ of 0.28g (Figure 4.23a), both the EL and NL lines matched the 'measured spectra reasonably well while in the case of $PGA_{Outcrop}$ of 0.55g (Figure 4.23b), only the NL predictions matched the 'measured spectra well. Here, an effort is made to calculate the area ratio (similar procedure followed in Section 4.7.1) between the EL and NL responses for both these cases ($PGA_{Outcrop}$ = 0.28g and 0.55g). It is observed that, in the case of $PGA_{Outcrop}$ of 0.28g (Figure 4.23a), the calculated area ratio between EL and NL

spectral responses fall within 10% (~6%) range which suggests that either the EL or the NL programs produces similar predictions. On the other hand, in the case of $PGA_{Outcrop}$ of 0.55g (Figure 4.23b), the area ratio between EL and NL lines were found to be above 10% (~13%) which suggests that the NL programs are expected to produce better prediction. This is a validation of the idea that the area ratio of computed spectral acceleration responses between EL and NL codes is a useful indicator for selecting the appropriate analysis procedure.

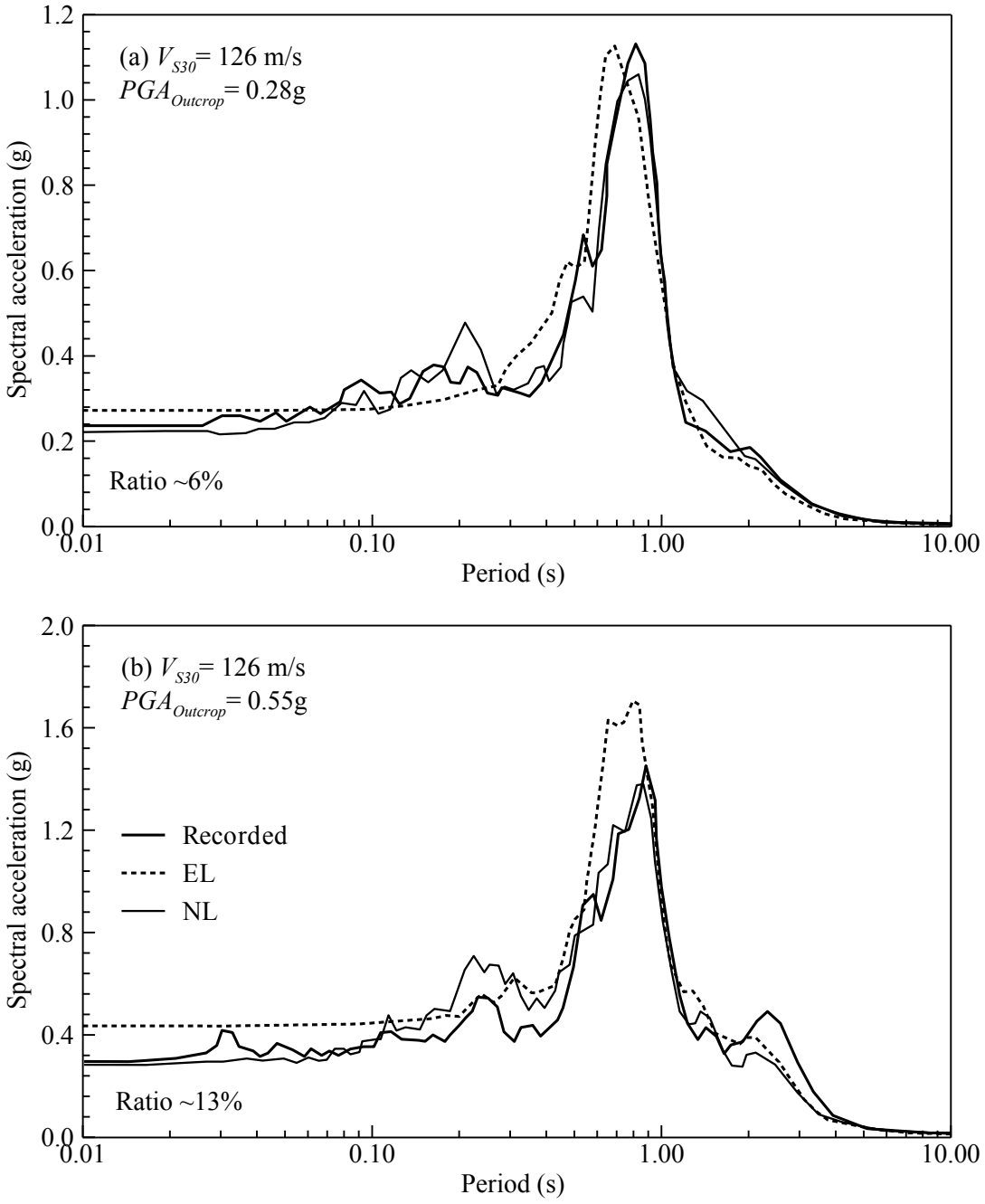

Figure 4.23: Validation of the idea of EL-NL area ratio as an indicator for selecting the most appropriate code: (a) $PGA_{Outcrop}$ =0.28g, (b) $PGA_{Outcrop}$ =0.55g. (Reproduced part of the Figure 95 from Brandenberg et al., 2013).

The primary limitations involved with the here developed threshold chart are: (i) it is developed based on the deviations of EL responses from the corresponding NL responses without the NL outcomes being validated with actual earthquake recordings (unavailable at this time) from the site; this agrees with the assumptions made in Assimaki and Li (2012) as they estimated errors associated with linear visco-elastic and equivalent linear model responses by setting nonlinear analysis responses as the benchmark, (ii) only the conditions specific to the Charleston, SC area is considered although a similar tool can also be generated for any other parts of the world by simply following and/or adjusting the procedure presented in Section 4.7.1, (iii) the variability seen in the responses from different NL codes suggests that the use of a NL code other than the here considered ones may have altered the thresholds suggested, and (iv) unreasonable implied shear strength may have computed by the NL codes which may have tampered the NL outcomes.

4.8 Conclusions

Based on a total of 18000 site response analyses with SHAKE2000, DMOD2000 and DEEPSOIL, three new seismic site factor models: SF-SK, SF-DM and SF-DS, respectively are developed and compared in this study. Both NL site factor models (SF-DM and SF-DS) predicted lower values than the EL model (i.e. SF-SK) even at the lowest loading intensities considered indicating the presence of nonlinearity even at that small loading level for softer profiles. The programs based on nonlinear theories generated much higher shear strain in the profile which implied larger hysteretic damping mostly for the softer profile cases. The difference observed in the computed surface

amplifications between the NL analysis programs i.e. between the SF-DM and SF-DS, may relate to the difference in the damping formulation implemented. However, the site factor models generated based on the NL programs falling below the recently proposed Aboye et al. (2013a) site factor model ensured adequacy and safety; and therefore supported the use of the Aboye et al. (2013a) site factor model for the Charleston, SC area.

Finally, a unique threshold chart was proposed based on the comparisons of the EL and NL analysis outcomes which provided a guideline for the practitioners in deciding for which conditions the application of a NL program over an EL program is warranted, in the case of a site specific response spectrum analysis for the Charleston, SC region.

CHAPTER 5

EFFECT OF MILD INFINITE GROUND SLOPE ON SEISMIC SITE RESPONSE FOR CHARLESTON, SOUTH CAROLINA

5.1 Introduction

Surface topography can significantly affect earthquake ground motion propagating from the bedrock to the ground surface. Evidences of such effects were observed during some past earthquake events such as: 1971 San Fernando earthquake (Boore, 1972), 1987 Whittier Narrows earthquake and 1999 Athens earthquake etc. (Assimaki, 2004). Structural damage concentrations were more abundant in areas with uneven topography (hills, slopes, canyons etc.). One of the commonly seen topographic features is mild infinitely sloping ground conditions where economic importance exists. These sloping ground conditions are often approximated to horizontal ground conditions so that the seismic site response analysis can be conducted using one-dimensional codes. The seismic site factors recommended by NEHRP (BSSC, 1995) were also developed based on one-dimensional analyses ignoring the two-dimensional effect due to sloping ground surface.

For the cases with ground inclination, a static shear stress is always active towards the downslope direction. This additional stress causes the horizontal ground deformation to accumulate in the downslope direction although a temporary deformation may be observed in the opposite direction during an earthquake event (Biscontin and Pestana, 2006; Kramer et al., 2011) and thus can significantly alter the propagating ground motion characteristics.

Numerous studies (Boore, 1972; Geli et al., 1988; Bard, 1999; Assimaki, 2004, Bouckovalas and Papadimitriou, 2005) have been done in the past for addressing the effect of steep slopes (hills, ridges, dams etc.) on ground motion characteristics. A general outcome/observation from all of these studies is that the earthquake motion amplifies at the crest of a steep slope. A more recent study by Assimaki and Jeong (2013) reveals that to effectively evaluate the effect of steep slope on earthquake ground motion acceleration, both of the soil stratigraphy and topography effects should be accounted for in a coupled manner. However, there has been scarcely any study that has solely focused on the effect of mild infinite slopes on earthquake motion characteristics. So far, mild infinite slopes under seismic events have been studied mostly to address the stability related problems (Hadj-Hamou and Kavazanjian, 1985; Taboada and Dobry, 1998; Mutsuo et al., 2002; Ko, 2001). To the author's knowledge, only a very few (Taboada and Dobry, 1998; Ko, 2001) have looked into, at least to some extent, the effect of mild infinite slopes on ground motion acceleration amplitudes. Taboada and Dobry (1998) summarized eleven centrifuge model tests performed at Rensselaer Polytechnic Institute (RPI) to investigate liquefaction and earthquake-induced lateral spreading in sand using a laminar box. Ko (2001) performed parametric study by varying ground inclination with a one dimensional ground response analysis program that has been modified to account for slope inclination. Both of these studies reveal an increase in computed surface acceleration with the increase of the slope angle until the onset of liquefaction. In this study, a correction factor is developed to modify the existing ADRS curve generated considering flat ground condition to account for mildly sloping ground condition.

Previously, this author as part of a research team has developed a seismic site factor provision for the horizontal ground condition of Charleston, SC region (Aboye et al., 2013a) which is going to be incorporated in the next version of the SCDOT Geotechnical Design Manual. Seismic site factors are the ratio of computed/recorded surface spectral acceleration, $S_{S\_T(\theta=0^o)}$ to the bedrock/outcropping spectral acceleration, $S_{T(\theta=0^o)}$ for a specific spectral period, T (SCDOT, 2008a). In Aboye et al. (2013a), one-dimensional site response analysis was used for generating surface spectral acceleration for the horizontal ground conditions. Here, an effort has been made to modify the surface spectral acceleration for horizontal ground condition to be applicable for the mildly sloping (infinite) ground conditions. For a mildly (infinite) sloping ground surface condition, two dimensional plain-strain modeling approach is required. The two-dimensional simulation results from the sloping ground cases ranging from: 1^o to 6^o, are compared with that of the horizontal ground (0^o) conditions; a set of slope adjustment factors are recommended. It is worthwhile to mention that this study doesn't consider slope failure or lateral spreading of any kind and their effect on the ground motion propagation. Moreover, the bedrock geometry i.e. basin effect of any kind is also beyond the scopes of this study although the basin geometry may significantly affect the seismic ground response (Semblat et al., 2002; Fernandez and Rix, 2008; Gvirtzman and Louie, 2010).

5.2 Topographic Variation of Charleston

Presented in Figure 5.1 is the topographic map of the location of interest of the study: Charleston, SC. The Charleston area lies at the lower part of the Atlantic Coastal

Plain. The gridlines represents the boundaries to the 7.5-minute quadrangles. The blue areas represent the ocean, rivers, lakes etc. The ground inclination angles (θ) were measured using the Digital Elevation Model data, collected from the SCDNR (South Carolina Department of Natural Resources) website (http://www.dnr.sc.gov/). The ground inclination was classified in five different ranges i.e. 0^o-1^o, 1^o-2^o, 2^o-4^o, 4^o-6^o and $> 6^o$. As seen in the figure, Charleston is relatively flat with most of the areas less than 1^o ground inclinations. However, in proximity of the depressions (i.e. rivers, channels or lakes) a few patches of green (1^o-2^o), red (2^o-4^o) and even yellow (4^o-6^o) are visible. This observation indicates the existence of sloping grounds where the seismic wave propagation characteristics may be altered. This also indicates the necessity of incorporating such specific topographic effect on the computed seismic site factors for the study area.

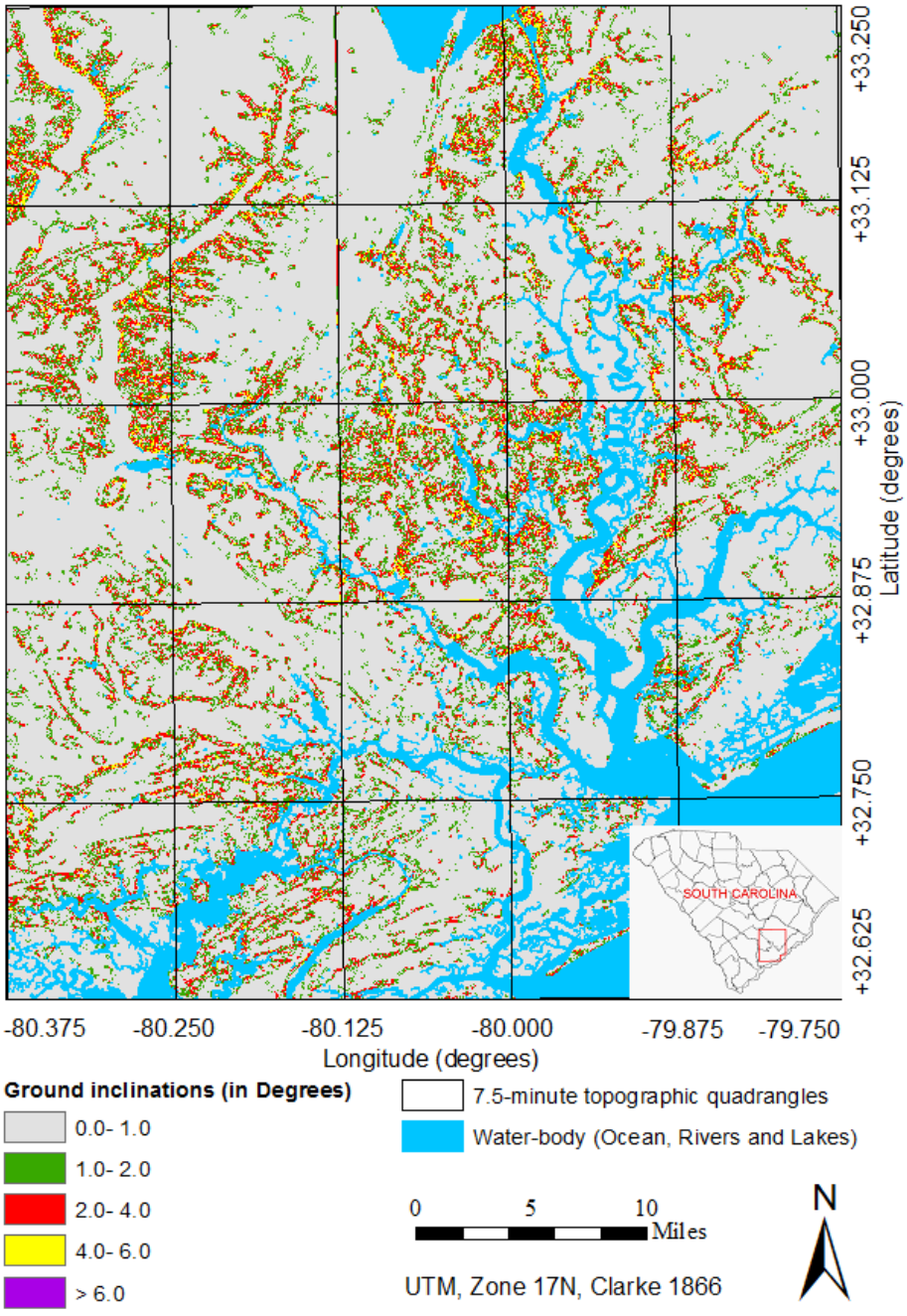

Figure 5.1: Topographic map of the Charleston, SC area showing the ground-surface inclination angles (Based on the Digital Elevation Model from SCDNR, 2006).

5.3 Soil Profile and Material properties

Figure 5.2 presents the eleven *Vs* profiles selected from Aboye et al. (2013a) for this study. These 137m deep profiles lay over the soft-rock half space with assumed *Vs* of 700 m/s for Charleston area. The 'dark' line in Figure 5.2 presents the 'reference/mean' V_S profile while all the other V_S profiles are generated by considering combinations of: 'mean±1σ' (σ = standard deviation) of the natural logarithm of V_S and also by assuming 0m, 10m, 20m and 30m Quaternary soil layer variations. During the selection of these eleven profiles from Aboye et al. (2013a), only the profiles with shear wave velocity V_{S30}>200 m/s were considered where V_{S30} is the average shear wave velocity at top 30 m which is defined as follows (Borcherdt, 1994):

$$V_{S30} = \frac{30}{\sum_{i=1}^{n} \frac{H_i}{V_{Si}}} \tag{5.1}$$

where H_i is the thickness of soil layer '*i*' in meter; V_{Si} is the shear wave velocity of layer '*i*' in m/s; and *n* is the number of soil layers in top 30 m from ground surface. Profiles with V_{S30}<200 m/s were found to be more prone to stability failure (mostly slips at layer interfaces) which is beyond the scopes of this study. The selected profiles have V_{S30} values ranging from 232 m/s to 543 m/s; eight of these are within the range of site class D (V_{S30} = 180 to 360 m/s) and the remaining three are in the site class C (V_{S30} = 360 to 700 m/s). The geometric and geotechnical parameters of the 'reference' soil profile are shown in Figure 5.2. These parameters include the soil layer thickness, total unit weight (γ_t), and plasticity index (PI). The shear modulus vs. shear strain (G/G_{max}-γ) and damping vs. shear strain (D-γ) curves are developed based on the Zhang et al. (2005) relationships and are

presented in Figure 5.3. Readers are suggested to visit Aboye et al. (2013a) for further information about soil profile generation.

The soil model used in OpenSees in this study requires the undrained shear strength (c_u) of soil as an input. Undrained shear strength is not a typical input for site response analysis and therefore it had to be determined from the available information. The procedure used to calculate the undrained shear strength is described in a later section of this chapter.

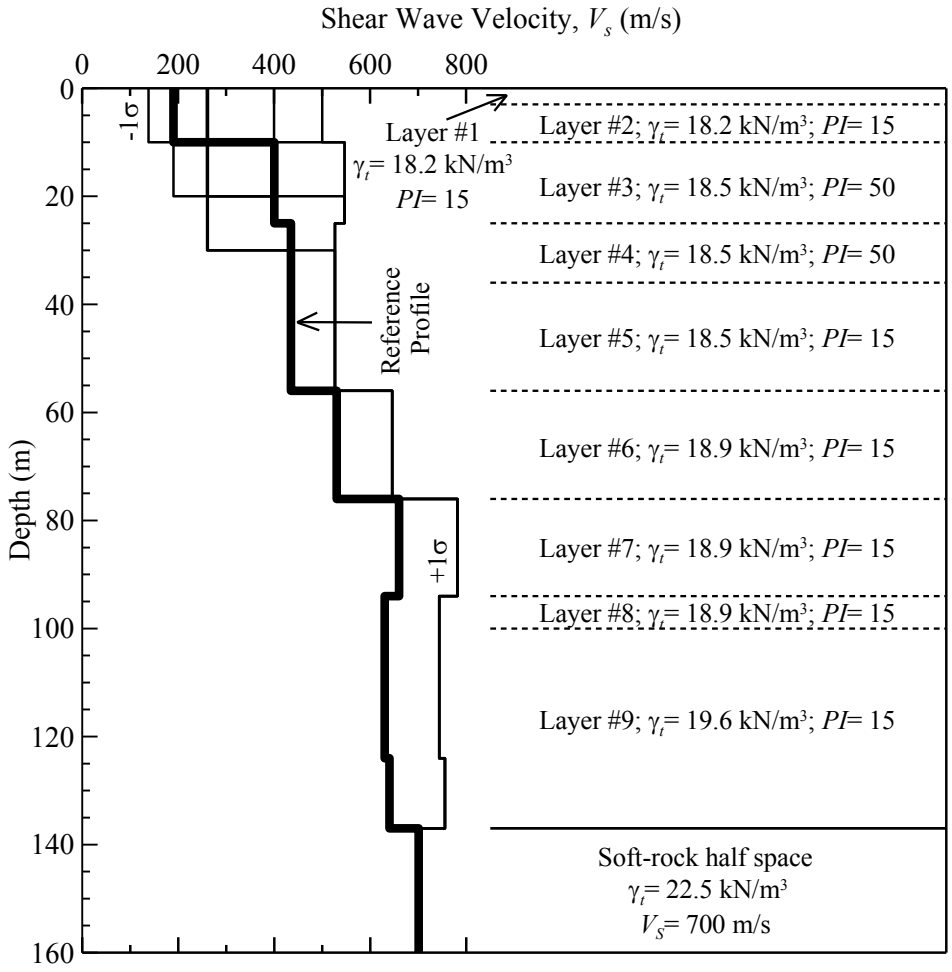

Figure 5.2: The eleven V_S profiles and corresponding material properties (γ_t in kN/m^3 and *PI*) for Charleston, SC area adopted from Aboye et al. (2013a).

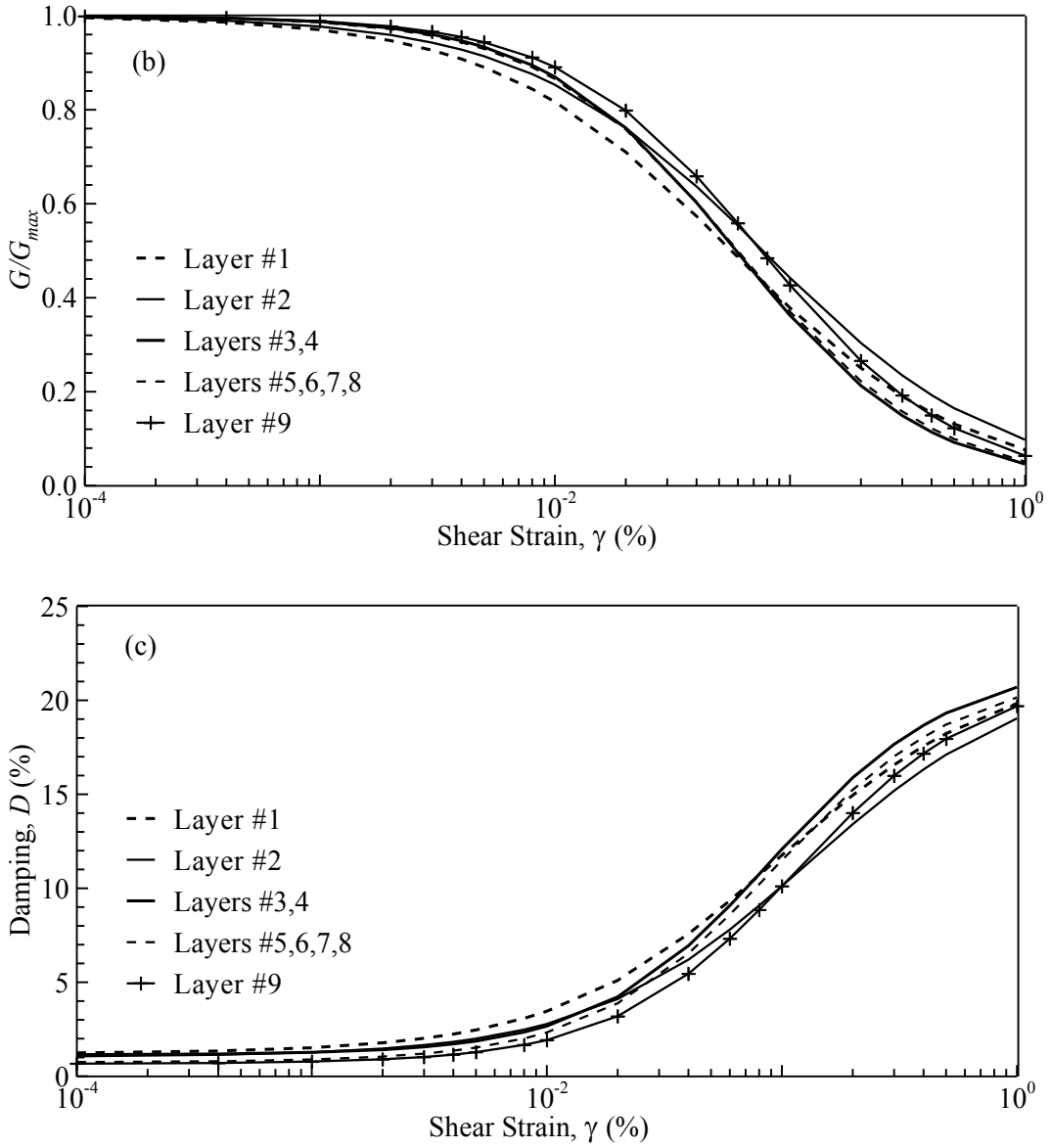

Figure 5.3: Soil dynamic properties: (a) the *G/Gmax-γ*; and (b) *D-γ* curves, based on Zhang et al. (2005) relationships.

5.4 Ground Motion

A single synthetic ground motion generated at the center of the Charleston quadrangle using Scenerio_PC was used in this study. Scenerio_PC uses a point-source

stochastic model (Atkinson and Boore, 1995) and the required inputs are the: (1) rock model, (2) earthquake moment magnitude, (3) site-to-source distance and (4) return period. A geologic realistic condition (Chapman and Talwani, 2002), very thick outcropping layer of soft rock (V_s = 700 m/s) half-space at 137 m depth, was selected as the rock model for the Scenerio_PC. A modal moment magnitude of 7.3, the site to source distance based on quadrangle location and a return period of 2% probability of exceedance in 50 years were used as inputs to the Scenerio_PC. The selected synthetic acceleration time history and corresponding response spectrum are presented in Figure 5.4. This motion was scaled to the peak ground acceleration ($S_{0.0sec}$) levels of: 0.1g, 0.2g, 0.3g, 0.4g and 0.5g, to be consistent with the previous works (Aboye et al., 2013a and the NEHRP site factors) so that the computed results could be compared. These five scaled ground motions are referred to as Motions-I to V, respectively, in this section.

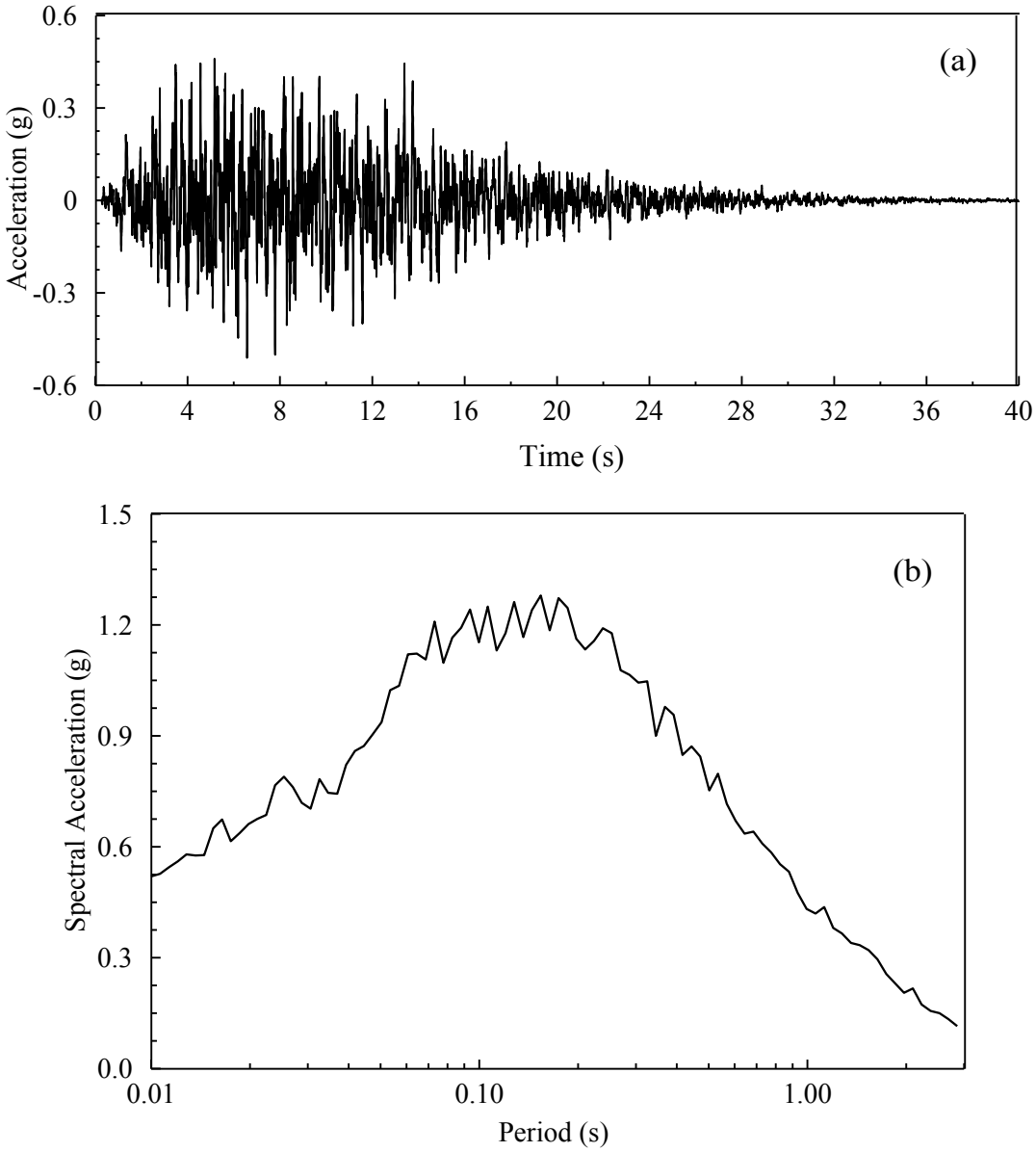

Figure 5.4: The synthetic ground motion generated for Charleston quadrangle: (a) the acceleration time history and (b) corresponding acceleration response spectra.

5.5 Finite Element Analysis

The mild infinite sloping grounds are simulated with OpenSees (Mckenna and Fenves, 2001). OpenSees is an open source finite element software framework developed under the auspice of the Pacific Earthquake Engineering Research (PEER) Centre. This software is capable of simulating complex structural and geotechnical systems in a coupled manner. It consists of numerous element types, constitutive models, boundary conditions and many other features useful for conducting dynamic analysis of various systems. At first the general finite element framework is discussed in this section. Later, the specifics about the soil constitutive model in OpenSees, the model building techniques and finally the unique calibration procedure that is developed to obtain the two-dimensional stress-strain model parameters (i.e. shear strength parameters) based on the inputs that are typically suitable for 1-D analysis are discussed.

5.5.1 General finite element technique

For many real world problems closed form solution is absent and numerical approaches such as finite element analysis is necessary to find appropriate solution of the system of equation. In finite element technique, a continuum is discretized into numerous elements with nodes at the boundaries. The soil displacement at a point of the continuum, $\{\mathbf{v}\}$ can be expressed using the nodal displacement of an element, $\{\mathbf{q}\}$ by

$$\{\mathbf{v}\} = [\mathbf{N}]\{\mathbf{q}\} \tag{5.2}$$

where $[\mathbf{N}]$ is the matrix of shape functions. The strain-displacement matrix $[\mathbf{B}]$ and the moduli matrix $[\mathbf{D}]$ can be defined by

$$\{\boldsymbol{\varepsilon}\} = [\mathbf{B}]\{\mathbf{q}\} \tag{5.3}$$

$$\{\boldsymbol{\sigma}\} = [\mathbf{D}]\{\boldsymbol{\varepsilon}\} \tag{5.4}$$

where $\{\boldsymbol{\varepsilon}\}$ and $\{\boldsymbol{\sigma}\}$ represent stress and strain tensors, respectively. Using the above strain-displacement and stress-strain relationships the element stiffness matrix, $[\mathbf{k_e}]$ and mass matrix, $[\mathbf{m_e}]$ can be expressed by

$$[\mathbf{k_e}] = \int_A [\mathbf{B}]^T [\mathbf{D}][\mathbf{B}] dA \tag{5.5}$$

$$[\mathbf{m_e}] = \rho \int_A [\mathbf{N}]^T [\mathbf{N}] dA \tag{5.5}$$

where ρ is the assumed uniform density of the element and A stands for the area of the element. The damping matrix $[\mathbf{c_e}]$ in nonlinear ground response analysis represents the viscous damping (or small strain damping) while the hysteretic damping is accounted for by the stiffness matrix variation. Finally, the dynamic equation of motion for the element can be expressed as

$$[\mathbf{m_e}]\{\ddot{\quad} \quad \dot{\quad} \quad \} = \{\mathbf{Q}\} \tag{5.6}$$

where $\{\mathbf{Q}\}$ is the element force vector. After developing the equations of motion for all the elements, the global equation of motion is developed as

$$[\mathbf{M}]\{\ddot{\quad} \quad \dot{\quad} \quad \} = \{\mathbf{R}\} \tag{5.7}$$

where $\{\mathbf{R}\}$ is the global nodal point force vector. The above global equation is solved using a numerical integration technique such as the Newmark's time integration technique. The model boundary conditions are necessary in obtaining the solution in finite element framework.

5.5.2 Soil constitutive model in OpenSees

A pressure independent type multi-yield-surface J2 plasticity model, representing the elasto-plastic nature of the stress-strain relationship of the soil, implemented in OpenSees by Elgamal et al. (2003), is used. The yield surface is assumed to follow the

Von Mises shape which is a function of undrained shear strength of soil. A purely deviatoric kinematic hardening rule (Prevost, 1985) is used to generate soil hysteretic response under cyclic loading. The nonlinear shear stress-strain backbone curve is approximated by a hyperbolic formula (Kondner, 1963) as shown in Equation 5.8:

$$\tau = \frac{G_{max}\gamma}{1+\left(\frac{\gamma}{\gamma_r}\right)} \tag{5.8}$$

where G_{max} is the small strain shear modulus, τ is the shear stress of the soil, γ is the shear strain, and γ_r represents the reference shear strain which is calculated as follows:

$$\gamma_r = \frac{\gamma_{max}\tau_{max}}{G_{max}\gamma_{max} - \tau_{max}} \tag{5.9}$$

where γ_{max} is the maximum shear strain, and τ_{max} is the shear strength of soil.

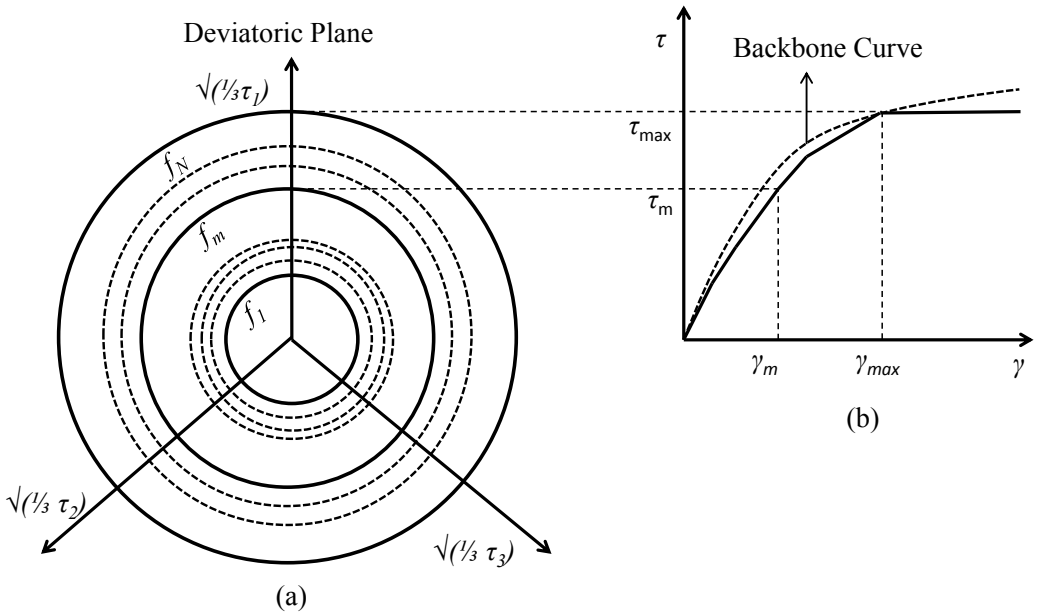

Figure 5.5: Multi-yield-surface J2 plasticity model: (a) Yield surface and (b) corresponding piece-wise linear representation of the backbone curve (reproduced from Gu et al., 2011).

In multi-yield-surface plasticity, the backbone curve (Equation 5.2) is replaced by a piecewise linear approximation. Figure 5.5(a) shows multiple yield surfaces in deviatoric plane and Figure 5.5(b) shows the corresponding shear stress-shear strain response. Here, each line segment on the backbone curve (in Figure 5.5b) stands for a yield surface ($f_i = 0$) (in Figure 5.5a) where i = 1, 2, 3,….m,….N; N is the total number of yield surfaces. An associative flow rule computes the plastic strain increments. The full Rayleigh damping formulation (Hudson et al., 1994) is implemented to incorporate the viscous damping to the system. A detailed overview of this soil model is available in Gu et al. (2011).

5.5.3 Model generation

Presented in Figure 5.6 is the schematic of the generalized 2-D model with all the inclined layers, layer numbers and numerical boundaries used to create the finite element mesh. This model was generated by setting the column AF in Figure 5.6 to represent the 137 m deep Charleston profiles (from Figure 5.2). Now, the ground surface slope, θ (0^o, 1^o, 2^o, 3^o, 4^o, 5^o and 6^o) is reduced with depth (i.e. layer boundaries) to merge with the surface of the perfectly horizontal (θ = 0^o) soft-rock at the bottom of the profile. This gradual variation of subsequent layer inclinations is to avoid the presence of low aspect ratio finite elements at the base of the model, especially at the corner where the model has the least thickness, thus avoiding any numerical instability during simulations. The method used in this study is similar to the example problem “Dynamic 2D effective stress analysis of slope” presented in OpenSees by Chrsitopher McGann and Pedro Arduino

from the University of Washington (http://opensees.berkeley.edu/wiki/index.php/Dynamic_2D_Effective_Stress_Analysis_of_Slop).

5.5.3.1 *Boundary conditions*

Utilizing appropriate boundary condition is critical to obtain realistic results, especially for dynamic analysis. In reality, the left and right vertical boundaries locate at an infinite distance from the center line. To reduce computational time without compromising the accuracy of the computed results, special techniques need to be employed to absorb the 2-D waves reaching the left and right boundaries. In these vertical boundaries, the displacement degrees of freedom of each node are tied together which ensures a periodic boundary condition. The nodes at the base of the model are fixed against vertical translation while those are tied together in the horizontal direction to allow equal horizontal displacement. In addition, extremely large thickness (10000 times larger thickness than the interior elements in the out-of-plane direction) is used in the absorbent boundary.

5.5.3.2 *Mesh and size sensitivity studies*

After the selection of boundary condition and orientation of the layers, it is necessary to conduct trial simulations to obtain appropriate element size (mesh sensitivity) and the domain size (size sensitivity) of the 2-D geometric model to ensure that the computed surface responses are independent of these user controlled parameters. For both the parametric studies, the reference profile (the dark line in Figure 5.2) with $\theta=6^{o}$ and Motion-V are used and the domain is discretized using 4-node quadrilateral elements.

Figure 5.7(a) presents the mesh sensitivity study. Here, three different meshes were considered: (1) with 6120 elements (mesh-1), (2) with 27132 elements (mesh-2) and (3) with 49480 elements (mesh-3). Then the computed surface spectral accelerations at Point A in Figure 5.6 are compared from the three meshes as shown in Figure 5.7(a). From this comparison it is found that the mesh-2 and mesh-3 lines fall on top of each other indicating that the number of elements in the second trial with 27132 elements is large enough to produce mesh independent results.

For the size sensitivity study, five trials are conducted using varying a and b combinations (see Figure 5.6): a = 3 and b = 20 m, a = 5 and b = 20 m, a = 6 and b = 20 m, a = 5 and b = 50 m, and a = 5 and b = 100 m. The computed surface spectral accelerations are then compared in Figure 5.7(b), evaluated and then the case with a = 5 and b = 50 m is selected.

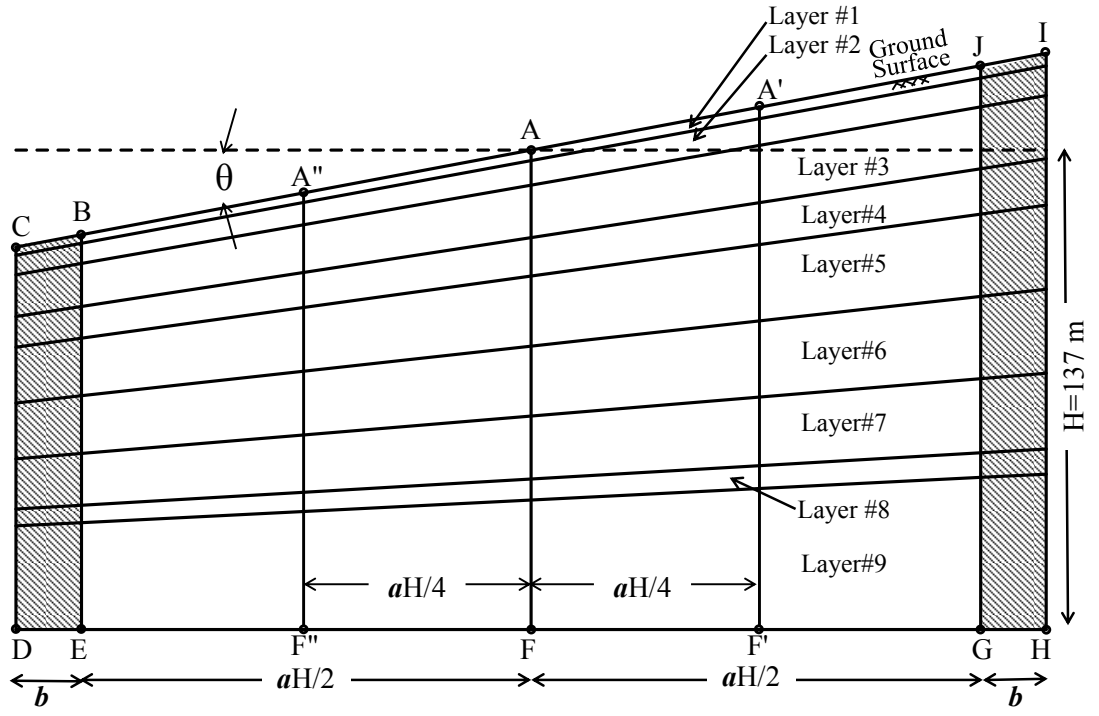

Figure 5.6: Generalized 2-D finite element model in OpenSees.

A Poisson's ratio of 0.33 is assumed for all the profiles. Simulations are conducted in two steps: (1) a static analysis to compute the initial stresses, and (2) a dynamic analysis to compute the earthquake responses. Total stress analysis is conducted for all the cases in this study. OpenSeesMP, the parallel version of OpenSees executable, is installed into the parallel cluster of Clemson University: the Palmetto Cluster and significantly reduced the duration of simulations. Further information about the parallel version is available on the OpenSees website (http://opensees.berkeley.edu/OpenSees/parallel/parallel.php).

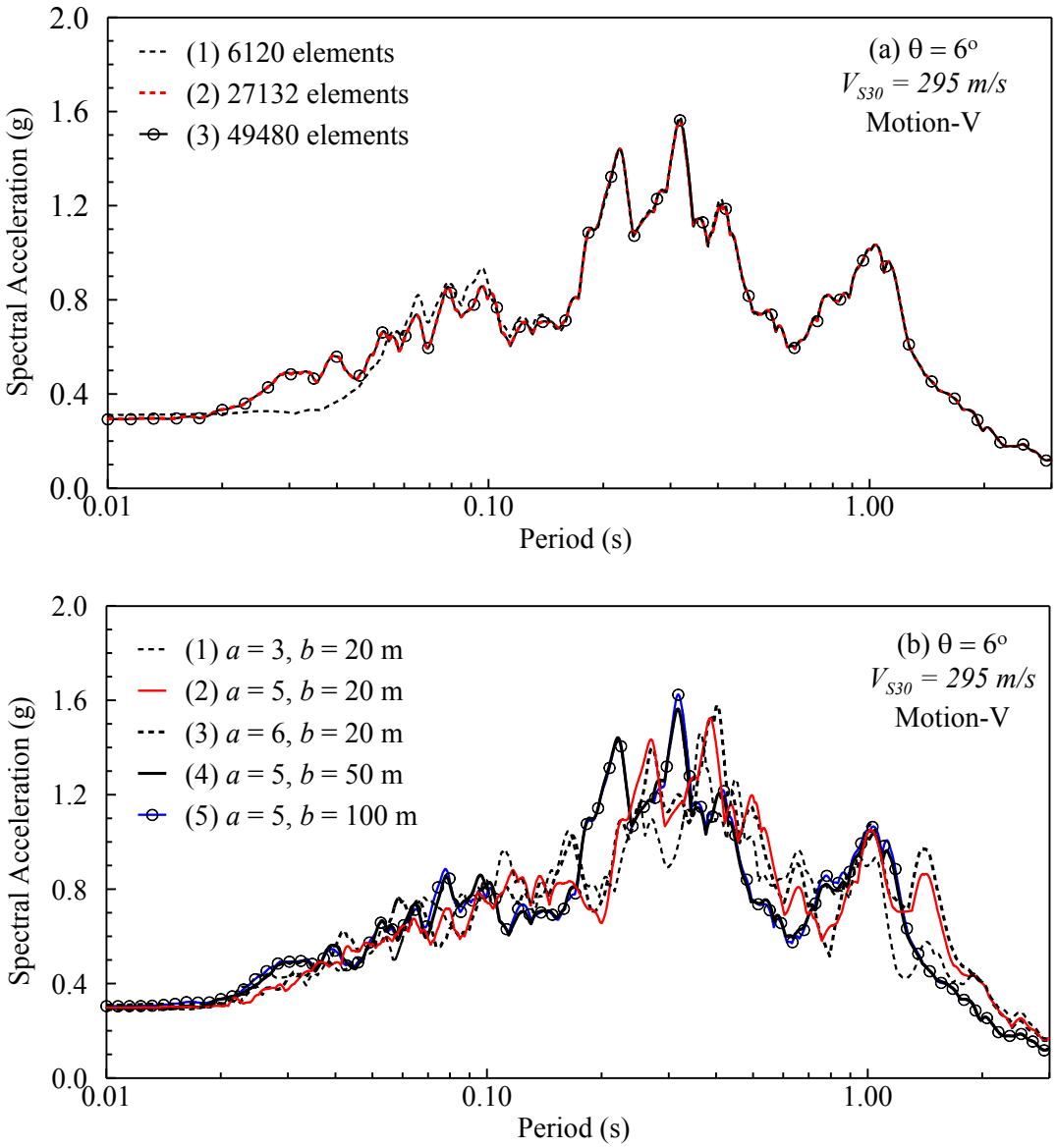

Figure 5.7: The surface response spectra from the numerical trials of: (a) mesh sensitivity study; and (b) domain size sensitivity study.

5.5.4 Parameter calibration: undrained shear strength

The constitutive model used in OpenSees requires the undrained shear strength or c_u as an input. This parameter had to be calibrated for each layers of all eleven profiles due to: (i) unavailability of the data for such deep profiles; (ii) to be consistent with the 1-D profiles presented in Aboye et al. (2013a) as currently these are the most representative

profiles of the area that are available; and (iii) this parameter calibration will allow the practitioners to be able to perform site response analysis of sloping ground conditions using the same sets of inputs as of a 1-D site response analysis (i.e. SHAKE2000, DMOD2000, DEEPSOIL etc.).

Calibration is conducted by matching the acceleration response spectra obtained at node A of Figure 5.6 using OpenSees and the 1-D program DEEPSOIL for each layer of the profiles. At first, the finite element model of a 30 m thick (as in H of Figure 5.6) single horizontal ($\theta = 0^o$) soil layer laying over the half-space is developed in OpenSees by following the similar procedure as section 5.5.3. For the Motion-V (scaled to $S_{0.0sec}$ of 0.5g), each model is simulated for a set of c_u values and for each case, the free field acceleration response spectra are recorded at node A (Figure 5.6). Finally the single c_u value that produces the best match of surface spectral responses computed from OpenSees with that of DEEPSOIL is selected as the calibrated c_u value for that specific soil layer. Similarly, calibrated c_u values are generated for all the soil layers from each of the eleven soil profile cases for this study. The layer thickness was selected as 30 m based on the following considerations: first, from a preliminary study it was seen that the thicker the layer is the more accurate the calibrated c_u it can produce; and secondly, an increasing thickness will turn the simulations numerically expensive. The calibrated c_u values are listed in Table 5.1 where the c_u values are grouped into three categories: the 'reference' or mean profile and its $\pm 1\sigma$ V_S variations as rest of the profiles considered here are different combinations of these three categories.

As seen in the Table 5.1, the calibrated c_u values, especially in the deeper layers (Tertiary) are large numbers. During the geotechnical explorations for the construction of Arthur Ravenel Jr. Bridge in Charleston area undrained shear strength was measured up to 240 kPa at the shallow (within 20 m from surface) Tertiary layers (known as Cooper Marl) as reported by Camp et al. (2002). Moreover, Santi (2006) suggests that the compressive strength of residual soil can go up to 1.0 MPa with anything beyond this value enters into the zone of weak rock. These support the possibility of existence of such higher shear strength obtained through the calibration procedure especially for the layers closer to the soft-rock boundary. However, it should be noted that this is the only parameter that could be adjusted to obtain comparable surface spectral responses from both 1-D and 2-D models which seems more critical in order to obtain reasonable results from actual simulations of 2-D cases.

Table 5.1: Calibrated undrained shear strength, c_u (kN/m2) values for all profile variations: Mean-1σ, Mean and Mean+1σ of V_S.

Layer #	Layer thickness (m)	Calibrated undrained shear strength, c_u (kN/m^2) of the profiles		
		Mean-1σ *Vs*	Mean *Vs*	Mean+1σ *Vs*
1	3	22	34	70
2	7	30	47	100
3	15	-	170	300
4	11	-	180	300
5	20	-	200	300
6	20	-	280	400
7	18	-	350	450
8	6	-	370	480
9	37	-	450	500
10	Soft-rock half space	-	-	-

Finally, by using the calibrated c_u values, computed spectral accelerations at the surface node A (see Figure 5.6) of each of the 137 m deep profiles for horizontal ground condition are compared with the corresponding 1-D DEEPSOIL outcomes; this is done for all eleven profiles. A sample case with 'reference' profile and Motion-V is presented in Figure 5.8 where a close match in the surface spectral accelerations from DEEPSOIL and OpenSees is obtained. Similar observations are made for all other profiles (Figures B.1-B.10 in Appendix B) and the obtained close match between these 1-D and 2-D models in general supported the acceptability of the calibrated parameters and their application for the later part of this study.

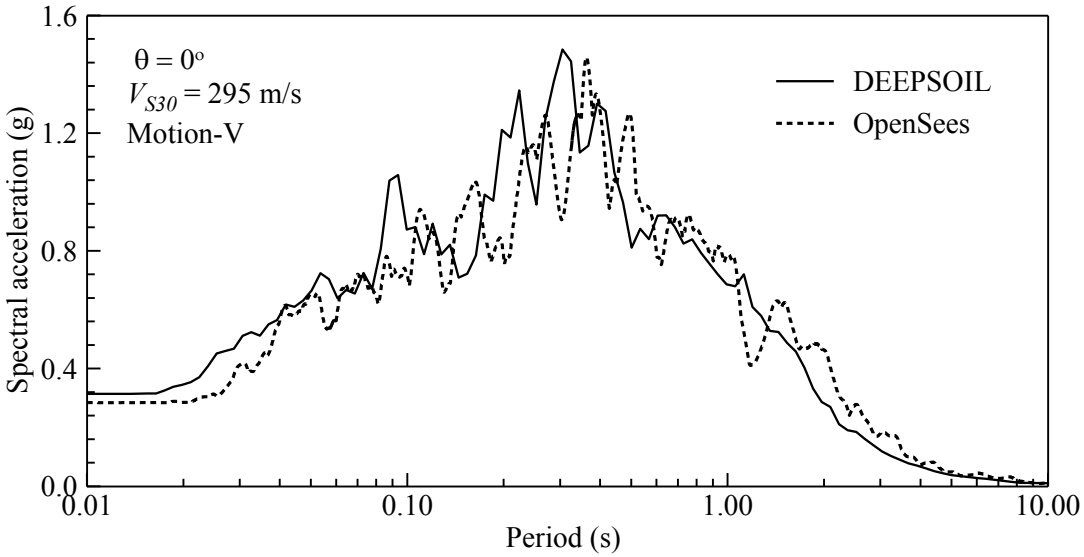

Figure 5.8: Sample validation study of the calibrated c_u values by comparing the spectral accelerations from OpenSees model with that of DEEPSOIL for the reference profile (V_{S30} = 295 m/s) with flat ground condition and Motion-V.

5.6 Results and Discussions

Among the 385 simulations 21 cases showed large shear strain accumulation and significant ground movement at the end of the earthquake excitation. It is believed that

the code is incapable of predicting such a large deformation accurately and therefore is not considered for developing adjustment factors. These failed cases consist of mostly softer soil profiles (mostly V_{S30} = 232 and 247 m/s) with relatively steeper slopes (mostly $\geq 4^0$) subjected to higher $S_{0.0sec}$ motions (i.e. 0.4g and 0.5g). These observations are consistent with the general understanding of the physics of slopes made of soft soils that are subjected to heavy shakings.

Plotted in Figure 5.9 is a sample case where the computed acceleration response spectra for the 'reference' profile (V_{S30} = 295 m/s) from all the sloping ground cases (0^o, 1^o, 2^o, 3^o, 4^o, 5^o and 6^o) with Motions-I and V or the $S_{0.0sec}$ levels of 0.1g and 0.5g, respectively. Overall, responses from the sloping ground cases are higher than that of horizontal ground case which indicates the importance of considering even such mild surface inclination in the site response analysis. Especially at higher periods (i.e. 0.6-1.0 sec), spectral accelerations are observed to become higher with the increase of surface inclination. At lower periods (i.e. <0.6 sec) no such trend is found although the sloping ground spectral accelerations are still higher than the flat ground responses; uncertainty at lower periods is a commonly observed feature in the recent site response studies (Stewart et al., 2008; Kottke, 2010; Zalachoris, 2014). Overall, the slope effect is more significant at smaller shaking (i.e. $S_{0.0sec}$ of 0.1g and 0.2g) and/or for stiffer profile cases; with the increased shaking ($S_{0.0sec}$ of 0.3g, 0.4g and 0.5g) and/or softer profile the system becomes more nonlinear thus greater damping is involved. Similar observations were also made for rest of the profiles which are presented in the Appendix in Figures B.11-B.21.

The computed surface spectal accelerations from the sloping ground cases were normalized by similar responses from the corresponding flat ground conditions, for all the profiles. These normalized spectral accelerations are divided into six spectral period ranges: 0.01, 0.01-0.4, 0.41-0.8, 0.81-1.2, 1.21-2.0 and 2.01-4.0 sec, following the exact same period ranges that are adopted for seismic site factors generation in Aboye et al. (2013a). Then the average of the ratio within each spectral period range is calcualted and assigned to the middle of each period range i.e. 0, 0.2, 0.6, 1.0, 1.6 and 3.0 sec periods. These averaged spectral ratio is referred to as the slope adjustment factor, K_θ in this section.

For all cases, K_θ vs. ground inclination plots were generated. A sample K_θ vs. ground inclination plot for the 'reference' profile (V_{S30} = 295 m/s) and for Motions-I to V, are presented in Figure 5.10; T = 0.0, 0.2, 0.6, 1.0, 1.6 and 3.0 sec cases are sorted in subplots 5.10(a)-5.10(f), respectively. No clear trend is observed for K_θ variation with slope in the low spectral period cases (i.e. T = 0.0, 0.2 and 0.6 sec) in the subplots (a)-(c) in Figure 5.10 while K_θ is increasing with slope inclination for T = 1.0 sec period (Figure 5.10d). This observation is consistent with the observation made in the original spectral acceleration values (Figure 5.9) as there the consistent amplitude increment was found only in the higher periods. As expected, only the smaller shaking cases produced larger values of K_θ among all, in general. The K_θ values also points to the fact that the spectral acclerations computed based on sloping ground conditions may produce upto 60-70% higher accleration values than that of the corresponding flat ground cases; such

observations proves the importance of considering such topographic variation during site response analysis for designing structures on slopeing grounds. Similar observations were also made for other profile cases as presented in Figures B.22-B.31 in Appendix B. However, there is a general increase of K_θ with the V_{S30} increment which is also an expected outcome as stiffer materials mean lesser damping and greater contrast in computed surface response for sloping ground conditions.

In order to find the reason behind the inconsistent nature of the spectral acceleration at lower periods, profile shear strains at different stages of the simulations are investigated. Figure 5.11 presents the computed shear strain along three columns: AF, A'F' and A"F", of the 'reference' profile (V_{S30} = 295 m/s) for 0^o and 5^o sloping ground cases after 4.1 sec and 6.9 sec of shaking with Motion-I (i.e. $S_{0.0sec}$ of 0.1g). All three columns show very similar shear strains throughout the profile during the entire shaking of the 0^o case (i.e. Figure 5.11b and 5.11d) while for the sloping ground condition they show significant differences (i.e. Figure 5.11c and 5.11e). Further investigation (i.e. displacement and acceleration time history at different nodes along each column) reveals that the differences in the depth of the profile at these three locations generate a mismatch in the mode of vibration; this imposes an in-phase and out-of-phase relative movement among these three columns during the earthquake shaking. Therefore, the 0^o case shows no strain difference due to uniform column depth while the 5^o case shows significant variation due to difference in column depth. These three columns represent how different locations of this long model (i.e. Figure 5.6) responded during the entire vibration; such in-phase out-of-phase relative movements could produce tension and compression,

especially during high frequency vibration, and thus could amplify or de-amplify the surface responses. Therefore, the model geometry may be the source of the inconsistencies (i.e. no clear trend in computed spectral acceleration with slope variation) observed in the surface spectral acceleration, especially at smaller periods (or at higher frequencies), which is certainly a limitation of this study.

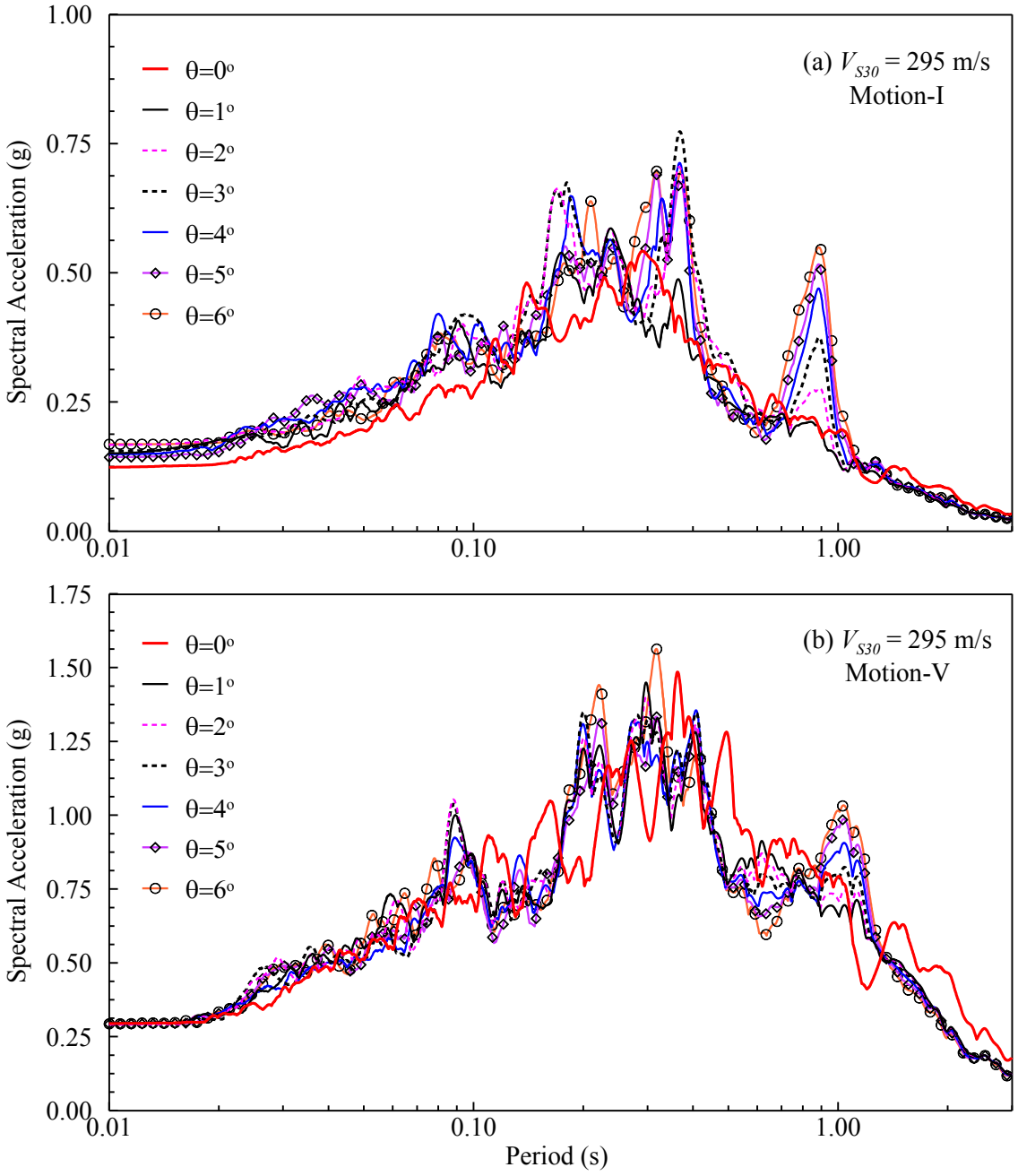

Figure 5.9: Sample acceleration response spectra for the reference profile (V_{S30} = 295 m/s) from all the sloping ground cases (0^o to 6^o) with (a) Motion-I ($S_{0.0sec}$= 0.1g); and (b) Motion-V ($S_{0.0sec}$= 0.5g).

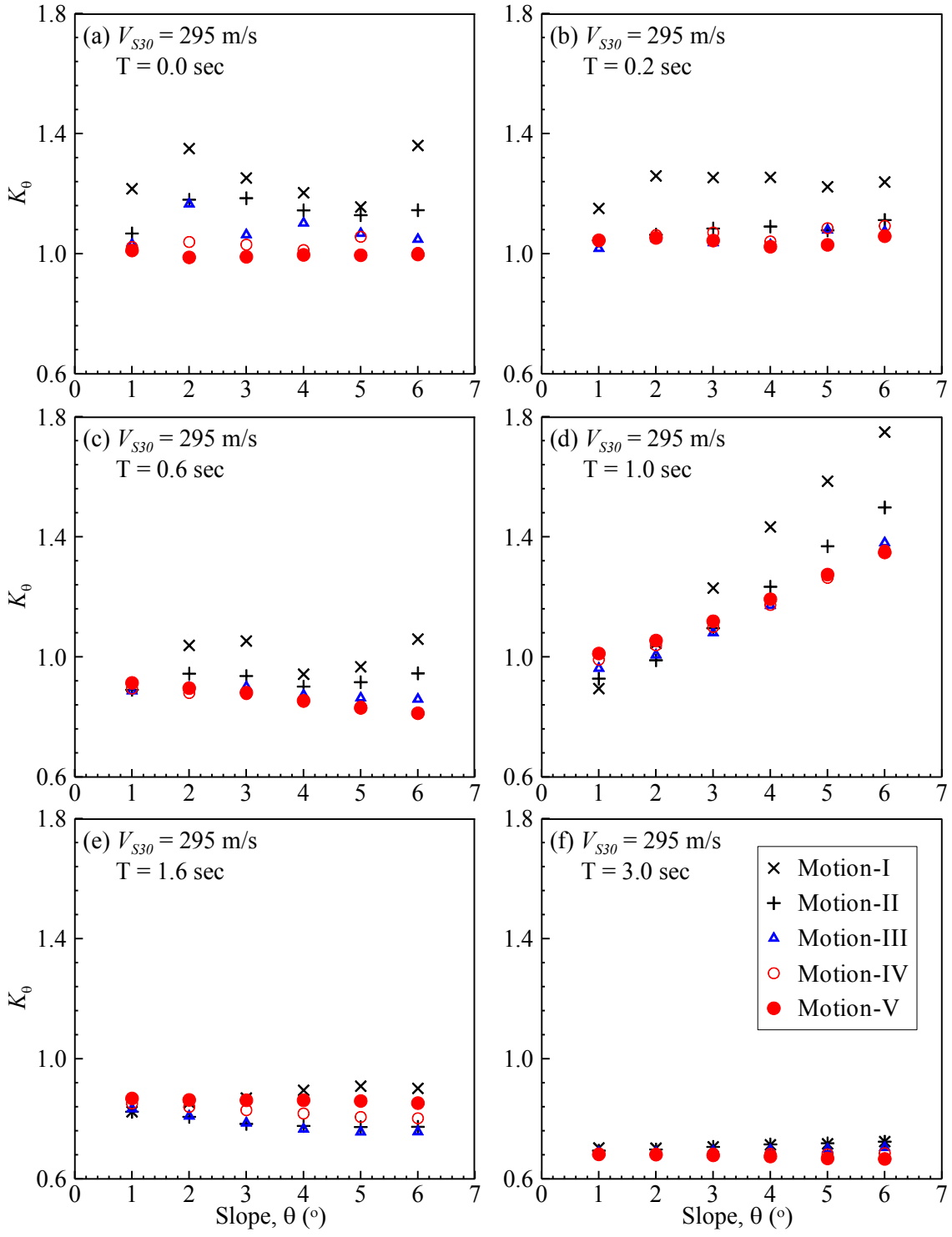

Figure 5.10: K_θ vs. θ plots for the reference profile (V_{S30} = 295 m/s) and Motions-I to V and also for period, T as (a) 0.0, (b) 0.2, (c) 0.6, (d) 1.0, (e) 1.6, and (f) 3.0 sec.

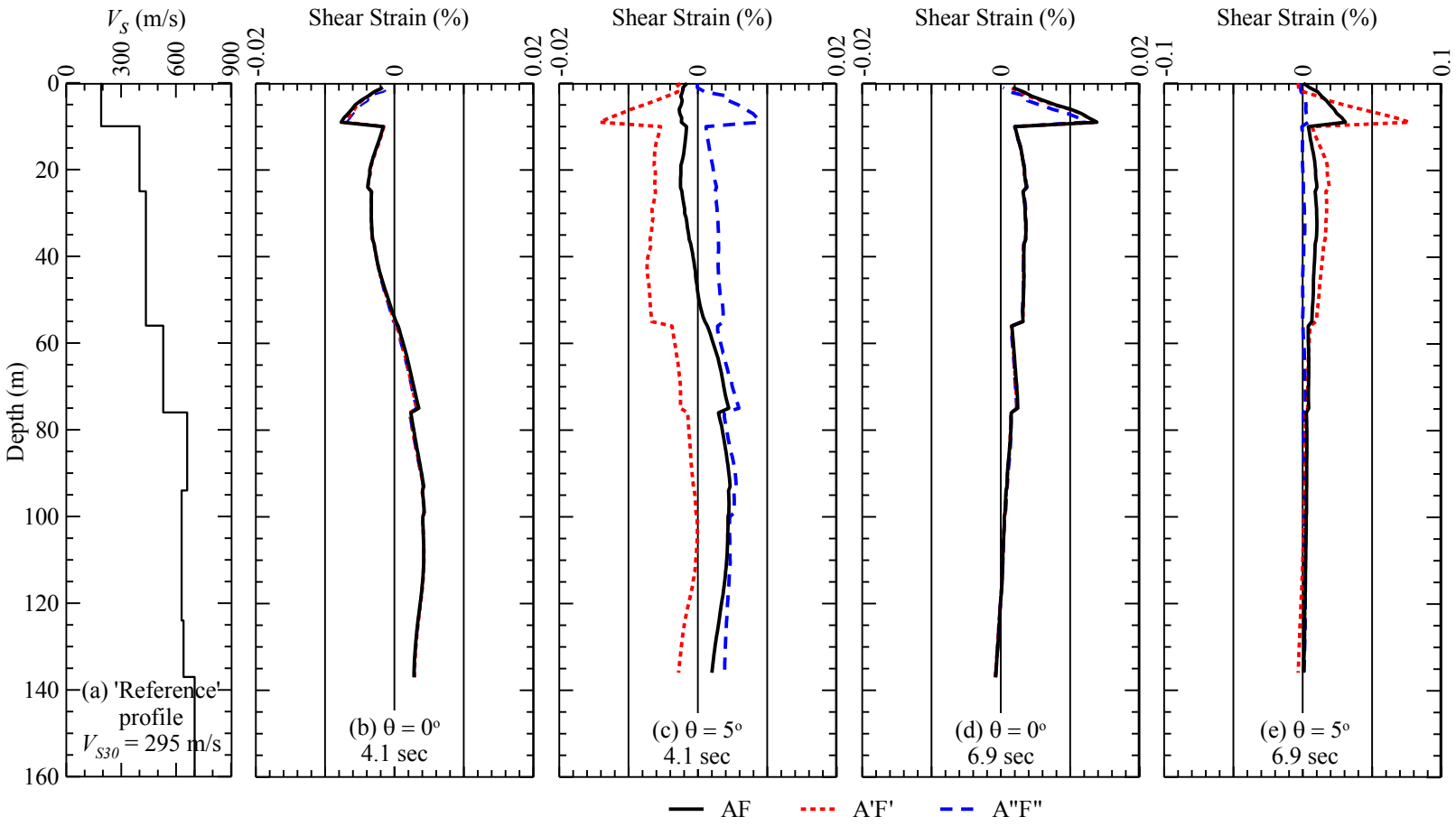

Figure 5.11: Computed shear strain along three columns: AF, A'F' and A"F" of the 'reference' profile (V_{S30} = 295 m/s) with Motion-I ($S_{0.0sec}$= 0.1g) after 4.1 sec of shaking of: (a) θ = 0° and (b) θ = 5° cases; and also after 6.9 sec of shaking of the same two: (a) θ = 0° and (b) θ = 5° cases.

5.7 Development of Guideline

Based on the above findings it is clear that mild surface inclination can alter the seismic surface response significantly. However, it is a very common practice to consider mildly sloping grounds as horizontal and determine the seismic site factors either from code provisions or site response analysis. The current code provisions also lack any such guideline and/or most typical one-dimensional site response software packages such as SHAKE2000, DMOD2000 and DEEPSOIL are incapable of simulating such scenario. In this Chapter, an effort is made to develop a guideline to obtain seismic spectral acceleration for mild infinitely sloping ground surface condition.

Table 5.2 presents the recommended slope adjustment factor, K_θ based on all simulations performed in this study. The computed K_θ are sorted for different ranges of values: K_θ<1.1, 1.1<K_θ<1.2, 1.2<K_θ<1.4, 1.4<K_θ<1.6, 1.6<K_θ<1.8 and K_θ>1.8, and are then plotted keeping θ as the horizontal and V_{S30} as the vertical axes using separate symbols representing each of the different ranges. Figure 5.12 presents such plots of K_θ vs. θ and V_{S30} for some selected cases where K_θ values are generally higher. Cases where K_θ values are rather insignificant for any slope inclination and V_{S30} combinations (within the considered range of this study) are assigned a constant number and listed in Table 5.2. For example, the case of T = 0.0 sec and Motion-I, K_θ values increase with slope inclination as well as V_{S30} and thus are plotted in Figure 5.12(a). The cases of T=0.0 sec and Motion-II to V produced K_θ values closer to 1.0 which indicates minimal variation

in spectral acceleration obtained in these cases from each of the sloped cases than horizontal conditions; these cases are assigned a constant K_θ and is listed in Table 5.2. Similarly, the rest of the subplots in Figure 5.12 have been populated with the cases where K_θ values are considerably high and vary with ground inclination as well as the V_{S30}: T = 0.6 sec and Motion-I cases in Figure 5.12(b); T = 0.6 sec and Motion-II cases in Figure 5.12(c); T = 1.0 sec and Motion-I cases in Figure 5.12(d); T = 1.0 sec and Motion-II cases in Figure 5.12(e); and T = 1.0 sec and Motion-III to V cases in Figure 5.12(f). Corresponding S_{Tsec} values are also listed for each of the T values and all five scaled motion levels. Based on these K_θ ranges from Figure 5.12, regions of uniform K_θ values can be distinguished and are plotted in Figure 5.13 using different shades. Using these shaded regions, K_θ values can be easily obtained from Figure 5.13 for a known set of θ and V_{S30} values. Therefore, together the Table 5.2 and Figure 5.13 deliver the recommended K_θ values. These K_θ values are only applicable within the range of values for θ, V_{S30}, S_{Tsec} and T combinations that are considered in this study.

Table 5.2: The slope adjustment factor, K_θ determination for a set of θ, V_{S30}, S_{Tsec} and T combinations.

Ground Slopes, θ	Spectral Period, T	Motion-I		Motion-II		Motion-III		Motion-IV		Motion-V	
		S_{Tsec}** (g)	K_θ	S_{Tsec} (g)	K_θ	S_{Tsec} (g)	K_θ	S_{Tsec} (g)	K_θ	S_{Tsec} (g)	K_θ
*1^o to 6^o****	0 sec	0.1	*5.13a	0.2	1.2	0.3	1.2	0.4	1.0	0.5	1.0
	0.2 sec	0.19	5.13a	0.38	1.2	0.57	1.2	0.76	1.0	0.95	1.0
	0.6 sec	0.14	5.13b	0.28	5.13c	0.43	1.2	0.57	1.2	0.71	1.0
	1.0 sec	0.09	5.13d	0.18	5.13e	0.27	5.13f	0.36	5.13f	0.45	5.13f
	1.6 sec	0.06	1.1	0.12	1.0	0.17	1.0	0.23	1.0	0.29	1.0
	3.0 sec	0.02	1.1	0.05	1.0	0.07	1.0	0.10	1.0	0.12	1.0

*Figure number

**Interpolated K_θ should be used between two specified S_{Tsec} ranges for each T

*** K_θ is 1.0 for all $\theta = 0^o$ case.

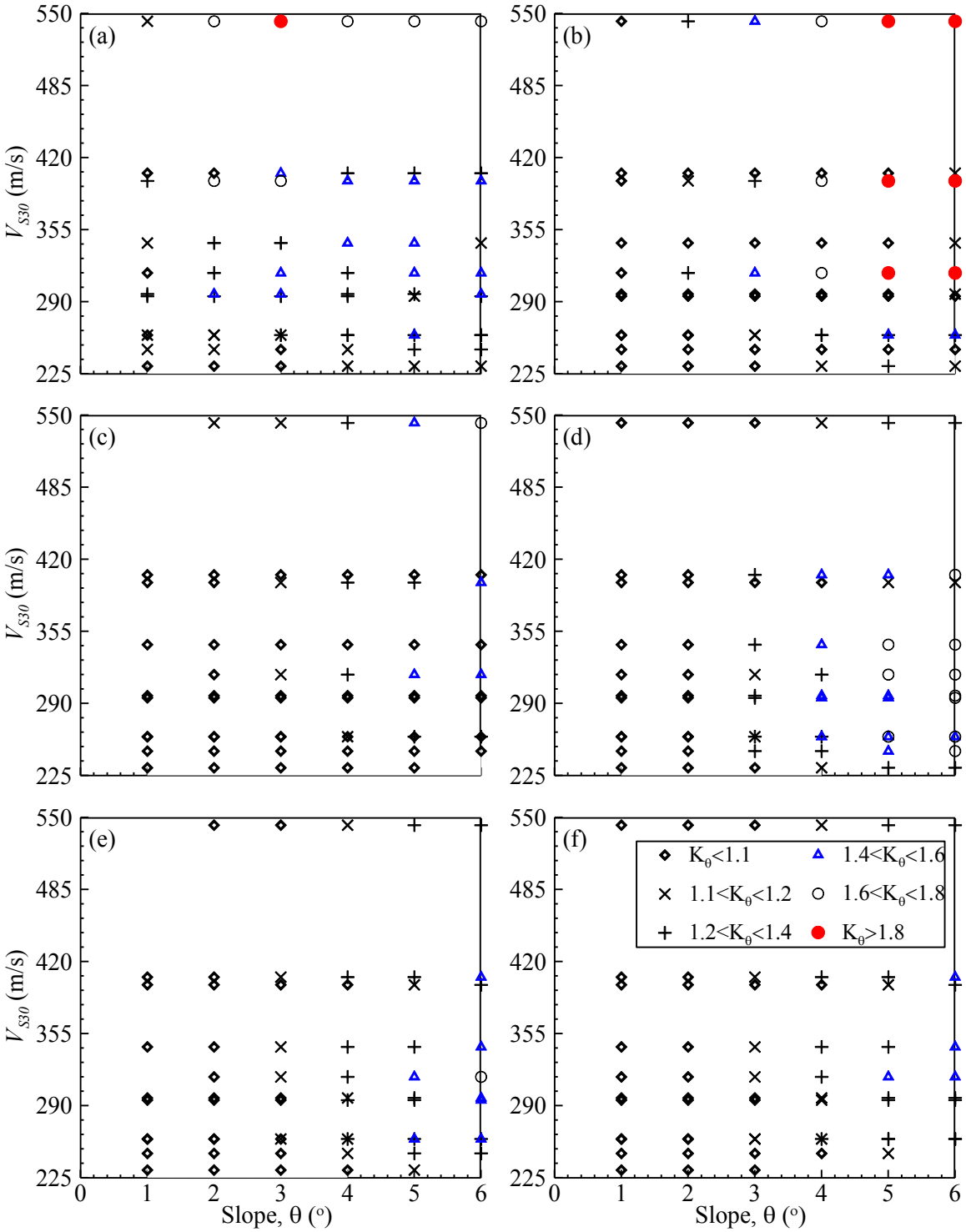

Figure 5.12: Scatters showing K_θ ranges with respect to the V_{S30} and θ variations for the cases: (a) T=0.0-0.2s and Motion-I; (b) T=0.6s and Motion-I; (c) T=0.6s and Motion-II; (d) T=1.0s and Motion-I; (e) T=1.0s and Motion-II; (f) T=1.0s and Motion-III to V.

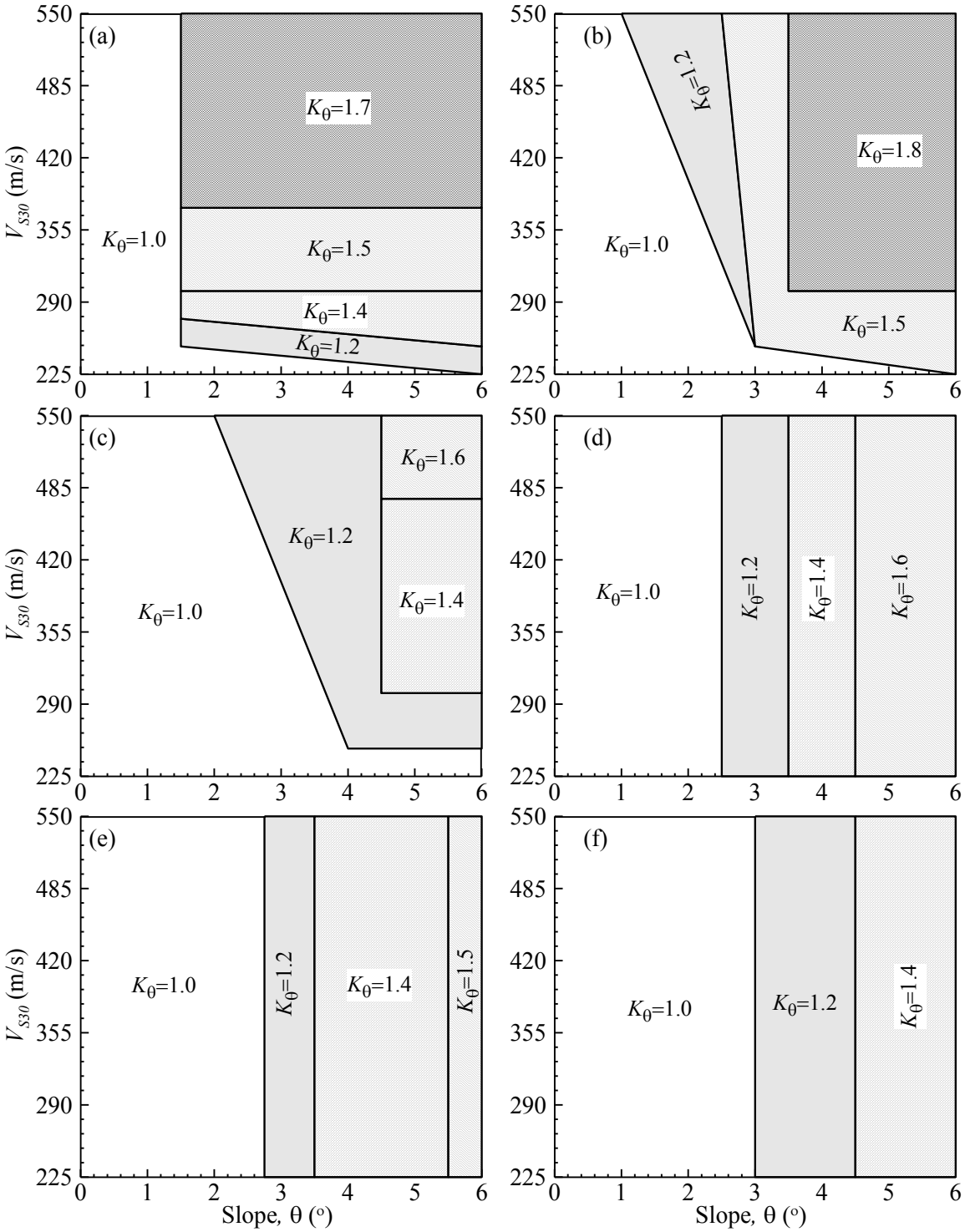

Figure 5.13: K_θ variation with V_{S30} and θ for the cases: (a) T=0.0-0.2s and Motion-I; (b) T=0.6s and Motion-I; (c) T=0.6s and Motion-II; (d) T=1.0s and Motion-I; (e) T=1.0s and Motion-II; (f) T=1.0s and Motion-III to V.

5.8 Application and Limitations

To obtain design spectral acceleration for a sloping ground ($\theta>0^o$) site at a specific period (i.e. T = 0.0, 0.2, 0.6, 1.0, 1.6 and 3.0 sec), $S_{S\_T(\theta)}$, the design spectral acceleration assuming flat ground ($\theta = 0^o$) surface at that period, $S_{S\_T(\theta=0^o)}$ has to be multiplied with the corresponding slope adjustment factor, K_θ from Table 5.2 as presented in the following equation:

$$S_{S\_T(\theta)} = K_\theta S_{S\_T(\theta=0^0)} \tag{5.10}$$

The flowchart in Figure 5.14 lists the required inputs and steps involved in generating $S_{S\_T(\theta)}$ values. At first, $S_{S\_T(\theta=0^o)}$ values are obtained from conventional site response analysis considering horizontal ground surface or by directly using site factors from the code provisions such as NEHRP (BSSC, 1995) or as proposed in Aboye et al. (2013a) for Charleston area. Ground inclination can be measured using different surveying techniques such as: using a total station reading or a clinometer. Another approach to obtain ground inclination can be by analyzing the Digital Elevation Model (DEM) data available in the SCDNR website. Soon a high resolution DEM based on LiDAR (Light Detection and Ranging) data will be available through SCDNR for Charleston, SC area. Using Table 5.2 and Figure 5.13, K_θ values can be obtained for a specific inclination and finally $S_{S\_T(\theta)}$ is calculated using Equation 5.10. Interestingly, apart from the parameters that are necessary for generating $S_{S\_T(\theta=0^o)}$, this method requires only a single additional parameter: θ, for $S_{S\_T(\theta)}$ generation.

This study is conducted over the mild infinite slopes ranging from 0^o-6^o. Thus, the recommendations made in this study cannot be applied in the cases of steep slopes such

as hills, dams, steep channel banks etc. Also, the ground inclination has to be continuous at-least for a comparable stretch of land as the finite element model in this study is developed considering almost a 700 m wide section with a single continuous inclination. Similarly, the recommended K_θ is only applicable for soil profiles with V_{S30} within 232 m/s - 543 m/s range. All the profiles and the single ground motion considered here is from Charleston region, the K_θ recommendations outside this zone may not produce adequate estimates.

This study assumes horizontal bedrock while the slopes of each layer are varied from slope θ at the surface and a perfectly horizontal ($\theta = 0^o$) bedrock boundary at the bottom of the profile (see Figure 5.6). As mentioned earlier, this was employed to avoid low aspect ratio elements at the base of the finite element model thus avoiding any numerical instability during simulations. The authors are fully aware that actual site conditions and the layering might be different and thus a bias on results is expected. Moreover, the model geometry has varying depth from the left to the right side due to the consideration of sloping ground surface and horizontal bedrock boundary. As discussed in the previous section, this has imposed a simultaneous in-phase out-of-phase movement at different locations of the profile and consequently affects the computed surface response which is certainly a limitation of such model. The soil shear strength had to be calibrated due to the lack of measurement data for such deep profiles from the site. Finally, a systematically designed validation study with field measurements and/or a centrifuge model test is required to evaluate the quality of the recommendations made here although none is available at this point.

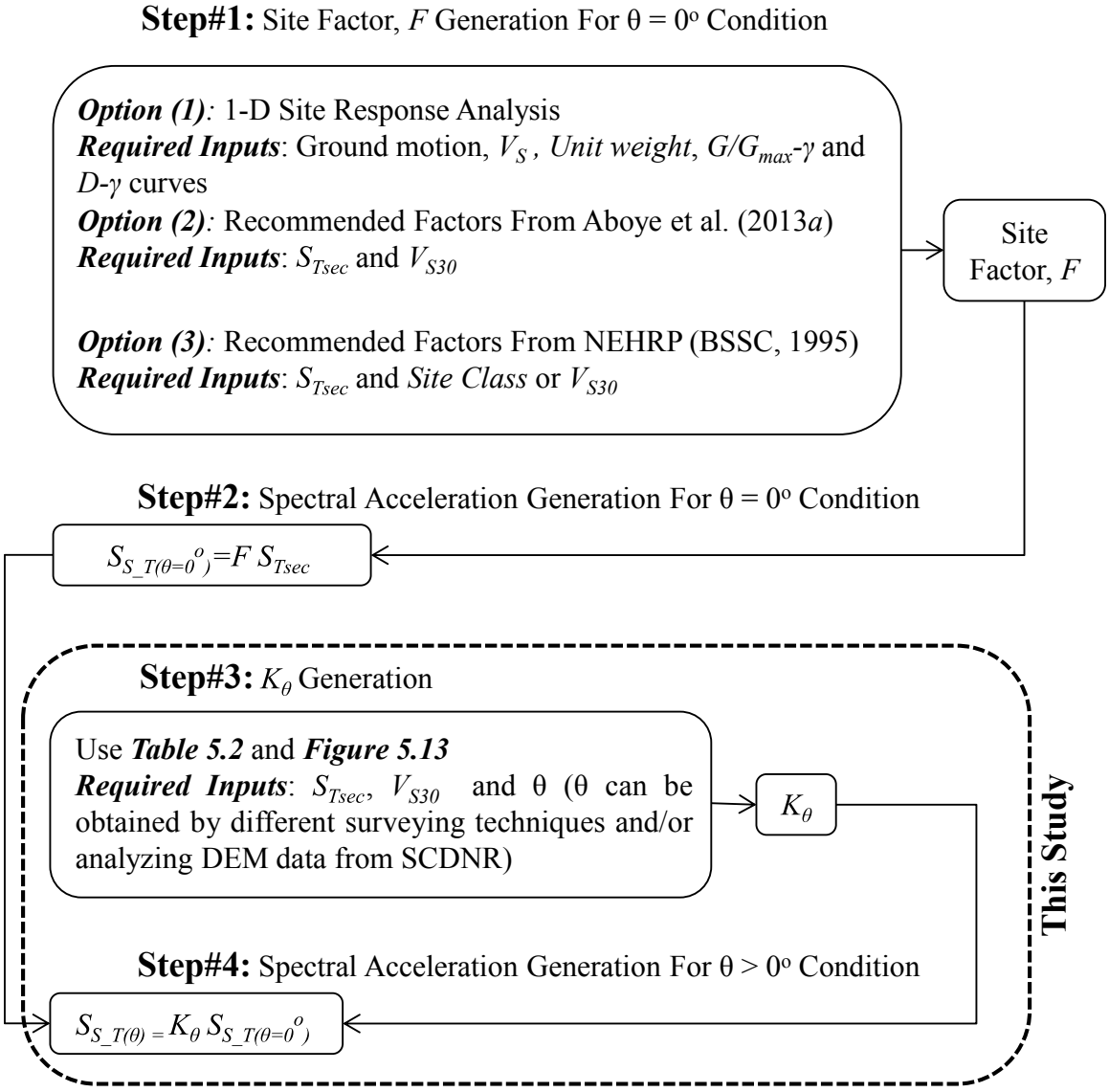

Figure 5.14: Flow chart of $S_{S\ T(\theta)}$ generation process.

5.9 Conclusions

This study explores the potential effect of ground slopes on the computed surface responses under an earthquake event. The study focused only on Charleston, SC region. A total of 385 two-dimensional finite element simulations were performed for this study

consisting of: seven ground inclinations (0^o, 1^o, 2^o, 3^o, 4^o, 5^o and 6^o), eleven V_S profiles representative of the area and one ground motion scaled to five different $S_{0.0sec}$ levels. Computed surface spectral accelerations are generally higher for sloping ground cases than the corresponding flat ground scenario which immediately justifies the importance of such study. Due to a known modeling limitation low period spectral accelerations (i.e. <0.6 sec periods) from sloping ground cases didn't produce a clear trend while in the higher periods (i.e. >0.6 sec period) spectral acceleration increases with surface inclination. The slope effect is more significant when the system behaves within the linear range i.e. stiffer profile and/or smaller loading; when the system behavior enters nonlinear zone damping becomes much higher which reduces the slope effect on the computed responses. Finally, the combined outcomes are used to develop a slope adjustment factor, K_θ which is multiplied to the surface spectral accelerations for 'Flat' ground case to obtain the surface spectral acceleration of a sloping ground condition. However, more works including extensive validation studies are required to fully understand this new branch of site response study.

CHAPTER 6

EFFECT OF SUDDEN CONTRAST OF SHEAR WAVE VELOCITY AT LAYER INTERFACES ON SEISMIC SITE RESPONSE ANALYSIS FOR CHARLESTON, SC

6.1 Introduction

Seismic site response analysis predicts the local site effect on the earthquake ground motion propagating from the bedrock to the ground surface. Shear wave velocity (V_S) is an important parameter for such analysis. Commonly, shear wave velocity measurements (from field tests such as: seismic cone, crosshole seismic, multichannel analysis of surface waves, refraction microtremor etc. or from the laboratory tests such as: resonant column tests, bender element test etc.) for a site are simplified by discretizing the whole profile with a number of homogeneous layers with a constant V_S value for each layer. Therefore, to represent an increased or decreased shear wave velocity in the immediate layers a sudden rise and drop of V_S values at the layer interfaces i.e. the V_S contrasts are inevitable. In this manner the geotechnical engineer compiles the 'working' V_S profile. This has been a wide spread practice in the community for decades as this simplification is advantageous to the general geotechnical engineering related computations (both analytical and numerical).

However, this assumption of sudden contrast of V_S in the layer interfaces is often unnatural; a gradual rise or drop is a better representation of the measured data for a lot of cases. On the other hand, such sudden changes in V_S incurs unrealistically high shear strain at those interface locations, especially on the softer side of the interface, during numerical simulations (Stewart et al., 2008; Kottke, 2010; Matasovic and Hashash, 2012;

Bozzano et al., 2012; Gouveia et al., 2012; Brandenberg et al., 2013). Similar shear strain concentration was also observed at interface locations while performing thousands of simulations in Chapter 3 and 4. Figure 6.1 presents a sample scenario of the shear strain-profile in the case of a typical Charleston, SC profile (reference profile as described in Chapter 3 and 4) and for a synthetic ground motion (a peak rock-outcropping ground acceleration or $PGA_{Outcrop}$ of 0.5g) generated for the area. Extensive amount of shear strain is observed in each of the three scenarios (i.e. time) captured (Figures 6.1b, 6.1c and 6.1d) during the simulation where the most prominent V_S contrast (Figure 6.1a) of the whole profile is located. Such excessive shear strain can cause a significant amount of energy loss during the seismic wave propagation through that interface which may eventually reduce the amplitude of the computed surface response (Gouveia et al., 2012).

Seismic site response analysis is performed to generate acceleration response spectra which is a plot of the maximum response of a set of SDOF (single-degree-of-freedom) systems with different periods and a specified (5% typically) damping, for a particular input ground motion (Kramer, 1996). The ratio of the computed acceleration response spectra at the ground surface (S_{Site}) and at rock-outcrop ($S_{Outcrop}$) is called the seismic site factors (F), for a specific spectral period (SCDOT, 2008a). These site factors are used to perform seismic analyses of structures. The most common site factors in practice are the NEHRP (BSSC, 1995) site factors. Chapter 3 presented the seismic site factor model for the Charleston, South Carolina area that has been developed and recommended to SCDOT (Aboye et al., 2011 and 2013a) based upon thousands of one-dimensional equivalent linear and nonlinear site response analysis results. There, the V_S

profiles were based on the assumption of sudden contrast at layer interfaces as adopted from the Andrus et al. (2006). Such simplification of the V_S profiles allowed the research group to perform thousands of numerical simulations and to make general recommendations over the area. However, a closer investigation on the V_S recordings of some other published works on this site (Chapman et al., 2006; Jaume, 2006) would suggest that a continuous change of V_S at some interfaces is a more appropriate approach. Figure 6.2 shows the seismic cone penetration (SCPT) measurements and the corresponding three-point running mean of SCPT velocities from two sites in Charleston area inside the campus of The Citadel, the military college of SC. The sites are referred to as: C1SC and C2SC and are presented in Figures 6.2(a) and (b), respectively. This figure is a reproduction of the work done by Jaume (2006). In the case of these profiles, the transitional zone between the Quaternary (Q) and Tertiary (T) aged layers (details on the Quaternary and Tertiary layers are in the following section) are 2-3m wide. The same transition has been represented as a sudden jump of V_S in Andrus et al. (2006), following the conventional approach.

In this chapter, a few representative V_S profiles of the Charleston, SC area from Chapters 3 and 4 have been adopted and then the profiles are altered to introduce different degrees of continuous variation of V_S at a few selected interface locations. These profiles were analyzed to compute seismic surface responses and were then compared. This investigation offers a scope to evaluate the implication of smoothening the key sudden interface V_S contrasts over the computed seismic surface response (i.e. site factors) for the area. Nevertheless, the intention of this study is not to improve/update any

of the currently available site factor provision, rather to raise awareness for this important matter which has been ignored for long in site response study.

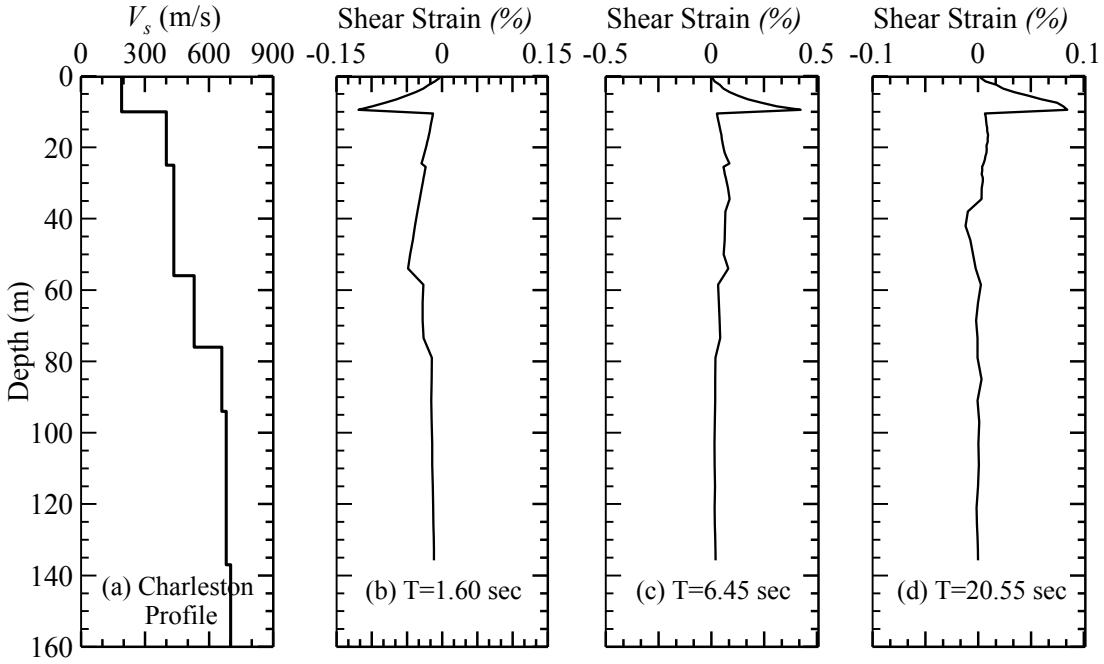

Figure 6.1: Profile shear strain–time history of a typical Charelston profile: (a) simplified V_S profile; (b) profile shear strain at T=1.60 sec; (b) profile shear strain at T=6.45 sec; (b) profile shear strain at T=20.55 sec. A ground motion with $PGA_{Outcrop}$ of 0.5g was used.

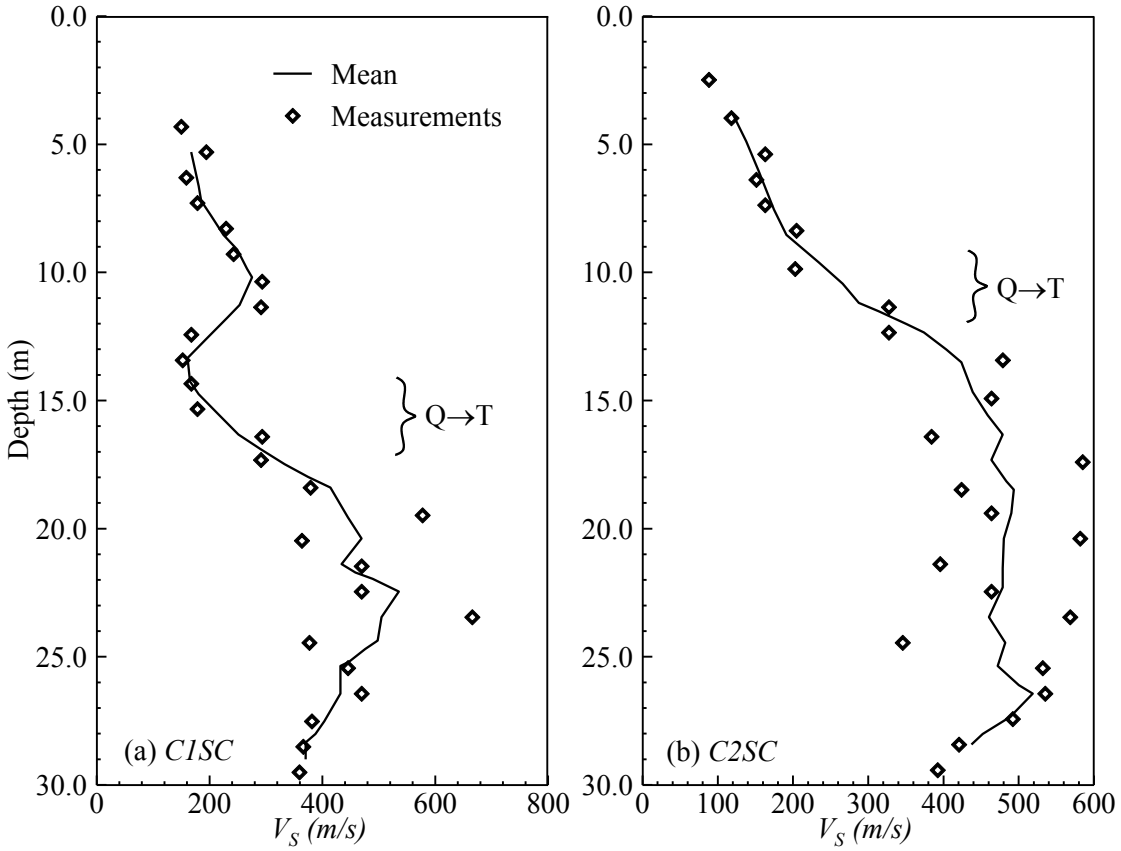

Figure 6.2: Sample V_S measurements with SCPT and the three-point running mean of SCPT velocities from the C1SC and C2SC sites are presented in (a) and (b), respectively. The transitional zone between the Quaternary (Q) and Tertiary (T) layers is also marked (Reproduction of Figure 5 from Jaume, 2006).

6.2 Soil Profile and Material properties

6.2.1 Shear wave velocity profiles

6.2.1.1 *Profiles with sudden contrast at the interface:*

The 137 m deep soil profile designated as the 'reference' or mean *Vs* profile along with its ±1σ (σ = standard deviation) same as Chapter 3 and 4 are adopted in this Chapter. Figure 6.3 presents all three V_S profiles: the mean and mean±1σ which were originally based on the data collected and compiled from Andrus et al. (2006) and also from suspension logger tests done by South Carolina Department of Transportation (SCDOT)

in 2006. In this Chapter, the 'mean' *Vs* profile (dark line in Figure 6.3) with sudden contrast is referred to as 'SC'; the 'mean+1σ' (on the right of the dark line in Figure 6.3) and the 'mean-1σ' (on the left of the dark line in Figure 6.3) cases are referred to as 'SC(+)' and 'SC(-)', respectively. Underneath these 137m deep profiles are the soft-rock half space with an assumed *Vs* = 700 m/s for the area. The other profile parameters such as: soil layers and thickness, total unit weight and plasticity index are also presented in Figure 6.3.

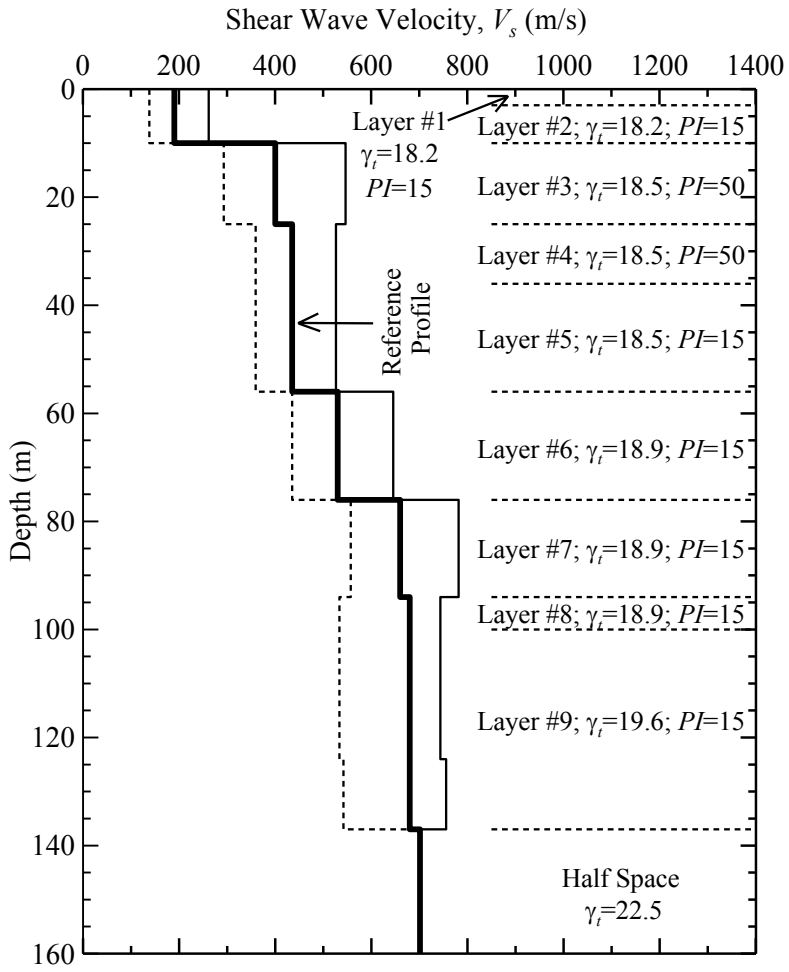

Figure 6.3: The shear wave velocity profiles: 'Mean' and it's ±1σ variations, based on Aboye et al. (2013a) for Charleston, SC area. These profiles have sudden stiffness contrasts at layer interfaces. The total unit weight (in kN/m^3) and plasticity index are listed for each layer.

6.2.1.2 *Altered/smoothened profiles:*

Three additional (hypotheitical) *Vs* profiles: Model-I (or M-I), Model-II (or M-II) and Model-III (or M-III), have been generated based on each of the SC, SC(+) and SC(-) profile cases from Figure 6.3. All three model variations for each of the SC, SC(+) and SC(-) profile cases are grouped and presented in the subplots (a), (b) and (c) of the Figures 6.4, respectively.

These nine hypothetical profiles were developed by smoothening the sudden *Vs* contrasts at 10m and 56m depth from the surface with different degrees of continuous variation. These are the two locations where significant *Vs* contrast exists in the profiles; especially the contrast at 10m depth is the interface between Quaternary and Tertiary strata. Based on the authors' experience, these two interfaces are the locations where large shear strain usually occurs which is the reason for selecting these two interfaces for smoothening.

Model-I (or M-I): In this case, smoothening was done by discretization of the each of the corresponding layers to eight 0.5m thick micro-layers, in conjunction with step-like *Vs*. M-I, M-I(+) and M-I(-) are the three variations generated based on the SC, SC(+) and SC(-) profile cases, respectively.

Model-II (or M-II): This model is similar to the Model-I except six-teen 0.5m thick micro-layers were adopted at each of the 10m and 56 deep interfaces. M-II, M-II(+) and M-II(-) are the three variations corresponding to the SC, SC(+) and SC(-) profile cases, respectively.

Model-III (or M-III): 1.0m thick micro-layers are extended throughout the corresponding layers on the both sides of the interfaces to replace those sudden contrasts with a continuous change of *Vs*. M-III, M-III(+) and M-III(-) are the three variations corresponding to the SC, SC(+) and SC(-) profile cases, respectively.

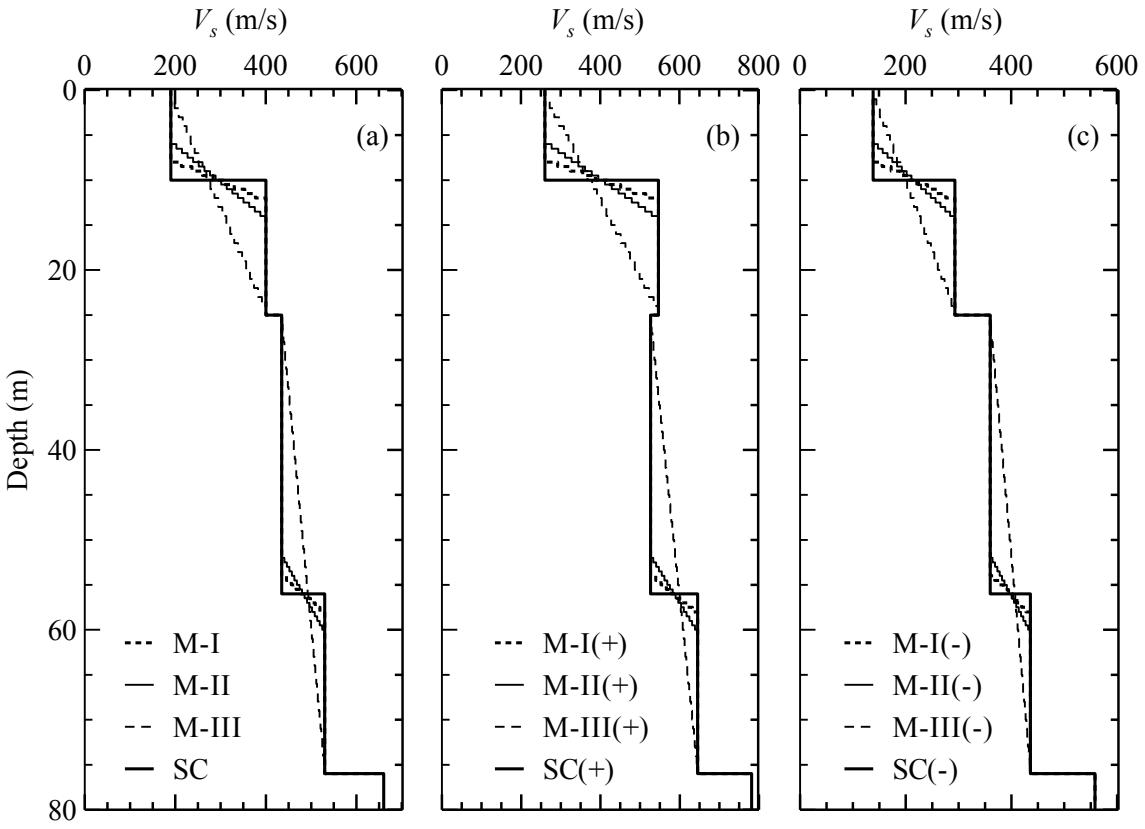

Figure 6.4: Three variations in shear wave velocity profiles are considered for each of the SC, SC(+) and SC(-) profile cases from Charleston and are presented in the subplots (a), (b) and (c), respectively. Only up-to 80m depth has been presented of these 137m deep profiles; below this depth no further variation has been implemented to the corresponding original profiles.

6.2.2 Modulus reduction and damping curves

Figures 6.5(a) and 6.5(b) present the G/G_{max}-γ and D-γ curves, respectively, for each of the nine layers. These curves were developed using the Zhang et al. (2005) relationships which are the function of soil plasticity index, mean effective confining pressure and geologic age. For the half space (V_S = 700 m/s), purely linear relationships for G/G_{max}-γ and D-γ were assumed and this was done by keeping G/G_{max} at 1 and D at 0.5% as constants for all γ values and standard deviations as in South Carolina Coastal Plain D = 0.5% is considered as representative for soft rock outcrop (SCDOT, 2008a).

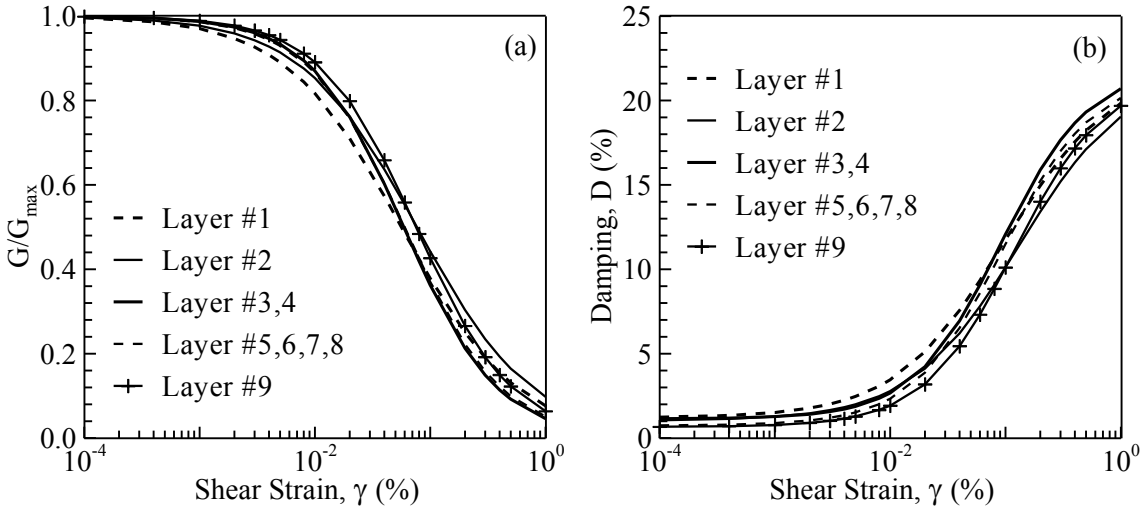

Figure 6.5: Soil dynamic properties: (a) the *G/Gmax-γ*; and (b) *D-γ* curves, based on Zhang et al. (2005) relationships.

Point to be noted that, in the micro-layers of each of the smoothened profiles only the *Vs* was varied. All other soil properties (i.e. G/G_{max}-γ and *D-γ* curves, unit weight) were kept the same as the corresponding profiles with sudden contrast although in reality, these properties are usually expected to vary in accordance with the *Vs* variation. This implies that in some of the micro-layers (above 10m and 56m interfaces) these properties are under-estimated and in the rest of the micro-layers those are over-estimated. Justifications to this assumption are: (i) as the micro-layers are symmetric (in the sense of both layer thickness and *Vs*) with respect to the original layer interface, the effect of over and under-estimated soil properties should have cancelled out each other or at-least to some extent; and (ii) the G/G_{max}-γ and *D-γ* curves in Figure 6.5(a) and 6.5(b) for different layers are very close and thus separate sets of G/G_{max}-γ and *D-γ* curves for each of the micro-layers would have produced negligible difference in surface response.

6.3 Ground Motion

The single ground motion used for this Chapter also appeared in Chapter 3 and 4. A computer program called Scenario_PC (Chapman, 2006) was employed to generate outcroppping motions for Charleston area as there was no actual strong motion record available. Scenario_PC was developed for South Carolina Department of Transportation (SCDOT) to perform seismic hazard analysis in this area. The acceleration time history and corresponding response spectra of the ground motion generated for the Charleston quadrangle are presented in the Figure 6.6. A return period of 2% probability of exceedance in 50 years and a modal moment magnitude of 7.3 were used as inputs for Scenerio_PC. This motion was then scaled to the peak ground accelerations ($PGA_{Outcrop}$) of 0.1g, 0.3g and 0.5g in this Chapter.

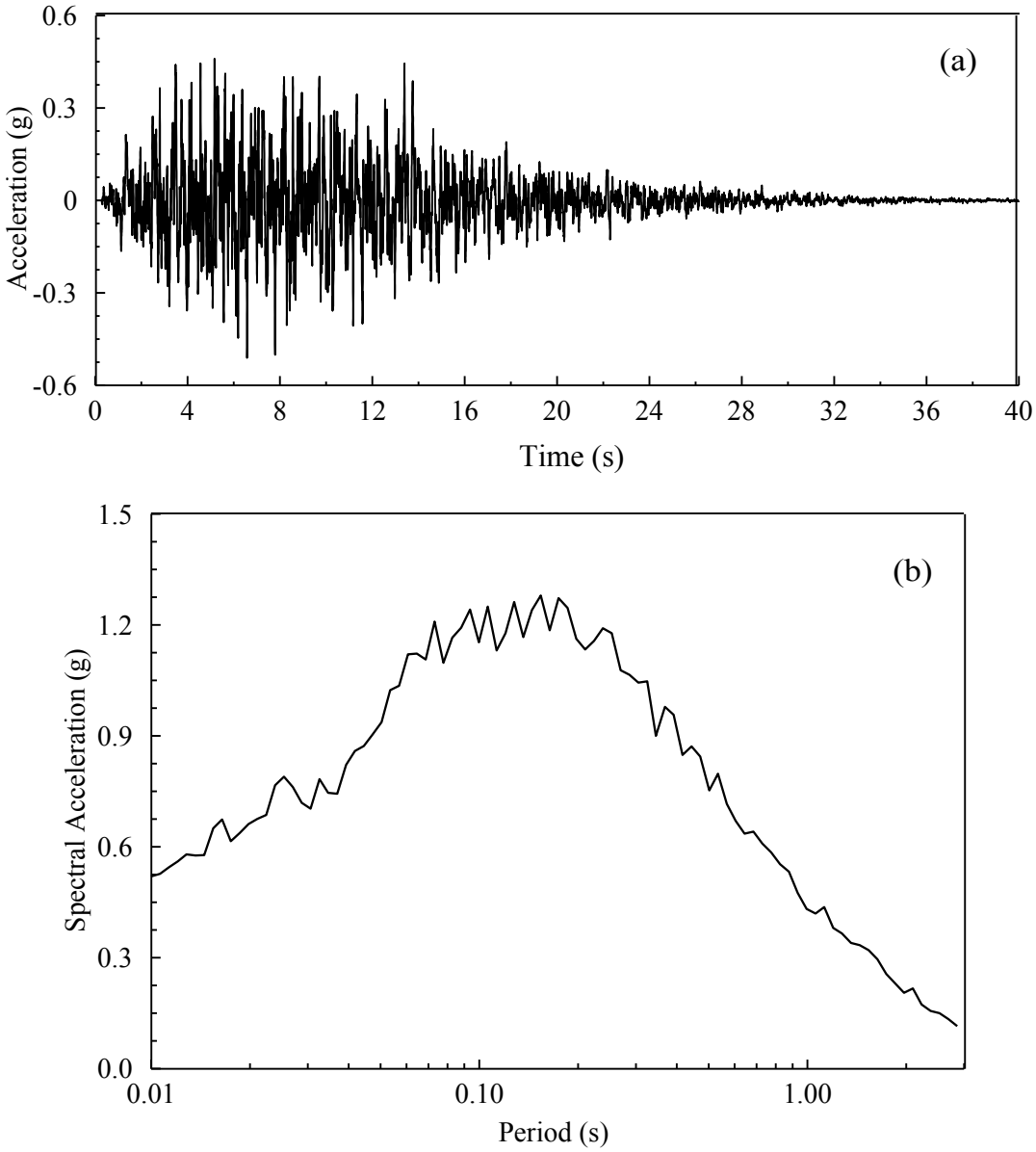

Figure 6.6: The ground motion generated for Charleston quadrangle: (a) acceleration time history and (b) acceleration response spectra.

6.4 Ground Response Analysis

DEEPSOIL v5.0 (Hashash et. al. 2011) is a widely accepted one-dimensional site response analysis program. Although it is capable of performing both nonlinear and equivalent linear total stress and effective stress analyses, only nonlinear total stress

capabilities are used. DEEPSOIL has an intuitive graphical user interface. It models the vertical propagation of horizontal shear wave through deep soil deposits using a multi-degree of freedom lumped-mass system. The dynamic equation of motion is solved by Newmark's β method.

DEEPSOIL implements the Modified KZ model (Matasovic and Vucetic, 1993a) to define the initial hyperbolic stress-strain backbone curve in the simulation. The normalized MKZ model is given by:

$$\tau^* = \frac{G^*_{max}\gamma}{1+\alpha\left(\frac{\gamma}{\gamma_r}\right)^s} \tag{1}$$

where α and s are two curve fitting constants added to the Kondner and Zelasko (1963) or KZ model, τ is the shear stress, γ is the shear strain, $\tau^* = \tau/\sigma'_{vc}$, $G^*_{max}=G_{max}/\sigma'_{vc}$, $\gamma_r=\tau_{max}/G_{max}$, σ'_{vc} is the initial vertical effective stress and G_{max} is the initial (maximum) shear modulus of the soil.

A modified reference shear strain definition (Hashash and Park, 2001) has been incorporated with the Modified KZ model:

$$\gamma_r = a\left(\frac{\sigma'_{vc}}{\sigma_{ref}}\right)^b \tag{2}$$

where σ'_{vc} = effective vertical stress, σ_{ref} = reference confining pressure and a and b are the curve fitting parameters. Hysteretic damping is calculated using the backbone curve considering the Masings criteria.

The ‘modulus reduction and damping fitting’ option in DEEPSOIL is selected for the MKZ model parameters (α and s) calibration. This option in DEEPSOIL employs a reduction factor (Phillips and Hashash, 2009) which modifies the extended Masing (1926) loading/unloading stress-strain relationship. This increases the flexibility of the model to match both the modulus reduction and damping curves simultaneously with better accuracy. A frequency independent small-strain damping (Phillips and Hashash, 2009) technique implemented in DEEPSOIL has been used.

On the other hand, SHAKE2000 (Ordóñez 2011) was developed by GeoMotions, LLC which is a widely used equivalent linear program. SHAKE2000 was developed based on the SHAKE program by Schnabel et al. (1972). In this method an equivalent linear shear modulus, G and an equivalent linear damping ratio, ξ are primarily determined by performing trial runs by the program. These properties are then kept constant for the final run of the entire earthquake excitation and thus this method cannot account for soil stiffness changes during an event. Therefore, an equivalent linear analysis is merely an approximation to the actual nonlinear behavior. Thus in the case of higher loading and/or induced shear strain, equivalent linear programs are unable to produce reasonable estimates. Equivalent linear method is more popular within practitioners because of simplicity, low computational requirement, and also availability of good documentation on usage protocol. With SHAKE2000 and DEEPSOIL, all profiles presented in Figures 6.3 and 6.4 are simulated for all three $PGA_{Outcrop}$ levels: 0.1g, 0.3g and 0.5g. Then the computed responses are compared.

6.5 Analysis Results

6.5.1 Comparison of acceleration response spectra

Acceleration response spectra from DEEPSOIL and SHAKE2000 at the ground surface level are computed for each of the cases. In Figure 6.7(a) and 6.7(b) and in Figure 6.8, DEEPSOIL outcomes for the 'mean' or SC profile and the corresponding altered models: M-I, II and III are presented, for $PGA_{Outcrop}$ of 0.1g, 0.3g and 0.5g, respectively. In Appendix C, Figures C.1(a) and C.1(b) and in Figure C.2, DEEPSOIL outcomes for the 'mean+1σ' or SC(+) profile and it's altered models: M-I(+), II(+) and III(+) are presented, for $PGA_{Outcrop}$ of 0.1g, 0.3g and 0.5g, respectively. In Figures C.3(a) and C.3(b) and in Figure C.4, DEEPSOIL outcomes for the 'mean-1σ' or SC(-) profile and it's altered models: M-I(-), II(-) and III(-) are presented, for $PGA_{Outcrop}$ of 0.1g, 0.3g and 0.5g, respectively. Similar plots based on the SHAKE2000 outcomes are also presented in the Appendix C Figures C.5- C.10.

Based on these figures, generally speaking, in each of the mean and mean±1σ cases, the M-I and M-II cases produced higher spectral acceleration peaks while the M-III cases are always on the lower side, in compared to the corresponding SC cases. Such difference becomes greater with the increase of $PGA_{Outcrop}$ from 0.1g to 0.5g. In the cases of M-I and M-II, an increased (due to smoothening) stiffness (or V_S) is present within 10m from the surface compared to the corresponding SC profile (see Figures 6.4a, 6.4b and 6.4c). Although there is a symmetric drop of stiffness below 10m, it is common that the shallowest profiles are more influential during wave propagation through the topsoil. Thus higher peaks are observed in these two cases: M-I and M-II, in-fact, the M-II cases

produced the highest peak. Additionally, there is one more symmetric stiffness increase at 56m depth interface which is also acting in favor of amplification of surface response, in these two cases.

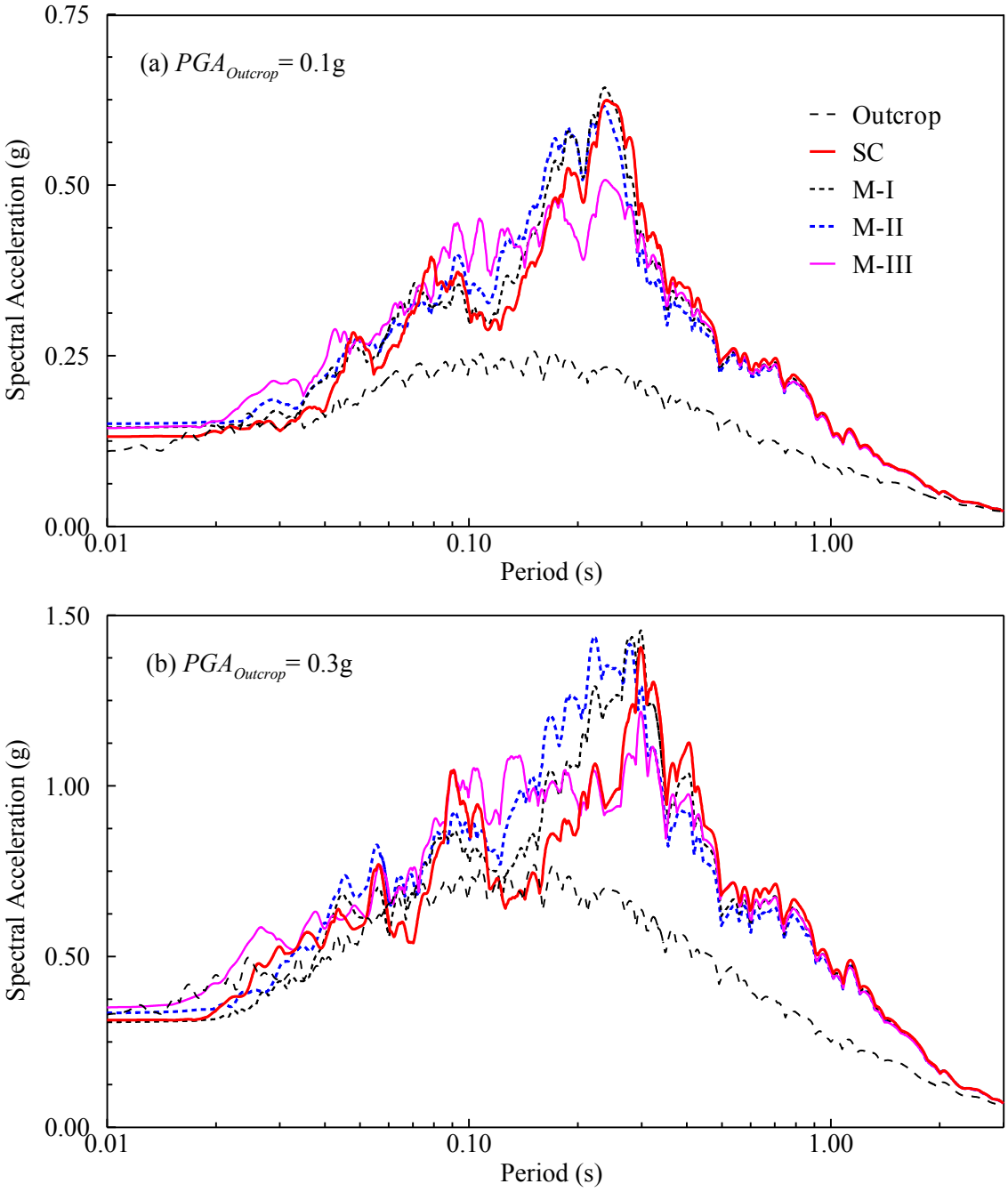

Figure 6.7: DEEPSOIL generated acceleration response spectra at surface level for profile variations presented in Figure 6.4(a) and for: (a) $PGA_{Outcrop}$ = 0.1g; and (b) $PGA_{Outcrop}$ = 0.3g.

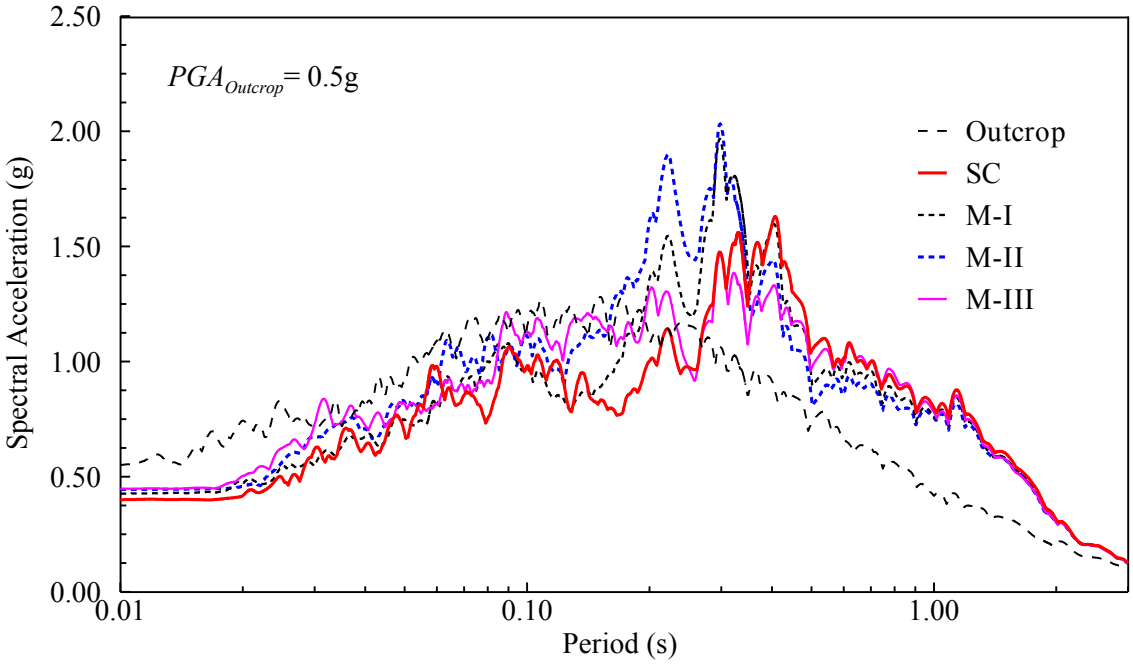

Figure 6.8: DEEPSOIL generated acceleration response spectra at surface level for profile variations presented in Figure 6.4(a) and for $PGA_{Outcrop}$ = 0.5g.

On the other hand, the stiffness changes for M-III models are not symmetric and there is a bigger drop of V_S below 10m interface (see Figures 6.4a, 6.4b and 6.4c), which is the Tertiary layer, has overwhelmed the minor stiffness increase within the top 10m. This has reduced the amplification of ground motion travelling through this 'softer' system and thus explains the eventual drop at the surface spectral acceleration than the corresponding SC cases. Point to be noted here that, such difference in the computed spectral accelerations between the altered models and the corresponding SC cases become more significant when the profile becomes softer i.e. the mean-1σ cases (SC(-), M-I(-), M-II(-), and M-III(-)) in Figures C.3-C.4, especially for $PGA_{Outcrop}$ of 0.5g while it's the opposite for stiffer profiles (e.g. Figures C.1-C.2). Softer profiles and/or higher loading push the system behavior more into nonlinear zone and that reflects on the

computed surface response differences. Similar behaviors were also seen in the SHAKE2000 responses (Figures C.5-C.10 in Appendix C). However, due to the limitation of SHAKE2000 in capturing the true nonlinear behavior, the differences observed between the altered and the corresponding SC cases are lesser compared to the DEEPSOIL outcomes, especially for the softer profiles (mean-1σ) and higher $PGA_{Outcrop}$ cases (i.e. Figure C.10).

6.5.2 Comparison of seismic site factors

Seismic site factors are also generated to observe the potential difference that could be obtained from the site response analyses considering both the 'smoothened V_S profile' and the typical 'V_S profile with sudden contrast'. Site factor, F was calculated for six spectral period ranges: ≤ 0.01 s for *T=0* sec period, 0.01-0.4 s for *T=0.2* sec period, 0.41-0.8 s for *T=0.6* sec period, 0.81-1.2 s for *T=1.0* sec period, 1.21-2.0 s for *T=1.6* sec period and 2.01-4.0 s for *T=3.0* sec period, which are the averaged values of the corresponding ranges. Then the site factors from the altered models (all mean and ±1σ variations of M-I, II and III), F_{Models}, are normalized by the site factors computed from the original profiles with sudden contrast (i.e. mean and ±1σ variations of SC profile) at interface locations, F_{SC}, and were plotted against $PGA_{Outcrop}$ values. Figure 6.9 presents the F_{Models}/F_{SC} vs. $PGA_{Outcrop}$ plots for all periods from the DEEPSOIL outcomes while in Figure C.11 of Appendix C presents the corresponding SHAKE2000 outcomes. F_{Models}/F_{SC} =1.0 line stands for the SC, SC(+) and SC(-) while the black, blue and red symbols stand for: M-I, II and III; M-I(+), II(+) and III(+); and M-I(-), II(-) and III(-), respectively.

As is seen in Figure 6.9, the lower periods such as T=0.0 and 0.2 sec cases, each of mean and ±1σ variations of the altered (M-I, II and III) cases produced higher ratios than unity, thus higher site factors than the corresponding SC (i.e. SC, SC(+) and SC(-)) profiles while it is the opposite in higher periods such as 0.6, 1.0, 1.6 and 3.0 sec cases. Especially, the soft altered models: M-I(-) and M-II(-), produced about 10-20% higher site factors than the SC(-) profile at T= 0.0, 0.2 and even at 0.6 sec periods for higher $PGA_{Outcrop}$ cases, proving the softer profiles to be the most critical. Similar behaviors were also observed in the SHAKE2000 responses (in Figure C.11 of Appendix C) although the lesser difference in computed surface spectral accelerations from SHAKE2000 kept these ratios (and/or site factors) lower than the corresponding DEEPSOIL cases.

6.5.3 Comparison of profile maximum shear strain

Plotted in Figure 6.10 are the maximum shear strains computed throughout the layers of the profiles: SC, M-I, II and III, using DEEPSOIL. For better visualization, the corresponding V_S profiles are also kept side-by-side for each case. For the SC profile (Figures 6.10(a) and 6.10(b)), high amount of shear strain are observed at the 10m and 56m deep layer interfaces as expected although the shallowest one i.e. at 10m depth, producing the highest among all point to the fact that the shallowest interfaces with significant stiffness contrast are more viable for such behavior. In the cases of M-I and M-II (Figures 6.10c-6.10f), a considerable amount of reduction in the interface maximum shear strains are observed, as compared to the SC case. This explains the higher peak spectral accelerations observed at the surface level for these two profile cases (see

Figures 6.7 and 6.8) than the SC case, as lower strain means lower system damping. In the case of M-III profile (Figures 6.10g and 6.10h), although the maximum shear strain reduces at 10m depth than the mean profile, a zone of increased shear strain is observed at locations where this profile has lesser stiffness than the SC profile (below 10m and 56m). This explains the smaller peak spectral response from this profile at the surface level as larger strain means higher hysteretic damping in the system. Similar high shear strain at layer interfaces also occurred for the stiffer (mean+1σ cases from Figure 6.4b) and softer (mean-1σ cases from Figure 6.4c) profile cases as presented in the Appendix C in Figures C.12 and C.13, respectively, although the stiffer profiles produced milder strain while the softer ones showed higher, as compared to the cases showed in Figure 6.10, in general.

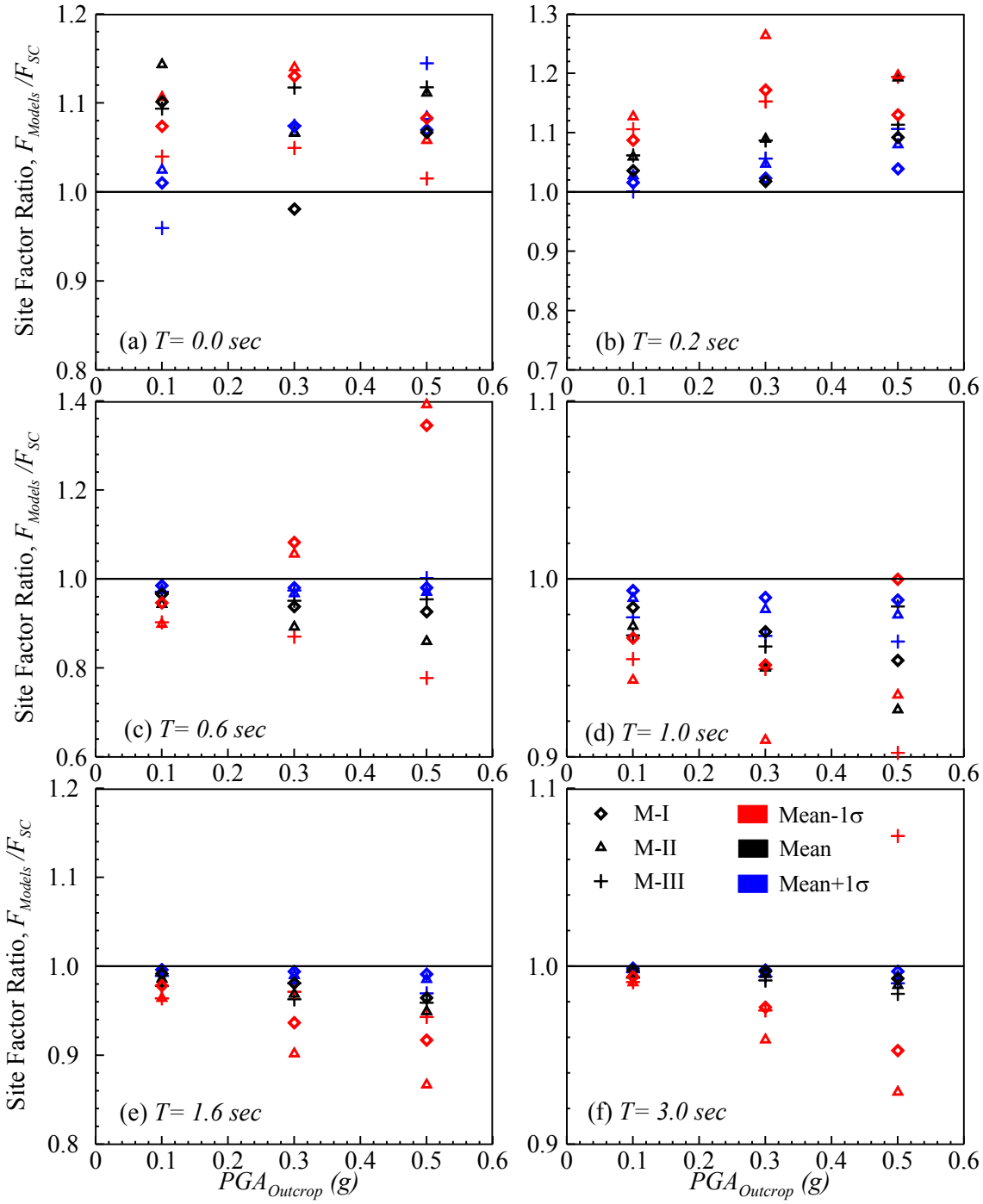

Figure 6.9: Site Factors Ratios vs. $PGA_{Outcrop}$ plots for the 'Mean' and it's ±1σ variations of all three models: M-I, II and II (see Figure 6.4) based on DEEPSOIL data points for: (a) T= 0.0 sec, (b) T= 0.2 sec, (c) T= 0.6 sec, (d) T= 1.0 sec, (e) T= 1.6 sec, and (f) *T= 3.0 sec*.

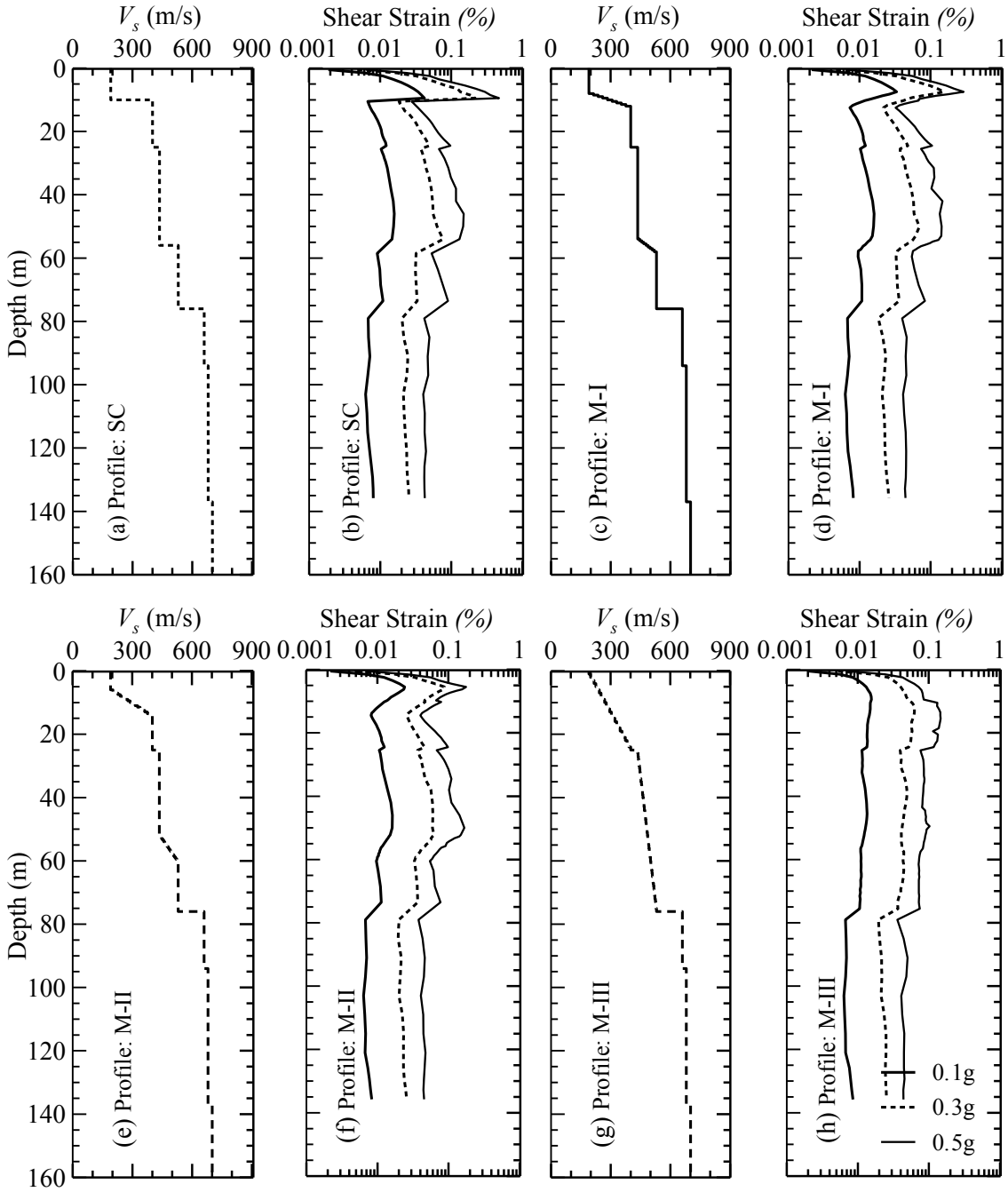

Figure 6.10: Profile maximum shear strains, based on DEEPSOIL data points, along with the corresponding V_S profiles from Figure 6.4(a) and for $PGA_{Outcrop}$ levels of 0.1, 0.3 and 0.5g. Subplots (a) and (b) are for the profile: SC; (c) and (d) for the profile M-I; (e) and (f) for the profile M-II; and, (g) and (h) for the profile M-III.

6.6 Discussions

Based on the plots presented in the previous section, even with a very mild deviation (e.g. cases M-I and M-II) from the originally compiled V_S profiles (i.e. with sudden contrast at interface locations or SC cases) could produce a considerably higher surface response; this leads to higher seismic site factors especially for lower period cases (mostly T=0.0 and 0.2 sec). Such behavior is expected to be prominent when the site in hand is relatively softer and/or greater shaking involved. In the case of sudden V_S variation, significant shear strain was observed at those interface locations, mostly at the shallowest interface (at 10m depth). This filters out (or dampens) a major portion of the wave energy transmitted through that interface and eventually produces smaller surface response.

With the shear strain increase, the system behavior becomes more and more nonlinear and the equivalent linear approach becomes more inadequate; a nonlinear code is required to simulate the system behavior properly. With the consideration of continuous variation of stiffness in the interface regions, much lower shear strains were obtained especially for the M-I and M-II cases. For example in Figure 6.10, in the case of $PGA_{Outcrop}$ of 0.5g, the SC profile has a maximum shear strain ~0.5% (Figure 6.10b), at the interface of 10m depth from surface, which requires a nonlinear analysis according to the recommendation made by Matasovic and Hashash (2012). Matasovic and Hashash (2012) claimed that the nonlinear and equivalent linear approaches start to diverge at 0.1-0.2% strain level and after 0.5%, responses calculated by equivalent linear approach are no more reliable. On the other hand, in the case of M-I and M-II, the same location in the

profile (at 10m depth from surface) show 0.3% and 0.1% strains, respectively; thus equivalent linear analysis is expected to produce adequate estimates for these two cases. In order to further investigate, the spectral accelerations computed based on the equivalent linear program SHAKE2000 and nonlinear program DEEPSOIL were plotted together and presented in Figures 6.11-6.12. As is seen, for $PGA_{Outcrop}$ of 0.1g, for each of the SC, M-I and M-II cases the computed spectral accelerations from SHAKE2000 and DEEPSOIL matched with great accuracy. On the other hand, for $PGA_{Outcrop}$ of 0.5g case, both codes produced significantly different responses in the case of SC profile (Figure 6.11a) as was expected due to high shear strain involved at interfaces. However, for the M-I and M-II cases in Figures 6.11(b) and 6.12, respectively, both the codes produced a good peak matching at $PGA_{Outcrop}$ level of 0.5g although in the lower periods both lines still differ considerably. Such small period mismatch between nonlinear and equivalent linear codes is also very common (Stewart et al., 2008). Therefore, profiles with smoothened V_S contrasts have a potential wider range of appropriateness for equivalent linear analysis, an additional benefit of this concept.

Moreover, based on the above responses, the author believes that this may potentially be a reason or even partly responsible for the under-predictions from several site response tools in compared to the recorded scenario which were observed by Kim and Hashash (2013) and Zalachoris (2014). The primary reasons are: first, both Kim and Hashash (2013) and Zalachoris (2014) observed the current site response tools fail to predict especially when system behavior is highly nonlinear i.e. higher loading and/or softer sites involved, especially at smaller periods. The smoothened V_S contrast cases also

produced significantly higher surface responses when the intense loading is involved and also within the smaller period ranges. Secondly, estimation of the soil dynamic properties such as G/G_{max}-γ and D-γ curves at large shear strain levels are always a challenge and is speculated by Zalachoris (2014) as a major cause of failed site response predictions of actual events. As the consideration of smoothed interface stiffness produces much lower profile shear strains, the deviation of G/G_{max}-γ and D-γ curves are also expected to be the minimum and a better accuracy in site response prediction is expected.

Another implication of this study is, it introduces a brand new research question to the geotechnical earthquake engineering community of how to approximate the limited shear wave velocity measurements. In order to fully understand the significance of this concept over the current practice of V_S measurements, extensive numerical investigations aided with sufficient laboratory and field validations are required. Parametric studies of the magnitude of the stiffness contrast, depth/location of the contrast and the total number of layer interfaces with significant contrasts in the profile etc. are necessary to properly estimate the potential effect of such stiffness contrasts in site response analysis. This may eventually revolutionize the current practice of collecting V_S measurements and the generation of the 'working' V_S profiles for the site specific response spectral analysis.

The observations made here indicate that large number of shear wave velocity measurements must be taken where significant contrast is expected to accurately predict the surface response using commonly used site response analysis programs. Nevertheless, in the light of the above findings, a few steps are suggested to follow during a site specific response spectrum analysis using the V_S profiles with interface contrasts, until a

more appropriate technique becomes available: first, a preliminary site response analysis has to be performed considering the V_S profile with conventional simplification (i.e. with sudden contrast at interfaces) of the measured data; if a large (as compared to the rest of the profile locations) shear strain at layer interface(s) has been developed then the V_S profile has to be smoothened at those locations which should also agree with the variation pattern of the measured V_S from the field tests; finally, site response analysis has to be performed again with the 'smoothened' profile and compared with that of the previous analysis (i.e. with interface contrast). These steps are expected to produce a reasonable surface response.

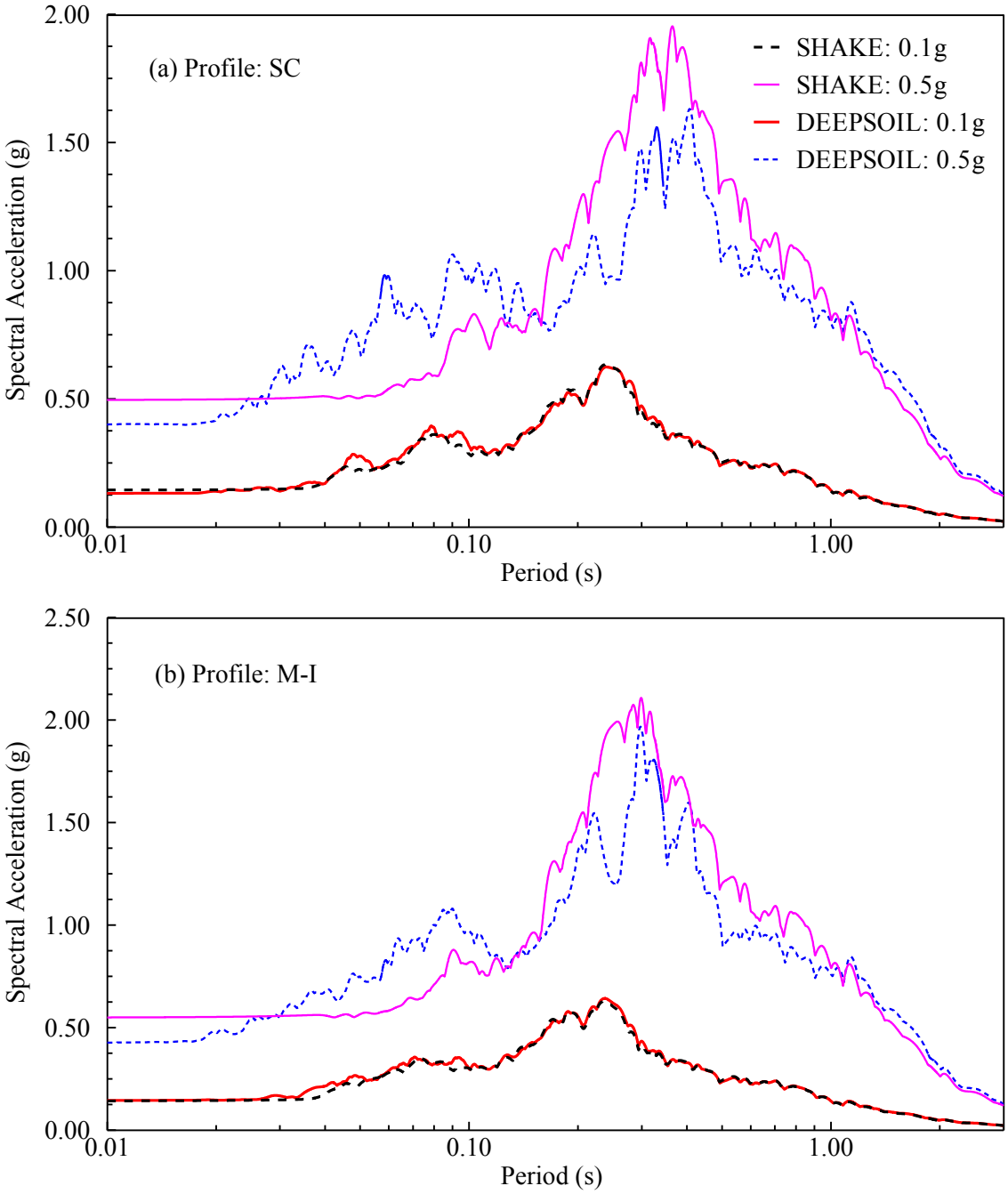

Figure 6.11: Comparison of SHAKE and DEEPSOIL spectral acceleration responses for the profiles (see Figure 6.4(a) for profile information): SC and M-I in subplots (a) and (b), respectively and for $PGA_{Outcrop}$ of 0.1g and 0.5g cases.

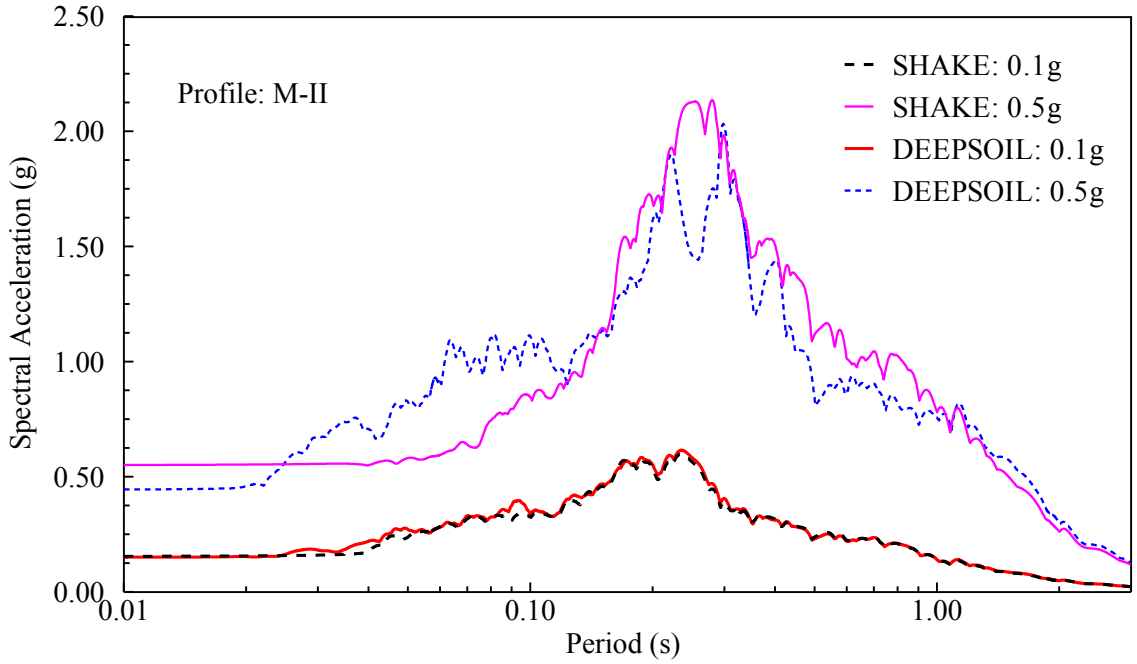

Figure 6.12: Comparison of SHAKE and DEEPSOIL spectral acceleration responses for the profiles (see Figure 6.4(a) for profile information) M-II and for $PGA_{Outcrop}$ of 0.1g and 0.5g cases

6.7 Conclusions

Three V_S profiles representative of the Charleston, SC area were considered and altered to replace a few selected sudden stiffness contrasts at layer interfaces with continuously varying V_S values. After analyzing these profiles with seismic site response tools: SHAKE2000 and DEEPSOIL, the outcomes were compared.

Overall, a general reduction in interface shear strains and increase in surface spectral accelerations especially at lower periods were observed from the altered (smoothened) profiles than the corresponding profiles with interface contrast. For softer profiles this difference in the computed site factors from the original and the altered profiles was observed to increase up to 20%. This shows the importance of such smoothening of the interface contrasts which may eventually revolutionize the current

practice of collecting V_S measurements and the generation of the 'working' V_S profiles for the site specific response spectral analysis. Additionally, such smoothening of V_S reduces the shear strain at interface locations; smaller shear strains mean reduced system nonlinearity and thus a potential much wider range of applicability of the equivalent linear approach for site response analysis is expected.

CHAPTER 7

REPERCUSSIONS OF NEW SEISMIC SITE FACTORS AND ADRS CURVES

7.1 Introduction

The development of models for site factors for the South Carolina Coastal Plain (SCCP) was described in earlier chapters (Chapters 3 and 4) in detail. It is observed that the newly recommended site factors are different from the site factors currently used by SCDOT (2008a) and the difference varies with the site class. The Acceleration Design Response Spectrum (ADRS) generated based on these new site factors are expected to be different than the ones generated using the current (AASHTO, 2011 and SCDOT, 2008a) site factors used by SCDOT. This could impose a great deal of impact on the seismic demand of existing and to-be-built highway structures (i.e. bridges) which will consequently impact the industry from an economic standpoint.

On this view, an attempt was made to apply the ADRS curves generated from AASHTO (2011) and the new site factors (Chapter 3), on actual highway structures to observe the differences in responses of interest. Thus the goal of this chapter is to implement ADRS curves from both the current (also referred to as "AASHTO, 2011" in this report) and 'Recommended' (i.e. the proposed site factor model as of Chapter 3) methods as one of the inputs on typical highway bridge structures and compare the responses to better understand the effect of the newly developed site factors on structural analysis outcome.

Two sample highway bridges are used in this study as listed in Table 7.1. They are: (1) the "LRFD Example Bridge", a Cast in Place (CIP) concrete box-girder bridge which is design example no. 8 in "Design examples: Recommended LRFD guidelines for the seismic design of highway bridges" (ATC/MCEER, 2003a); and (2) the "Russell Creek Bridge", a to-be-built concrete deck-girder bridge over the Russell Creek River in Charleston County, SC. The LRFD Example Bridge was analyzed using SAP2000 version 14.2.2 (CSI, 2009) for NEHRP site classes C, D and E. For site classes D and E, the site factors corresponding to Charleston, SC are used because these two site classes are the most frequently encountered in that area. For site class C, site factors corresponding to Columbia are used. On the other hand, the Russell Creek Bridge is analyzed using CSiBridge version 15 (CSI, 2011) for site class D (site factors corresponding to Charleston), following the original design consideration. First, ADRS curves corresponding to each site class are generated using the AASHTO (2011) and 'Recommended' site factors. Then, multi-modal response spectrum (MMRS) analysis results obtained by applying the AASHTO (2011) and 'Recommended' ADRS curves on these two bridges were compared at intermediate bents. For the LRFD Example Bridge, forces, moments and displacements are compared at the top and bottom of all four intermediate bent columns. For the Russell Creek Bridge, forces, moments and displacements are compared at the top of the piles of all nine intermediate bents. Two different load combinations are used for each bridge. Finally, a parametric study is conducted for the LRFD Example Bridge to investigate the effect of fixity of the foundations (fixed and springs) because the original LRFD Design Example uses

foundation springs, whereas, SCDOT (2008b) suggests the application of fixed-base for pile foundations. Details are provided in subsequent sections.

Table 7.1: List of sample highway bridges considered.

Sample No.	Bridge name	Location	Number of spans	Deck type	Pier type	Abutment type	Foundation type	Site Class
1	LRFD Example Bridge	Puget Sound region of Washington State	5	Concrete box girder	Two column integral bent	Stub type	Concrete piles	Analyzed for Site Classes C, D and E
2	Russell Creek Bridge	Charleston County, SC	10	Concrete I-girder	Pile bent	Pile bent	Concrete piles	Site Class D

7.2 Generation of ADRS Curves for LRFD Example Bridge Analysis

For the ADRS curve generation, the site factors for Charleston area are selected for the site classes D and E and on the other hand for site class C, Columbia area is selected. The depth to the B-C boundary is assumed as 137 m for Charleston (see reference profile for Charleston in Chapter 2) and 30 m for Columbia area. The depth to the B-C boundary is one of the parameters to be used in the proposed site factor model.

Seven different ADRS curves were used in this chapter. The first three ADRS curves (I, II and III) were generated based on AASHTO (2011) for site classes C, D and E, respectively. ADRS-IV, V, VI and VII were generated based on the newly proposed model for the SCCP (Chapter 3). ADRS-IV is for site class C with V_{S30} of 385 m/s, and depth to soft-rock equal to 30 m, which was assumed for the Columbia area in Chapter 3 (thus both K_{H1} and K_{H2} are equal to 1.0). ADRS-V is for site class D with V_{S30} of 293 m/s, and depth to soft-rock equal to 137 m which was assumed for Charleston in Chapter 2.

ADRS-VI is the maximum possible ADRS curve in site class D using the proposed model and also for the location (i.e. the input motion). This ADRS curve was developed by using the site factor model developed in Chapter 3 and calculating the maximum possible site factors for spectral periods of 0, 0.2 and 1.0 s. The maximum ADRS was used to produce the maximum difference between the 'Recommended' and AASHTO (2011) ADRS curves and observe its impact on the structural response. ADRS-VII is for site class E with V_{S30} of 183 m/s which is the highest V_{S30} within site class E. Based on the simulations conducted in this study, site factors were found to generally decrease with decreasing V_{S30} within site class E. In contrast, the AASHTO (2011) and SCDOT (2008a) site factors are constants considering the middle range values within each site class. Thus by selecting 183 m/s as V_{S30}, the 'Recommended' model is expected to produce the highest response (i.e. ADRS curve and also the structural responses) within site class E. Then by comparing that with the corresponding similarly generated AASHTO (2011) ADRS curve outcome should produce the maximum plausible difference scenario with respect to the structural response.

The ADRS curves (IV, V, VI and VII) generated using the newly recommended site factors for SCCP (Chapters 3) are compared with the ADRS curves (I, II and III) based on the AASHTO (2011) site factors (AASHTO, 2011 and SCDOT, 2008a) in Figure 7.1. Noticeably, in Figure 7.1 ADRS curves II and V fall very close to each other while ADRS curves II and VI and ADRS curves III and VII show larger differences. The amplitude of ADRS-I is greater than ADRS-IV for spectral periods <0.5 s (0-0.5 s) and

lesser for periods beyond 0.5 s. Similar inter-relationships are also expected to be reflected on the respective bridge responses presented in later sections.

Table 7.2 presents the site factors based on the seven ADRS curves generated. The spectral accelerations listed in the Table 7.2, $PGA_{B\text{-}C}$, S_s and S_1, and respective site factors, F_{PGA}, F_a and F_v, corresponding to periods of 0, 0.2 and 1.0 s, respectively. Charleston SEE ground motion (2% probability of exceedance in 50 years) with moment magnitude of 7.3 was generated by Scenerio_PC (Chapman, 2006). This motion was then used to compute the acceleration response at the B-C boundary i.e. $S_{B\text{-}C}$, which are then multiplied by the corresponding site factors to calculate the surface spectral acceleration i.e. S_{site}, for different periods. S_{site} values are then used for ADRS curves generation following procedures defined in SCDOT (2008a) and AASHTO (2011). Figure 7.2 presents the procedure followed to develop three-point ADRS curves. For detailed step-by-step procedures, readers are suggested to visit SCDOT (2008a), from where the figure was originally adopted.

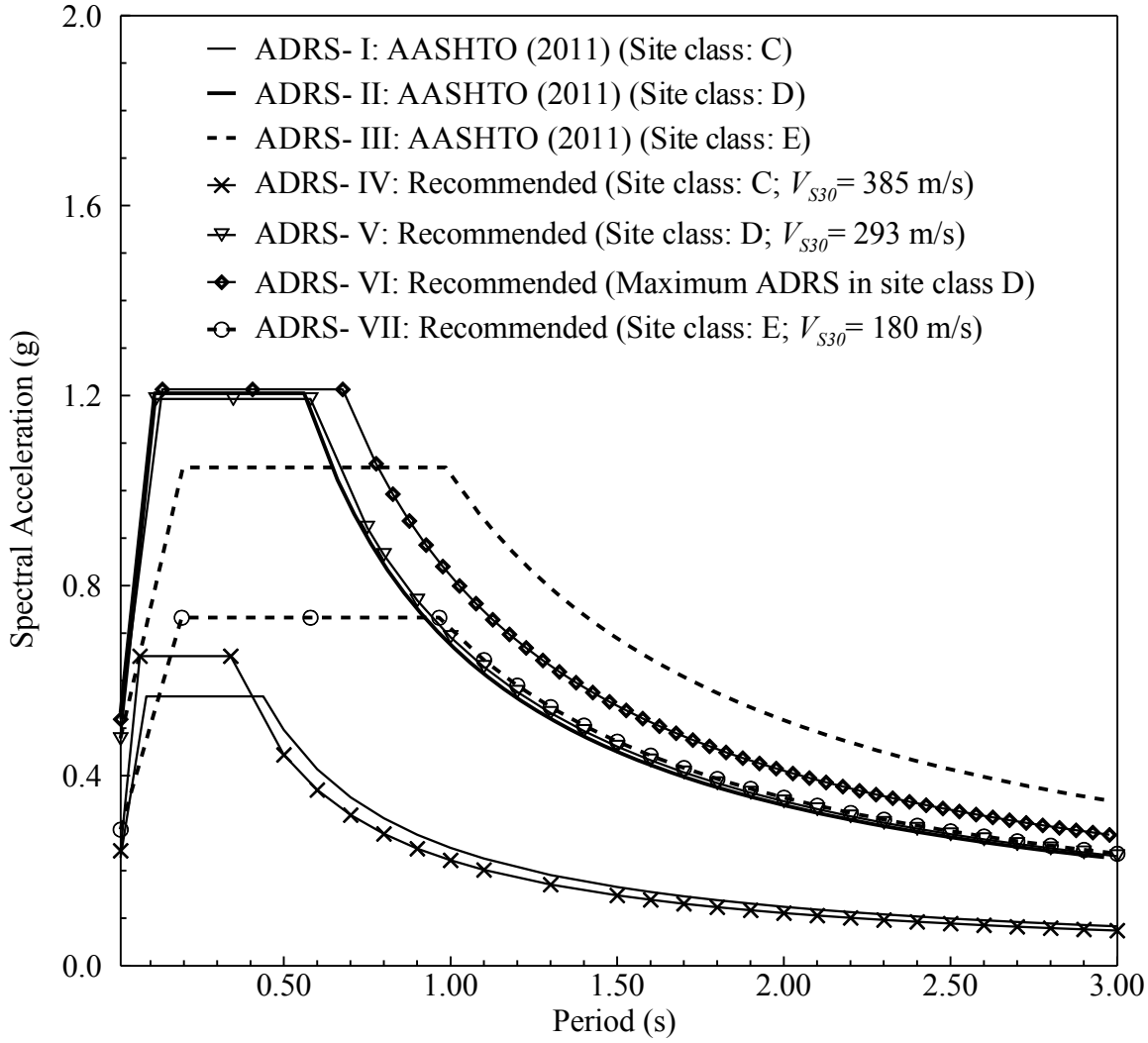

Figure 7.1: ADRS curves used in this Chapter based on an SEE motion for Charleston generated by Scenario_PC.

Table 7.2: Site factors corresponding to all seven ADRS curves considered.

ADRS curve	Spectral accelerations at B-C boundary			Site factors		
	$PGA_{B\text{-}C}$	S_s	S_1	F_{PGA}	F_a	F_v
I	0.190	0.472	0.151	1.200	1.200	1.650
II	0.532	1.165	0.431	1.000	1.034	1.569
III	0.532	1.165	0.431	0.900	0.900	2.400
IV	0.190	0.472	0.151	1.278	1.380	1.475
V	0.532	1.165	0.431	0.877	1.024	1.607
VI	0.532	1.165	0.431	0.975	1.041	1.910
VII	0.532	1.165	0.431	0.539	0.629	1.644

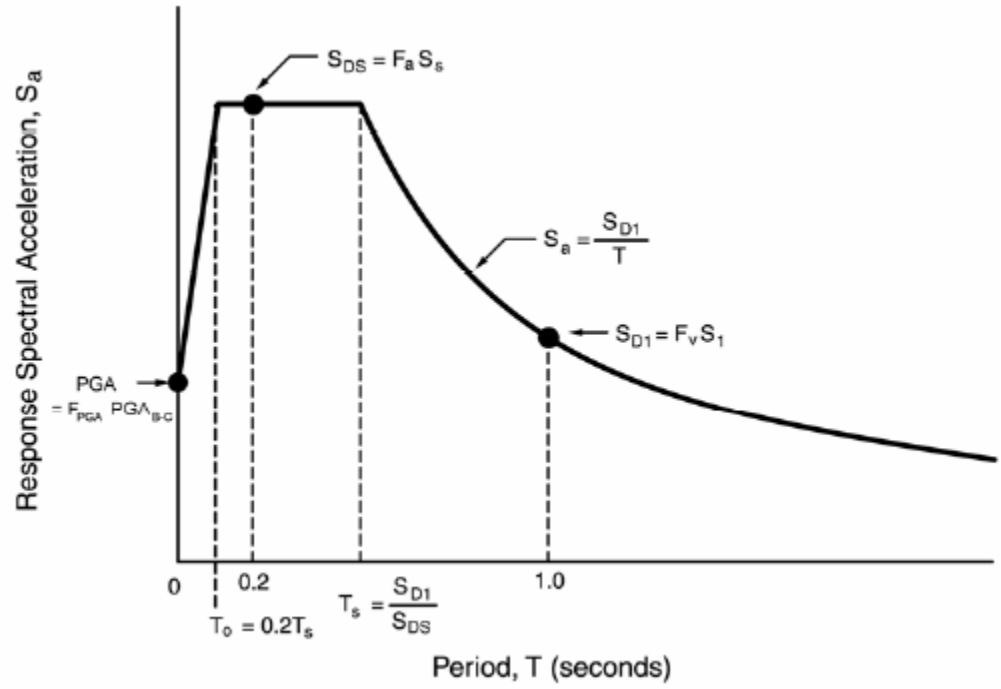

Figure 7.2: Three-point ADRS curve development methodology (SCDOT, 2008a).

7.3 LRFD Example Bridge and Modeling Procedure

7.3.1 Problem description

The bridge is a five-span CIP Concrete Box-Girder with two-column bents and no skew. Each span is about 100 ft long, totaling a 500 ft long structure (abutment to

abutment). A schematic diagram of the bridge is shown in Figure 7.3 and Table 7.3 presents the column and foundation seal height. The four bents are attached to the box-girder superstructure with integrated cross-beams. On the other end, the two circular columns of each bent are integrated with pile caps. Figure 7.4 shows a cross-section of the bridge superstructure-bent system. Stub-type abutment with an assumption of free longitudinal (in global X direction) translation is assumed on both sides of the bridge.

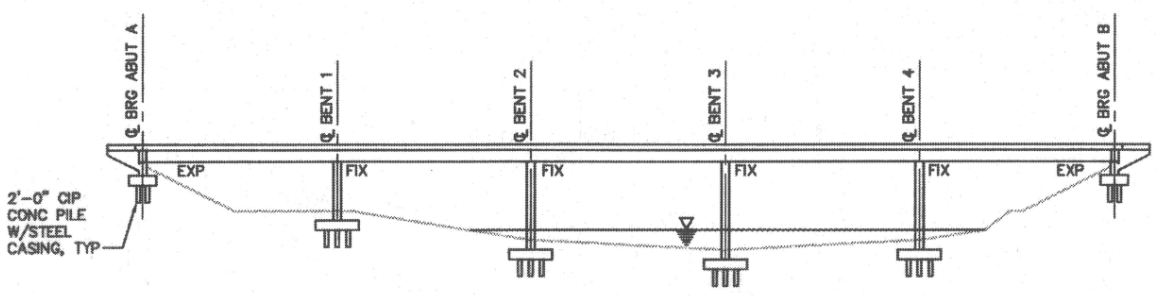

Figure 7.3: Schematic diagram of the LRFD Example Bridge (ATC/MCEER, 2003a).

Table 7.3: Bent details of LRFD Example Bridge.

Bents	Column Height (ft)	Pile Cap Seal Depth (ft)
1	30	3
2	45	4
3	50	6
4	45	4

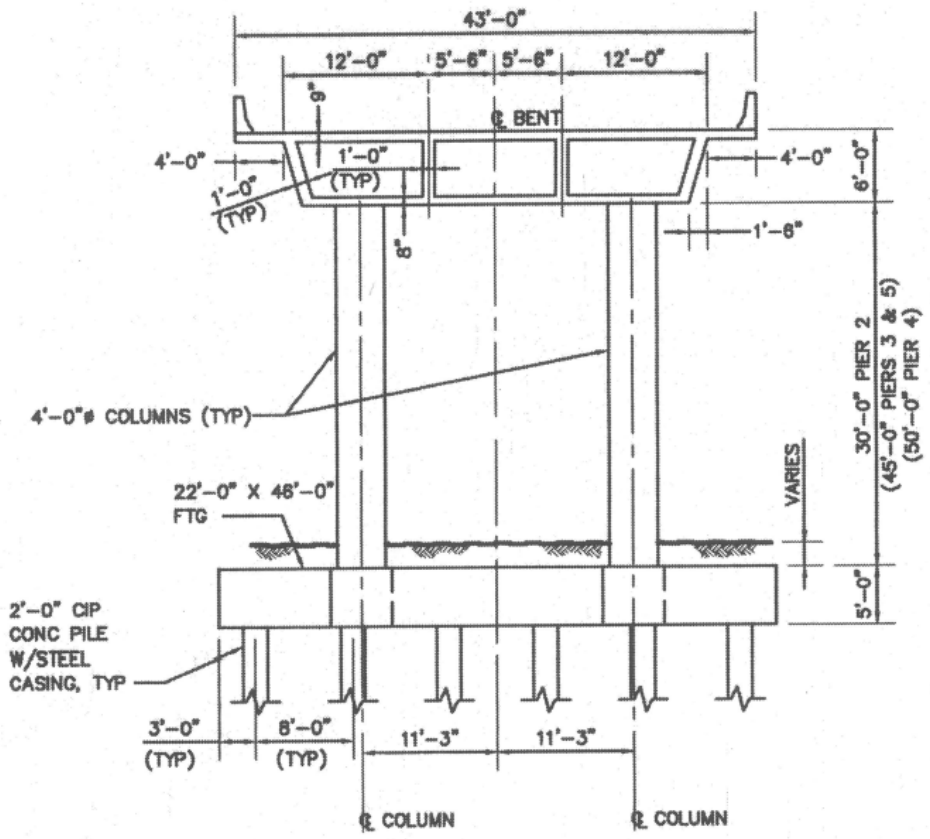

Figure 7.4: LRFD Example Bridge cross-section at an intermediate pier (ATC/MCEER, 2003a).

7.3.2 Analysis tool: SAP2000 version 14.2.2

The three dimensional bridge analysis model of the LRFD Example Bridge is generated with the widely used structural analysis program SAP2000 (CSI, 2009). SAP2000 is capable of performing elastic response spectrum analysis of three dimensional structures, which is the requirement for this study. SAP2000 version 14.2.2 uses object-based-modeling technique. This particular modeling technique involves development of the object based geometry of the structure through an intuitive graphical interface and automatic conversion of the object-based model into the analysis model (i.e., finite element model consisting of the traditional elements and nodes). Smart

graphical environment, helpful object-based modeling option and MMRS analysis capability on three dimensional structures –all together helped make the decision to use SAP2000 for this study.

7.3.3 Modeling in SAP2000

In this sub-section, modeling of the three dimensional bridge system in SAP2000 is described. The numerical model is developed following the procedure described in the design example (Example 8) from the LRFD guidelines (ATC/MCEER, 2003a). In the guidelines, foundation springs are used to represent the piles. However, for this analysis, fixed column bases are used instead due to: (i) SCDOT (2008b) suggests the use of fixed base in the case of deep foundations; (ii) it is a widely accepted procedure among practitioners; and (iii) the use of fixed column base makes the bridge response independent of soil-pile interaction. Therefore, ADRS curves generated for South Carolina conditions could be used for a bridge model that has been borrowed from the West Coast of US without misrepresenting the subsurface soil-pile conditions. In a later part of this chapter, the same bridge is modeled with foundation springs to evaluate the effect of using foundation springs instead of fixed supports. Thus addressing both of the 'with' and 'without' spring modeling approaches helps covering the interest of a wide range of practicing community. However, in this sub-section, discussion is limited to the modeling of the bridge using fixed support. Modeling with foundation springs will be discussed under a parametric study section (Section 7.7.1) to show the effect of support conditions in the computed responses.

Figure 7.5 presents the details of an interior bent including all its frame elements assumed for the SAP2000 model used in the LRFD example (ATC/MCEER, 2003a). This configuration is used to develop the actual bridge model for this study. The model used for this study is presented in Figures 7.6 and 7.7. Figure 7.6 presents a similar bent as drawn in Figure 7.5 modeled in SAP2000, showing the elements and node numbers referred to in this study. Figure 7.7 presents the 3-D frame or 'spine' model of the bridge developed in SAP2000 using fixed base condition.

As is seen in the Figures 7.5, 7.6 and 7.7, the bridge deck section is represented with a straight line consisting of frame elements and individual elements are assigned for the other components of the structure (i.e., cross-beams and columns). For the deck, four elements per span are provided while for the columns, three elements which covers the entire length -as required by SCDOT (2008b) are used. Both the column tops are connected to the cap beam element using rigid links. The bottom nodes of the seal elements are connected to the node with springs by using the rigid link elements again. The only difference from the bent model presented in Figure 7.5 to the model in Figure 7.6 are: the model in Figure 7.6 skips the elements representing the pile cap, the seal element, the rigid link connecting the two columns with the foundation springs and obviously the foundation springs. Rather, the column bases are restrained for displacements at all directions (fixed base) as shown in Figure 7.6.

Necessary frame member properties i.e. cross-sectional area, density and inertias in all three directions are listed in Table 7.4 which is directly adopted from the LRFD guideline's design example. Also adopted from the example are the total dead load

including the self-weight, which is 2.35 kips per linear foot of superstructure, and a foundation spring stiffness of 375 kips/ft, which are used to model the backfill at each of the abutments.

Table 7.4: Section properties for the LRFD Example Bridge model (ATC/MCEER, 2003a).

Properties	Structural Elements				
	Bridge Deck	Bent Cap Beam	Bent Columns	Pile Caps	Seals
Cross sectional area (ft^2)	72	27	12.57	506	196
Moment of inertia in Global X direction, I_X (ft^4)	1,177	10,000	5	109,634	6,403
Moment of inertia in Global Y direction, I_Y (ft^4)	401	10,000	5	89225	89225
Moment of inertia in Global Z direction, I_Z (ft^4)	9,697	10,000	10	20,409	20,409
Density (lb/ft^3)	180	150	150	150	140

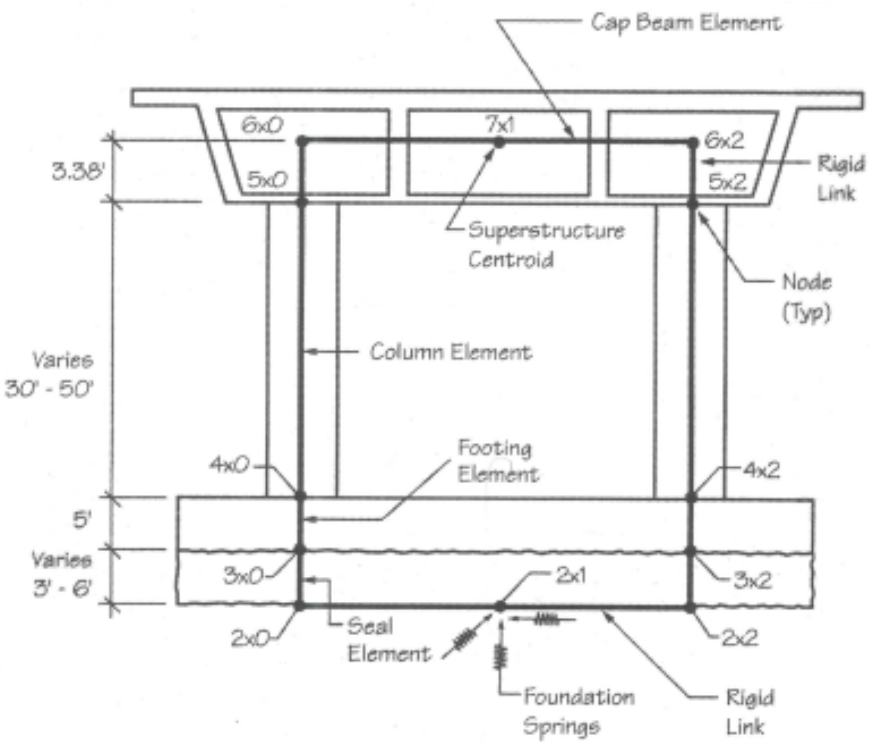

Figure 7.5: Intermediate bent details in the model with foundation springs of LRFD Example Bridge (ATC/MCEER, 2003a).

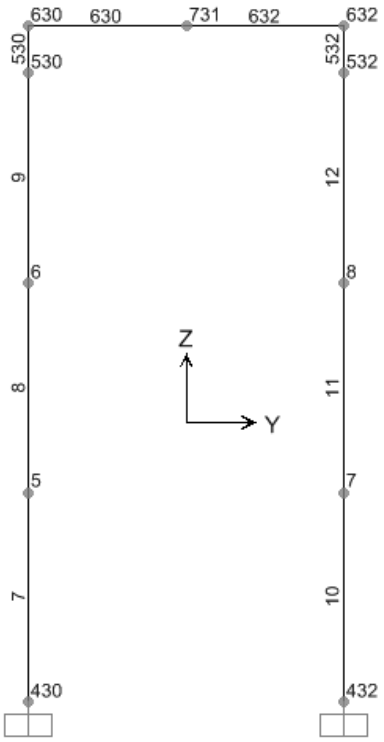

Figure 7.6: Intermediate bent details with frame elements and joint numbers in the case of fixed column base for a sample bent of LRFD Example Bridge (screen capture of SAP2000 model).

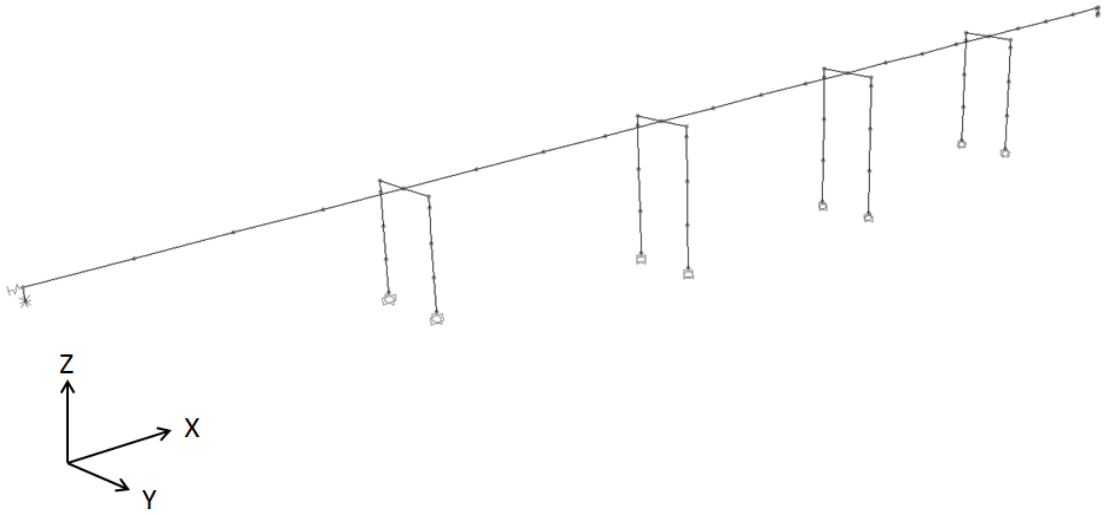

Figure 7.7: 3-D 'spine' model of the bridge in the case of fixed column base of LRFD Example Bridge (screen capture of SAP2000 model).

Readers are suggested to visit the original design example in the LRFD guidelines (ATC/MCEER, 2003a) for further information about the bridge system and the modeling technique.

7.4 LRFD Example Bridge Analysis Procedure

Multi-Modal Response Spectral (MMRS) analysis is selected for this study. The analysis is performed according to the procedure described in LRFD bridge design specification (ATC/MCEER, 2003b) and also meets the requirements defined in the SCDOT Seismic Design Specification of Highway Bridges (SCDOT, 2008b). Because this method considers a wide band of spectral period by producing different structural modes with different periods, the effect of using different ADRS curves will be determined for a broad range of spectral periods.

The major steps of the MMRS analysis procedure are presented below.

Step 1: By performing modal analysis of the entire structure, the mode shapes, corresponding periods and the mass participations are determined. The total mass participation should be above 90% for the considered number of modes. From this requirement, the required number of modes for modal analysis is determined.

Step 2: Using the periods obtained from previous step, corresponding spectral acceleration values are obtained using the ADRS curve that were defined for this analysis. These accelerations are then multiplied with the corresponding mass contributions to calculate the base shears of the different modes.

Step 3: Base shears from all the modes are then combined using several statistical sums and applied at the base of the structure for the seismic analysis of the structure which is a static type analysis in this case.

In MMRS analysis, structural modes of vibrations are estimated in two directions: longitudinal (global X direction) and transverse (global Y direction). Then the Complete Quadratic Combination (CQC) rule is applied to combine the different modal responses and to estimate the 'enveloping' response of the structural components: EQ_{LONG} (for longitudinal direction) and EQ_{TRANS} (for transverse direction). Responses from these two directions are then further combined using the 100%-30% rule (SCDOT, 2008b) to generate the load or displacement combinations to aid in estimating seismic design demands over the structure. The 100%-30% combination rule is defined as:

Table 7.5: Cases considered for the comparison between the AASHTO (2011) and 'Recommended' model.

Case #	Foundation Type	ADRS curve generation	
		ADRS curve used	Site class considered
1	Fixed	I and IV	C[(1)] with V_{S30} = 385 m/s
2	Fixed	II and V	D[(2)] with V_{S30} = 295 m/s
3	Fixed	II and VI	Maximum possible ADRS curve within Site Class D
4	Fixed	III and VII	E[(3)] with V_{S30} = 180 m/s

(1) Site class C is ranging from 360 to 760 m/s
(2) Site class D is ranging from 180 to 360 m/s
(3) Site class E is ranging from 0 to 180 m/s

Load Case 1 or LC1= 100% of EQ_{LONG}+ 30% of EQ_{TRANS}

Load Case 2 or LC2= 30% of EQ_{LONG}+ 100% of EQ_{TRANS}

These LC1 and LC2 are calculated and compared between desired cases for all the intermediate bent columns at the top and bottom positions. This entire process (from model generation to the calculation of LC1 and LC2) is done through a single run with SAP2000 for this study.

Table 7.5 presents the cases considered in estimating the repercussions of the new site factor model. The bridge model developed in Section 7.3.3 with fixed column base-type is selected. The recommended site factor model used to generate ADRS curves IV, V, VI and VII, are applied on the structure and the analysis outcomes are compared with the similar outcomes based on the respective AASHTO (2011) ADRS curves I, II and III.

7.5 LRFD Example Bridge Analysis Results and Discussions

The complete analysis results in terms of forces, moments and displacements at all the columns for Cases #1 to #4 are presented in tabular and graphical formats in the Appendix D. In this section, selected structural responses are reported and compared.

Tables D.1 and D.2 in Appendix D present the natural periods of vibrations and the corresponding mass participations for the first 40 modes (including longitudinal and transverse vibration) for the bridge model with the fixed base and with foundation springs, respectively. For both models, the cumulative mass participation attained above 90% in both directions which is the minimum requirement according to both ATC/MCEER (2003b) and SCDOT (2008b).

Column forces, moments and displacements in longitudinal (global X direction) and transverse (global Y direction) directions are obtained for the load and displacement combinations LC1 and LC2. The AASHTO and 'Recommended' cases are compared in terms of percentage differences in structural response for LC1 and LC2 at the column top and bottom positions and at all the bents and are presented both graphically and tabular formats. This section and Appendix D jointly present all the tables and necessary figures oriented to all of these analysis cases this study involved.

Now the analysis outcomes from the four cases (listed in Table 7.5) oriented to the comparison between the AASHTO (2011) and the 'Recommended' model will be presented. For Case#1, Tables D.3 and D.4 present the comparison of the computed structural responses (forces and moments) based on AASHTO (2011) and 'Recommended' models with respect to the load combinations LC1 and LC2 and their

percentage differences for all the column tops and bottom locations, respectively. In Tables D.5, the comparison between displacements from AASHTO (2011) and 'Recommended' models with respect to the load combinations LC1 and LC2 (and also by stating their percentage differences) for all the column top positions are presented. Similarly, comparisons of the load combinations for forces, moments and displacements are presented in Tables D.6- D.14 for the Cases #2-4.

The overall percentage differences (for LC1 and LC2) between the AASHTO (2011) and the 'Recommended' model obtained from the results presented in Appendix D are summarized as bar chart in Figure 7.8 for deriving the general conclusion. For Case#1, the differences in the column outcomes predicted with the 'Recommended' and the AASHTO (2011) ADRS curves are around 10% with AASHTO (2011) predicting conservative estimate. The AASHTO (2011) ADRS curve fall above the 'Recommended' ADRS curve at periods higher than approximately 0.5 s, as reported earlier (see Figure 7.1). Since the first few modes of vibration of the LRFD design bridge have frequencies greater than 0.5 s and those modes cover the largest share in mass participation in the analysis (see Table D.1), the AASHTO (2011) outcomes are higher than that of the 'Recommended' outcomes. For Case#2, all the column outcomes predicted with the 'Recommended' ADRS curve are only 2-3% higher than that predicted from the AASHTO (2011) ADRS curve (Figure 7.8). Such an observation is expected since the 'Recommended' and the AASHTO (2011) ADRS curves corresponding to the profile with V_{S30} of 295 m/s (site class D) are nearly identical (see Figure 7.1). In Case#3, which compares the maximum possible 'Recommended' ADRS curve within site class D with

the AASHTO (2011) site class D curve, the 'Recommended' produced about 21% higher estimate than the AASHTO (2011) case. This comparison suggests that the design forces/displacements computed using the 'Recommended' curves can be up to 21% higher than that of the AASHTO (2011) curves for similar transportation structures in SCCP (e.g. Charleston). For Case#4, the AASHTO (2011) and the 'Recommended' ADRS curves for site class E are compared. Because the design spectral acceleration for site class E is much higher for the AASHTO ADRS than that of the 'Recommended', the predicted column outcomes are about 31% lower for the 'Recommended' ADRS curve. Thus more economical design is expected in site class E for SCCP locations using the 'Recommended' site factor models.

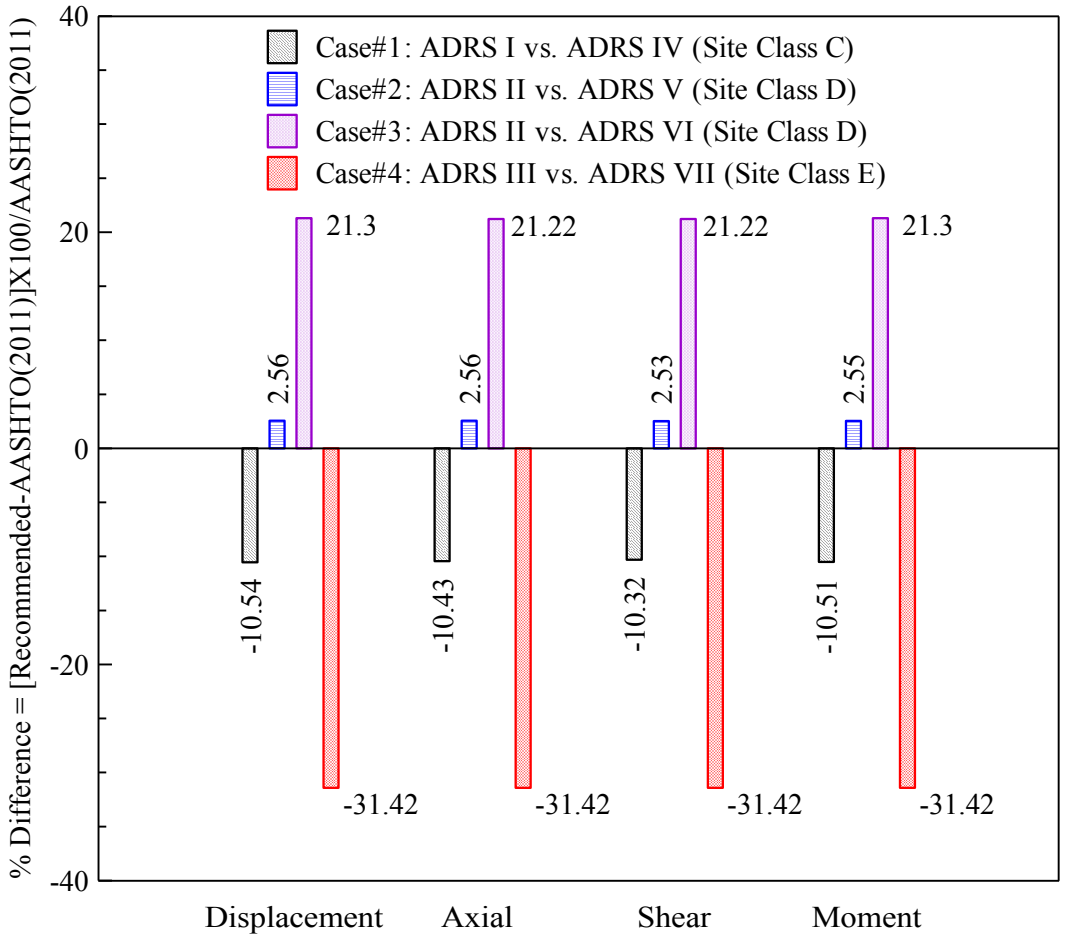

Figure 7.8: Generalized comparison results between the AASHTO (2011) and 'Recommended' model based on column forces, moments or displacement combinations LC1 and LC2.

7.6 Parametric Study

Parametric studies are performed in this section to investigate the effect of different techniques that can be used to model the bridge foundation in SAP2000. Discussed in this section are: adjustments made to the previous bridge model to convert the foundation system to springs; development of a set of parametric test cases; and finally presented are the parametric study outcomes and related discussions.

7.6.1 Addition of foundation springs

This time the same bridge (developed in Section 7.3.3) is taken and the fixed column bases are modified to include the foundations springs. This modeling modification of the same three dimensional bridge system in SAP2000 is described in this sub-section.

To include spring elements in the bridge model, the procedure described in the LRFD example (ATC/MCEER, 2003a) is followed. As discussed in the Section 7.3.3 of this chapter and also presented in Figure 7.5, all the required elements are added to the existing SAP2000 model systematically. First, all the restraints at the foundation base nodes are removed, then the elements representing the pile cap and foundation seal are introduced, and finally the seal elements are connected by rigid links to a node to which all the foundation springs are then attached. The foundation springs are consisted of three translational and three rotational springs. Figure 7.9 presents an interior bent modeled in SAP2000 environment with foundation springs and Figure 7.10 shows the whole 3-D frame or 'spine' model of the bridge including the foundation springs with their directions. The frame member properties (for the added frame member also) are

presented in Tables 7.3 and 7.4 while the foundation spring stiffness properties are listed in Table 7.6, which are directly adopted from the LRFD guideline's design example (ATC/MCEER, 2003a). Readers are suggested to visit the original design example in the LRFD guidelines (ATC/MCEER, 2003a) for further information about the bridge system and modeling technique.

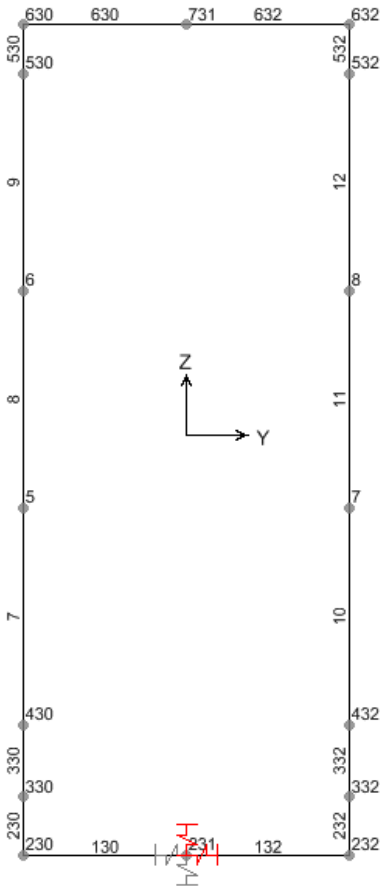

Figure 7.9: Intermediate bent details with frame elements and joint numbers with foundation springs for a sample bent (screen capture of SAP2000 model).

Table 7.6: Foundation spring stiffness.

	Translational stiffness			Rotational stiffness		
	Axial	Longitudinal	Lateral	Axial	Longitudinal	Lateral
Global	UY	UX	UZ	RY	RX	RZ
Pier #	K_{11} (k/ft)	K_{22} (k/ft)	K_{33} (k/ft)	K_{44} (k-ft/rad)	K_{55} (k-ft/rad)	K_{66} (k-ft/rad)
1	7.30E+04	0.00E+00	1.60E+05	0.00E+00	2.99E+07	0.00E+00
2	3.21E+05	3.33E+05	2.47E+05	1.19E+07	4.74E+07	1.19E+09
3	3.31E+05	3.43E+05	2.73E+05	1.31E+07	5.24E+07	1.23E+09
4	4.47E+05	4.59E+05	2.86E+05	1.37E+07	5.50E+07	1.68E+09
5	3.31E+05	3.43E+05	2.73E+05	1.31E+07	5.24E+07	1.23E+09
6	7.30E+04	0.00E+00	1.60E+05	0.00E+00	2.99E+07	0.00E+00

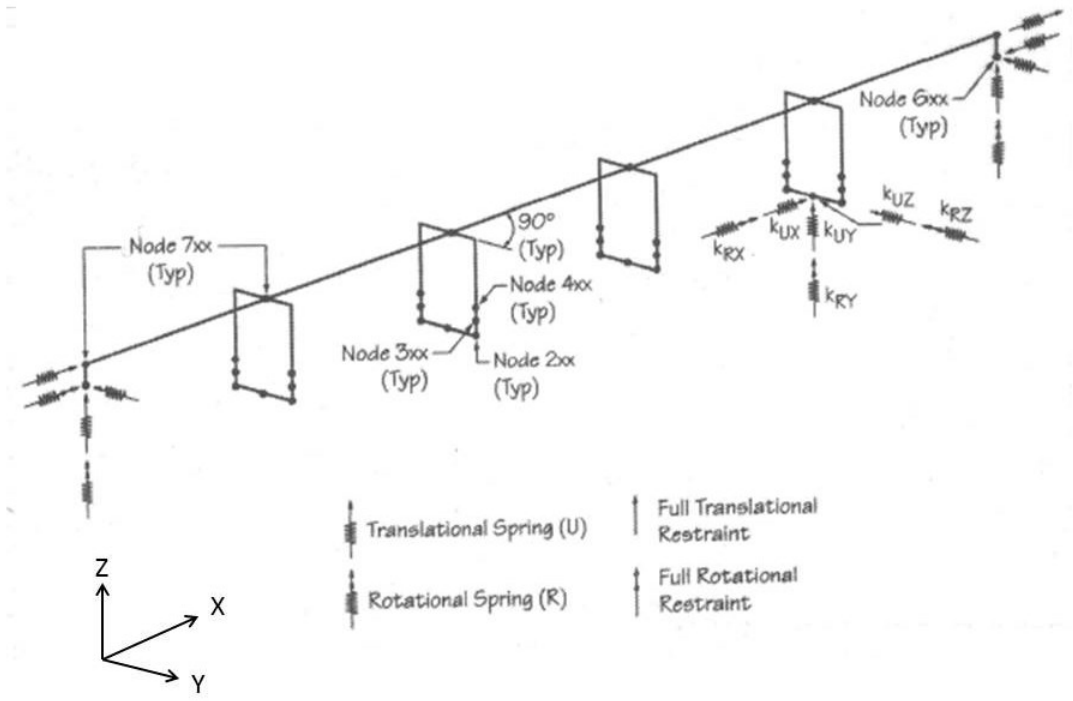

Figure 7.10: 3-D 'spine' model of the bridge in the case of model with foundation spring directions (ATC/MCEER, 2003a).

7.6.2 Test cases considered

The numerical test cases considered in this section are presented in Table 7.7. The objective of these tests is to study the effect of using foundation springs instead of fixed base in the analysis. The ADRS curves used for the parametric studies are: IV, V, VI and VII. These ADRS curves are applied on both bridge models (with fixed support and with foundation springs) and the responses are compared. The numerical tests corresponding to these four ADRS curves are referred to as Test # 1, 2, 3 and 4, respectively. The site class and the V_{S30} used for developing corresponding ADRS curves are shown in Table 7.7. It is worth noting that: (i) both 'with' and 'without' spring bridge models are subjected to the ADRS curves developed considering typical V_{S30} values for corresponding site classes and (ii) the foundation springs are adopted from the LRFD guideline's design example (ATC/MCEER, 2003a) which are developed for a different site (the Puget Sound region of Washington State). Therefore, the conclusions made based on the responses computed 'with' spring bridge model in this study are expected to have a bias.

Table 7.7: Parametric study test cases.

Test #	Parameters considered in the compared cases					
	Case #1			Case #2		
	Foundation Type	ADRS curve generation		Foundation Type	ADRS curve generation	
		ADRS curve used	Site class considered		ADRS curve used	Site class considered
1	Fixed	IV	C[(1)] with V_{S30} = 385 m/s	Foundation Springs	IV	C[(1)] with V_{S30} = 385 m/s
2	Fixed	V	D[(2)] with V_{S30} = 295 m/s	Foundation Springs	V	D[(2)] with V_{S30} = 295 m/s
3	Fixed	VI	Maximum possible ADRS curve within Site Class D	Foundation Springs	VI	Maximum possible ADRS curve within Site Class D
4	Fixed	VII	E[(3)] with V_{S30} = 180 m/s	Foundation Springs	VII	E[(3)] with V_{S30} = 180 m/s

(1) Site class C is ranging from 360 to 760 m/s
(2) Site class D is ranging from 180 to 360 m/s
(3) Site class E is ranging from 0 to 180 m/s

7.6.3 Parametric study results and discussions

This sub-section presents the parametric study (test cases presented in Table 7.7) outcomes. The natural periods of vibrations and the corresponding mass participations for the first 40 modes (including longitudinal and transverse vibration) for the bridge model described in Section 7.7.1 is presented in Table D.2 in Appendix D. The cumulative mass participation attained is above 90% in both directions which is the minimum requirement according to both ATC/MCEER (2003b) and SCDOT (2008b).

For each analysis, column forces (Shear X, Shear Y and Axial), moments (Moments X and Moment Y) and displacements in longitudinal (global X-direction) and transverse (global Y-direction) directions are obtained with the load and displacement combinations LC1 and LC2. The foundation spring model is compared to the fixed support model in terms of the percentage difference in the column forces and moments at the column top and bottom positions and the displacement at the column top position only, at each bent and for each of the load cases LC1 and LC2 and are presented in Tables D.15 - D.26.

For Case#1, Tables D.15 and D.16 present the comparison of the computed structural responses (forces and moments) based on with spring and fixed based models with respect to the load combinations LC1 and LC2 and their percentage differences for all the column tops and bottom locations, respectively. Table D.17 presents similar comparison for the displacements at the columns tops. Similarly, comparisons of the load combinations for forces, moments and displacements are presented in Tables D.17- D.26 for the Test cases #2-4.

Summarized in Table 7.8 are the approximate ranges of percentage difference in column response (force, moment and displacement) for all four numerical tests, based on the responses tabulated in the Appendix D. The percentage difference values indicate the sensitivity of the MMRS analysis outcomes to the foundation type and support condition (i.e., comparison between the cases with fixed column bases and the cases with foundation springs). For the Tests #1- #4, the differences in the computed outcomes are between -6.0 and 7.5% for the combinations LC1 and LC2 which indicates that the computed responses are less sensitive to the support condition of the columns for the loading and soil conditions considered in this study. Therefore, the simplified approach (fixed column base) used in this study gives reasonable results.

Table 7.8: Parametric study results. Comparison was done based on column forces, moments or displacement combinations i.e. LC1 and LC2.

Test #	Parameters considered in the compared cases						% Difference[3] between Case #1 and Case #2 (Approx.)
	Case #1			Case #2			
	Foundation Type	ADRS curve generation		Foundation Type	ADRS curve generation		
		ADRS curve used	Site class considered		ADRS curve used	Site class considered	
1	Fixed	IV	C[1] with V_{S30} = 385 m/s	Foundation Springs	IV	C[1] with V_{S30} = 385 m/s	-5.5 to 7.5%
2	Fixed	V	D[2] with V_{S30} = 295 m/s	Foundation Springs	V	D[2] with V_{S30} = 295 m/s	-6 to 6%
3	Fixed	VI	Maximum possible ADRS curve within Site Class D	Foundation Springs	VI	Maximum possible ADRS curve within Site Class D	-6 to 4%
4	Fixed	VII	E[3] with V_{S30} = 180 m/s	Foundation Springs	VII	E[3] with V_{S30} = 180 m/s	-6 to 2%

(1) Site class C is ranging from 360 to 760 m/s
(2) Site class D is ranging from 180 to 360 m/s
(3) Site class E is ranging from 0 to 180 m/s
(4) % Difference (in column Forces, Moments or Displacement combinations: LC1 and LC2) = [Case #2- Case #1] X 100/ Case #1. A negative value represents greater Case #2 outcomes.

7.7 Russell Creek Bridge Analysis

This section covers the analysis of a 510 ft long concrete I-Girder bridge, the Russell Creek Bridge, in Charleston County, SC. This to-be-built highway structure on SC 174 will be constructed over the Russell Creek River. A CSiBridge model of Russell Creek Bridge developed by the SCDOT engineers during its design phase was adopted in this study to perform MMRS analysis. The analysis results obtained by applying the ADRS curves generated using the AASHTO (2011) and 'Recommended' factors are compared.

7.7.1 Generation of ADRS curves for Russell Creek bridge analysis

During the design phase of the Russell Creek Bridge, the ADRS curves corresponding to the FEE and SEE motions based on AASHTO (2011) site factors were generated and used. Figure 7.11 presents the 'Design' (AASHTO, 2011 factors) and 'Recommended' (based on Chapter 3) ADRS curves based on factors for both FEE and SEE cases and used in this study. Table 7.9 presents the spectral accelerations ($PGA_{B\text{-}C}$, S_s and S_1) and the site factors (F_{PGA}, F_s and F_a) corresponding to 0, 0.2 and 1.0 s periods, respectively, from which the ADRS curves are generated. This bridge site has a measured average shear wave velocity in the upper 30 m (V_{S30}) of 218 m/s which indicates the bridge site is in site class D (SCDOT, 2008a). As is seen in Figure 7.11, in the case of FEE motions, the both the 'Design' and 'Recommended' lines are close to each other over the entire period range. On the other hand, in the case of SEE motions, the 'Design' line is much higher than its 'Recommended' counterpart.

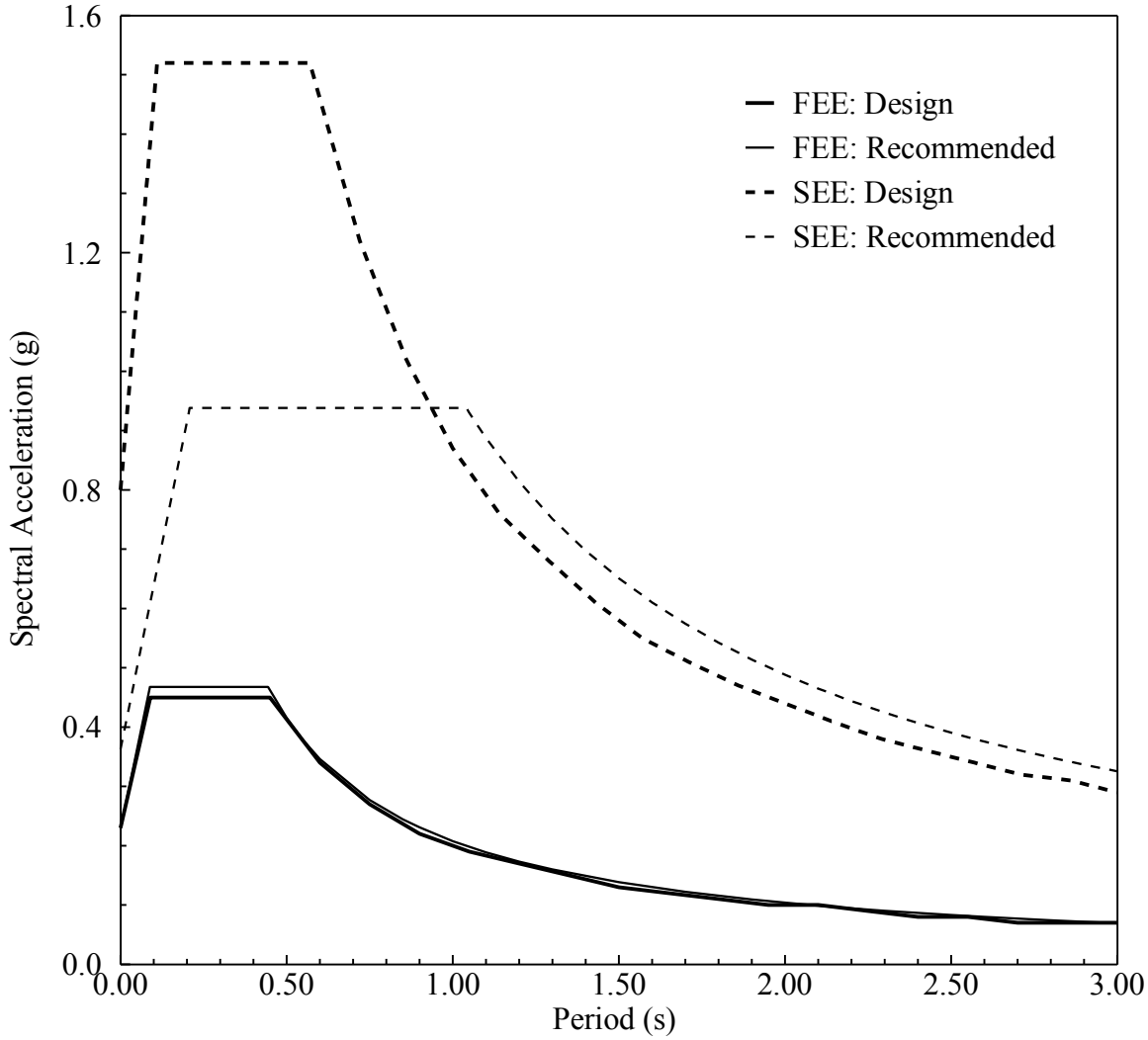

Figure 7.11: ADRS curves used for Russell Creek Bridge.

Table 7.9: Required parameters to generate site factors.

ADRS #	Type	V_{S100ft} (Site Class)	Spectral accelerations at B-C boundary			Site factors		
			PGA_{B-C}	S_s	S_1	F_{PGA}	F_a	F_v
1	FEE: Design	218 m/s (Site Class: D)	0.152	0.288	0.084	1.515	1.560	2.400
2	FEE: Recommended					1.503	1.622	2.474
3	SEE: Design		0.803	1.522	0.581	1.000	1.000	1.500
4	SEE: Recommended					0.452	0.616	1.681

7.7.2 Problem description

A schematic diagram and cross section of the Russell Creek Bridge are shown in Figures 7.12 and 7.13, respectively. The bridge is a concrete I-Girder bridge with 10 spans supported on 9 intermediate bents and pile-bent type abutments at both ends. Span length varies from 45 ft to 55 ft. The bents consist of 3 to 7 concrete piles. Bents #1 through #8 have 7 piles made of 24 inch (square) pre-stressed concrete while Bent #9 and the abutments are supported by 3 drilled shafts of 42 inch diameter. Table 7.10 presents the interior bent details including the pile lengths. Bridge I-Girders are integrated with the deck slab above. The super-structure dead load is transmitted to the piles through the bent cap beams on which the I-Girders are supported through the bearings. These elastomeric type bearings are assigned fixity for translations and rotations in all directions at the abutments while at the interior bents only rotations are allowed.

Table 7.10: Bent details of Russell Creek Bridge.

Bent #	Pile length (ft)	Number of Piles in the bent
1	32.0	7
2	31.9	7
3	32.9	7
4	33.3	7
5	33.8	7
6	33.8	7
7	33.0	7
8	32.3	7
9	46.5	3 (Drilled shaft)

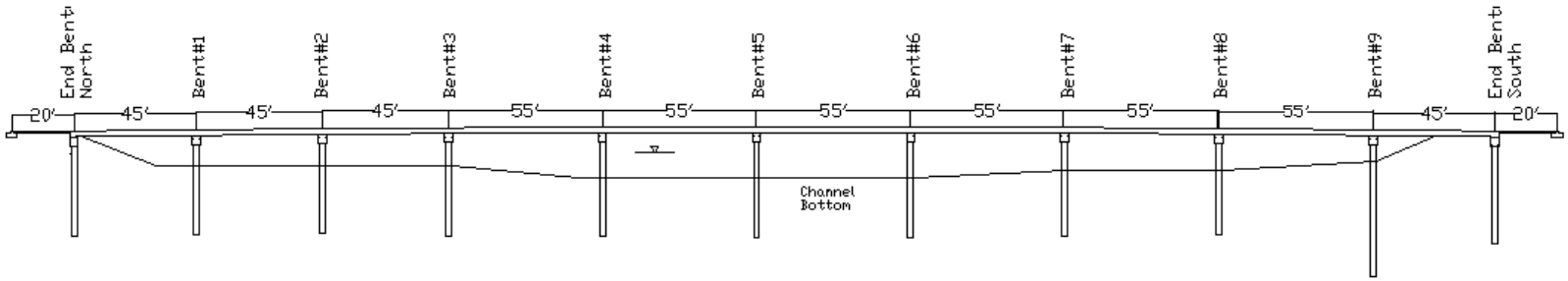

Figure 7.12: Schematic diagram of Russell Creek Bridge.

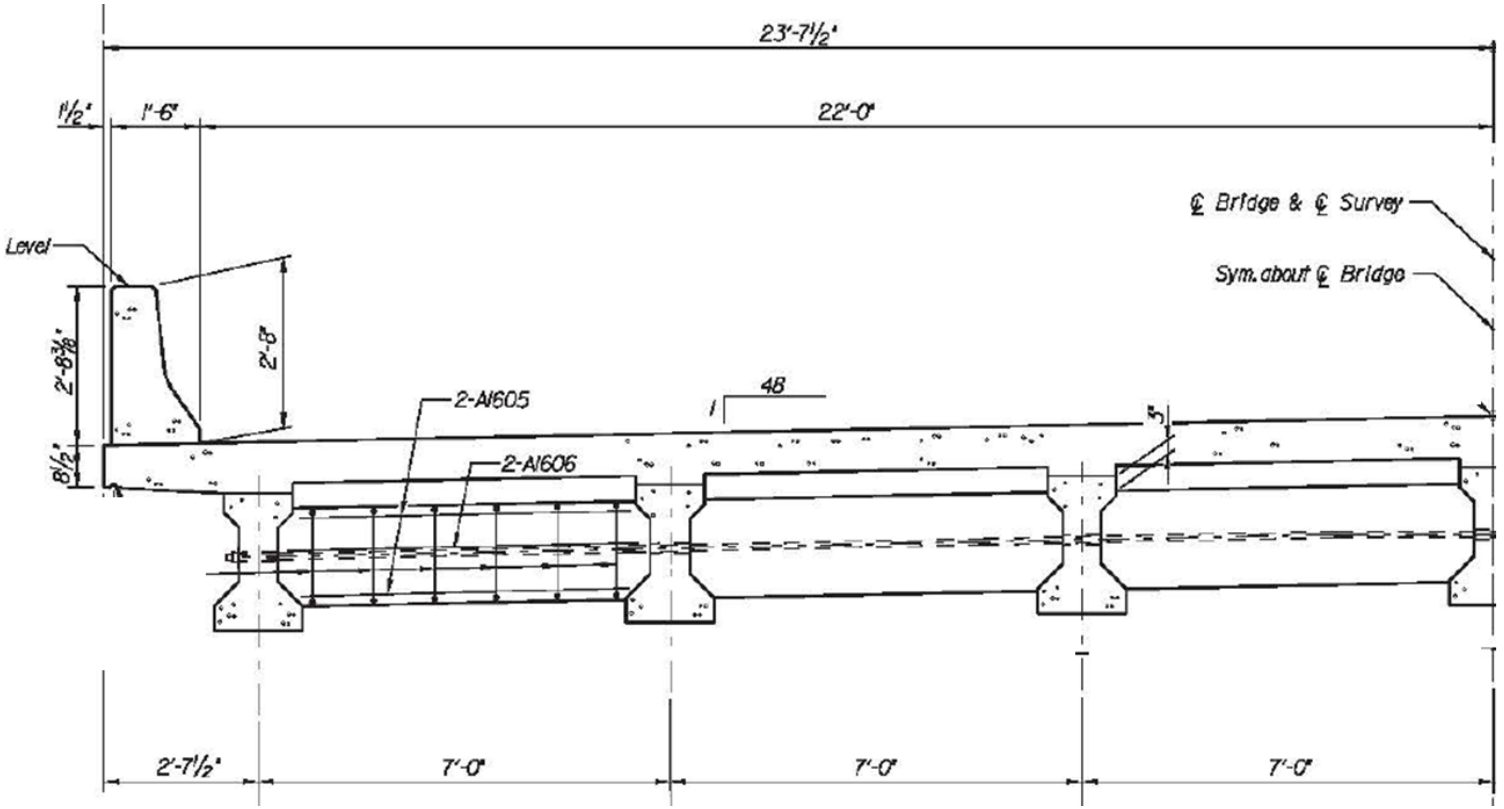

Figure 7.13: Russell Creek Bridge deck cross-section at an interior bent.

7.7.3 Analysis tool (CSiBridge version 15.0) and model generation

CSiBridge, a special purpose software for modeling, analysis, and design of bridges, is used to analyze the Russell Creek Bridge as the original analyses of this bridge is also conducted using CSiBridge before constructing it. This software is widely used by practicing engineers, including the SCDOT.

Figures 7.14 and 7.15 present the intermediate bent details and 3-D model of the bridge in CSiBridge, respectively. In the 3-D spine model in Figure 7.15, the bridge deck including the I-Girders are represented by the bridge layout line (layout lines define the bridge alignments in CSiBridge) made of frame elements which extend longitudinally in the global X direction. As shown in Figure 7.14, the girder bottom is resting on the bearings placed on top of the bent cap beams. The cap beam is represented by frame elements and is connected to the bearings by rigid links. At the bents, piles are represented with frame elements with fixed bases. All the frame member properties such as cross-sectional area, density and inertias in all three directions of the girder, cap, beam and the pile sections are listed in Table 7.11.

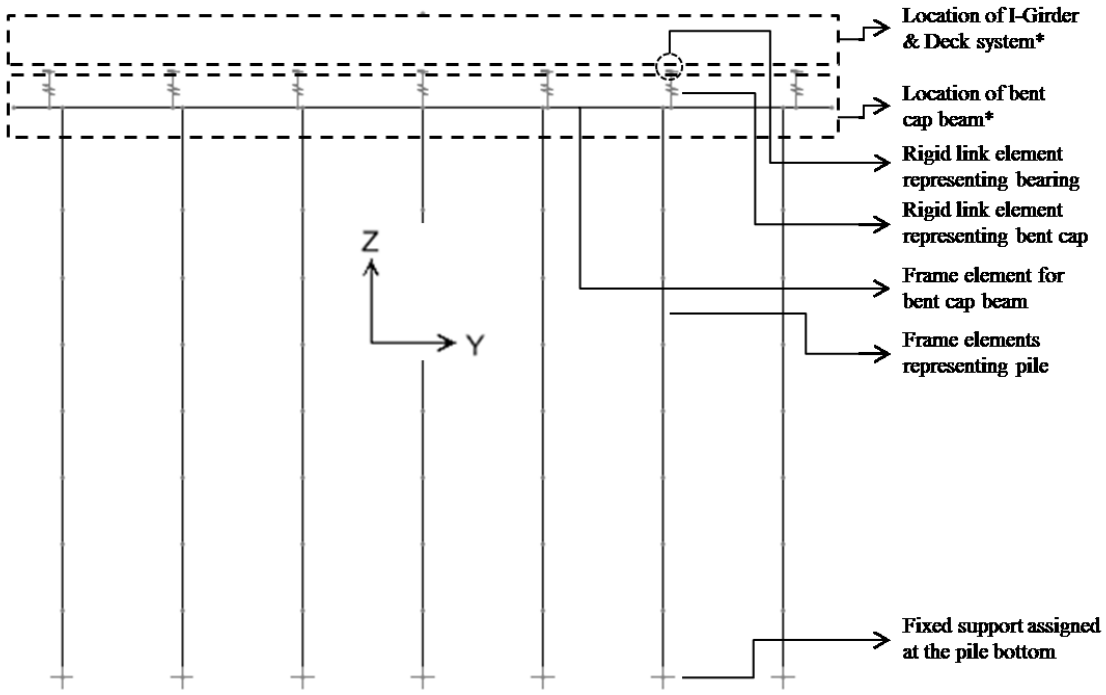

*Broken lines are drawn externally (outside of CSiBridge environment) to locate the specific bridge elements.

Figure 7.14: Intermediate bent details of Russell Creek Bridge (screen capture from CSiBridge model).

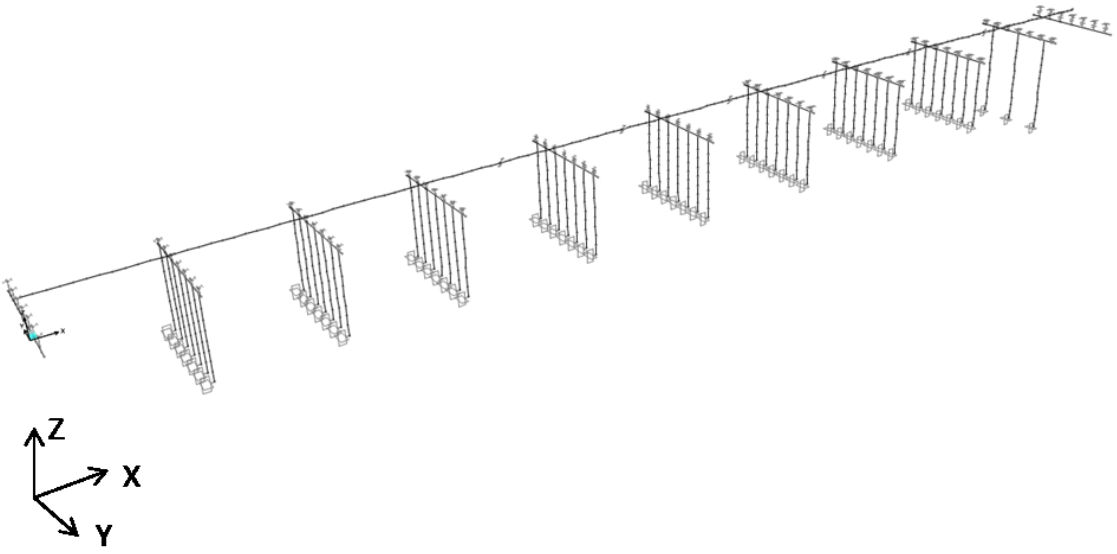

Figure 7.15: 3-D 'spine' model of Russell Creek Bridge (screen capture from CSiBridge model).

Table 7.11: Section properties used for Russell Creek Bridge model.

Properties	Structural Elements			
	I-Girder (Each)	Bent Cap Beam	Pile details	
			24" (square section) Pre-stressed Concrete Pile	42" Dia. Drilled Shaft
Cross sectional area (ft^2)	2.31	14.00	3.99	8.67
Moment of inertia in Global X direction, I_X (ft^4)	0.37	18.67	2.25	23.93
Moment of inertia in Global Y direction, I_Y (ft^4)	1.28	27.19	1.33	5.98
Moment of inertia in Global Z direction, I_Z (ft^4)	0.25	14.29	1.33	5.98
Density (lb/ft^3)	150.00	150.00	150.00	150.00

7.7.4 Results and discussions

Similar to the LRFD Example Bridge, MMRS analysis is performed for the Russell Creek Bridge. In the modal analyses, cracked section stiffness properties are used for the concrete section.

The bridge responses (forces, moments and displacements) at the top of the middle pile for all nine bents were computed by applying both 'Design' and 'Recommended' FEE and SEE ADRS curves in the longitudinal and transverse directions. The analyzed results from the 'Design' and 'Recommended' cases are compared (with respect to both FEE and SEE) to understand the effect of new site factors on the to-be-built bridge. Table D.27 in Appendix D presents the natural periods of vibration and the corresponding mass participations for the first 60 modes (longitudinal and transverse) of vibration. It was confirmed that the cumulative mass participation attained was above 90% in both directions (translation in Global X and Y).

Similar to the LRFD Example Bridge study, the forces, moments, and displacements in both longitudinal (global X direction) and transverse (global Y direction) directions are obtained and then the load and displacement combinations LC1 and LC2 are computed. These recordings are taken at each intermediate bent at the middle piles where the pile and cap beam connects to each-other. The percentage differences in LC1 and LC2 are calculated for all the cases and compared in Tables D.28 – D.31 in Appendix D, similar to Section 7.5.

Table D.28 present the comparison between analyses results (forces and moments) from the 'Design' and 'Recommended' FEE cases with respect to the load combinations LC1 and LC2 and also by stating their percentage differences for all the column tops and bottoms. Similarly, presented in Table D.29 are the displacements from the 'Design' and 'Recommended' FEE cases with respect to the load combinations LC1 and LC2 and also their percentage differences for all the column top positions. Similarly, the comparisons in the cases of SEE motion are presented in similar Tables D.30 - D.31 in Appendix D.

The overall percentage differences (for LC1 and LC2) between the responses computed based on ADRS curves with 'Design' and 'Recommended' factors presented in Appendix D are summarized as form of a bar chart in Figure 7.16 for deriving the general conclusion. In the case of FEE motion, the ADRS curves with 'Design' and 'Recommended' factors produced almost identical results with a margin of 1-4% with respect to the percentage difference in forces, moments and displacements. On the other hand, the results for 'Design' are found to be conservative with a large margin of 38-50%

than that of ‘Recommended’ for the SEE cases. As the FEE based ‘Design’ and ‘Recommended’ ADRS curves are similar (Figure 7.11), it was expected that MMRS analysis would also produce similar responses. In contrast, the SEE based ‘Design’ and ‘Recommended’ ADRS curves showed significant difference and similar trend is observed in the MMRS analysis outcomes.

Therefore with respect to FEE motion, the demand estimated through the ‘Design’ curve satisfied the demand estimated using the ‘Recommended’ model. The ‘Recommended’ model would have produced a considerably smaller design demand in the case of SEE motion for this site condition, and therefore a more economic design.

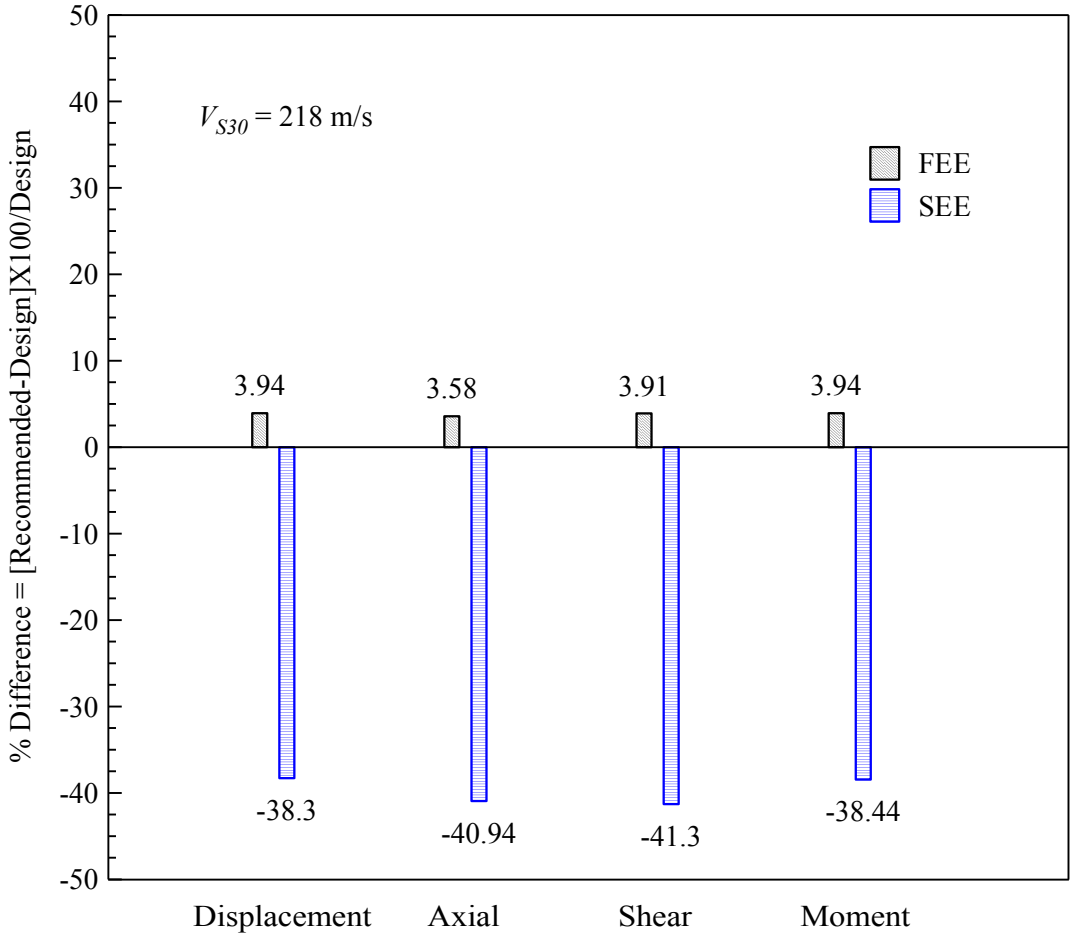

Figure 7.16: Generalized comparison of structural responses obtained using the 'Design' and 'Recommended' ADRS curves based on the column forces, moments or displacement combinations LC1 and LC2.

7.8 Conclusions

The LRFD Example Bridge and Russell Creek Bridge were analyzed for seismic performance using SAP2000 and CSiBridge, respectively, by applying the ADRS curves generated based on the 'Recommended' and the current (AASHTO, 2011) site factors. Based on the computed results, the following observations were made:

LRFD Example Bridge:

- For site class C (in Columbia using V_{S30} of 385 m/s), the AASHTO (2011) produced conservative results compared to the 'Recommended' model. This indicates further cost reduction is possible if the 'Recommended' factors are used.
- For site class D (in Charleston), the 'Recommended' model is expected to generate more conservative design forces/moments and displacements of the structural components than the AASHTO (2011) would have. Two different cases modeled based on the 'Recommended' factors produced seismic demands from 2 to 3% (using V_{S30} of 295 m/s) to 20-22% (for maximum ADRS within site class D) more than the respective cases modeled with AASHTO (2011) ADRS curves.
- For site class E (in Charleston using V_{S30} of 180 m/s), the cases based on 'Recommended' factors predicted approximately 31% less design forces/moments and displacements of the structural components than the AASHTO (2011) would have required, possibility for a more economical design option for the softer sites in SCCP.
- A sensitivity study was performed to investigate the effect of fixed versus spring foundation types. Results from both the approaches fell within a close range proving no practical bias on the analysis outcomes. Thus this sensitivity study confirmed that the MMRS analysis outcomes using fixed column base are valid.

Russell Creek Bridge:

- In the case of Russell Creek Bridge, a Site Class D, the analysis with the 'Recommended' site factors produced similar (1-4%) responses (forces, moments and displacement) compared to that of the AASHTO (2011) site factors in the case of FEE motion. This indicates that the original design is satisfactory with respect to the new site factors. However, in the case of SEE motion, the analysis with the 'Recommended' factors produced significantly lower (38-50%) responses. Therefore, the use of 'Recommended' site factors has the potential to significantly reduce the project cost for bridges similar to the Russell Creek Bridge in Site Class D.

CHAPTER 8

APPLICATIONS OF SITE RESPONSE ANALYSIS

This author was part of two additional site response studies: (i) the seismic site response analysis of unsaturated soils; and (ii) the effect of ground motions with different moment magnitudes over the computed surface response. In both studies, performing site response analysis using several programs such as: DEEPSOIL, DMOD2000 and OpenSees were the responsibilities of this author.

8.1 Ravichandran et al. (2012 and 2015)

In this study, a numerically stable and computationally efficient finite element model for analyzing dynamic response of unsaturated soil profiles in terms of total stresses is introduced. The highly nonlinear, fully-coupled governing differential equations are simplified by neglecting the relative accelerations and velocities of the pore fluids and the simplified formulation is improved by incorporating an external viscous damping formulation for unsaturated soil. The surface spectral accelerations computed using the proposed model (TeraUDysac simulation) is then qualitatively compared with that of DEEPSOIL and PLAXIS as no experimental data sets for unsaturated soil conditions were available for comparison and/or validation of this new model. As part of the group, this author was responsible for performing the DEEPSOIL simulations.

Figure 8.1 presents the finite element mesh of a soil-pile system which was simulated with the newly proposed unsaturated soil model. Node N3 represents the free-filed condition and the spectral accelerations computed from each of DEEPSOIL,

PLAXIS and the new unsaturated model (TeraUDysac) were compared at that point of the model. The engineering properties of Minco silt were used for the soil profile. The Figure 8.2 presents the ground motion used in the study.

Figure 8.3(a) and 8.3(b) present the comparison of the computed surface spectral accelerations from the DEEPSOIL, PLAXIS and the new unsaturated model (TeraUDysac) for two degrees of saturation: 70% and 20%, respectively. Based on the these comparisons, while the TeraUDysac predictions are close to the PLAXIS predictions, the DEEPSOIL predictions are much higher than that of other two codes. The possible reasons are: (i) none of the PLAXIS and DEEPSOIL programs have capabilities to model unsaturated soil conditions, and (ii) the one-dimensional approximation is DEEPSOIL while both the PLAXIS and TeraUDysac approximates two-dimensional plain strain condition.

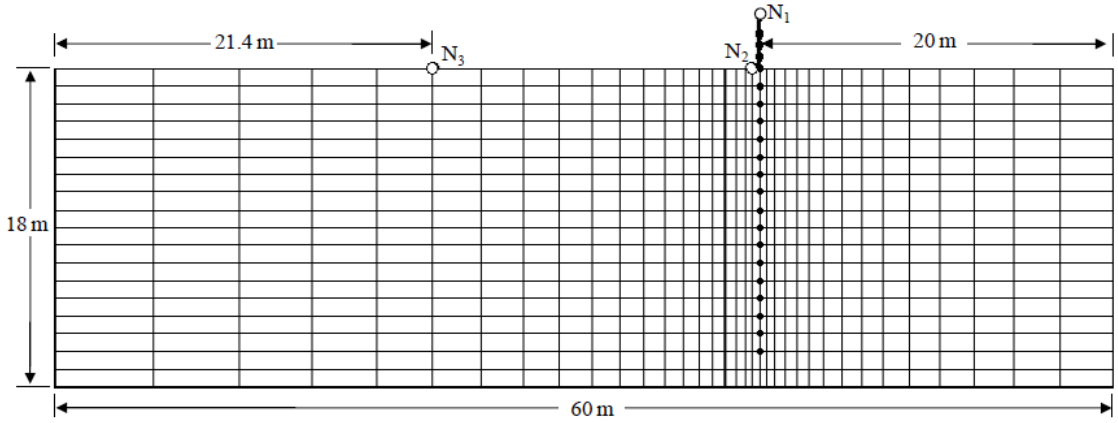

Figure 8.1: Finite element mesh showing the nodes where responses were recorded (Ravichandran et al., 2013).

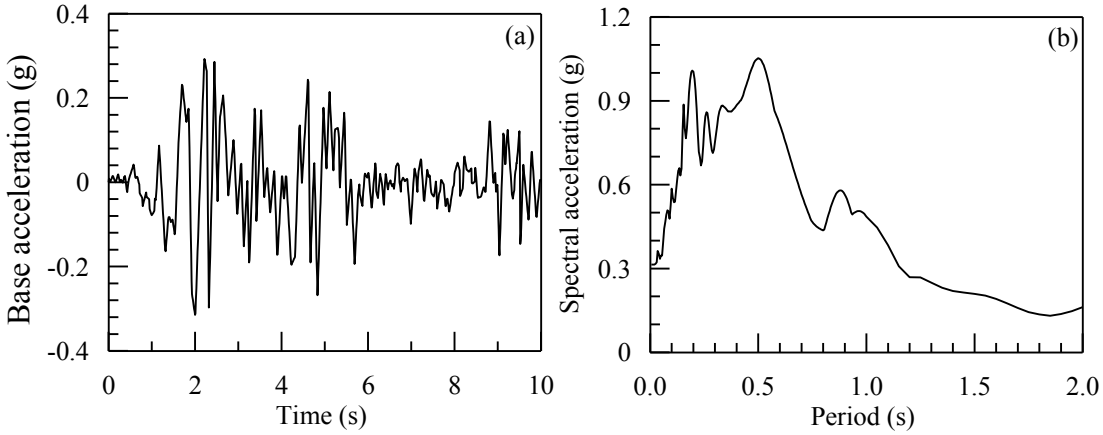

Figure 8.2: Base shaking (used as scaled down by 5.0) (a) Acceleration-time history and (b) Spectral acceleration (Ravichandran et al., 2015)

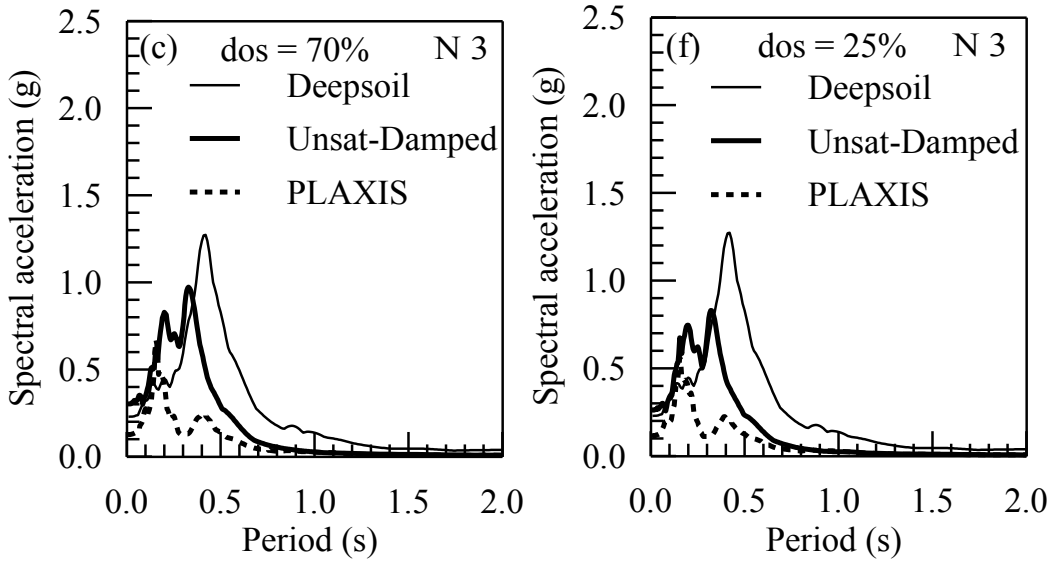

Figure 8.3: Comparison of Unsaturated-Damped Simplified (TeraUDysac), DEEPSOIL and PLAXIS predictions (Ravichandran et al., 2015)

8.2 Bhuiyan et al. (2013)

The comparison of the seismic ground responses computed from different nonlinear programs: DMOD2000, DEEPSOIL and OpenSees are conducted in this study. Additionally, the effect of synthetically generated ground motions based on a set of moment magnitudes on the computed surface responses is also explored. The Charleston reference profile as described in Section 4.3 was adopted for this study. Figure 8.4 presents all four ground motions generated for the Charleston, SC region with Scenario_PC corresponding to the moment magnitudes, M_w of 5.0, 6.0, 7.3 and 8.0.

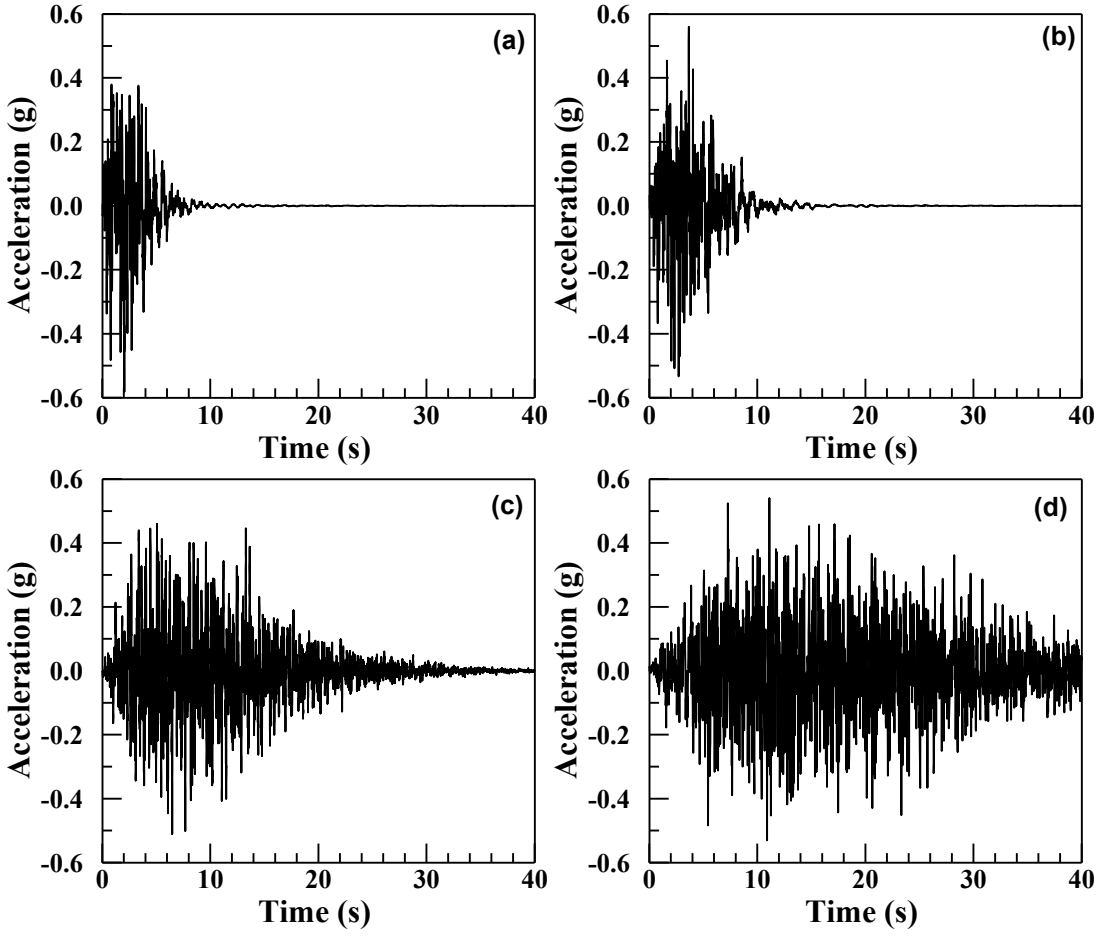

Figure 8.4: Input acceleration time histories for different magnitudes (Bhuiyan et al., 2013).

The modeling techniques of each of the site response analysis programs: DMOD2000, DEEPSOIL and OpenSees are already described in previous chapters (Chapters 4 and 5). Figure 8.5 presents the comparison of the computed surface spectral accelerations from these three programs. The results show that all three codes computed similar responses overall. However, there is a slight difference in the low period range (<0.2 sec period). In fact, the DMOD2000 and DEEPSOIL lines reasonable match even in the shorter periods due to the implementation of the same soil constitutive model (i.e. MKZ model) in both these codes. On the other hand, in OpenSees, has different soil model (multi-yield surface J2 plasticity model) is implemented and thus the outcome is slightly different than the other two at lower periods.

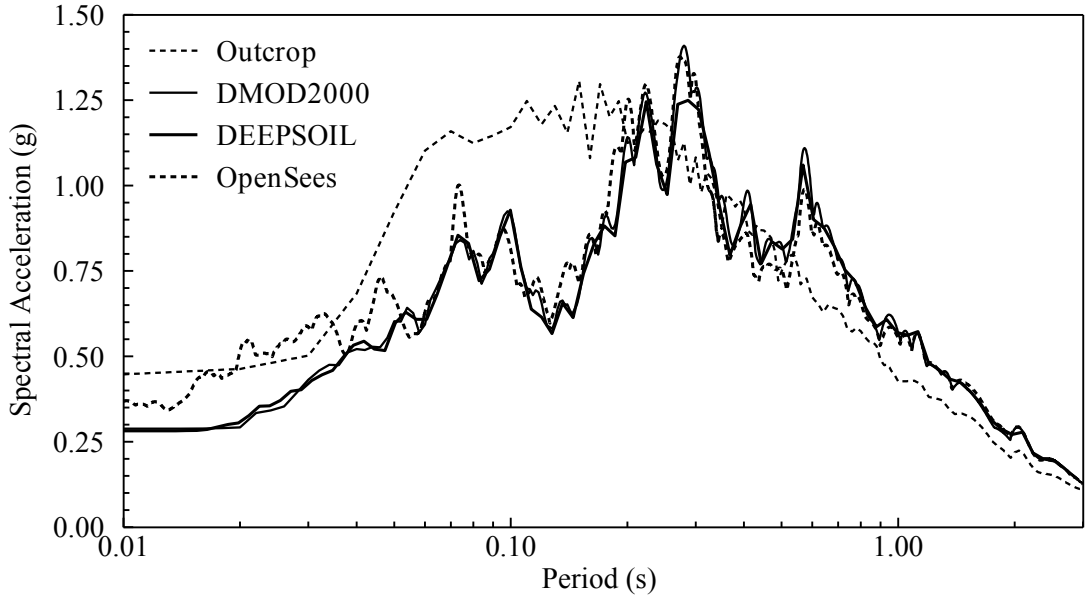

Figure 8.5: Comparison of results from several site response analyses programs (Bhuiyan et al., 2013).

OpenSees is also used to explore the effect of synthetic ground motions generated based on different moment magnitudes on the computed surface response for the same soil profile from Charleston. Figure 8.6 presents the comparison of the computed surface spectral accelerations using moment magnitudes of 5.0, 6.0, 7.3 and 8.0. The results show that the spectral acceleration values increase with the increasing magnitude of the input motion at the lower periods (<0.2 sec period). However, for higher periods, no clear trend was observed with moment magnitude variation.

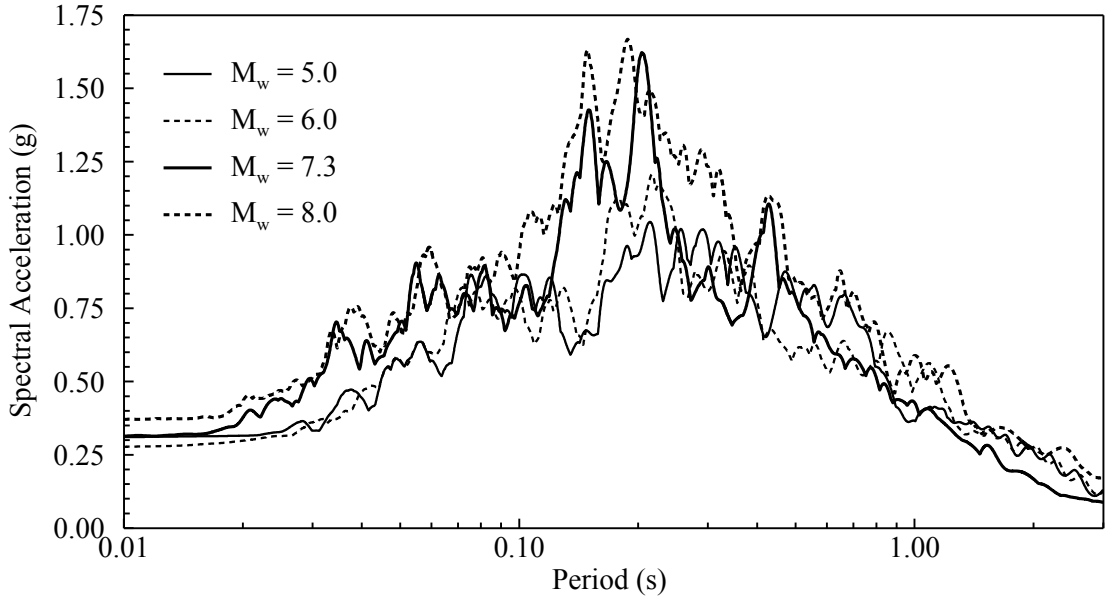

Figure 8.6: Comparison of results from 2-D analyses with OpenSees and variations of input motion characteristics for a model with 5^o ground slope (Bhuiyan et al., 2013).

CHAPTER 9

CONCLUSIONS AND RECOMMENDATIONS

9.1 Conclusions

This dissertation over-all contributes to the existing knowledge base of seismic ground response studies. Presented in Chapter 3 are the nonlinear time domain one dimensional site response analysis outcomes from DMOD2000. 17000 DMOD2000 simulations were performed for all four locations selected from the SCCP: Charleston, Myrtle Beach, Columbia and Aiken. The simulation results were used to develop a new seismic site factor provision for the region. This new seismic site factor model has already been proposed for the next version of the SCDOT Geotechnical Design Manual.

Based on a total of 18000 site response simulations with SHAKE2000, DMOD2000 and DEEPSOIL, three new seismic site factor models were developed and compared in Chapter 4. Both the NL site factor models predicted lower amplitudes than that of the EL generally for the softer profiles. The NL programs generated much higher shear strain and therefore larger hysteretic damping was imposed mostly for the softer profile cases which caused the NL lines to fall below the EL lines. The differences in the computed responses (and also the site factor models) observed between the NL programs are possibly due to the difference in the damping formulation used and/or unrealistic implied shear strength estimated by the program. However, the proposed Aboye et al. (2013a) site factor model predicting higher values than the site factor models generated based on the NL programs ensured adequacy and safety of the proposed model for

engineering applications in this area. Finally, a unique threshold chart was proposed based on the comparisons of the EL and NL analysis outcomes to provide a simple guideline for the practitioners to select the appropriate program between the NL or EL types for the Charleston, SC region.

The study presented in Chapter 5 explored the potential effect of ground slopes on the computed seismic surface responses for Charleston, SC region. A total of 385 two-dimensional finite element simulations were performed for this study consisting of seven ground inclinations (0^o, 1^o, 2^o, 3^o, 4^o, 5^o and 6^o), eleven V_S profiles representative of the area and one ground motion scaled to five different $PGA_{Outcrop}$ levels. Computed surface spectral accelerations were generally higher for sloping ground cases than the corresponding flat ground scenario, which immediately justifies the importance of considering even minor ground slopes into site response study. At the higher periods (i.e. >0.6 sec period) spectral acceleration increased with surface inclination although in the low periods (i.e. <0.6 sec periods) spectral accelerations from sloping ground cases didn't produce a clear trend due to a known modeling limitation. However, the slope effect on ground response has been found to be reduced for higher base shaking and/or softer profiles due to increased damping. Finally, the simulation outcomes are used to develop a set of slope adjustment factors, K_θ as a function of ground inclination, profile V_{S30} and $S_{Outcrop}$ values. The K_θ values are used to modify the surface spectral accelerations from level ground case to obtain the surface spectral acceleration of a sloping ground condition.

In Chapter 6, three V_S profiles representative of the Charleston, SC area were altered to replace a few interface stiffness contrasts with continuously varying V_S values. These profiles were analyzed with seismic site response analysis programs SHAKE2000 and DEEPSOIL. The computed surface responses were compared to evaluate the implication of sudden stiffness contrast at layer interfaces on the computed surface responses. Overall, a general reduction in interface shear strains and increase in surface spectral accelerations especially at lower periods were observed from the altered (smoothened) profiles than the corresponding profiles with interface contrast. For softer profiles this difference in the computed site factors from the original and the altered profiles was observed to increase up to 20%. This shows the importance of such smoothening of the interface contrasts which may eventually revolutionize the current practice of collecting V_S measurements and the generation of the 'working' V_S profiles for the site specific response spectral analysis. Additionally, such smoothening of V_S reduces the shear strain at interface locations; smaller shear strains mean reduced system nonlinearity and thus a potential much wider range of applicability of the equivalent linear approach for site response analysis is expected.

The repercussion of the newly generated site factor model for the South Carolina Coastal Plain (SCCP) has been discussed in Chapter 7. The earthquake loading, generated based on both the new and the current (NEHRP) site factors, were applied on two highway bridge structures to compare the structural responses computed using a Multi-Modal Response Spectrum analysis with SAP2000 and CSiBridge software. Differences in computed structural design demands were observed from these two site factor

provisions. The AASHTO (2011) produced slightly conservative results (about 10%) compared to the 'Recommended' model in the case of site class C. For site class D, the difference between the AASHHTO (2011) and the 'Recommended' model was observed to vary between -40% to 20% (negative value stands for higher AASHTO responses and vice versa). For site class E, the 'Recommended' site factors predicted approximately 31% less design demand than the AASHTO (2011). Therefore, the analysis results from both these bridges showed a wide band of variation from site to site which proves the significance of this update of the site factor provision on the seismic design demand of highway structures.

Finally, a few studies where site response analyses were applied by this author are described in Chapter 8.

9.2 Recommendations

The recommended future works are as follows:

1. Although site response analysis has been practiced in the community for decades, with the increased availability of the vertical array recordings from different parts of the world, it's only recently that a few validation and verification efforts being available (Borja et al., 1999; Lee et al., 2006; Stewart et al., 2008; Kottke, 2010; Kaklamanos et al., 2013 and 2015; Kim and Hashash, 2013; and Zalachoris, 2014). While developing the threshold chart for the selection of an EL or a NL analysis in Chapter 4, the NL responses were assumed as the reference (i.e. true response) while comparing with the EL responses. A comprehensive validation

study with the help of recorded scenario (i.e. vertical array recordings) is highly recommended to validate and/or update the threshold chart.

2. The slope adjustment factors developed in Chapter 5 are very unique in nature as to the authors knowledge no such study (both experimental and numerical) has ever been conducted. However, the major issue is: these factors are completely based on numerical computations with no experimental validation. A systematically designed validation study with centrifuge model test is highly recommended.
3. The observed effect of smoothening of the V_S contrast is recommended to be validated by performing systematically designed centrifuge model tests. If the centrifuge test results agree with the numerical predictions, this will encourage further investigation and may revolutionize the current practice of collecting V_S measurements for different geotechnical applications.
4. Two of the very recent studies: Kim and Hashash (2013) and Zalachoris (2014), found lack of conservativeness in the responses computed using site response analyses of the both equivalent linear and nonlinear-types, especially when large profile shear strain (softer sites and/or large intensity of motion) is involved. Such occurring can be due to a cumulative effect from several sources: improper soil-layer properties and ground motion characteristics, incompetency of numerical model or even due to some assumptions/simplifications made during the process. The sudden contrast of V_S in the layer interfaces can potentially be a major source of such under-prediction while simulated with the popular site

response tools, given that the layer interface has rather gradual variation of V_S in reality. The V_S profiles that were found to produce unconservative site response predictions by both Kim and Hashash (2013) and Zalachoris (2014) are recommended to be evaluated for the above potential source of error.

APPENDICES

APPENDIX A

SUMMARY OF THE RESULTS FROM THE COMPARISON OF NONLINEAR AND EQUIVALENT LINEAR SITE RESPONSE ANALYSES IN CHARLESTON, SOUTH CAROLINA PRESENTED IN CHAPTER 4

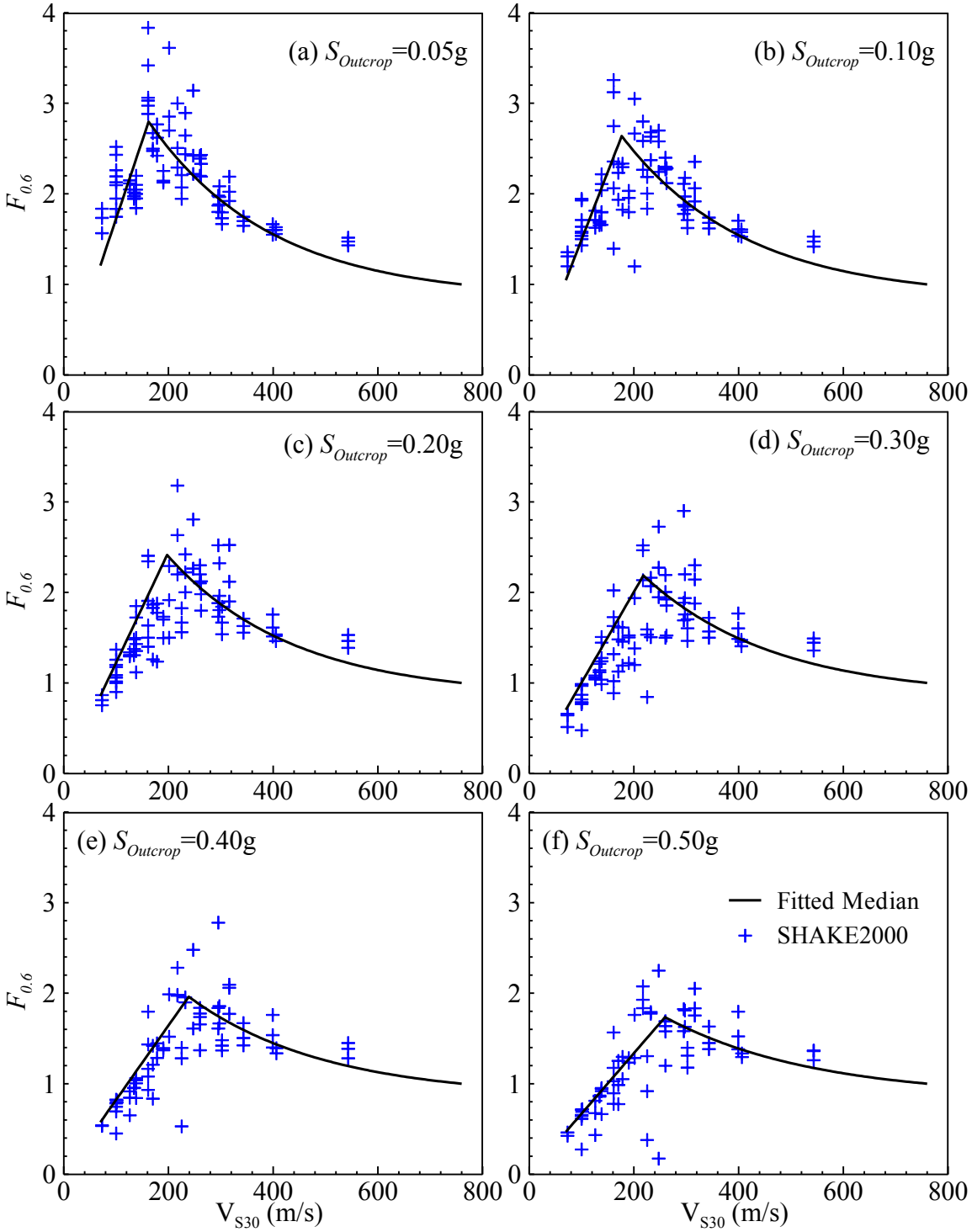

Figure A.1: Site Factor model based on SHAKE2000 data points for $F_{0.6}$ for $S_{Outcrop}$ of (a) 0.05g, (b) 0.1g, (c) 0.2g, (d) 0.3g, (e) 0.4g and (f) 0.5g.

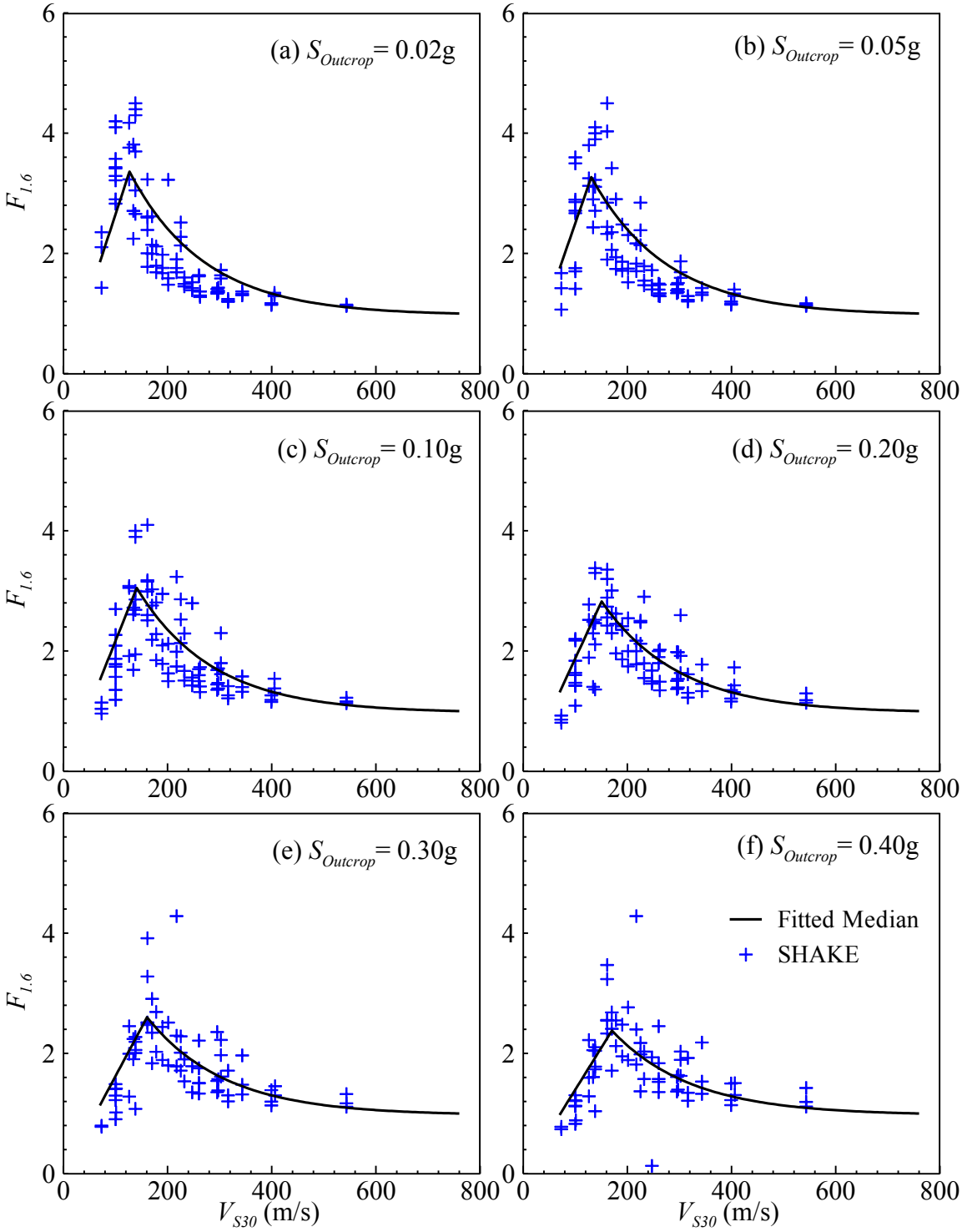

Figure A.2: Site Factor model based on SHAKE2000 data points for $F_{1.6}$ and $S_{Outcrop}$ of (a) 0.02g, (b) 0.05g, (c) 0.1g, (d) 0.2g, (e) 0.3g and (f) 0.4g.

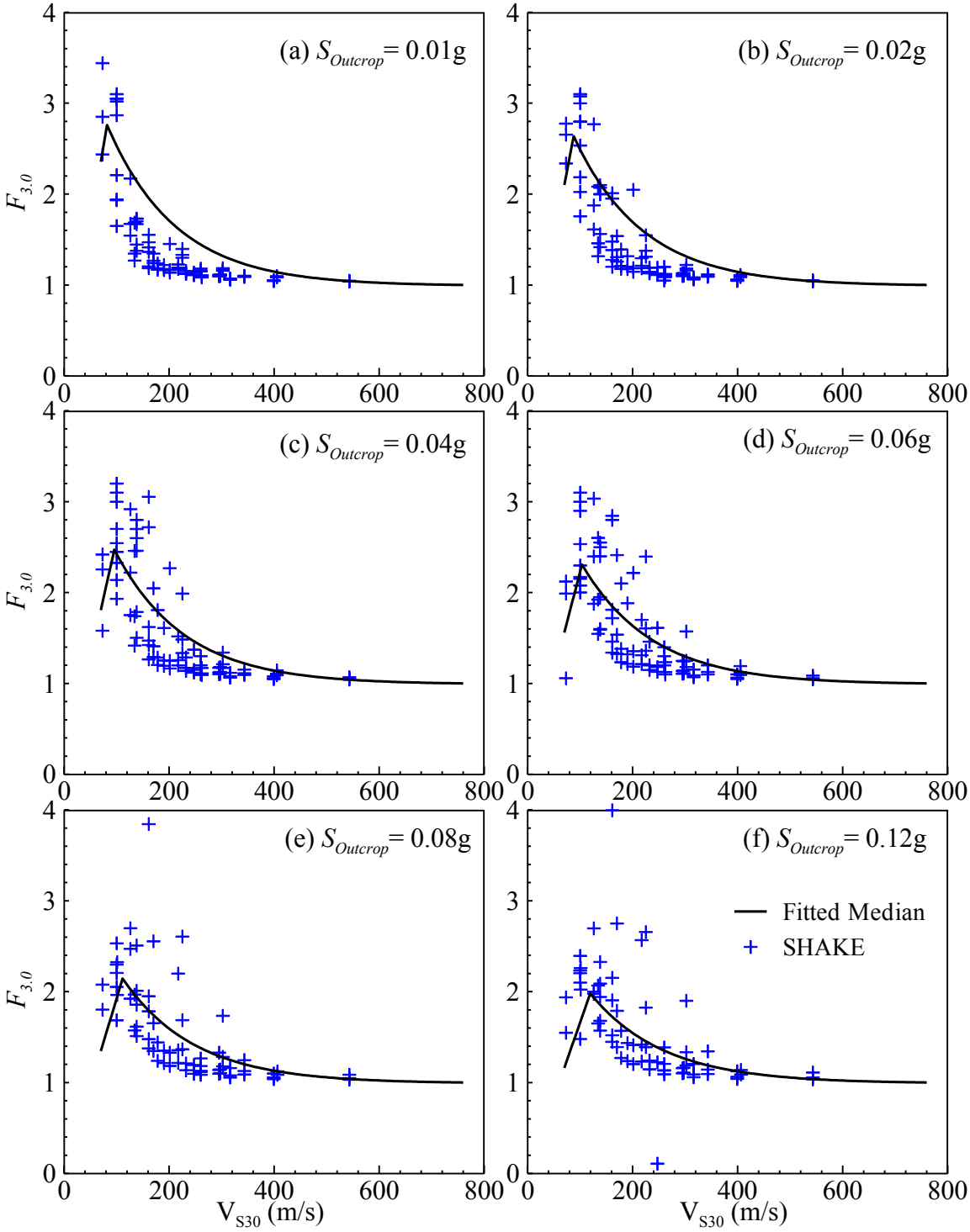

Figure A.3: Site Factor model based on SHAKE2000 data points for $F_{3.0}$ and $S_{Outcrop}$ of (a) 0.01g, (b) 0.02g, (c) 0.04g, (d) 0.06g, (e) 0.08g and (f) 0.12g.

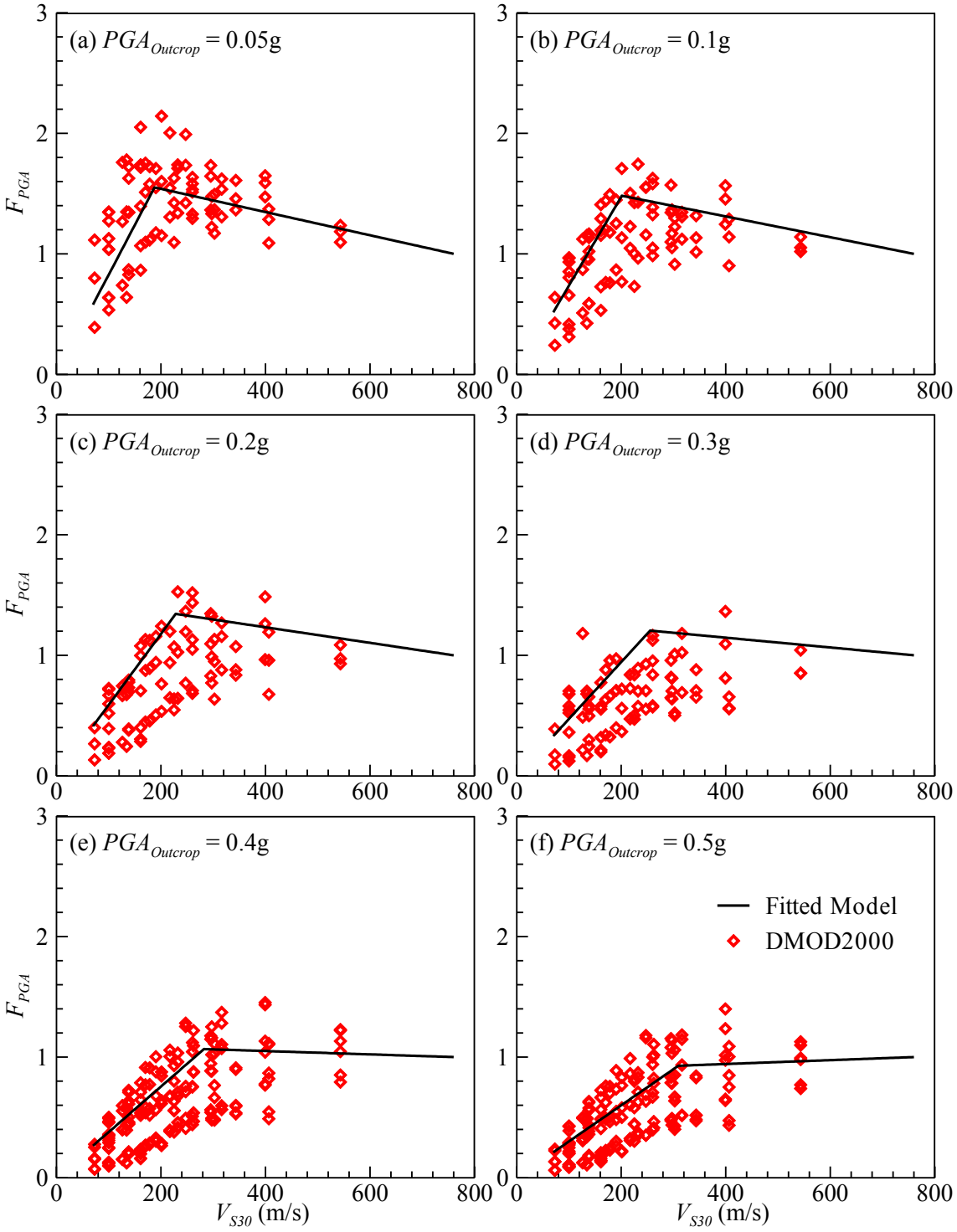

Figure A.4: Site Factor model based on DMOD2000 data points for F_{PGA} and $PGA_{Outcrop}$ of (a) 0.05g, (b) 0.1g, (c) 0.2g, (d) 0.3g, (e) 0.4g, and (f) 0.5g.

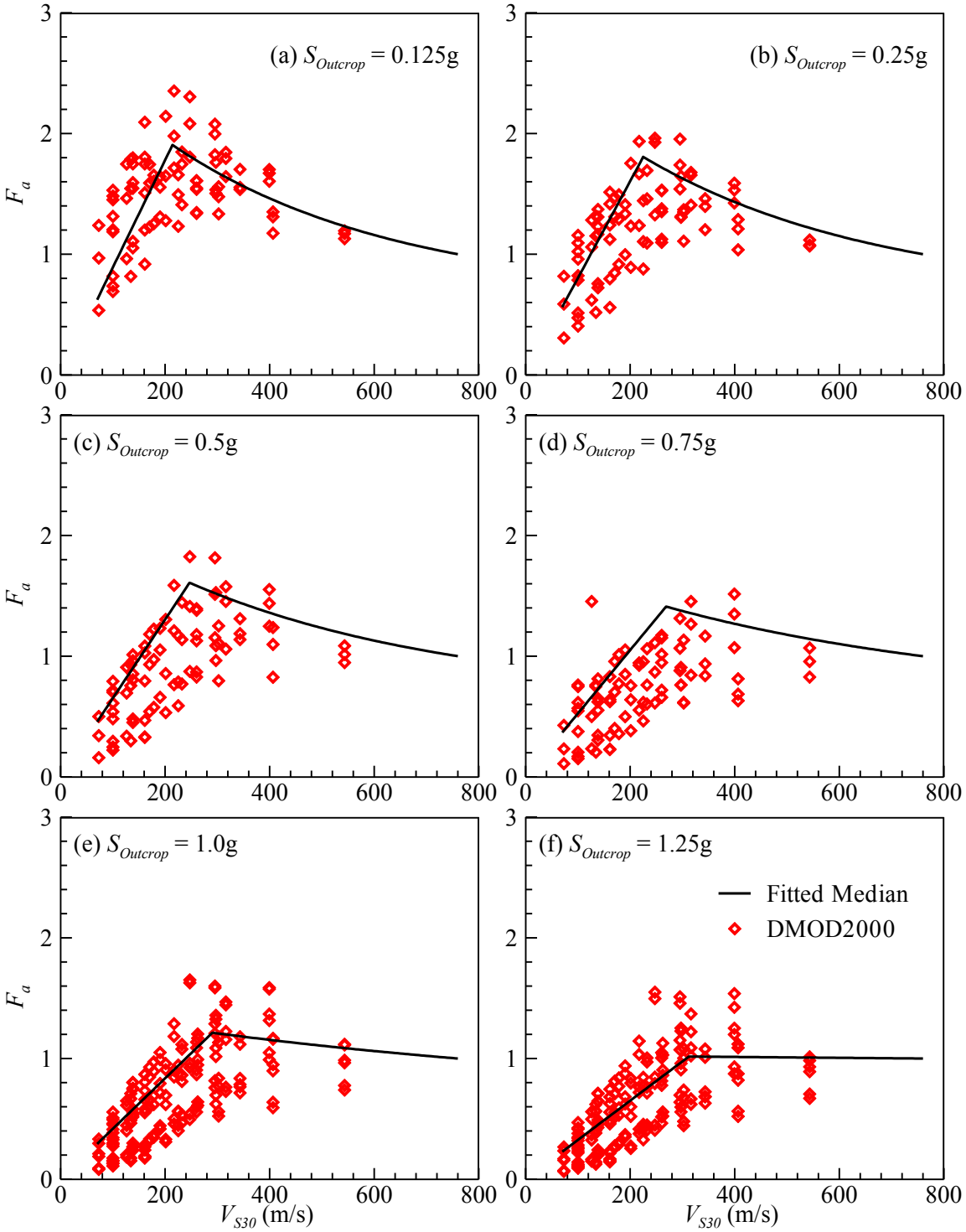

Figure A.5: Site Factor model based on DMOD2000 data points for F_a or $F_{0.2}$ and $S_{Outcrop}$ of (a) 0.125g, (b) 0.25g, (c) 0.5g, (d) 0.75g, (e) 1.0g, and (f) 1.25g.

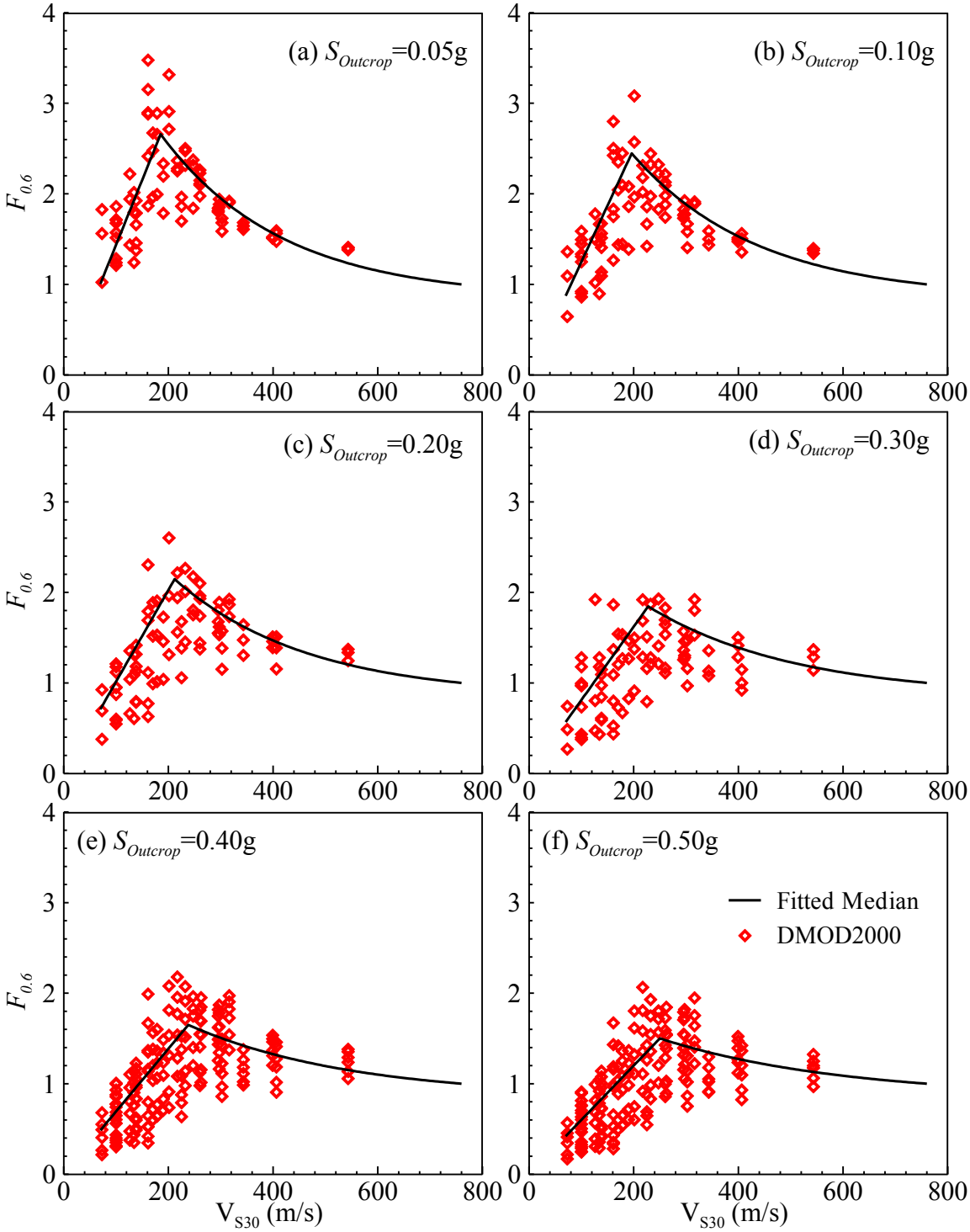

Figure A.6: Site Factor model based on DMOD2000 data points for $F_{0.6}$ for $S_{Outcrop}$ of (a) 0.05g, (b) 0.1g, (c) 0.2g, (d) 0.3g, (e) 0.4g and (f) 0.5g.

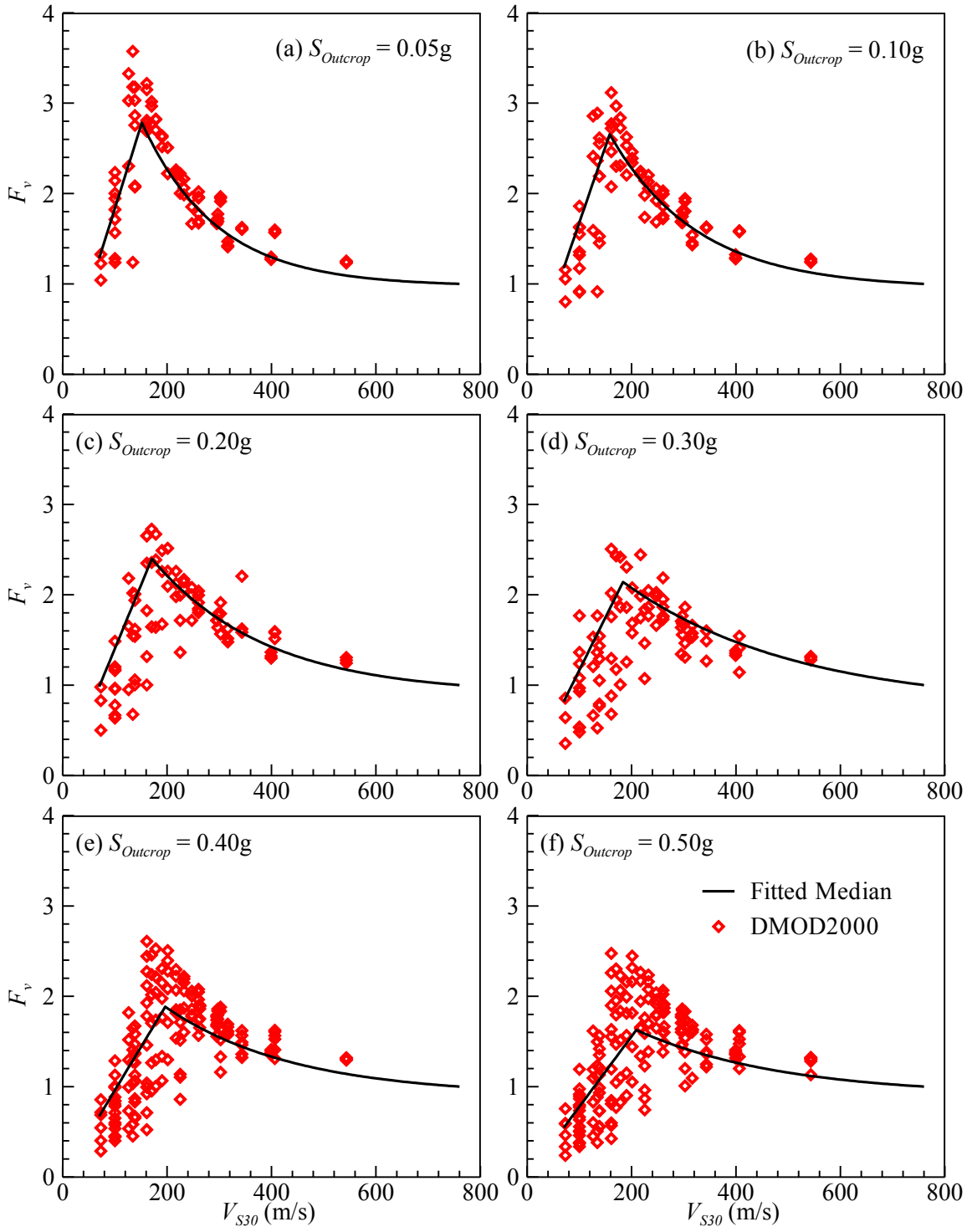

Figure A.7: Site Factor model based on DMOD2000 data points for F_v or $F_{1.0}$ and $S_{Outcrop}$ of (a) 0.05g, (b) 0.1g, (c) 0.2g, (d) 0.3g, (e) 0.4g, and (f) 0.5g

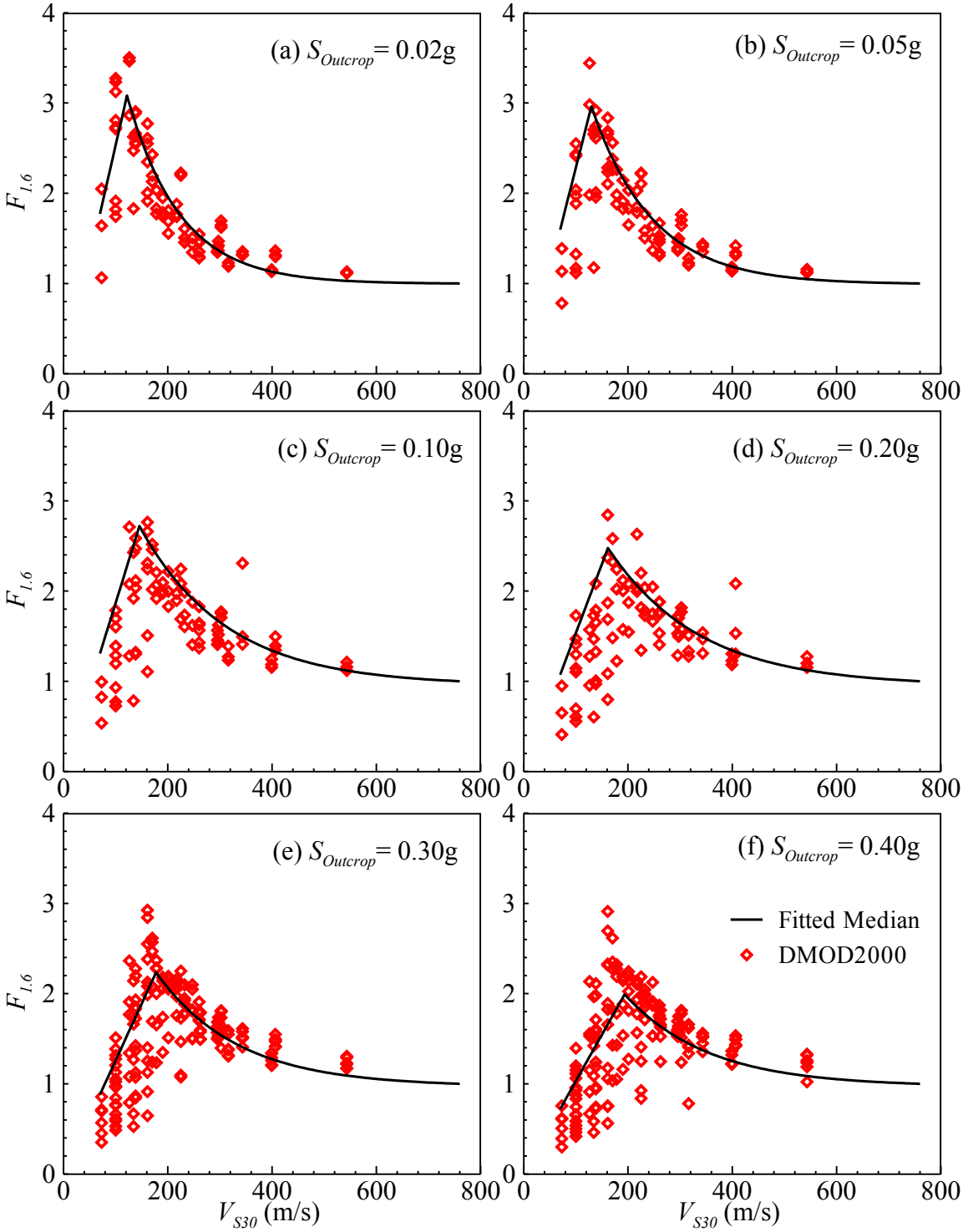

Figure A.8: Site Factor model based on DMOD2000 data points for $F_{1.6}$ and $S_{Outcrop}$ of (a) 0.02g, (b) 0.05g, (c) 0.1g, (d) 0.2g, (e) 0.3g and (f) 0.4g.

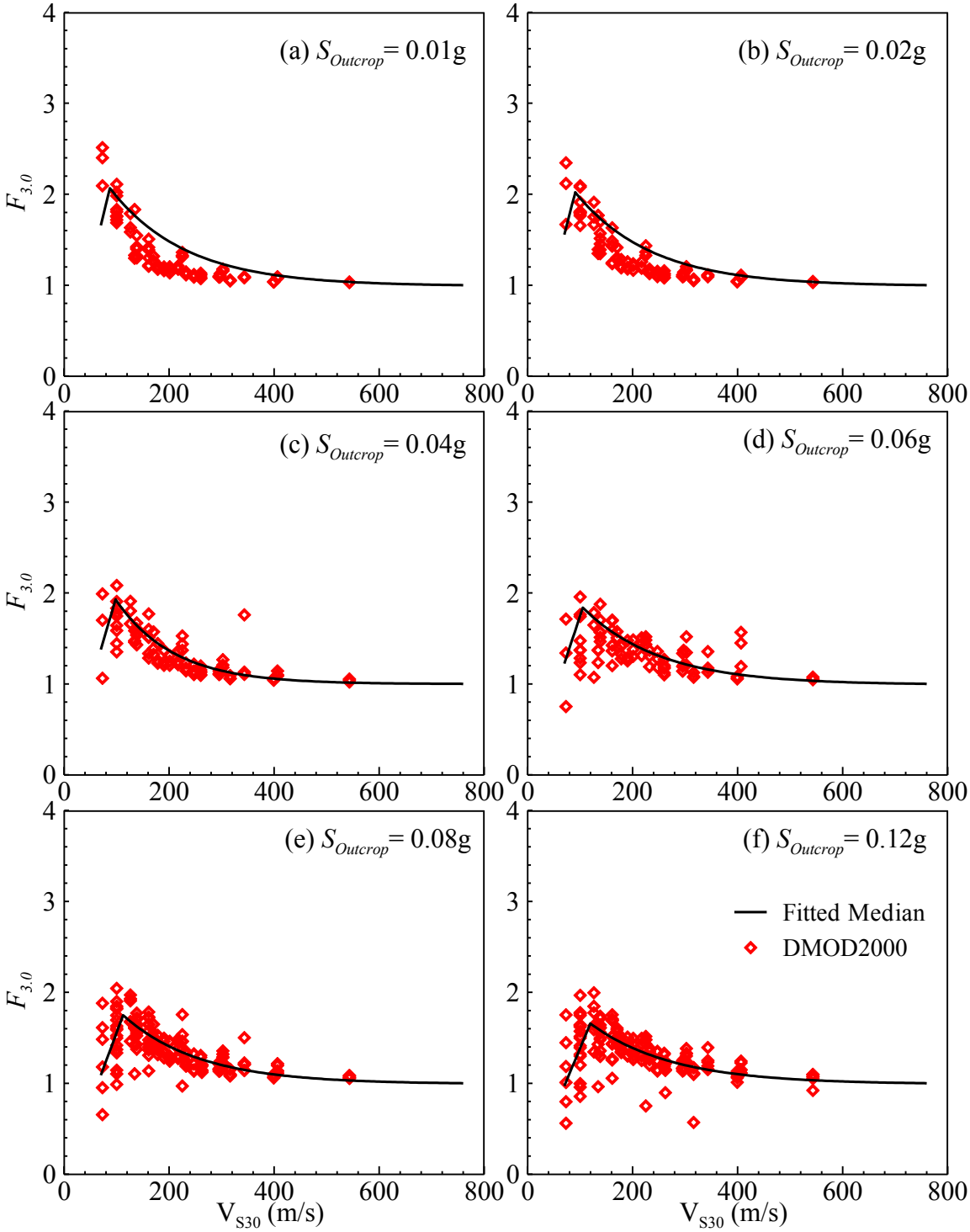

Figure A.9: Site Factor model based on DMOD2000 data points for $F_{3.0}$ and $S_{Outcrop}$ of (a) 0.01g, (b) 0.02g, (c) 0.04g, (d) 0.06g, (e) 0.08g and (f) 0.12g.

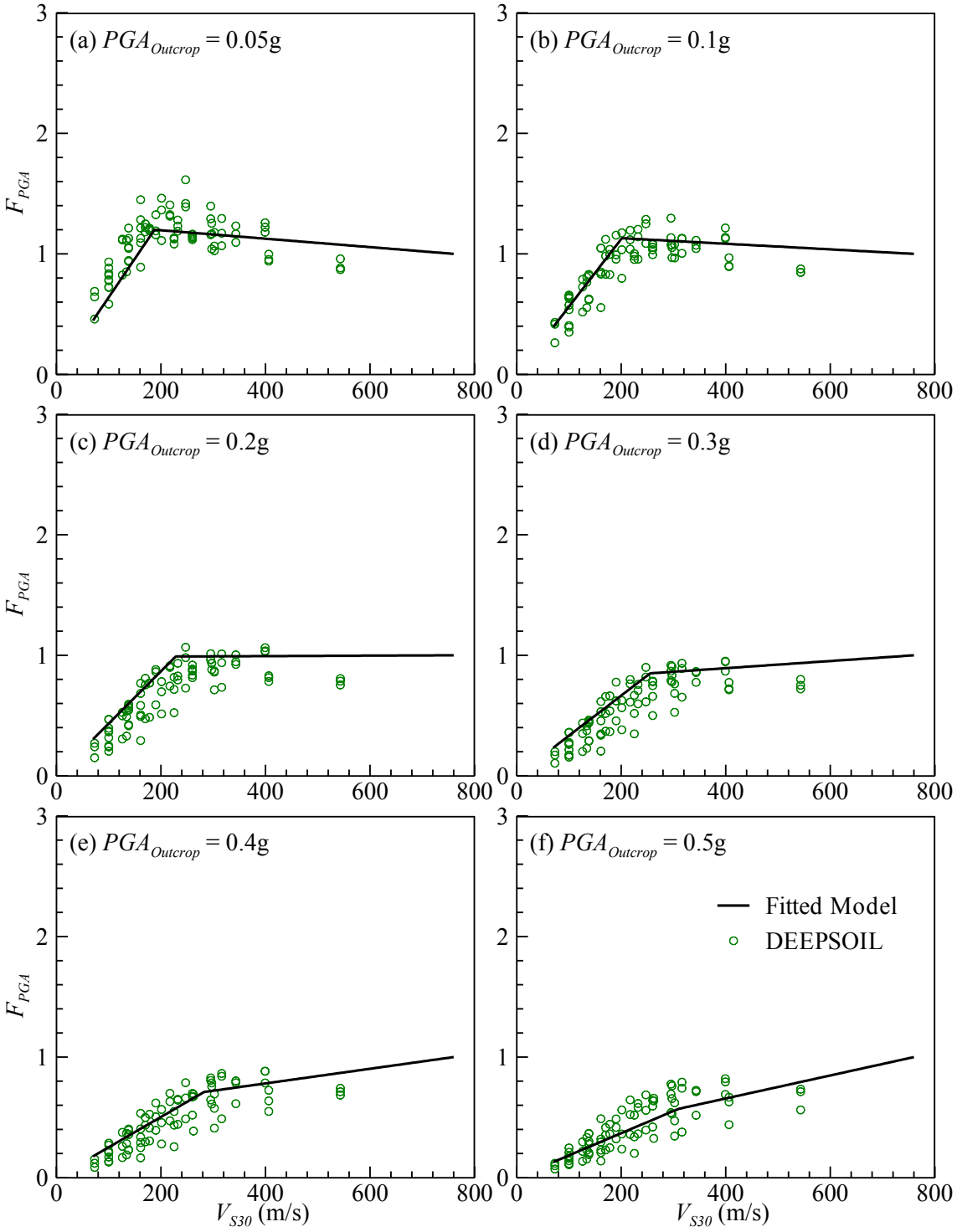

Figure A.10: Site Factor model based on DEEPSOIL data points for F_{PGA} and $PGA_{Outcrop}$ of (a) 0.05g, (b) 0.1g, (c) 0.2g, (d) 0.3g, (e) 0.4g, and (f) 0.5g.

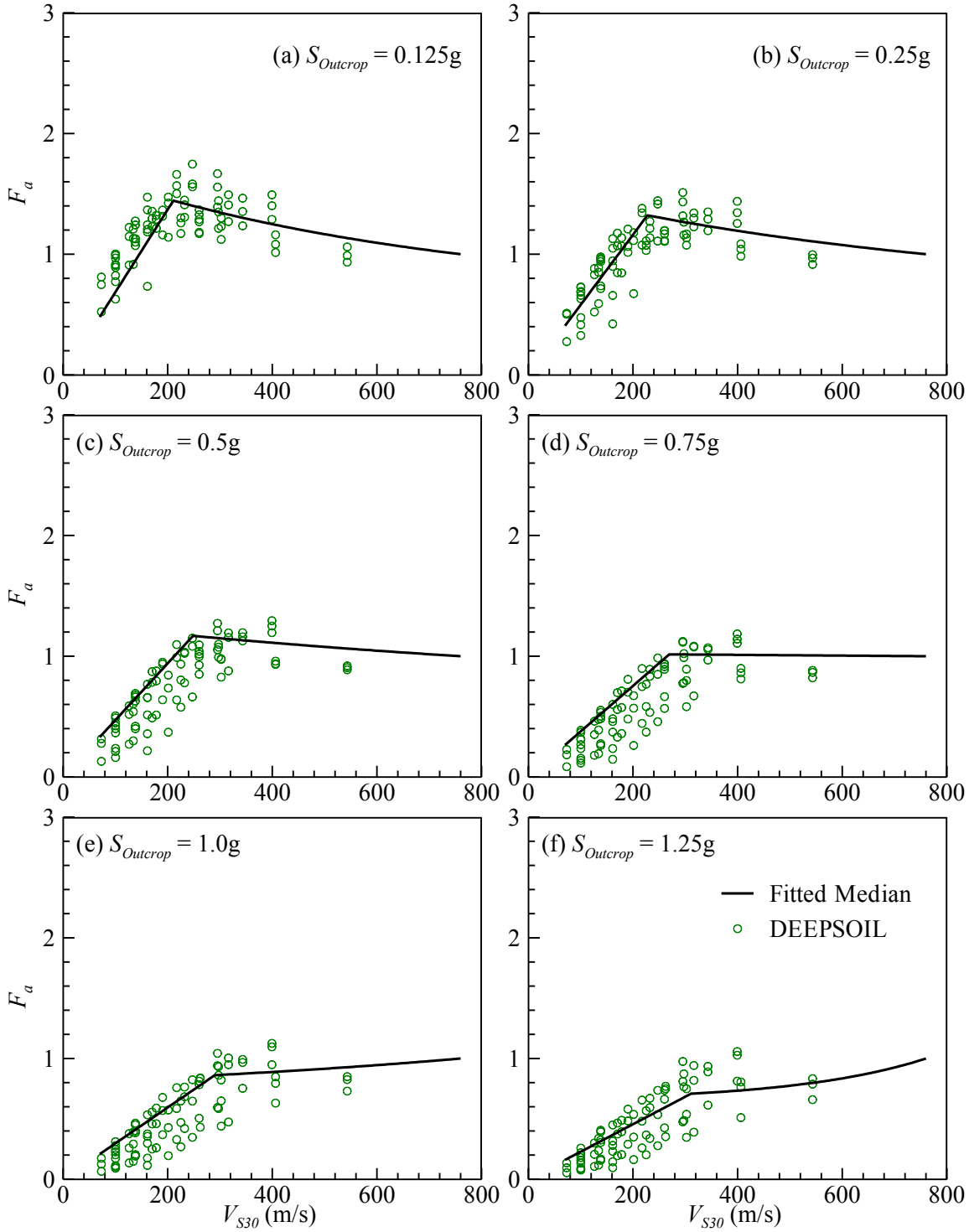

Figure A.11: Site Factor model based on DEEPSOIL data points for F_a or $F_{0.2}$ and $S_{Outcrop}$ of (a) 0.125g, (b) 0.25g, (c) 0.5g, (d) 0.75g, (e) 1.0g, and (f) 1.25g.

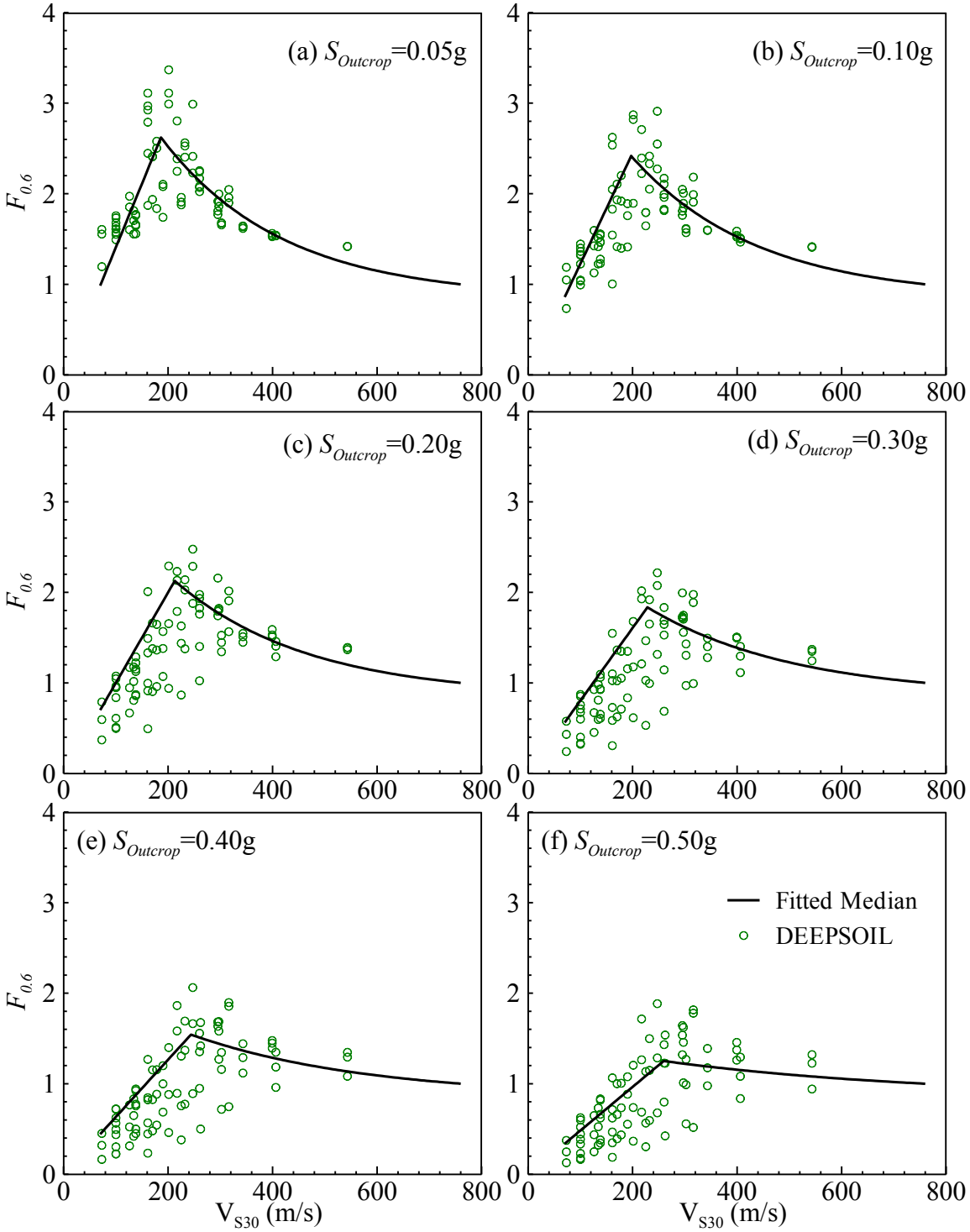

Figure A.12: Site Factor model based on DEEPSOIL data points for $F_{0.6}$ for $S_{Outcrop}$ of (a) 0.05g, (b) 0.1g, (c) 0.2g, (d) 0.3g, (e) 0.4g and (f) 0.5g.

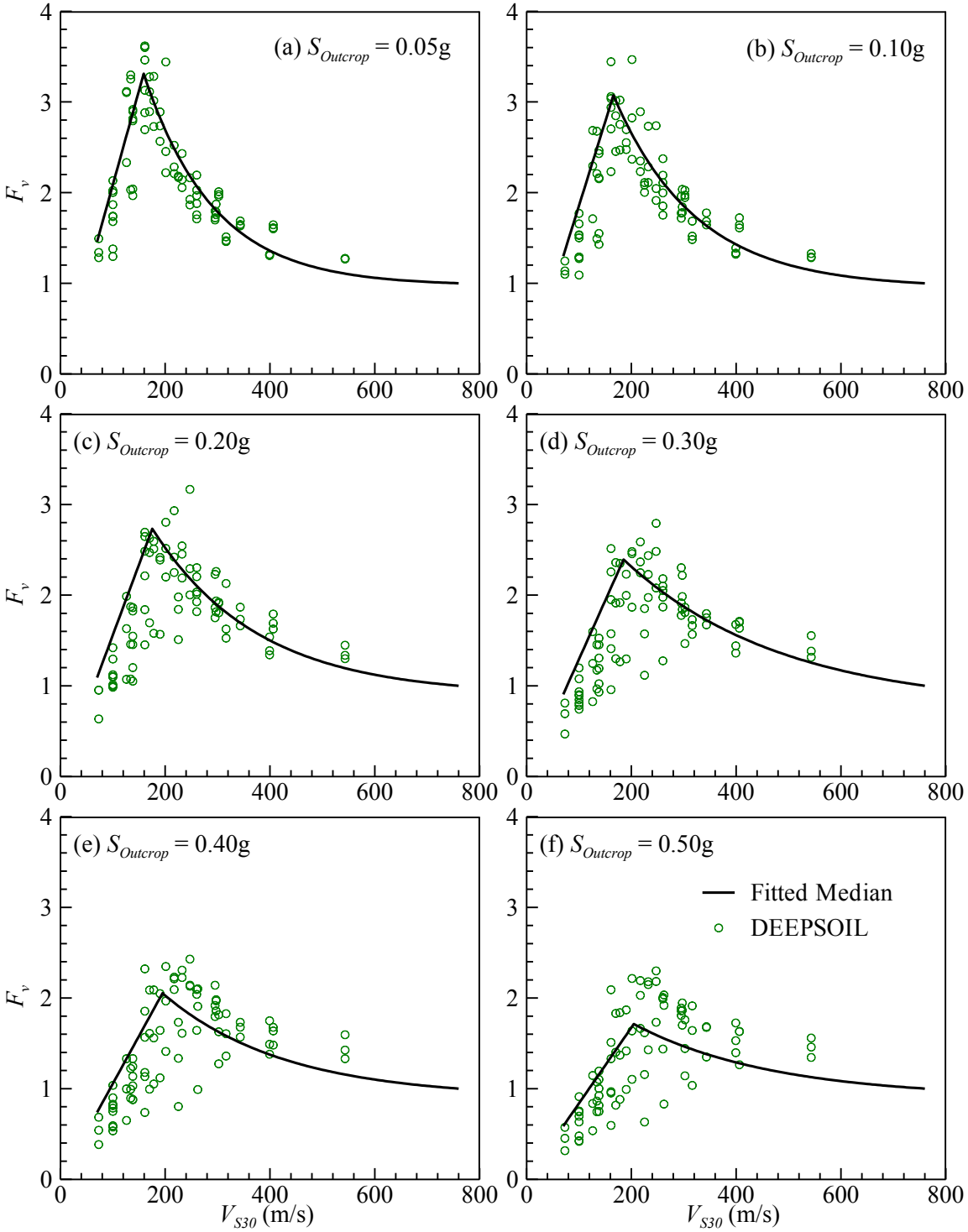

Figure A.13: Site Factor model based on DEEPSOIL data points for F_v or $F_{1.0}$ and $S_{Outcrop}$ of (a) 0.05g, (b) 0.1g, (c) 0.2g, (d) 0.3g, (e) 0.4g, and (f) 0.5g

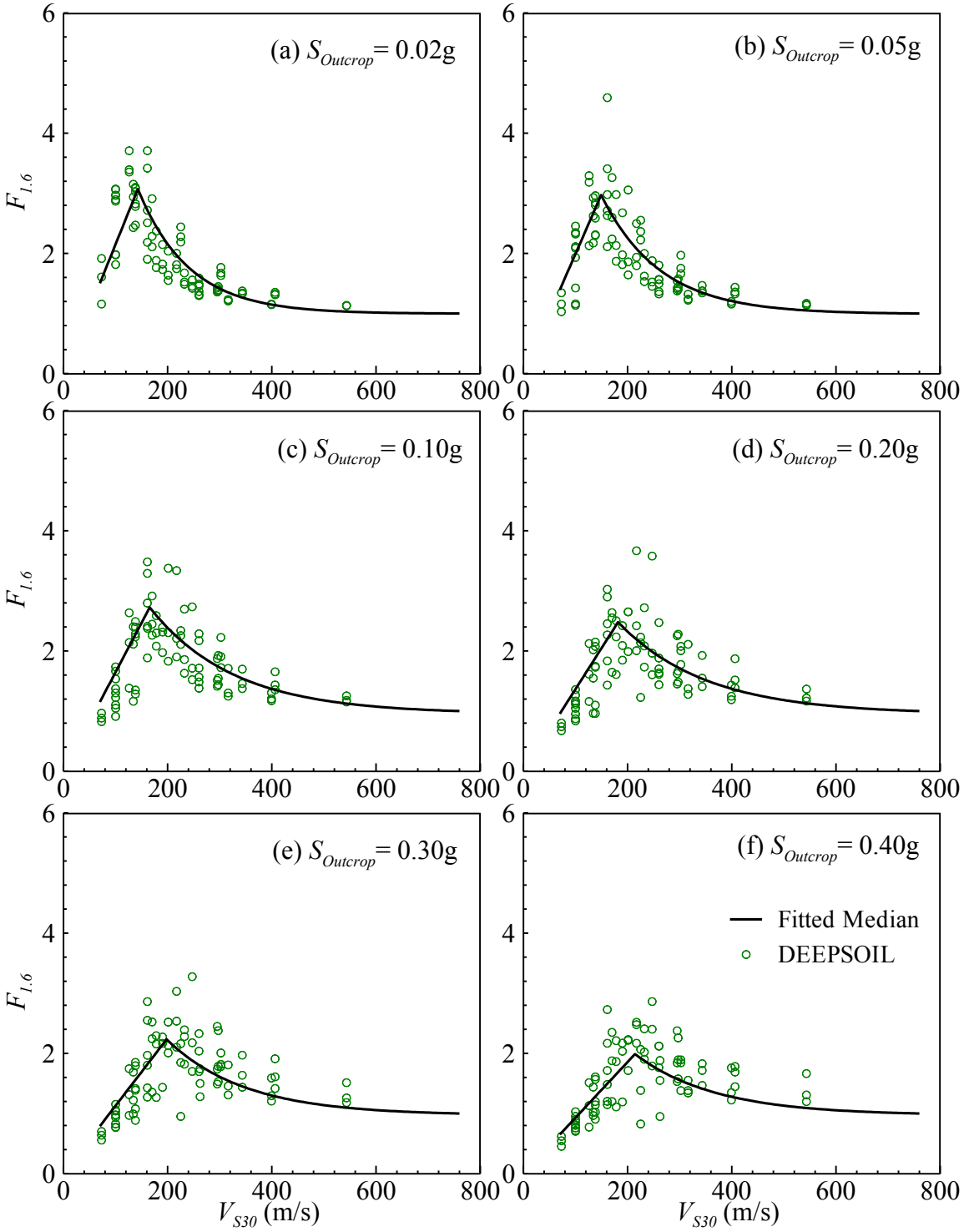

Figure A.14: Site Factor model based on DEEPSOIL data points for $F_{1.6}$ and $S_{Outcrop}$ of (a) 0.02g, (b) 0.05g, (c) 0.1g, (d) 0.2g, (e) 0.3g and (f) 0.4g.

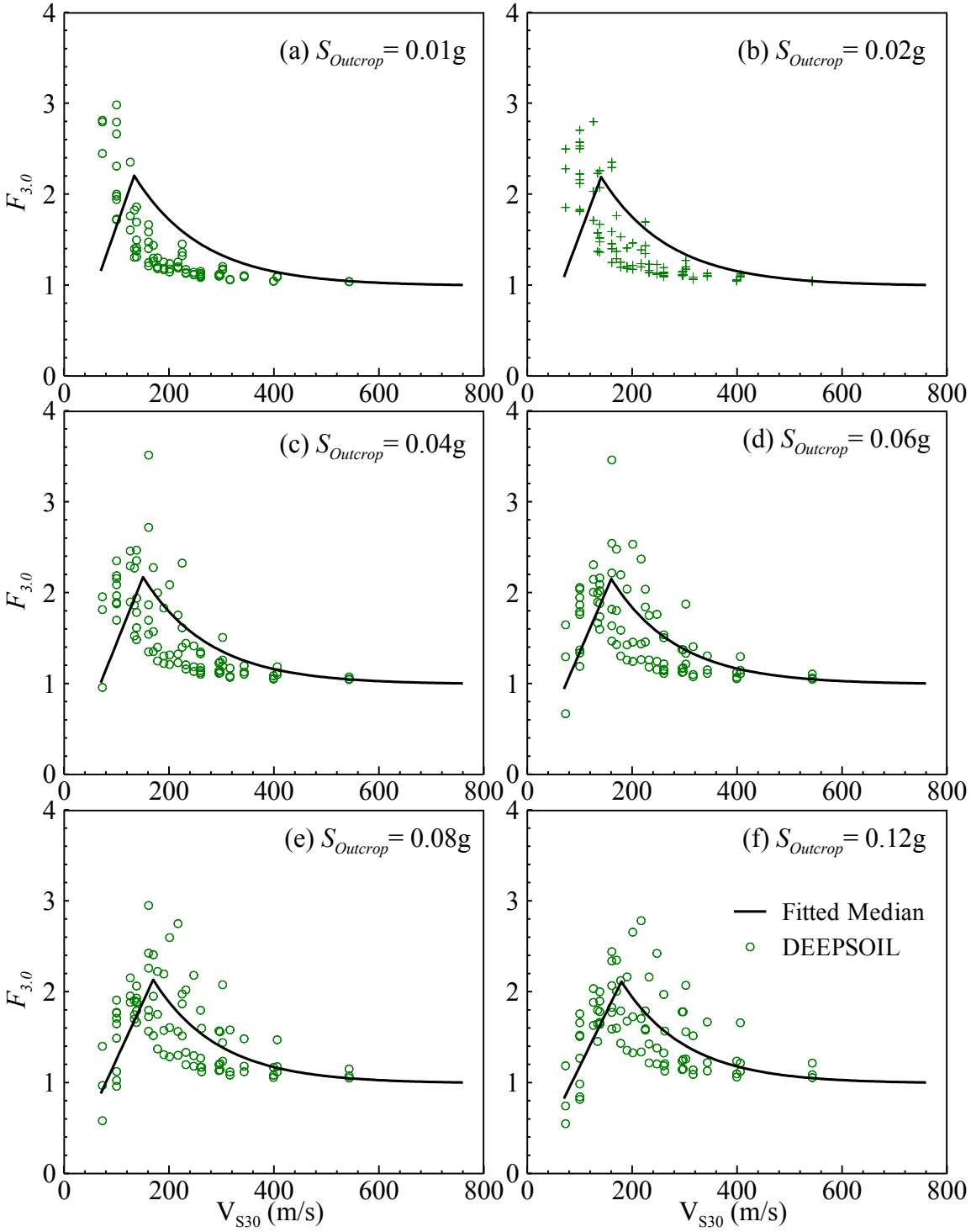

Figure A.15: Site Factor model based on DEEPSOIL data points for $F_{3.0}$ and $S_{Outcrop}$ of (a) 0.01g, (b) 0.02g, (c) 0.04g, (d) 0.06g, (e) 0.08g and (f) 0.12g.

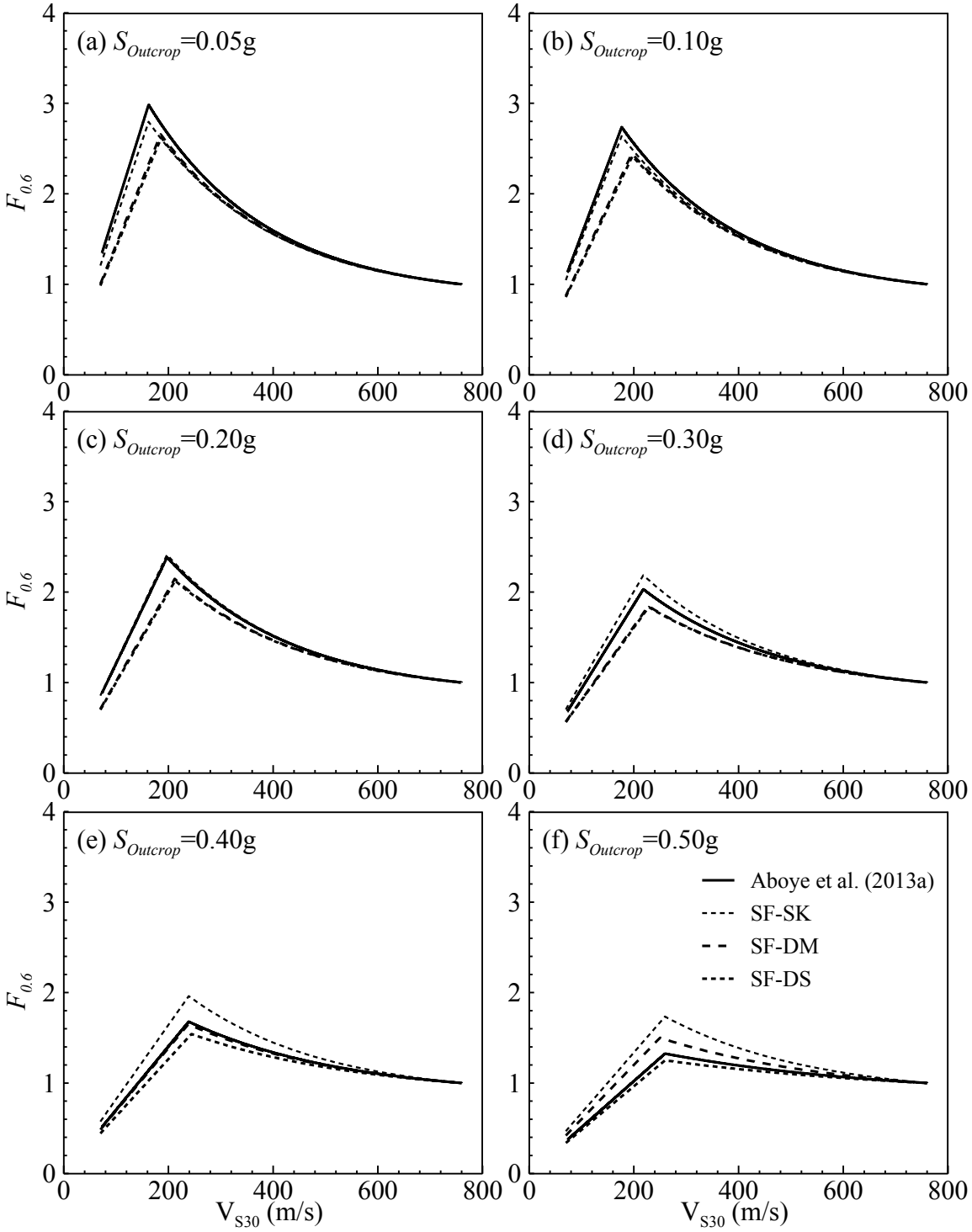

Figure A.16: Comparison of the site factor models based on Aboye et al. (2013a), SHAKE2000, DMOD2000 and DEEPSOIL in the case of $F_{0.6}$ for $S_{Outcrop}$ of (a) 0.05g, (b) 0.1g, (c) 0.2g, (d) 0.3g, (e) 0.4g and (f) 0.5g.

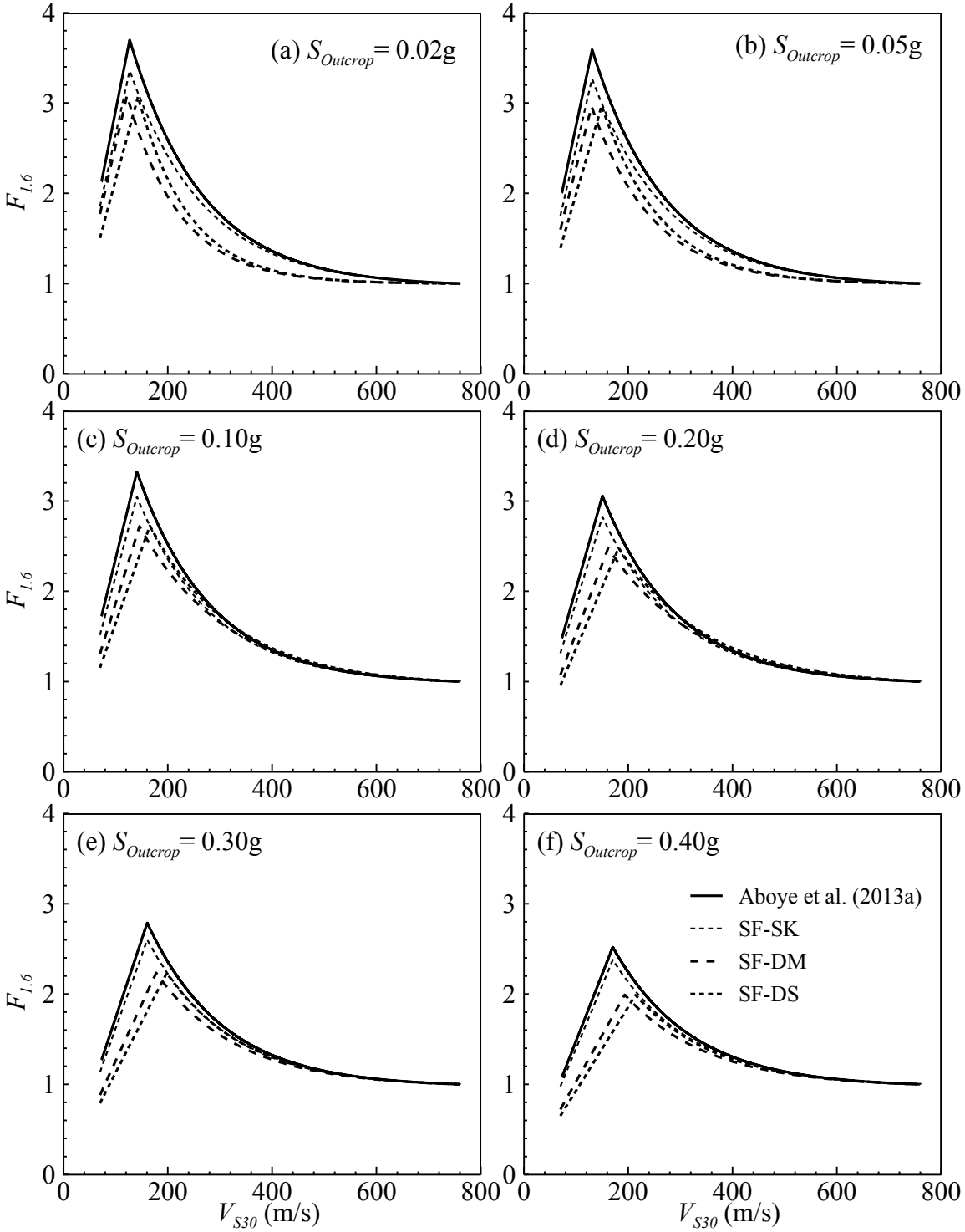

Figure A.17: Comparison of the site factor models based on Aboye et al. (2013a), SHAKE2000, DMOD2000 and DEEPSOIL in the case of $F_{1.6}$ for $S_{Outcrop}$ of (a) 0.02g, (b) 0.05g, (c) 0.1g, (d) 0.2g, (e) 0.3g and (f) 0.4g.

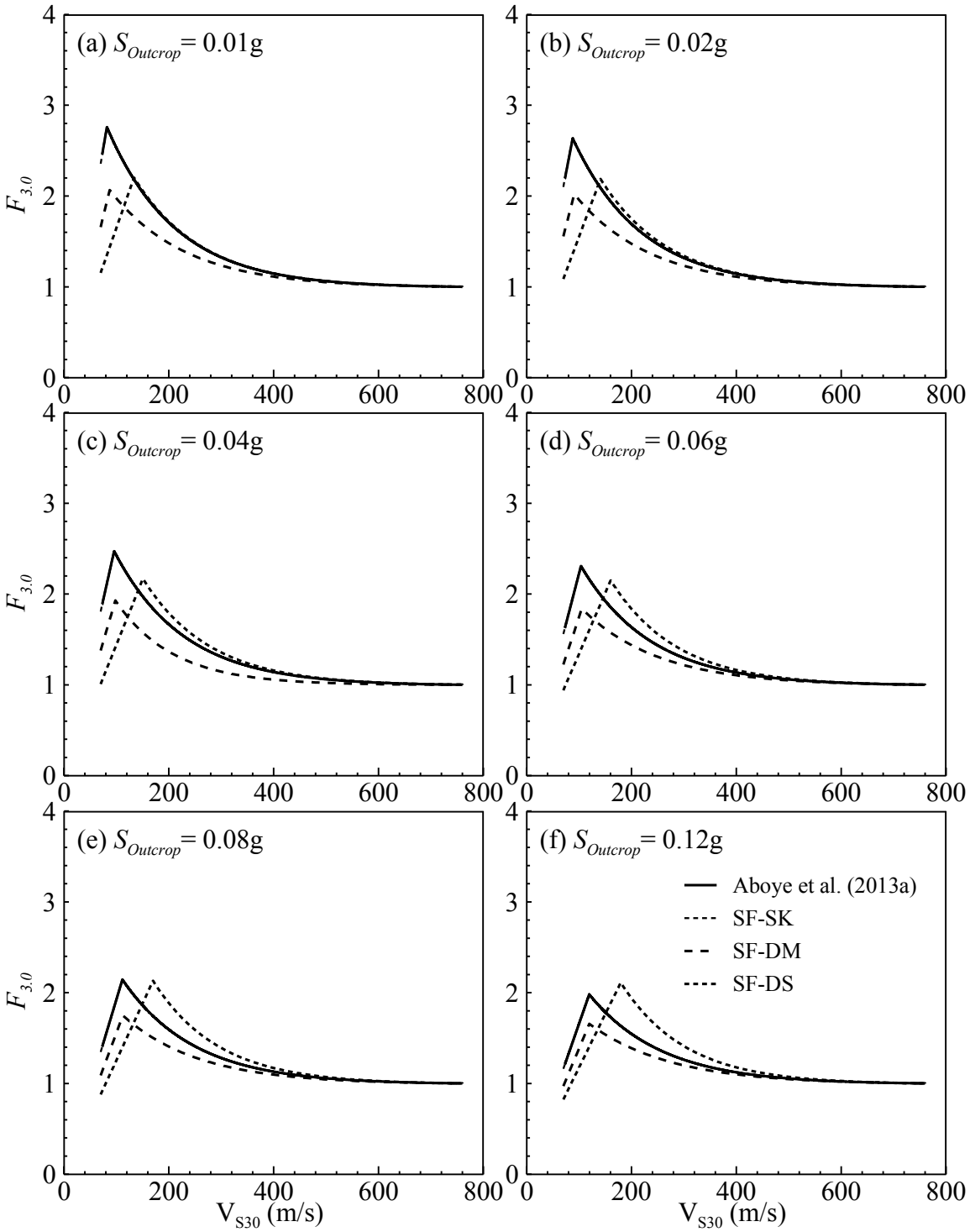

Figure A.18: Comparison of the site factor models based on Aboye et al. (2013a), SHAKE2000, DMOD2000 and DEEPSOIL in the case of $F_{3.0}$ for $S_{Outcrop}$ of (a) 0.01g, (b) 0.02g, (c) 0.04g, (d) 0.06g, (e) 0.08g and (f) 0.12g.

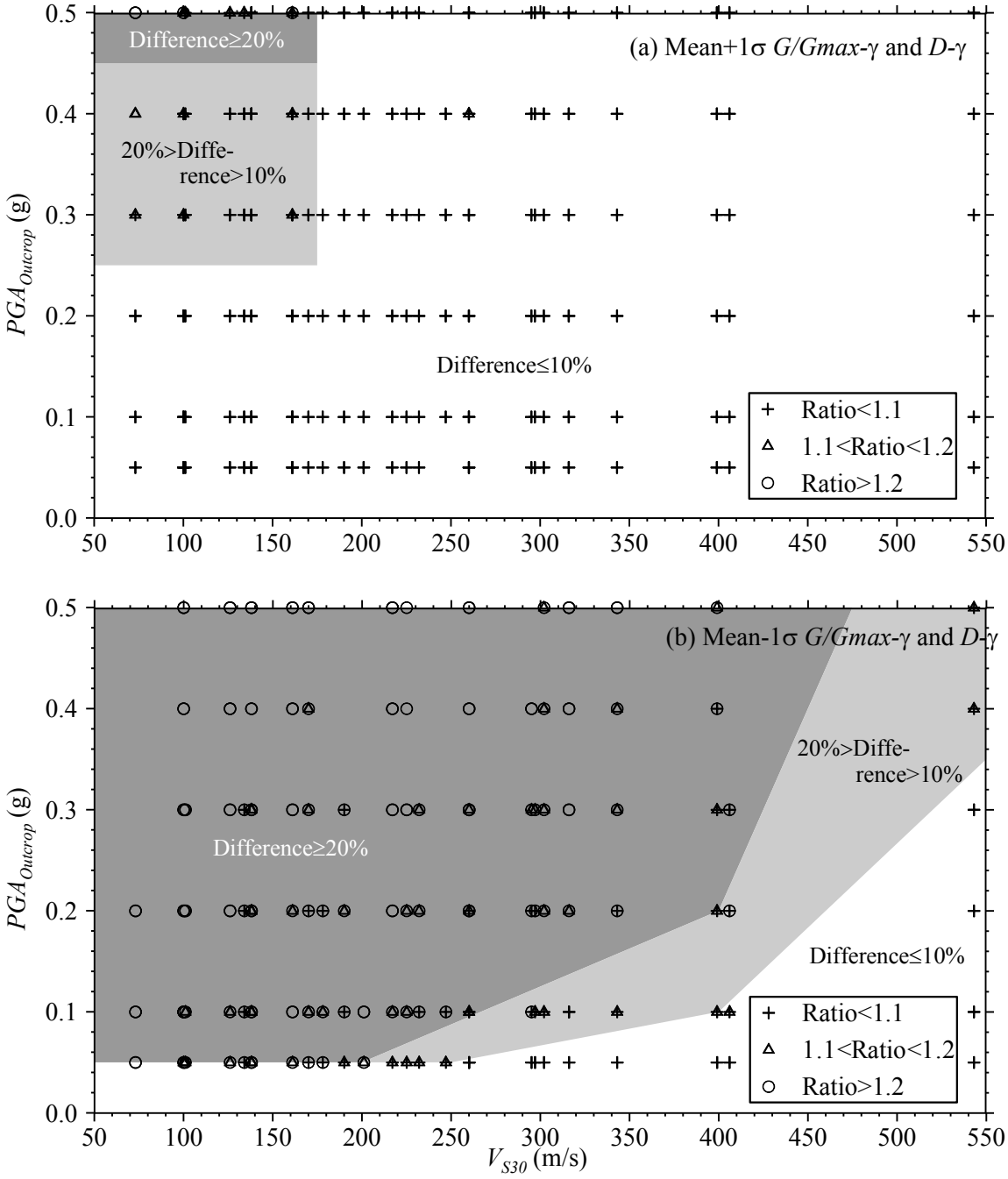

Figure A.19: Threshold chart developed with regions showing variation of the area ratios between the EL (SHAKE2000) and NL codes (DMOD2000 and DEEPSOIL) for a range of V_{S30} and $PGA_{Outcrop}$ considered for the (a) mean+1σ and (b) mean-1σ of G/G_{max}-γ and D-γ.

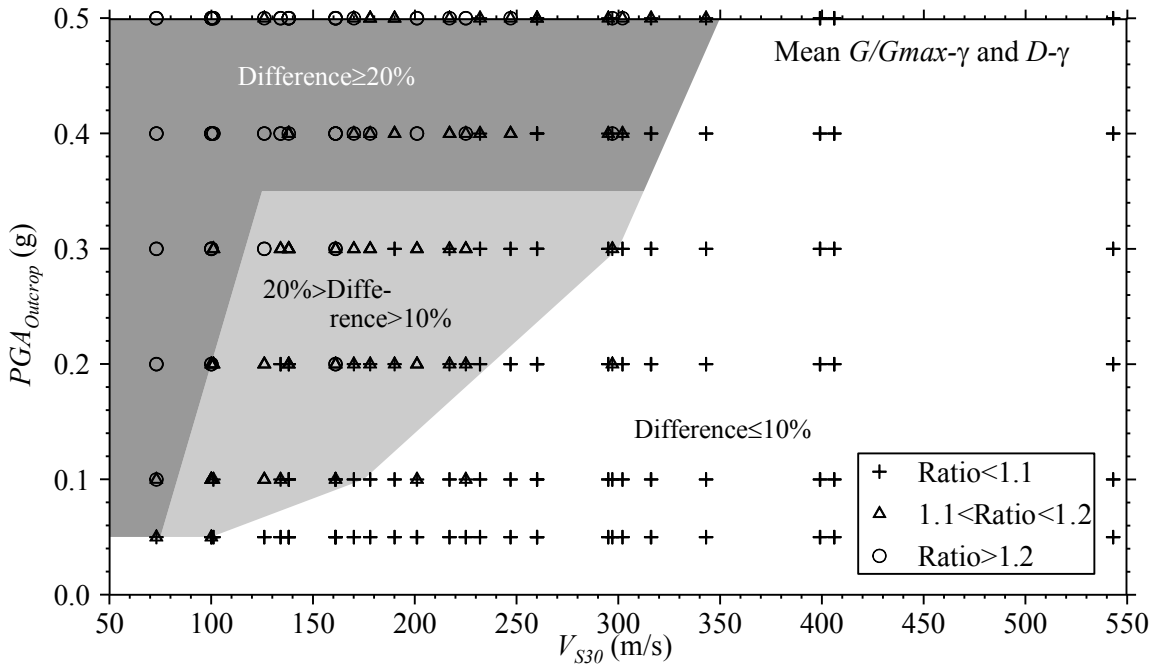

Figure A.20: Threshold chart developed for the mean G/G_{max}-γ and D-γ cases considering 0-4 sec spectral period band of respective response spectral acclerations while computing the area ratios.

APPENDIX B

SUMMARY OF THE RESULTS OF THE SITE RESPONSE ANALYSIS OF MILD INFINITE GROUND SLOPES PRESENTED IN CHAPTER 5

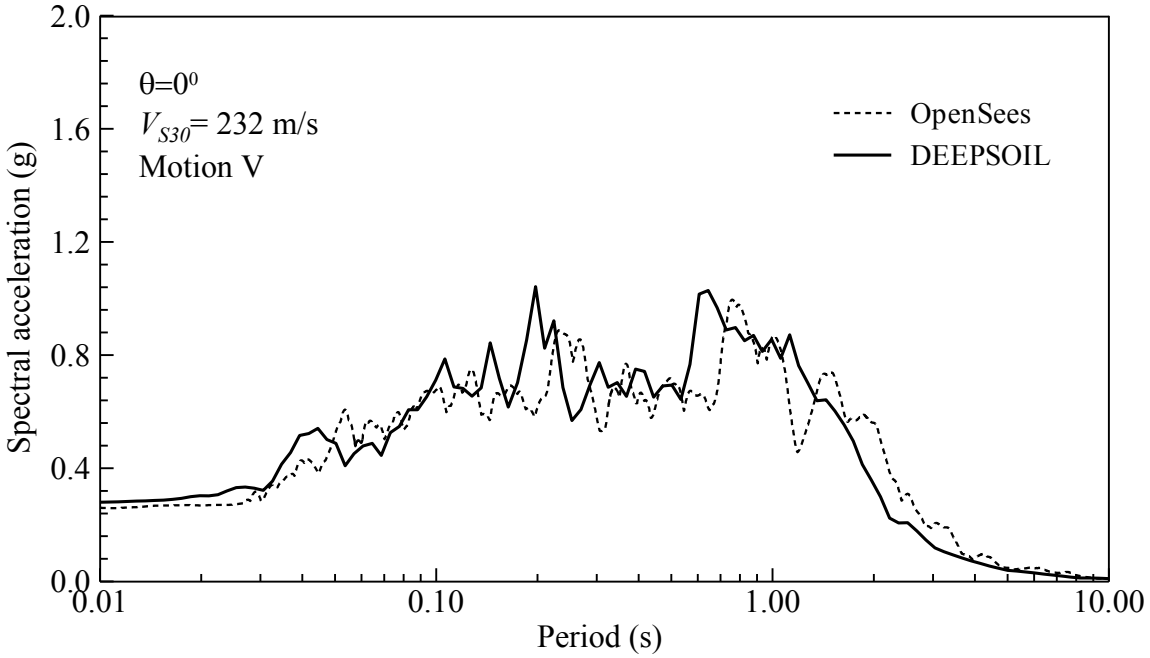

Figure B.1: Sample validation study of the calibrated c_u values by comparing the spectral accelerations from OpenSees model with that of DEEPSOIL for the profile with V_{S30} = 232 m/s for flat ground condition and Motion-V.

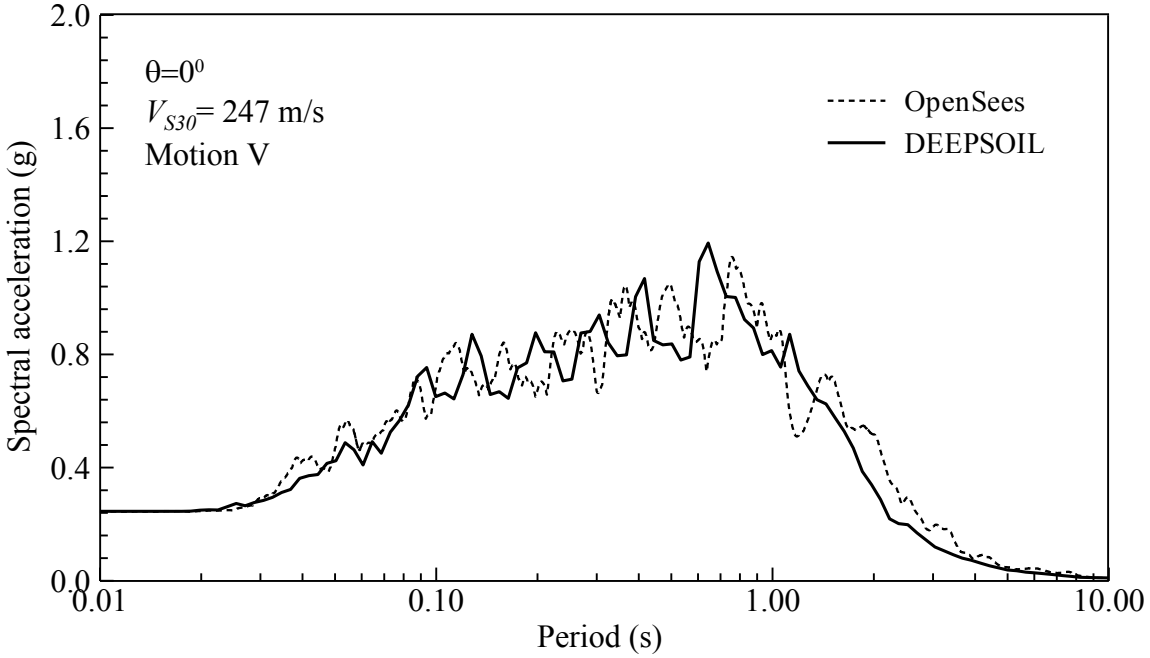

Figure B.2: Sample validation study of the calibrated c_u values by comparing the spectral accelerations from OpenSees model with that of DEEPSOIL for the profile with V_{S30} = 247 m/s for flat ground condition and Motion-V.

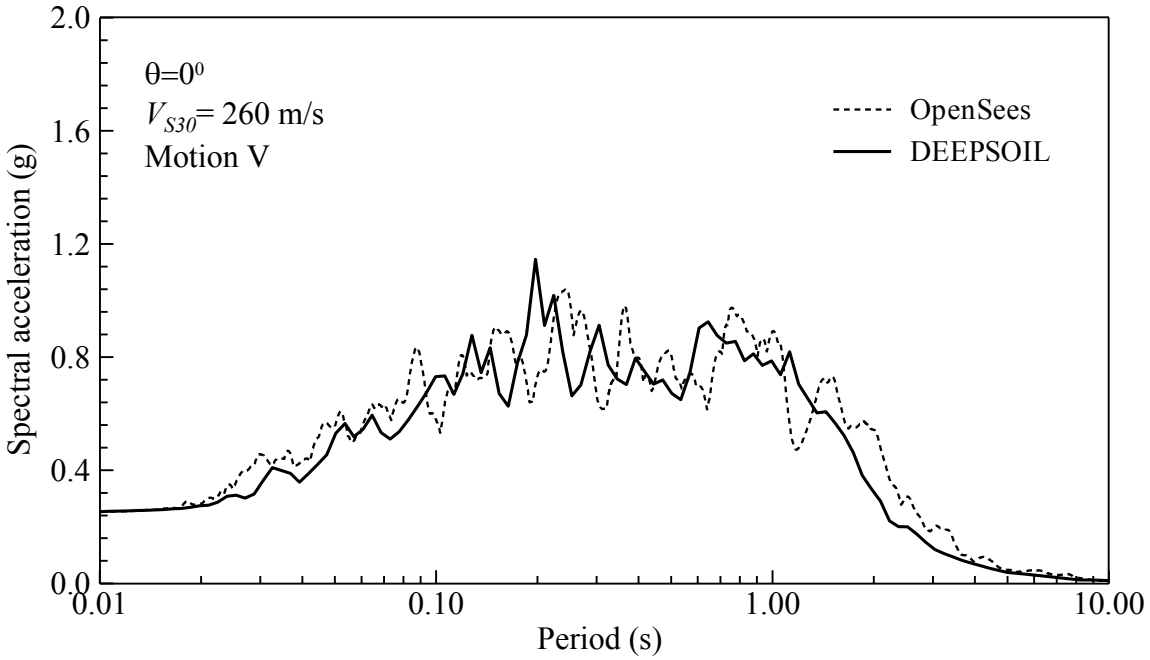

Figure B.3: Sample validation study of the calibrated c_u values by comparing the spectral accelerations from OpenSees model with that of DEEPSOIL for the profile with V_{S30} = 260 m/s for flat ground condition and Motion-V.

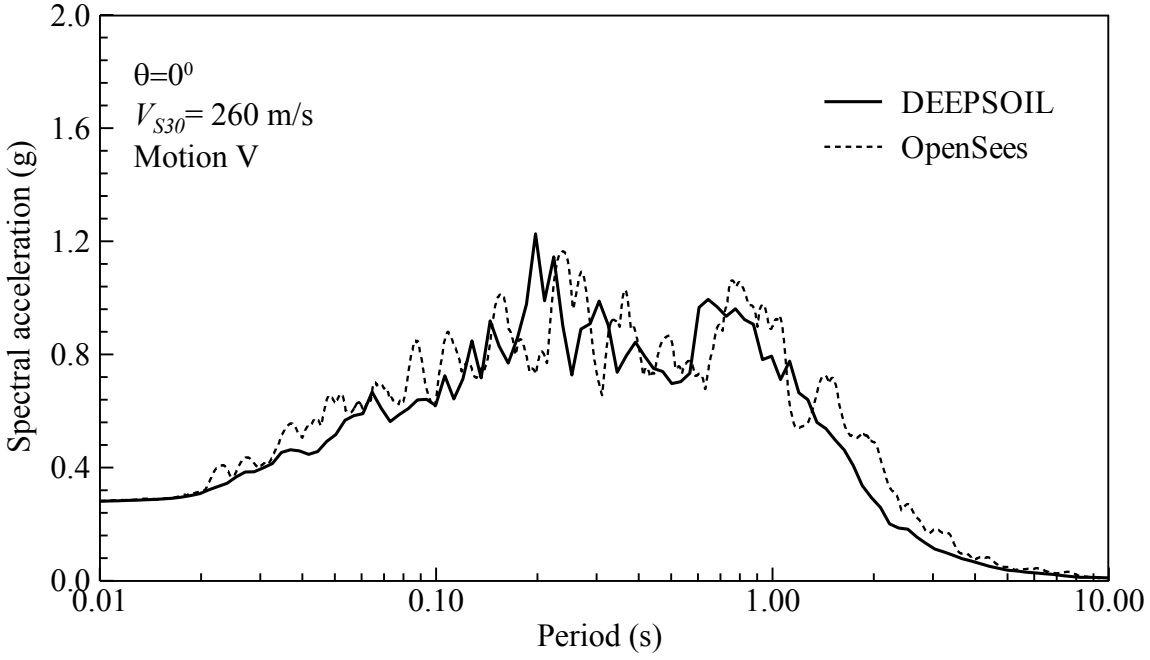

Figure B.4: Sample validation study of the calibrated c_u values by comparing the spectral accelerations from OpenSees model with that of DEEPSOIL for the profile with V_{S30} = 260 m/s for flat ground condition and Motion-V.

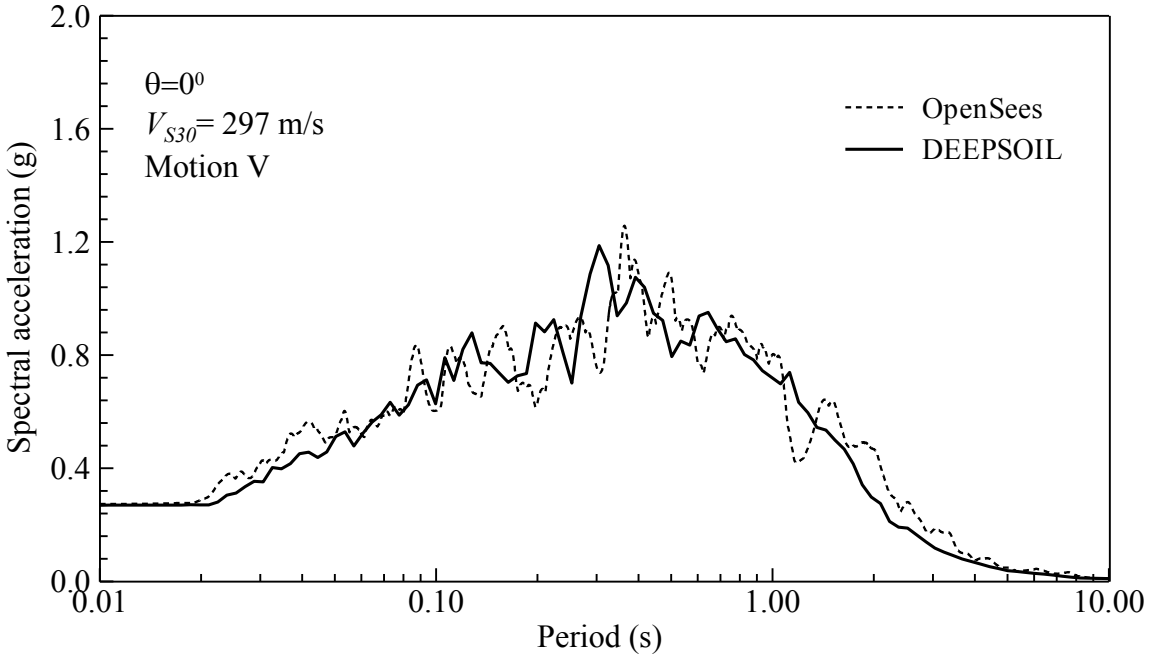

Figure B.5: Sample validation study of the calibrated c_u values by comparing the spectral accelerations from OpenSees model with that of DEEPSOIL for the profile with V_{S30} = 297 m/s for flat ground condition and Motion-V.

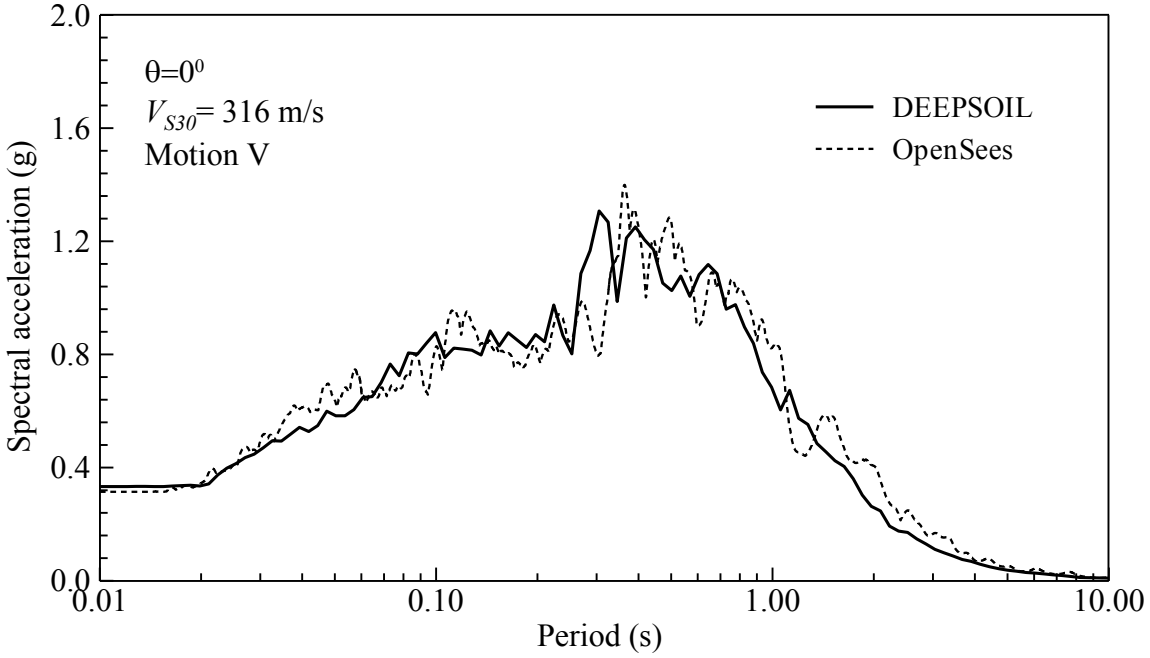

Figure B.6: Sample validation study of the calibrated c_u values by comparing the spectral accelerations from OpenSees model with that of DEEPSOIL for the profile with V_{S30} = 316 m/s for flat ground condition and Motion-V.

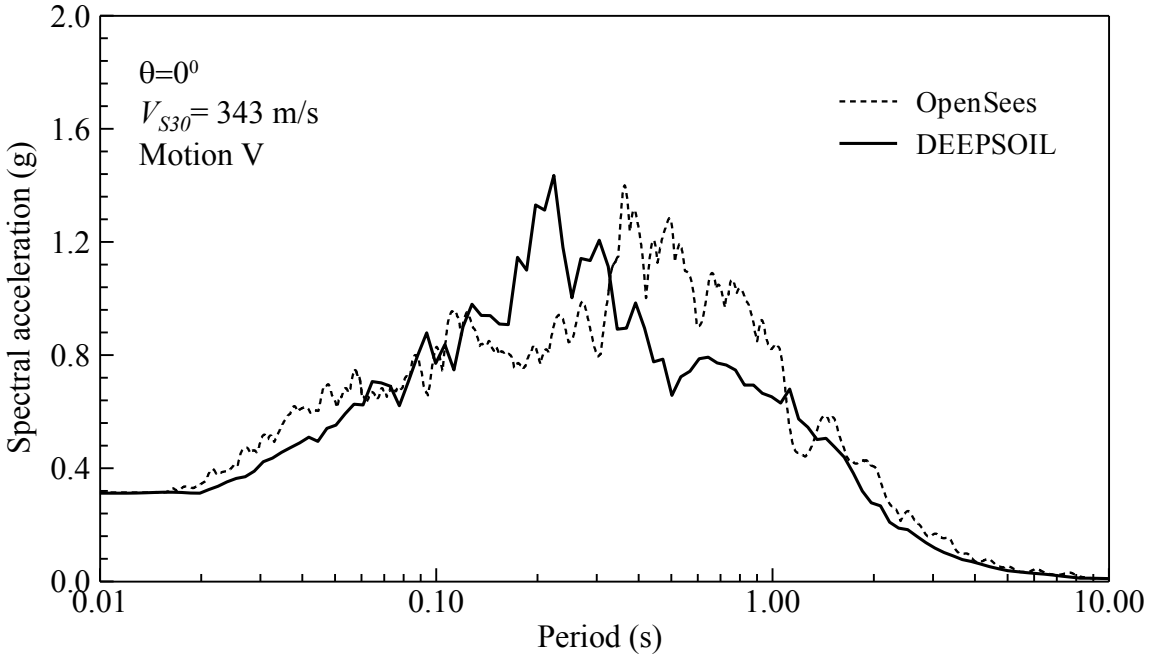

Figure B.7: Sample validation study of the calibrated c_u values by comparing the spectral accelerations from OpenSees model with that of DEEPSOIL for the profile with V_{S30} = 343 m/s for flat ground condition and Motion-V.

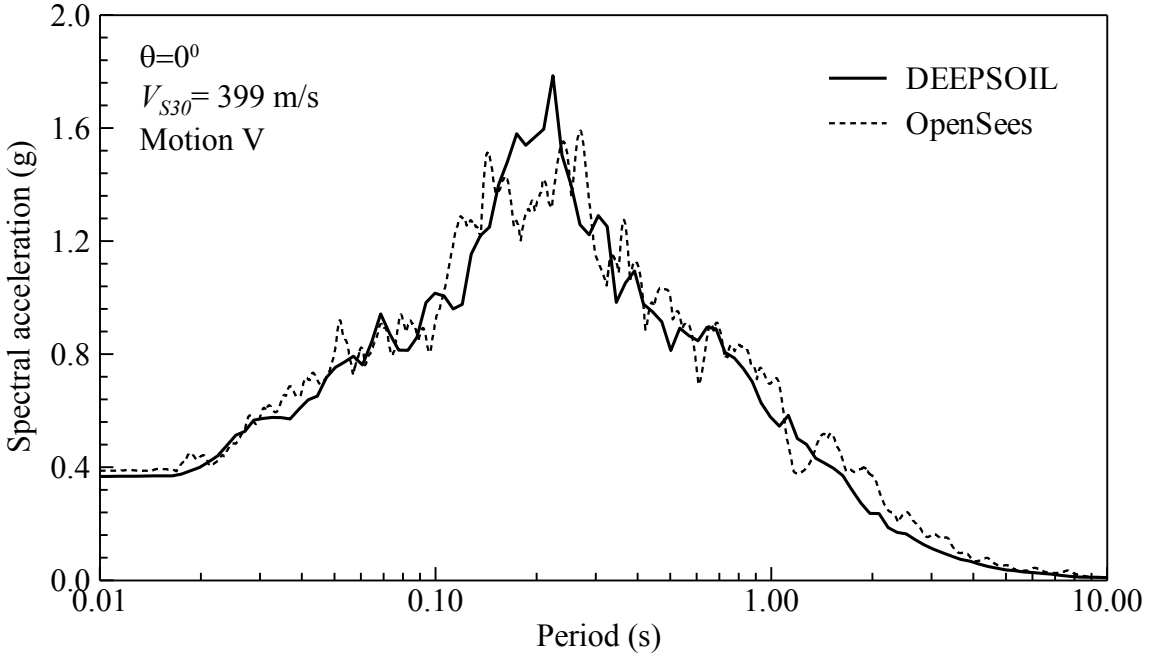

Figure B.8: Sample validation study of the calibrated c_u values by comparing the spectral accelerations from OpenSees model with that of DEEPSOIL for the profile with V_{S30} = 399 m/s for flat ground condition and Motion-V.

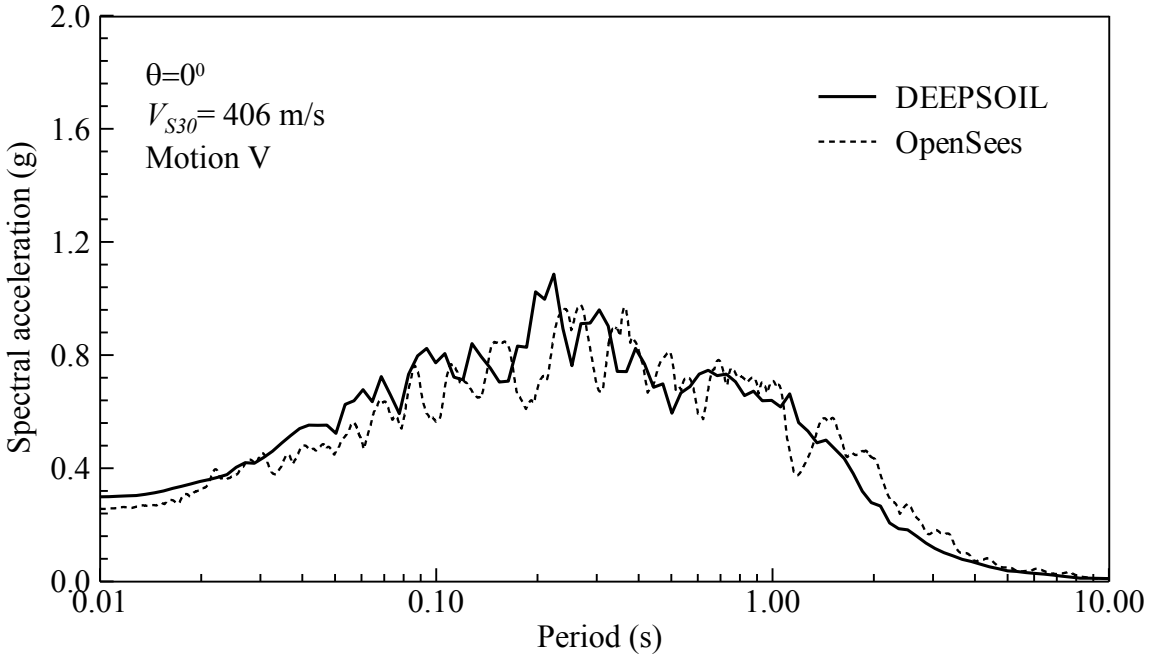

Figure B.9: Sample validation study of the calibrated c_u values by comparing the spectral accelerations from OpenSees model with that of DEEPSOIL for the profile with V_{S30} = 406 m/s for flat ground condition and Motion-V.

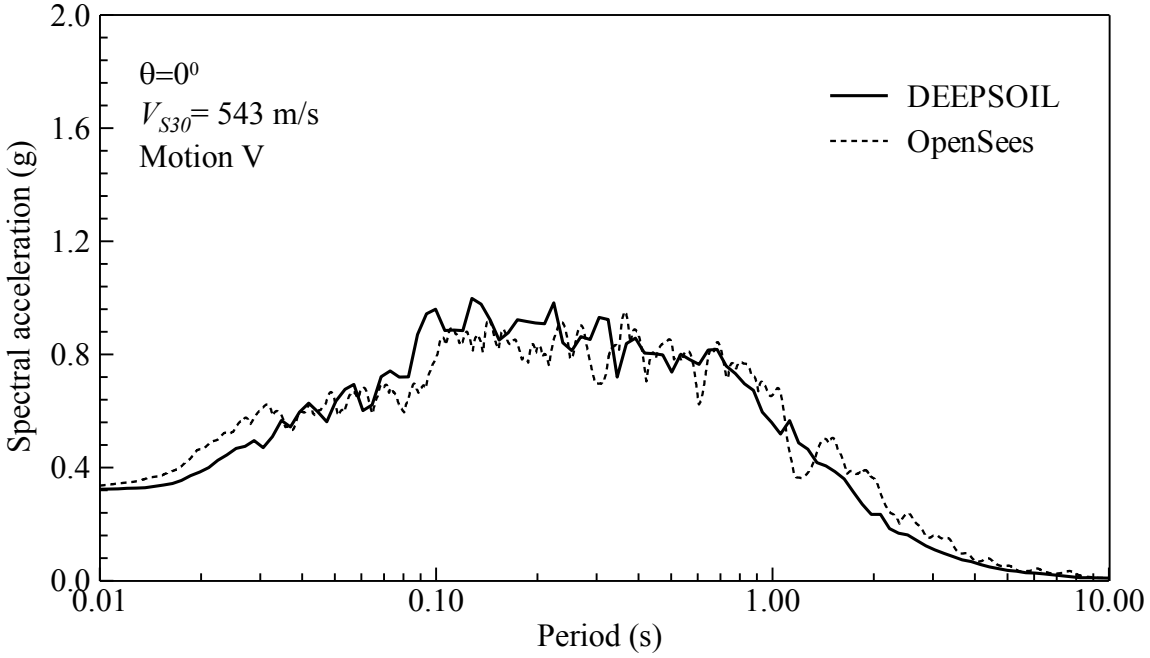

Figure B.10: Sample validation study of the calibrated c_u values by comparing the spectral accelerations from OpenSees model with that of DEEPSOIL for the profile with V_{S30} = 543 m/s for flat ground condition and Motion-V.

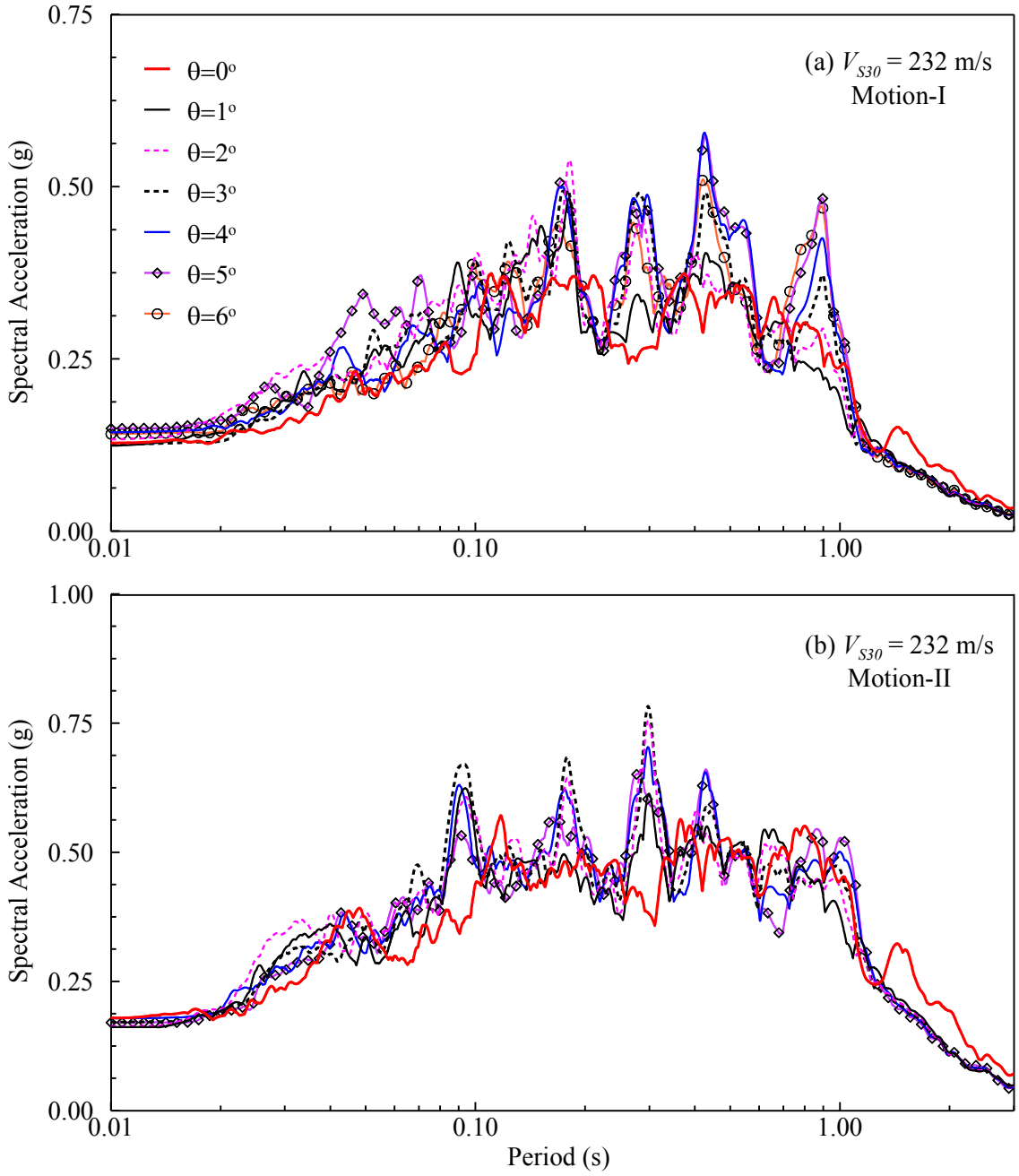
θ=0°
θ=1°
θ=2°
θ=3°
θ=4°
θ=5°
θ=6°
(a) V_{S30} = 232 m/s
Motion-I
(b) V_{S30} = 232 m/s
Motion-II
Spectral Acceleration (g)
Period (s)
0.00
0.25
0.50
0.75
1.00
0.01
0.10
1.00

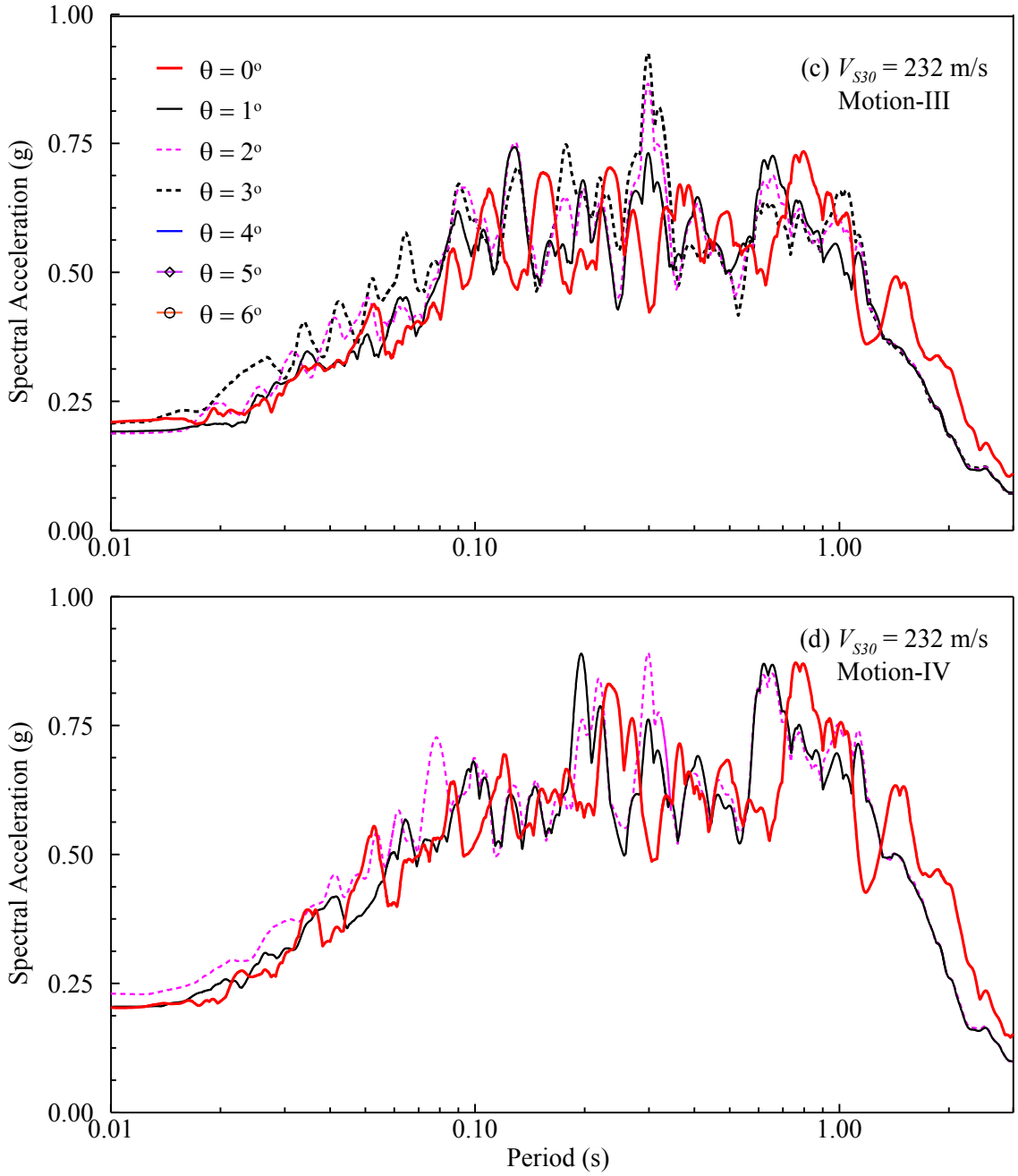
θ = 0°
θ = 1°
θ = 2°
θ = 3°
θ = 4°
θ = 5°
θ = 6°
(c) V_{S30} = 232 m/s
Motion-III
(d) V_{S30} = 232 m/s
Motion-IV
Spectral Acceleration (g)
Period (s)
1.00
0.75
0.50
0.25
0.00
0.01
0.10
1.00

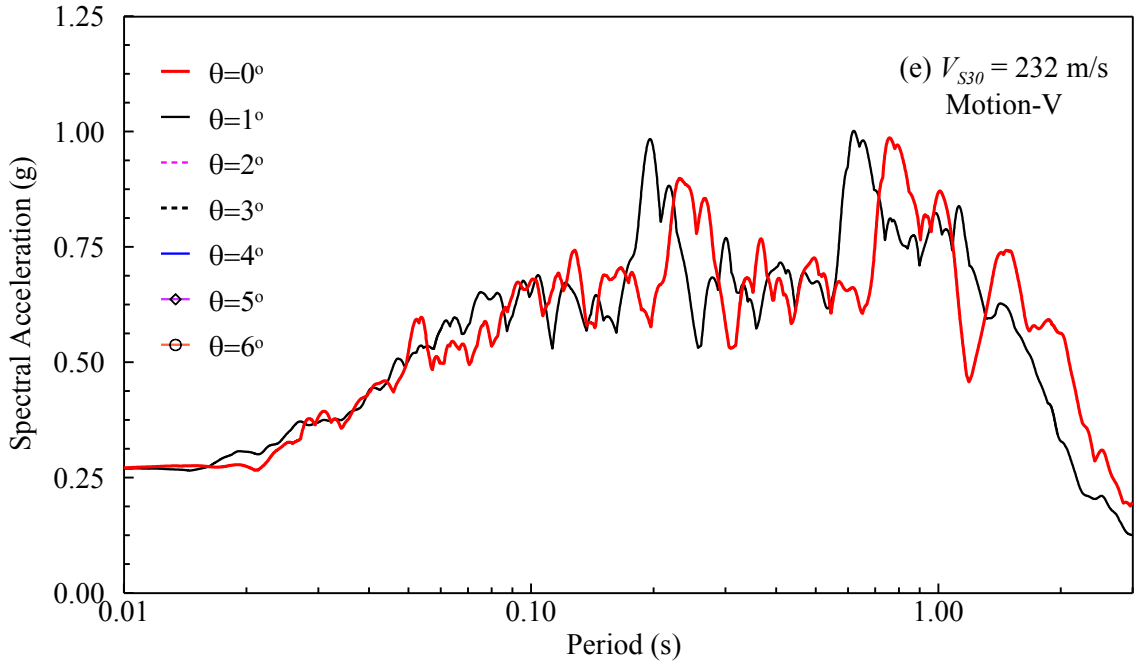

Figure B.11: Sample acceleration response spectra for the profile with V_{S30} =232 m/s from all the sloping ground cases (0^0, 1^0, 2^0, 3^0, 4^0, 5^0, 6^0) with (a) $PGA_{Outcrop}$= 0.1g, (b) $PGA_{Outcrop}$= 0.2g, (c) $PGA_{Outcrop}$= 0.3g, (d) $PGA_{Outcrop}$= 0.4g, and (e) $PGA_{Outcrop}$= 0.5g.

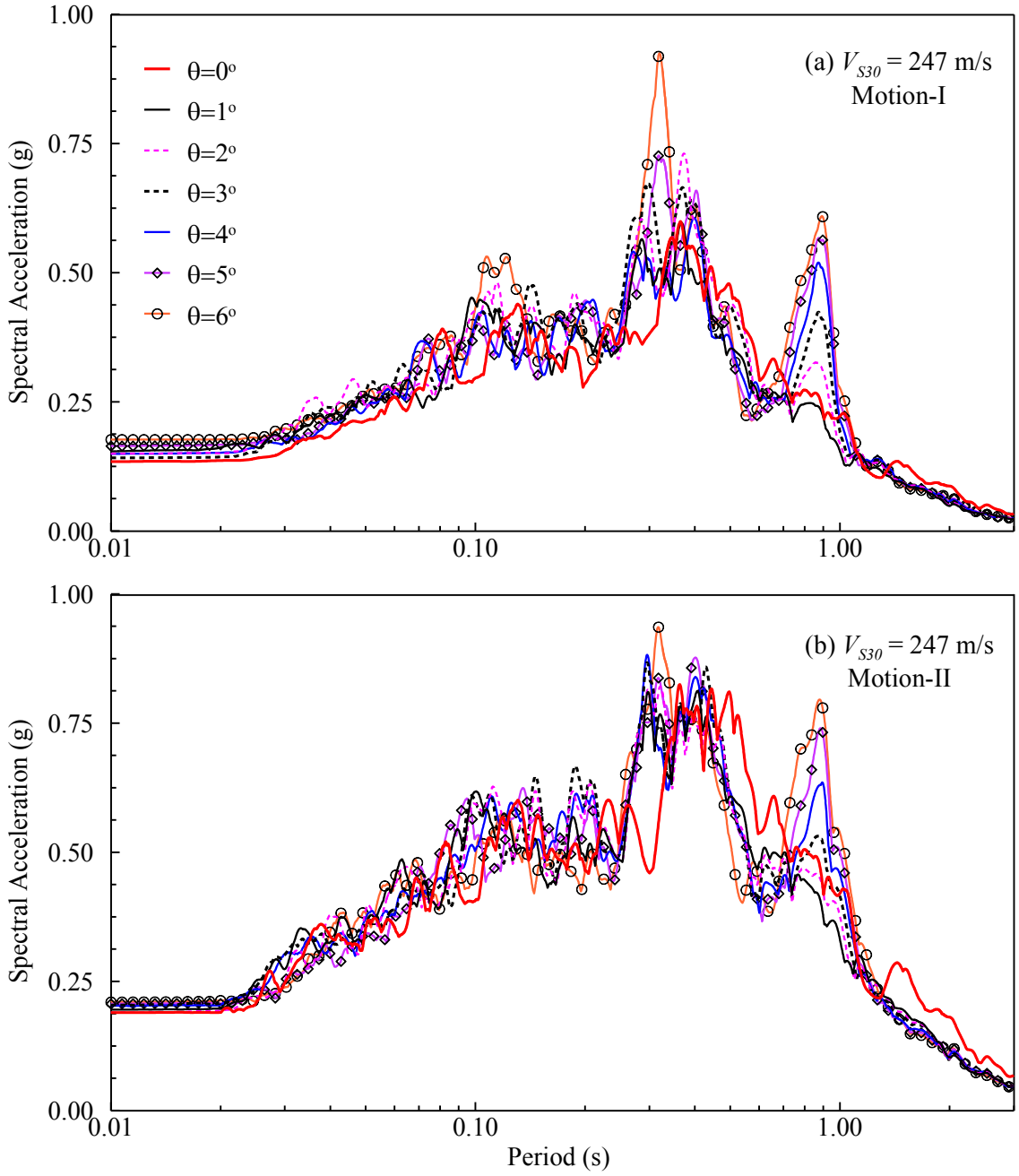
1.00
0.75
0.50
0.25
0.00
Spectral Acceleration (g)
θ=0°
θ=1°
θ=2°
θ=3°
θ=4°
θ=5°
θ=6°
(a) V_{S30} = 247 m/s
Motion-I
0.01
0.10
1.00
(b) V_{S30} = 247 m/s
Motion-II
Period (s)

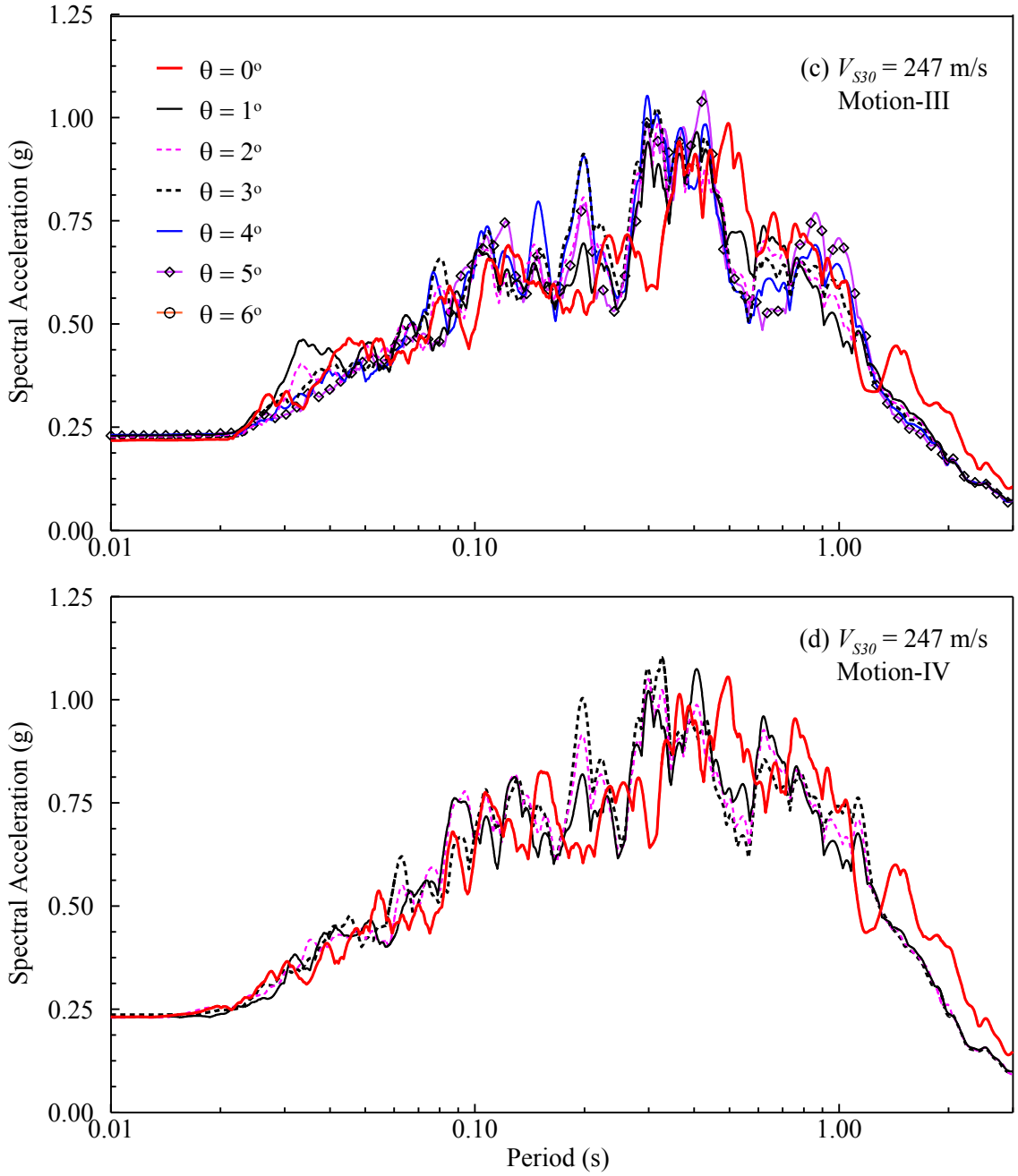
θ = 0°
θ = 1°
θ = 2°
θ = 3°
θ = 4°
θ = 5°
θ = 6°
(c) V_{S30} = 247 m/s
Motion-III
(d) V_{S30} = 247 m/s
Motion-IV
Spectral Acceleration (g)
Period (s)
0.00
0.25
0.50
0.75
1.00
1.25
0.01
0.10
1.00

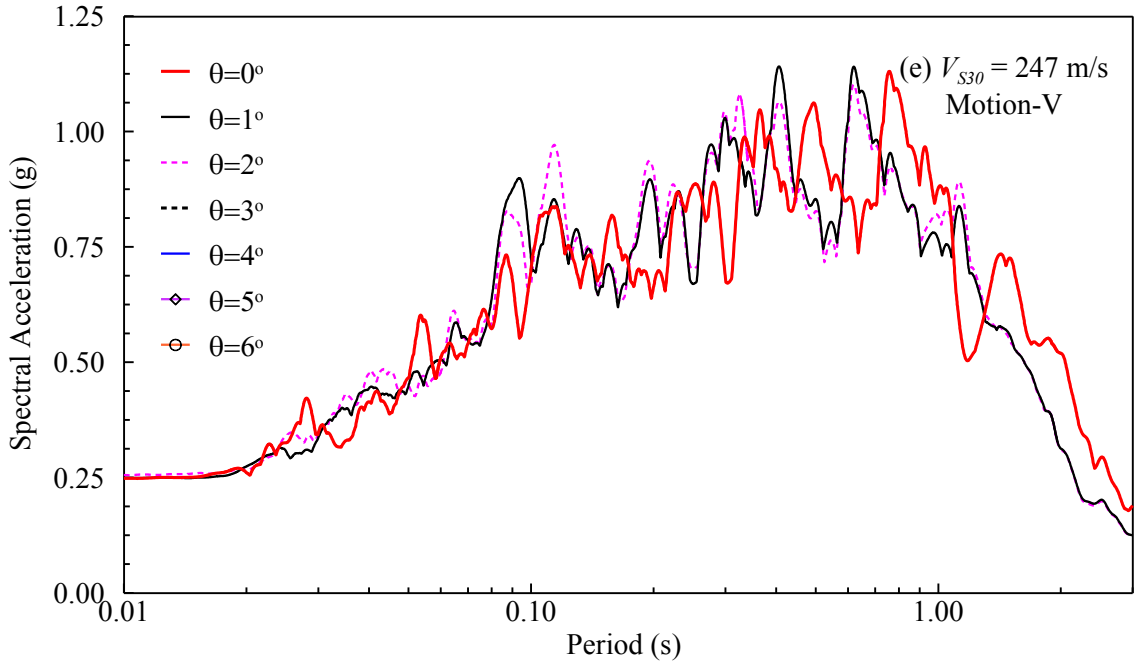

Figure B.12: Sample acceleration response spectra for the profile with V_{S30} =247 m/s from all the sloping ground cases (0^0, 1^0, 2^0, 3^0, 4^0, 5^0, 6^0) with (a) $PGA_{Outcrop}$= 0.1g, (b) $PGA_{Outcrop}$= 0.2g, (c) $PGA_{Outcrop}$= 0.3g, (d) $PGA_{Outcrop}$= 0.4g, and (e) $PGA_{Outcrop}$= 0.5g.

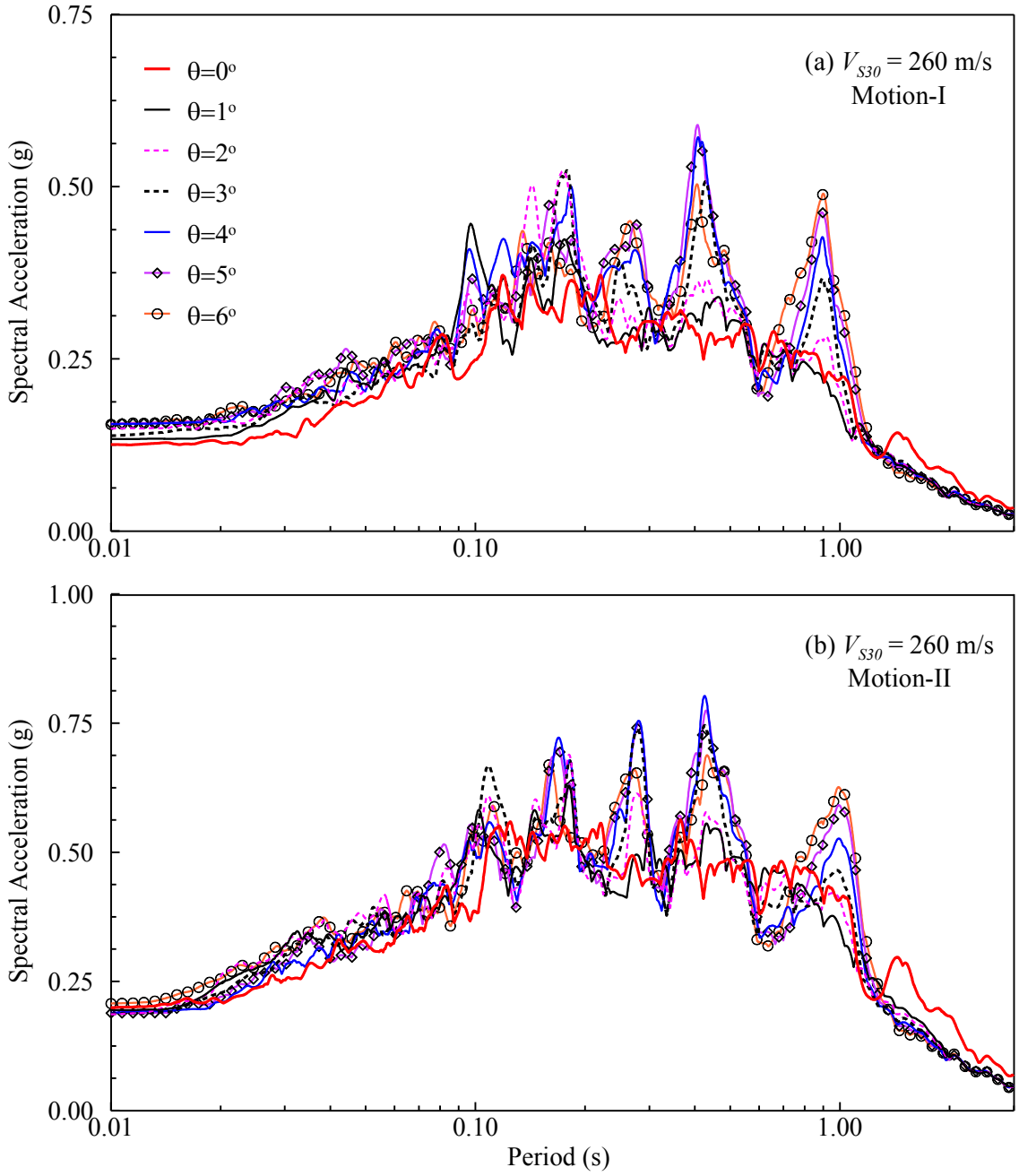
θ=0°
θ=1°
θ=2°
θ=3°
θ=4°
θ=5°
θ=6°
(a) V_{S30} = 260 m/s
Motion-I
(b) V_{S30} = 260 m/s
Motion-II
Spectral Acceleration (g)
Period (s)
0.00
0.25
0.50
0.75
1.00
0.01
0.10
1.00

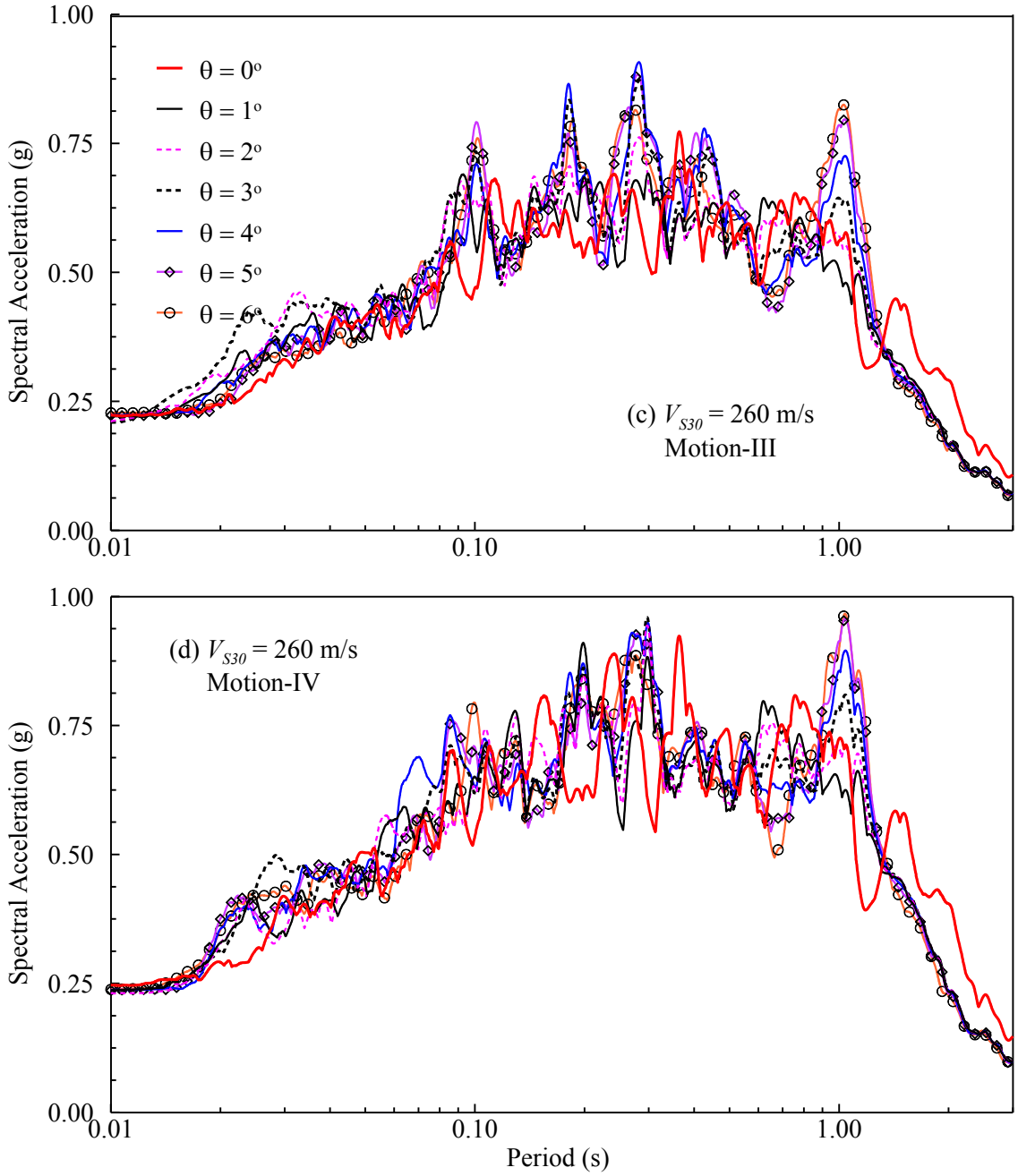
1.00
0.75
0.50
0.25
0.00
Spectral Acceleration (g)
θ = 0°
θ = 1°
θ = 2°
θ = 3°
θ = 4°
θ = 5°
θ = 6°
(c) V_{S30} = 260 m/s
Motion-III
0.01
0.10
1.00
(d) V_{S30} = 260 m/s
Motion-IV
Period (s)

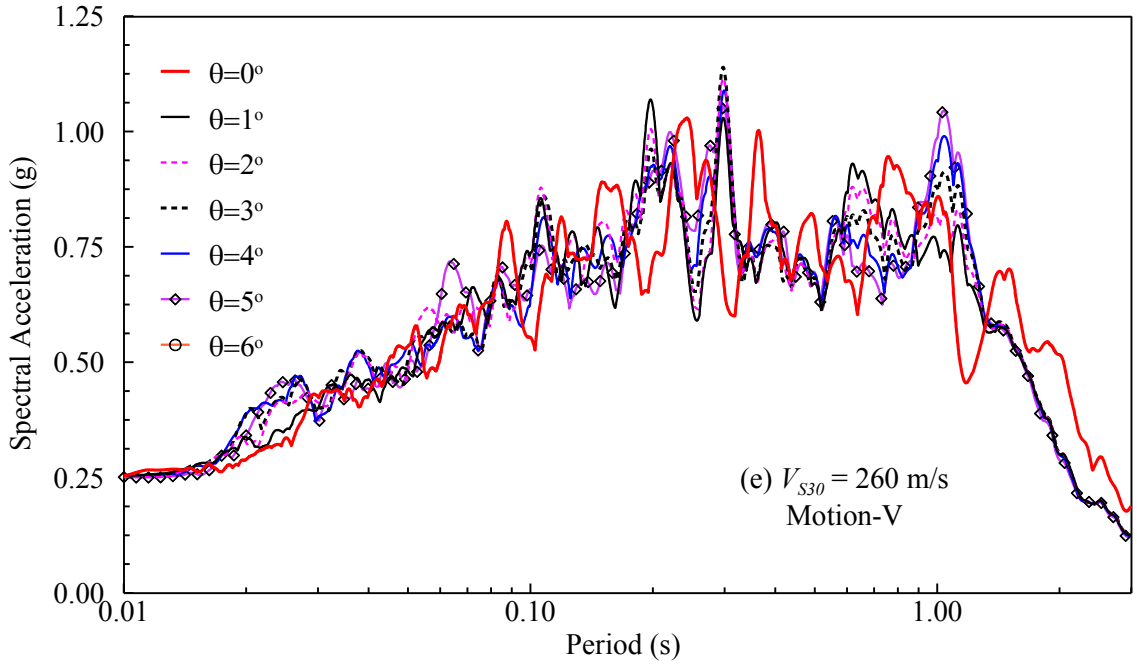

Figure B.13: Sample acceleration response spectra for the profile with V_{S30} =260 m/s from all the sloping ground cases (0^0, 1^0, 2^0, 3^0, 4^0, 5^0, 6^0) with (a) $PGA_{Outcrop}$= 0.1g, (b) $PGA_{Outcrop}$= 0.2g, (c) $PGA_{Outcrop}$= 0.3g, (d) $PGA_{Outcrop}$= 0.4g, and (e) $PGA_{Outcrop}$= 0.5g.

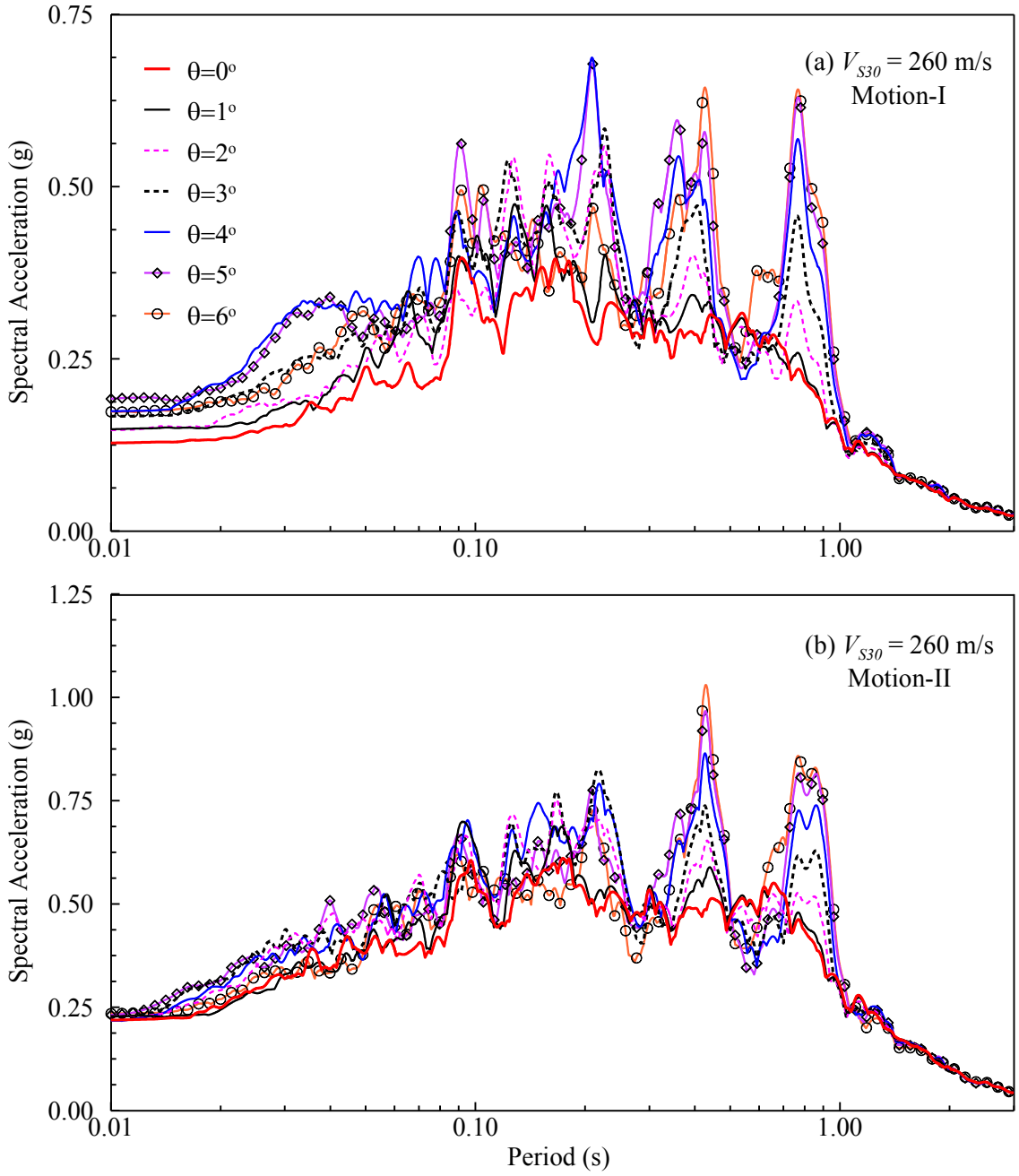
0.75
0.50
0.25
0.00
Spectral Acceleration (g)
θ=0°
θ=1°
θ=2°
θ=3°
θ=4°
θ=5°
θ=6°
(a) V_{S30} = 260 m/s
Motion-I
0.01
0.10
1.00
1.25
1.00
0.75
0.50
0.25
0.00
Spectral Acceleration (g)
(b) V_{S30} = 260 m/s
Motion-II
0.01
0.10
1.00
Period (s)

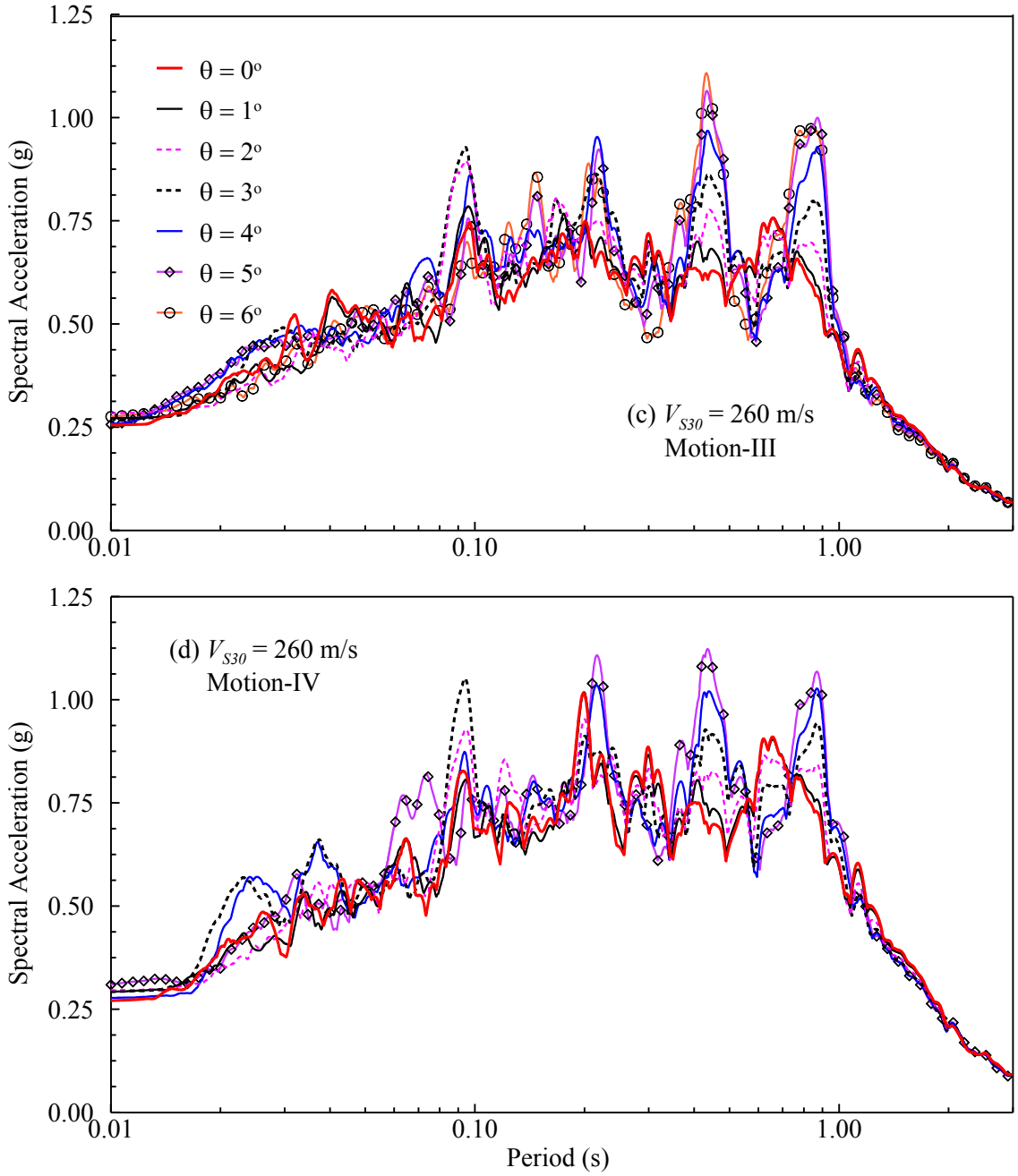
θ = 0°
θ = 1°
θ = 2°
θ = 3°
θ = 4°
θ = 5°
θ = 6°
(c) V_{S30} = 260 m/s
Motion-III
(d) V_{S30} = 260 m/s
Motion-IV
Spectral Acceleration (g)
Period (s)
0.00
0.25
0.50
0.75
1.00
1.25
0.01
0.10
1.00

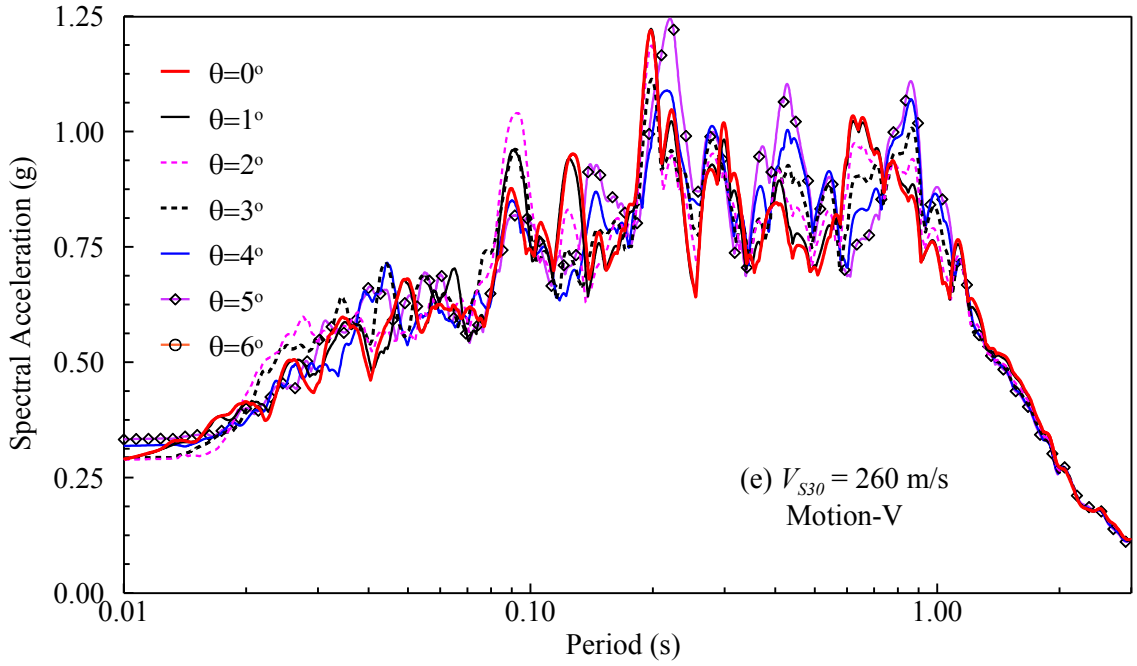

Figure B.14: Sample acceleration response spectra for the profile with V_{S30} =260 m/s from all the sloping ground cases (0^0, 1^0, 2^0, 3^0, 4^0, 5^0, 6^0) with (a) $PGA_{Outcrop}$= 0.1g, (b) $PGA_{Outcrop}$= 0.2g, (c) $PGA_{Outcrop}$= 0.3g, (d) $PGA_{Outcrop}$= 0.4g, and (e) $PGA_{Outcrop}$= 0.5g.

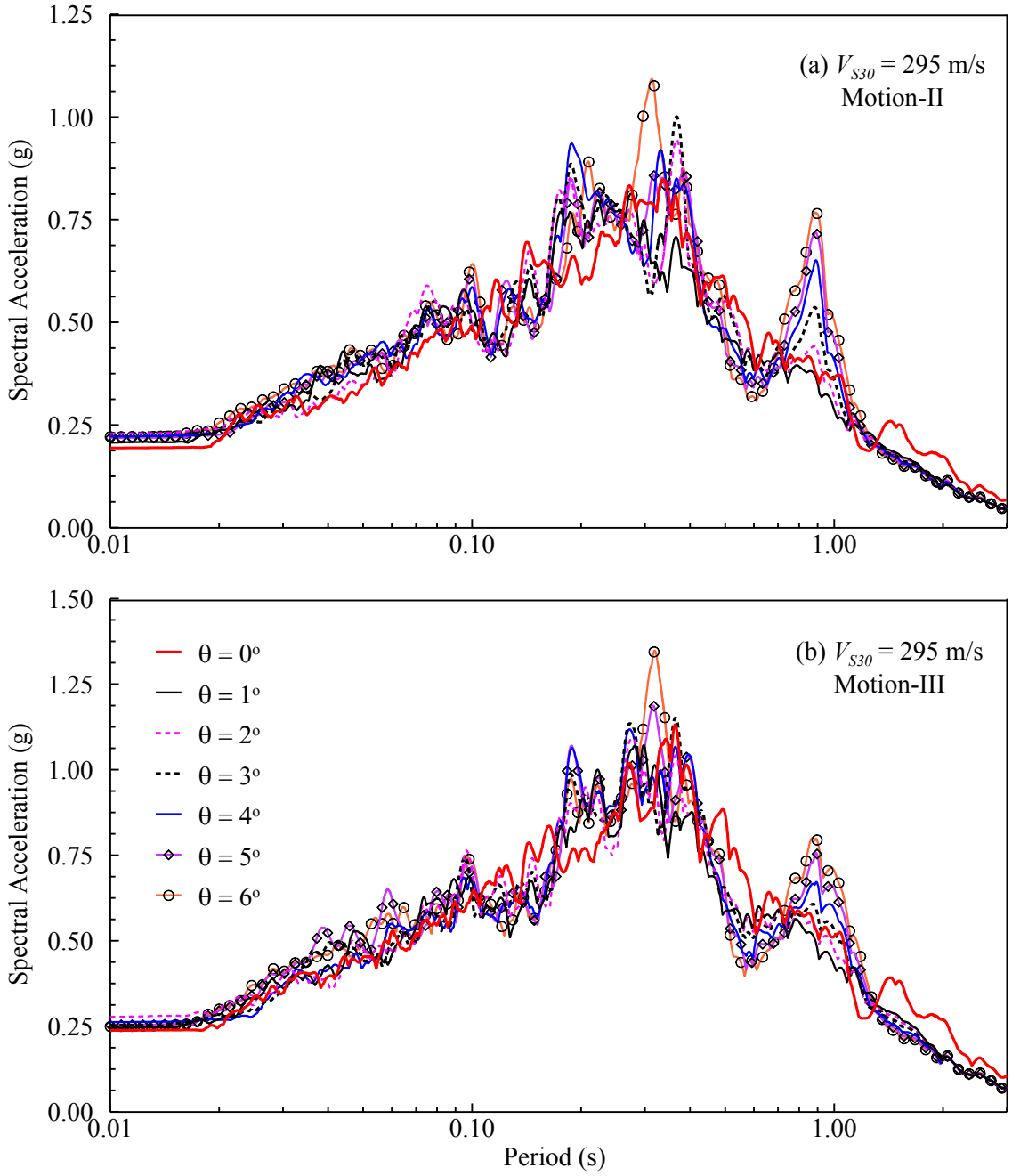
(a) V_{S30} = 295 m/s
Motion-II
(b) V_{S30} = 295 m/s
Motion-III
θ = 0°
θ = 1°
θ = 2°
θ = 3°
θ = 4°
θ = 5°
θ = 6°
Spectral Acceleration (g)
Period (s)
0.00
0.25
0.50
0.75
1.00
1.25
1.50
0.01
0.10
1.00

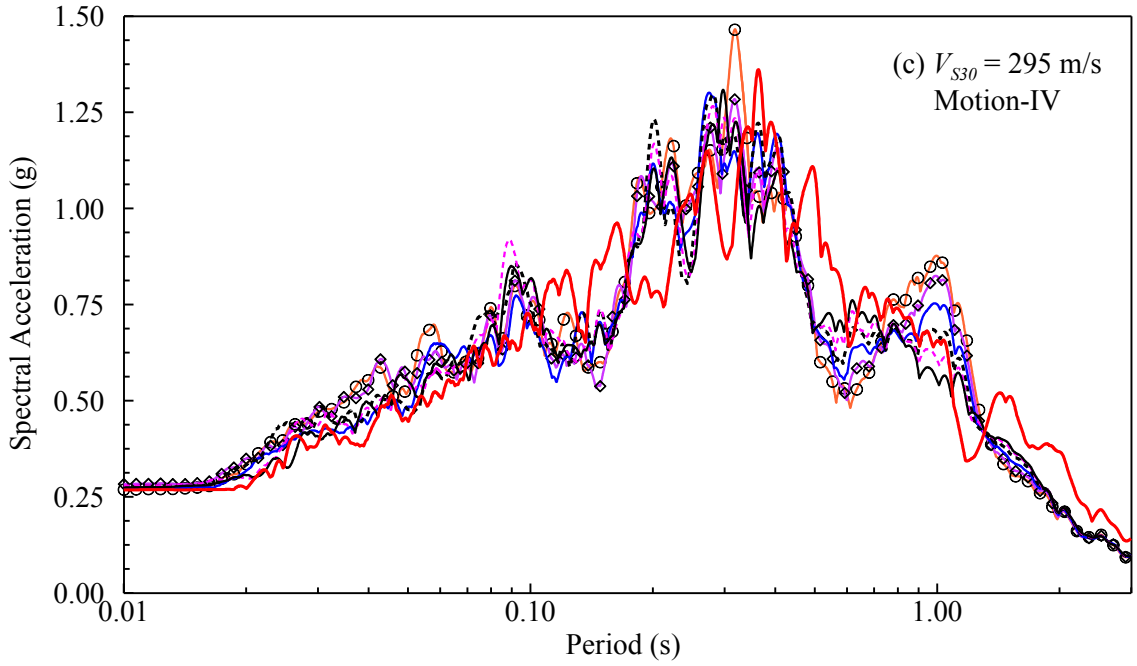

Figure B.15: Sample acceleration response spectra for the profile with V_{S30} =295 m/s from all the sloping ground cases (0^0, 1^0, 2^0, 3^0, 4^0, 5^0, 6^0) with (a) $PGA_{Outcrop}$= 0.2g, (b) $PGA_{Outcrop}$= 0.3g, and (c) $PGA_{Outcrop}$= 0.4g.

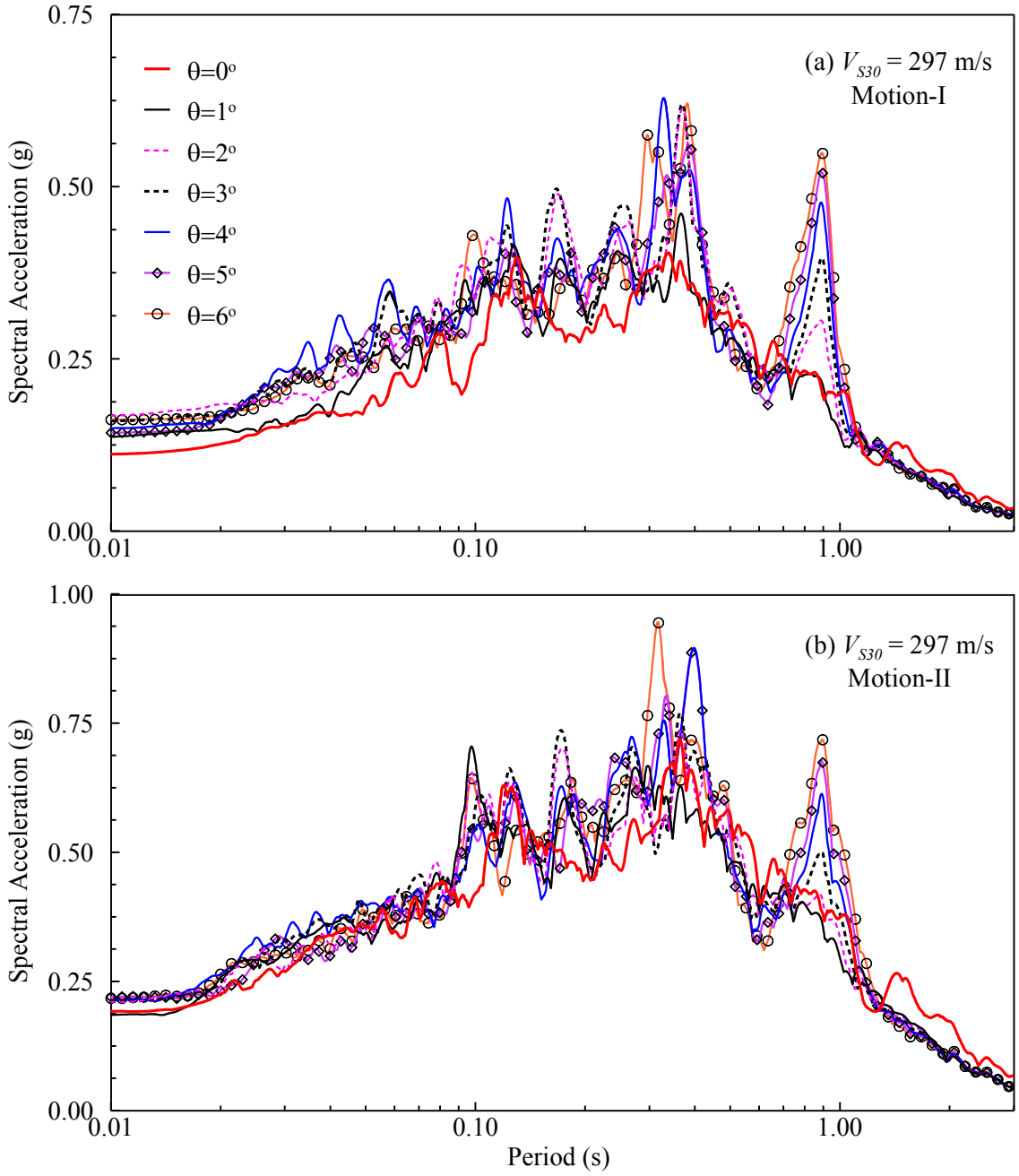
θ=0°
θ=1°
θ=2°
θ=3°
θ=4°
θ=5°
θ=6°
(a) V_{S30} = 297 m/s
Motion-I
(b) V_{S30} = 297 m/s
Motion-II
Spectral Acceleration (g)
Period (s)
0.00
0.25
0.50
0.75
1.00
0.01
0.10
1.00

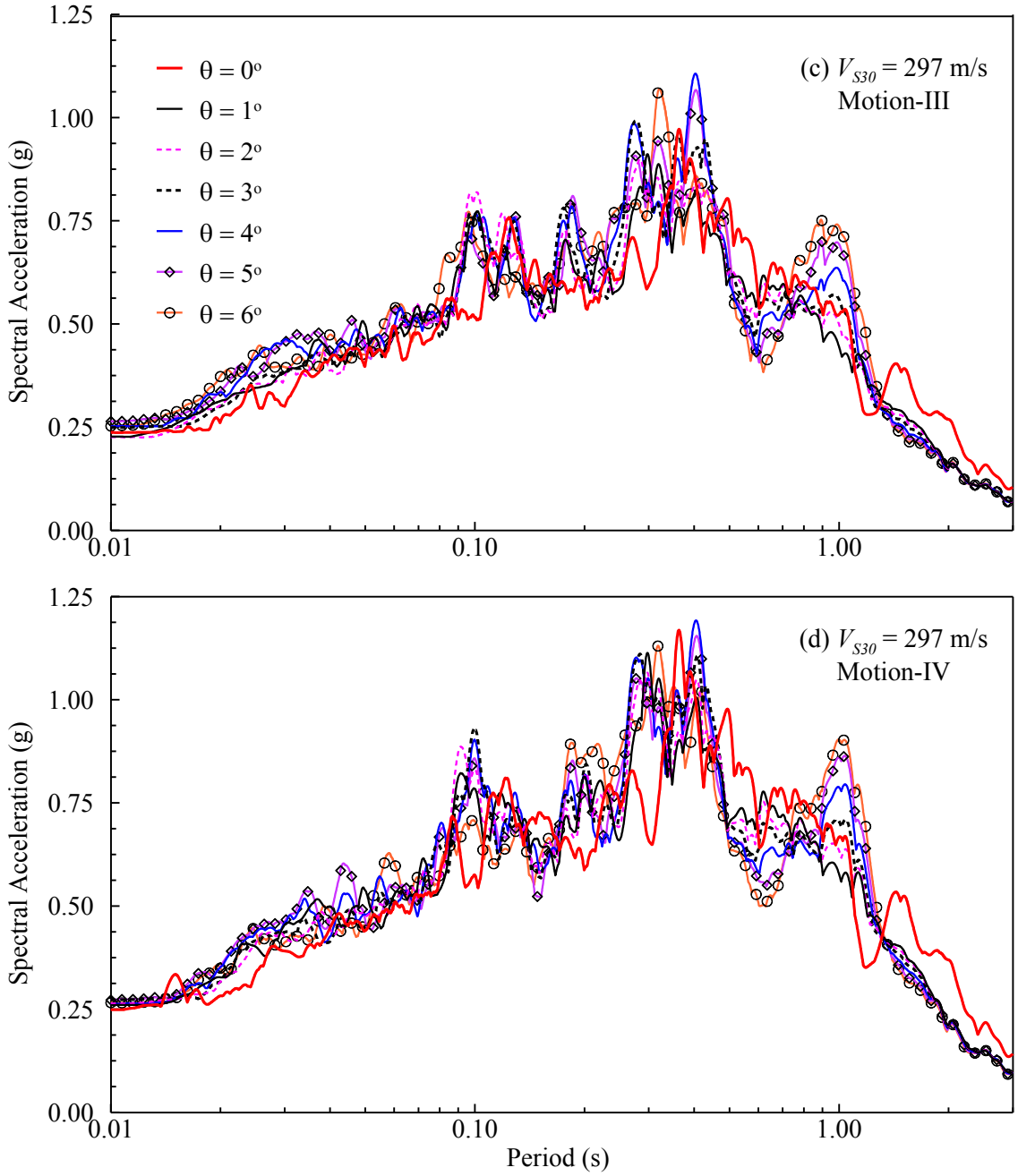
θ = 0°
θ = 1°
θ = 2°
θ = 3°
θ = 4°
θ = 5°
θ = 6°
(c) V_{S30} = 297 m/s
Motion-III
(d) V_{S30} = 297 m/s
Motion-IV
Spectral Acceleration (g)
Period (s)
0.00
0.25
0.50
0.75
1.00
1.25
0.01
0.10
1.00

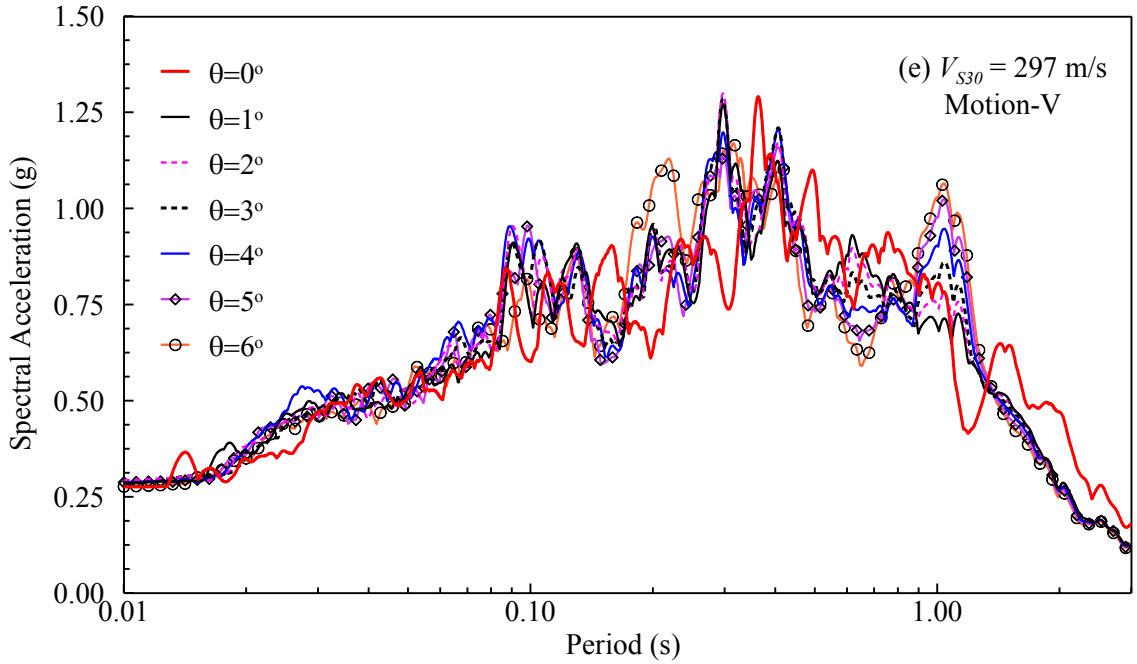

Figure B.16: Sample acceleration response spectra for the profile with V_{S30} =297 m/s from all the sloping ground cases (0^0, 1^0, 2^0, 3^0, 4^0, 5^0, 6^0) with (a) $PGA_{Outcrop}$= 0.1g, (b) $PGA_{Outcrop}$= 0.2g, (c) $PGA_{Outcrop}$= 0.3g, (d) $PGA_{Outcrop}$= 0.4g, and (e) $PGA_{Outcrop}$= 0.5g.

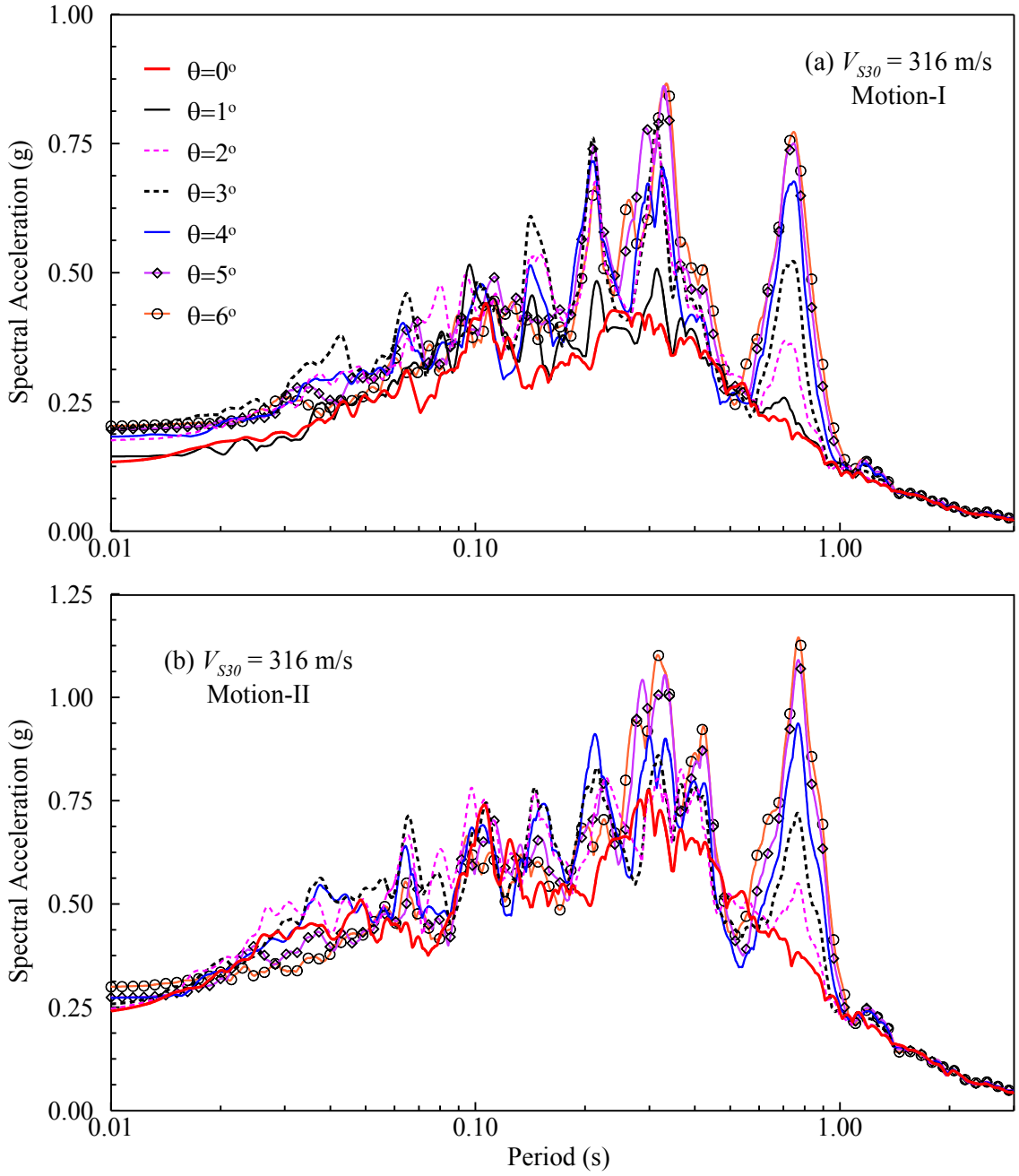
1.00
0.75
0.50
0.25
0.00
Spectral Acceleration (g)
θ=0°
θ=1°
θ=2°
θ=3°
θ=4°
θ=5°
θ=6°
(a) V_{S30} = 316 m/s
Motion-I
0.01
0.10
1.00
1.25
1.00
0.75
0.50
0.25
0.00
Spectral Acceleration (g)
(b) V_{S30} = 316 m/s
Motion-II
0.01
0.10
1.00
Period (s)

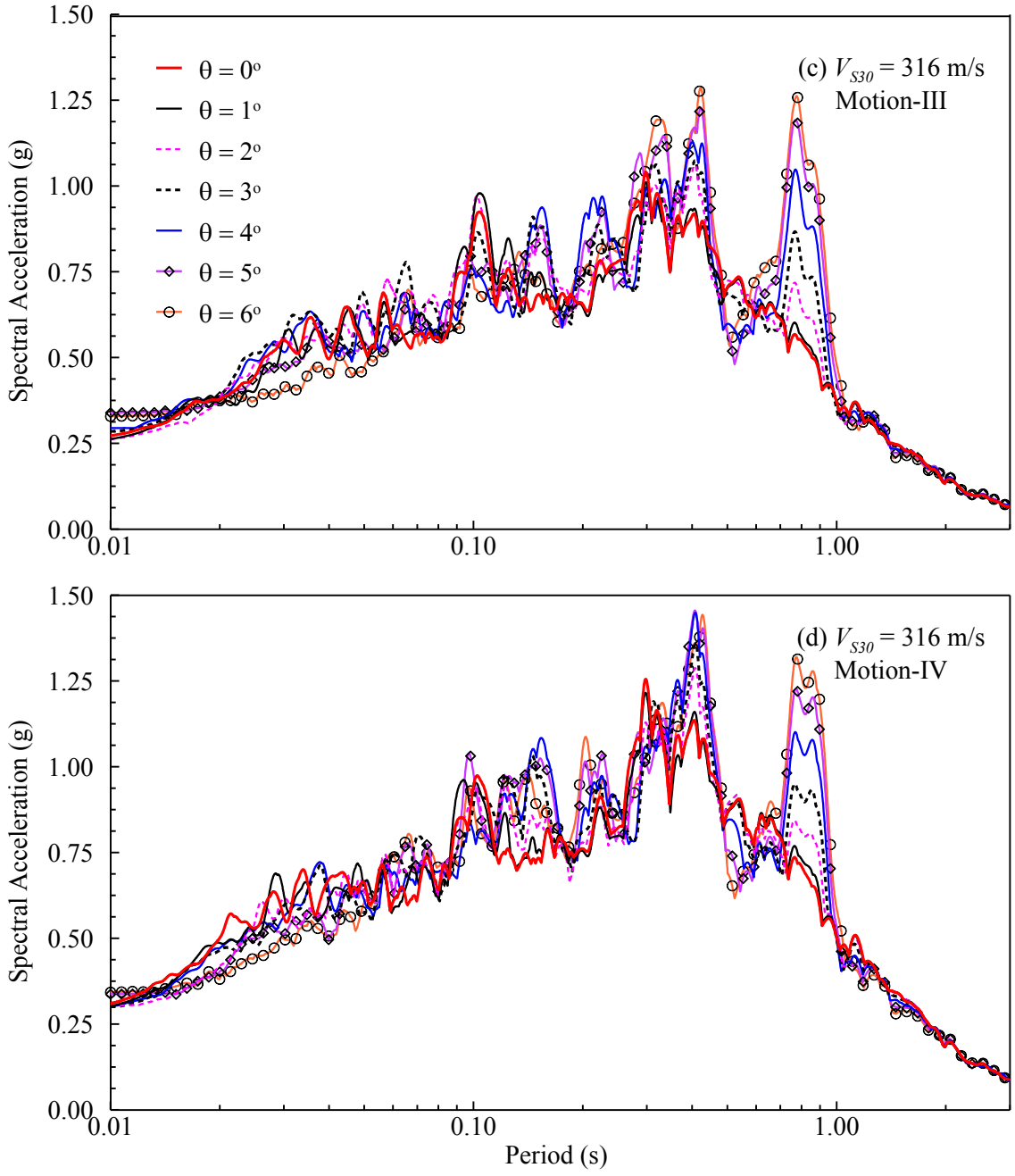
θ = 0°
θ = 1°
θ = 2°
θ = 3°
θ = 4°
θ = 5°
θ = 6°
(c) V_{S30} = 316 m/s
Motion-III
(d) V_{S30} = 316 m/s
Motion-IV
Spectral Acceleration (g)
Period (s)
1.50
1.25
1.00
0.75
0.50
0.25
0.00
0.01
0.10
1.00

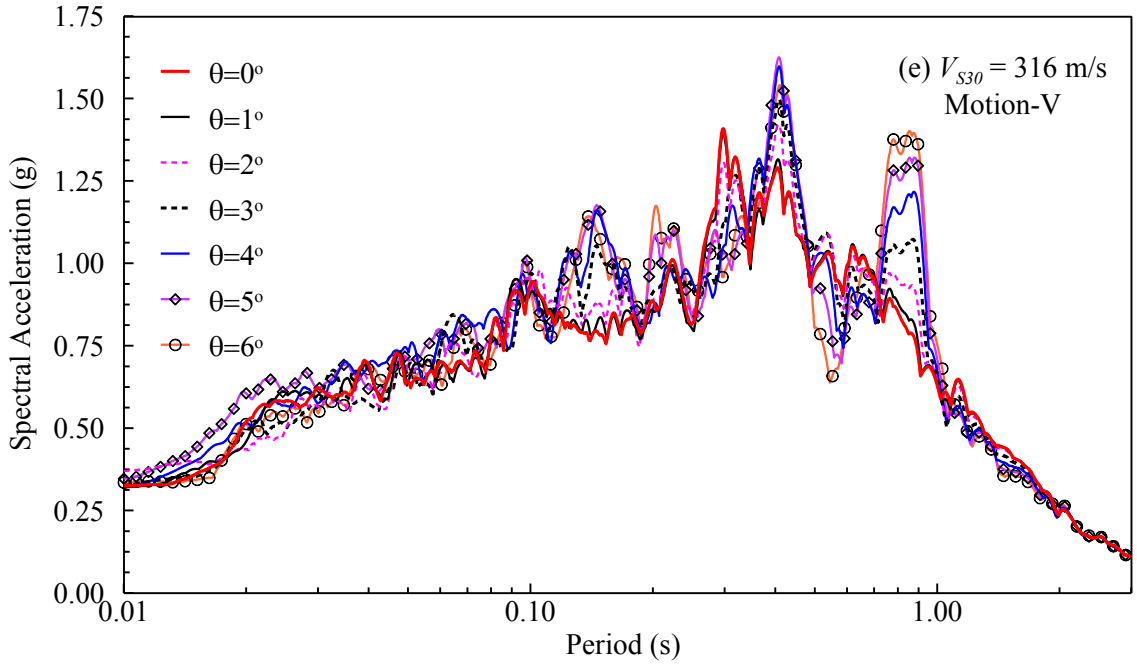

Figure B.17: Sample acceleration response spectra for the profile with V_{S30} =316 m/s from all the sloping ground cases (0^0, 1^0, 2^0, 3^0, 4^0, 5^0, 6^0) with (a) $PGA_{Outcrop}$= 0.1g, (b) $PGA_{Outcrop}$= 0.2g, (c) $PGA_{Outcrop}$= 0.3g, (d) $PGA_{Outcrop}$= 0.4g, and (e) $PGA_{Outcrop}$= 0.5g.

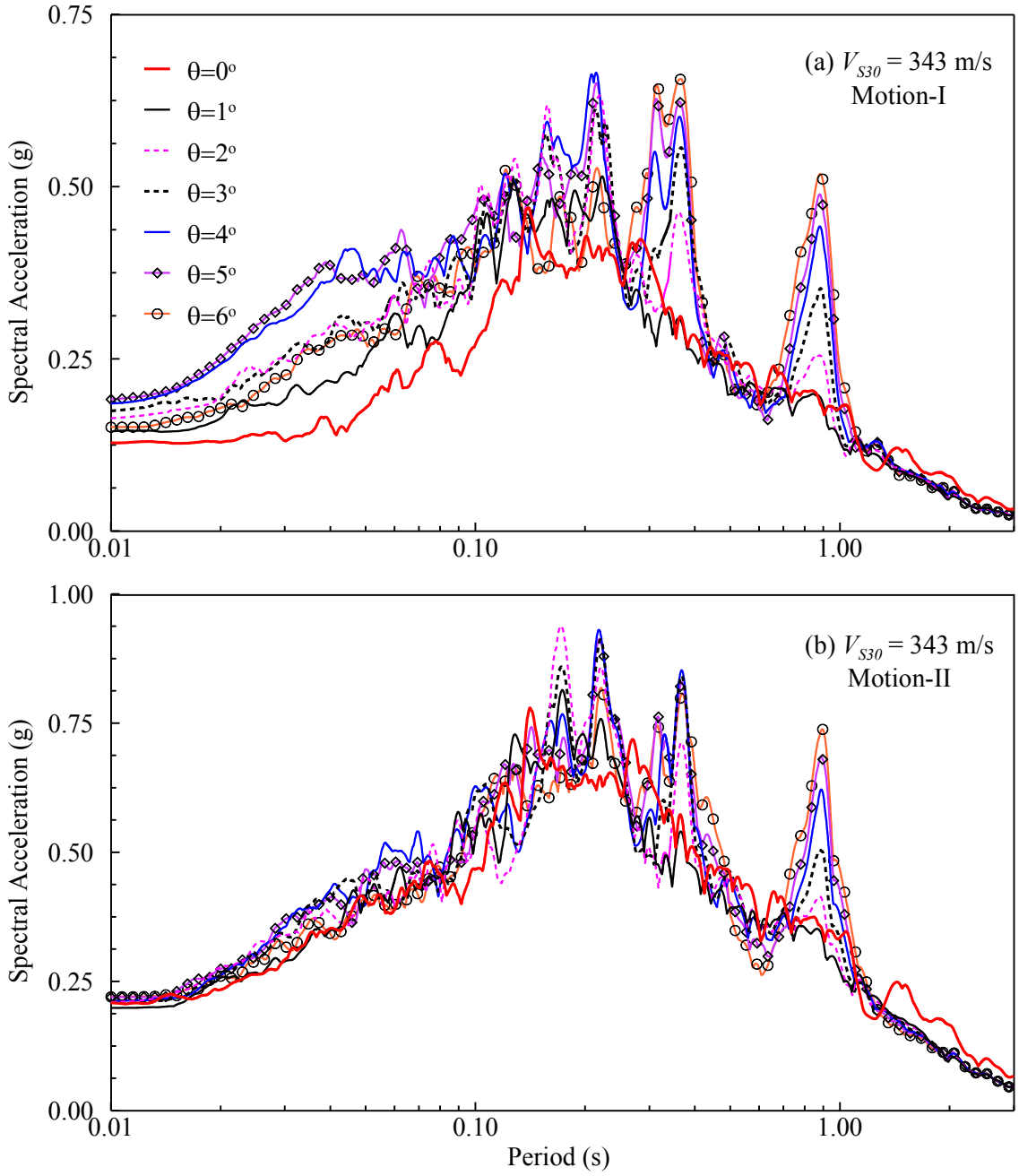
θ=0°
θ=1°
θ=2°
θ=3°
θ=4°
θ=5°
θ=6°
(a) V_{S30} = 343 m/s
Motion-I
(b) V_{S30} = 343 m/s
Motion-II
Spectral Acceleration (g)
Period (s)
0.00
0.25
0.50
0.75
1.00
0.01
0.10
1.00

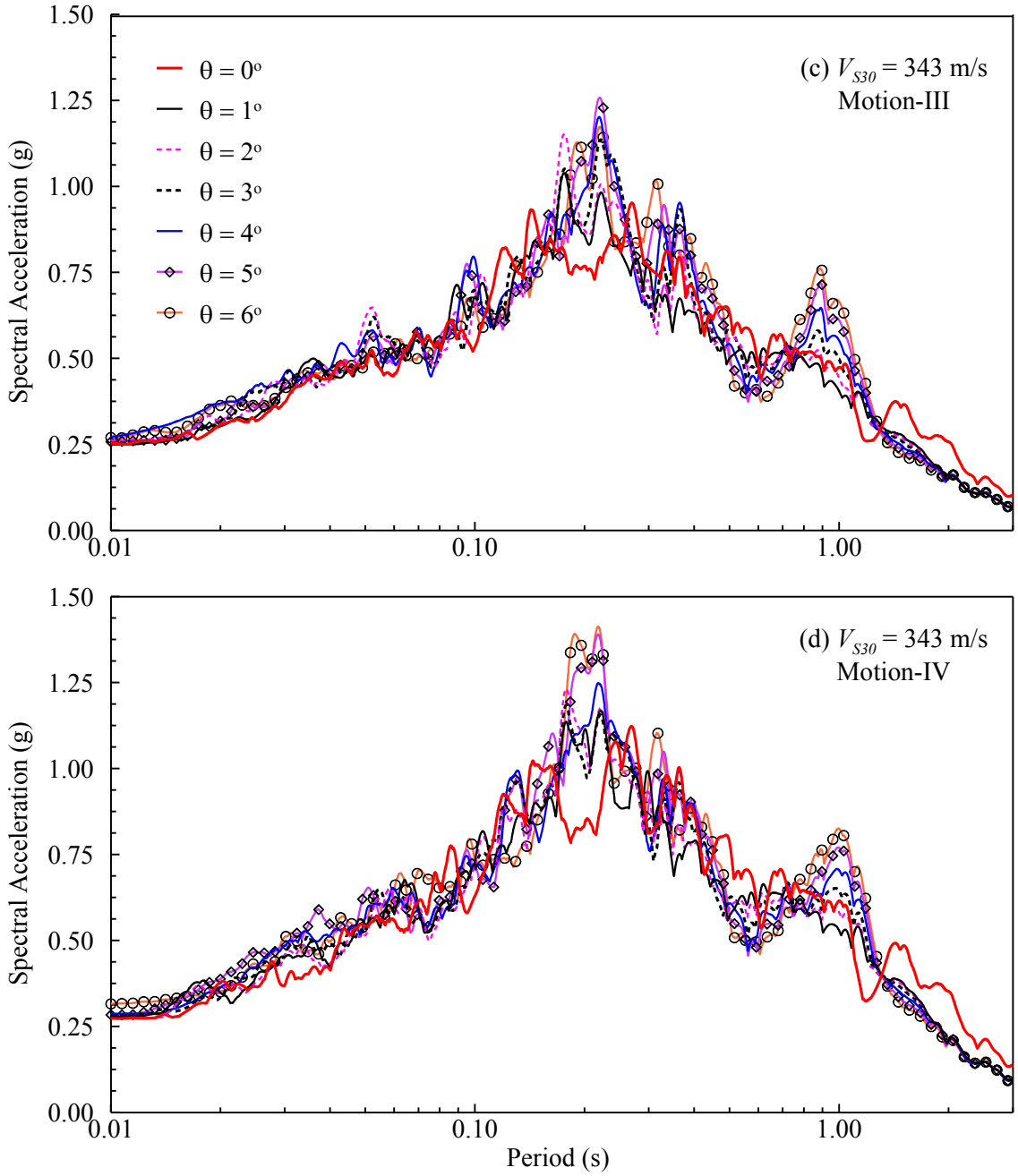
θ = 0°
θ = 1°
θ = 2°
θ = 3°
θ = 4°
θ = 5°
θ = 6°
(c) V_{S30} = 343 m/s
Motion-III
(d) V_{S30} = 343 m/s
Motion-IV
Spectral Acceleration (g)
Period (s)
1.50
1.25
1.00
0.75
0.50
0.25
0.00
0.01
0.10
1.00

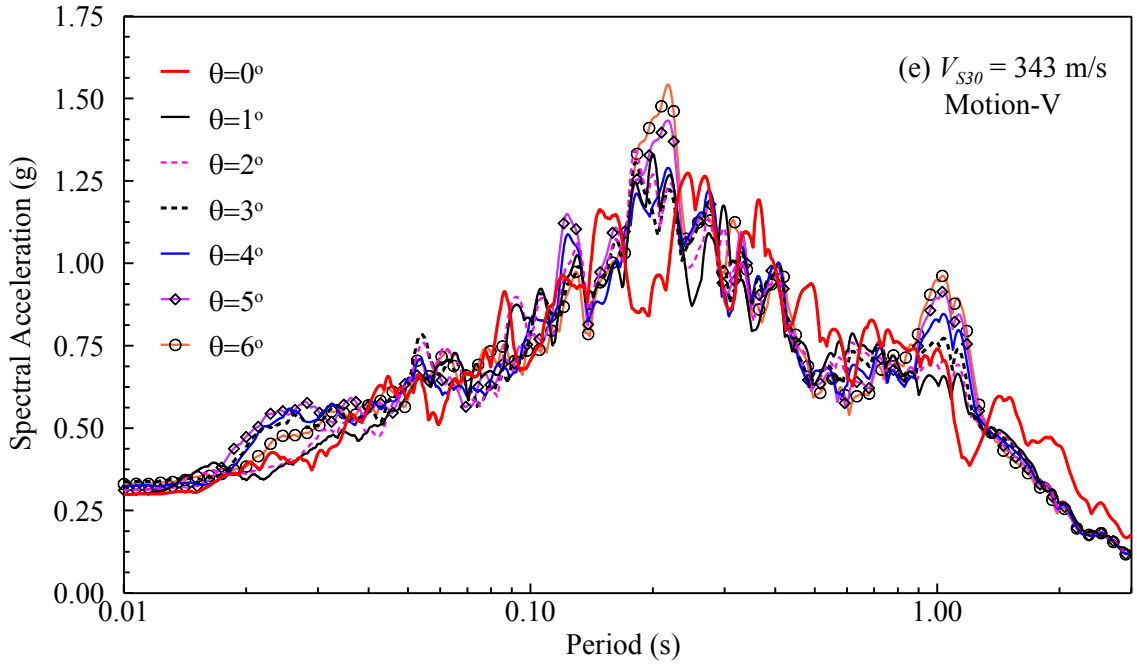

Figure B.18: Sample acceleration response spectra for the profile with V_{S30} =343 m/s from all the sloping ground cases (0^0, 1^0, 2^0, 3^0, 4^0, 5^0, 6^0) with (a) $PGA_{Outcrop}$= 0.1g, (b) $PGA_{Outcrop}$= 0.2g, (c) $PGA_{Outcrop}$= 0.3g, (d) $PGA_{Outcrop}$= 0.4g, and (e) $PGA_{Outcrop}$= 0.5g.

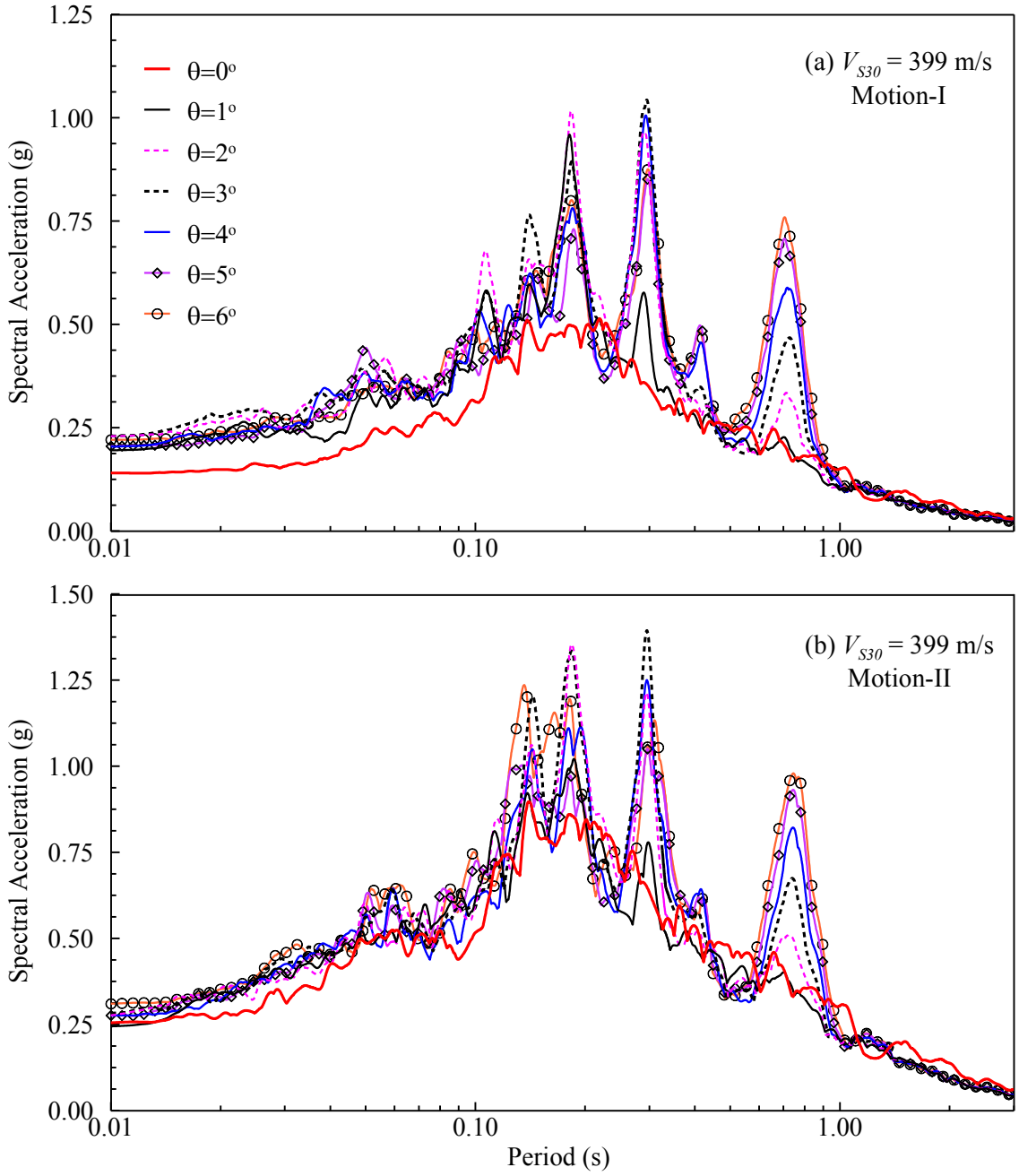
θ=0°
θ=1°
θ=2°
θ=3°
θ=4°
θ=5°
θ=6°
(a) V_{S30} = 399 m/s
Motion-I
(b) V_{S30} = 399 m/s
Motion-II
Spectral Acceleration (g)
Period (s)
0.00
0.25
0.50
0.75
1.00
1.25
1.50
0.01
0.10
1.00

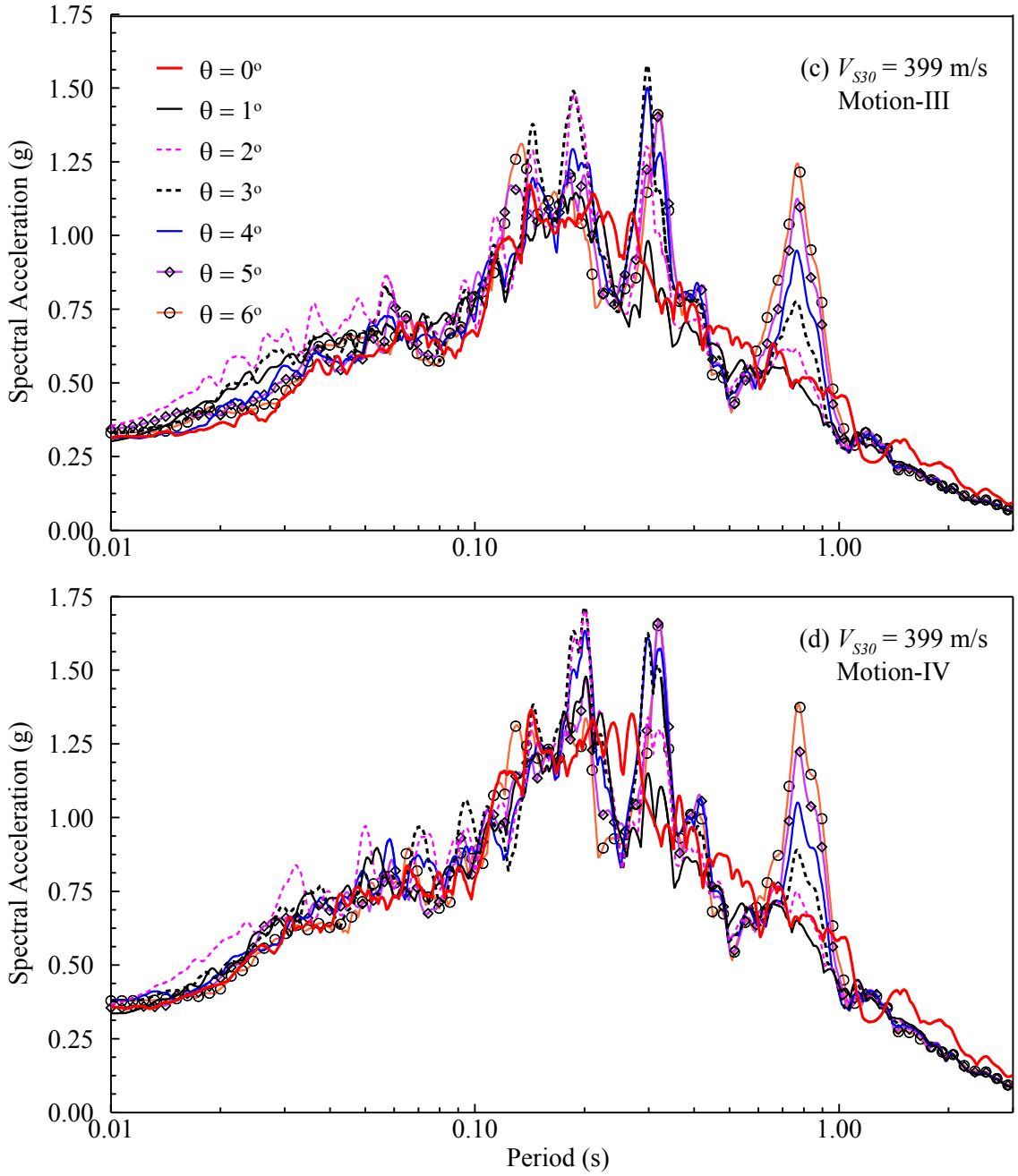
θ = 0°
θ = 1°
θ = 2°
θ = 3°
θ = 4°
θ = 5°
θ = 6°
(c) V_{S30} = 399 m/s
Motion-III
(d) V_{S30} = 399 m/s
Motion-IV
Spectral Acceleration (g)
Period (s)
0.00
0.25
0.50
0.75
1.00
1.25
1.50
1.75
0.01
0.10
1.00

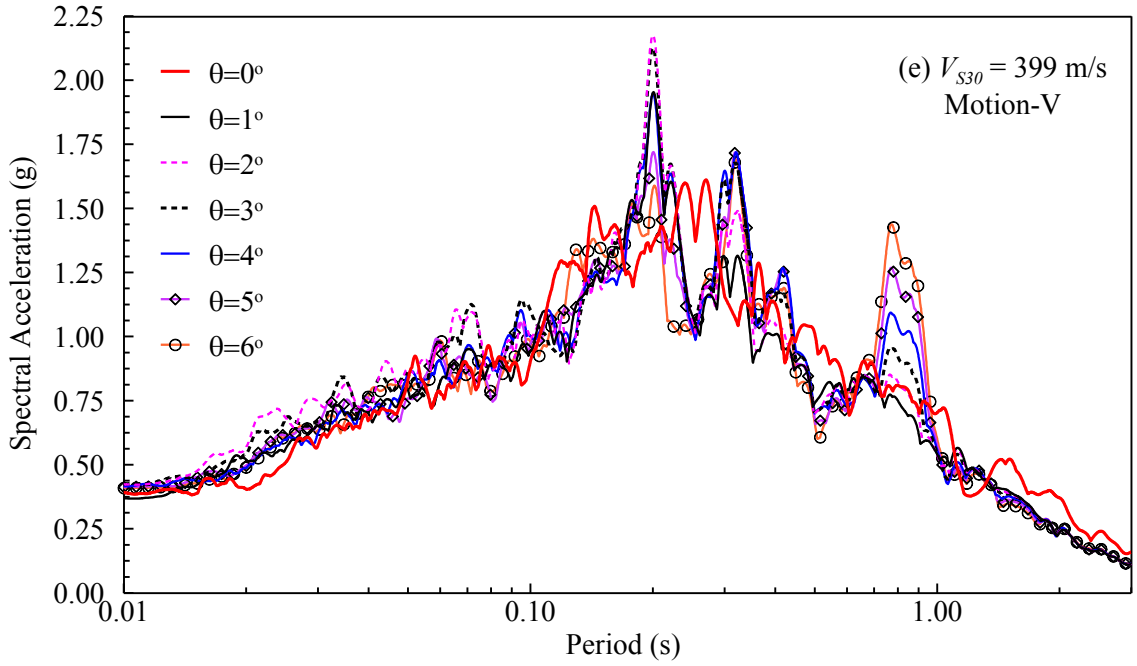

Figure B.19: Sample acceleration response spectra for the profile with V_{S30} =399 m/s from all the sloping ground cases (0^0, 1^0, 2^0, 3^0, 4^0, 5^0, 6^0) with (a) $PGA_{Outcrop}$= 0.1g, (b) $PGA_{Outcrop}$= 0.2g, (c) $PGA_{Outcrop}$= 0.3g, (d) $PGA_{Outcrop}$= 0.4g, and (e) $PGA_{Outcrop}$= 0.5g.

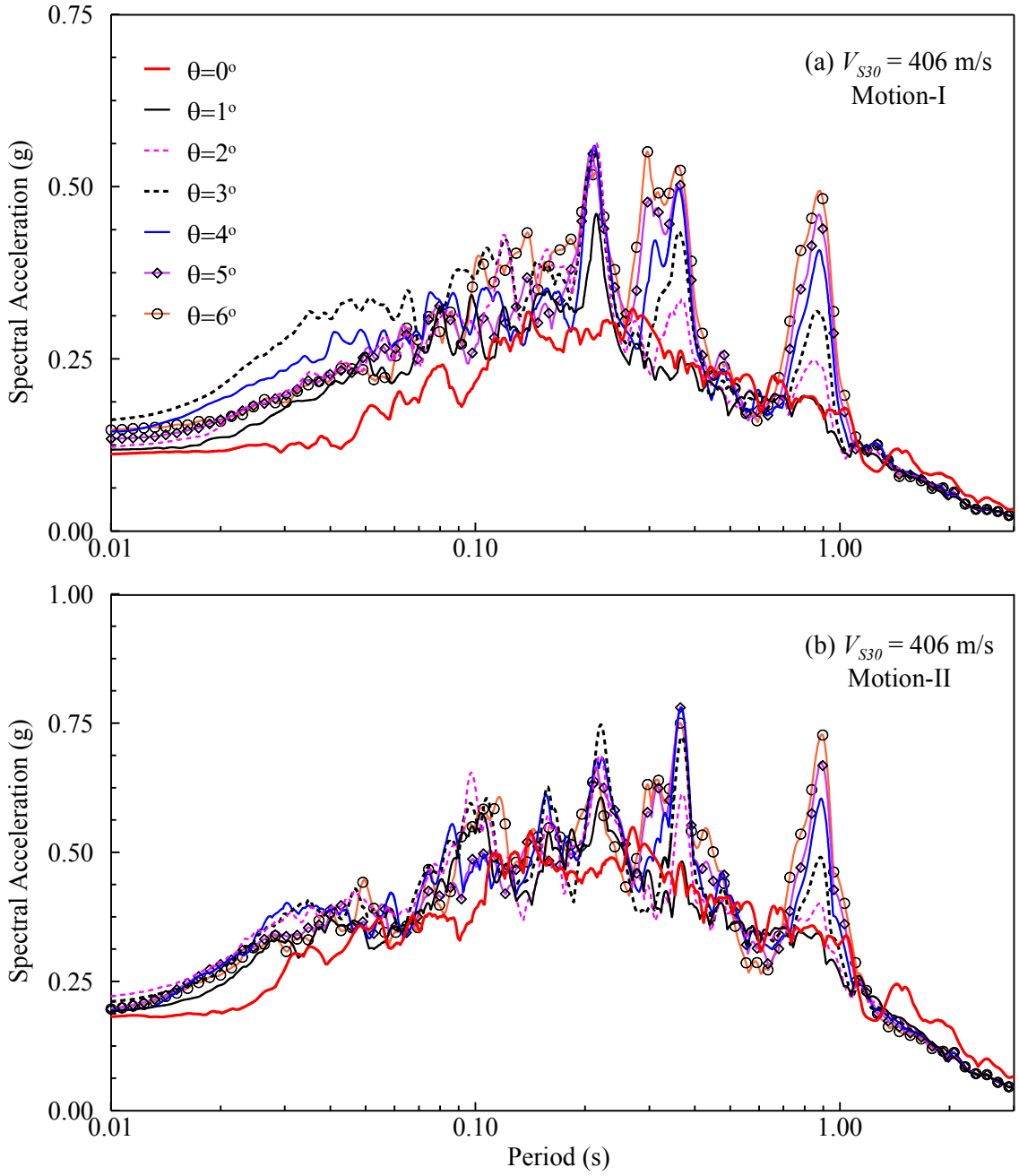
θ=0°
θ=1°
θ=2°
θ=3°
θ=4°
θ=5°
θ=6°
(a) V_{S30} = 406 m/s
Motion-I
(b) V_{S30} = 406 m/s
Motion-II
Spectral Acceleration (g)
Period (s)
0.00
0.25
0.50
0.75
1.00
0.01
0.10
1.00

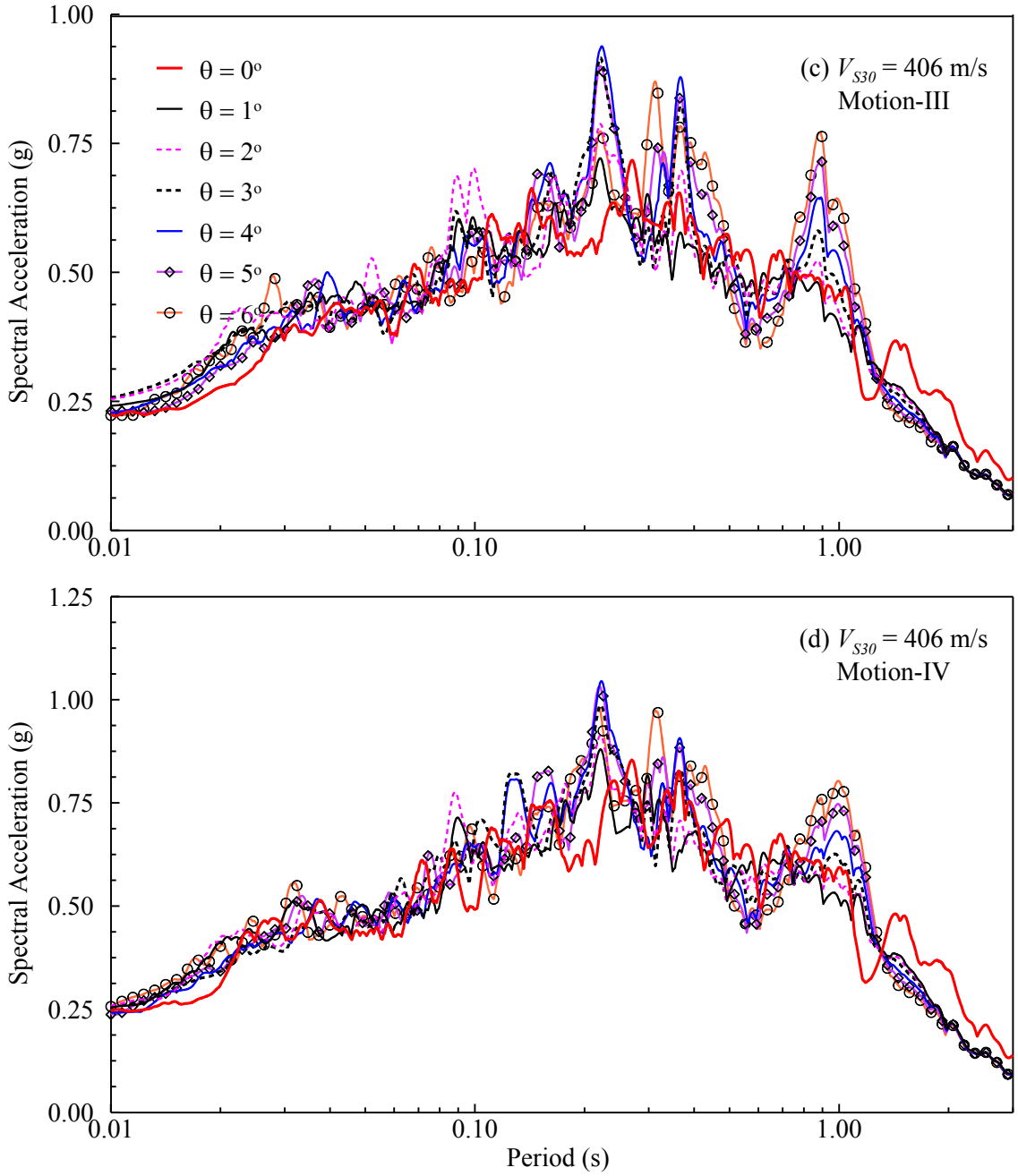
θ = 0°
θ = 1°
θ = 2°
θ = 3°
θ = 4°
θ = 5°
θ = 6°
(c) V_{S30} = 406 m/s
Motion-III
(d) V_{S30} = 406 m/s
Motion-IV
Spectral Acceleration (g)
Period (s)
0.00
0.25
0.50
0.75
1.00
1.25
0.01
0.10
1.00

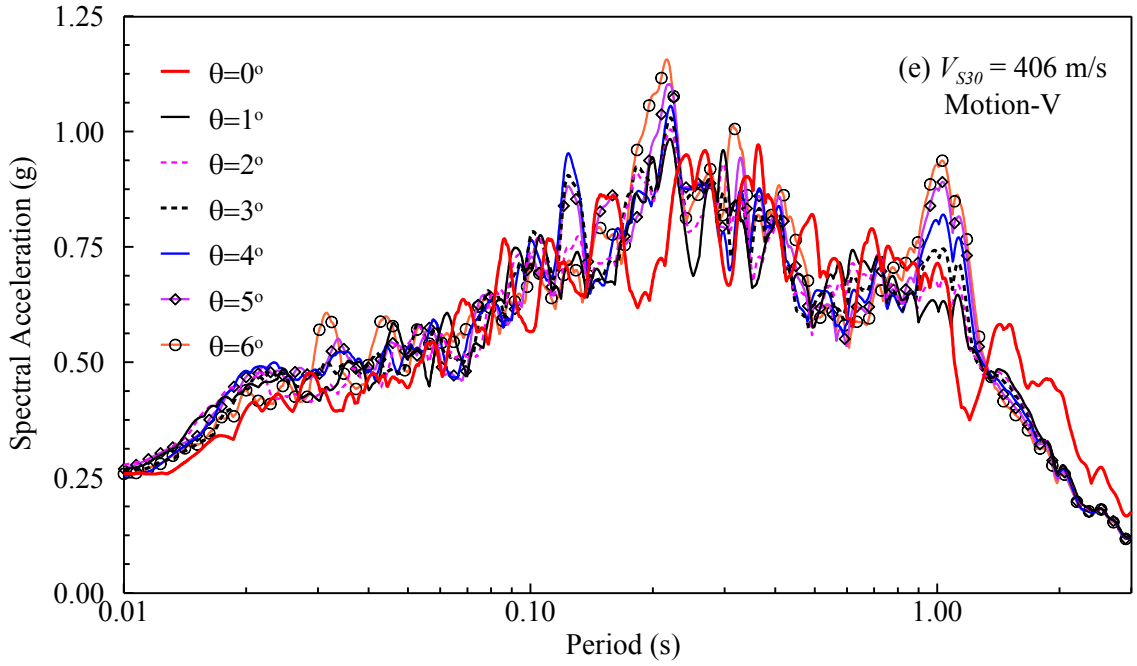

Figure B.20: Sample acceleration response spectra for the profile with V_{S30} =406 m/s from all the sloping ground cases (0^0, 1^0, 2^0, 3^0, 4^0, 5^0, 6^0) with (a) $PGA_{Outcrop}$= 0.1g, (b) $PGA_{Outcrop}$= 0.2g, (c) $PGA_{Outcrop}$= 0.3g, (d) $PGA_{Outcrop}$= 0.4g, and (e) $PGA_{Outcrop}$= 0.5g.

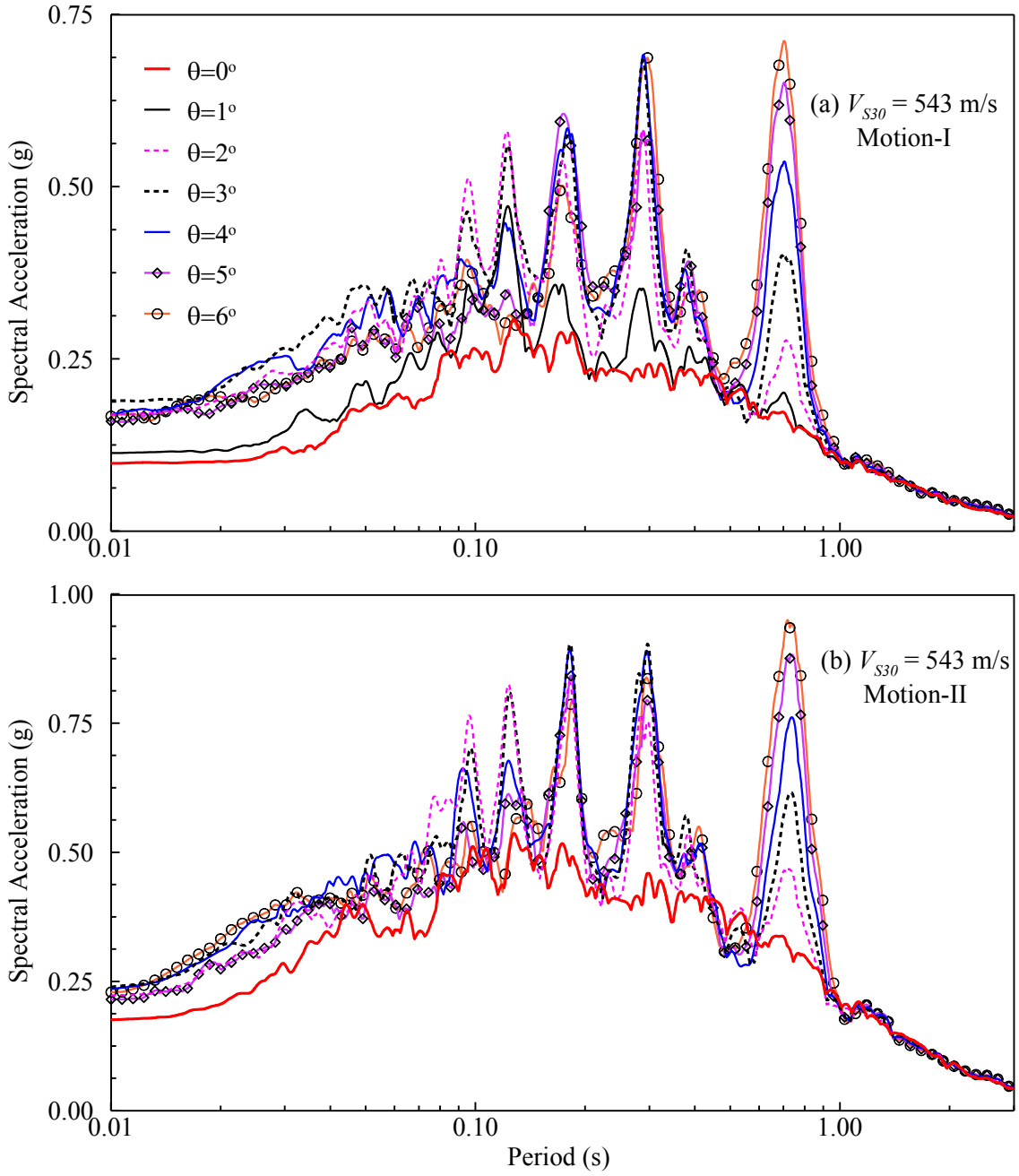
θ=0°
θ=1°
θ=2°
θ=3°
θ=4°
θ=5°
θ=6°
(a) V_{S30} = 543 m/s
Motion-I
(b) V_{S30} = 543 m/s
Motion-II
Spectral Acceleration (g)
Period (s)
0.00
0.25
0.50
0.75
1.00
0.01
0.10
1.00

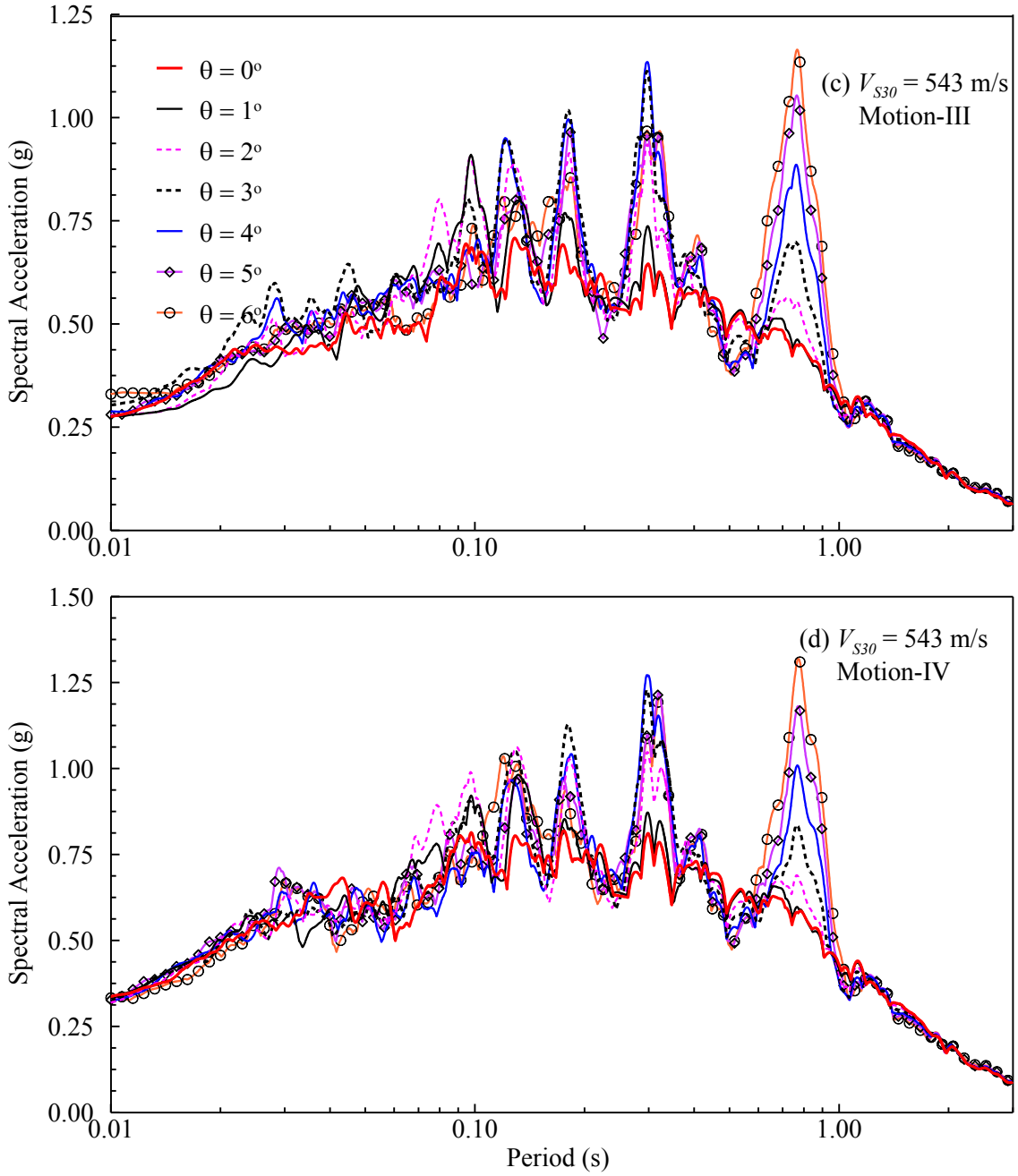
θ = 0°
θ = 1°
θ = 2°
θ = 3°
θ = 4°
θ = 5°
θ = 6°
(c) V_{S30} = 543 m/s
Motion-III
(d) V_{S30} = 543 m/s
Motion-IV
Spectral Acceleration (g)
Period (s)
0.00
0.25
0.50
0.75
1.00
1.25
1.50
0.01
0.10
1.00

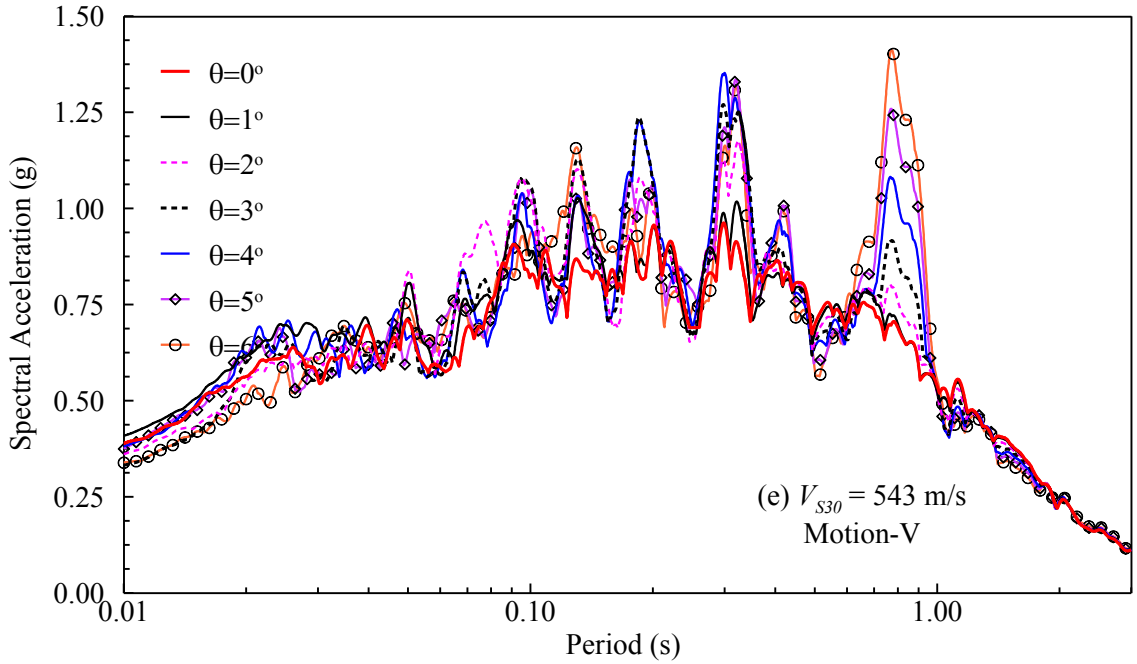

Figure B.21: Sample acceleration response spectra for the profile with V_{S30} =543 m/s from all the sloping ground cases (0^0, 1^0, 2^0, 3^0, 4^0, 5^0, 6^0) with (a) $PGA_{Outcrop}$= 0.1g, (b) $PGA_{Outcrop}$= 0.2g, (c) $PGA_{Outcrop}$= 0.3g, (d) $PGA_{Outcrop}$= 0.4g, and (e) $PGA_{Outcrop}$= 0.5g.

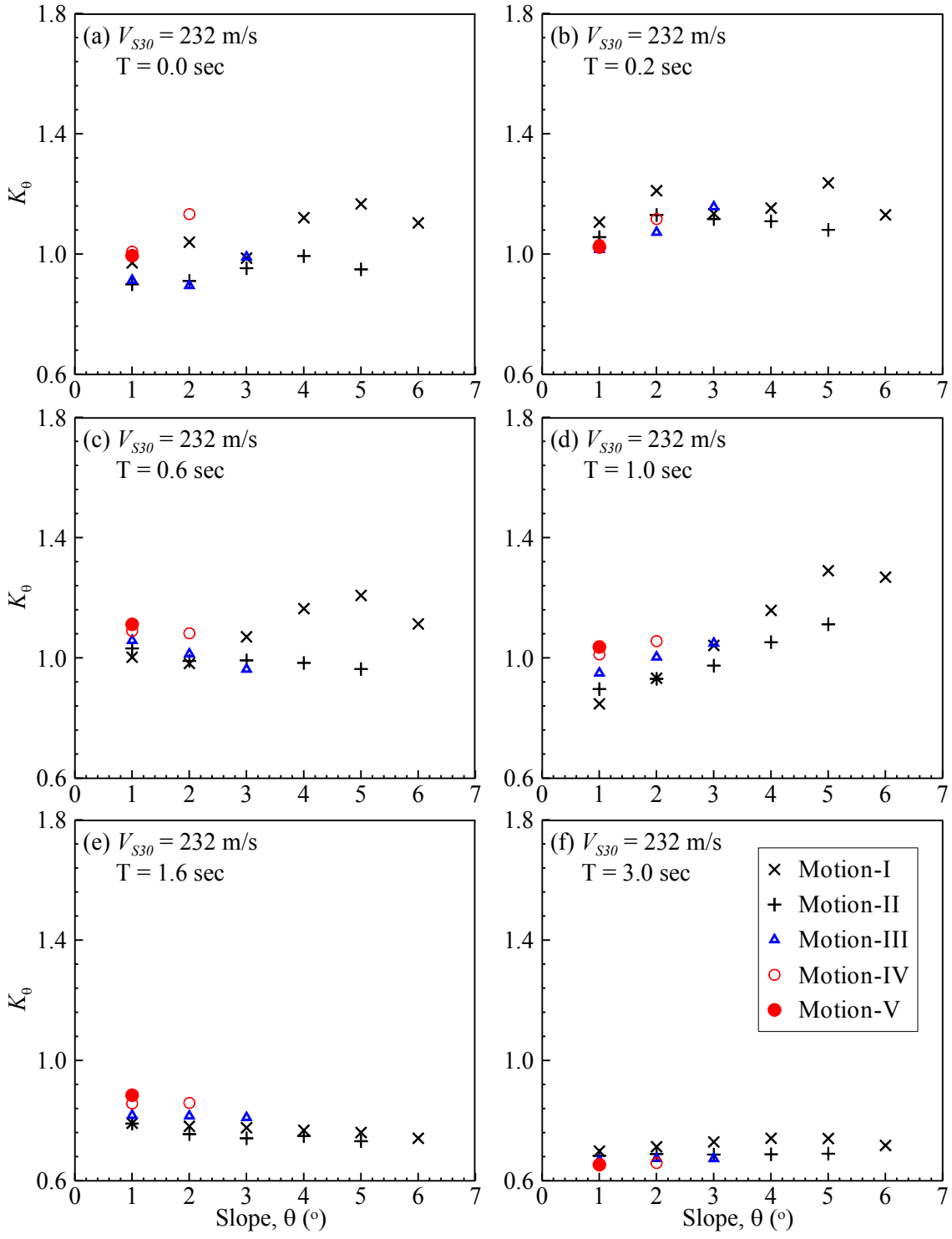

Figure B.22: K_θ vs. θ plots for the profile with V_{S30} = 232 m/s and Motions-I to V and also for the periods, T of (a) 0.0, (b) 0.2, (c) 0.6, (d) 1.0, (e) 1.6, and (f) 3.0 sec.

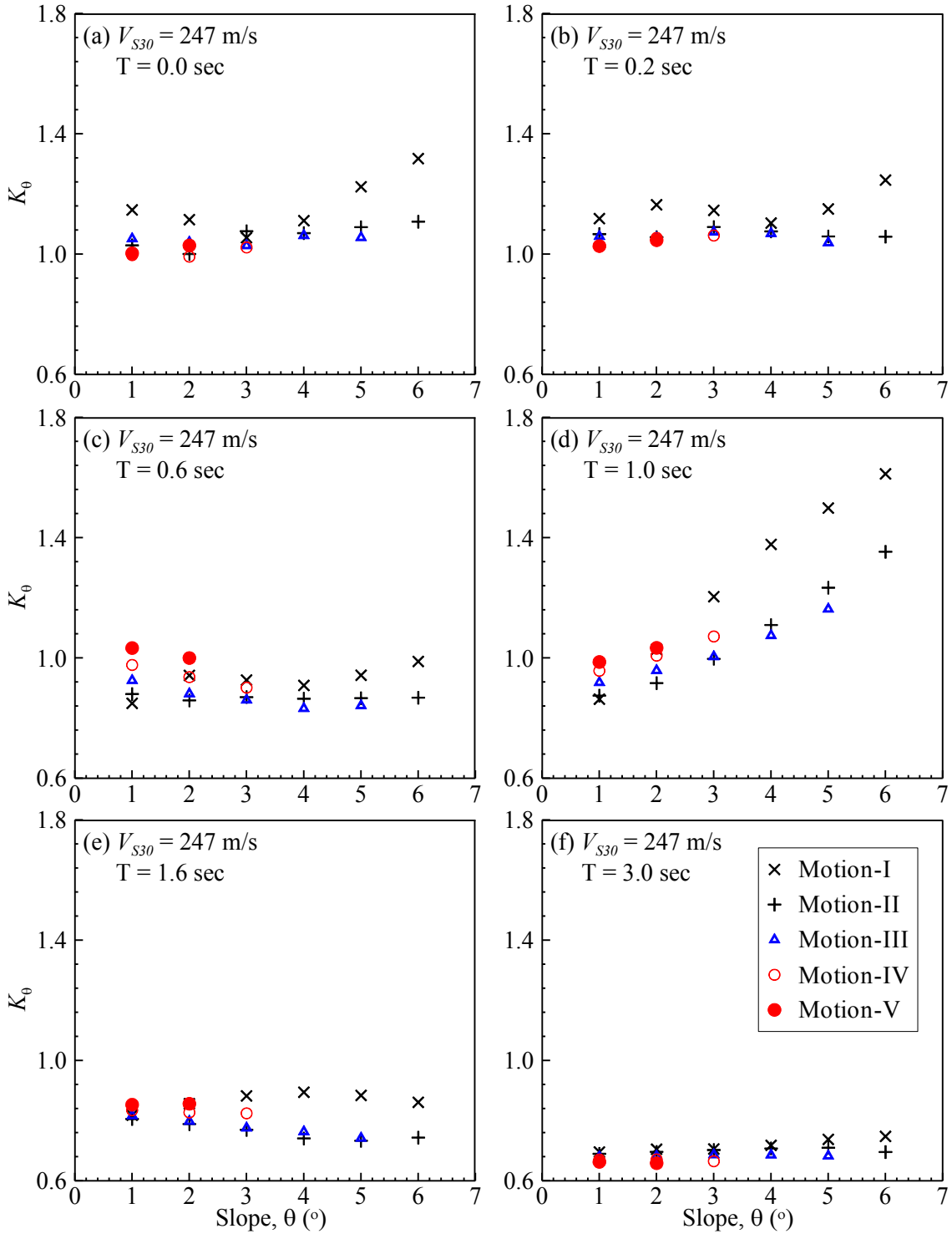

Figure B.23: K_θ vs. θ plots for the profile with V_{S30} = 247 m/s and Motions-I to V and also for the periods, T of (a) 0.0, (b) 0.2, (c) 0.6, (d) 1.0, (e) 1.6, and (f) 3.0 sec.

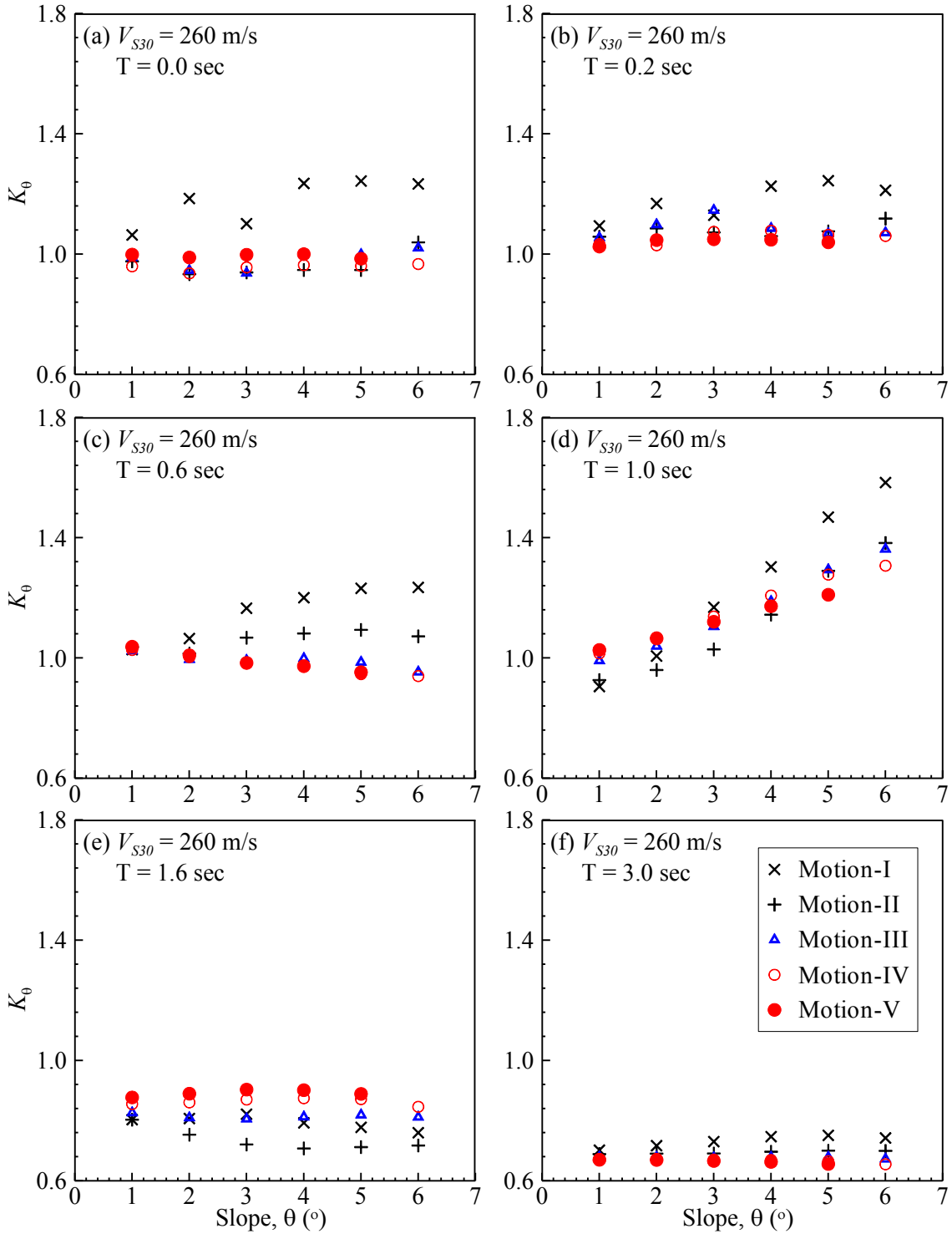

Figure B.24: K_θ vs. θ plots for the profile with V_{S30} = 260 m/s and Motions-I to V and also for the periods, T of (a) 0.0, (b) 0.2, (c) 0.6, (d) 1.0, (e) 1.6, and (f) 3.0 sec.

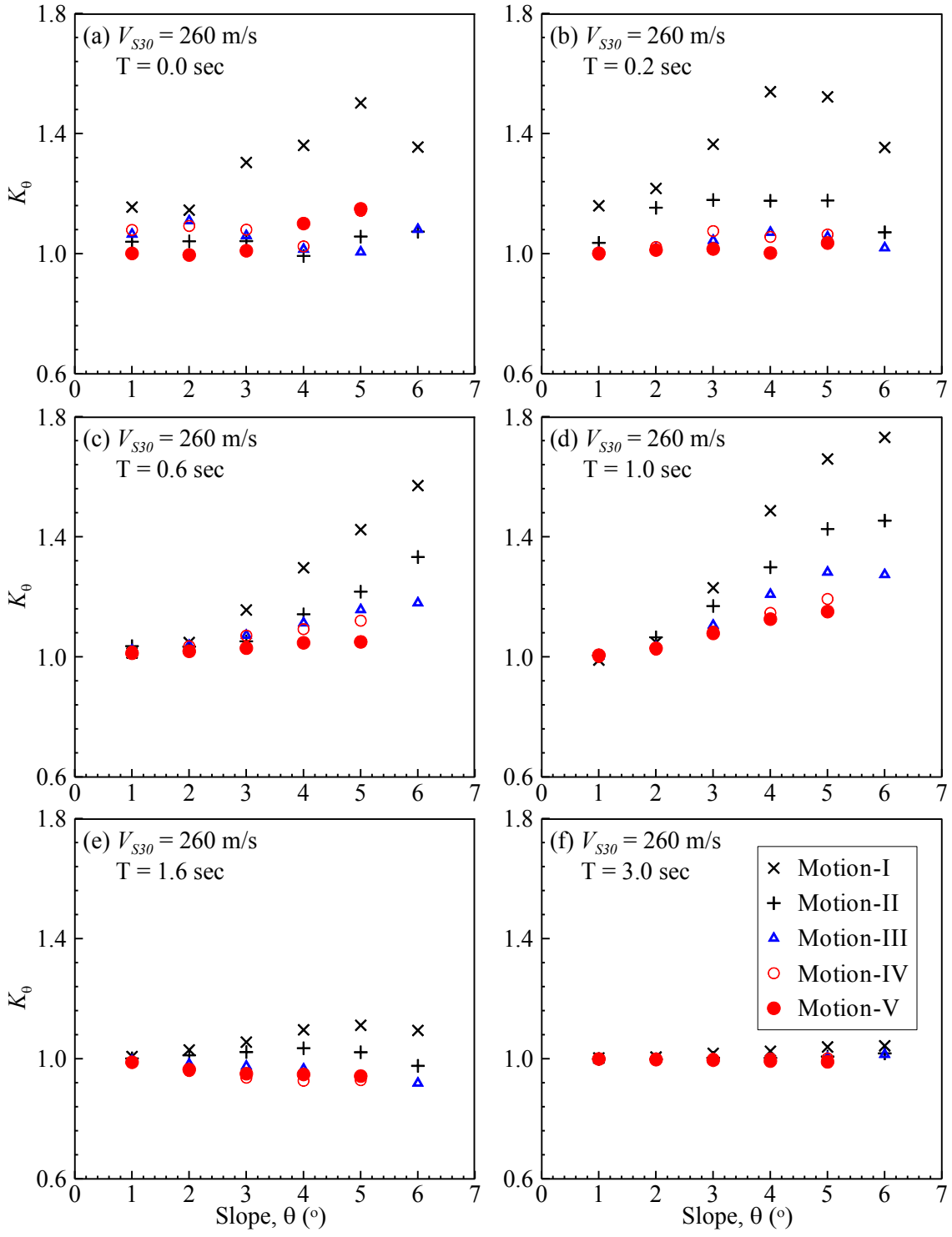

Figure B.25: K_θ vs. θ plots for the profile with V_{S30} = 260 m/s and Motions-I to V and also for the periods, T of (a) 0.0, (b) 0.2, (c) 0.6, (d) 1.0, (e) 1.6, and (f) 3.0 sec.

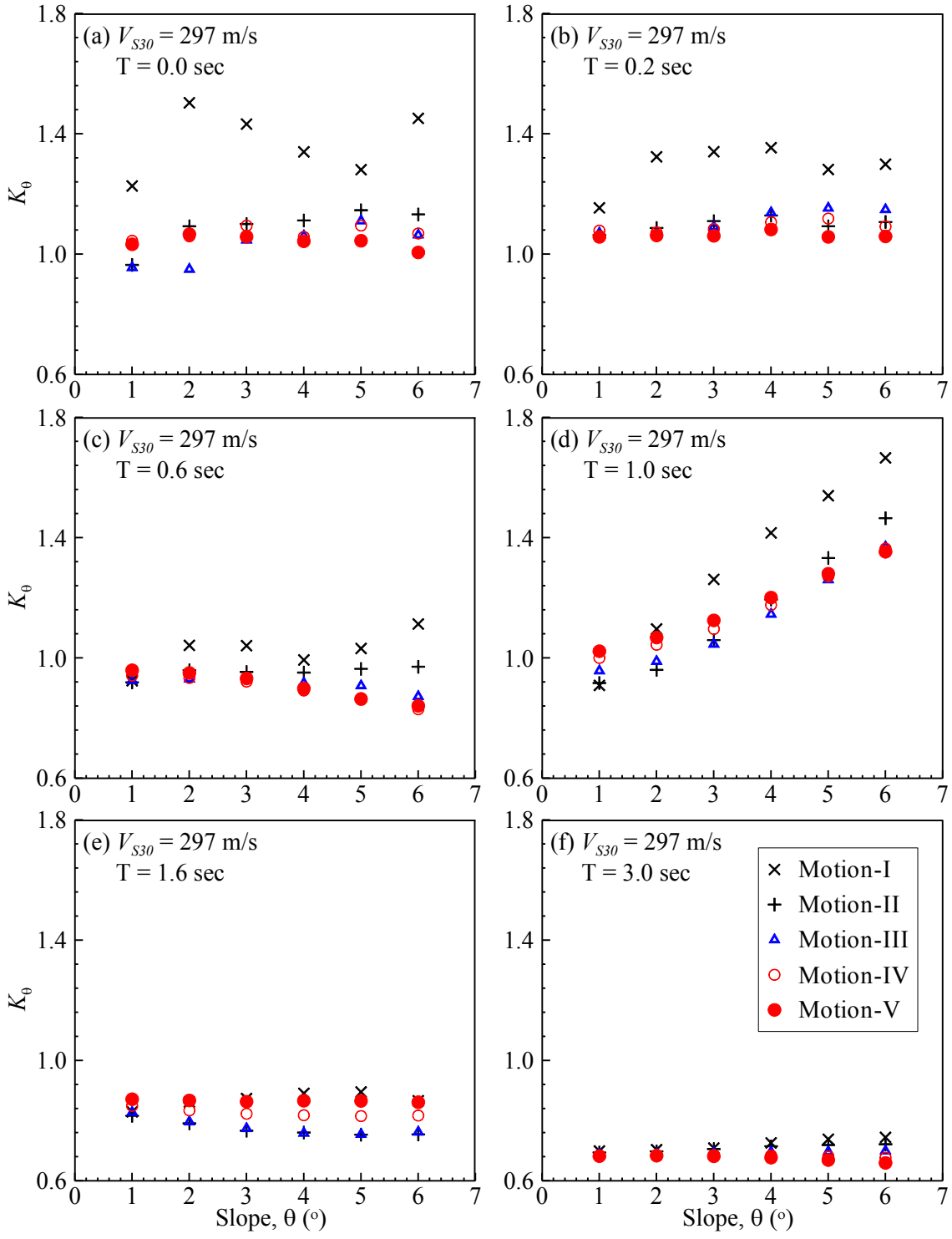

Figure B.26: K_θ vs. θ plots for the profile with V_{S30} = 297 m/s and Motions-I to V and also for the periods, T of (a) 0.0, (b) 0.2, (c) 0.6, (d) 1.0, (e) 1.6, and (f) 3.0 sec.

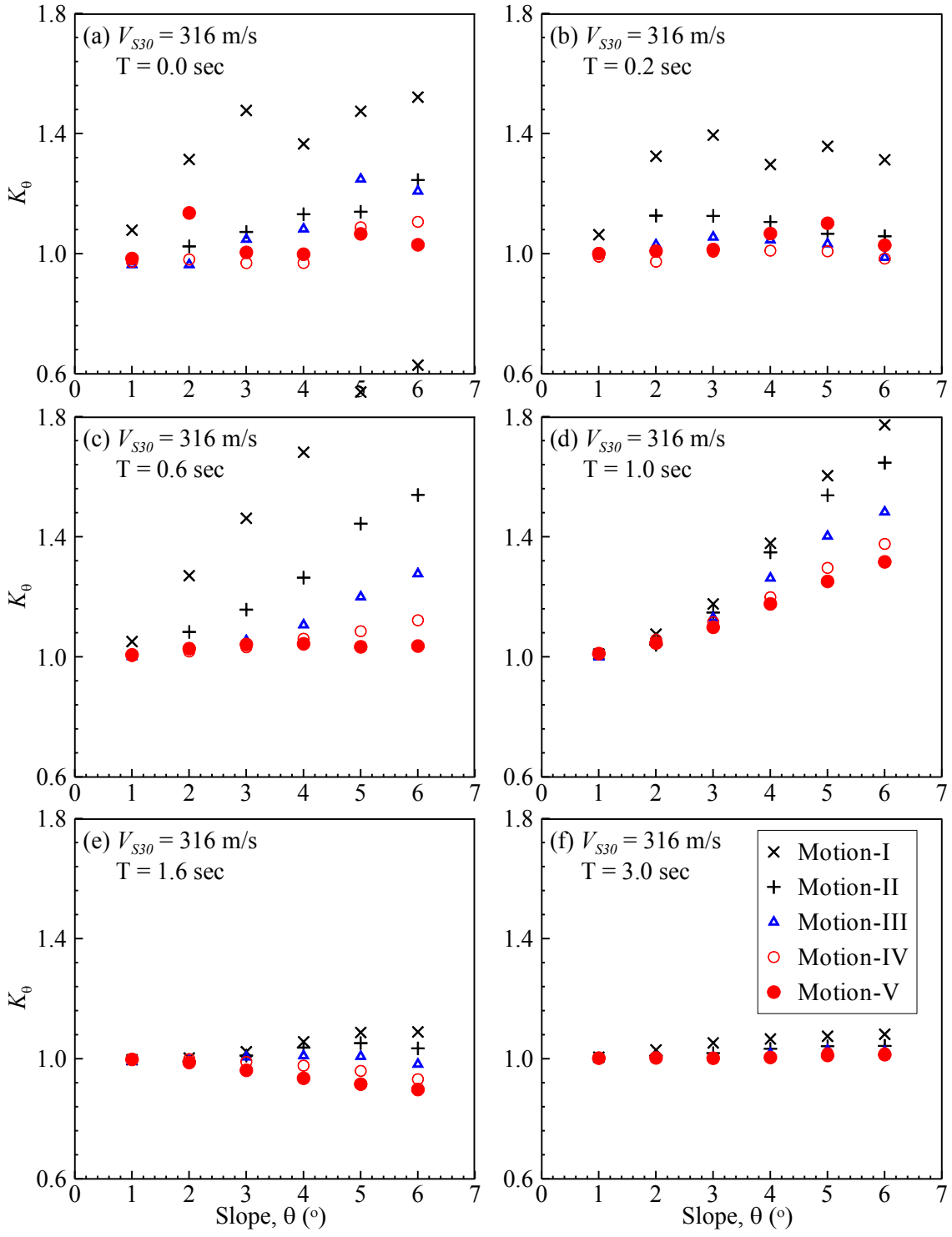

Figure B.27: K_θ vs. θ plots for the profile with V_{S30} = 316 m/s and Motions-I to V and also for the periods, T of (a) 0.0, (b) 0.2, (c) 0.6, (d) 1.0, (e) 1.6, and (f) 3.0 sec.

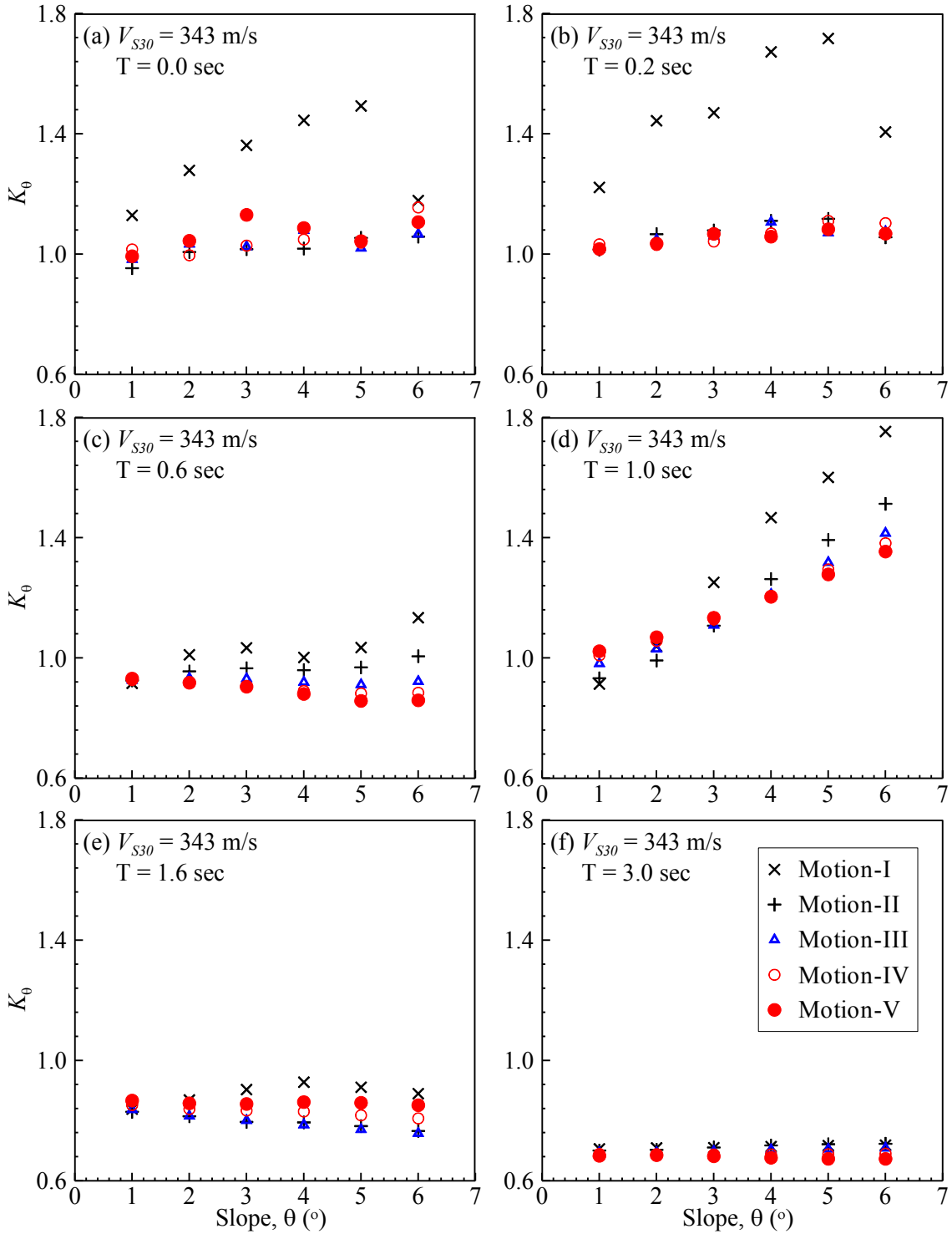

Figure B.28: K_θ vs. θ plots for the profile with V_{S30} = 343 m/s and Motions-I to V and also for the periods, T of (a) 0.0, (b) 0.2, (c) 0.6, (d) 1.0, (e) 1.6, and (f) 3.0 sec.

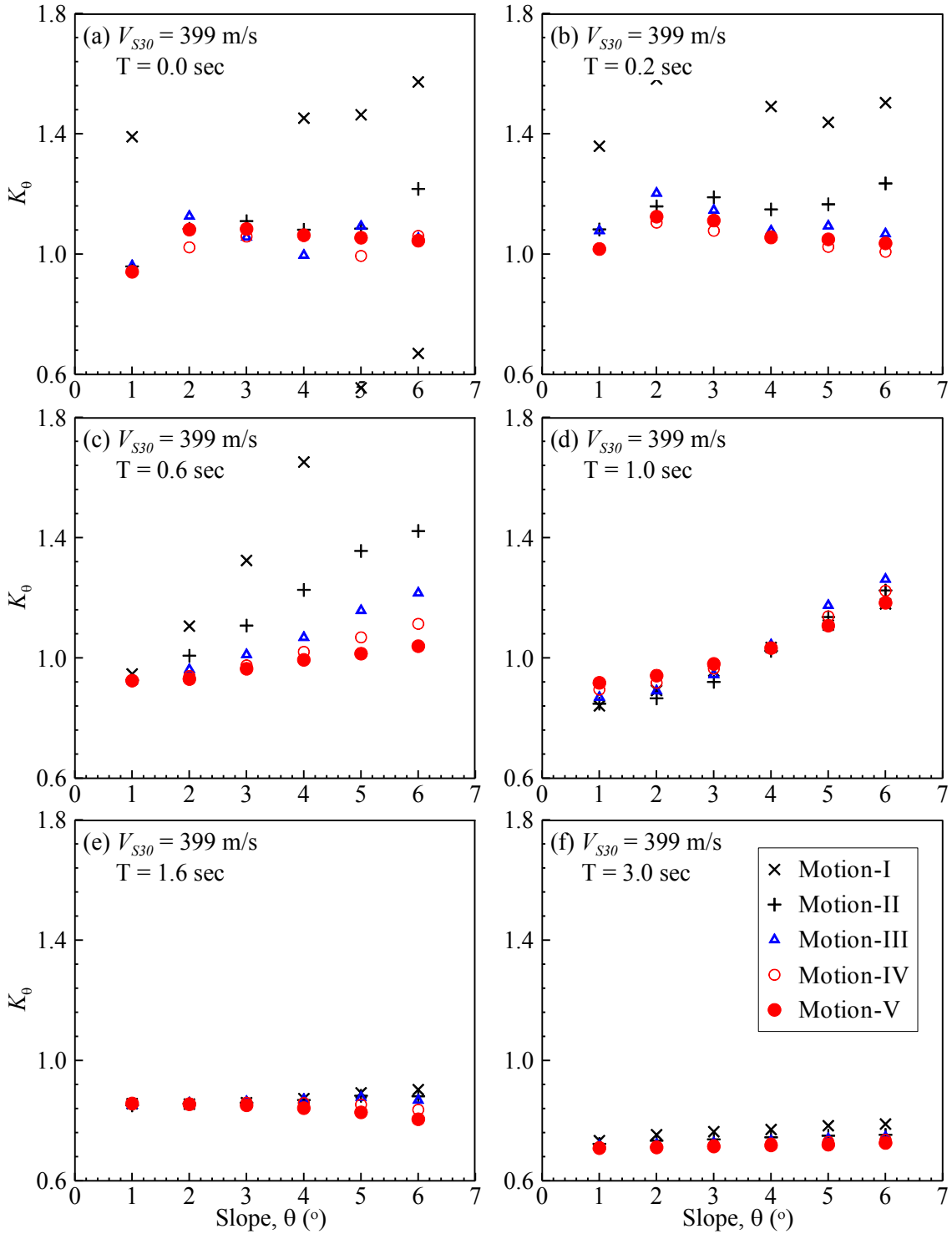

Figure B.29: K_θ vs. θ plots for the profile with V_{S30} = 399 m/s and Motions-I to V and also for the periods, T of (a) 0.0, (b) 0.2, (c) 0.6, (d) 1.0, (e) 1.6, and (f) 3.0 sec.

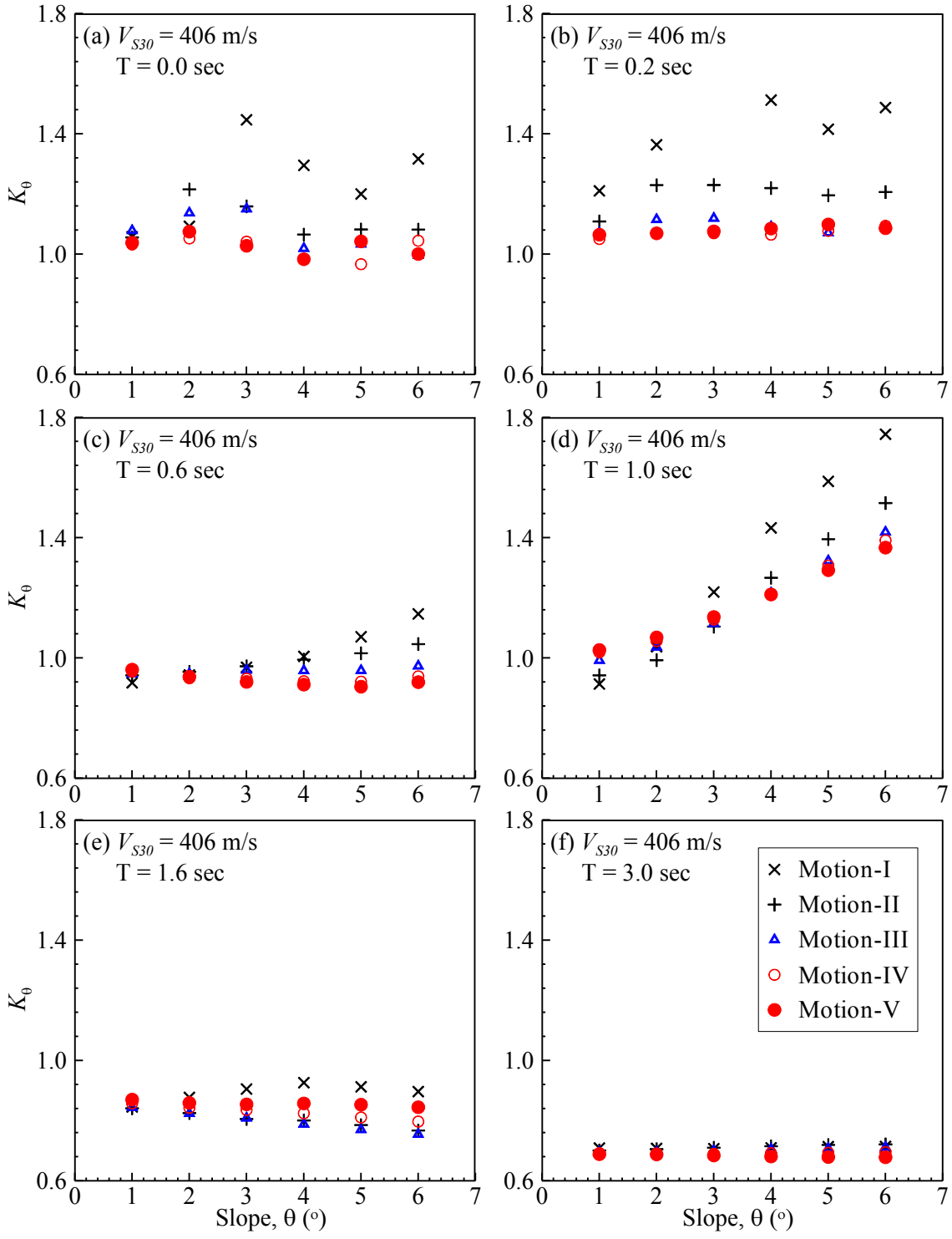

Figure B.30: K_θ vs. θ plots for the profile with V_{S30} = 406 m/s and Motions-I to V and also for the periods, T of (a) 0.0, (b) 0.2, (c) 0.6, (d) 1.0, (e) 1.6, and (f) 3.0 sec.

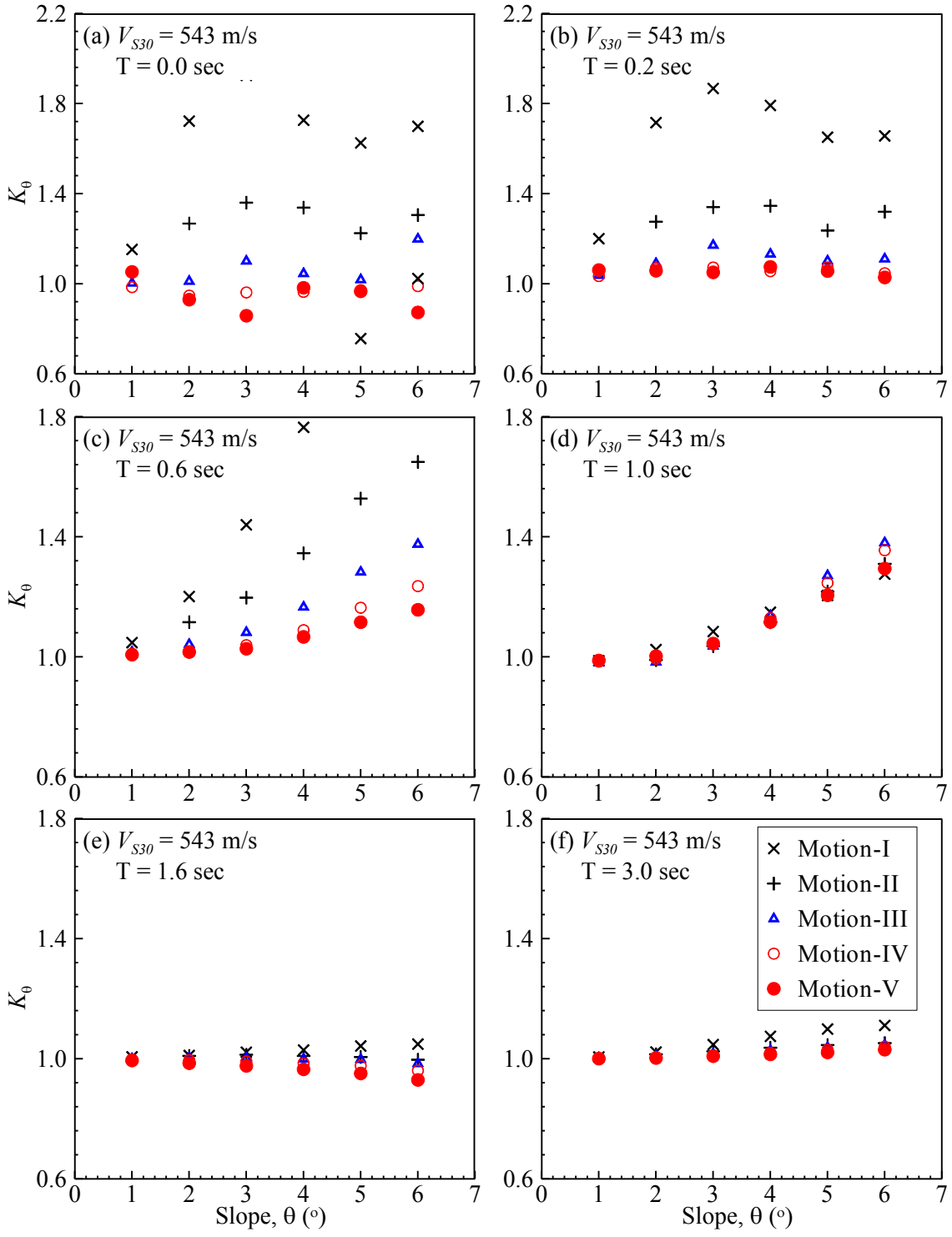

Figure B.31: K_θ vs. θ plots for the profile with V_{S30} = 543 m/s and Motions-I to V and also for the periods, T of (a) 0.0, (b) 0.2, (c) 0.6, (d) 1.0, (e) 1.6, and (f) 3.0 sec.

APPENDIX C

SUMMARY OF THE ANALYSIS RESULTS PERFORMED TO EVALUATE THE EFFECT OF SUDDEN SHEAR WAVE VELOCITY CONTRAST AT LAYER INTERFACES ON SEISMIC SITE RESPONSE ANALYSIS FOR CHARLESTON, SC PRESENTED IN CHAPTER 6

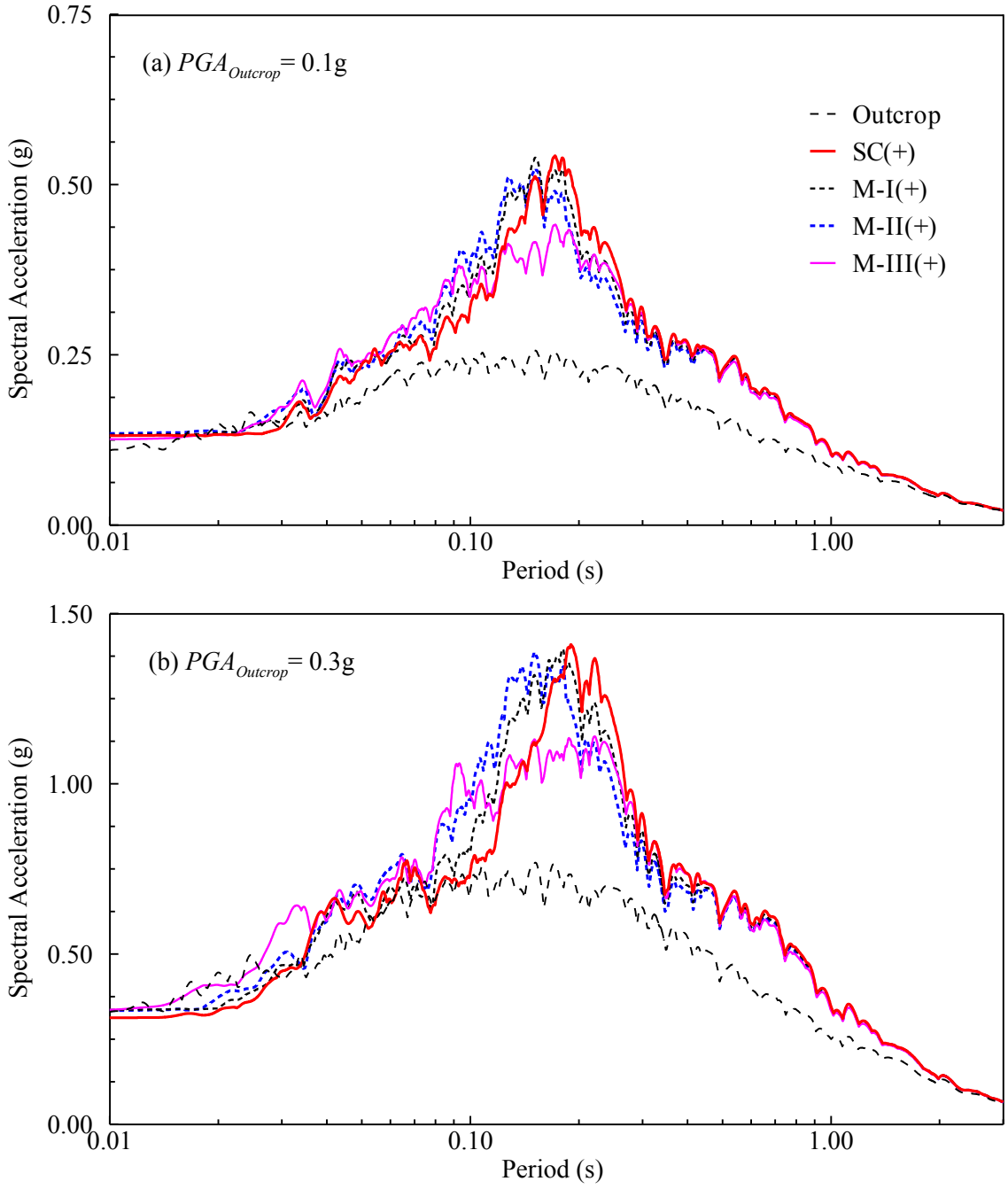

Figure C.1: DEEPSOIL generated acceleration response spectra at surface level for profile variations presented in Figure 6.3(b) and for: (a) $PGA_{Outcrop}$= 0.1g and (b) $PGA_{Outcrop}$= 0.3g.

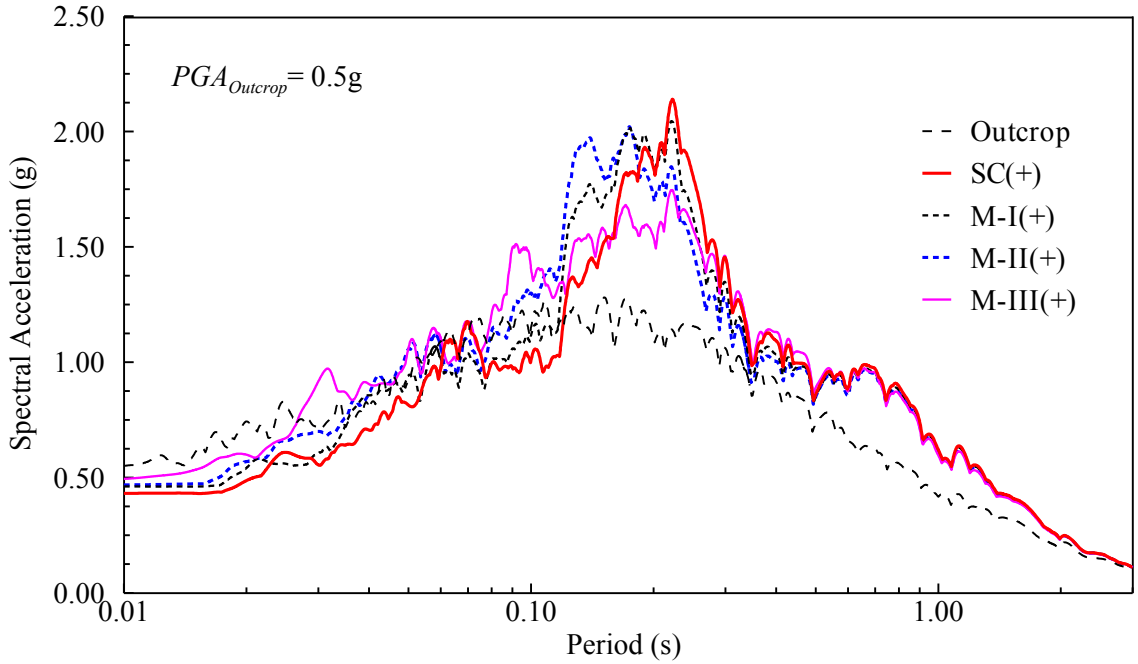

Figure C.2: DEEPSOIL generated acceleration response spectra at surface level for profile variations presented in Figure 6.3(b) and for $PGA_{Outcrop}$ of 0.5g.

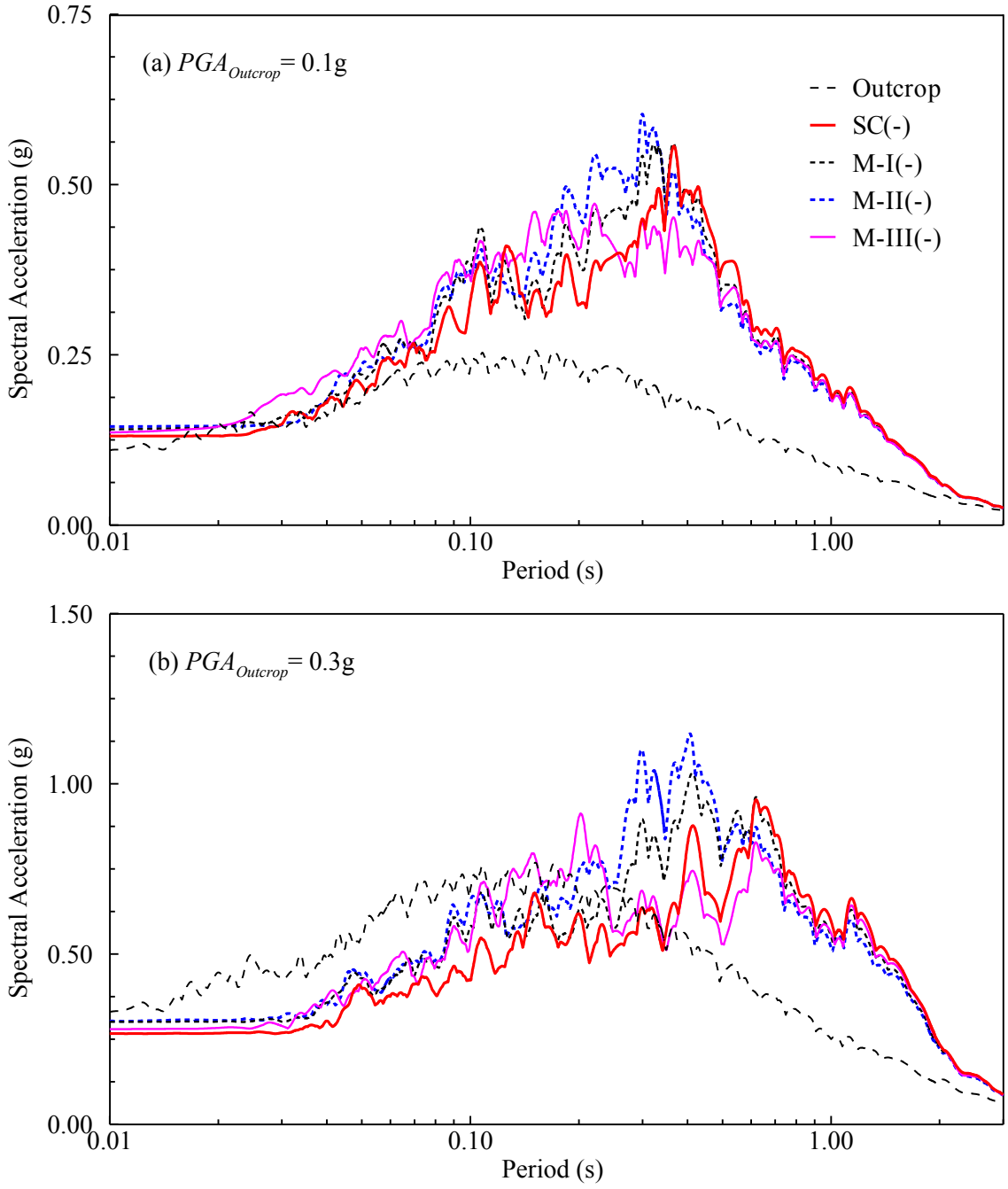

Figure C.3: DEEPSOIL generated acceleration response spectra at surface level for profile variations presented in Figure 6.3(c) and for: (a) $PGA_{Outcrop}$= 0.1g and (b) $PGA_{Outcrop}$= 0.3g.

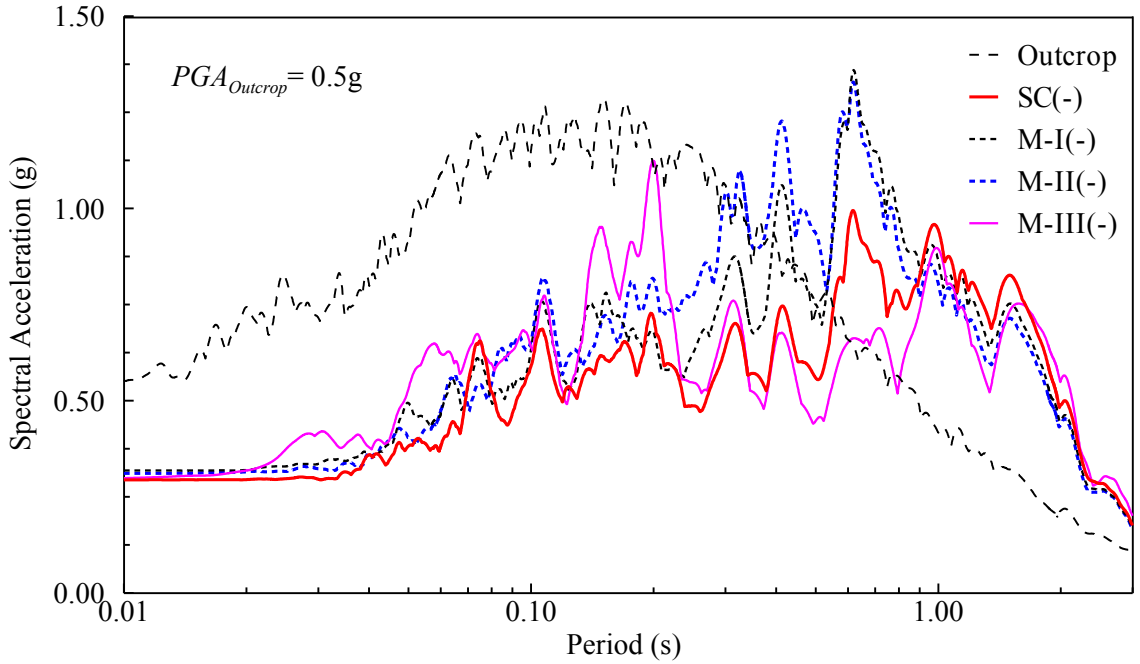

Figure C.4: DEEPSOIL generated acceleration response spectra at surface level for profile variations presented in Figure 6.3(c) and for $PGA_{Outcrop}$ of 0.5g.

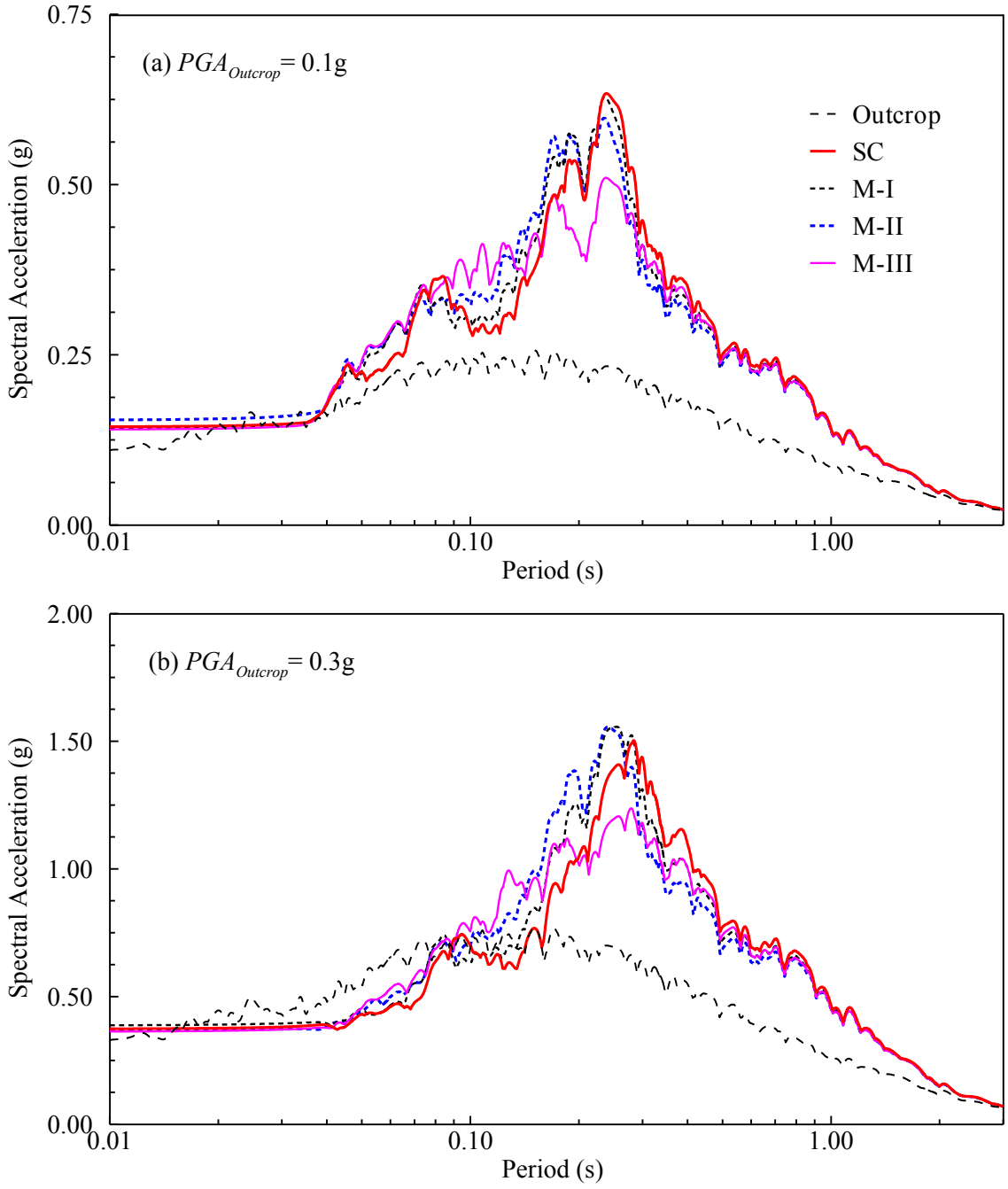

Figure C.5: SHAKE generated acceleration response spectra at surface level for profile variations presented in Figure 6.3(a) and for: (a) $PGA_{Outcrop}$= 0.1g and (b) $PGA_{Outcrop}$= 0.3g.

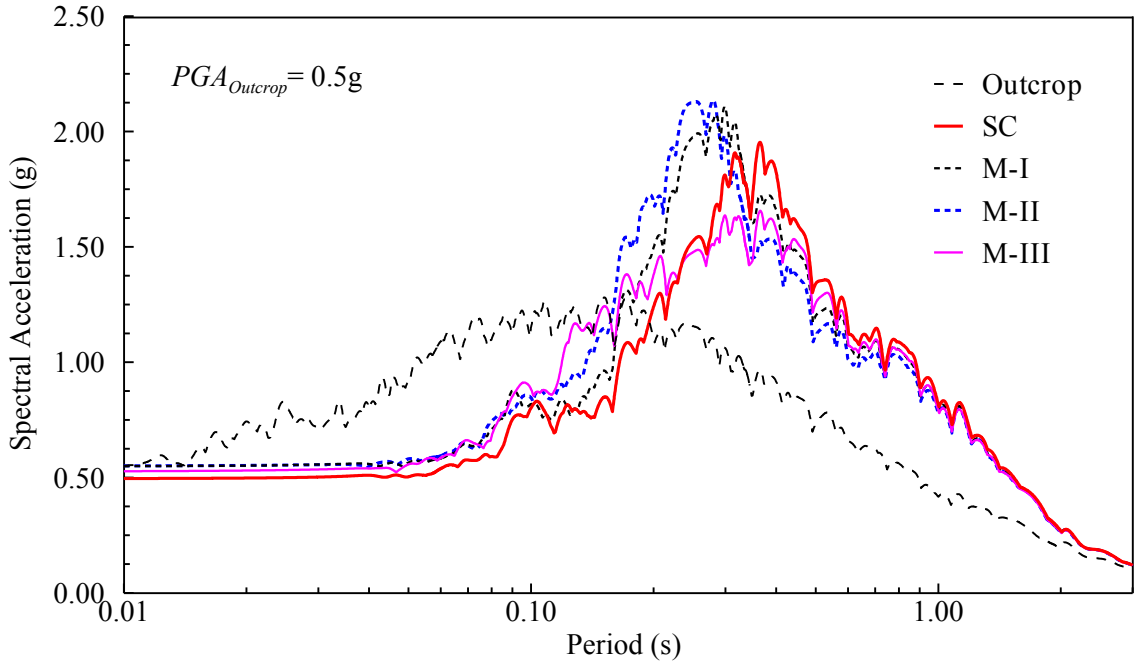

Figure C.6: SHAKE generated acceleration response spectra at surface level for profile variations presented in Figure 6.3(b) and for $PGA_{Outcrop}$ of 0.5g.

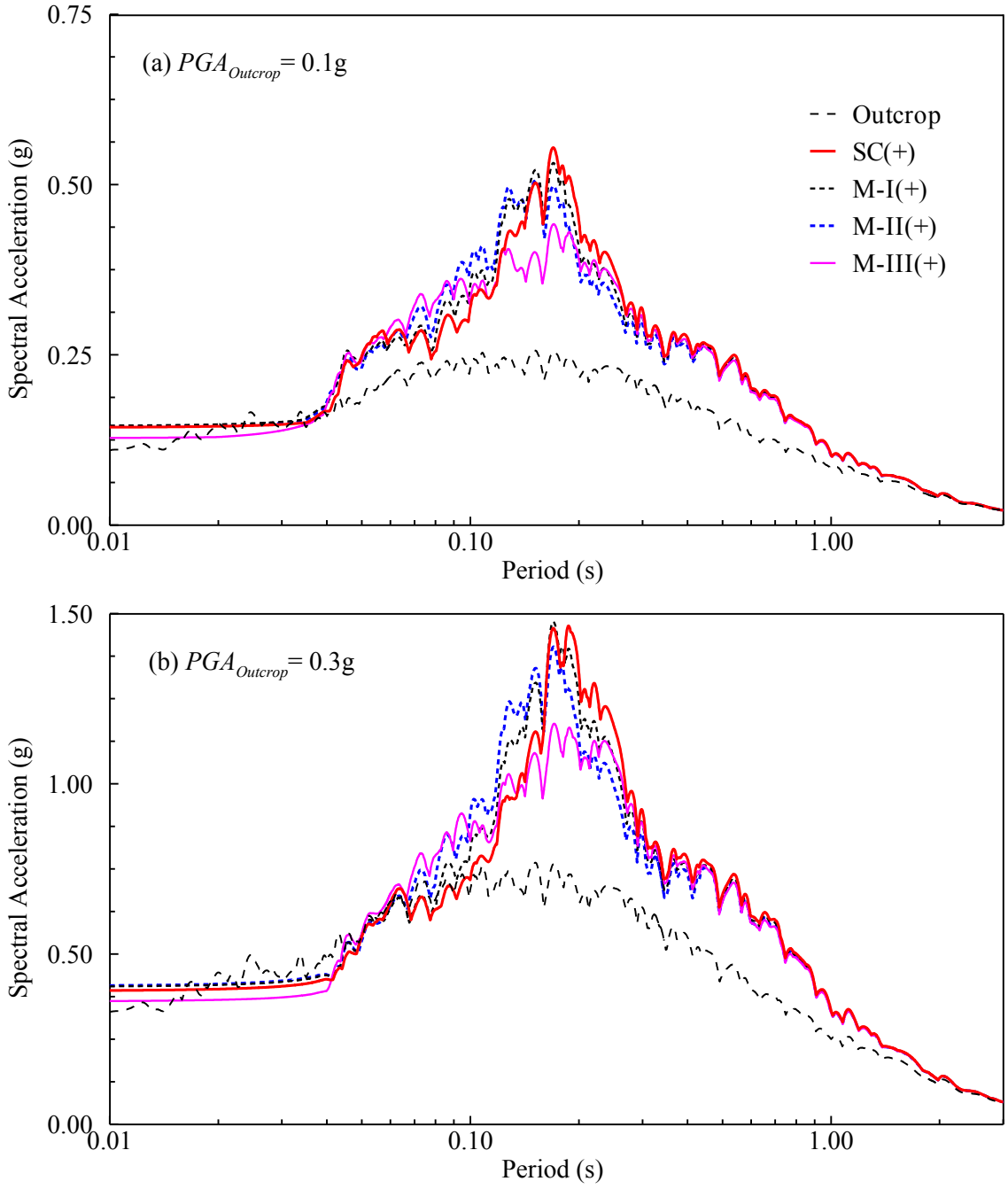

Figure C.7: SHAKE generated acceleration response spectra at surface level for profile variations presented in Figure 6.3(b) and for: (a) $PGA_{Outcrop}$= 0.1g and (b) $PGA_{Outcrop}$= 0.3g.

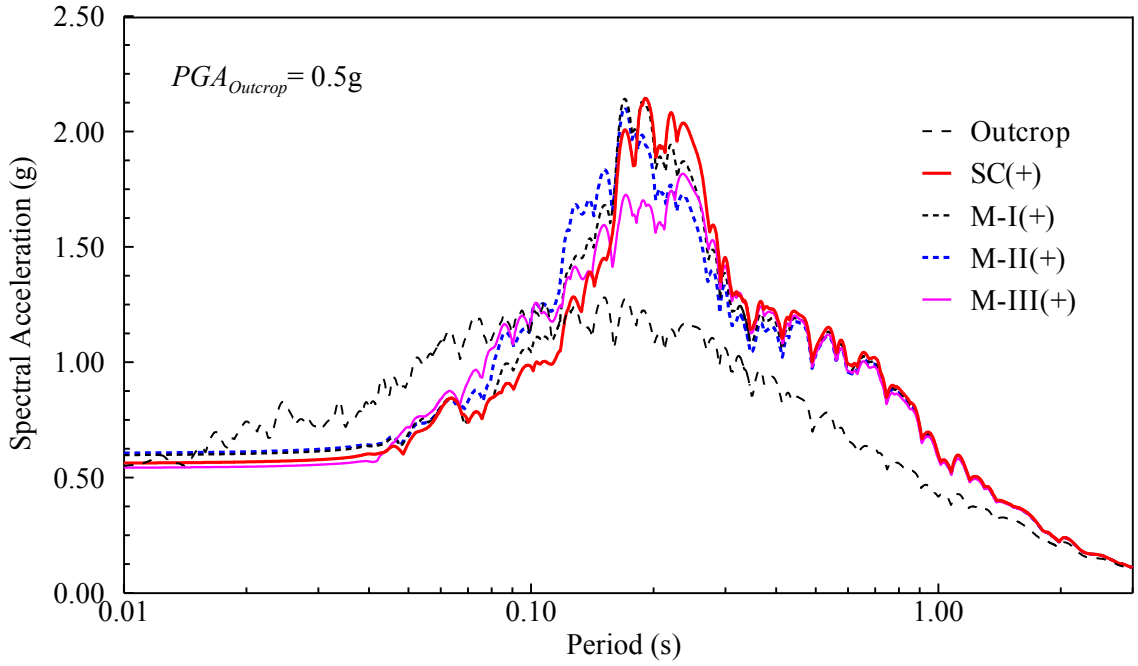

Figure C.8: SHAKE generated acceleration response spectra at surface level for profile variations presented in Figure 6.3(b) and for $PGA_{Outcrop}$ of 0.5g.

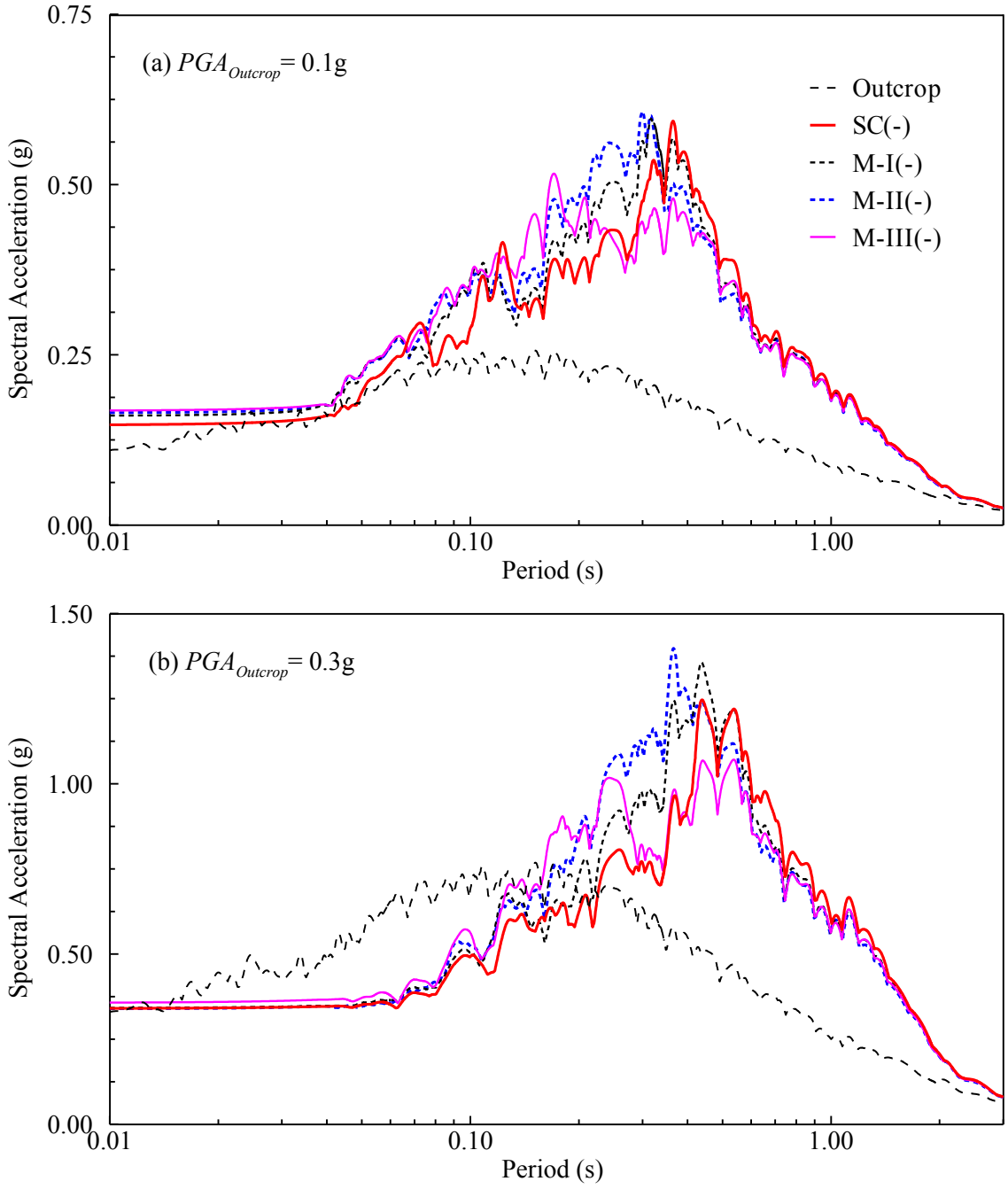

Figure C.9: SHAKE generated acceleration response spectra at surface level for profile variations presented in Figure 6.3(c) and for: (a) $PGA_{Outcrop}$= 0.1g and (b) $PGA_{Outcrop}$= 0.3g.

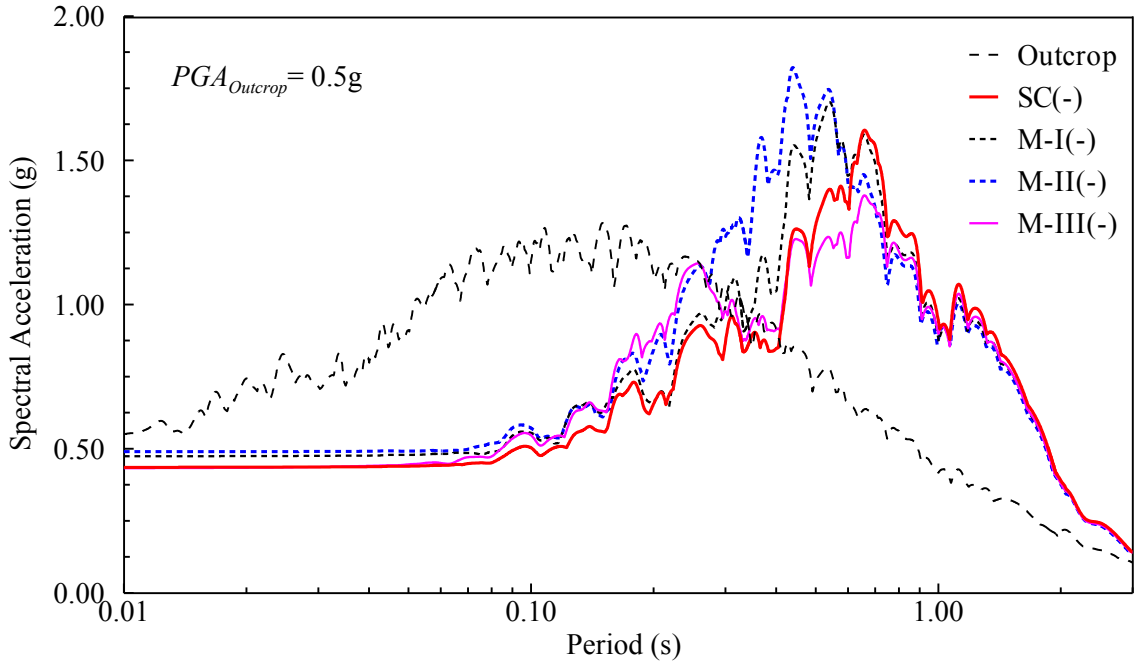

Figure C.10: SHAKE generated acceleration response spectra at surface level for profile variations presented in Figure 6.3(c) and for $PGA_{Outcrop}$ of 0.5g.

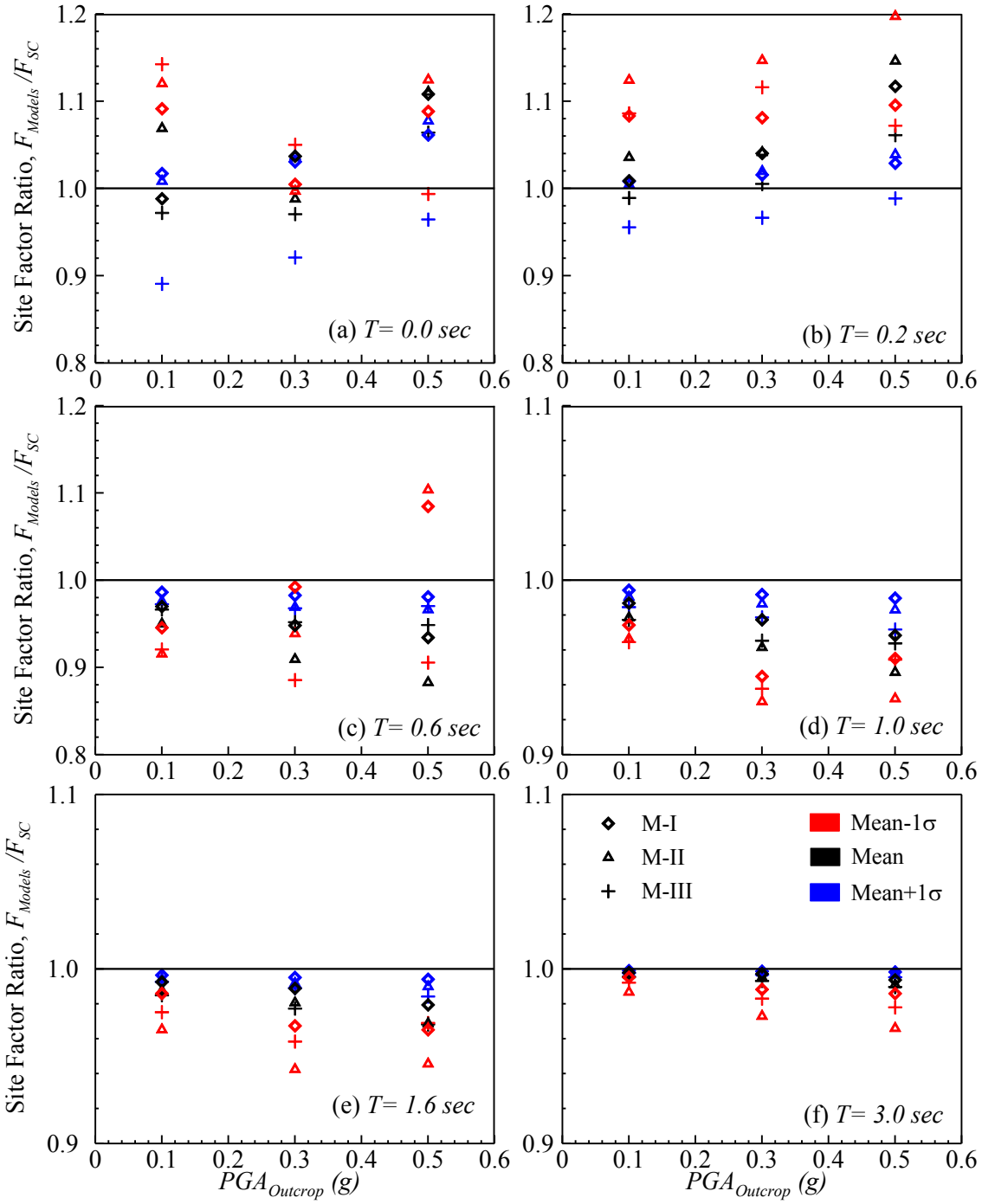

Figure C.11: Site Factors Ratios vs. $PGA_{Outcrop}$ plots for the 'Mean' and it's ±1σ variations of all three models: M-I, II and II (see Figure 6.3) based on SHAKE data points for: (a) *T= 0.0 sec*, (b) *T= 0.2 sec*, (c) *T= 0.6 sec*, (d) *T= 1.0 sec*, (e) *T= 1.6 sec*, and (f) *T= 3.0 sec*.

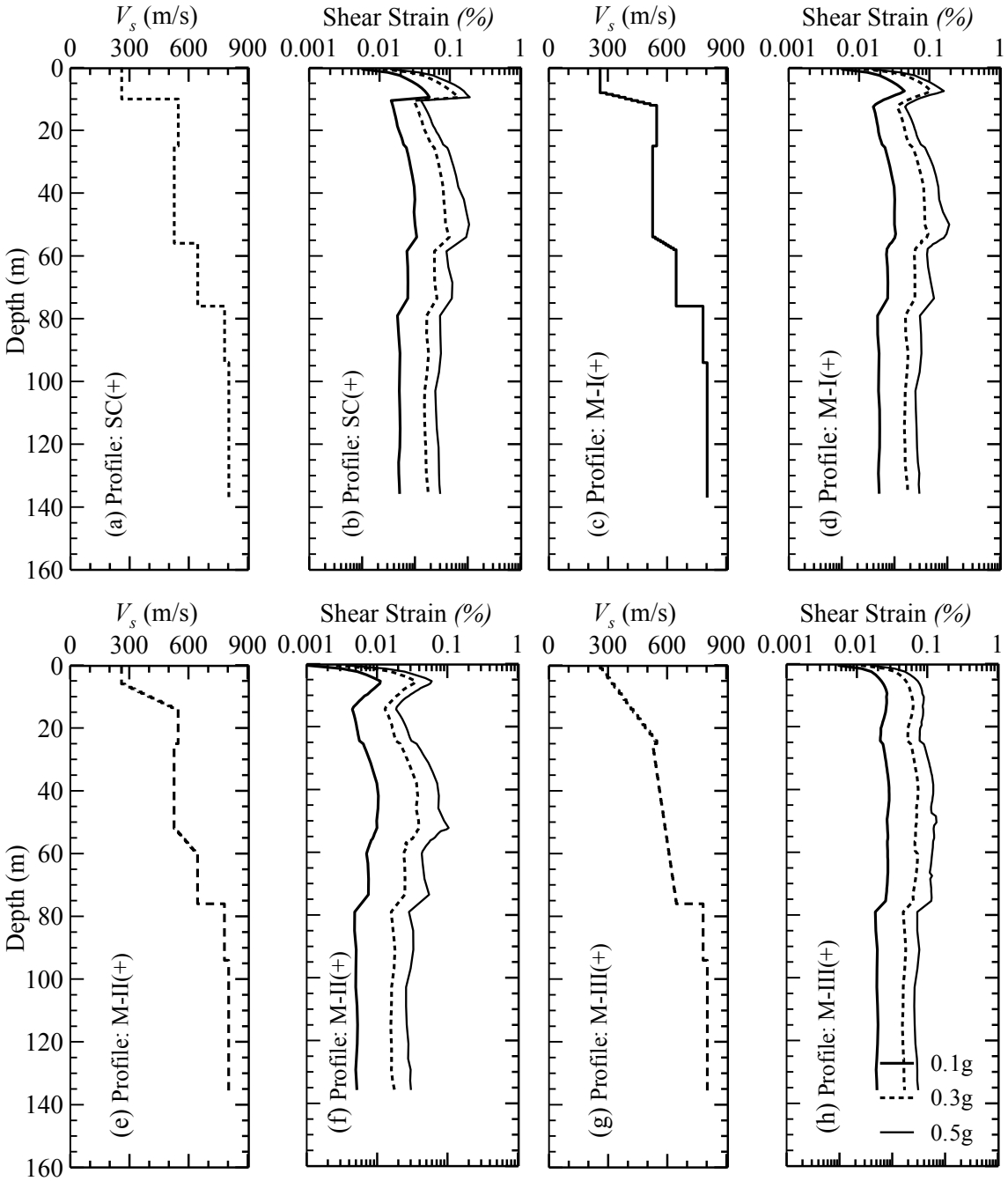

Figure C.12: Profile maximum shear strains, based on DEEPSOIL data points, along with the corresponding V_S profiles from Figure 6.3(b) and for $PGA_{Outcrop}$ levels of 0.1, 0.3 and 0.5g. Subplots (a) and (b) are for the profile: SC(+); (c) and (d) for the profile M-I(+); (e) and (f) for the profile M-II(+); and, (g) and (h) for the profile M-III(+).

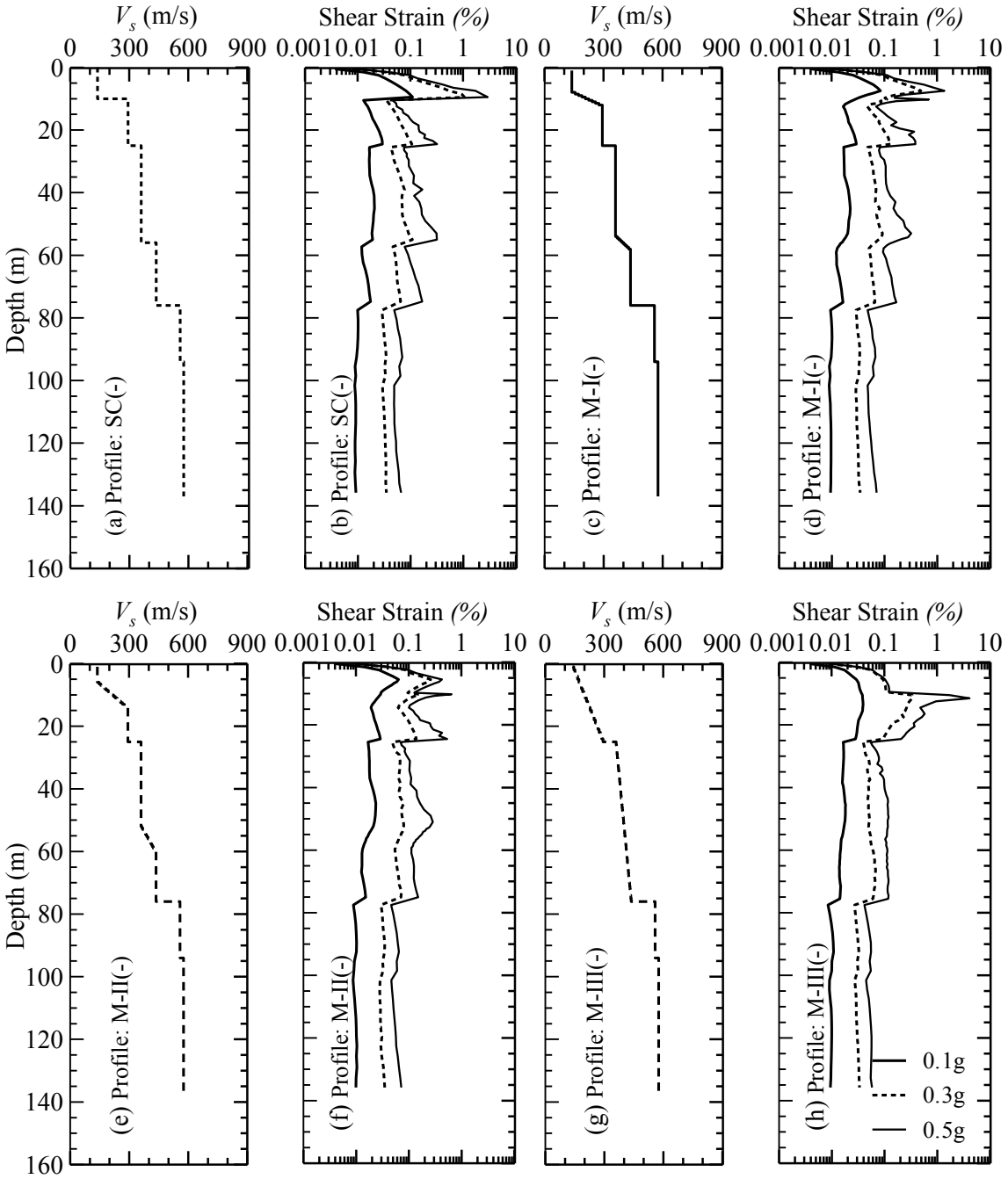

Figure C.13: Profile maximum shear strains, based on DEEPSOIL data points, along with the corresponding V_S profiles from Figure 6.3(c) and for $PGA_{Outcrop}$ levels of 0.1, 0.3 and 0.5g. Subplots (a) and (b) are for the profile: SC(-); (c) and (d) for the profile M-I(-); (e) and (f) for the profile M-II(-); and, (g) and (h) for the profile M-III(-).

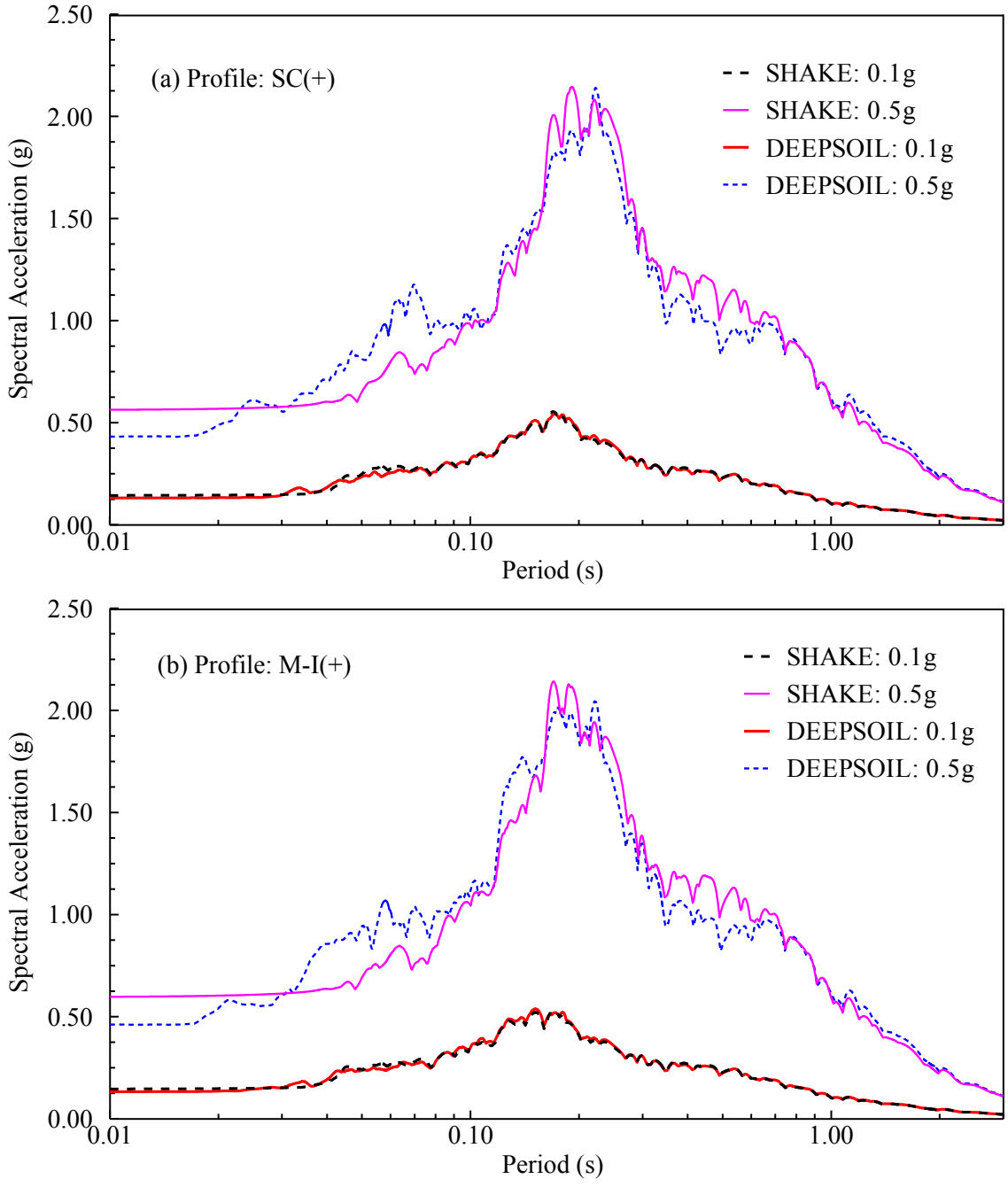

Figure C.14: Comparison of SHAKE and DEEPSOIL spectral acceleration responses for the profiles (see Figure 6.3(b) for profile information): SC(+) and M-I(+) in subplots (a) and (b), respectively and for $PGA_{Outcrop}$ of 0.1g and 0.5g cases.

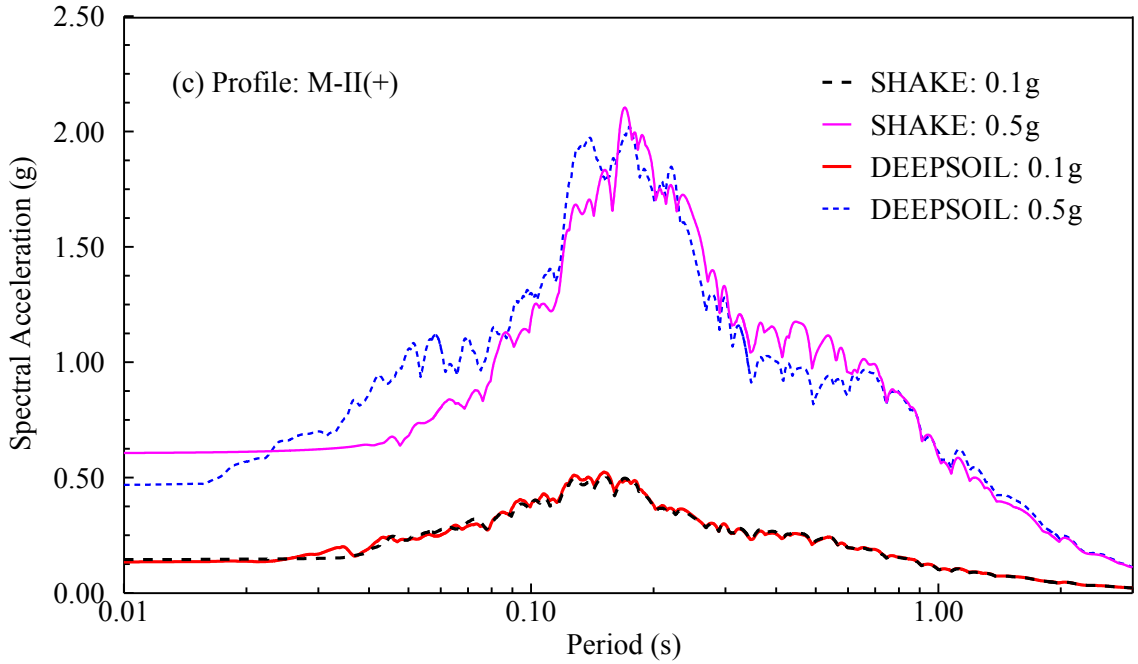

Figure C.15: Comparison of SHAKE and DEEPSOIL spectral acceleration responses for the profile M-II(+) (see Figure 6.3(b) for profile information) and for $PGA_{Outcrop}$ of 0.1g and 0.5g cases.

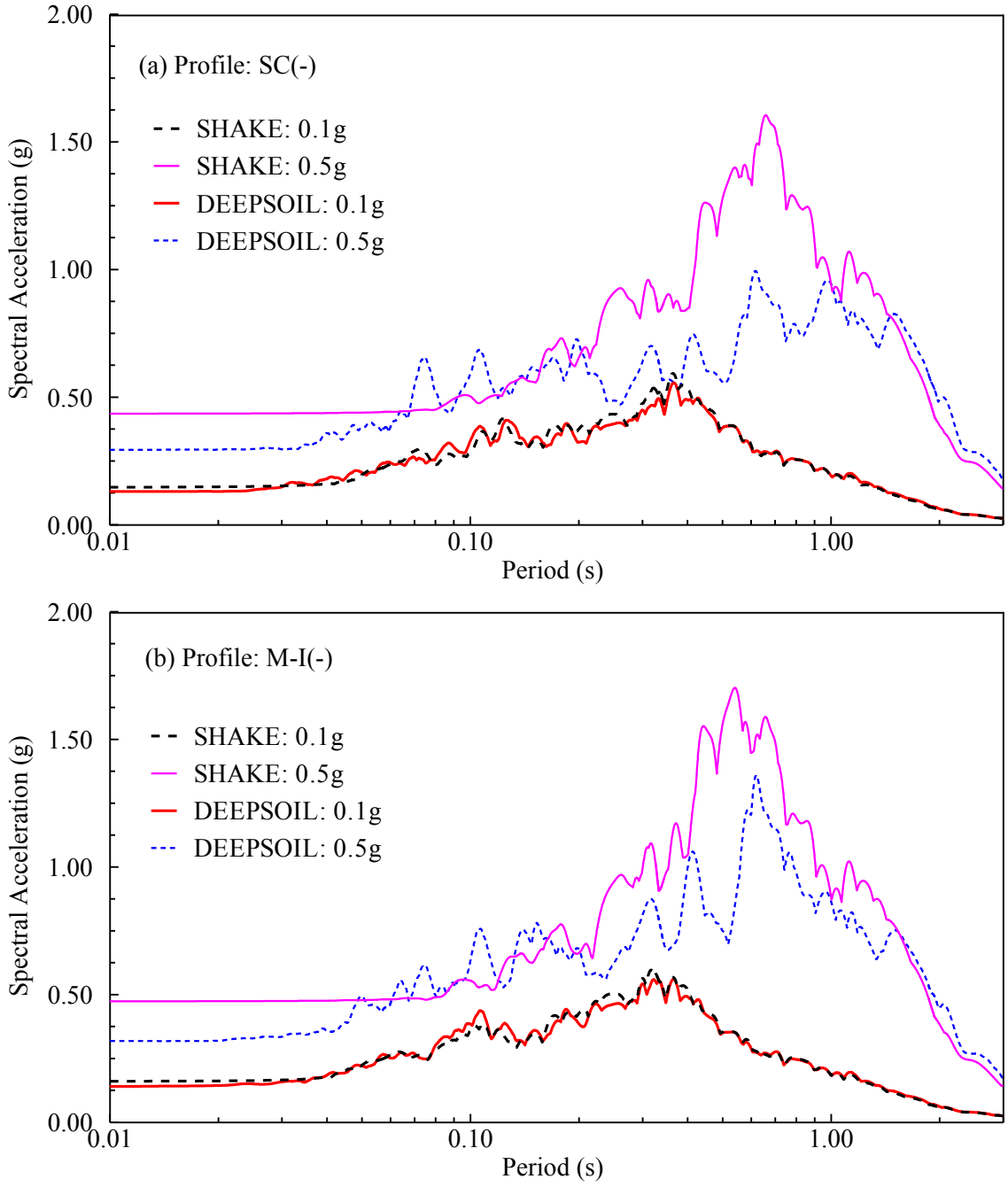

Figure C.16: Comparison of SHAKE and DEEPSOIL spectral acceleration responses for the profiles (see Figure 6.3(c) for profile information): SC(-) and M-I(-) in subplots (a) and (b), respectively and for $PGA_{Outcrop}$ of 0.1g and 0.5g cases.

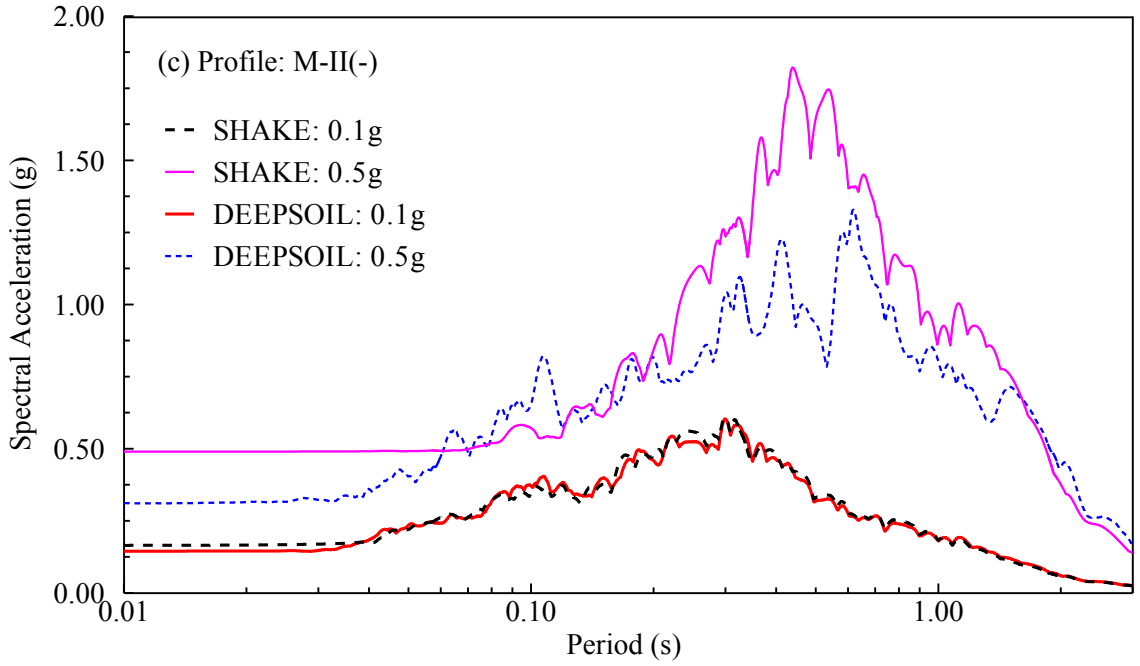

Figure C.17: Comparison of SHAKE and DEEPSOIL spectral acceleration responses for the profile M-II(-) (see Figure 6.3(b) for profile information) and for $PGA_{Outcrop}$ of 0.1g and 0.5g cases.

APPENDIX D

SUMMARY OF MODEL INFORMATION, ANALYSIS RESULTS, AND COMPARISON WITH ASSHTO (2011) FOR REPERCUSSION STUDY PRESENTED IN CHAPTER 7

Table D.1: Modal periods and participating mass (Fixed base).

Modes	Period (sec)	Participating mass					
		Individual Mode (Percent)			Cumulative Sum (Percent)		
		UX	UY	UZ	UX	UY	UZ
1	1.605524	0.00%	68.17%	0.00%	0.00%	68.17%	0.00%
2	1.3625	98.40%	0.00%	0.00%	98.40%	68.17%	0.00%
3	1.030894	0.00%	3.48%	0.00%	98.40%	71.65%	0.00%
4	0.668836	0.00%	15.23%	0.00%	98.40%	86.89%	0.00%
5	0.442127	0.00%	0.21%	0.00%	98.40%	87.09%	0.00%
6	0.274762	0.00%	2.33%	0.00%	98.40%	89.42%	0.00%
7	0.203888	0.00%	0.00%	0.00%	98.40%	89.42%	0.00%
8	0.151085	0.00%	1.01%	0.00%	98.40%	90.43%	0.00%
9	0.117486	0.00%	0.01%	0.00%	98.40%	90.44%	0.00%
10	0.110662	0.02%	0.00%	0.00%	98.41%	90.44%	0.00%
11	0.104737	0.00%	0.08%	0.00%	98.41%	90.52%	0.00%
12	0.103904	0.00%	0.00%	0.00%	98.41%	90.52%	0.00%
13	0.10376	0.34%	0.00%	0.00%	98.75%	90.52%	0.00%
14	0.103604	0.00%	0.10%	0.00%	98.75%	90.62%	0.00%
15	0.093127	0.00%	0.17%	0.00%	98.75%	90.79%	0.00%
16	0.08709	0.00%	0.00%	54.27%	98.75%	90.79%	54.28%
17	0.085262	0.00%	0.02%	0.00%	98.75%	90.81%	54.28%
18	0.084654	0.00%	0.13%	0.00%	98.75%	90.94%	54.28%
19	0.084322	0.35%	0.00%	2.64%	99.10%	90.94%	56.92%
20	0.084193	0.00%	0.00%	0.00%	99.10%	90.94%	56.92%
21	0.084187	0.01%	0.00%	0.10%	99.11%	90.94%	57.02%
22	0.083777	0.35%	0.00%	1.64%	99.45%	90.94%	58.65%
23	0.083469	0.00%	0.03%	0.00%	99.45%	90.96%	58.65%
24	0.082231	0.00%	0.99%	0.00%	99.45%	91.96%	58.65%
25	0.081093	0.00%	0.00%	0.92%	99.46%	91.96%	59.57%
26	0.07255	0.00%	0.00%	26.39%	99.46%	91.96%	85.96%
27	0.069316	0.00%	0.00%	0.00%	99.46%	91.96%	85.96%
28	0.065467	0.00%	0.00%	2.88%	99.46%	91.96%	88.84%
29	0.060783	0.00%	0.29%	0.00%	99.46%	92.24%	88.84%
30	0.056545	0.00%	0.00%	2.23%	99.46%	92.24%	91.07%
31	0.055103	0.01%	0.00%	0.00%	99.47%	92.24%	91.07%
32	0.051975	0.00%	0.01%	0.00%	99.47%	92.25%	91.07%
33	0.045713	0.00%	0.22%	0.00%	99.47%	92.47%	91.07%
34	0.044889	0.00%	0.04%	0.00%	99.47%	92.52%	91.07%
35	0.044715	0.00%	0.00%	0.00%	99.47%	92.52%	91.07%
36	0.044692	0.08%	0.00%	0.00%	99.55%	92.52%	91.07%
37	0.04412	0.00%	0.05%	0.00%	99.55%	92.57%	91.07%
38	0.039936	0.00%	0.05%	0.00%	99.55%	92.62%	91.07%
39	0.038071	0.08%	0.00%	0.03%	99.63%	92.62%	91.10%
40	0.03803	0.00%	0.02%	0.00%	99.63%	92.64%	91.10%

* UX, UY and UZ represent respective mass participations in Global three directions

Table D.2: Modal periods and participating mass (with Foundation Spring).

Modes	Period (sec)	Participating mass					
		Individual Mode (Percent)			Cumulative Sum (Percent)		
		UX	UY	UZ	UX	UY	UZ
1	1.610791	0.00%	45.67%	0.00%	0.00%	45.67%	0.00%
2	1.370173	65.80%	0.00%	0.00%	65.80%	45.67%	0.00%
3	1.035744	0.00%	2.34%	0.00%	65.80%	48.01%	0.00%
4	0.672964	0.00%	10.38%	0.00%	65.80%	58.38%	0.00%
5	0.445255	0.00%	0.14%	0.00%	65.80%	58.52%	0.00%
6	0.277953	0.00%	1.80%	0.00%	65.80%	60.32%	0.00%
7	0.20747	0.00%	0.00%	0.00%	65.80%	60.32%	0.00%
8	0.15439	0.00%	1.03%	0.00%	65.80%	61.35%	0.00%
9	0.132092	0.00%	0.00%	79.26%	65.80%	61.35%	79.26%
10	0.126357	0.00%	0.00%	2.77%	65.81%	61.35%	82.03%
11	0.120668	0.00%	0.01%	0.00%	65.81%	61.36%	82.03%
12	0.112764	0.01%	0.00%	9.46%	65.81%	61.36%	91.49%
13	0.11072	0.04%	0.00%	0.27%	65.85%	61.36%	91.76%
14	0.105942	0.00%	0.23%	0.00%	65.85%	61.59%	91.76%
15	0.104987	0.56%	0.00%	0.09%	66.41%	61.59%	91.85%
16	0.104272	0.00%	0.10%	0.00%	66.41%	61.69%	91.85%
17	0.104228	0.00%	0.00%	0.00%	66.41%	61.69%	91.85%
18	0.095921	0.00%	0.57%	0.00%	66.41%	62.26%	91.85%
19	0.091662	0.02%	0.00%	0.00%	66.43%	62.26%	91.85%
20	0.086596	0.00%	2.98%	0.00%	66.43%	65.24%	91.85%
21	0.086438	1.53%	0.00%	0.02%	67.96%	65.24%	91.87%
22	0.086064	0.00%	1.17%	0.00%	67.96%	66.41%	91.87%
23	0.085723	0.87%	0.00%	0.01%	68.83%	66.41%	91.87%
24	0.085625	0.00%	0.73%	0.00%	68.83%	67.13%	91.87%
25	0.084534	0.00%	0.00%	0.00%	68.83%	67.13%	91.87%
26	0.084534	0.00%	0.00%	0.00%	68.83%	67.13%	91.87%
27	0.084248	0.00%	1.35%	0.00%	68.83%	68.48%	91.87%
28	0.076822	0.00%	0.07%	0.00%	68.83%	68.55%	91.87%
29	0.07206	0.00%	0.22%	0.00%	68.83%	68.77%	91.87%
30	0.070286	0.00%	9.40%	0.00%	68.83%	78.17%	91.87%
31	0.069931	0.06%	0.00%	2.62%	68.88%	78.17%	94.49%
32	0.069319	0.00%	0.00%	0.00%	68.88%	78.17%	94.49%
33	0.069026	0.00%	11.40%	0.00%	68.88%	89.57%	94.49%
34	0.067641	0.00%	9.73%	0.00%	68.88%	99.30%	94.49%
35	0.062743	0.00%	0.03%	0.00%	68.88%	99.32%	94.49%
36	0.06215	6.39%	0.00%	0.00%	75.27%	99.32%	94.49%
37	0.06194	2.01%	0.00%	0.00%	77.28%	99.32%	94.49%
38	0.061681	4.60%	0.00%	0.00%	81.88%	99.32%	94.49%
39	0.061607	9.20%	0.00%	0.00%	91.08%	99.32%	94.50%
40	0.059434	8.33%	0.00%	0.00%	99.41%	99.32%	94.50%

* UX, UY and UZ represent respective mass participations in Global three directions

Table D.3: Analyses results from Case#1 at column top (Seismic loading in both longitudinal and transverse directions, LC1 and LC2) (Also presented in Chapter 6).

		FORCES AND MOMENTS														
		Longitudinal (Global X direction)						Transverse (Global Y direction)						Axial (kips)		
		Shear X (kips)			Moment Y (kips-ft)			Shear Z (kips)			Moment X (kips-ft)					
Support/ Location	Load Case	AASHTO (2011)	Rec.	Difference (%)*	AASHTO (2011)	Rec.	Difference (%)*	AASHTO (2011)	Rec.	Difference (%)*	AASHTO (2011)	Rec.	Difference (%)*	AASHTO (2011)	Rec.	Difference (%)*
Bent 1 Col	LC1	345	308	-10.56	5183	4636	-10.56	44	40	-10.53	668	597	-10.55	90	81	-10.44
	LC2	123	110	-10.47	1848	1655	-10.45	148	132	-10.56	2225	1990	-10.56	236	211	-10.55
Bent 2 Col	LC1	102	91	-10.37	2326	2081	-10.53	31	28	-10.35	699	625	-10.53	100	90	-10.39
	LC2	40	36	-10.33	917	820	-10.50	103	92	-10.36	2330	2084	-10.53	241	216	-10.51
Bent 3 Col	LC1	72	65	-10.08	1843	1650	-10.49	33	29	-10.46	837	748	-10.55	86	77	-10.30
	LC2	25	22	-9.48	628	563	-10.37	110	98	-10.46	2789	2495	-10.55	271	242	-10.53
Bent 4 Col	LC1	102	91	-10.33	2328	2083	-10.52	33	30	-10.36	760	680	-10.53	86	77	-10.25
	LC2	40	36	-10.01	908	813	-10.43	111	100	-10.37	2532	2265	-10.54	246	220	-10.50

* % Difference (in column Forces, Moments or Displacement combinations: LC1 and LC2) = [Recommended- AASHTO (2011)] X 100/ AASHTO (2011). A negative value represents greater AASHTO (2011) outcomes.

Rec.: Based on ADRS curves developed using the recommended site factors.

Table D.4: Analyses results from Case#1 at column bottom (Seismic loading in both longitudinal and transverse directions, LC1 and LC2).

		FORCES AND MOMENTS														
		Longitudinal (Global X direction)						Transverse (Global Y direction)						Axial (kips)		
		Shear X (kips)			Moment Y (kips-ft)			Shear Z (kips)			Moment X (kips-ft)					
Support/ Location	Load Case	AASHTO (2011)	Rec.	Difference (%)*	AASHTO (2011)	Rec.	Difference (%)*	AASHTO (2011)	Rec.	Difference (%)*	AASHTO (2011)	Rec.	Difference (%)*	AASHTO (2011)	Rec.	Difference (%)*
Bent 1 Col	LC1	348	312	-10.56	5220	4669	-10.56	46	41	-10.52	682	610	-10.55	90	81	-10.43
	LC2	124	111	-10.40	1861	1667	-10.42	152	136	-10.56	2271	2031	-10.56	236	211	-10.55
Bent 2 Col	LC1	107	96	-10.37	2384	2133	-10.52	32	29	-10.36	717	642	-10.53	100	90	-10.37
	LC2	43	38	-10.18	944	846	-10.41	107	96	-10.36	2390	2138	-10.53	241	216	-10.50
Bent 3 Col	LC1	78	70	-10.10	1914	1714	-10.45	35	31	-10.46	866	775	-10.55	86	77	-10.19
	LC2	27	25	-9.24	662	595	-10.04	117	104	-10.46	2887	2582	-10.55	271	242	-10.51
Bent 4 Col	LC1	107	96	-10.33	2386	2135	-10.51	35	31	-10.37	781	699	-10.53	86	78	-10.22
	LC2	42	38	-9.88	931	835	-10.34	117	104	-10.38	2603	2329	-10.54	246	221	-10.49

* % Difference (in column Forces, Moments or Displacement combinations: LC1 and LC2) = [Recommended- AASHTO (2011)] X 100/ AASHTO (2011). A negative value represents greater AASHTO (2011) outcomes.

Rec.: Based on ADRS curves developed using the recommended site factors.

Table D.5: Analyses results from Case#1 at column top (Seismic loading in both longitudinal and transverse directions, LC1 and LC2).

		DISPLACEMENTS					
		Global X (ft)			Global Y (ft)		
Support/ Location	Load Case	AASHTO (2011)	Proposed	Difference (%)*	AASHTO (2011)	Proposed	Difference (%)*
Bent 1 Col	LC1	0.2838	0.2539	-10.5608	0.0372	0.0332	-10.5650
	LC2	0.1012	0.0906	-10.4364	0.1238	0.1108	-10.5650
Bent 2 Col	LC1	0.2887	0.2582	-10.5673	0.0877	0.0784	-10.5747
	LC2	0.1141	0.1021	-10.5041	0.2922	0.2613	-10.5749
Bent 3 Col	LC1	0.2844	0.2543	-10.5561	0.1302	0.1164	-10.5753
	LC2	0.0975	0.0874	-10.3833	0.4340	0.3881	-10.5755
Bent 4 Col	LC1	0.2891	0.2586	-10.5667	0.0953	0.0853	-10.5755
	LC2	0.1127	0.1008	-10.4960	0.3178	0.2842	-10.5756

* % Difference (in column Forces, Moments or Displacement combinations: LC1 and LC2) = [Proposed- AASHTO (2011)] X 100/ AASHTO (2011). A negative value represents greater AASHTO (2011) outcomes.

Table D.6: Analyses results from Case#2 at column top (Seismic loading in both longitudinal and transverse directions, LC1 and LC2) (Also presented in Chapter 6).

		FORCES AND MOMENTS														
		Longitudinal (Global X direction)						Transverse (Global Y direction)						Axial (kips)		
		Shear X (kips)			Moment Y (kips-ft)			Shear Z (kips)			Moment X (kips-ft)					
Support/ Location	Load Case	AASHTO (2011)	Rec.	Difference (%)*	AASHTO (2011)	Rec.	Difference (%)*	AASHTO (2011)	Rec.	Difference (%)*	AASHTO (2011)	Rec.	Difference (%)*	AASHTO (2011)	Rec.	Difference (%)*
Bent 1 Col	LC1	935	958	2.49	14052	14402	2.49	120	124	3.19	1813	1871	3.20	245	252	2.97
	LC2	333	341	2.47	5008	5132	2.47	400	413	3.19	6040	6233	3.20	639	659	3.11
Bent 2 Col	LC1	275	282	2.49	6304	6462	2.50	84	86	2.37	1902	1947	2.38	272	278	2.40
	LC2	108	111	2.53	2486	2550	2.56	279	286	2.37	6340	6491	2.38	656	672	2.38
Bent 3 Col	LC1	195	199	2.45	4993	5118	2.49	90	92	2.38	2278	2332	2.39	233	238	2.38
	LC2	66	68	2.48	1701	1745	2.57	298	306	2.38	7592	7774	2.39	737	754	2.38
Bent 4 Col	LC1	276	283	2.47	6309	6466	2.49	91	93	2.41	2067	2117	2.43	234	240	2.41
	LC2	108	110	2.44	2461	2522	2.47	303	310	2.41	6890	7058	2.43	670	686	2.42

* % Difference (in column Forces, Moments or Displacement combinations: LC1 and LC2) = [Recommended- AASHTO (2011)] X 100/ AASHTO (2011). A negative value represents greater AASHTO (2011) outcomes.

Rec.: Based on ADRS curves developed using the recommended site factors.

Table D.7: Analyses results from Case#2 at column bottom (Seismic loading in both longitudinal and transverse directions, LC1 and LC2).

		FORCES AND MOMENTS														
		Longitudinal (Global X direction)						Transverse (Global Y direction)						Axial (kips)		
		Shear X (kips)			Moment Y (kips-ft)			Shear Z (kips)			Moment X (kips-ft)					
Support/ Location	Load Case	AASHTO (2011)	Rec.	Difference (%)*	AASHTO (2011)	Rec.	Difference (%)*	AASHTO (2011)	Rec.	Difference (%)*	AASHTO (2011)	Rec.	Difference (%)*	AASHTO (2011)	Rec.	Difference (%)*
Bent 1 Col	LC1	944	968	2.49	14151	14503	2.49	124	127	3.21	1850	1909	3.21	245	252	2.97
	LC2	337	345	2.46	5043	5168	2.46	411	425	3.22	6165	6363	3.21	640	659	3.11
Bent 2 Col	LC1	290	298	2.49	6460	6621	2.50	87	89	2.37	1952	1998	2.38	272	278	2.40
	LC2	115	118	2.55	2558	2624	2.56	291	297	2.37	6505	6659	2.38	656	672	2.38
Bent 3 Col	LC1	211	216	2.46	5184	5313	2.49	95	97	2.39	2357	2414	2.39	233	239	2.37
	LC2	74	75	2.49	1788	1833	2.56	317	325	2.39	7858	8046	2.39	737	755	2.38
Bent 4 Col	LC1	290	298	2.47	6466	6626	2.49	95	97	2.44	2125	2177	2.44	234	240	2.41
	LC2	114	116	2.43	2522	2585	2.47	317	325	2.44	7083	7256	2.44	670	686	2.42

* % Difference (in column Forces, Moments or Displacement combinations: LC1 and LC2) = [Recommended- AASHTO (2011)] X 100/ AASHTO (2011). A negative value represents greater AASHTO (2011) outcomes.

Rec.: Based on ADRS curves developed using the recommended site factors.

Table D.8: Analyses results from Case#2 at column top (Seismic loading in both longitudinal and transverse directions, LC1 and LC2).

		DISPLACEMENTS					
		Global X (ft)			Global Y (ft)		
Support/ Location	Load Case	AASHTO (2011)	Proposed	Difference (%)*	AASHTO (2011)	Proposed	Difference (%)*
Bent 1 Col	LC1	0.7695	0.7886	2.4889	0.1009	0.1041	3.2077
	LC2	0.2742	0.2809	2.4643	0.3362	0.3469	3.2076
Bent 2 Col	LC1	0.7827	0.8023	2.5004	0.2386	0.2443	2.3816
	LC2	0.3093	0.3173	2.5639	0.7954	0.8143	2.3815
Bent 3 Col	LC1	0.7708	0.7901	2.5011	0.3544	0.3629	2.3940
	LC2	0.2641	0.2710	2.5812	1.1814	1.2097	2.3938
Bent 4 Col	LC1	0.7839	0.8035	2.4900	0.2595	0.2658	2.4403
	LC2	0.3056	0.3131	2.4760	0.8650	0.8862	2.4405

* % Difference (in column Forces, Moments or Displacement combinations: LC1 and LC2) = [Proposed- AASHTO (2011)] X 100/ AASHTO (2011). A negative value represents greater AASHTO (2011) outcomes.

Table D.9: Analyses results from Case#3 at column top (Seismic loading in both longitudinal and transverse directions, LC1 and LC2).

		FORCES AND MOMENTS														
		Longitudinal (Global X direction)						Transverse (Global Y direction)						Axial (kips)		
		Shear X (kips)			Moment Y (kips-ft)			Shear Z (kips)			Moment X (kips-ft)					
Support/ Location	Load Case	AASHTO (2011)	Rec.	Difference (%)*	AASHTO (2011)	Rec.	Difference (%)*	AASHTO (2011)	Rec.	Difference (%)*	AASHTO (2011)	Rec.	Difference (%)*	AASHTO (2011)	Rec.	Difference (%)*
Bent 1 Col	LC1	935	1135	21.44	14052	17065	21.44	120	145	20.64	1813	2187	20.65	245	296	20.86
	LC2	333	404	21.39	5008	6079	21.38	400	483	20.66	6040	7287	20.65	639	772	20.75
Bent 2 Col	LC1	275	334	21.36	6304	7655	21.42	84	102	21.36	1902	2310	21.42	272	330	21.37
	LC2	108	131	21.27	2486	3017	21.33	279	339	21.36	6340	7698	21.42	656	797	21.41
Bent 3 Col	LC1	195	236	21.19	4993	6061	21.39	90	109	21.37	2278	2765	21.41	233	282	21.34
	LC2	66	80	20.85	1701	2063	21.26	298	362	21.37	7592	9218	21.41	737	895	21.41
Bent 4 Col	LC1	276	335	21.35	6309	7661	21.43	91	110	21.32	2067	2509	21.37	234	284	21.27
	LC2	108	131	21.20	2461	2987	21.37	303	367	21.32	6890	8362	21.37	670	813	21.37

* % Difference (in column Forces, Moments or Displacement combinations: LC1 and LC2) = [Recommended- AASHTO (2011)] X 100/ AASHTO (2011). A negative value represents greater AASHTO (2011) outcomes.
Rec.: Based on ADRS curves developed using the recommended site factors.

Table D.10: Analyses results from Case#3 at column bottom (Seismic loading in both longitudinal and transverse directions, LC1 and LC2).

		FORCES AND MOMENTS														
		Longitudinal (Global X direction)						Transverse (Global Y direction)						Axial (kips)		
		Shear X (kips)			Moment Y (kips-ft)			Shear Z (kips)			Moment X (kips-ft)					
Support/ Location	Load Case	AASHTO (2011)	Rec.	Difference (%)*	AASHTO (2011)	Rec.	Difference (%)*	AASHTO (2011)	Rec.	Difference (%)*	AASHTO (2011)	Rec.	Difference (%)*	AASHTO (2011)	Rec.	Difference (%)*
Bent 1 Col	LC1	944	1147	21.44	14151	17185	21.44	124	149	20.62	1850	2232	20.63	245	296	20.86
	LC2	337	408	21.36	5043	6121	21.37	411	496	20.63	6165	7437	20.64	640	772	20.74
Bent 2 Col	LC1	290	352	21.36	6460	7844	21.42	87	106	21.35	1952	2369	21.41	272	330	21.36
	LC2	115	140	21.19	2558	3102	21.28	291	353	21.35	6505	7898	21.41	656	797	21.41
Bent 3 Col	LC1	211	256	21.20	5184	6292	21.38	95	115	21.36	2357	2862	21.40	233	283	21.31
	LC2	74	89	20.71	1788	2165	21.10	317	385	21.36	7858	9540	21.41	737	895	21.40
Bent 4 Col	LC1	290	352	21.35	6466	7851	21.42	95	115	21.30	2125	2579	21.36	234	284	21.26
	LC2	114	138	21.14	2522	3060	21.33	317	384	21.30	7083	8597	21.36	670	813	21.37

* % Difference (in column Forces, Moments or Displacement combinations: LC1 and LC2) = [Recommended- AASHTO (2011)] X 100/ AASHTO (2011). A negative value represents greater AASHTO (2011) outcomes.

Rec.: Based on ADRS curves developed using the recommended site factors.

Table D.11: Analyses results from Case#3 at column top (Seismic loading in both longitudinal and transverse directions, LC1 and LC2).

		DISPLACEMENTS					
		Global X (ft)			Global Y (ft)		
Support/ Location	Load Case	AASHTO (2011)	Proposed	Difference (%)*	AASHTO (2011)	Proposed	Difference (%)*
Bent 1 Col	LC1	0.7695	0.9344	21.4416	0.1009	0.1217	20.6461
	LC2	0.2742	0.3328	21.3772	0.3362	0.4056	20.6466
Bent 2 Col	LC1	0.7827	0.9505	21.4341	0.2386	0.2898	21.4302
	LC2	0.3093	0.3753	21.3216	0.7954	0.9658	21.4300
Bent 3 Col	LC1	0.7708	0.9360	21.4300	0.3544	0.4304	21.4186
	LC2	0.2641	0.3203	21.2605	1.1814	1.4345	21.4184
Bent 4 Col	LC1	0.7839	0.9520	21.4428	0.2595	0.3150	21.3800
	LC2	0.3056	0.3709	21.3932	0.8650	1.0500	21.3800

* % Difference (in column Forces, Moments or Displacement combinations: LC1 and LC2) = [Proposed- AASHTO (2011)] X 100/ AASHTO (2011). A negative value represents greater AASHTO (2011) outcomes.

Table D.12: Analyses results from Case#4 at column top (Seismic loading in both longitudinal and transverse directions, LC1 and LC2).

		FORCES AND MOMENTS														
		Longitudinal (Global X direction)						Transverse (Global Y direction)						Axial (kips)		
		Shear X (kips)			Moment Y (kips-ft)			Shear Z (kips)			Moment X (kips-ft)					
Support/ Location	Load Case	AASHTO (2011)	Rec.	Difference (%)*	AASHTO (2011)	Rec.	Difference (%)*	AASHTO (2011)	Rec.	Difference (%)*	AASHTO (2011)	Rec.	Difference (%)*	AASHTO (2011)	Rec.	Difference (%)*
Bent 1 Col	LC1	1429	980	-31.45	21492	14732	-31.45	157	108	-31.07	2359	1626	-31.07	336	231	-31.21
	LC2	509	349	-31.46	7649	5243	-31.46	523	360	-31.07	7863	5420	-31.07	851	586	-31.14
Bent 2 Col	LC1	420	288	-31.45	9622	6596	-31.45	128	88	-31.52	2908	1992	-31.52	415	284	-31.50
	LC2	163	112	-31.43	3736	2562	-31.42	426	292	-31.52	9693	6638	-31.52	1003	687	-31.52
Bent 3 Col	LC1	296	203	-31.45	7618	5223	-31.45	137	94	-31.51	3473	2379	-31.51	355	243	-31.51
	LC2	99	68	-31.42	2551	1750	-31.41	455	312	-31.51	11577	7929	-31.51	1125	770	-31.51
Bent 4 Col	LC1	421	289	-31.45	9645	6612	-31.45	138	94	-31.50	3130	2144	-31.49	355	243	-31.49
	LC2	164	112	-31.46	3749	2570	-31.46	459	314	-31.50	10432	7147	-31.49	1017	697	-31.50

* % Difference (in column Forces, Moments or Displacement combinations: LC1 and LC2) = [Recommended- AASHTO (2011)] X 100/ AASHTO (2011). A negative value represents greater AASHTO (2011) outcomes.
Rec.: Based on ADRS curves developed using the recommended site factors.

Table D.13: Analyses results from Case#4 at column bottom (Seismic loading in both longitudinal and transverse directions, LC1 and LC2).

		FORCES AND MOMENTS														
		Longitudinal (Global X direction)						Transverse (Global Y direction)						Axial (kips)		
		Shear X (kips)			Moment Y (kips-ft)			Shear Z (kips)			Moment X (kips-ft)					
Support/ Location	Load Case	AASHTO (2011)	Rec.	Difference (%)*	AASHTO (2011)	Rec.	Difference (%)*	AASHTO (2011)	Rec.	Difference (%)*	AASHTO (2011)	Rec.	Difference (%)*	AASHTO (2011)	Rec.	Difference (%)*
Bent 1 Col	LC1	1444	990	-31.45	21642	14835	-31.45	160	110	-31.06	2402	1656	-31.06	336	231	-31.21
	LC2	514	352	-31.46	7701	5278	-31.46	534	368	-31.05	8005	5519	-31.06	851	586	-31.14
Bent 2 Col	LC1	442	303	-31.45	9856	6756	-31.45	133	91	-31.52	2983	2043	-31.52	415	284	-31.50
	LC2	172	118	-31.41	3832	2628	-31.42	444	304	-31.52	9943	6809	-31.52	1004	687	-31.52
Bent 3 Col	LC1	321	220	-31.44	7905	5419	-31.44	145	99	-31.51	3591	2460	-31.51	355	243	-31.51
	LC2	109	75	-31.39	2665	1828	-31.40	483	331	-31.51	11972	8199	-31.51	1125	770	-31.51
Bent 4 Col	LC1	443	304	-31.45	9883	6774	-31.45	143	98	-31.49	3212	2201	-31.49	355	244	-31.49
	LC2	172	118	-31.46	3838	2631	-31.46	478	328	-31.49	10708	7336	-31.49	1017	697	-31.50

* % Difference (in column Forces, Moments or Displacement combinations: LC1 and LC2) = [Recommended- AASHTO (2011)] X 100/ AASHTO (2011). A negative value represents greater AASHTO (2011) outcomes.
Rec.: Based on ADRS curves developed using the recommended site factors.

Table D.14: Analyses results from Case#4 at column top (Seismic loading in both longitudinal and transverse directions, LC1 and LC2).

		DISPLACEMENTS					
		Global X (ft)			Global Y (ft)		
Support/ Location	Load Case	AASHTO (2011)	Proposed	Difference (%)*	AASHTO (2011)	Proposed	Difference (%)*
Bent 1 Col	LC1	1.1768	0.8067	-31.4510	0.1311	0.0904	-31.0624
	LC2	0.4187	0.2870	-31.4594	0.4371	0.3013	-31.0623
Bent 2 Col	LC1	1.1946	0.8189	-31.4465	0.3649	0.2499	-31.5185
	LC2	0.4641	0.3183	-31.4197	1.2162	0.8329	-31.5185
Bent 3 Col	LC1	1.1765	0.8066	-31.4455	0.5403	0.3700	-31.5102
	LC2	0.3953	0.2712	-31.4046	1.8010	1.2335	-31.5102
Bent 4 Col	LC1	1.1986	0.8216	-31.4510	0.3927	0.2690	-31.4924
	LC2	0.4655	0.3191	-31.4581	1.3089	0.8967	-31.4923

* % Difference (in column Forces, Moments or Displacement combinations: LC1 and LC2) = [Proposed- AASHTO (2011)] X 100/ AASHTO (2011). A negative value represents greater AASHTO (2011) outcomes.

Table D.15: Analyses results from Test#1 at column top (Seismic loading in both longitudinal and transverse directions, LC1 and LC2).

		FORCES AND MOMENTS														
		Longitudinal						Transverse						Axial (kips)		
		Shear X (kips)			Moment Y (kips-ft)			Shear Z (kips)			Moment X (kips-ft)					
Support/ Location	Load Test	Case#1	Case#2	Difference (%)*	Case#1	Case#2	Difference (%)*	Case#1	Case#2	Difference (%)*	Case#1	Case#2	Difference (%)*	Case#1	Case#2	Difference (%)*
Bent 1 Col	LC1	308	306	-0.87	4636	4604	-0.69	40	40	0.11	597	597	-0.02	81	78	-4.00
	LC2	110	109	-0.58	1655	1648	-0.40	132	132	0.20	1990	1990	0.02	211	209	-1.02
Bent 2 Col	LC1	91	94	2.84	2081	2095	0.68	28	29	4.79	625	632	1.04	90	85	-5.28
	LC2	36	37	3.37	820	827	0.80	92	96	4.74	2084	2105	1.02	216	216	0.29
Bent 3 Col	LC1	65	67	3.23	1650	1663	0.82	29	30	1.34	748	750	0.27	77	75	-2.65
	LC2	22	23	4.72	563	570	1.22	98	99	1.20	2495	2500	0.20	242	242	-0.27
Bent 4 Col	LC1	91	95	3.43	2083	2100	0.80	30	31	4.01	680	684	0.71	77	77	-0.40
	LC2	36	39	7.45	813	827	1.69	100	104	3.96	2265	2281	0.69	220	223	0.91

* % Difference (in column Forces, Moments or Displacement combinations: LC1 and LC2) = [Case#2- Case#1] X 100/ Case#1. A negative value represents greater Case#1 outcomes.

Table D.16: Analyses results from Test#1 at column bottom (Seismic loading in both longitudinal and transverse directions, LC1 and LC2).

		FORCES AND MOMENTS														
		Longitudinal						Transverse						Axial (kips)		
		Shear X (kips)			Moment Y (kips-ft)			Shear Z (kips)			Moment X (kips-ft)					
Support/ Location	Load Test	Case#1	Case#2	Difference (%)*	Case#1	Case#2	Difference (%)*	Case#1	Case#2	Difference (%)*	Case#1	Case#2	Difference (%)*	Case#1	Case#2	Difference (%)*
Bent 1 Col	LC1	312	309	-0.87	4669	4616	-1.13	41	41	-0.03	610	609	-0.16	81	78	-4.00
	LC2	111	111	-0.53	1667	1654	-0.77	136	136	0.06	2031	2029	-0.12	211	209	-1.03
Bent 2 Col	LC1	96	98	2.17	2133	2141	0.38	29	30	4.29	642	648	0.98	90	85	-5.15
	LC2	38	39	2.77	846	850	0.58	96	100	4.25	2138	2159	0.96	216	217	0.40
Bent 3 Col	LC1	70	72	1.79	1714	1721	0.43	31	32	0.86	775	776	0.22	77	75	-2.29
	LC2	25	26	3.16	595	601	0.94	104	105	0.71	2582	2586	0.15	242	242	-0.17
Bent 4 Col	LC1	96	99	2.72	2135	2146	0.50	31	32	3.54	699	703	0.66	78	77	-0.19
	LC2	38	40	6.41	835	847	1.44	104	108	3.50	2329	2344	0.64	221	223	1.03

* % Difference (in column Forces, Moments or Displacement combinations: LC1 and LC2) = [Case#2- Case#1] X 100/ Case#1. A negative value represents greater Case#1 outcomes.

Table D.17: Analyses results from Test#1 at column top (Seismic loading in both longitudinal and transverse directions, LC1 and LC2).

		DISPLACEMENTS					
		Global X (ft)			Global Y (ft)		
Support/ Location	Load Test	Case#1	Case#2	Difference (%)*	Case#1	Case#2	Difference (%)*
Bent 1 Col	LC1	0.2539	0.2560	0.8351	0.0332	0.0338	1.6523
	LC2	0.0906	0.0915	0.9458	0.1108	0.1126	1.6515
Bent 2 Col	LC1	0.2582	0.2603	0.8072	0.0784	0.0790	0.8318
	LC2	0.1021	0.1028	0.7357	0.2613	0.2635	0.8321
Bent 3 Col	LC1	0.2543	0.2564	0.8237	0.1164	0.1171	0.5437
	LC2	0.0874	0.0882	0.9072	0.3881	0.3902	0.5435
Bent 4 Col	LC1	0.2586	0.2607	0.8020	0.0853	0.0858	0.6229
	LC2	0.1008	0.1016	0.7507	0.2842	0.2859	0.6222

* % Difference (in column Forces, Moments or Displacement combinations: LC1 and LC2) = [Case#2- Case#1] X 100/ Case#1.
A negative value represents greater Case#1 outcomes.

Table D.18: Analyses results from Test#2 at column top (Seismic loading in both longitudinal and transverse directions, LC1 and LC2).

		FORCES AND MOMENTS														
		Longitudinal						Transverse						Axial (kips)		
		Shear X (kips)			Moment Y (kips-ft)			Shear Z (kips)			Moment X (kips-ft)					
Support/ Location	Load Test	Case#1	Case#2	Difference (%)*	Case#1	Case#2	Difference (%)*	Case#1	Case#2	Difference (%)*	Case#1	Case#2	Difference (%)*	Case#1	Case#2	Difference (%)*
Bent 1 Col	LC1	958	948	-0.97	14402	14293	-0.75	124	124	-0.18	1871	1868	-0.12	252	242	-4.09
	LC2	341	339	-0.69	5132	5107	-0.49	413	413	-0.12	6233	6227	-0.09	659	652	-1.12
Bent 2 Col	LC1	282	282	-0.11	6462	6469	0.11	86	86	0.05	1947	1950	0.12	278	261	-6.06
	LC2	111	111	-0.01	2550	2553	0.14	286	286	0.01	6491	6497	0.10	672	666	-0.81
Bent 3 Col	LC1	199	201	0.75	5118	5138	0.39	92	92	0.26	2332	2334	0.07	238	229	-3.78
	LC2	68	69	1.37	1745	1755	0.55	306	306	0.19	7774	7777	0.04	754	750	-0.61
Bent 4 Col	LC1	283	284	0.62	6466	6483	0.26	93	94	0.63	2117	2119	0.06	240	237	-1.35
	LC2	110	117	6.31	2522	2558	1.43	310	312	0.61	7058	7062	0.06	686	687	0.04

* % Difference (in column Forces, Moments or Displacement combinations: LC1 and LC2) = [Case#2- Case#1] X 100/ Case#1. A negative value represents greater Case#1 outcomes.

Table D.19: Analyses results from Test#2 at column bottom (Seismic loading in both longitudinal and transverse directions, LC1 and LC2).

		FORCES AND MOMENTS														
		Longitudinal						Transverse						Axial (kips)		
		Shear X (kips)			Moment Y (kips-ft)			Shear Z (kips)			Moment X (kips-ft)					
Support/ Location	Load Test	Case#1	Case#2	Difference (%)*	Case#1	Case#2	Difference (%)*	Case#1	Case#2	Difference (%)*	Case#1	Case#2	Difference (%)*	Case#1	Case#2	Difference (%)*
Bent 1 Col	LC1	968	958	-0.95	14503	14333	-1.17	127	127	-0.14	1909	1907	-0.13	252	242	-4.07
	LC2	345	343	-0.67	5168	5123	-0.86	425	424	-0.08	6363	6356	-0.11	659	652	-1.12
Bent 2 Col	LC1	298	297	-0.09	6621	6613	-0.13	89	89	0.06	1998	2000	0.11	278	262	-6.02
	LC2	118	118	0.02	2624	2622	-0.05	297	298	0.02	6659	6666	0.09	672	667	-0.80
Bent 3 Col	LC1	216	218	0.66	5313	5320	0.14	97	98	0.27	2414	2415	0.06	239	230	-3.45
	LC2	75	76	1.17	1833	1840	0.35	325	325	0.19	8046	8048	0.03	755	750	-0.58
Bent 4 Col	LC1	298	299	0.55	6626	6627	0.01	97	98	0.63	2177	2178	0.05	240	237	-1.29
	LC2	116	123	5.60	2585	2616	1.23	325	327	0.61	7256	7259	0.04	686	687	0.06

* % Difference (in column Forces, Moments or Displacement combinations: LC1 and LC2) = [Case#2- Case#1] X 100/ Case#1. A negative value represents greater Case#1 outcomes.

Table D.20: Analyses results from Test#2 at column top (Seismic loading in both longitudinal and transverse directions, LC1 and LC2).

		DISPLACEMENTS					
		Global X (ft)			Global Y (ft)		
Support/ Location	Load Test	Case#1	Case#2	Difference (%)*	Case#1	Case#2	Difference (%)*
Bent 1 Col	LC1	0.7886	0.7948	0.7905	0.1041	0.1058	1.6669
	LC2	0.2809	0.2833	0.8661	0.3469	0.3527	1.6671
Bent 2 Col	LC1	0.8023	0.8084	0.7653	0.2443	0.2463	0.8313
	LC2	0.3173	0.3194	0.6836	0.8143	0.8211	0.8317
Bent 3 Col	LC1	0.7901	0.7962	0.7774	0.3629	0.3649	0.5439
	LC2	0.2710	0.2732	0.8134	1.2097	1.2163	0.5441
Bent 4 Col	LC1	0.8035	0.8096	0.7596	0.2658	0.2675	0.6237
	LC2	0.3131	0.3153	0.6939	0.8862	0.8917	0.6234

* % Difference (in column Forces, Moments or Displacement combinations: LC1 and LC2) = [Case#2- Case#1] X 100/ Case#1.
A negative value represents greater Case#1 outcomes.

Table D.21: Analyses results from Test#3 at column top (Seismic loading in both longitudinal and transverse directions, LC1 and LC2).

		FORCES AND MOMENTS														
		Longitudinal						Transverse						Axial (kips)		
		Shear X (kips)			Moment Y (kips-ft)			Shear Z (kips)			Moment X (kips-ft)					
Support/ Location	Load Test	Case#1	Case#2	Difference (%)*	Case#1	Case#2	Difference (%)*	Case#1	Case#2	Difference (%)*	Case#1	Case#2	Difference (%)*	Case#1	Case#2	Difference (%)*
Bent 1 Col	LC1	1135	1124	-0.97	17065	16937	-0.75	145	145	0.14	2187	2191	0.20	296	284	-3.93
	LC2	404	401	-0.70	6079	6049	-0.49	483	484	0.19	7287	7303	0.22	772	765	-0.86
Bent 2 Col	LC1	334	334	-0.06	7655	7664	0.13	102	102	0.06	2310	2312	0.10	330	310	-6.08
	LC2	131	131	0.04	3017	3022	0.18	339	339	0.03	7698	7705	0.09	797	790	-0.82
Bent 3 Col	LC1	236	237	0.53	6061	6083	0.35	109	109	0.16	2765	2766	0.04	282	271	-4.18
	LC2	80	81	0.99	2063	2073	0.50	362	363	0.10	9218	9219	0.01	895	889	-0.68
Bent 4 Col	LC1	335	336	0.41	7661	7677	0.21	110	111	0.35	2509	2509	0.01	284	280	-1.46
	LC2	131	136	4.11	2987	3016	0.96	367	369	0.34	8362	8363	0.01	813	813	-0.04

* % Difference (in column Forces, Moments or Displacement combinations: LC1 and LC2) = [Case#2- Case#1] X 100/ Case#1. A negative value represents greater Case#1 outcomes.

Table D.22: Analyses results from Test#3 at column bottom (Seismic loading in both longitudinal and transverse directions, LC1 and LC2).

		FORCES AND MOMENTS														
		Longitudinal						Transverse						Axial (kips)		
		Shear X (kips)			Moment Y (kips-ft)			Shear Z (kips)			Moment X (kips-ft)					
Support/ Location	Load Test	Case#1	Case#2	Difference (%)*	Case#1	Case#2	Difference (%)*	Case#1	Case#2	Difference (%)*	Case#1	Case#2	Difference (%)*	Case#1	Case#2	Difference (%)*
Bent 1 Col	LC1	1147	1136	-0.95	17185	16983	-1.17	149	149	0.19	2232	2236	0.19	296	284	-3.91
	LC2	408	406	-0.67	6121	6068	-0.87	496	498	0.24	7437	7452	0.21	772	766	-0.85
Bent 2 Col	LC1	352	352	-0.04	7844	7834	-0.12	106	106	0.07	2369	2372	0.09	330	310	-6.05
	LC2	140	140	0.08	3102	3102	-0.02	353	353	0.05	7898	7904	0.08	797	790	-0.81
Bent 3 Col	LC1	256	257	0.48	6292	6298	0.10	115	116	0.17	2862	2863	0.03	283	272	-3.91
	LC2	89	90	0.88	2165	2171	0.31	385	385	0.11	9540	9540	0.00	895	889	-0.65
Bent 4 Col	LC1	352	354	0.37	7851	7848	-0.04	115	116	0.37	2579	2579	0.00	284	280	-1.42
	LC2	138	143	3.65	3060	3083	0.75	384	386	0.36	8597	8596	0.00	813	813	-0.02

* % Difference (in column Forces, Moments or Displacement combinations: LC1 and LC2) = [Case#2- Case#1] X 100/ Case#1. A negative value represents greater Case#1 outcomes.

Table D.23: Analyses results from Test#3 at column top (Seismic loading in both longitudinal and transverse directions, LC1 and LC2).

		DISPLACEMENTS					
		Global X (ft)			Global Y (ft)		
Support/ Location	Load Test	Case#1	Case#2	Difference (%)*	Case#1	Case#2	Difference (%)*
Bent 1 Col	LC1	0.9344	0.9418	0.7908	0.1217	0.1241	1.9873
	LC2	0.3328	0.3356	0.8586	0.4056	0.4136	1.9868
Bent 2 Col	LC1	0.9505	0.9578	0.7706	0.2898	0.2921	0.8138
	LC2	0.3753	0.3780	0.7173	0.9658	0.9737	0.8140
Bent 3 Col	LC1	0.9360	0.9433	0.7820	0.4304	0.4326	0.5324
	LC2	0.3203	0.3230	0.8483	1.4345	1.4421	0.5325
Bent 4 Col	LC1	0.9520	0.9593	0.7606	0.3150	0.3170	0.6286
	LC2	0.3709	0.3735	0.6928	1.0500	1.0566	0.6285

* % Difference (in column Forces, Moments or Displacement combinations: LC1 and LC2) = [Case#2- Case#1] X 100/ Case#1.
A negative value represents greater Case#1 outcomes.

Table D.24: Analyses results from Test#4 at column top (Seismic loading in both longitudinal and transverse directions, LC1 and LC2).

		FORCES AND MOMENTS														
		Longitudinal						Transverse						Axial (kips)		
		Shear X (kips)			Moment Y (kips-ft)			Shear Z (kips)			Moment X (kips-ft)					
Support/ Location	Load Test	Case#1	Case#2	Difference (%)*	Case#1	Case#2	Difference (%)*	Case#1	Case#2	Difference (%)*	Case#1	Case#2	Difference (%)*	Case#1	Case#2	Difference (%)*
Bent 1 Col	LC1	980	970	-0.98	14732	14621	-0.75	108	108	0.12	1626	1629	0.17	231	221	-4.30
	LC2	349	346	-0.71	5243	5216	-0.51	360	361	0.16	5420	5431	0.19	586	581	-0.90
Bent 2 Col	LC1	288	288	-0.02	6596	6604	0.13	88	88	0.10	1992	1994	0.12	284	267	-6.08
	LC2	112	112	0.03	2562	2566	0.15	292	292	0.08	6638	6645	0.11	687	682	-0.79
Bent 3 Col	LC1	203	204	0.29	5223	5239	0.30	94	94	0.07	2379	2379	0.02	243	232	-4.78
	LC2	68	68	0.50	1750	1756	0.37	312	312	0.03	7929	7929	0.01	770	765	-0.73
Bent 4 Col	LC1	289	289	0.15	6612	6622	0.16	94	94	0.06	2144	2143	-0.06	243	240	-1.62
	LC2	112	114	1.58	2570	2581	0.43	314	314	0.06	7147	7143	-0.06	697	696	-0.13

* % Difference (in column Forces, Moments or Displacement combinations: LC1 and LC2) = [Case#2- Case#1] X 100/ Case#1. A negative value represents greater Case#1 outcomes.

Table D.25: Analyses results from Test#4 at column bottom (Seismic loading in both longitudinal and transverse directions, LC1 and LC2).

		FORCES AND MOMENTS														
		Longitudinal						Transverse						Axial (kips)		
		Shear X (kips)			Moment Y (kips-ft)			Shear Z (kips)			Moment X (kips-ft)					
Support/ Location	Load Test	Case#1	Case#2	Difference (%)*	Case#1	Case#2	Difference (%)*	Case#1	Case#2	Difference (%)*	Case#1	Case#2	Difference (%)*	Case#1	Case#2	Difference (%)*
Bent 1 Col	LC1	990	980	-0.96	14835	14661	-1.18	110	111	0.17	1656	1659	0.17	231	221	-4.29
	LC2	352	350	-0.69	5278	5231	-0.89	368	369	0.20	5519	5529	0.18	586	581	-0.89
Bent 2 Col	LC1	303	303	-0.01	6756	6748	-0.12	91	91	0.11	2043	2045	0.11	284	267	-6.07
	LC2	118	118	0.05	2628	2626	-0.06	304	304	0.10	6809	6816	0.10	687	682	-0.79
Bent 3 Col	LC1	220	221	0.27	5419	5422	0.05	99	99	0.08	2460	2460	0.01	243	232	-4.61
	LC2	75	75	0.47	1828	1831	0.16	331	331	0.04	8199	8199	-0.01	770	765	-0.71
Bent 4 Col	LC1	304	304	0.14	6774	6768	-0.09	98	98	0.08	2201	2199	-0.06	244	240	-1.60
	LC2	118	120	1.42	2631	2637	0.22	328	328	0.08	7336	7331	-0.07	697	696	-0.12

* % Difference (in column Forces, Moments or Displacement combinations: LC1 and LC2) = [Case#2- Case#1] X 100/ Case#1. A negative value represents greater Case#1 outcomes.

Table D.26: Analyses results from Test#4 at column top (Seismic loading in both longitudinal and transverse directions, LC1 and LC2).

		DISPLACEMENTS					
		Global X (ft)			Global Y (ft)		
Support/ Location	Load Test	Case#1	Case#2	Difference (%)*	Case#1	Case#2	Difference (%)*
Bent 1 Col	LC1	0.8067	0.8131	0.7879	0.0904	0.0922	1.9569
	LC2	0.2870	0.2894	0.8412	0.3013	0.3072	1.9570
Bent 2 Col	LC1	0.8189	0.8252	0.7651	0.2499	0.2519	0.8276
	LC2	0.3183	0.3205	0.6795	0.8329	0.8398	0.8279
Bent 3 Col	LC1	0.8066	0.8128	0.7754	0.3700	0.3721	0.5421
	LC2	0.2712	0.2733	0.7943	1.2335	1.2402	0.5420
Bent 4 Col	LC1	0.8216	0.8279	0.7571	0.2690	0.2707	0.6186
	LC2	0.3191	0.3212	0.6722	0.8967	0.9022	0.6185

* % Difference (in column Forces, Moments or Displacement combinations: LC1 and LC2) = [Case#2- Case#1] X 100/ Case#1.
A negative value represents greater Case#1 outcomes.

Table D.27: Modal periods and participating mass.

Modes	Period (sec)	Participating mass					
		Individual Mode (Percent)			Cumulative Sum (Percent)		
		UX	UY	UZ	UX	UY	UZ
1	0.535865	1.064E-19	0.68604	8.063E-18	1.064E-19	0.68604	8.063E-18
2	0.24793	4.214E-18	0.00001769	5.897E-17	4.321E-18	0.68606	6.704E-17
3	0.215441	0.94503	1.607E-16	0.000000169	0.94503	0.68606	0.000000169
4	0.172805	0.000001627	1.769E-14	0.00002019	0.94503	0.68606	0.00002036
5	0.160199	8.539E-07	1.415E-14	0.00338	0.94503	0.68606	0.0034
6	0.151785	5.053E-16	0.1945	1.423E-14	0.94503	0.88056	0.0034
7	0.146294	9.508E-09	5.485E-13	0.00005753	0.94503	0.88056	0.00346
8	0.14293	0.00006324	2.443E-14	0.00047	0.94509	0.88056	0.00393
9	0.142318	0.00007235	6.992E-14	0.00001237	0.94517	0.88056	0.00394
10	0.139284	0.00001039	1.127E-15	0.00006948	0.94518	0.88056	0.00401
11	0.137672	0.00001807	6.979E-14	2.777E-07	0.94519	0.88056	0.00401
12	0.136094	0.000003261	1.687E-15	0.00217	0.9452	0.88056	0.00618
13	0.132799	0.00002533	3.855E-13	0.00207	0.94522	0.88056	0.00826
14	0.13198	0.0001	3.896E-14	0.01661	0.94532	0.88056	0.02487
15	0.130891	0.00017	5.657E-17	0.00569	0.94549	0.88056	0.03056
16	0.128469	0.004	3.038E-14	0.00035	0.94949	0.88056	0.03091
17	0.123114	0.00001656	5.042E-14	0.00000141	0.94951	0.88056	0.03091
18	0.117701	0.000002602	8.883E-13	0.34615	0.94951	0.88056	0.37706
19	0.109126	5.83E-14	5.607E-07	2.332E-12	0.94951	0.88056	0.37706
20	0.107872	1.086E-08	1.949E-15	0.00642	0.94951	0.88056	0.38348
21	0.097127	7.219E-07	6.994E-15	0.13491	0.94951	0.88056	0.51839
22	0.091965	3.802E-14	0.00097	2.256E-11	0.94951	0.88152	0.51839
23	0.091833	1.2E-13	0.00001931	1.597E-12	0.94951	0.88154	0.51839
24	0.089486	6.824E-15	0.00213	2.58E-11	0.94951	0.88368	0.51839
25	0.088176	8.845E-14	0.00044	1.076E-11	0.94951	0.88412	0.51839
26	0.087722	1.624E-16	0.00045	6.447E-11	0.94951	0.88457	0.51839
27	0.086453	2.46E-16	0.03297	3E-13	0.94951	0.91754	0.51839
28	0.085525	0.00236	1.051E-13	0.01447	0.95188	0.91754	0.53286
29	0.084296	1.459E-15	0.00214	1.258E-11	0.95188	0.91968	0.53286
30	0.083704	1.33E-13	0.00046	5.282E-12	0.95188	0.92014	0.53286
31	0.083064	0.00014	5.027E-13	0.05461	0.95201	0.92014	0.58747
32	0.08299	8.055E-14	0.00157	1.788E-13	0.95201	0.92172	0.58747
33	0.08201	2.181E-09	2.176E-13	1.115E-10	0.95201	0.92172	0.58747
34	0.082002	6.769E-09	2.43E-13	6.399E-09	0.95201	0.92172	0.58747
35	0.081623	2.277E-14	0.00166	1.821E-14	0.95201	0.92338	0.58747
36	0.081455	0.000006467	4.02E-14	0.08397	0.95202	0.92338	0.67143
37	0.081405	2.02E-14	0.000000181	5.528E-13	0.95202	0.92338	0.67143
38	0.081383	7.127E-13	0.000001006	1.331E-11	0.95202	0.92338	0.67143
39	0.081155	3.967E-12	2.292E-12	3.642E-10	0.95202	0.92338	0.67143
40	0.081147	9.633E-15	4.505E-13	6.573E-13	0.95202	0.92338	0.67143

(Continued)

Modes	Period (sec)	Participating mass					
		Individual Mode (Percent)			Cumulative Sum (Percent)		
		UX	UY	UZ	UX	UY	UZ
41	0.081072	4.675E-13	5.084E-09	2.063E-16	0.95202	0.92338	0.67143
42	0.081045	3.081E-13	2.085E-08	8.122E-19	0.95202	0.92338	0.67143
43	0.081011	2.708E-11	3.204E-12	5.193E-12	0.95202	0.92338	0.67143
44	0.08098	1.739E-11	4.909E-14	1.186E-10	0.95202	0.92338	0.67143
45	0.08074	8.501E-14	1.566E-12	5.488E-12	0.95202	0.92338	0.67143
46	0.080737	2.564E-13	2.029E-10	3.618E-12	0.95202	0.92338	0.67143
47	0.080718	3.65E-14	2.112E-08	6.044E-13	0.95202	0.92338	0.67143
48	0.080698	8.771E-13	4.1E-13	5.267E-13	0.95202	0.92338	0.67143
49	0.080697	1.514E-13	9.528E-13	7.444E-12	0.95202	0.92338	0.67143
50	0.080694	4.753E-13	2.037E-08	3.93E-12	0.95202	0.92338	0.67143
51	0.080689	6.918E-13	1.461E-12	7.424E-14	0.95202	0.92338	0.67143
52	0.080687	3.198E-14	4.769E-09	2.096E-12	0.95202	0.92338	0.67143
53	0.080687	4.098E-14	5.374E-09	5.713E-12	0.95202	0.92338	0.67143
54	0.080684	8.8E-14	8.188E-09	1.703E-12	0.95202	0.92338	0.67143
55	0.080683	6.916E-14	1.368E-12	5.859E-12	0.95202	0.92338	0.67143
56	0.080679	2.652E-13	2.891E-14	1.373E-11	0.95202	0.92338	0.67143
57	0.079821	1.12E-13	0.00008122	5.859E-13	0.95202	0.92346	0.67143
58	0.079548	1.04E-09	1.982E-13	1.233E-09	0.95202	0.92346	0.67143
59	0.078941	2.652E-14	9.681E-07	5.015E-14	0.95202	0.92346	0.67143
60	0.078689	1.142E-12	2.741E-14	2.497E-12	0.95202	0.92346	0.67143

* UX, UY and UZ represent respective mass participations in Global three directions

Table D.28: Analyses results in case of FEE at pile (middle) top (Seismic loading in both longitudinal and transverse directions, LC1 and LC2).

		FORCES AND MOMENTS														
		Longitudinal						Transverse						Axial (kips)		
		Shear X (kips)			Moment Y (kips-ft)			Shear Y (kips)			Moment X (kips-ft)					
Bent #	Load Case	Des.	Prop.	Difference (%)	Des.	Prop.	Difference (%)	Des.	Prop.	Difference (%)	Des.	Prop.	Difference (%)	Des.	Prop.	Difference (%)
1	LC1	1	1	3.96	15	16	3.94	1	1	2.24	10	10	0.63	1	1	3.94
	LC2	0	0	3.96	5	5	3.94	2	2	2.24	32	32	0.63	0	0	3.94
2	LC1	1	1	3.99	16	17	3.94	1	1	0.78	22	22	0.39	1	1	3.95
	LC2	0	0	3.99	5	5	3.94	4	4	0.78	73	73	0.39	0	0	3.95
3	LC1	1	1	3.92	18	19	3.94	2	2	0.68	34	34	0.41	0	0	3.85
	LC2	0	0	3.92	5	6	3.94	6	6	0.68	114	115	0.41	0	0	3.85
4	LC1	1	1	3.92	19	20	3.94	2	2	0.40	47	47	0.38	0	0	3.85
	LC2	0	0	3.92	6	6	3.94	7	7	0.40	156	157	0.38	0	0	3.85
5	LC3	2	2	3.90	20	21	3.94	2	2	0.72	51	52	0.41	0	0	3.30
	LC4	0	0	3.90	6	6	3.94	8	8	0.72	171	172	0.41	0	0	3.30
6	LC5	2	2	4.00	20	21	3.94	2	2	0.52	48	49	0.39	0	0	4.13
	LC6	0	0	4.00	6	6	3.94	8	8	0.52	161	162	0.39	0	0	4.13
7	LC7	1	1	3.95	18	19	3.94	2	2	0.62	40	40	0.41	1	1	3.81
	LC8	0	0	3.95	6	6	3.94	7	7	0.62	132	132	0.41	0	0	3.81
8	LC9	1	1	3.93	17	17	3.94	1	1	0.74	25	25	0.39	1	1	3.99
	LC10	0	0	3.93	5	5	3.94	4	4	0.74	82	82	0.39	0	0	3.99
9	LC11	1	1	3.60	32	33	3.92	4	4	0.46	107	107	0.45	3	3	3.91
	LC12	0	0	3.60	10	10	3.92	14	14	0.46	355	357	0.45	1	1	3.91

Table D.29: Analyses results in case of FEE at pile (middle) top (Seismic loading in both longitudinal and transverse directions, LC1 and LC2).

		DISPLACEMENTS					
		Global X (ft)			Global Y (ft)		
Bent #	Load Case	Design	Proposed	Difference (%)	Design	Proposed	Difference (%)
1	LC1	0.0157	0.0163	3.9406	0.0060	0.0061	0.5669
	LC2	0.0047	0.0049	3.9406	0.0201	0.0202	0.5669
2	LC1	0.0170	0.0177	3.9408	0.0140	0.0141	0.4282
	LC2	0.0051	0.0053	3.9408	0.0467	0.0469	0.4282
3	LC1	0.0184	0.0191	3.9432	0.0232	0.0233	0.3879
	LC2	0.0055	0.0057	3.9432	0.0773	0.0776	0.3879
4	LC1	0.0194	0.0201	3.9375	0.0326	0.0327	0.3808
	LC2	0.0058	0.0060	3.9375	0.1087	0.1091	0.3808
5	LC3	0.0199	0.0207	3.9394	0.0370	0.0371	0.3843
	LC4	0.0060	0.0062	3.9394	0.1234	0.1238	0.3843
6	LC5	0.0197	0.0205	3.9406	0.0349	0.0350	0.3811
	LC6	0.0059	0.0062	3.9406	0.1162	0.1167	0.3811
7	LC7	0.0187	0.0195	3.9370	0.0269	0.0270	0.3821
	LC8	0.0056	0.0058	3.9370	0.0898	0.0901	0.3821
8	LC9	0.0173	0.0180	3.9406	0.0159	0.0160	0.4149
	LC10	0.0052	0.0054	3.9406	0.0530	0.0532	0.4149
9	LC11	0.0146	0.0152	3.9361	0.0059	0.0059	0.5731
	LC12	0.0044	0.0045	3.9361	0.0195	0.0197	0.5731

Table D.30: Analyses results in case of SEE at pile (middle) top (Seismic loading in both longitudinal and transverse directions, LC1 and LC2).

		FORCES AND MOMENTS														
		Longitudinal						Transverse						Axial (kips)		
		Shear X (kips)			Moment Y (kips-ft)			Shear Y (kips)			Moment X (kips-ft)					
Bent #	Load Case	Des.	Prop.	Difference (%)	Des.	Prop.	Difference (%)	Des.	Prop.	Difference (%)	Des.	Prop.	Difference (%)	Des.	Prop.	Difference (%)
1	LC1	4	2	-44.09	52	32	-38.75	2	1	-43.66	37	23	-38.89	3	2	-38.53
	LC2	1	1	-44.09	15	9	-38.75	8	5	-43.66	123	75	-38.89	1	1	-38.54
2	LC1	4	2	-42.43	55	34	-38.54	5	3	-39.08	86	53	-38.29	2	1	-38.65
	LC2	1	1	-42.44	17	10	-38.54	15	9	-39.08	287	177	-38.29	1	0	-38.65
3	LC1	4	3	-39.16	61	38	-38.34	7	4	-39.00	134	83	-38.35	2	1	-39.09
	LC2	1	1	-39.16	18	11	-38.34	22	14	-39.00	447	276	-38.35	0	0	-39.09
4	LC1	5	3	-38.55	65	40	-38.29	9	5	-38.34	184	114	-38.29	1	1	-39.89
	LC2	1	1	-38.55	20	12	-38.29	29	18	-38.34	614	379	-38.29	0	0	-39.90
5	LC3	5	3	-38.40	68	42	-38.28	9	6	-39.05	201	124	-38.36	0	0	-46.26
	LC4	2	1	-38.40	20	13	-38.28	32	19	-39.05	670	413	-38.36	0	0	-46.27
6	LC5	5	3	-38.40	67	42	-38.28	9	5	-38.62	190	117	-38.32	1	1	-40.66
	LC6	2	1	-38.40	20	12	-38.28	29	18	-38.62	632	390	-38.32	0	0	-40.67
7	LC7	4	3	-39.01	62	39	-38.33	8	5	-38.93	155	96	-38.36	2	1	-39.68
	LC8	1	1	-39.01	19	12	-38.33	25	16	-38.93	517	319	-38.36	1	0	-39.68
8	LC9	4	2	-41.92	57	35	-38.51	5	3	-38.98	97	60	-38.30	3	2	-41.48
	LC10	1	1	-41.92	17	10	-38.51	17	10	-38.98	322	199	-38.30	1	1	-41.48
9	LC11	4	2	-49.61	108	67	-38.64	17	10	-38.47	417	257	-38.41	9	5	-44.19
	LC12	1	1	-49.61	33	20	-38.64	55	34	-38.47	1391	857	-38.41	3	2	-44.19

Table D.31: Analyses results in case of SEE at pile (middle) top (Seismic loading in both longitudinal and transverse directions, LC1 and LC2).

		DISPLACEMENTS					
		Global X (ft)			Global Y (ft)		
Bent #	Load Case	Design	Proposed	Difference (%)	Design	Proposed	Difference (%)
1	LC1	0.0530	0.0327	-38.3131	0.0235	0.0144	-38.6562
	LC2	0.0159	0.0098	-38.3131	0.0784	0.0481	-38.6562
2	LC1	0.0575	0.0355	-38.2992	0.0549	0.0339	-38.3770
	LC2	0.0173	0.0106	-38.2992	0.1831	0.1128	-38.3770
3	LC1	0.0621	0.0383	-38.2884	0.0911	0.0562	-38.2977
	LC2	0.0186	0.0115	-38.2884	0.3037	0.1874	-38.2977
4	LC1	0.0655	0.0404	-38.2828	0.1281	0.0791	-38.2841
	LC2	0.0196	0.0121	-38.2828	0.4270	0.2635	-38.2841
5	LC3	0.0673	0.0415	-38.2796	0.1453	0.0897	-38.2910
	LC4	0.0202	0.0125	-38.2796	0.4844	0.2989	-38.2910
6	LC5	0.0667	0.0412	-38.2798	0.1369	0.0845	-38.2865
	LC6	0.0200	0.0123	-38.2798	0.4565	0.2817	-38.2865
7	LC7	0.0633	0.0391	-38.2873	0.1058	0.0653	-38.2871
	LC8	0.0190	0.0117	-38.2873	0.3525	0.2175	-38.2871
8	LC9	0.0585	0.0361	-38.2969	0.0624	0.0385	-38.3524
	LC10	0.0175	0.0108	-38.2969	0.2080	0.1282	-38.3524
9	LC11	0.0493	0.0304	-38.2844	0.0229	0.0140	-38.6705
	LC12	0.0148	0.0091	-38.2844	0.0762	0.0467	-38.6705

BIBLIOGRAPHY

Aboye, S. A, Andrus, R. D., Ravichandran, N., Bhuiyan, A., and Harman, N., (2013a). Seismic Site Factors and Design Response Spectra Based on Conditions in Charleston, South Carolina. *Earthquake Spectra* (in print).

Aboye, S. A., Andrus, R. D., Ravichandran, N., Bhuiyan, A. H., and Harman, N. E., (2013b). Amplitude- and V_{S30}- based Seismic Site Factor Model for Myrtle Beach South Carolina, *Proc., 7th National Seismic Conference on Bridges and Highways*, *MCEER*, University of Buffalo, NY, May 20-22, Oakland, CA.

Aboye, S., Andrus, R. D., Ravichandran, N., Bhuiyan, A. and Harman, N., (2011). Site factors for estimating peak ground acceleration in Charleston, South Carolina, based on V_{S30}. *Proc., 4th IASPEI/IAEE International Symposium: Effects of Surface Geology on Seismic Motion*, University of California Santa Barbara, CA, August 23-26, http://esg4.eri.ucsb.edu/.

Aboye, S., Andrus, R. D., Ravichandran, N., Bhuiyan, A. H., Martin, J. R. and Harman, N. (2014). A New Seismic Site Coefficient Model Based on Conditions in the South Carolina Coastal Plain. *Bulletin of the Seismological Society of America (BSSA)*, 104(6), 2866-2883.

Afacan, K. B., Brandenberg, S. J., and Stewart, J. P. (2013). Centrifuge modeling studies of site response in soft clay over wide strain range. *Journal of Geotechnical and Geoenvironmental Engineering*, 140(2). (http://dx.doi.org/10.1061/(ASCE)GT.1943-5606.0001014)

American Association of State Highway and Transportation Officials (AASHTO), (2011). *LRFD Bridge Design Specifications, AASHTO 2nd Edition,* Washington, D.C.

American Society of Civil Engineers (ASCE), 2010. *Minimum Design Loads for Buildings and Other Structures, ASCE standard 7-10*, Reston, VA, 650 p.

Andrus, R. D., Fairbanks, C. D., Zhang, J., Camp III, W. M., Casey, T. J., Cleary, T. J., and Wright, W. B. (2006). Shear-wave velocity and seismic response of near-surface sediments in Charleston, South Carolina. *Bull. Seism. Soc. Am.*, (Vol. 95(5)), pp. 1897-1914.

Andrus, R. D., Ravichandran, N., Aboye, S., Bhuiyan, A. H., and Martin, J. R. (2014). Seismic Site Coefficients and Accleration Design Response Spectra Based on Conditions in South Carolina. Final Report to SCDOT, FHWA-SC-14-02, Glenn Dept. of Civil Engg., 367 p.

Ardoino, F., Traverso, C. M., and Parker, E. J. (2008). Evaluation of Site Response for Deepwater Field. *Geotechnical Earthquake Engineering and Soil Dynamics* IV (pp. 1-10). ASCE.

Assimaki, D. (2004). Topography effects in the 1999 Athens earthquake: Engineering issues in seismology. PhD Dissertation, Department of Civil and Environmental Engineering, Massachusetts Institute of Technology.

Assimaki, D., and Jeong, S. (2013). Ground-Motion Observations at Hotel Montana during the M 7.0 2010 Haiti Earthquake: Topography or Soil Amplification?. *Bulletin of the Seismological Society of America*, *103*(5), 2577-2590.

Assimaki, D., and Li, W. (2012). Site-and ground motion-dependent nonlinear effects in seismological model predictions. *Soil Dynamics and Earthquake Engineering*, 32(1), 143-151. doi:10.1016/j.soildyn.2011.06.013

ATC/MCEER. (2003a). Design Examples: Recommended LRFD guidelines for the seismic design of highway bridges, Report No. MCEER/ATC-49, Applied Technology Council and Multidisciplinary Center for Earthquake Engineering Research Center, Redwood City, CA.

ATC/MCEER. (2003b). Specifications: Recommended LRFD guidelines for the seismic design of highway bridges, Report No. MCEER/ATC-49, Applied Technology Council and Multidisciplinary Center for Earthquake Engineering Research Center, Redwood City, CA.

Atkinson, G. M., and Boore, D. M. (1995). Ground motion relations for eastern North America, *Bull. Seism. Soc. Am.*, 85(1), 17-30.

Bard, P. Y. (1999). Local effects on strong ground motion: physical basis and estimation methods in view of microzoning studies. In *Proc. Advanced Study Course "Seismotectonic and Microzonation Techniques in Earthquake Engineering,"* Kefallinia, Greece.

Bhuiyan, M. H., Ravichandran, N., Andrus, R. D., and Aboye, S. A., (2013). Comparison of nonlinear one-dimensional and two-dimensional site response analysis tools for Charleston, SC. *Proc., 2013 Geo-Congress: Stability and Performance of Slopes and Embankments III, Geotechnical Special Publication No. 231*, ASCE, San Diego, CA, March 3-7, 1240-1249.

Biscontin, G. and and J.M. Pestana. (2006). Factors Affecting Seismic Response of Submarine Slopes. *Natural Hazards and Earth System Sciences*, Vol. 6 (1), pp. 97-107.

Biscontin, G., and Pestana, J. M. (2006). Factors affecting seismic response of submarine slopes. *Natural Hazards and Earth System Science*, *6*(1), 97-107.

Bollinger, G. A. (1977). Reinterpretation of the intensity data for the 1886 Charleston, South Carolina, earthquake, *Studies Related to the Charleston, South Carolina, Earthquake of 1886: A Preliminary Report*, *U.S.G.S. Prof. Paper 1028*, Reston, VA, D. W. Rankin (editor), 17-32.

Boore, D. M. (1972). A note on the effect of simple topography on seismic SH waves. *Bulletin of the seismological Society of America*, 62(1):275–284.

Borcherdt, R. D. (1994). Estimates of site-dependent response spectra for design (methodology and justification), *Earthquake Spectra*, 10(4), 617-653.

Borcherdt, R. D., and Glassmoyer, G. (1992). On the characteristics of local geology and their influence on ground motions generated by the Loma Prieta earthquake in the San Francisco Bay region, California, *Bull. Seism. Soc. Am.*, 82(2), 603-641.

Borja, R. I., H. Y. Chao, F. J. Montans, C. Lin (1999). Nonlinear Ground Response at Lotung LSST site. *Journal of Geotechnical and Geoenvironmental Engineering*, 125(3), 187-197.

Bouckovalas, G. D., and Papadimitriou, A. G. (2005). Numerical evaluation of slope topography effects on seismic ground motion. *Soil Dynamics and Earthquake Engineering*, *25*(7), 547-558.

Bozzano, F., Martino, S., Giacomi, A. C., Lenti, L., Martini, G., and D'Avila, M. S. (2012) Numerical modeling of nonlinear dynamic shear strains in heterogeneous soils by 1D-3C finite element SWAP_3C. *Proc. of the 15th world conference on earthquake engineering*, Lisbon, Portugal.

Brandenberg, S.J., Stewart, J.P., and Afacan, K. (2013). Influence of Liquefaction on Earthquake Ground Motions. Final Report for USGS, Award Number G12AP20098.

Building Seismic Safety Council (BSSC) (1995). NEHRP Recommended Provisions for Seismic Regulations for New Buildings (1994 edition), *Federal Emergency Management Agency, FEMA* 222A/223A, Building Seismic Safety Council, Washington, D.C.

Building Seismic Safety Council (BSSC) (2010). NEHRP Recommended Provisions for Seismic Regulations for New Buildings and Other Structures (2009 edition), Fe*deral Emergency Management Agency, FEMA P-749*, Building Seismic Safety Council, Washington, D.C.

Camp, W., Brown, D., and Mayne, P. (2002). Construction Method Effects on Axial Drilled Shaft Performance. *Deep Foundations* 2002: pp. 193-208. Doi: 10.1061/40601(256)14

Chapman, M. C. (2006). User's guide to SCENARIO_PC and SCDOTSHAKE. Report to the South Carolina Department of Transportation, Columbia, SC.

Chapman, M. C., and Talwani, P. (2002). Seismic hazard mapping for bridge and highway design, Report to the South Carolina Department of Transportation, Columbia, SC.

*Chapman, M. C., Martin, J. R., Olgun, C. G., and Beale, J. N., (*2006*).* Site-response models for Charleston, South Carolina and vicinity developed from shallow geotechnical investigations*, Bull. Seism. Soc. Am.*, 96(2)*,* 467-489.

Clough, R. W., and Penzien, J. (1993) Dynamics of structures. Vol. xxii. New York: McGraw- Hill.

CSI (2009). CSI Analysis Reference Manual. Version 14.2.2, Computers and Structures Inc. California, USA.

Dobry, R., Martin, G. M., Parra, E., and Bhattacharya, A., (1994). Development of site-dependent ratios of elastic response spectra (RRS) and site categories for building seismic codes, *Proc. NCEER, SEAOC, BSSC Workshop on Site Response during Earthquakes and Seismic Code Provisions*, University of Southern California, Los Angeles, CA, November 18 - 20, 1992.

Durá-Gómez, I., and Talwani, P. (2009). Finding faults in the Charleston area, South Carolina: 1. Seismological data. Seismological Research Letters, 80(5), 883-900. doi: 10.1785/gssrl.80.5.883

Elgamal, A., Yang, Z., Parra, E., and Ragheb A. (2003). Modeling of cyclic mobility in saturated cohesionless soil. Int. J. Plasticity 19, pp. 883–905.

Fernandez, J. A., and Rix, G. J. (2008). Basin Effects in the Upper Mississippi Embayment. In *Geotechnical Earthquake Engineering and Soil Dynamics IV*(pp. 1-10). ASCE.

Geli, L., Bard, P. Y., and Jullien, B. (1988). The effect of topography on earthquake ground motion: a review and new results. *Bulletin of the Seismological Society of America*, *78*(1), 42-63.

Gouveia, F., Gomes, R. C., Lopes, I. F., and Author, A. B. (2012) Influence of stiffness contrast in non-horizontally layered ground on site effects. *Proc. of the 15th world conference on earthquake engineering,* Lisbon, Portugal.

Gu, Q., Conte, J.P., Yang, Z., and Elgamal, A. (2011). Consistent tangent moduli for multi-yield-surface J2 plasticity model. *Comput. Mech.* 48, 1 (July 2011), 97-120.

Gvirtzman, Z., and Louie, J. N. (2010). 2D analysis of earthquake ground motion in Haifa Bay, Israel. *Bulletin of the Seismological Society of America*, *100*(2), 733-750.

Hadj-Hamou, T., and Kavazanjian Jr, E. (1985). Seismic stability of gentle infinite slopes. *Journal of Geotechnical Engineering*, *111*(6), 681-697.

Hartzell, S., Bonilla, L. F., and Williams, R. A. (2004). Prediction of nonlinear soil effects. *Bulletin of the Seismological Society of America,* 94(5), 1609-1629. (http://www.civil.utah.edu/~bartlett/CVEEN6330/ NONLINVSEQL.pdf)

Hashash, Y. M., Phillips, C., & Groholski, D. R. (2010). Recent advances in nonlinear site response analysis. In *Fifth International Conference in Recent Advances in Geotechnical Earthquake Engineering and Soil Dynamics*.

Hashash, Y.M.A. (2011). DEEPSOIL v5.0, User Manual and Tutorial. University of Illinois at Urbana-Champaign, Urbana, IL, < www.illinois.edu/~deepsoil >.

Hashash, Y.M.A. and D. Park (2001). Nonlinear one-dimensional seismic ground motion propagation in the Mississippi embayment. *Eng. Geology*, Amsterdam, 62(1–3), 185–206.

Hudson, M., I.M. Idriss, and M. Beikae (1994). QUAD4M – A computer program to evaluate the seismic response of soil structures using finite element procedures and incorporating a compliant base. Center for Geotechnical Modeling, Dept. Civil and Envir. Eng., Univ. of Calif., Davis, CA.

Idriss, I. M., and Sun, J. I. (1992). SHAKE91: A computer program for conducting equivalent linear seismic response analyses of horizontally layered soil deposits. Department of Civil and Environmental Engineering, University of California Davis.

International Codes Council, Inc. (ICC). (2012). International Building Code (IBC), Falls Church, VA, 328 pp.

Jaume, S. C. (2006). Shear wave velocity profiles via seismic cone penetration test and refraction microtremor techniques at ANSS strong motion sites in Charleston, South Carolina. *Seismological Research Letters* 77.6 (2006): 771-779.

Johnston, A. C., (1996). Seismic moment assessment of earthquakes in stable continental regions, III. New Madrid 1811-1812, Charleston 1886 and Lisbon 1755. *Geophys. J. Int.*, 126(2), 314–344.

Joyner, W. B., Fumal, T. E., and Glassmoyer, G., (1994). Empirical spectral response ratios for strong motion data from the 1989 Loma Prieta, California, earthquake, *Proc. NCEER, SEAOC, BSSC Workshop on Site Response during Earthquakes and Seismic Code Provisions*, University of Southern California, Los Angeles, CA, November 18 - 20, 1992.

Kaklamanos, J., Baise, L. G., Thompson, E. M., and Dorfmann, L. (2015). Comparison of 1D linear, equivalent-linear, and nonlinear site response models at six KiK-net validation sites. *Soil Dynamics and Earthquake Engineering*, 69, 207-219. doi:10.1016/j.soildyn.2014.10.016

Kaklamanos, J., Bradley, B. A., Thompson, E. M., and Baise, L. G. (2013). Critical Parameters Affecting Bias and Variability in Site-Response Analyses Using KiK-net Downhole Array Data. *Bulletin of the Seismological Society of America*, 103(3), 1733-1749. doi: 10.1785/0120120166

Kim, B., and Hashash, Y. M. (2013). Site response analysis using downhole array recordings during the March 2011 Tohoku-Oki earthquake and the effect of long-duration ground motions. *Earthquake Spectra*, *29*(s1), S37-S54.

Kim, B., Hashash, Y. M., Kottke, A. R., Assimaki, D., Li, W., Rathje, E. M., Campbell, K. W., Silva, W. J. and Stewart, J. P. (2013). A predictive model for the relative differences between nonlinear and equivalent-linear site response analyses. In *Proceedings of the 22nd International Conference in Structural Mechanics in Reactor Technology*, San Francisco, California, 18–23 August.

Ko, C. P. (2001). Fully coupled site response analysis for mild sloping ground. M.Sc. thesis. Hongkong University of Science and Technology, Hongkong.

Kondner R.L. (1963). Hyperbolic stress-strain response: cohesive soils. *J Soil Mech Found Div* (ASCE) 89(SM1):115–143

Kondner, R. L., and J.S. Zelasko (1963). A hyperbolic stress-strain formulation of sands. *Proc. of 2nd Pan American Conference on Soil Mechanics and Foundation Engineering*, Sao Paulo, Brasil, 289–324.

Kottke, A. R. (2010). A Comparison of Seismic Site Response Methods. *Ph.D. Dissertation, University of Texas at Austin*, Austin, Texas.

Kramer, S.L. and Paulsen, S.B. (2004). Practical Use of Geotechnical Site Response Models. *Proceedings, International Workshop on Uncertainties in Nonlinear*

Soil Properties and their Impact on Modeling Dynamic Soil Response, University of California, Berkeley.

Kramer, S.L., (1996). Geotechnical Earthquake Engineering. Prentice Hall, Upper Saddle River, N.J.

Kramer, S.L.,Hartvigsen. A.J., Sideras. S.S. and Ozener. P.T. (2011). Site Response Modeling in Liquefiable Soil Deposits. *4th IASPEI / IAEE International Symposium*, August, 2011,University of California, Santa Barbara, CA.

Kwok, A. O. L., Stewart, J. P., and Hashash, Y. M. A. (2008). Nonlinear ground-response analysis of Turkey Flat shallow stiff-soil site to strong ground motion. *Bulletin of Seismological Society of America,* 98(1), 331–343. doi: 10.1785/0120070009

Kwok, O.L.A., J.P. Stewart, Y.M.A. Hashash, N. Matasovic, R.M. Pyke, Z.L. Wang, and Z. Yang (2007). Use of exact solutions of wave propagation problems to guide implementationof nonlinear seismic ground response analysis procedures. *J. of Geotech. & Geoenvir. Eng.*,ASCE, 133, no. 11, 1385–1398

Lee, C-P., Y-B. Tsai, and K-L. Wen (2006). Analysis of Nonlinear Site Response using the LSST Downhole Accelerometer Array Data. *Soil Dynamics and Earthquake Engineering*, 26, 435-460

Lee, M. K., and Finn, W. D. L. (1978). DESRA-2, Dynamic effective stress response analysis of soil deposits with energy transmitting boundary including assessment of liquefaction potential. *Soil Mechanics Series*, No. 36, Department of Civil Engineering, University of British Columbia, Vancouver, Canada.

Lester, A. P., and Chapman, M. C., (2005). An examination of site response in Columbia, South Carolina, *Seism. Res. Lett.*, 76(1), 118 p.

Li, X., Wang, Z. L., and Shen, C. K. (1997). SUMDES. A nonlinear procedure for response analysis of horizontally layered sites subjected to multi-directional earthquake loading. Department of Civil Engineering, University of California at Davis.

Masing, G. (1926). Eignespannungen und Verfestigung beim Messing. *Second International Congress on Applied Mechanics*, Zurich, Switzerland, 332-335.

Matasovic, N. (1993). Seismic response of composite horizontally-layered soil deposits. Ph.D. Thesis, University of California, Los Angeles.

Matasovic, N. and Vucetic, M. (1993a). Cyclic Characterization of Liquefiable Sands. *J. of Geotech. Eng*., ASCE, 119(11), 1805-1822. (http://dx.doi.org/10.1061/(ASCE)0733-9410(1993)119:11(1805))

Matasovic, N. and Vucetic, M. (1993b). Seismic response of horizontally layered soil deposits. Report No. ENG 93-182, School of Engineering and Applied Science, University of California, Los Angeles.

Matasovic, N. and Y. Hashash (2012). NCHRP428: Practices and procedures for site-specific evaluations of earthquake ground motions (A synthesis of highway practice). National Cooperative Highway Research Program, Transportation Research Board, Washington, D.C. (http://onlinepubs.trb.org/onlinepubs/nchrp/nchrp_syn_428.pdf)

Matasović, N., and Ordóñez, G. A., (2011). D-MOD2000: A Computer program for seismic response analysis of horizontally layered soil deposits, Earthfill Dams and Solid Waste Landfills, User's Manual, Geomotions, LLC, Lacey, WA, 172 p., http://www.geomotions.com.

Matsuo, O., Saito, Y., Sasaki, T., Kondoh, K., and Sato, T. (2002). Earthquake-induced flow slides of fills and infinite slopes. *Soils and foundations*, *42*(1), 89-104.

McCartan, L., Lemon, E. M., and Weems, R. E. (1984). Geologic Map of the area between Charleston and Orangeburg, South Carolina. USGS Misc. Investigations Series Map I-1472, Reston, VA.

McKenna, F., and Fenves, G. L. (2001). The OpenSees Command Language Manual: Version 1.2. PEER Center, University of California at Berkely.

Newmark, N. M. (1959). A Method of Computation for Structural Dynamics. *Journal of the Engineering Mechanics Division*, 85, 67-94.

Odum, J. K., Williams, R. A., Stepheson, W. J., and Worley, D. M., (2003). Near-surface S-wave and P-wave seismic velocities of primary geological formations on the Piedmont and Atlantic Coastal Plain of South Carolina, US, *U.S.G.S., Reston, VA, Open-file Report 03-043,* 14 p.

Ordóñez, G. A., (2011). SHAKE2000: A computer program for the 1D analysis of geotechnical earthquake engineering problems, user's manual, Geomotions, LLC, Lacey, WA.

Park, D., and Y. M. A. Hashash (2004). Estimation of Nonlinear Seismic Site Effects for Deep Deposits of the Mississippi Embayment. Technical Report, National Science Foundation, Mid America Earthquake Center.

Phillips, C., and Hashash, Y. (2009). Damping formulation for nonlinear 1D site response analyses. *Soil Dynamics and Earthquake Engineering*, 29(7), 1143-1158.

Prevost, J. H. (1989). DYNA1D: A computer program for nonlinear site response analysis, technical documentation. National Center of Earthquake Engineering Research, Sunny at Buffalo, NY.

Prevost, J.H. (1985). A simple plasticity theory for frictional cohesionless soils. *Soil Dyn. Earthquake Eng*., 4(1), 9-17.

Ravichandran, N., Bhuiyan, A. H., and Huggins, E. L. (2012). Dynamic Analysis of Unsaturated Soil-Pile System Using Improved Simplified Finite Element Formulation. *Proc., 2012 Geo-Congress: State of the Art and Practice in Geotechnical Engineering, ASCE*, Oakland, CA. March 25-29, (March 2013; http://ascelibrary.org/doi/abs/10.1061/9780784412121.252)

Ravichandran, N., Krishnapillai, H., Bhuiyan, A. H., and Huggins, E. (2015). A Simplified Finite Element Model for Site Response Analysis of Unsaturated Soil Profiles. *International Journal of Geomechanics.* (Accepted)

Santi, P. M. (2006). Field methods for characterizing weak rock for engineering. *Environmental & Engineering Geoscience*, *12*(1), 1-11.

Schnabel, P. B., Lysmer, J. L., and Seed, H. B. (1972). SHAKE: A computer program for earthquake response analysis of horizontally layered sites. EERC-72/12, Earthquake Engineering Research Center, Berkeley, CA.

Seed, R. B., Dickenson, S., and Mok, C. M., 1994. Site effects on strong shaking and seismic risk: recent developments and their impact on seismic design codes and practice, *Proc. of the ASCE Structures Congress XII,* vol. 1, Atlanta, GA, 573–578.

Semblat, J. F., Dangla, P., Kham, M., and Duval, A. M. (2002). Seismic site effects for shallow and deep alluvial basins: in-depth motion and focusing effect. *Soil Dynamics and Earthquake Engineering*, *22*(9), 849-854.

Seyhan, E., and Stewart, J. P. (2014). Semi-empirical nonlinear site amplification from NGA-West 2 data and simulations. *Earthquake Spectra*, 30(3), 1241-1256.

Silva, W., Wang, I., Siegel, T., Gregor, N., Darragh, R. and Lee, R., (2003). Ground motion and liquefaction simulation of the 1886 Charleston, South Carolina, earthquake, *Bull. Seism. Soc. Am.,* 93 (6), 2717-2736.

South Carolina Department of Natural Resources (SCDNR). (2005). Generalized geologic map of South Carolina, South Carolina Department of Natural Resources and South Carolina Geological Survey, Columbia, SC.

South Carolina Department of Natural Resources (SCDNR). (2006). Statewide Digital Elevation Model for South Carolina. South Carolina Department of Natural Resources and South Carolina Geological Survey, Columbia, SC.

South Carolina Department of Transportation (SCDOT). (2008a). Geotechnical Design Manual. Version 1.0. South Carolina Department of Transportation, Columbia, SC.

South Carolina Department of Transportation (SCDOT). (2008b). SCDOT Seismic Design Specification of Highway Bridges. Version 2.0. South Carolina Department of Transportation, Columbia, SC.

Stewart, J.P. and O.L.A. Kwok. (2008). Nonlinear seismic ground response analysis: code usageprotocols and verification against vertical array data. *Proc. 4th Decennial GeotechnicalEarthquake Engineering and Soil Dynamics* Conference, ASCE, Sacramento, CA

Stewart, J.P., Kwok, A.O., Hashash, Y.M.A., Matasovic, N., Pyke, R., Wang, Z., and Yang, Z. (2008). Benchmarking of nonlinear geotechnical ground response analysis procedures. Report PEER 2008/04, Pacific Earthquake Engineering Research Center, University of California, Berkeley.

Stewart, J.P., O.L.A. Kwok, Y.M.A. Hashash, N. Matasovic, R. Pyke, Z.L. Wang, and Z. Yang (2006). Overcoming hurdles that limit the application of nonlinear seismic ground response analysis in engineering practice. *5th National Seismic Conference on Bridges and Highways*, San Francisco, CA

Taboada-Urtuzuástegui, V. M., and Dobry, R. (1998). Centrifuge modeling of earthquake-induced lateral spreading in sand. *Journal of Geotechnical and Geoenvironmental Engineering*, *124*(12), 1195-1206.

Talwani, P., and Schaeffer, W. T. (2001). Recurrence rates of large earthquakes in the South Carolina Coastal Plain based on paleoliquefaction data. *Journal of Geophysical Research: Solid Earth* (1978–2012), 106(B4), 6621-6642. doi: 10.1029/2000JB900398

Tokimatsu, K., and Sugimoto, R. (2008). Strain-Dependent Soil Properties Estimated from Downhole Array Recordings at Kashiwazaki-Kariwa Nuclear Power Plant During the 2007 Niigata-Ken Chuetsu-Oki Earthquake. *Geotechnical Earthquake Engineering and Soil Dynamics IV* (pp.1-10). ASCE. (http://ascelibrary.org/doi/pdf/10.1061/40975(318)25)

Wheeler, R. L., and Cramer, C. H. (2000). Preliminary estimate of the amplification of possible earthquake ground motion at a site in Charleston County, South Carolina, *U.S.G.S., Reston, VA, Open-file Report 00-048.*

Zalachoris, G. (2014). Evaluation of one-dimensional site response methodologies using borehole arrays, Ph.D. Dissertation, The University of Texas at Austin, Austin, TX.

Zhang J., Andrus, R. D., and Juang, C. H. (2008). Model uncertainty in normalized shear modulus and damping relationships. *Jour. Geotech. and Geoenviron. Engrg*, 134 (1), pp. 24-36.

Zhang, J., Andrus, R. D., and Juang, C. H. (2005). Normalized shear modulus and material damping ratio relationships. *Journal of geotechnical and geoenvironmental engineering,* 131(4), 453-464. http://dx.doi.org/10.1061/(ASCE)1090-0241(2005)131:4(453)